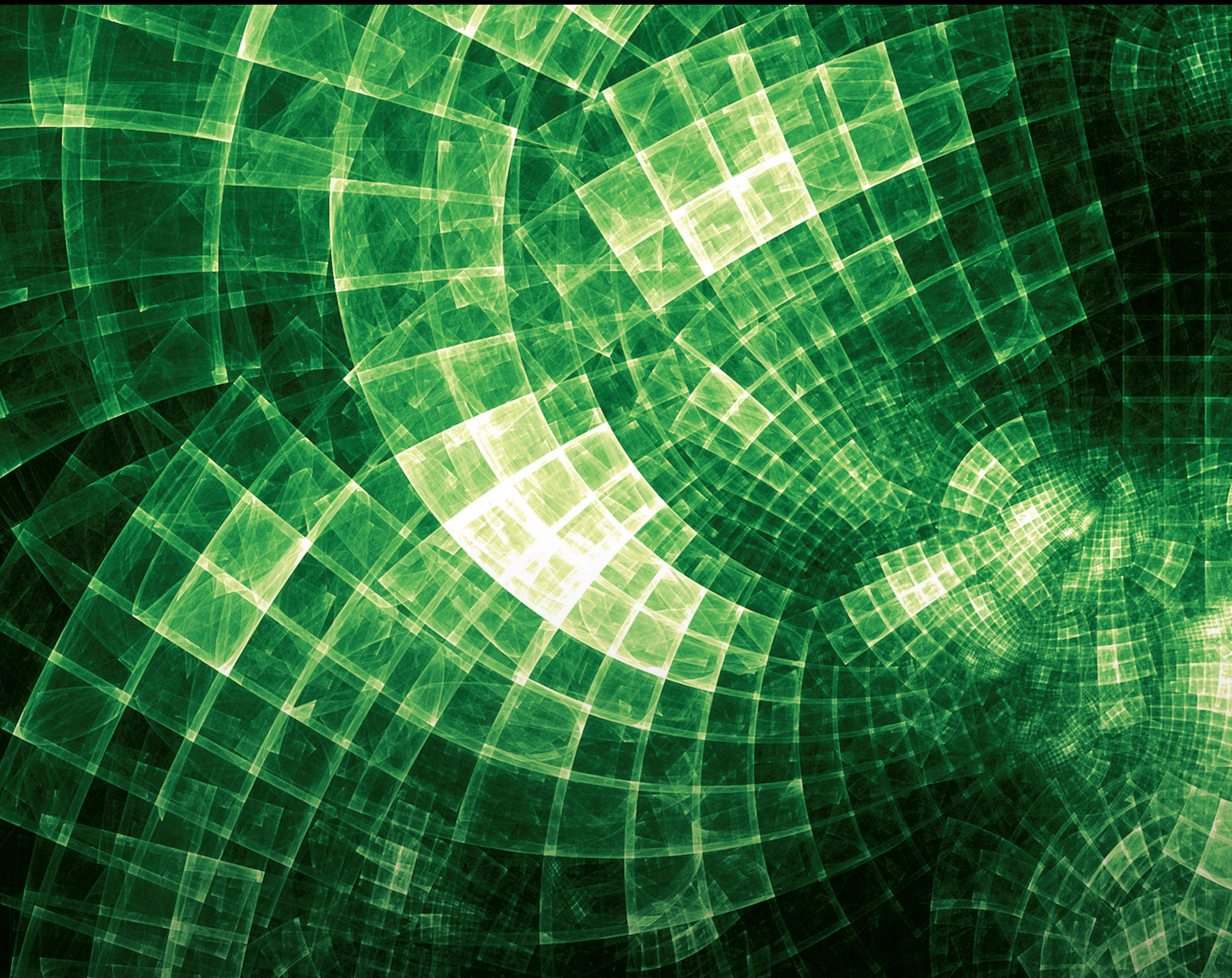


Mathematical Aspects of Computational Methods for Fractional Differential Equations

Lead Guest Editor: Arzu Akbulut

Guest Editors: Melike Kaplan and Dipankar Kumar





Mathematical Aspects of Computational Methods for Fractional Differential Equations

Journal of Mathematics

**Mathematical Aspects of Computational
Methods for Fractional Differential
Equations**

Lead Guest Editor: Arzu Akbulut

Guest Editors: Melike Kaplan and Dipankar Kumar



Copyright © 2023 Hindawi Limited. All rights reserved.

This is a special issue published in "Journal of Mathematics." All articles are open access articles distributed under the Creative Commons Attribution License, which permits unrestricted use, distribution, and reproduction in any medium, provided the original work is properly cited.

Chief Editor

Jen-Chih Yao, Taiwan

Algebra

SEÇİL ÇEKEN , Turkey
Faranak Farshadifar , Iran
Marco Fontana , Italy
Genni Fragnelli , Italy
Xian-Ming Gu, China
Elena Guardo , Italy
Li Guo, USA
Shaofang Hong, China
Naihuan Jing , USA
Xiaogang Liu, China
Xuanlong Ma , China
Francisco Javier García Pacheco, Spain
Francesca Tartarone , Italy
Fernando Torres , Brazil
Zafar Ullah , Pakistan
Jiang Zeng , France

Geometry

Tareq Al-shami , Yemen
R.U. Gobithaasan , Malaysia
Erhan Güler , Turkey
Ljubisa Kocinac , Serbia
De-xing Kong , China
Antonio Masiello, Italy
Alfred Peris , Spain
Santi Spadaro, Italy

Logic and Set Theory

Ghous Ali , Pakistan
Kinkar Chandra Das, Republic of Korea
Jun Fan , Hong Kong
Carmelo Antonio Finocchiaro, Italy
Radomír Halaš, Czech Republic
Ali Jaballah , United Arab Emirates
Baoding Liu, China
G. Muhiuddin , Saudi Arabia
Basil K. Papadopoulos , Greece
Musavarah Sarwar, Pakistan
Anton Setzer , United Kingdom
R Sundareswaran, India
Xiangfeng Yang , China

Mathematical Analysis

Ammar Alsinai , India
M.M. Bhatti, China
Der-Chen Chang, USA
Phang Chang , Malaysia
Mengxin Chen, China
Genni Fragnelli , Italy
Willi Freeden, Germany
Yongqiang Fu , China
Ji Gao , USA
A. Ghareeb , Egypt
Victor Ginting, USA
Azhar Hussain, Pakistan
Azhar Hussain , Pakistan
Ömer Kişi , Turkey
Yi Li , USA
Stefan J. Linz , Germany
Ming-Sheng Liu , China
Dengfeng Lu, China
Xing Lü, China
Gaetano Luciano , Italy
Xiangyu Meng , USA
Dimitri Mugnai , Italy
A. M. Nagy , Kuwait
Valeri Obukhovskii, Russia
Humberto Rafeiro, United Arab Emirates
Luigi Rarità , Italy
Hegazy Rezk, Saudi Arabia
Nasser Saad , Canada
Mohammad W. Alomari, Jordan
Guotao Wang , China
Qiang Wu, USA
Çetin YILDIZ , Turkey
Wendong Yang , China
Jun Ye , China
Agacik Zafer, Kuwait

Operations Research

Ada Che , China
Nagarajan Deivanayagam Pillai, India
Sheng Du , China
Nan-Jing Huang , China
Chiranjibe Jana , India
Li Jin, United Kingdom
Mehmet Emir Koksal, Turkey
Palanivel M , India





Stanislaw Migorski , Poland
Predrag S. Stanimirović , Serbia
Balendu Bhooshan Upadhyay, India
Ching-Feng Wen , Taiwan
K.F.C. Yiu , Hong Kong
Liwei Zhang, China
Qing Kai Zhao, China

Probability and Statistics






Mario Abundo, Italy
Antonio Di Crescenzo , Italy
Jun Fan , Hong Kong
Jiancheng Jiang , USA
Markos Koutras , Greece
Fawang Liu , Australia
Barbara Martinucci , Italy
Yonghui Sun, China
Niansheng Tang , China
Efthymios G. Tsionas, United Kingdom
Bruce A. Watson , South Africa
Ding-Xuan Zhou , Hong Kong

Contents




On the Global Well-Posedness for a Hyperbolic Model Arising from Chemotaxis Model with Fractional Laplacian Operator

Oussama Melkemi , Mohammed S. Abdo , M.A. Aiyashi , and M. Daher Albalwi 
Research Article (10 pages), Article ID 1140032, Volume 2023 (2023)



Exploring the Analytical Solutions to the Economical Model via Three Different Methods

M. Raheel, Khalid K. Ali , Asim Zafar , Ahmet Bekir , Omar Abu Arqub , and Marwan Abukhaled 
Research Article (15 pages), Article ID 1416097, Volume 2023 (2023)

Fractional Optimal Control Model of SARS-CoV-2 (COVID-19) Disease in Ghana

Samuel Okyere , Joseph Ackora-Prah , Kwaku Forkuoh Darkwah, Francis Tabi Oduro, and Ebenezer Bonyah 
Research Article (25 pages), Article ID 3308529, Volume 2023 (2023)



Analytical and Approximate Solutions of the Nonlinear Gas Dynamic Equation Using a Hybrid Approach

Muhammad Nadeem  and Mouad M. H. Ali 
Research Article (7 pages), Article ID 3136490, Volume 2023 (2023)



Obtaining the Soliton Type Solutions of the Conformable Time-Fractional Complex Ginzburg-Landau Equation with Kerr Law Nonlinearity by Using Two Kinds of Kudryashov Methods

Arzu Akbulut 
Research Article (6 pages), Article ID 4741219, Volume 2023 (2023)




A New Efficient Method for Solving System of Weakly Singular Fractional Integro-Differential Equations by Shifted Sixth-Kind Chebyshev Polynomials

S. Yaghoubi, H. Aminikhah , and K. Sadri 
Research Article (18 pages), Article ID 9087359, Volume 2022 (2022)




Two Computational Strategies for the Approximate Solution of the Nonlinear Gas Dynamic Equations

Muhammad Nadeem  and Mouad M. H. Ali 
Research Article (7 pages), Article ID 8130940, Volume 2022 (2022)

Mathematical Modeling of Coronavirus Dynamics with Conformable Derivative in Liouville-Caputo Sense

Ebenezer Bonyah , Zakia Hammouch , and Mehmet Emir Koksali 
Research Article (12 pages), Article ID 8353343, Volume 2022 (2022)

Modeling Drug Concentration Level in Blood Using Fractional Differential Equation Based on Psi-Caputo Derivative

Muath Awadalla , Yves Yannick Yameni Noupoue, Kinda Abu Asbeh , and Nouredine Ghiloufi 
Research Article (8 pages), Article ID 9006361, Volume 2022 (2022)



Impact of Multiplicative Noise on the Exact Solutions of the Fractional-Stochastic Boussinesq-Burger System

Wael W. Mohammed , Farah M. Al-Askar, and M. El-Morshedy 
Research Article (10 pages), Article ID 9288157, Volume 2022 (2022)

Solution of Space-Time Fractional Differential Equations Using Aboodh Transform Iterative Method

Michael A. Awuya , Gbenga O. Ojo , and Nazim I. Mahmudov 
Research Article (14 pages), Article ID 4861588, Volume 2022 (2022)



Bivariate Chebyshev Polynomials to Solve Time-Fractional Linear and Nonlinear KdV Equations

Azam Zahrani , Mashaallah Matinfar , and Mostafa Eslami 
Research Article (12 pages), Article ID 6554221, Volume 2022 (2022)

An Efficient Numerical Scheme for Solving Multiorder Tempered Fractional Differential Equations via Operational Matrix

Abiodun Ezekiel Owoyemi , Chang Phang , and Yoke Teng Toh 
Research Article (9 pages), Article ID 7628592, Volume 2022 (2022)




The Fractional Series Solutions for the Conformable Time-Fractional Swift-Hohenberg Equation through the Conformable Shehu Daftardar-Jafari Approach with Comparative Analysis

Muhammad Imran Liaqat , and Eric Okyere 
Research Article (20 pages), Article ID 3295076, Volume 2022 (2022)




Computational Insights of Bioconvective Third Grade Nanofluid Flow past a Riga Plate with Triple Stratification and Swimming Microorganisms

Safak Kayikci 
Research Article (12 pages), Article ID 6378721, Volume 2022 (2022)

A Class of Symmetric Fractional Differential Operator Formed by Special Functions

Ibtisam Aldawish , Rabha W. Ibrahim , and Suzan J. Obaiys 
Research Article (10 pages), Article ID 8339837, Volume 2022 (2022)

A Semianalytical Approach for the Solution of Nonlinear Modified Camassa-Holm Equation with Fractional Order

Jiahua Fang , Muhammad Nadeem , and Hanan A. Wahash 
Research Article (8 pages), Article ID 5665766, Volume 2022 (2022)

Research Article

On the Global Well-Posedness for a Hyperbolic Model Arising from Chemotaxis Model with Fractional Laplacian Operator

Oussama Melkemi ¹, Mohammed S. Abdo ², M.A. Aiyashi ³ and M. Daher Albalwi ⁴

¹Laboratory of Partial Differential Equations and Applications, University Batna 2, Batna 05000, Algeria

²Department of Mathematics, Hodeidah University, P.O. Box 3114, Al-Hudaydah, Yemen

³Department of Mathematics, Faculty of Science, Jazan University, Jazan 45142, Saudi Arabia

⁴Yanbu Industrial College, The Royal Commission for Jubail and Yanbu, 30436, Riyadh, Saudi Arabia

Correspondence should be addressed to Mohammed S. Abdo; msabdo@hoduniv.net.ye

Received 25 August 2022; Revised 11 October 2022; Accepted 24 November 2022; Published 9 May 2023

Academic Editor: Arzu Akbulut

Copyright © 2023 Oussama Melkemi et al. This is an open access article distributed under the Creative Commons Attribution License, which permits unrestricted use, distribution, and reproduction in any medium, provided the original work is properly cited.

Several cells and microorganisms, such as bacteria and somatic, have many essential features, one of which can be modeled by the chemotaxis system, which we consider to be our main interest in this article. More precisely, we studied the hyperbolic system derived from the chemotaxis model with fractional dissipation, which is a generalization for the hyperbolic system with classical dissipation. The results of this article are divided into two parts. In the first part, we used energy methods to obtain the existence of small solutions in the Besov spaces. The second one deals with the optimal decay of perturbed solutions using a refined time-weighted energy combined with the Littlewood-Paley decomposition technique. To the authors' best knowledge, this type of system (with fractional dissipation) has not been studied in the literature.

1. Introduction

This present article aims to study the hyperbolic chemotaxis system, which is governed by the following Cauchy problem:

$$\begin{cases} \partial_t \tilde{p} + \omega \Lambda^\sigma \tilde{p} = \operatorname{div}(\tilde{p}q) & \text{if } (t, x) \in \mathbb{R}_+ \times \mathbb{R}^d, \\ \partial_t q + \lambda \Lambda^\sigma q = \nabla(\tilde{p} + \lambda|q|^2) & \text{if } (t, x) \in \mathbb{R}_+ \times \mathbb{R}^d, \\ (\tilde{p}, q)|_{t=0} = (\tilde{p}_0, q_0), \end{cases} \quad (1)$$

where $\tilde{p}(t, x)$ represents the cell density, $q(t, x) = -(\nabla v/v)$ with v is the chemical concentration, $\omega > 0$ and $\lambda \geq 0$ describe the cell and chemical diffusion coefficients, respectively, and the fractional operator $\Lambda^\sigma = (-\Delta)^{\sigma/2}$ denotes the fractional Laplacian operator. In the whole space \mathbb{R}^d , the operator Λ^σ is defined via the following Fourier transform:

$$(\widehat{\Lambda^\sigma f})(\xi) \triangleq |\xi|^\sigma (\widehat{f})(\xi). \quad (2)$$

Chemotaxis model (1) describes the ability of free-moving organisms to react to chemical substances or their concentration differences with specific, directed movements. On the other hand, the fractional dissipation has several applications in the molecular biology, we mention as an example the anomalous diffusion and chemical attraction to organisms in semiconductor growth, see for instance [1]. It is well known that the fractional chemotaxis system (1) is derived from the following canonical formulation of the famous ‘‘Keller-Segel’’ model [2, 3]:

$$\begin{cases} \partial_t u = -\omega \Lambda^\sigma u - \operatorname{div}(\chi u \nabla \Psi(v)) & \text{if } (t, x) \in \mathbb{R}_+ \times \mathbb{R}^d, \\ \partial_t v = -\lambda \Lambda^\sigma v + f(u, v) & \text{if } (t, x) \in \mathbb{R}_+ \times \mathbb{R}^d, \\ (p, q)|_{t=0} = (p_0, q_0), \end{cases} \quad (3)$$

where χ is a constant that represents the chemosensitivity; when the coefficient $\chi > 0$, we say that the system is attractive and in the case when the coefficient $\chi < 0$, the system is repulsive. The function Ψ describes the mechanism of signal detection. In the situation, when the function $\Psi(u) = \nabla(\Lambda^{-\sigma/2}u)$ with $\sigma \in (1, 2]$ Biler and Wu [4] investigated system (3) in the Besov spaces. In particular, they have established the local existence and uniqueness of solutions. Later, Zhai [5] studied the system in the case when $f(u, v) = u$; more precisely, Zhai [5] showed that system (3) admits a mild solutions. There is a large literature on the analysis of system (3), we refer the reader to [6–10] and the references therein. For the case, when $\lambda = 0$, then system (1) turns out to be the hyperbolic-parabolic chemotaxis; in this context, when the fractional Laplacian operator is substituted by the classical Laplacian operator, Zhang and Zhu [11] investigated the Cauchy problem for system (1) $\sigma = 2, \lambda = 0$ with small initial data. Lately, Jun et al. [12] explored the global existence of system (1) $\sigma = 2, \lambda = 0$ with large initial data. Recently, Hao [13] showed that system (1) $\sigma = 2, \lambda = 0$ admits a unique solution near to some constant equilibrium state in the critical hybrid Besov spaces $B^{d/2-2}(\mathbb{R}^d) \times B^{d/2-2, d/2-1}(\mathbb{R}^d)$. In their very recent work Nie and Yuan [14] investigated the well-posedness and the ill-posedness in the critical Besov spaces $B_{p,q}^{d/2-2}(\mathbb{R}^d) \times B_{p,q}^{d/2-1}(\mathbb{R}^d)$. For this hyperbolic-parabolic system, there have been a large number of results concerning the long-time dynamics to the solutions, blow-up phenomenon, and the existence of global solutions (see for instance, [15–19]). Here, we focus on the chemically diffusible model corresponding to the case of $\lambda > 0$. As far as we know, the results obtained for the Hyperbolic model (1) $\lambda > 0$ are less compared to Hyperbolic-Parabolic model (1) $\lambda = 0$. In the situation, when the fractional Laplacian is changed by the full Laplacian operator, Tao et al. [20] proved that system (1) $\lambda > 0$ is globally well posed; moreover, they have obtained the long-time behavior, and diffusion limit of one-dimensional large-amplitude classical solutions on finite intervals subject to the Neumann-Dirichlet boundary conditions. Thereafter, in [21], Li and Zhao explored the same issues of [20] but for the Dirichlet-Dirichlet boundary conditions. Wang et al. [22] investigated the global existence, asymptotic decay rates, and diffusion convergence rate of small solutions in the Sobolev framework. Recently, Martinez et al. [23] proved a set of results, such as, the global asymptotic stability of constant ground states and the explicit decay rate of solutions. More recently, Wu and Su [24] showed that system (1) $\sigma = 2$ admits global solution and also they have obtained a decay rate of solutions in the Besov spaces. For the traveling wave solution of problem (1) with $\sigma = 2$ and its nonlinear stability, see the series of papers [25–28].

Stimulated by the above works, especially with [24], the main objective of this article is to investigate system (1) with

the fractional Laplacian operator Λ^σ , with $\sigma \in (1, 2)$. To be more precise, we have the following two outcomes:

Theorem 1. *Assume that $1 < \sigma < 2, d \geq 2$ and $v \in [1, \infty]$. Let $(\pi_0, q_0) \in \dot{B}_{2,v}^\alpha$. We assume that there exists a constant $\epsilon > 0$ such that*

$$\|\pi_0\|_{\dot{B}_{2,v}^\alpha} + \|q_0\|_{\dot{B}_{2,v}^\alpha} \leq \epsilon, \quad (4)$$

where $\alpha = d/2 - \sigma + 1$ and $\pi_0 = \tilde{p}_0 - \bar{p}$, for some equilibrium state $\bar{p} > 0$. Then, system (1) admits a global unique solution (\tilde{p}, q) satisfying for any $T > 0$:

$$\tilde{p} - \bar{p}, q \in L^\infty\left(0, T; \dot{B}_{2,v}^{(d/2)-\sigma+1}\right) \cap L^1\left(0, T; \dot{B}_{2,v}^{(d/2)+1}\right). \quad (5)$$

Remark 1. From the identity $\dot{B}_{2,2}^s \approx \dot{H}^s$, then for $v = 2$, Theorem 1 implies the global well-posedness in the scale of (homogeneous) Sobolev spaces.

Our existence theorem is based on the energy estimates. Due to the presence of the terms $\operatorname{div}(\tilde{p}q)$ and $\nabla(|q|^2)$, we established with the help of Bony's decomposition (see the next section) a product estimates, thus we can get the a priori estimates of our system, which leads us to get the global small solutions in $\dot{B}_{2,v}^{(d/2)-\sigma+1}$.

The second result of this article deals with the time decay rates of strong solutions for system (1), which is given as follows:

Theorem 2. *Let $1 < \sigma < 2, d \geq 2$ and $v \in [1, \infty]$. Let $(\tilde{p}_0 - \bar{p}, q_0) \in B_{2,1}^\alpha \cap \dot{B}_{1,\infty}^0$. There exists a constants $\epsilon > 0$ such that if*

$$\|\pi_0\|_{B_{2,1}^\alpha \cap \dot{B}_{1,\infty}^0} + \|q_0\|_{B_{2,1}^\alpha \cap \dot{B}_{1,\infty}^0} \leq \epsilon, \quad (6)$$

where $\alpha = (d/2) - \sigma + 1$ and $\pi_0 = \tilde{p}_0 - \bar{p}$, then system (1) has a unique global solution as follows:

$$\pi, q \in L^\infty\left(0, T; B_{2,1}^{(d/2)-\sigma+1}\right), \quad (7)$$

where $\pi = \tilde{p} - \bar{p}$. Furthermore, there exists a positive constant M_0 such that

$$\|(\pi, q)\|_{B_{2,1}^{(d/2)-\sigma+1}} \leq M_0 (1+t)^{-(d/2)\sigma}. \quad (8)$$

Remark 2. Theorem 2 gives the optimal decay of solutions for system (1) due to embedding $B_{2,1}^{(d/2)-\sigma+1} \rightarrow L^2$.

Remark 3. In the sequel and for the simplicity we assume (without loss of generality) $\lambda = \omega = \bar{p} = 1$.

The content of this article is arranged as follows. We introduced the notations and some useful definitions and results in Section 2, then we reformulated system (1) and we established some useful a priori estimates in section 3.

Section 4 is devoted to the proof of the existence of solutions. Finally, we proved Theorem 2 in Section 5.

1.1. Notation. C or M stands for some positive constant and may represent different values in different lines, the notation $X \leq Y$ means that there exist a constant $M_0 > 0$ such that $X \leq M_0 Y$, where M_0 is a constant depending on the initial data.

2. Preparatory

In this section, we recall some ingredients, such as the famous Littlewood–Paley operators and Bony decomposition, also some function spaces will be introduced.

2.1. Littlewood–Paley Theory. We start this section by giving the definition of the dyadic partition of unity.

Definition 1. There exists $(\chi, \psi) \in \mathfrak{D}(\mathbb{R}^2) \times \mathfrak{D}(\mathbb{R}_*^2)$ such that

$$\text{For all } \xi \in \mathbb{R}^2, \chi(\xi) + \sum_{q \in \mathbb{N}} \psi(2^q \xi) = 1. \tag{9}$$

For every $f \in \mathcal{S}'(\mathbb{R}^d)$, we defined the operators $\dot{\Delta}_\zeta$, and \dot{S}_ζ as follows. Let $\zeta \in \mathbb{Z}$

$$\begin{aligned} \dot{\Delta}_\zeta b &\triangleq \psi(2^{-\zeta} \partial) b, \\ \dot{S}_\zeta b &\triangleq \chi(2^{-\zeta} \partial) b, \end{aligned} \tag{10}$$

$$\dot{T}_a b = \sum_q \dot{S}_{q-1} a \dot{\Delta}_q b, \mathfrak{R}(a, b) = \sum_q \dot{\Delta}_q \tilde{\Delta}_q b \text{ with } \tilde{\Delta}_q = \dot{\Delta}_{q-1} + \dot{\Delta}_q + \dot{\Delta}_{q+1}. \tag{14}$$

The next result is the famous Bernstein inequality, for the proof see [29].

Proposition 1. *Let $1 \leq \theta \leq \vartheta \leq \infty$. Assume $H \in L^\theta$, then for every $\iota \in \mathbb{N}^d$, there exists constants M_1, M_2 such that*

$$\begin{aligned} \text{supp } \widehat{H} \subset \{|\xi| \leq A_0 2^q\} &\Rightarrow \|\partial^\iota H\|_{L^\vartheta} \leq M_1 2^{q(|\iota|+d(1/\theta-1/\vartheta))} \|H\|_{L^\theta}, \\ \text{supp } \widehat{H} \subset \{A_1 2^q \leq |\xi| \leq A_0 2^q\} &\Rightarrow \|H\|_{L^\vartheta} \leq M_2 2^{-qk} \sup_{|\iota|=k} \partial^\iota H \|H\|_{L^\theta}. \end{aligned} \tag{15}$$

Now, we recall the definitions of homogeneous and nonhomogeneous Besov spaces.

Definition 2. For $(\eta, \theta) \in \mathbb{R} \times [1, +\infty]$ and $1 \leq \nu < \infty$. The homogeneous Besov space $\dot{B}_{\theta, \nu}^\eta$ is defined as the set of all tempered distributions $a \in \mathcal{S}'(\mathbb{R}^d)$ such that:

$$\|a\|_{\dot{B}_{\theta, \nu}^\eta} \triangleq \left(2^{q\eta} \|\dot{\Delta}_q a\|_{L^\theta} \right)_{\ell^\nu(\mathbb{Z})} < \infty. \tag{16}$$

Besides, if $\nu = \infty$

and Δ_ζ as follows:

$$\Delta_{-1} b \triangleq \chi(\partial) f, \text{ and for all } \zeta \geq 0, \Delta_\zeta b \triangleq \psi(2^{-\zeta} \partial) b. \tag{11}$$

By the definition of localization operators above, we have some interesting properties as follows:

(1) The formal Littlewood–Paley decomposition:

$$b = \sum_{\zeta \in \mathbb{Z}} \dot{\Delta}_\zeta b, \text{ for all } b \in \mathcal{S}'(\mathbb{R}^d). \tag{12}$$

(2) The quasiorthogonality:

- (i) If $|\zeta - \kappa| \geq 2$, then $\dot{\Delta}_\kappa \dot{\Delta}_\zeta b = 0$;
- (ii) if $|\zeta - \kappa| \geq 5$, then $\dot{\Delta}_\kappa (\dot{S}_\zeta b \dot{\Delta}_\zeta b) = 0$.

The paradifferential calculus plays a key role in the proof of the existence result, and its given by the following definition:

(i) Bony decomposition

For $a, b \in \mathcal{S}'(\mathbb{R}^d)$, we have the following equation:

$$ab = \mathfrak{T}_a b + \mathfrak{T}_b a + \mathfrak{R}(a, b), \tag{13}$$

with

$$\|a\|_{\dot{B}_{\theta, \infty}^\eta} \triangleq \sup_{q \in \mathbb{Z}} \left(2^{q\eta} \|\dot{\Delta}_q a\|_{L^\theta} \right) < \infty. \tag{17}$$

Definition 3. For $(\eta, \theta) \in \mathbb{R} \times [1, +\infty]$ and $1 \leq \nu < \infty$. The nonhomogeneous Besov space $B_{\theta, \nu}^\eta$ is defined as the set of all tempered distributions $a \in \mathcal{S}'(\mathbb{R}^d)$ such that

$$\|a\|_{B_{\theta, \nu}^\eta} \triangleq \left(2^{q\eta} \|\Delta_q a\|_{L^\theta} \right)_{\ell^\nu(\mathbb{Z})} < \infty. \tag{18}$$

Besides, if $\nu = \infty$

$$\|a\|_{B_{\theta, \infty}^\eta} \triangleq \sup_{q \in \mathbb{N} \cup \{-1\}} \left(2^{q\eta} \|\Delta_q a\|_{L^\theta} \right) < \infty. \tag{19}$$

The following spaces are introduced by Chemin and Lerner in [30]:

Definition 4. We assume that $\tau > 0$ and $\zeta \geq 1$, the space $L_T^\zeta B_{\theta, \nu}^\eta$ is the set of $a \in \mathcal{S}'(\mathbb{R}^d)$ such that

$$\|a_{L_\tau^\zeta \dot{B}_{\theta,v}^\eta}\| \triangleq \left\| \left(2^{q\eta} \|\dot{\Delta}_q a\|_{L^\theta} \right)_{\ell^r(\mathbb{Z})} \right\|_{L_\tau^\zeta} < \infty, \quad (20)$$

and the space $\tilde{L}_\tau^\zeta \dot{B}_{\theta,\infty}^\eta$ is the space $a \in \mathcal{S}'(\mathbb{R}^d)$ such that

$$\|a\|_{\tilde{L}_\tau^\zeta \dot{B}_{\theta,\infty}^\eta} \triangleq \left(2^{q\eta} \|\dot{\Delta}_q a\|_{L_\tau^\zeta L^\theta} \right)_{\ell^r(\mathbb{Z})} < \infty. \quad (21)$$

As a consequence of the last definition, we have the following embedding. Let $\epsilon > 0$, then we have the following equation:

$$\begin{aligned} L_\tau^\zeta \dot{B}_{\theta,v}^\eta &\rightarrow \tilde{L}_\tau^\zeta \dot{B}_{\theta,v}^\eta, \forall v \geq \zeta, \\ \tilde{L}_\tau^\zeta \dot{B}_{\theta,v}^\eta &\rightarrow L_\tau^\zeta \dot{B}_{\theta,v}^\eta, \forall \zeta \geq v. \end{aligned} \quad (22)$$

The following Lemma is useful in our contribution, for more details see [31].

Lemma 1. (i) Let $\nu_1, \nu_2 > 0$ satisfying $\max\{\nu_1, \nu_2\} > 1$. Then

$$\int_0^{\tau'} \left(1 + \tau' - \tau \right)^{-\nu_1} (1 + \tau)^{-\nu_2} d\tau \leq M_{\nu_1, \nu_2} \left(1 + \tau' \right)^{-\min\{\nu_1, \nu_2\}}, \quad \tau' > 0. \quad (23)$$

(ii) Let $\nu_1, \nu_2 > 0$ and $b \in L^\infty((0, \infty))$. Then

$$\int_0^{\tau'} \left(1 + \tau' - \tau \right)^{-\nu_1} (1 + \tau)^{-\nu_2} b(\tau) d\tau \leq M_{\nu_1, \nu_2} \left(1 + \tau' \right)^{-\min\{\nu_1, \nu_2\}} \int_0^{\tau'} |b(\tau)| d\tau, \tau' > 0. \quad (24)$$

We finished this section by establishing a product estimate.

Lemma 2. Let $\sigma \in (1, 2), v \in [1, \infty]$ and $u, v \in \dot{B}_{2,v}^{(d/2)-\sigma+1} \cap \dot{B}_{2,v}^{(d/2)+1}$. Then $uv \in \dot{B}_{2,v}^{(d/2)-\sigma+2}$ and we have the following equation:

$$\|uv\|_{\dot{B}_{2,v}^{(d/2)-\sigma+2}} \leq C \left(\|u\|_{\dot{B}_{2,v}^{(d/2)-\sigma+1}} \|v\|_{\dot{B}_{2,v}^{(d/2)+1}} + \|v\|_{\dot{B}_{2,v}^{(d/2)-\sigma+1}} \|u\|_{\dot{B}_{2,v}^{(d/2)+1}} \right). \quad (25)$$

Proof. By using the Bony decomposition (13), we split the term uv as follows:

$$uv = \mathfrak{T}_u v + \mathfrak{T}_v u + \mathfrak{R}(u, v). \quad (26)$$

From the property (2) part (ii), we have the following equation:

$$\begin{aligned} \|\dot{\Delta}_\kappa(uv)\|_{L^2} &= \sum_{|\kappa-\kappa| \leq 4} \|\dot{\Delta}_\kappa(\dot{S}_{\kappa-1} u \dot{\Delta}_\kappa v)\|_{L^2} + \sum_{|\kappa-\kappa| \leq 4} \|\dot{\Delta}_\kappa(\dot{S}_{\kappa-1} v \dot{\Delta}_\kappa u)\|_{L^2} \\ &+ \sum_{\substack{l \geq \kappa-3 \\ |l| \leq 1}} \|\dot{\Delta}_\kappa(\dot{\Delta}_\kappa u \dot{\Delta}_{\kappa-l} v)\|_{L^2}. \end{aligned} \quad (27)$$

Multiplying equation (27) by $2^{\kappa((d/2)+2-\sigma)}$ and taking the ℓ^v norm we find out that

$$\begin{aligned} \|uv\|_{\dot{B}_{2,v}^{(d/2)-\sigma+2}} &\leq \left\| \left(2^{\kappa((d/2)-\sigma+2)} \sum_{|\kappa-\kappa| \leq 4} \|\dot{\Delta}_\kappa(\dot{S}_{\kappa-1} u \dot{\Delta}_\kappa v)\|_{L^2} \right)_{\kappa \in \mathbb{Z}} \right\|_{\ell^v(\mathbb{Z})} \\ &+ \left\| \left(2^{\kappa((d/2)-\sigma+2)} \sum_{|\kappa-\kappa| \leq 4} \|\dot{\Delta}_\kappa(\dot{S}_{\kappa-1} v \dot{\Delta}_\kappa u)\|_{L^2} \right)_{\kappa \in \mathbb{Z}} \right\|_{\ell^v(\mathbb{Z})} \\ &+ \left\| \left(2^{\kappa((d/2)-\sigma+2)} \sum_{\substack{\kappa \geq \kappa-3 \\ |l| \leq 1}} \|\dot{\Delta}_\kappa(\dot{\Delta}_\kappa u \dot{\Delta}_{\kappa-l} v)\|_{L^2} \right)_{\kappa \in \mathbb{Z}} \right\|_{\ell^v(\mathbb{Z})} \\ &\triangleq \mathbb{K}_1 + \mathbb{K}_2 + \mathbb{K}_3. \end{aligned} \quad (28)$$

For the first term \mathbb{K}_1 we used Hölder inequality and Young inequality and obtained the following equation:

$$\begin{aligned} \mathbb{K}_1 &\leq \left\| \left(2^{\kappa((d/2)-\sigma+2)} \sum_{\kappa' \leq \kappa-2} \|\dot{\Delta}_{\kappa'} u\|_{L^\infty} \|\dot{\Delta}_{\kappa} v\|_{L^2} \right)_{\kappa \in \mathbb{Z}} \right\|_{\ell^v(\mathbb{Z})} \\ &\leq \left\| \left(\sum_{\kappa' \leq \kappa-2} 2^{(\kappa'-\kappa)(\sigma-1)} 2^{\kappa'(1-\sigma)} \|\dot{\Delta}_{\kappa'} u\|_{L^\infty} 2^{\kappa((d/2)+1)} \|\dot{\Delta}_{\kappa} v\|_{L^2} \right)_{\kappa \in \mathbb{Z}} \right\|_{\ell^v(\mathbb{Z})} \\ &\leq \|u\|_{\dot{B}_{\infty, \infty}^{1-\sigma}} \|v\|_{\dot{B}_{2, v}^{(d/2)+1}}. \end{aligned} \tag{29}$$

Similarly, we obtain the following equation:

$$\mathbb{K}_2 \leq \|u\|_{\dot{B}_{2, v}^{(d/2)+1}} \|v\|_{\dot{B}_{\infty, \infty}^{1-\sigma}}. \tag{30}$$

Taking advantage of Young inequality and the Hölder inequality, it holds that

$$\begin{aligned} \mathbb{K}_3 &\leq \left\| \left(2^{\kappa((d/2)-\sigma+2)} \sum_{\substack{\zeta \geq \kappa-3 \\ |l| \leq 1}} \|\dot{\Delta}_{\zeta} u\|_{L^\infty} \|\dot{\Delta}_{\zeta-l} v\|_{L^2} \right)_{\kappa \in \mathbb{Z}} \right\|_{\ell^v(\mathbb{Z})} \\ &\leq \left\| \left(\sum_{\zeta \geq \kappa-3, |l| \leq 1} 2^{(1-\sigma)\zeta} \|\dot{\Delta}_{\zeta} u\|_{L^\infty} 2^{((d/2)+1)(\zeta-l)} \|\dot{\Delta}_{\zeta-l} v\|_{L^2} 2^{((d/2)+2-\sigma)(\kappa-\zeta)} \right)_{\kappa \in \mathbb{Z}} \right\|_{\ell^v(\mathbb{Z})} \\ &\leq \|u\|_{\dot{B}_{\infty, \infty}^{1-\sigma}} \|v\|_{\dot{B}_{2, v}^{(d/2)+1}}. \end{aligned} \tag{31}$$

By the Besov embedding $\dot{B}_{2, v}^{(d/2)-\sigma+1} \rightarrow \dot{B}_{\infty, \infty}^{-\sigma+1}$, we get the desired result. \square

$$\begin{cases} \partial_t \pi + \Lambda^\sigma \pi - \operatorname{div} q = F & \text{if } (t, x) \in \mathbb{R}_+ \times \mathbb{R}^d, \\ \partial_t q + \Lambda^\sigma q - \nabla \pi = H & \text{if } (t, x) \in \mathbb{R}_+ \times \mathbb{R}^d, \\ (\pi, q)|_{t=0} = (\pi_0, q_0). \end{cases} \tag{33}$$

3. Reformulation of System and the A Priori Estimate

In this paragraph, we reformulated the original system (1), where we will assume (without loss of generality) that the equilibrium state $\bar{p} = 1$ and we set $\pi = \bar{p} - 1$, the system becomes as follows:

$$\begin{cases} \partial_t \pi + \Lambda^\sigma \pi = \operatorname{div}(\pi q) + \operatorname{div} q & \text{if } (t, x) \in \mathbb{R}_+ \times \mathbb{R}^d, \\ \partial_t q + \Lambda^\sigma q = \nabla(\pi + |q|^2) & \text{if } (t, x) \in \mathbb{R}_+ \times \mathbb{R}^d, \\ (\pi, q)|_{t=0} = (\pi_0, q_0). \end{cases} \tag{32}$$

We note that system (33) is given by the following equation:

$$\begin{cases} \partial_t \mathbb{V} + L_\sigma \mathbb{V} = \mathbb{G} & \text{if } (t, x) \in \mathbb{R}_+ \times \mathbb{R}^d, \\ \mathbb{V}|_{t=0} = \mathbb{V}_0, \end{cases} \tag{34}$$

where $\mathbb{V}(t) = (\pi(t), q(t))^T$, $\mathbb{G} = (F, H)^T$ and

$$L_\sigma = \begin{pmatrix} \Lambda^\sigma & -\operatorname{div} \\ -\nabla & \Delta^\sigma \end{pmatrix}. \tag{35}$$

Next, we prove the A priori estimate for system (32).

3.1. A Priori Estimate

We will study the a priori estimates for linearized system (32) with general source term as follows:

Proposition 2. *We assume that (π, q) is a regular solution for the system (32), then for all $t \in [0, T)$,*

$$\begin{aligned}
& \|\pi\|_{\dot{B}_{2,v}^{(d/2)-\sigma+1}} + \|q\|_{\dot{B}_{2,v}^{(d/2)-\sigma+1}} + \int_0^t \|\pi(\tau)\|_{\dot{B}_{2,v}^{(d/2)+1}} + \|q(\tau)\|_{\dot{B}_{2,v}^{(d/2)+1}} d\tau \\
& \leq \|\pi_0\|_{\dot{B}_{2,v}^{(d/2)-\sigma+1}} + \|q_0\|_{\dot{B}_{2,v}^{(d/2)-\sigma+1}} \\
& \quad + \|F\|_{L_t^1 \dot{B}_{2,v}^{(d/2)-\sigma+1}} + \|H\|_{L_t^1 \dot{B}_{2,v}^{(d/2)-\sigma+1}}.
\end{aligned} \tag{36}$$

Proof. Let $k \in \mathbb{Z}$ and we set $(\pi_k, q_k) = (\dot{\Delta}_k \pi, \dot{\Delta}_k q)$ and $(F_k, H_k) = (\dot{\Delta}_k (\operatorname{div} \pi q), \dot{\Delta}_k (\nabla (|q|^2)))$.

We observed that (π_k, q_k) solves the following system:

$$\begin{cases} \partial_t \pi_k + \Lambda^\sigma \pi_k = \operatorname{div} q_k + F_k \\ \partial_t q_k + \Lambda^\sigma q_k = \nabla \pi_k + H_k. \end{cases} \tag{37}$$

Taking the L^2 -scalar product of equation (37), we found out that

$$\begin{cases} \frac{1}{2} \frac{d}{dt} \|\pi_k(t)\|_{L^2}^2 + \|\Lambda^{\sigma/2} \pi_k(t)\|_{L^2}^2 = (\operatorname{div} q_k, \pi_k) + (F_k, \pi_k) \\ \frac{1}{2} \frac{d}{dt} \|q_k(t)\|_{L^2}^2 + \|\Lambda^{\sigma/2} q_k(t)\|_{L^2}^2 = (\nabla \pi_k, q_k) + (H_k, q_k). \end{cases} \tag{38}$$

For simplicity, we set $X^2(t) \triangleq \|\pi_k(t)\|_{L^2}^2 + \|q_k(t)\|_{L^2}^2$. According to the identity $(\nabla \pi_k, q_k) = (\operatorname{div} q_k, \pi_k)$ and Bernstein's Lemma, we get the following equation:

$$\frac{1}{2} \frac{d}{dt} X^2(t) + 2^{\sigma k} X^2(t) \leq (\|F_k\|_{L^2} + \|H_k\|_{L^2}) X(t). \tag{39}$$

Thus,

$$\frac{1}{2} \frac{d}{dt} X(t) + 2^{\sigma k} X(t) \leq \|F_k\|_{L^2} + \|H_k\|_{L^2}. \tag{40}$$

Multiplying equation (40) by $2^{k((d/2)-\sigma+1)}$ and taking the ℓ^v norm over $k \in \mathbb{Z}$, we obtained the following equation:

$$\begin{aligned}
& \frac{1}{2} \frac{d}{dt} \left(\|\pi\|_{\dot{B}_{2,v}^{(d/2)-\sigma+1}} + \|q\|_{\dot{B}_{2,v}^{(d/2)-\sigma+1}} \right) + \|\pi(t)\|_{\dot{B}_{2,v}^{(d/2)+1}} \\
& \quad + \|q(t)\|_{\dot{B}_{2,v}^{(d/2)+1}} d\tau \leq \|F\|_{\dot{B}_{2,v}^{(d/2)-\sigma+1}} + \|H\|_{\dot{B}_{2,v}^{(d/2)-\sigma+1}}.
\end{aligned} \tag{41}$$

Integrating the above estimate with respect to time, hence, we get the desired result. \square

4. Existence

For the proof of the existence part, we are going to use the classical Friedrichs' regularization method combined with the energy method. First, we define the spectral cutoff as follows. Let $\mu > 0$

$$\widehat{\mathbb{J}}_\mu a(\omega) \triangleq \mathbf{1}_{B_\mu} \widehat{a}(\omega), \tag{42}$$

where $B_\mu = \{x \in \mathbb{R}^d / |x| \leq \mu\}$ and $\mathbf{1}_{B_\mu}$ denotes the characteristic function on the ball B_μ . We define the following equation:

$$L_\mu^2 \triangleq \{a \in L^2 : \operatorname{supp} \widehat{a} \subset B(0, \mu)\}. \tag{43}$$

We consider the following approximate system:

$$\begin{cases} \partial_t \pi_\mu + \Lambda^\sigma \pi_\mu = F_\mu & \text{if } (t, x) \in \mathbb{R}_+ \times \mathbb{R}^d, \\ \partial_t q_\mu + \Lambda^\sigma q_\mu = \nabla \pi_\mu + H_\mu & \text{if } (t, x) \in \mathbb{R}_+ \times \mathbb{R}^d, \\ (\pi_\mu, q_\mu)|_{t=0} = (\mathbb{J}_\mu \pi_0, \mathbb{J}_\mu q_0), \end{cases} \tag{44}$$

where $F_\mu = \mathbb{J}_\mu (\operatorname{div} (\pi q))$ and $H_\mu = \mathbb{J}_\mu (\nabla (|q|^2))$.

The usual (Cauchy Lipschitz) theorem guarantees that system (44) admits a unique regular solution $C([0, T_\mu^*], L_\mu^2)$.

Denote

$$\|(\pi, q)\|_{\mathcal{X}_t^{(d/2), \sigma}} \triangleq \|(\pi, q)\|_{L_t^\infty \dot{B}_{2,v}^{(d/2)-\sigma+1}} + \|(\pi, q)\|_{L_t^1 \dot{B}_{2,v}^{(d/2)+1}}. \tag{45}$$

Let

$$T_\mu \triangleq \sup \left\{ T \in (0, T_\mu^*) : \|(\pi_\mu, q_\mu)\|_{\mathcal{X}_T^{(d/2), \sigma}} \leq M \widetilde{C} \|(\pi_0, q_0)\|_{\dot{B}_{2,v}^{(d/2)-\sigma+1}} \right\}, \tag{46}$$

where $\widetilde{C} \geq 2$ and $M = (1/2C\widetilde{C}^2 \|(\pi_0, q_0)\|_{\dot{B}_{2,v}^{(d/2)-\sigma+1}})$, thus we have $T_\mu > 0$. From Lemma 2.5, we deduce that

$$\begin{aligned}
& \|F_\mu\|_{L_t^1 \dot{B}_{2,v}^{(d/2)+1-\sigma}} \leq C \|(\pi_\mu, q_\mu)\|_{L_t^1 \dot{B}_{2,v}^{(d/2)+2-\sigma}} \\
& \leq C \left(\|q_\mu\|_{L_t^\infty \dot{B}_{2,v}^{(d/2)-\sigma+1}} \|(\pi_\mu, q_\mu)\|_{L_t^1 \dot{B}_{2,v}^{(d/2)+1}} + \|(\pi_\mu, q_\mu)\|_{L_t^\infty \dot{B}_{2,v}^{(d/2)-\sigma+1}} \|q_\mu\|_{L_t^1 \dot{B}_{2,v}^{(d/2)+1}} \right) \\
& \leq C \|(\pi_\mu, q_\mu)\|_{L_t^\infty \dot{B}_{2,v}^{(d/2)-\sigma+1}} \|(\pi_\mu, q_\mu)\|_{L_t^1 \dot{B}_{2,v}^{(d/2)+1}}.
\end{aligned} \tag{47}$$

In a similar way,

$$\begin{aligned} \|H_\mu\|_{L_t^1 \dot{B}_{2,v}^{(d/2)+1-\sigma}}^{-1} &\leq C \|q_\mu q_\mu\|_{L_t^1 \dot{B}_{2,v}^{(d/2)+2-\sigma}}^{-1} \\ &\leq C \left(\|q_\mu\|_{L_t^\infty \dot{B}_{2,v}^{(d/2)-\sigma+1}} \|q_\mu\|_{L_t^1 \dot{B}_{2,v}^{(d/2)+1}} \right). \end{aligned} \quad (48)$$

Hence,

$$\begin{aligned} \|(\pi_\mu, q_\mu)\|_{\mathcal{X}_t^{(d/2),\sigma}} &\leq \tilde{C} \left(\|(\pi_0, q_0)\|_{\dot{B}_{2,v}^{(d/2)-\sigma+1}} + C \|(\pi_\eta, q_\eta)\|_{\mathcal{X}_t^{(d/2),\sigma}}^2 \right) \\ &\leq \tilde{C} \|(\pi_0, q_0)\|_{\dot{B}_{2,v}^{(d/2)-\sigma+1}} \left(1 + C (M\tilde{C})^2 \|(\pi_0, q_0)\|_{\dot{B}_{2,v}^{(d/2)-\sigma+1}} \right), \end{aligned} \quad (49)$$

where $C \geq 2$. We choose $\|(\pi_0, q_0)\|_{\dot{B}_{2,v}^{(d/2)-\sigma+1}} < 1/4\tilde{C}^2 C$. Therefore, $1 + M^2\tilde{C}^2 C \|(\pi_0, q_0)\|_{\dot{B}_{2,v}^{(d/2)-\sigma+1}} < M$. Then, for any $T < T_\mu$, we have $\|(\pi_\mu, q_\mu)\|_{\mathcal{X}_t^{(d/2),\sigma}} \leq \tilde{C} M \|(\pi_0, q_0)\|_{\dot{B}_{2,v}^{(d/2)-\sigma+1}} \leq (1/4)$. Our next aim is to prove that $T_\mu = T_\mu^*$; previously, we showed that $\|(\pi_\mu, q_\mu)\|_{\mathcal{X}_t^{(d/2),\sigma}} \leq M\tilde{C} \|(\pi_0, q_0)\|_{\dot{B}_{2,v}^{(d/2)-\sigma+1}}$ for all $T_\mu < T_\mu^*$. By the continuity argument, we can get $\|(\pi_\mu, q_\mu)\|_{\mathcal{X}_{T+\delta}^{(d/2),\sigma}} \leq M\tilde{C} \|(\pi_0, q_0)\|_{\dot{B}_{2,v}^{(d/2)-\sigma+1}}$, for a sufficiently small constant $\delta > 0$, which contradicts the definition of T_μ . Next, we will show that system (44) admits global solutions. For this aim, we assumed that $T^* < +\infty$, we have $\|(\pi_\mu, q_\mu)\|_{\mathcal{X}_t^{(d/2),\sigma}} \leq M\tilde{C} \|(\pi_0, q_0)\|_{\dot{B}_{2,v}^{(d/2)-\sigma+1}}$. On the other hand, we have $\pi_\mu, q_\mu \in \tilde{L}^\infty([0, T_\mu^*]; \dot{B}_{2,v}^{(d/2)-\sigma+1})$, then we have $\|(\pi_\mu, q_\mu)\|_{L^\infty([0, T_\mu^*]; L_v^2)} < +\infty$. By the Cauchy-Lipschitz Theorem we can continue the solution beyond the time T_μ^* and this contradicts the definition of T_μ^* . Hence, $T_\mu^* = +\infty$. By standard arguments, we can show that $(\pi_\mu, q_\mu)_{\mu > 0}$ converges to the solution (π, q) which solves system (32) and here we omit the details.

5. Optimal Decay of Solutions

To know more about the asymptotic behavior of the solutions obtained in the previous results, we studied in this section the optimal temporal decay of perturbed solution in terms of $B_{2,1}^{(d/2)-\sigma+1}$ norm, where we will estimate low frequencies and high frequencies separately. For the low frequencies, we use the good behavior of the semigroup $\mathcal{A}_\sigma(\rho)$. Regarding the high frequencies, we make use of the Fourier localization method.

Proof of Theorem 2. We assume that $\mathbb{V}(t) \triangleq (\pi(t), q(t))^T$ is a smooth solution for system (33) and $(F, H) \triangleq (\operatorname{div}(\pi q), \nabla(|q|^2))^T$. Then, employing Duhamel's principle, we found out that

$$\mathbb{V}(\rho) = \mathcal{A}_\sigma(\rho) \mathbb{V}_0 + \int_0^\rho \mathcal{A}_\sigma(\rho) \mathbb{G}(\mathbb{V}(\gamma)) d\gamma, \quad (50)$$

where $\mathbb{V}_0 = (\pi_0, q_0)^T$, $\mathbb{G}(\mathbb{V}(\rho)) = (F, H)$ and $\mathcal{A}_\sigma(\rho)$ is the semigroup associated with the LHS of system (33), which is given by the following equation:

$$\mathcal{A}_\sigma(\rho) b = F^{-1} \left(e^{\hat{L}_\sigma(\xi) \hat{b}} \right), \quad (51)$$

where

$$\hat{L}_\sigma(\xi) = \begin{pmatrix} |\xi|^\sigma & -i\xi \\ -\xi^T & |\xi|^\sigma I_d \end{pmatrix}, \quad (52)$$

where I_d represents the identity matrix of the d dimension. For convenience, we denoted the following equation:

$$\begin{aligned} W_{\text{low}}(t) &\triangleq \sup_{\gamma \in [0,t]} (1+\gamma)^{d/2\sigma} \|\Delta_{-1} \mathbb{V}(\gamma)\|_{L^2} \\ W_{\text{high}}(t) &\triangleq \sup_{\gamma \in [0,t]} (1+\gamma)^{d/2\sigma} \sum_{k \geq 0} 2^{d/2-\sigma+1} \|\Delta_k \mathbb{V}(\gamma)\|_{L^2}, \end{aligned} \quad (53)$$

therefore,

$$\|\mathbb{V}(t)\|_{B_{2,1}^{(d/2)-\sigma+1}} \leq (1+\gamma)^{-d/2\sigma} (W_{\text{low}}(t) + W_{\text{high}}(t)). \quad (54)$$

Since Δ_k coincides with $\dot{\Delta}_k$ for all $k \geq 0$, then

$$\begin{aligned} W_{\text{low}}(t) &\leq \sup_{\gamma \in [0,t]} (1+t)^{d/2\sigma} \left\| \mathcal{A}_\sigma(\gamma) \Delta_{-1} \mathbb{V}_0 \right\|_{L^2} + \sup_{\gamma \in [0,t]} (1+t)^{d/2\sigma} \int_0^\gamma \left\| \mathcal{A}_\sigma(\gamma-\gamma') \Delta_{-1} \mathbb{G}(\mathbb{V}(\gamma')) \right\|_{L^2}, \\ W_{\text{high}}(t) &\leq \sup_{\gamma \in [0,t]} (1+t)^{d/2\sigma} \sum_{k \geq 0} 2^{d/2-\sigma+1} \left\| \mathcal{A}_\sigma(\tau) \dot{\Delta}_k \mathbb{V}_0 \right\|_{L^2} + \sup_{\gamma \in [0,t]} (1+t)^{d/2\sigma} \sum_{k \geq 0} 2^{d/2-\sigma+1} \left\| \mathcal{A}_\sigma(\tau-\tau') \dot{\Delta}_k \mathbb{G}(\mathbb{V}(\tau')) \right\|_{L^2}. \end{aligned} \quad (55)$$

By virtue of [1], Lemma 2.4, we have the following equation:

$$\|\mathcal{A}_\sigma(t)\dot{\Delta}_k \mathbb{V}_0\|_{L^2} = \left\| \left(\mathcal{A}_\sigma(t) \widehat{\Delta}_k \mathbb{V}_0 \right)_{L^2} \right\| \leq C e^{-c_0 t 2^{\sigma k}} \|\dot{\Delta}_k \mathbb{V}_0\|_{L^2}. \quad (56)$$

We also have the following equation:

$$\begin{aligned} \|\mathcal{A}_\sigma(t)\Delta_{-1} \mathbb{V}_0\|_{L^2} &\leq \sum_{k' \leq 0} \|\mathcal{A}_\sigma(t)\dot{\Delta}_{k'} \Delta_{-1} \mathbb{V}_0\|_{L^2} \\ &\leq \sum_{k' \leq 0} \|\mathcal{A}_\sigma(t)\dot{\Delta}_{k'} \mathbb{V}_0\|_{L^2}. \end{aligned} \quad (57)$$

In view of Bernstein's Lemma, we obtained the following equation:

$$\|\mathcal{A}_\sigma(t)\Delta_{-1} \mathbb{V}_0\|_{L^2} \leq \sum_{k' \leq 0} 2^{k' d/2} e^{-c_0 t 2^{\sigma k'}} \|\dot{\Delta}_{k'} \mathbb{V}_0\|_{L^1}. \quad (58)$$

Multiplying both sides by $t^{d/2\sigma}$, according to [1], Lemma 2.35, we concluded that

$$\begin{aligned} t^{d/2\sigma} \|\mathcal{A}_\sigma(t)\Delta_{-1} \mathbb{V}_0\|_{L^2} &\leq C \|\mathbb{V}_0\|_{\dot{B}_{1,\infty}^1} \sum_{k' \in \mathbb{Z}} t^{d/2\sigma} 2^{k' d/2} e^{-c_0 t 2^{\sigma k'}} \\ &\leq C \|\mathbb{V}_0\|_{\dot{B}_{1,\infty}^1}. \end{aligned} \quad (59)$$

In a similar way, we also get the following equation:

$$\begin{aligned} \|\mathcal{A}_\sigma(t)\Delta_{-1} \mathbb{V}_0\|_{L^2} &\leq \sum_{k' \leq 0} 2^{k' d/2} e^{-c_0 t 2^{\sigma k'}} \|\dot{\Delta}_{k'} \mathbb{V}_0\|_{L^1} \\ &\leq \|\mathbb{V}_0\|_{\dot{B}_{1,\infty}^1} \sum_{k' \leq 0} 2^{k' d/2} \\ &\leq C \|\mathbb{V}_0\|_{\dot{B}_{1,\infty}^1}. \end{aligned} \quad (60)$$

Summing up equations (59) and (60), we deduced the following equation:

$$\|\mathcal{A}_\sigma(t)\Delta_{-1} \mathbb{V}_0\|_{L^2} \leq C(1+t)^{-d/2\sigma} \|\mathbb{V}_0\|_{\dot{B}_{1,\infty}^0}. \quad (61)$$

For the high frequencies, we have the following equation:

$$\begin{aligned} t^{d/2\sigma} \sum_{k \geq 0} \|\mathcal{A}_\sigma(t)\dot{\Delta}_k \mathbb{V}_0\|_{L^2} &\leq C \sum_{k \geq 0} t^{d/2\sigma} e^{-c_0 t 2^{\sigma k}} \|\dot{\Delta}_k \mathbb{V}_0\|_{L^2} \\ &\leq C \|\mathbb{V}_0\|_{\dot{B}_{2,1}^{d/2-\sigma+1}}. \end{aligned} \quad (62)$$

Similarly, we get the following equation:

$$\begin{aligned} \sum_{k \geq 0} \|\mathcal{A}_\sigma(t)\dot{\Delta}_k \mathbb{V}_0\|_{L^2} &\leq C \sum_{k \geq 0} e^{-c_0 t 2^{\sigma k}} \|\dot{\Delta}_k \mathbb{V}_0\|_{L^2} \\ &\leq C \|\mathbb{V}_0\|_{\dot{B}_{2,1}^{d/2-\sigma+1}}. \end{aligned} \quad (63)$$

Consequently,

$$\sum_{k \geq 0} \|\mathcal{A}_\sigma(t)\dot{\Delta}_k \mathbb{V}_0\|_{L^2} \leq C(1+t)^{d/2\sigma} \|\mathbb{V}_0\|_{\dot{B}_{2,1}^{d/2-\sigma+1}}. \quad (64)$$

According to Hölder inequality, we obtained the following equation:

$$\begin{aligned} \|\mathbb{G}(\mathbb{V})\|_{L^1} &\leq \|\operatorname{div}(\pi q)\|_{L^1} + \|\nabla(|q|^2)\|_{L^1} \\ &\leq \|\nabla \pi\|_{L^2} \|q\|_{L^2} + \|\pi\|_{L^2} \|\operatorname{div} q\|_{L^2} + \|\nabla q\|_{L^2} \|q\|_{L^2} \\ &\leq \mathbb{J}_1 + \mathbb{J}_2 + \mathbb{J}_3. \end{aligned} \quad (65)$$

By using the Besov embedding $(B_{2,1}^s \rightarrow L^2)$ for $s \geq 0$, we found that

$$\begin{aligned} \mathbb{J}_1 &\leq \|q\|_{\dot{B}_{2,1}^{(d/2)-\sigma+1}} \left(\|\Delta_{-1} \nabla \pi\|_{L^2} + \left\| \sum_{\kappa \geq 0} \Delta_\kappa \nabla \pi \right\|_{\dot{B}_{2,1}^{(d/2)}} \right) \\ &\leq \|q\|_{\dot{B}_{2,1}^{(d/2)-\sigma+1}} \left(\|\pi\|_{\dot{B}_{2,1}^{(d/2)-\sigma+1}} + \|\pi\|_{\dot{B}_{2,1}^{(d/2)+1}} \right) \\ &\leq \|\mathbb{V}\|_{\dot{B}_{2,1}^{(d/2)-\sigma+1}} \left(\|\mathbb{V}\|_{\dot{B}_{2,1}^{(d/2)-\sigma+1}} + \|\mathbb{V}\|_{\dot{B}_{2,1}^{(d/2)+1}} \right). \end{aligned} \quad (66)$$

In a similar way, we bound $\mathbb{J}_2, \mathbb{J}_3$. Thus, we get the following equation:

$$\|\mathbb{G}(\mathbb{V})\|_{L^1} \leq \|\mathbb{V}\|_{\dot{B}_{2,1}^{(d/2)-\sigma+1}} \left(\|\mathbb{V}\|_{\dot{B}_{2,1}^{(d/2)-\sigma+1}} + \|\mathbb{V}\|_{\dot{B}_{2,1}^{(d/2)+1}} \right). \quad (67)$$

According to equations (61) and (64) and Lemma 1, we infer that

$$\begin{aligned} \int_0^\gamma \|\mathcal{A}_\sigma(\gamma-z)\Delta_{-1} \mathbb{G}(\mathbb{V}(z))\|_{L^2} dz &\leq \int_0^\gamma (1+\gamma-z)^{-d/2\sigma} \|\mathbb{G}(\mathbb{V}(z))\|_{\dot{B}_{\infty,1}^0} dz \\ &\leq \int_0^\gamma (1+\gamma-z)^{-d/2\sigma} \|\mathbb{G}(\mathbb{V}(z))\|_{L^1} dz \\ &\leq \int_0^\gamma (1+\gamma-z)^{-d/2\sigma} (1+z)^{-d/2\sigma} W(\gamma) \left((1+z)^{-d/2\sigma} W(\tau) + \|\mathbb{V}\|_{\dot{B}_{2,1}^{d/2+1}} \right) dz \\ &\leq (1+\gamma)^{-d/2\sigma} W(\tau) \|\mathbb{V}\|_{L_t^1 \dot{B}_{2,1}^{d/2+1}} + (1+\gamma)^{-d/2\sigma} W^2(\tau). \end{aligned} \quad (68)$$

We used equations (47) and (48) with $(v=1)$ and obtained the following equation:

$$\begin{aligned} \|\mathbb{G}(\mathbb{V}(z))\|_{\dot{B}_{2,1}^{(d/2)-\sigma+1}} &\leq \|\operatorname{div}(\pi q)\|_{\dot{B}_{2,1}^{(d/2)-\sigma+1}} + \|\nabla(|q|^2)\|_{\dot{B}_{2,1}^{(d/2)-\sigma+1}} \\ &\leq \|\mathbb{V}\|_{\dot{B}_{2,1}^{(d/2)-\sigma+1}} \|\mathbb{V}\|_{\dot{B}_{2,1}^{(d/2)+1}}, \end{aligned} \quad (69)$$

where we have used also the embedding $B_{2,1}^{(d/2)-\sigma+1} \rightarrow B_{2,1}^{(d/2)-\sigma+1}$. According to equation (64) and Lemma 1, we found out that

$$\begin{aligned} \sum_{k \geq 0} 2^{k((d/2)-\sigma+1)} \int_0^\gamma \|\mathcal{A}_\sigma(\gamma-z)\Delta_k \mathbb{G}(\mathbb{V}(z))\|_{L^2} ds &\leq \int_0^\gamma (1+\gamma-z)^{-(d/2\sigma)} \|\mathbb{G}(\mathbb{V}(z))\|_{\dot{B}_{2,1}^{(d/2)-\sigma+1}} dz \\ &\leq \int_0^\gamma (1+\gamma-z)^{-(d/2\sigma)} (1+z)^{-(d/2\sigma)} W(\gamma) \|\mathbb{V}(z)\|_{\dot{B}_{2,1}^{(d/2)+1}} dz \\ &\leq (1+\gamma)^{-(d/2\sigma)} W(\gamma) \|\mathbb{V}(z)\|_{L_t^1 \dot{B}_{2,1}^{(d/2)+1}}. \end{aligned} \tag{70}$$

In view of equations (61) and (64), we deduced the following equation:

$$\begin{aligned} W(t) &\leq C \|\mathbb{V}_0\|_{\dot{B}_{\infty,1}^0 \cap \dot{B}_{2,1}^{(d/2)-\sigma+1}} + \sup_{\gamma \in [0,t]} \int_0^\gamma \|\Delta_{-1} \mathcal{A}_\sigma(\gamma-z)\mathbb{G}(\mathbb{V}(z))\|_{L^2} dz \\ &\quad + \sup_{\gamma \in [0,t]} \int_0^\gamma \sum_{k \geq 0} 2^{k((d/2)-\sigma+1)} \int_0^\gamma \|\mathcal{A}_\sigma(\gamma-z)\Delta_k \mathbb{G}(\mathbb{V}(z))\|_{L^2} dz. \end{aligned} \tag{71}$$

Putting equations (68) and (70) into equation (71), we obtained the following equation:

$$W(t) \leq \|\mathbb{V}_0\|_{\dot{B}_{\infty,1}^0 \cap \dot{B}_{2,1}^{(d/2)-\sigma+1}} + W(t) \|\mathbb{V}_0\|_{\dot{B}_{\infty,1}^0 \cap \dot{B}_{2,1}^{(d/2)-\sigma+1}} + W^2(t). \tag{72}$$

A bootstrapping argument implies that there is $\epsilon > 0$ such that, if $\|\mathbb{V}_0\|_{\dot{B}_{\infty,1}^0 \cap \dot{B}_{2,1}^{(d/2)-\sigma+1}} < \epsilon$, then for all $t \geq 0$,

$$W(t) \leq M_0 \epsilon, \tag{73}$$

for some positive constant M_0 . Then, the Proof of Theorem 2 is now achieved. \square

6. Conclusions

More or less recently, several methodologies have been proposed to describe behaviors of some complex world problems emerging in several applications, especially in molecular biology. The chemotaxis model gains increasing interest from mathematicians; so far, the problem of existence and uniqueness of classical solutions to system (1) (with fractional dissipation Λ^σ or classical dissipation $-\Delta$) in multidimensions $d > 1$ remains an open problem. In this work, we were able to give a positive answer regarding the existence of classical solutions with small initial data lying in the Besov spaces; also, we managed to get the optimal temporal decay of strong solutions. In the future direction, it will be interesting to study the current model on recent fractional derivatives, then demonstrate the effect of the fractional order through some simulations.

Data Availability

No underlying data was collected or produced in this study.

Disclosure

This work was conducted during our work at Hodeidah University.

Conflicts of Interest

The authors declare that they have no conflicts of interest.

References

- [1] A. Pekalski and K. Sznajd-Weron, "Anomalous diffusion. From basics to applications," *Lecture Notes in Phys*, Vol. 519, Springer, Berlin, Germany, 1999.
- [2] E. F. Keller and L. A. Segel, "Initiation of slime mold aggregation viewed as an instability," *Journal of Theoretical Biology*, vol. 26, no. 3, pp. 399–415, 1970.
- [3] E. F. Keller and L. A. Segel, "Model for chemotaxis," *Journal of Theoretical Biology*, vol. 30, no. 2, pp. 225–234, 1971.
- [4] P. Biler and G. Wu, "Two-dimensional chemotaxis models with fractional diffusion," *Mathematical Methods in the Applied Sciences*, vol. 32, no. 1, pp. 112–126, 2009.
- [5] Z. Zhai, "Global well-posedness for nonlocal fractional Keller–Segel systems in critical Besov spaces," *Nonlinear Analysis: Theory, Methods & Applications*, vol. 72, no. 6, pp. 3173–3189, 2010.
- [6] P. Biler and G. Karch, "Blow up of solutions to generalized Keller–Segel model," *Journal of Evolution Equations*, vol. 10, no. 2, pp. 247–262, 2010.

- [7] V. Calevez, B. Perthame, and M. Sharifi Tabar, “Modified Keller–Segel system and critical mass for the log interaction kernel,” in *Stochastic Analysis and Pde, AMS, Contemp. Math*, G. Q. Chen, Ed., vol. 429, pp. 45–62, Springer, Berlin, Germany, 2007.
- [8] H. Kozono and Y. Sugiyama, “Global strong solution to the semi-linear Keller–Segel system of parabolic–parabolic type with small data in scale invariant spaces,” *Journal of Differential Equations*, vol. 247, pp. 1–32, 2009.
- [9] Y. Sugiyama and H. Kunii, “Global existence and decay properties for a degenerate Keller–Segel model with a power factor in drift term,” *Journal of Differential Equations*, vol. 227, no. 1, pp. 333–364, 2006.
- [10] Z. Zhai, “Well-posedness for two types of generalized Keller–Segel system of chemotaxis in critical Besov spaces,” *Communications on Pure and Applied Analysis*, vol. 10, no. 1, pp. 287–308, 2010.
- [11] M. Zhang and C. Zhu, “Global existence of solutions to a hyperbolic-parabolic system,” *Proceedings of the American Mathematical Society*, vol. 135, no. 04, pp. 1017–1027, 2007.
- [12] G. Jun, X. Jixiong, Z. Huijiang, and Z. Changjiang, “Global solutions to a hyperbolic-parabolic coupled system with large initial data,” *Acta Mathematica Scientia*, vol. 29, no. 3, pp. 629–641, 2009.
- [13] C. Hao, “Global well-posedness for a multidimensional chemotaxis model in critical Besov spaces,” *Zeitschrift für Angewandte Mathematik und Physik*, vol. 63, no. 5, pp. 825–834, 2012.
- [14] Y. Nie and J. Yuan, “Well-posedness and ill-posedness of a multidimensional chemotaxis system in the critical Besov spaces,” *Nonlinear Analysis*, vol. 196, Article ID 111782, 2020.
- [15] X. Guan, S. Wang, Y. Lv, and F. Xu, “The optimal convergence rates for the multi-dimensional chemotaxis model in critical Besov spaces,” *Acta Applicandae Mathematica*, vol. 143, no. 1, pp. 91–104, 2016.
- [16] B. D. Sleeman and H. A. Levine, “A system of reaction diffusion equations arising in the theory of reinforced random walks,” *SIAM Journal on Applied Mathematics*, vol. 57, no. 3, pp. 683–730, 1997.
- [17] D. Li, T. Li, and K. Zhao, “ON a hyperbolic–parabolic system modeling chemotaxis,” *Mathematical Models and Methods in Applied Sciences*, vol. 21, no. 08, pp. 1631–1650, 2011.
- [18] F. Xu, X. Li, and C. Wang, “The large-time behavior of the multi-dimensional hyperbolic-parabolic model arising from chemotaxis,” *Journal of Mathematical Physics*, vol. 60, no. 9, Article ID 091509, 2019.
- [19] W. Xie, Y. Zhang, Y. Xiao, and W. Wei, “Global existence and convergence rates for the strong solutions in H^2 to the 3D chemotaxis model,” *Journal of Applied Mathematics*, vol. 2013, Article ID 391056, 9 pages, 2013.
- [20] Y. Tao, L. Wang, and Z. Wang, “Large-time behavior of a parabolic-parabolic chemotaxis model with logarithmic sensitivity in one dimension,” *Discrete & Continuous Dynamical Systems - B*, vol. 18, no. 3, pp. 821–845, 2013.
- [21] H. Li and K. Zhao, “Initial-boundary value problems for a system of hyperbolic balance laws arising from chemotaxis,” *Journal of Differential Equations*, vol. 258, no. 2, pp. 302–338, 2015.
- [22] Z.-A. Wang, Z. Xiang, and P. Yu, “Asymptotic dynamics on a singular chemotaxis system modeling onset of tumor angiogenesis,” *Journal of Differential Equations*, vol. 260, no. 3, pp. 2225–2258, 2016.
- [23] V. R. Martinez, Z. Wang, and K. Zhao, “Asymptotic and viscous stability of large-amplitude solutions of a hyperbolic system arising from biology,” *Indiana University Mathematics Journal*, vol. 67, no. 4, pp. 1383–1424, 2018.
- [24] X. Wu and K. Su, “Global existence and optimal decay rate of solutions to hyperbolic chemotaxis system in Besov spaces,” *Discrete & Continuous Dynamical Systems - B*, vol. 26, p. 6057, 2021.
- [25] J. Li, T. Li, and Z.-A. Wang, “Stability of traveling waves of the Keller–Segel system with logarithmic sensitivity,” *Mathematical Models and Methods in Applied Sciences*, vol. 24, no. 14, pp. 2819–2849, 2014.
- [26] T. Li and Z.-A. Wang, “Nonlinear stability of traveling waves to a hyperbolic-parabolic system modeling chemotaxis,” *SIAM Journal on Applied Mathematics*, vol. 70, no. 5, pp. 1522–1541, 2010.
- [27] T. Li and Z.-A. Wang, “Nonlinear stability of large amplitude viscous shock waves of a generalized hyperbolic-parabolic system arising in chemotaxis,” *Mathematical Models and Methods in Applied Sciences*, vol. 20, no. 11, pp. 1967–1998, 2010.
- [28] T. Li and Z.-A. Wang, “Asymptotic nonlinear stability of traveling waves to conservation laws arising from chemotaxis,” *Journal of Differential Equations*, vol. 250, no. 3, pp. 1310–1333, 2011.
- [29] H. Bahouri, J.-Y. Chemin, and R. Danchin, “Fourier analysis and nonlinear partial differential equations,” *Grundlehren der Mathematischen Wissenschaften*, Vol. 343, Springer, Berlin, Germany, 2011.
- [30] J.-Y. Chemin and N. Lerner, “Flow of nlvf-Stokes equations,” *Journal of Differential Equations*, vol. 121, no. 2, pp. 314–328, 1995.
- [31] M. Okita, “Optimal decay rate for strong solutions in critical spaces to the compressible Navier-Stokes equations,” *Journal of Differential Equations*, vol. 257, no. 10, pp. 3850–3867, 2014.

Research Article

Exploring the Analytical Solutions to the Economical Model via Three Different Methods

M. Raheel,^{1,2} Khalid K. Ali ,³ Asim Zafar ,² Ahmet Bekir ,⁴ Omar Abu Arqub ,⁵
and Marwan Abukhaled ⁶

¹Department of Mathematics and Statistics, Institute of Southern Punjab, Multan, Pakistan

²Department of Mathematics, CUI, Vehari Campus, Vehari, Pakistan

³Mathematics Department, Faculty of Science, Al-Azhar University, Nasr, Cairo, Egypt

⁴Neighbourhood of Akcaglan, Imarli Street, Number: 28/4, Eskisehir 26030, Turkey

⁵Department of Mathematics, Faculty of Science, Al-Balqa Applied University, As-Salt, Jordan

⁶Department of Mathematics and Statistics, American University of Sharjah, Sharjah, UAE

Correspondence should be addressed to Ahmet Bekir; bekirahmet@gmail.com

Received 9 November 2022; Revised 22 January 2023; Accepted 5 April 2023; Published 22 April 2023

Academic Editor: Francisco J. Garcia Pacheco

Copyright © 2023 M. Raheel et al. This is an open access article distributed under the Creative Commons Attribution License, which permits unrestricted use, distribution, and reproduction in any medium, provided the original work is properly cited.

In this article, the analytical solutions of economically important model named as the Ivancevic option pricing model (IOPM) along new definition of derivative have been explored. For this purpose, \exp_a function, extended sinh-Gordon equation expansion (EShGEE) and extended (G'/G) -expansion methods have been utilized. The resulting solutions are dark, bright, dark-bright, periodic, singular, and other kinds of solutions. These solutions are obtained and also verified by a Mathematica tool. Some of the gained results are explained by 2-D, 3-D, and contour plots.

1. Introduction

Many mathematical models have been developed in many areas of sciences in the form of nonlinear partial differential equations (NLPDEs). Numerous techniques are made to gain exact solutions of NLPDEs such as generalized exponential rational function scheme (GERFS) [1–4], $(m + 1/G)$ -expansion and Adomian decomposition schemes [5], new generalized expansion method [6], simplest equation and Kudryashov's new function techniques [7], modified simple equation scheme [8], modified Kudryashov simple equation technique [9], first integral technique [10], Bäcklund transformation scheme [11], extended Jacobi elliptic function expansion technique [12], and extended (G/G) -expansion and improved (G'/G) -expansion schemes [13].

In modern century, one of the most studied fields from all over the world is the economy or finance. Therefore, such problems were studied to be explained

and investigated by using scientific norms. Thus, such works introduce more intellectual ways for the user. Therefore, to observe financial market is highly important. Deeper properties of the modeling of a global financial market produce global informative systems. Especially, these dynamical systems can be used for deep investigation of the productions. The first step is to treatment its mathematical models being either complex-valued or real values with wave function. Therefore, many models were developed by experts in extracting their wave distributions in today and future direction. In our study, we use three methods \exp_a function, extended sinh-Gordon equation expansion (EShGEE), and extended (G'/G) -expansion methods. These methods have various applications. Likely, some new kind of analytical results of perturbed Gerdjikov–Ivanov model (pGIM) have been achieved by using \exp_a function and extended tanh function expansion methods in [14]. By applying \exp_a function and hyperbolic function methods, various

types of wave solutions of two nonlinear Schrödinger equations are gained in [15]. New trigonometry and hyperbolic function type soliton solutions of (2 + 1)-dimensional hyperbolic and cubic-quintic nonlinear Schrödinger equations are achieved by applying extended sinh-Gordon equation expansion technique in [16]. Bright, dark, and bright-dark soliton solutions of generalized nonlinear Schrödinger equation have been determined by utilizing extended sinh-Gordon equation expansion approach in [17]. Some exact solitons of (2 + 1)-dimensional that improved the Eckhaus equation are calculated by using extended (G'/G)-expansion technique in [18]. Different types of exact solitons of time-fractional parabolic equations are obtained by using extended (G'/G)-expansion scheme in [19].

Our considering model is one of the important and interesting economical models, namely, the Ivancevic option pricing model (IOPM). It can be possible to derive the Ivancevic option pricing model by using the Brownian movement like the Black–Scholes option pricing model. The Ivancevic option pricing model is an adaptive-wave model which is a nonlinear wave alternative for the standard Black–Scholes option-pricing model, representing controlled Brownian behavior of financial markets, which is formally defined by adaptive nonlinear Schrodinger (NLS) equations, defining the option-pricing wave function in terms of the stock price and time. In the literature, few techniques have been used on this model to get different exact solutions. For example, new solutions have been achieved in this model by applying the fractionally reduced differential transform technique in [20]. Dark, bright, dark-bright, complex, travelling, periodic, trigonometric, and hyperbolic function solutions have been achieved by applying rational sine-Gordon expansion scheme and modified exponential method in [21]. Rogue wave and dark wave solitons of the Ivancevic option pricing equation have been obtained by using the trial function method in [22].

The fundamental purpose of the work is to explore analytical solutions of the truncated M-fractional Ivancevic option pricing model based on \exp_a function, extended sinh-Gordon equation expansion, and extended (G'/G)-expansion methods.

The paper is structured as follows: The brief introduction of model has been given in Section 2, together with other useful properties and characterizations. Section 3 contains the description of methodologies. The mathematical analysis of model and its analytical solutions have been provided in Section 4. Section 5 some solutions have been represented through different types of graphics. Finally, Section 6 contains some discussion about the graphs and conclusion of our research.

2. Model Description

Scholes and Robert Merton published their now-well-known option pricing formula which would have an important effect on the development of quantitative finance. In their model, typically known as Black–Scholes, the value of an

option depends on the future volatility of a stock rather than on its expected return. The Ivancevic option pricing model is an adaptive-wave model which is a nonlinear wave alternative for the standard Black–Scholes option-pricing model, representing controlled Brownian behavior of financial markets, which is formally defined by adaptive nonlinear Schrodinger (NLS) equations, defining the option-pricing wave.

Let's assume the M-fractional Ivancevic option pricing model (IOPM) [22] given as follows:

$${}_t D_{M,t}^{\epsilon,\rho} q + \frac{\delta}{2} D_{M,2s}^{2\epsilon,\rho} q + \Omega q |q|^2 = 0, \quad \iota = \sqrt{-1}, \quad (1)$$

where $D_{M,t}^{\epsilon,\rho} q = \lim_{\tau \rightarrow 0} \rho q(t E_\rho(\tau t^{1-\epsilon})) - q(t)/\tau, 0 < \epsilon < 1, \rho > 0.$

This model was first developed by Ivancevic [23] to fulfill both behavioral and efficient markets. Here, $q = q(s, t)$ describes the option price wave profile. While t is time variable and s is asset price of the model. Parameter δ represents the volatility which shows either stochastic process itself or only a constant. Where $\Omega = \Omega(r, \omega)$ is called Landau coefficient which describes adaptive market potential. In nonadaptive simplest case, Ω and r become equal which shows the interest rate while in adaptive case, $\Omega(r, \omega)$ may be connected to market temperature and it depends on the set of tractable parameters $\{W_i\}$. In third term, $|q|^2$ shows the probability density function which denotes the potential field.

3. Description of Methodologies

3.1. Summary of \exp_a Function Scheme. Here, we will give complete concept of this scheme.

Assuming the nonlinear partial differential equation (PDE),

$$G(q, q^2 q_t, q_x, q_{tt}, q_{xx}, q_{xt}, \dots) = 0. \quad (2)$$

Equation (2) transformed into nonlinear partial differential equation as follows:

$$\Lambda(Q, Q', Q'', \dots) = 0. \quad (3)$$

By using following transformations,

$$q(x, y, t) = Q(\zeta), \quad \zeta = ax + by + rt. \quad (4)$$

Considering root of equation (3) is shown in [24–27].

$$Q(\zeta) = \frac{\alpha_0 + \alpha_1 d^\zeta + \dots + \alpha_m d^{m\zeta}}{\beta_0 + \beta_1 d^\zeta + \dots + \beta_m d^{m\zeta}}, \quad d \neq 0, 1, \quad (5)$$

where α_i and $\beta_i (0 \leq i \leq m)$ are undetermined. Positive integral value of m is calculated by utilizing homogenous balance technique in equation (3). Putting equation (5) into equation (3) gives

$$\wp(d^\zeta) = \ell_0 + \ell_1 d^\zeta + \dots + \ell_i d^{t\zeta} = 0. \quad (6)$$

Taking $\ell_i (0 \leq i \leq t)$ in equation (6) equal to 0, a set of algebraic equations is gained which is given as

$$\ell_i = 0, \text{ where } i = 0, \dots, t. \tag{7}$$

By using the got roots, we attain analytical results of equation (2).

3.2. *Detail of Extended Sinh-Gordon Equation Expansion Method (EShGEEM).* Here, we will describe main steps of this technique.

Step 1:

Let a nonlinear partial differential equation be given as

$$Z(f, D_{M,t}^{\alpha,\gamma} f^2, f^2 f_x, f_y, f_{yy}, f_{xx}, f_{xy}, f_{xt}, \dots) = 0, \tag{8}$$

where $f = f(x, y, t)$ denotes the wave function.

Assuming the travelling wave transformation,

$$f(x, y, t) = F(\xi), \xi = x - \nu y + \frac{\Gamma(\gamma + 1)}{\alpha} (\kappa t^\alpha). \tag{9}$$

Inserting equation (9) into equation (8), we attain the nonlinear ODE given as

$$Z(F(\xi), F^2(\xi)F'(\xi), F''(\xi), \dots) = 0. \tag{10}$$

Step 2:

Assuming the results of equation (9) in the series form,

$$F(p) = \alpha_0 + \sum_{i=1}^m (\beta_i \sinh(p) + \alpha_i \cosh(p))^i. \tag{11}$$

Here, $\alpha_0, \alpha_i,$ and β_i ($i = 1, 2, 3, \dots, m$) are unknowns. Consider a function p of ξ that satisfies the following equation:

$$\frac{dp}{d\xi} = \sinh(p). \tag{12}$$

Natural number m can be attained with the use of homogenous balance approach. Equation (12) is gained from sinh-Gordon equation as shown as

$$q_{xt} = \kappa \sinh(\nu). \tag{13}$$

By what being present in [28], we get the results of equation (13) given as follows:

$$\sinh p(\xi) = \pm \csc h(\xi) \text{ or } \cosh p(\xi) = \pm \coth(\xi). \tag{14}$$

In addition,

$$\sinh p(\xi) = \pm \operatorname{sech}(\xi) \text{ or } \cosh p(\xi) = \pm \tanh(\xi), \tag{15}$$

where $\iota^2 = -1$.

Step 3:

Using equation (11) with equation (13) into equation (10), we get the algebraic equations involving $p^{i,k}(\xi) \sinh^l p(\xi) \cosh^m p(\xi)$ ($k = 0, 1; l = 0, 1; m =$

$0, 1, 2, \dots$). We take the every coefficient of $p^{i,k}(\xi) \sinh^l p(\xi) \cosh^m p(\xi)$ equal to 0, to attain system of algebraic equations having $\nu, \kappa, \alpha_0, \alpha_i$ and β_i ($i = 1, 2, 3, \dots, m$).

Step 4:

By solving the obtained system of algebraic equations, one may obtain value of $\nu, \kappa, \alpha_0, \alpha_i$ and β_i .

Step 5:

By achieved solutions, equations (14) and (15), we get the wave solitons of equation (10) shown as

$$F(\xi) = \alpha_0 + \sum_{i=1}^m (\pm \beta_i \operatorname{csch}(\xi) \pm \alpha_i \coth(\xi))^i, \tag{16}$$

$$F(\xi) = \alpha_0 + \sum_{i=1}^m (\pm \iota \beta_i \operatorname{sech}(\xi) \pm \alpha_i \tanh(\xi))^i. \tag{17}$$

3.3. *Explanation of Extended (G'/G)-Expansion Method.* Here, we will represent some main steps of method given in [13].

Step 1: Considering the nonlinear PDE,

$$Z(f, D_{M,t}^{\alpha,\gamma} f, f^2 f_x, f_y, f_{yy}, f_{xx}, f_{xy}, f_{xt}, \dots) = 0, \tag{18}$$

where $f = f(x, y, t)$ denotes the wave profile.

Considering the travelling wave transformations:

Step 2:

$$f(x, y, t) = F(\xi), \xi = x - \nu y + \frac{\Gamma(\gamma + 1)}{\alpha} (\kappa t^\alpha). \tag{19}$$

Using equation (19) along equation (18), we attain the nonlinear ODE as follows:

$$Z(F(\xi), F^2(\xi)F'(\xi), F''(\xi), \dots) = 0. \tag{20}$$

Step 3:

Assuming the results of equation (20) in the series form given as

$$F(\xi) = \sum_{i=-m}^m \alpha_i \left(\frac{G'(\xi)}{G(\xi)} \right)^i. \tag{21}$$

In equation (21), α_0 and α_i , ($i = \pm 1, \pm 2, \pm 3, \dots, \pm m$) are undetermined and $\alpha_i \neq 0$. Applying homogenous balance technique into equation (20), natural number m can be obtained.

Function $G = G(\xi)$ satisfies the Riccati differential equation.

$$dGG'' - aG^2 - bGG' - c(G')^2 = 0, \tag{22}$$

where $a, b, c,$ and d are constants.

Step 4:

When $b \neq 0$ and $b^2 + 4a(d - c) > 0$, then

Considering equation (22) has roots in the form:

$$\left(\frac{G'(\xi)}{G(\xi)}\right) = \frac{b}{2(d-c)} + \frac{\sqrt{-4a(c-d) + b^2}}{2(d-c)} \left(\frac{C_1 \sinh\left(\xi\sqrt{-4ac + 4ad + b^2}/2d\right) + C_2 \cosh\left(\xi\sqrt{-4a(c-d) + b^2}/2d\right)}{C_1 \cosh\left(\xi\sqrt{-4ac + 4ad + b^2}/2d\right) + C_2 \sinh\left(\xi\sqrt{-4ac + 4ad + b^2}/2d\right)} \right). \quad (23)$$

When $b \neq 0$ and $b^2 + 4ad - 4ac < 0$, then

$$\left(\frac{G'(\xi)}{G(\xi)}\right) = \frac{b}{2(d-c)} + \frac{\sqrt{4ac - 4ad - b^2}}{2(d-c)} \left(\frac{C_2 \cos\left(\xi\sqrt{4ac - 4ad - b^2}/2d\right) - C_1 \sin\left(\xi\sqrt{4ac - 4ad - b^2}/2d\right)}{C_1 \cos\left(\xi\sqrt{4ac - 4ad - b^2}/2d\right) + C_2 \sin\left(\xi\sqrt{4ac - 4ad - b^2}/2d\right)} \right). \quad (24)$$

When $b \neq 0$ and $b^2 + 4a(d - c) = 0$, then

When $b = 0$ and $a(d - c) > 0$, then

$$\left(\frac{G'(\xi)}{G(\xi)}\right) = \frac{b}{2(d-c)} + \frac{dD}{(d-c)(C - D\xi)}. \quad (25)$$

$$\left(\frac{G'(\xi)}{G(\xi)}\right) = \frac{\sqrt{ad - ac}}{(d-c)} \left(\frac{C_1 \sinh(\xi\sqrt{ad - ac}/d) + C_2 \cosh(\xi\sqrt{a(d-c)}/d)}{C_1 \cosh(\xi\sqrt{ad - ac}/d) + C_2 \sinh(\xi\sqrt{a(d-c)}/d)} \right). \quad (26)$$

When $b = 0$ and $a(d - c) < 0$, then

$$\left(\frac{G'(\xi)}{G(\xi)}\right) = \frac{\sqrt{a(c-d)}}{d-c} \left(\frac{C_2 \cos(\xi\sqrt{ac - ad}/d) - C_1 \sin(\xi\sqrt{a(c-d)}/d)}{C_1 \cos(\xi\sqrt{ac - ad}/d) + C_2 \sin(\xi\sqrt{a(c-d)}/d)} \right), \quad (27)$$

where $a, b, c, d, C_1,$ and C_2 are constants.

attain a set of algebraic equations involving $\nu, \kappa, \alpha_i, (i = 0, \pm 1, \pm 2, \dots, \pm m)$, and other parameters.

Step 5:

Step 6:

Putting equation (21) with equation (22) into equation (20) and collecting coefficients of each power of $(G'(\xi)/G(\xi))$. Taking every coefficient equal to 0, we

Finding the gain system of equations with the use of the tool.

Step 7:

Putting the attained solutions into the equation (21) and we gain analytical solutions of equation (18).

4. Mathematical Treatment of Model

Suppose the travelling wave transform given as

$$q(s, t) = Q(\zeta) \times \exp\left(i\left(\frac{\Gamma(\varrho + 1)}{\epsilon} (\mu s^\epsilon + \rho t^\epsilon)\right)\right), \zeta = \frac{\Gamma(\varrho + 1)}{\epsilon} (\lambda s^\epsilon + \tau t^\epsilon), \tag{28}$$

where $Q(\zeta)$ shows the amplitude of wave function while ρ and τ represent the time velocity. Parameters μ and λ are obtaining from asset price of the product.

Using equation (28) into equation (1), we gain real part and imaginary part given as

Real part:

$$2\Omega Q^3 + \delta \lambda^2 Q'' - (\delta \mu^2 + 2\rho)Q = 0. \tag{29}$$

Imaginary part:

$$(\delta \mu \lambda + \tau)Q' = 0. \tag{30}$$

From equation (30), we get the velocity of wave function given as follows:

$$\tau = -\delta \mu \lambda. \tag{31}$$

Utilizing the homogenous balance method into equation (29), we achieve $m = 1$

Now, we will gain the exact solutions of equation (29) by using three abovementioned methods.

4.1. Analytical Solutions via \exp_a Function Technique.

Equation (5) changes into the following for $m = 1$:

$$Q(\zeta) = \frac{\alpha_0 + \alpha_1 d^\zeta}{\beta_0 + \beta_1 d^\zeta}. \tag{32}$$

Inserting equation (32) into equation (29), a system of equations is achieved. By solving the system, we obtain different solution sets given as follows:

Set 1:

$$\left\{ \alpha_0 = -\frac{i\beta_0 \sqrt{\delta} \lambda \log(d)}{2\sqrt{\Omega}}, \alpha_1 = \frac{i\beta_1 \sqrt{\delta} \lambda \log(d)}{2\sqrt{\Omega}}, \rho = -\frac{1}{4} \delta (\lambda^2 \log^2(d) + 2\mu^2) \right\}. \tag{33}$$

From equations (28), (32) and (33), we get

$$q(s, t) = -\frac{i\sqrt{\delta} \lambda \log(d)}{2\sqrt{\Omega}} \left(\frac{\beta_0 - \beta_1 d^\zeta}{\beta_0 + \beta_1 d^\zeta} \right) \times \exp\left(i\left(\mu \frac{\Gamma(\varrho + 1)}{\epsilon} s^\epsilon - \frac{1}{4} \delta (\lambda^2 \log^2(d) + 2\mu^2) \frac{\Gamma(\varrho + 1)}{\epsilon} t^\epsilon\right)\right). \tag{34}$$

Set 2:

$$\left\{ \alpha_0 = \frac{i\beta_0 \sqrt{\delta} \lambda \log(d)}{2\sqrt{\Omega}}, \alpha_1 = -\frac{i\beta_1 \sqrt{\delta} \lambda \log(d)}{2\sqrt{\Omega}}, \rho = -\frac{1}{4} \delta (\lambda^2 \log^2(d) + 2\mu^2) \right\}. \tag{35}$$

From equations (28), (32) and (35), we get

$$q(s, t) = \frac{i\sqrt{\delta}\lambda \log(d)}{2\sqrt{\Omega}} \left(\frac{\beta_0 - \beta_1 d^i}{\beta_0 + \beta_1 d^i} \right) \times \exp\left(i \left(\mu \frac{\Gamma(\varrho + 1)}{\epsilon} s^\epsilon - \frac{1}{4} \delta (\lambda^2 \log^2(d) + 2\mu^2) \frac{\Gamma(\varrho + 1)}{\epsilon} t^\epsilon \right) \right). \tag{36}$$

Where $\zeta = \lambda\Gamma(\varrho + 1)/\epsilon(s^\epsilon - \delta\mu t^\epsilon)$.

4.2. *Exact Solutions through EShGEEM.* For $m = 1$, equations (9), (16) and (17) and become

$$Q(\zeta) = \alpha_0 \pm \beta_1 \operatorname{csch}(\zeta) \pm \alpha_1 \operatorname{coth}(\zeta), \tag{37}$$

$$Q(\zeta) = \alpha_0 \pm i\beta_1 \operatorname{sech}(\zeta) \pm \alpha_1 \operatorname{tanh}(\zeta), \tag{38}$$

$$Q(\zeta) = \alpha_0 + \beta_1 \sinh(p) + \alpha_1 \cosh(p). \tag{39}$$

Here, α_0, α_1 , and β_1 are undetermined. Utilizing equation (39) into equation (29), we attain algebraic equations containing $\alpha_0, \alpha_1, \beta_1$ and other parameters. By using the Mathematica tool, we get different solution sets given as

Set 1:

$$\left\{ \alpha_0 = 0, \alpha_1 = -\frac{i\sqrt{\delta}\lambda}{\sqrt{\Omega}}, \beta_1 = 0, \rho = -\frac{1}{2} \delta (2\lambda^2 + \mu^2) \right\}. \tag{40}$$

From equations (28), (37) and (40), we get

$$q_1(s, t) = \mp \frac{i\sqrt{\delta}\lambda}{\sqrt{\Omega}} \operatorname{coth}(\zeta) \times \exp\left(i \left(\mu \frac{\Gamma(\varrho + 1)}{\epsilon} s^\epsilon - \frac{1}{2} \delta (2\lambda^2 + \mu^2) \frac{\Gamma(\varrho + 1)}{\epsilon} t^\epsilon \right) \right). \tag{41}$$

From equations (28), (38), and (40), we get

$$q_2(s, t) = \mp \frac{i\sqrt{\delta}\lambda}{\sqrt{\Omega}} \operatorname{tanh}(\zeta) \times \exp\left(i \left(\mu \frac{\Gamma(\varrho + 1)}{\epsilon} s^\epsilon - \frac{1}{2} \delta (2\lambda^2 + \mu^2) \frac{\Gamma(\varrho + 1)}{\epsilon} t^\epsilon \right) \right). \tag{42}$$

Set 2:

$$\left\{ \alpha_0 = 0, \alpha_1 = \frac{i\sqrt{\delta}\lambda}{\sqrt{\Omega}}, \beta_1 = 0, \rho = -\frac{1}{2} \delta (2\lambda^2 + \mu^2) \right\}. \tag{43}$$

From equations (28), (37), and (43), we get

$$q_1(s, t) = \pm \frac{i\sqrt{\delta}\lambda}{\sqrt{\Omega}} \operatorname{coth}(\zeta) \times \exp\left(i \left(\mu \frac{\Gamma(\varrho + 1)}{\epsilon} s^\epsilon - \frac{1}{2} \delta (2\lambda^2 + \mu^2) \frac{\Gamma(\varrho + 1)}{\epsilon} t^\epsilon \right) \right). \tag{44}$$

From equations (28), (38), and (43), we get

$$q_2(s, t) = \pm \frac{i\sqrt{\delta}\lambda}{\sqrt{\Omega}} \operatorname{tanh}(\zeta) \times \exp\left(i \left(\mu \frac{\Gamma(\varrho + 1)}{\epsilon} s^\epsilon - \frac{1}{2} \delta (2\lambda^2 + \mu^2) \frac{\Gamma(\varrho + 1)}{\epsilon} t^\epsilon \right) \right). \tag{45}$$

Set 3:

$$\left\{ \alpha_0 = 0, \alpha_1 = -\frac{i\sqrt{\delta}\lambda}{2\sqrt{\Omega}}, \beta_1 = -\frac{i\sqrt{\delta}\lambda}{2\sqrt{\Omega}}, \rho = -\frac{1}{4} \delta (\lambda^2 + 2\mu^2) \right\}. \tag{46}$$

From equations (28), (37), and (46) we get

$$q_1(s, t) = \mp \frac{i\sqrt{\delta}\lambda}{2\sqrt{\Omega}} (\operatorname{coth}(\zeta) + \operatorname{csch}(\zeta)) \times \exp\left(i \left(\mu \frac{\Gamma(\varrho + 1)}{\epsilon} s^\epsilon - \frac{1}{4} \delta (\lambda^2 + 2\mu^2) \frac{\Gamma(\varrho + 1)}{\epsilon} t^\epsilon \right) \right). \tag{47}$$

From equations (28), (38), and (46), we get

$$q_2(s, t) = \mp \frac{i\sqrt{\delta}\lambda}{2\sqrt{\Omega}} (i \operatorname{sech}(\zeta) + \operatorname{tanh}(\zeta)) \times \exp\left(i \left(\mu \frac{\Gamma(\varrho + 1)}{\epsilon} s^\epsilon - \frac{1}{4} \delta (\lambda^2 + 2\mu^2) \frac{\Gamma(\varrho + 1)}{\epsilon} t^\epsilon \right) \right). \tag{48}$$

Set 4:

$$\left\{ \alpha_0 = 0, \alpha_1 = \frac{i\sqrt{\delta}\lambda}{2\sqrt{\Omega}}, \beta_1 = -\frac{i\sqrt{\delta}\lambda}{2\sqrt{\Omega}}, \rho = -\frac{1}{4} \delta (\lambda^2 + 2\mu^2) \right\}. \tag{49}$$

From equations (28), (37), and (49), we get

$$q_1(s, t) = \frac{i\sqrt{\delta}\lambda}{2\sqrt{\Omega}} (\pm \coth(\zeta) \mp \operatorname{csch}(\zeta)) \times \exp\left(i\left(\mu \frac{\Gamma(\varrho+1)}{\epsilon} s^\epsilon - \frac{1}{4}\delta(\lambda^2 + 2\mu^2) \frac{\Gamma(\varrho+1)}{\epsilon} t^\epsilon\right)\right). \tag{50}$$

From equations (28), (38), and (49), we get

$$q_2(s, t) = \frac{i\sqrt{\delta}\lambda}{2\sqrt{\Omega}} (\pm \tanh(\zeta) \mp i \operatorname{sech}(\zeta)) \times \exp\left(i\left(\mu \frac{\Gamma(\varrho+1)}{\epsilon} s^\epsilon - \frac{1}{4}\delta(\lambda^2 + 2\mu^2) \frac{\Gamma(\varrho+1)}{\epsilon} t^\epsilon\right)\right). \tag{51}$$

Set 5:

$$\left\{ \alpha_0 = 0, \alpha_1 = -\frac{i\sqrt{\delta}\lambda}{2\sqrt{\Omega}}, \beta_1 = \frac{i\sqrt{\delta}\lambda}{2\sqrt{\Omega}}, \rho = -\frac{1}{4}\delta(\lambda^2 + 2\mu^2) \right\}. \tag{52}$$

From equations (28), (37), and (52), we get

$$q_1(s, t) = -\frac{i\sqrt{\delta}\lambda}{2\sqrt{\Omega}} (\pm \coth(\zeta) \mp \operatorname{csch}(\zeta)) \times \exp\left(i\left(\mu \frac{\Gamma(\varrho+1)}{\epsilon} s^\epsilon - \frac{1}{4}\delta(\lambda^2 + 2\mu^2) \frac{\Gamma(\varrho+1)}{\epsilon} t^\epsilon\right)\right). \tag{53}$$

From equations (28), (38), and (52), we get

$$q_2(s, t) = -\frac{i\sqrt{\delta}\lambda}{2\sqrt{\Omega}} (\pm \tanh(\zeta) \mp i \operatorname{sech}(\zeta)) \times \exp\left(i\left(\mu \frac{\Gamma(\varrho+1)}{\epsilon} s^\epsilon - \frac{1}{4}\delta(\lambda^2 + 2\mu^2) \frac{\Gamma(\varrho+1)}{\epsilon} t^\epsilon\right)\right). \tag{54}$$

Set 6:

$$\left\{ \alpha_0 = 0, \alpha_1 = \frac{i\sqrt{\delta}\lambda}{2\sqrt{\Omega}}, \beta_1 = \frac{i\sqrt{\delta}\lambda}{2\sqrt{\Omega}}, \rho = -\frac{1}{4}\delta(\lambda^2 + 2\mu^2) \right\}. \tag{55}$$

From equations (28), (37), and (55), we get

$$q_1(s, t) = \pm \frac{i\sqrt{\delta}\lambda}{2\sqrt{\Omega}} (\coth(\zeta) + \operatorname{csch}(\zeta)) \times \exp\left(i\left(\mu \frac{\Gamma(\varrho+1)}{\epsilon} s^\epsilon - \frac{1}{4}\delta(\lambda^2 + 2\mu^2) \frac{\Gamma(\varrho+1)}{\epsilon} t^\epsilon\right)\right). \tag{56}$$

From equations (28), (38), and (55), we get

$$q_2(s, t) = \pm \frac{i\sqrt{\delta}\lambda}{2\sqrt{\Omega}} (i \operatorname{sech}(\zeta) + \tanh(\zeta)) \times \exp\left(i\left(\mu \frac{\Gamma(\varrho+1)}{\epsilon} s^\epsilon - \frac{1}{4}\delta(\lambda^2 + 2\mu^2) \frac{\Gamma(\varrho+1)}{\epsilon} t^\epsilon\right)\right). \tag{57}$$

Set 7:

$$\left\{ \alpha_0 = 0, \alpha_1 = 0, \beta_1 = -\frac{i\sqrt{\delta}\lambda}{\sqrt{\Omega}}, \rho = \frac{1}{2}\delta(\lambda^2 - \mu^2) \right\}. \tag{58}$$

By using equations (28), (37), and (58), we obtain

$$q_1(s, t) = \mp \frac{i\lambda\sqrt{\delta}}{\sqrt{\Omega}} \operatorname{csch}(\zeta) \times \exp\left(i\left(\mu \frac{\Gamma(\varrho+1)}{\epsilon} s^\epsilon + \frac{1}{2}\delta(\lambda^2 - \mu^2) \frac{\Gamma(\varrho+1)}{\epsilon} t^\epsilon\right)\right). \tag{59}$$

From equations (28), (38) and (58), we get

$$q_2(s, t) = \pm \frac{\sqrt{\delta}\lambda}{\sqrt{\Omega}} \operatorname{sech}(\zeta) \times \exp\left(i\left(\mu \frac{\Gamma(\varrho+1)}{\epsilon} s^\epsilon + \frac{1}{2}\delta(\lambda^2 - \mu^2) \frac{\Gamma(\varrho+1)}{\epsilon} t^\epsilon\right)\right). \tag{60}$$

Set 8:

$$\left\{ \alpha_0 = 0, \alpha_1 = 0, \beta_1 = \frac{i\sqrt{\delta}\lambda}{\sqrt{\Omega}}, \rho = \frac{1}{2}\delta(\lambda^2 - \mu^2) \right\}. \tag{61}$$

From equations (28), (37) and (61), we get

$$q_1(s, t) = \pm \frac{i\sqrt{\delta}\lambda}{\sqrt{\Omega}} \operatorname{csch}(\zeta) \times \exp\left(i\left(\mu \frac{\Gamma(\varrho+1)}{\epsilon} s^\epsilon + \frac{1}{2}\delta(\lambda^2 - \mu^2) \frac{\Gamma(\varrho+1)}{\epsilon} t^\epsilon\right)\right). \tag{62}$$

From equations (28), (38), and (61), we get

$$q_2(s, t) = \mp \frac{\sqrt{\delta}\lambda}{\sqrt{\Omega}} \operatorname{sech}(\zeta) \times \exp\left(i\left(\mu \frac{\Gamma(\varrho+1)}{\epsilon} s^\epsilon + \frac{1}{2}\delta(\lambda^2 - \mu^2) \frac{\Gamma(\varrho+1)}{\epsilon} t^\epsilon\right)\right), \tag{63}$$

where $\zeta = \lambda\Gamma(\varrho+1)/\epsilon(s^\epsilon - \delta\mu)t^\epsilon$.

4.3. Analytical Solutions via Extended (G'/G)-Expansion Technique. Equation (21) changes into following form for $m = 1$:

$$Q(\zeta) = \alpha_{-1} \left(\frac{G'(\zeta)}{G(\zeta)} \right)^{-1} + \alpha_0 + \alpha_1 \left(\frac{G'(\zeta)}{G(\zeta)} \right), \quad (64)$$

where α_{-1}, α_0 and α_1 are undetermined.

Inserting equation (64) along equation (22) into equation (29) and manipulating the set having $\alpha_{-1}, \alpha_0, \alpha_1$ and other parameters, we gain different sets of solutions given as

Set 1:

$$\left\{ \alpha_{-1} = -\frac{ia\sqrt{\delta}\lambda}{d\sqrt{\Omega}}, \alpha_0 = -\frac{ib\sqrt{\delta}\lambda}{2d\sqrt{\Omega}}, \alpha_1 = 0, \rho = -\frac{\delta(4a\lambda^2(d-c) + b^2\lambda^2 + 2d^2\mu^2)}{4d^2} \right\}. \quad (65)$$

From equations (23), (28), (64), and (65), we get

$$\begin{aligned} q(s, t) = & -\frac{i\sqrt{\delta}\lambda}{d\sqrt{\Omega}} \left(\frac{b}{2} + a \left(\frac{b}{2(d-c)} \right. \right. \\ & \left. \left. + \frac{\sqrt{-4ac + 4ad + b^2}}{2(d-c)} \left(\frac{C_1 \sinh(\zeta \sqrt{-4ac + 4ad + b^2}/2d) + C_2 \cosh(\zeta \sqrt{-4ac + 4ad + b^2}/2d)}{C_1 \cosh(\zeta \sqrt{-4ac + 4ad + b^2}/2d) + C_2 \sinh(\zeta \sqrt{-4ac + 4ad + b^2}/2d)} \right) \right)^{-1} \\ & \times \exp \left(i \left(\mu \frac{\Gamma(\varrho + 1)}{\epsilon} s^\epsilon - \frac{\delta(4a\lambda^2(d-c) + b^2\lambda^2 + 2d^2\mu^2)}{4d^2} \frac{\Gamma(\varrho + 1)}{\epsilon} t^\epsilon \right) \right). \end{aligned} \quad (66)$$

From equations (24), (28), (64), and (65), we get

$$\begin{aligned} q(s, t) = & -\frac{i\sqrt{\delta}\lambda}{d\sqrt{\Omega}} \left(\frac{b}{2} + a \left(\frac{b}{2(d-c)} \right. \right. \\ & \left. \left. + \frac{\sqrt{4ac - 4ad - b^2}}{2(d-c)} \left(\frac{C_2 \cos(\zeta \sqrt{4ac - 4ad - b^2}/2d) - C_1 \sin(\zeta \sqrt{4ac - 4ad - b^2}/2d)}{C_1 \cos(\zeta \sqrt{4ac - 4ad - b^2}/2d) + C_2 \sin(\zeta \sqrt{4ac - 4ad - b^2}/2d)} \right) \right)^{-1} \\ & \times \exp \left(i \left(\mu \frac{\Gamma(\varrho + 1)}{\epsilon} s^\epsilon - \frac{\delta(4a\lambda^2(d-c) + b^2\lambda^2 + 2d^2\mu^2)}{4d^2} \frac{\Gamma(\varrho + 1)}{\epsilon} t^\epsilon \right) \right). \end{aligned} \quad (67)$$

From equations (26), (28), (64), and (65), we get

$$\begin{aligned} q(s, t) = & -\frac{ia\sqrt{\delta}\lambda}{d\sqrt{\Omega}} \left(\frac{\sqrt{ad - ac}}{(d-c)} \left(\frac{C_1 \sinh(\zeta \sqrt{ad - ac}/d) + C_2 \cosh(\zeta \sqrt{ad - ac}/d)}{C_1 \cosh(\zeta \sqrt{ad - ac}/d) + C_2 \sinh(\zeta \sqrt{ad - ac}/d)} \right) \right)^{-1} \\ & \times \exp \left(i \left(\mu \frac{\Gamma(\varrho + 1)}{\epsilon} s^\epsilon - \frac{\delta(4a\lambda^2(d-c) + 2d^2\mu^2)}{4d^2} \frac{\Gamma(\varrho + 1)}{\epsilon} t^\epsilon \right) \right). \end{aligned} \quad (68)$$

From equations (27), (28), (64), and (65), we get

$$q(s, t) = \frac{ia\sqrt{\delta}\lambda}{d\sqrt{\Omega}} \left(\frac{\sqrt{ac-ad}}{d-c} \left(\frac{C_2 \cos(\zeta\sqrt{ac-ad}/d) - C_1 \sin(\zeta\sqrt{ac-ad}/d)}{C_1 \cos(\zeta\sqrt{ac-ad}/d) + C_2 \sin(\zeta\sqrt{ac-ad}/d)} \right) \right)^{-1} \times \exp \left(\iota \left(\mu \frac{\Gamma(\varrho+1)}{\epsilon} s^\epsilon - \frac{\delta(4a\lambda^2(d-c) + 2d^2\mu^2)}{4d^2} \frac{\Gamma(\varrho+1)}{\epsilon} t^\epsilon \right) \right). \tag{69}$$

Set 2:

$$\left\{ \alpha_{-1} = \frac{ia\sqrt{\delta}\lambda}{d\sqrt{\Omega}}, \alpha_0 = \frac{ib\sqrt{\delta}\lambda}{2d\sqrt{\Omega}}, \alpha_1 = 0, \rho = -\frac{\delta(4a\lambda^2(d-c) + b^2\lambda^2 + 2d^2\mu^2)}{4d^2} \right\}. \tag{70}$$

From equations (23), (28), (64), and (70), we get

$$q(s, t) = \frac{\iota\sqrt{\delta}\lambda}{d\sqrt{\Omega}} \left(\frac{b}{2} + a \left(\frac{b}{2(d-c)} + \frac{\sqrt{-4ac+4ad+b^2}}{2(d-c)} \left(\frac{C_1 \sinh(\zeta\sqrt{-4ac+4ad+b^2}/2d) + C_2 \cosh(\zeta\sqrt{-4ac+4ad+b^2}/2d)}{C_1 \cosh(\zeta\sqrt{-4ac+4ad+b^2}/2d) + C_2 \sinh(\zeta\sqrt{-4ac+4ad+b^2}/2d)} \right) \right)^{-1} \right) \times \exp \left(\iota \left(\mu \frac{\Gamma(\varrho+1)}{\epsilon} s^\epsilon - \frac{\delta(4a\lambda^2(d-c) + b^2\lambda^2 + 2d^2\mu^2)}{4d^2} \frac{\Gamma(\varrho+1)}{\epsilon} t^\epsilon \right) \right). \tag{71}$$

From equations (24), (28), (64), and (70), we get

$$q(s, t) = \frac{\iota\sqrt{\delta}\lambda}{d\sqrt{\Omega}} \left(\frac{b}{2} + a \left(\frac{b}{2(d-c)} + \frac{\sqrt{4ac-4ad-b^2}}{2(d-c)} \left(\frac{C_2 \cos(\zeta\sqrt{4ac-4ad-b^2}/2d) - C_1 \sin(\zeta\sqrt{4ac-4ad-b^2}/2d)}{C_1 \cos(\zeta\sqrt{4ac-4ad-b^2}/2d) + C_2 \sin(\zeta\sqrt{4ac-4ad-b^2}/2d)} \right) \right)^{-1} \right) \times \exp \left(\iota \left(\mu \frac{\Gamma(\varrho+1)}{\epsilon} s^\epsilon - \frac{\delta(4a\lambda^2(d-c) + b^2\lambda^2 + 2d^2\mu^2)}{4d^2} \frac{\Gamma(\varrho+1)}{\epsilon} t^\epsilon \right) \right). \tag{72}$$

From equations (26), (28), (64), and (70), we get

$$q(s, t) = \frac{ia\sqrt{\delta}\lambda}{d\sqrt{\Omega}} \left(\frac{\sqrt{ad-ac}}{(d-c)} \left(\frac{C_1 \sinh(\zeta\sqrt{ad-ac}/d) + C_2 \cosh(\zeta\sqrt{ad-ac}/d)}{C_1 \cosh(\zeta\sqrt{ad-ac}/d) + C_2 \sinh(\zeta\sqrt{ad-ac}/d)} \right) \right)^{-1} \times \exp \left(\iota \left(\mu \frac{\Gamma(\varrho+1)}{\epsilon} s^\epsilon - \frac{\delta(4a\lambda^2(d-c) + 2d^2\mu^2)}{4d^2} \frac{\Gamma(\varrho+1)}{\epsilon} t^\epsilon \right) \right). \tag{73}$$

From equations (27), (28), (64), and (70), we get

$$q(s, t) = \frac{ia\sqrt{\delta}\lambda}{d\sqrt{\Omega}} \left(\frac{\sqrt{ac-ad}}{d-c} \left(\frac{C_2 \cos(\zeta\sqrt{ac-ad}/d) - C_1 \sin(\zeta\sqrt{ac-ad}/d)}{C_1 \cos(\zeta\sqrt{ac-ad}/d) + C_2 \sin(\zeta\sqrt{ac-ad}/d)} \right) \right)^{-1} \times \exp \left(i \left(\mu \frac{\Gamma(\varrho+1)}{\epsilon} s^\epsilon - \frac{\delta(4a\lambda^2(d-c) + 2d^2\mu^2)}{4d^2} \frac{\Gamma(\varrho+1)}{\epsilon} t^\epsilon \right) \right). \tag{74}$$

Set 3:

$$\left\{ \alpha_{-1} = 0, \alpha_0 = \frac{ib\sqrt{\delta}\lambda}{2d\sqrt{\Omega}}, \alpha_1 = -\frac{i\sqrt{\delta}\lambda(c-d)}{d\sqrt{\Omega}}, \rho = -\frac{\delta(4a\lambda^2(d-c) + b^2\lambda^2 + 2d^2\mu^2)}{4d^2} \right\}. \tag{75}$$

From equations (23), (28), (64), and (75), we get

$$q(s, t) = \frac{-i\sqrt{\delta}\lambda}{d\sqrt{\Omega}} \left(\frac{b}{2} - \left(\frac{\sqrt{-4ac+4ad+b^2}}{2} \left(\frac{C_1 \sinh(\zeta\sqrt{-4ac+4ad+b^2}/2d) + C_2 \cosh(\zeta\sqrt{-4ac+4ad+b^2}/2d)}{C_1 \cosh(\zeta\sqrt{-4ac+4ad+b^2}/2d) + C_2 \sinh(\zeta\sqrt{-4ac+4ad+b^2}/2d)} \right) \right) \right) \times \exp \left(i \left(\mu \frac{\Gamma(\varrho+1)}{\epsilon} s^\epsilon - \frac{\delta(4a\lambda^2(d-c) + b^2\lambda^2 + 2d^2\mu^2)}{4d^2} \frac{\Gamma(\varrho+1)}{\epsilon} t^\epsilon \right) \right). \tag{76}$$

From equations (24), (28), (64), and (75), we get

$$q(s, t) = \frac{i\sqrt{\delta}\lambda}{d\sqrt{\Omega}} \left(\frac{b}{2} + (-d+c) \left(\frac{b}{2(-c+d)} + \frac{\sqrt{-4ad+4ac-b^2}}{2(-c+d)} \left(\frac{C_2 \cos(\zeta\sqrt{-4ad+4ac-b^2}/2d) - C_1 \sin(\zeta\sqrt{-4ad+4ac-b^2}/2d)}{C_1 \cos(\zeta\sqrt{-4ad+4ac-b^2}/2d) + C_2 \sin(\zeta\sqrt{-4ad+4ac-b^2}/2d)} \right) \right) \right) \times \exp \left(i \left(\mu \frac{\Gamma(\varrho+1)}{\epsilon} s^\epsilon - \frac{\delta(4a\lambda^2(d-c) + b^2\lambda^2 + 2d^2\mu^2)}{4d^2} \frac{\Gamma(\varrho+1)}{\epsilon} t^\epsilon \right) \right). \tag{77}$$

From equations (26), (28), (64), and (75), we get

$$q(s, t) = -\frac{\iota(c-d)\sqrt{\delta}\lambda}{d\sqrt{\Omega}} \left(\frac{\sqrt{a(d-c)}}{(d-c)} \left(\frac{C_1 \sinh(\zeta\sqrt{ad-ac}/d) + C_2 \cosh(\zeta\sqrt{ad-ac}/d)}{C_1 \cosh(\zeta\sqrt{ad-ac}/d) + C_2 \sinh(\zeta\sqrt{ad-ac}/d)} \right) \right) \times \exp\left(\iota\left(\mu\frac{\Gamma(\varrho+1)}{\epsilon}s^\epsilon - \frac{\delta(4a\lambda^2(d-c) + 2d^2\mu^2)}{4d^2}\frac{\Gamma(\varrho+1)}{\epsilon}t^\epsilon\right)\right). \quad (78)$$

From equations (27), (28), (64), and (75), we get

$$q(s, t) = -\frac{\iota(c-d)\sqrt{\delta}\lambda}{d\sqrt{\Omega}} \left(\frac{\sqrt{ac-ad}}{d-c} \left(\frac{C_2 \cos(\zeta\sqrt{ac-ad}/d) - C_1 \sin(\zeta\sqrt{ac-ad}/d)}{C_1 \cos(\zeta\sqrt{ac-ad}/d) + C_2 \sin(\zeta\sqrt{ac-ad}/d)} \right) \right) \times \exp\left(\iota\left(\mu\frac{\Gamma(\varrho+1)}{\epsilon}s^\epsilon - \frac{\delta(4a\lambda^2(d-c) + 2d^2\mu^2)}{4d^2}\frac{\Gamma(\varrho+1)}{\epsilon}t^\epsilon\right)\right). \quad (79)$$

Set 4:

$$\left\{ \alpha_{-1} = 0, \alpha_0 = \frac{\iota b\sqrt{\delta}\lambda}{2d\sqrt{\Omega}}, \alpha_1 = \frac{\iota\sqrt{\delta}\lambda(c-d)}{d\sqrt{\Omega}}, \rho = -\frac{\delta(4a\lambda^2(d-c) + b^2\lambda^2 + 2d^2\mu^2)}{4d^2} \right\}. \quad (80)$$

From equations (23), (28), (64), and (80), we get

$$q(s, t) = \frac{\iota\sqrt{\delta}\lambda}{d\sqrt{\Omega}} \left(\frac{b}{2} + (c-d) \left(\frac{b}{2(d-c)} + \frac{\sqrt{-4ac+4ad+b^2}}{2(d-c)} \left(\frac{C_1 \sinh\left(\zeta\sqrt{-4ac+4ad+b^2}/2d\right) + C_2 \cosh\left(\zeta\sqrt{-4ac+4ad+b^2}/2d\right)}{C_1 \cosh\left(\zeta\sqrt{-4ac+4ad+b^2}/2d\right) + C_2 \sinh\left(\zeta\sqrt{-4ac+4ad+b^2}/2d\right)} \right) \right) \right) \times \exp\left(\iota\left(\mu\frac{\Gamma(\varrho+1)}{\epsilon}s^\epsilon - \frac{\delta(4a\lambda^2(d-c) + b^2\lambda^2 + 2d^2\mu^2)}{4d^2}\frac{\Gamma(\varrho+1)}{\epsilon}t^\epsilon\right)\right). \quad (81)$$

From equations (24), (28), (64), and (80), we get

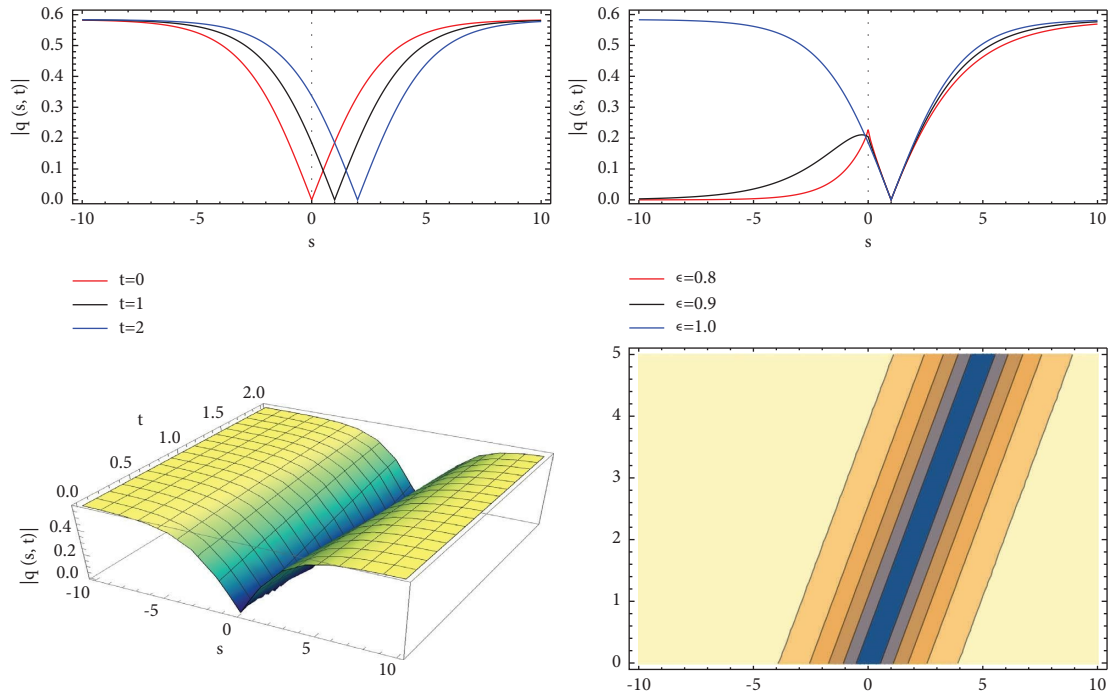


FIGURE 1: Structure of (34) for $\delta = 0.5, \lambda = 0.3, \varrho = 0.1, \mu = 2, \Omega = 0.7, \beta_0 = 0.1, \beta_1 = 0.1, d = 0.1, \epsilon = 1$.

$$\begin{aligned}
 q(s, t) = & \frac{i\sqrt{\delta}\lambda}{d\sqrt{\Omega}} \left(\frac{b}{2} + (c-d) \left(\frac{b}{2(d-c)} \right. \right. \\
 & + \frac{\sqrt{4ac-4ad-b^2}}{2(d-c)} \left(\frac{C_2 \cos\left(\zeta\sqrt{4ac-4ad-b^2}/2d\right) - C_1 \sin\left(\zeta\sqrt{4ac-4ad-b^2}/2d\right)}{C_1 \cos\left(\zeta\sqrt{-4ad+4ac-b^2}/2d\right) + C_2 \sin\left(\zeta\sqrt{-4ad+4ac-b^2}/2d\right)} \right) \left. \right) \\
 & \times \exp\left(i \left(\mu \frac{\Gamma(\varrho+1)}{\epsilon} s^\epsilon - \frac{\delta(4a\lambda^2(-c+d) + b^2\lambda^2 + 2d^2\mu^2)}{4d^2} \frac{\Gamma(\varrho+1)}{\epsilon} t^\epsilon \right) \right).
 \end{aligned} \tag{82}$$

From equations (26), (28), (64), and (80), we get

$$\begin{aligned}
 q(s, t) = & \frac{i(c-d)\sqrt{\delta}\lambda}{d\sqrt{\Omega}} \left(\frac{\sqrt{ad-ac}}{(d-c)} \left(\frac{C_1 \sinh(\zeta\sqrt{ad-ac}/d) + C_2 \cosh(\zeta\sqrt{ad-ac}/d)}{C_1 \cosh(\zeta\sqrt{ad-ac}/d) + C_2 \sinh(\zeta\sqrt{ad-ac}/d)} \right) \right) \\
 & \times \exp\left(i \left(\mu \frac{\Gamma(\varrho+1)}{\epsilon} s^\epsilon - \frac{\delta(4a\lambda^2(d-c) + 2d^2\mu^2)}{4d^2} \frac{\Gamma(\varrho+1)}{\epsilon} t^\epsilon \right) \right).
 \end{aligned} \tag{83}$$

From equations (27), (28), (64), and (80), we get

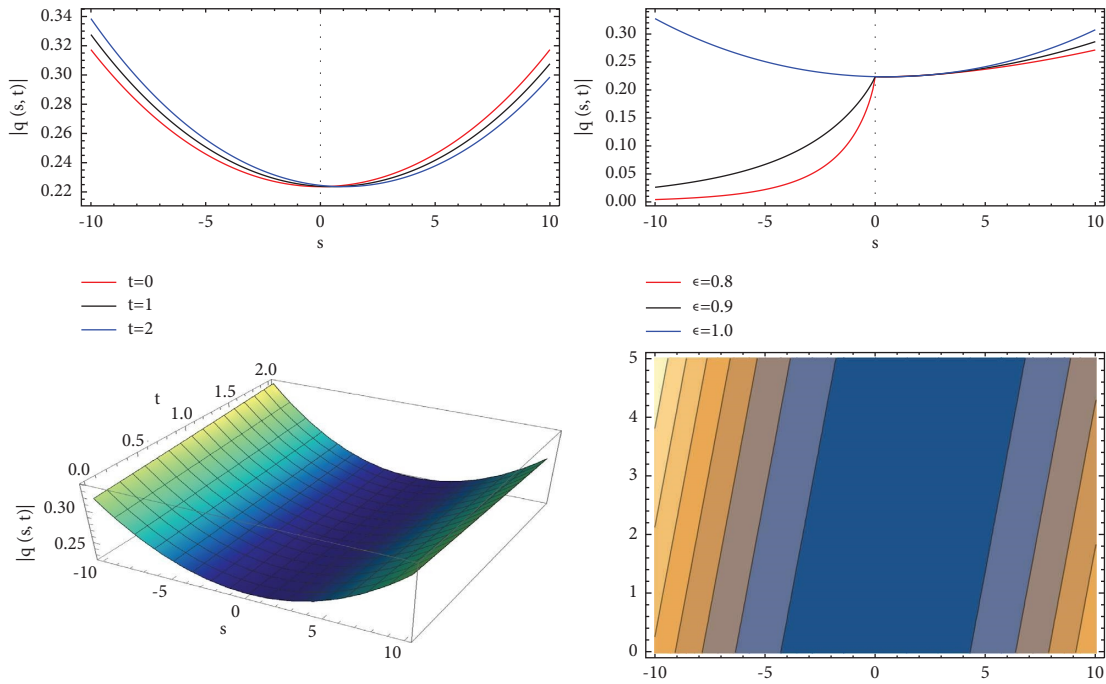


FIGURE 2: Structure of (41) for $\delta = 0.5, \lambda = 0.1, \rho = 0.5, \mu = 1, \Omega = 0.1, \epsilon = 1$.

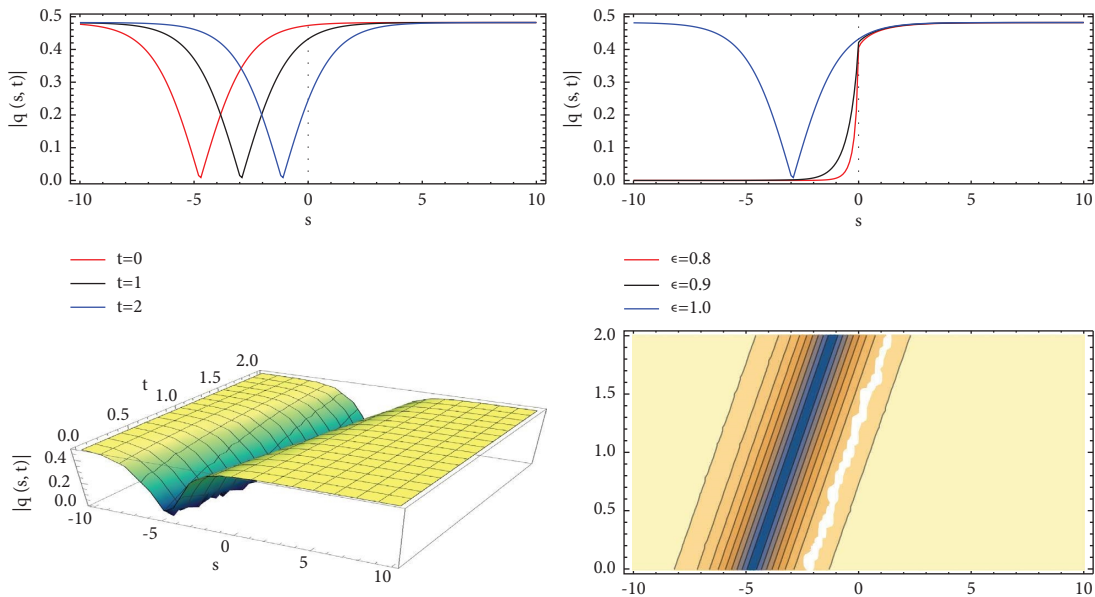


FIGURE 3: Structure of (66) for $\delta = 0.3, \lambda = 0.4, \rho = 0.5, \mu = 6, \Omega = 0.4, d = 0.17, a = 0.1, c = 0.01, b = 0.4, C_1 = 0.4, C_2 = 0.5$.

$$\begin{aligned}
 q(s, t) = & \frac{i(c-d)\sqrt{\delta}\lambda}{d\sqrt{\Omega}} \left(\frac{\sqrt{ac-ad}}{d-c} \left(\frac{C_2 \cos(\zeta\sqrt{ac-ad}/d) - C_1 \sin(\zeta\sqrt{ac-ad}/d)}{C_1 \cos(\zeta\sqrt{ac-ad}/d) + C_2 \sin(\zeta\sqrt{ac-ad}/d)} \right) \right) \\
 & \times \exp \left(i \left(\mu \frac{\Gamma(\rho+1)}{\epsilon} s^\epsilon - \frac{\delta(4a\lambda^2(d-c) + 2d^2\mu^2)}{4d^2} \frac{\Gamma(\rho+1)}{\epsilon} t^\epsilon \right) \right).
 \end{aligned}
 \tag{84}$$

Here, $\zeta = \lambda\Gamma(\rho+1)/\epsilon(s^\epsilon - \delta\mu t^\epsilon)$ for all above-mentioned solutions.

5. Illustrations with Graphics

In this portion, we will represent some 2-D, 3-D, and contour structures that help us to classify the type of results. Figures 1–3 show some of the analytical solutions. In Figure 1, we apply our technique to represent the plot of (34) for $\delta = 0.5, \lambda = 0.3, \varrho = 0.1, \mu = 2, \Omega = 0.7, \beta_0 = 0.1, \beta_1 = 0.1, d = 0.1, \epsilon = 1$. Furthermore, Figure 2 denotes the plot of (41) $\delta = 0.5, \lambda = 0.1, \varrho = 0.5, \mu = 1, \Omega = 0.1, \epsilon = 1$. Finally, the plot of (66) for $\delta = 0.3, \lambda = 0.4, \varrho = 0.5, \mu = 6, \Omega = 0.4, d = 0.17, a = 0.1, c = 0.01, b = 0.4, C_1 = 0.4, C_2 = 0.5$ is presented in Figure 3. We see that the wave retains its shape over time, moves to the right, and breaks by changing the value of ϵ .

Through our analysis of the forms presented in the previous section, we can reach important results as follows: First, in Figure 1, we apply the \exp_a function technique to represent the plot of (34) at $\delta = 0.5, \lambda = 0.3, \varrho = 0.1, \mu = 2, \Omega = 0.7, \beta_0 = 0.1, \beta_1 = 0.1, d = 0.1, \epsilon = 1$. Further, Figure 2 denotes the plot of (41) at $\delta = 0.5, \lambda = 0.1, \varrho = 0.5, \mu = 1, \Omega = 0.1, \epsilon = 1$ using EShGEE technique. Finally, the plot of (66) for $\delta = 0.3, \lambda = 0.4, \varrho = 0.5, \mu = 6, \Omega = 0.4, d = 0.17, a = 0.1, c = 0.01, b = 0.4, C_1 = 0.4, C_2 = 0.5$ presented in Figure 3 using the extended (G'/G) -expansion technique.

6. Conclusion

In this article, we obtain modernistic analytical solutions to the Ivancevic option pricing model along M-fractional derivative by utilizing \exp_a function, extended sinh-Gordon equation expansion, and extended (G'/G) -expansion methods. The achieved results are also verified and demonstrated with different plots by Mathematica tool. The obtained results are also explained graphically by 2-dimensional, 3-dimensional, and contour plots. Finally, it is suggested that to deal with the other fractional nonlinear PDEs, the \exp_a function, extended sinh-Gordon equation expansion, and extended (G'/G) -expansion methods are very helpful, reliable, and straight forward. The results achieved in this paper may be useful for the progress in the supplementary analyzing of this model.

Data Availability

The datasets generated during and/or analyzed during the current study are available from the corresponding author upon reasonable request.

Conflicts of Interest

The authors declare that they have no conflicts of interest.

Authors' Contributions

All authors have contributed equally to this work. All authors have read and agreed to the published version of the manuscript.

Acknowledgments

The work in this study was supported, in part, by the Open Access Program from the American University of Sharjah.

References

- [1] B. Ghanbari, M. S. Osman, and D. Baleanu, "Generalized exponential rational function method for extended Zakharov–Kuznetsov equation with conformable derivative," *Modern Physics Letters A*, vol. 34, no. 20, Article ID 1950155, 2019.
- [2] A. Neirameh and M. Eslami, "New solitary wave solutions for fractional Jaulent–Miodek hierarchy equation," *Modern Physics Letters B*, vol. 36, no. 7, Article ID 2150612, 2022.
- [3] R. I. Nuruddeen, K. S. Aboodh, and K. K. Ali, "Analytical Investigation of Soliton Solutions to Three quantum zakharov-kuznetsov Equations," *Communications in Theoretical Physics*, vol. 70, no. 4, pp. 405–412, 2018.
- [4] A. Saha, K. K. Ali, H. Rezazadeh, and Y. Ghatani, "Analytical optical pulses and bifurcation analysis for the traveling optical pulses of the hyperbolic nonlinear Schrödinger equation," *Optical and Quantum Electronics*, vol. 53, no. 3, p. 150, 2021.
- [5] H. F. Ismael, İ. Okumuş, T. Aktürk, H. Bulut, and M. S. Osman, "Analyzing study for the 3D potential Yu–Toda–Sasa–Fukuyama equation in the two-layer liquid medium," *Journal of Ocean Engineering and Science*, 2022.
- [6] A. S. Muhannad, K. K. Ali, K. R. Raslan, H. Rezazadeh, and A. Bekir, "Exact solutions of the conformable fractional EW and MEW equations by a new generalized expansion method," *Journal of Ocean Engineering and Science*, vol. 5, no. 3, pp. 223–229, 2020.
- [7] S. El-Ganaini, M. O. Al-Amr, and O. Mohammed, "New abundant solitary wave structures for a variety of some nonlinear models of surface wave propagation with their geometric interpretations," *Mathematical Methods in the Applied Sciences*, vol. 45, no. 11, pp. 7200–7226, 2022.
- [8] M. O. Al-Amr, H. Rezazadeh, K. K. Ali, A. Korkmazki, and A. Korkmaz, "N1-soliton solution for Schrödinger equation with competing weakly nonlocal and parabolic law nonlinearities," *Communications in Theoretical Physics*, vol. 72, no. 6, Article ID 65503, 2020.
- [9] N. M. Rasheed, M. O. Al-Amr, E. A. Az-Zo'bi et al., "Stable optical solitons for the Higher-order Non-Kerr NLSE via the modified simple equation method," *Mathematics*, vol. 9, no. 16, p. 1986, 2021.
- [10] M. Eslami and H. Rezazadeh, "The first integral method for Wu–Zhang system with conformable time-fractional derivative," *Calcolo*, vol. 53, no. 3, pp. 475–485, 2016.
- [11] H. Rezazadeh, D. Kumar, A. Neirameh, M. Eslami, and M. Mirzazadeh, "Applications of three methods for obtaining optical soliton solutions for the Lakshmanan–Porsezian–Daniel model with Kerr law nonlinearity," *Pramana*, vol. 94, no. 1, p. 39, 2020.
- [12] A. Zafar, M. Raheel, M. Mirzazadeh, and M. Eslami, "Different soliton solutions to the modified equal-width wave equation with Beta-time fractional derivative via two different methods," *Revista Mexicana de Física*, vol. 68, no. 1, p. 1, 2021.
- [13] S. Sahoo, S. Saha Ray, and M. A. Abdou, "New exact solutions for time-fractional Kaup–Kupershmidt equation using improved (G'/G) - expansion and extended (G'/G) - expansion methods," *Alexandria Engineering Journal*, vol. 59, no. 5, pp. 3105–3110, 2020.
- [14] A. Zafar, K. K. Ali, M. N. Raheel, K. S. Nisar, and A. Bekir, "Abundant M-fractional optical solitons to the perturbed

- Gerdjikov–Ivanov equation treating the mathematical nonlinear optics,” *Optical and Quantum Electronics*, vol. 54, no. 1, p. 25, 2022.
- [15] A. Zafar, A. Bekir, M. Raheel, and H. Rezazadeh, “Investigation for optical soliton solutions of two nonlinear Schrödinger equations via two concrete finite series methods,” *International Journal of Algorithms, Computing and Mathematics*, vol. 6, no. 3, p. 65, 2020.
- [16] A. R. Seadawy, D. Kumar, and A. K. Chakrabarty, “Dispersive optical soliton solutions for the hyperbolic and cubic-quintic nonlinear Schrödinger equations via the extended sinh-Gordon equation expansion method,” *The European Physical Journal Plus*, vol. 133, no. 5, p. 182, 2018.
- [17] A. Safaei Bezagabadi and M. A. Bolorizadeh, “Analytic combined bright-dark, bright and dark solitons solutions of generalized nonlinear Schrödinger equation using extended sinh-Gordon equation expansion method,” *Results in Physics*, vol. 30, Article ID 104852, 2021.
- [18] N. Taghizadeh, M. Noori, R. Seyyedeh, M. Noori, and B. Seyyedeh, “Application of the extended (G'/G) -expansion method to the improved Eckhaus equation, applications and applied mathematics,” *International Journal*, vol. 9, no. 1, p. 24, 2014.
- [19] M. Ekici, “Soliton and other solutions of nonlinear time fractional parabolic equations using extended (G'/G) -expansion method,” *Optik*, vol. 130, pp. 1312–1319, 2017.
- [20] R. M. Jena, S. Chakraverty, and D. Baleanu, “A novel analytical technique for the solution of time-fractional Ivancevic option pricing model,” *Physica A: Statistical Mechanics and Its Applications*, vol. 550, Article ID 124380, 2020.
- [21] Q. Chen, H. M. Baskonus, W. Gao, and E. Ilhan, “Soliton theory and modulation instability analysis: the Ivancevic option pricing model in economy,” *Alexandria Engineering Journal*, vol. 61, no. 10, pp. 7843–7851, 2022.
- [22] Y.-Q. Chen, Y.-H. Tang, J. Manafian, H. Rezazadeh, and M. S. Osman, “Dark wave, rogue wave and perturbation solutions of Ivancevic option pricing model,” *Nonlinear Dynamics*, vol. 105, no. 3, pp. 2539–2548, 2021.
- [23] V. G. Ivancevic, “Adaptive-wave alternative for the black-scholes option pricing model,” *Cogn. Comput.*, vol. 2, no. 1, pp. 17–30, 2010.
- [24] A. T. Ali and E. R. Hassan, “General Exp_a -function method for nonlinear evolution equations,” *Applied Mathematics and Computation*, vol. 217, no. 2, pp. 451–459, 2010.
- [25] E. M. E. Zayed and A. G. Al-Nowehy, “Generalized kudryashov method and general exp_a function method for solving a high order nonlinear Schrödinger equation,” *J. Space Explor.*, vol. 6, pp. 1–26, 2017.
- [26] K. Hosseini, Z. Ayati, and R. Ansari, “New exact solutions of the Tzitzéica-type equations in non-linear optics using the exp_a function method,” *Journal of Modern Optics*, vol. 65, no. 7, pp. 847–851, 2018.
- [27] A. Zafar, “The exp_a function method and the conformable time-fractional KdV equations,” *Nonlinear Engineering*, vol. 8, no. 1, pp. 728–732, 2019.
- [28] X. L. Yang and J. S. Tang, “Travelling wave solutions for Konopelchenko-Dubrovsky equation using an extended sinh-Gordon equation expansion method,” *Communications in Theoretical Physics*, vol. 50, Article ID 10471051, 2008.

Research Article

Fractional Optimal Control Model of SARS-CoV-2 (COVID-19) Disease in Ghana

Samuel Okyere ¹, Joseph Ackora-Prah ¹, Kwaku Forkuoh Darkwah,¹
Francis Tabi Oduro,² and Ebenezer Bonyah ^{3,4}

¹Department of Mathematics, Kwame Nkrumah University of Science and Technology, Kumasi, Ghana

²African Institute of Mathematical Sciences, Accra, Ghana

³Department of Mathematics Education, Akyem Pokuonua University of Skills Training and Entrepreneurial Development, Kumasi, Ghana

⁴Department of Mathematics, Faculty of Science and Technology, Universitas Airlangga, Surabaya 60115, Indonesia

Correspondence should be addressed to Samuel Okyere; okyere2015@gmail.com

Received 28 June 2022; Revised 18 August 2022; Accepted 6 April 2023; Published 21 April 2023

Academic Editor: Arzu Akbulut

Copyright © 2023 Samuel Okyere et al. This is an open access article distributed under the Creative Commons Attribution License, which permits unrestricted use, distribution, and reproduction in any medium, provided the original work is properly cited.

Research focus on optimal control problems brought on by fractional differential equations has been extensively applied in practice. However, because they are still open ended and challenging, a number of problems with fractional mathematical modeling and problems with optimal control require additional study. Using fractional-order derivatives defined in the Atangana–Baleanu–Caputo sense, we alter the integer-order model that has been proposed in the literature. We prove the solution's existence, uniqueness, equilibrium points, fundamental reproduction number, and local stability of the equilibrium points. The operator's numerical approach was put into practice to obtain a numerical simulation to back up the analytical conclusions. Fractional optimum controls were incorporated into the model to identify the most efficient intervention strategies for controlling the disease. Utilizing actual data from Ghana for the months of March 2020 to March 2021, the model is validated. The simulation's results show that the fractional operator significantly affected each compartment and that the incidence rate of the population rose when $\nu \geq 0.6$. The examination of the most effective control technique discovered that social exclusion and vaccination were both very effective methods for halting the development of the illness.

1. Introduction

The large family of viruses known as coronaviruses is responsible for a number of illnesses, including the Middle East respiratory syndrome (MERS), common cold, and severe acute respiratory syndrome (SARS-CoV-2). Never have humans been previously exposed to this novel coronavirus strain [1]. When an infected person coughs, breathes, sneezes, or talks, tiny droplets or particles, such as aerosols, are discharged into the air and transmit the disease [2, 3]. The illness's usual symptoms include fever, coughing, exhaustion, shortness of breath, or other breathing problems, as well as loss of taste and smell [4–6]. Over 6 million

people had died, and there were over 513 million confirmed infections worldwide as of May 1, 2022. Africa as a whole has recorded 11 million confirmed cases, with Ghana accounting for 161, 173 of those cases [7].

Numerous scholars have created models for the realization and control of the spread of transmissible illnesses in a population [8]. The representation of infectious diseases using fractional calculus has attracted a lot of attention lately. Examples include malaria [9], TB [10, 11], syphilis [12], chickenpox [13], and most recently COVID-19 [8, 14–23]. Fractional calculus, which is a generalization of differentiation and integration of integer orders, has been proposed to address several of the constraints of integer

order derivatives [14]. The fractional order may be able to depict more complex dynamics and include memory effects, which are prevalent in many real-world occurrences, in comparison to the integer model [10, 15]. Using data from China, Italy, and France, Bahloul et al. [16] proposed a fractional-order SEIQRDP model to study the COVID-19 pandemic. To examine the illness transmission in Spain, the researchers in Ref. [17] proposed a new SEIRS dynamical model that uses the fractional-order derivative and adds the vaccine rate. The authors of Ref. [18] presented a Caputo fractional SIR epidemic model taking a nonlinear incidence rate into consideration. Regarding the fractal-fractional Atangana–Baleanu derivative, Khan and Atangana [19] considered a fractional model to describe the transmission of COVID-19 while accounting for the isolation and quarantine of individuals.

There are several real-world uses for research on optimum control problems brought on by fractional differential equations. However, there are a number of difficulties and problems with fractional mathematical modeling as well as challenges with optimal control that need further study. A general formulation for the optimal control problem for a family of fuzzy fractional differential systems connected to SIR and SEIR epidemic models was developed by Das and Samanta [24] using real data from Italy and South Korea. Khan et al. [8] explored a fractional COVID-19 epidemic model that included fractional optimum control and had a convex incidence rate in the sense of Atangana–Baleanu and Caputo. Baba and Bilgehan [21] devised a fractional optimum control issue that incorporates public awareness and treatment for the disease outbreak using a mathematical model with a fractional-order derivative in the Caputo sense. Nabi et al. [22] created a compartmental model combining all workable nonpharmaceutical intervention options using the classical and Caputo–Fabrizio fractional-order derivatives to study illness transmission in Bangladesh and India. The age structure and fractional-order derivatives were used to create a more accurate version of the conventional SEIR model [23]. They expanded on their methods by including follow-up controls, diagnostics, and awareness programs. In Japan, Das and Samanta [24] suggested a susceptible-asymptomatic-infectious-recovered (SAIR) compartmental model inside a fractional-order framework that included the best possible management of social distance.

We propose a fractional-order derivative defined in the Atangana–Baleanu–Caputo sense in the current study to investigate the model presented in [20]. The nonlocal characteristic of the virus dynamics is not sufficiently captured by the classical model proposed in [20]. Because the Atangana–Baleanu and Caputo derivatives have a number of desired properties, such as nonlocality and non-singularity in their kernels, and because this operator can only accurately represent the crossover behavior of the

model, it was decided to utilize them to design the model. Other operators without similar qualities, such as Caputo and Caputo–Fabrizio, may or may not adequately explain the dynamics of the coronavirus [19]. Several articles using the Atangana–Baleanu–Caputo derivation are linked and can be found in [13, 25–27].

The following sections then make up the remainder of the paper. In Section 2, we create and analyze a mathematical model that makes use of the fractional-order derivative as established by Atangana, Baleanu, and Caputo. Section 3 identifies the qualitative traits of the model. We identify equilibrium locations, their stability, and the fundamental reproduction number. We incorporate time-dependent optimal control into the constructed model and analyze the optimal control model in Section 4. The numerical framework of the fractional-order model is provided in Section 5, and the numerical analysis is then presented in Section 6. In section 7, the numerical investigation of the optimal control model is presented. Finally, in Section 8, we explain and illustrate the results of our suggested model.

2. Model Formulation

In this section, utilizing the fractional-order derivatives derived in the Atangana–Baleanu in Caputo sense, we alter the model given in [20] to incorporate a compartment for quarantine individuals. The fractional-order operator is defined as ν , where $0 < \nu \leq 1$. Susceptible individuals (S), exposed (E), asymptomatic (I_A), symptomatic (I_S), vaccinated (V), quarantined (Q), and recovered (R) are the seven classifications that make up the model. The main premise of the model formulation is that, in contrast to [20], where only the asymptomatic transmits the virus, both symptomatic and asymptomatic persons spread the virus when they come into touch with susceptible individuals. Other presumptions in [20].

The susceptible population are recruited at the rate Ω and die at a rate μ . These individuals get exposed to the disease when they come in contact with the asymptomatic and symptomatic at a rate β . After being exposed to the disease, they either progress to the asymptomatic class at the rate $(1 - \alpha)\varphi$ or the symptomatic class at the rate $\alpha\varphi$. Both asymptomatic and symptomatic get quarantined at the rates ρ and τ , respectively. Those vaccinated according to this model do not get infected but may join the susceptible class at a rate Γ . The parameters μ and δ are the natural and the disease-induced death rates, respectively. The parameters σ , θ , and γ are the rate of recovery for the asymptomatic, symptomatic, and quarantine class, respectively. The schematic diagram of the model is displayed in Figure 1.

The following fractional derivatives describe the model.

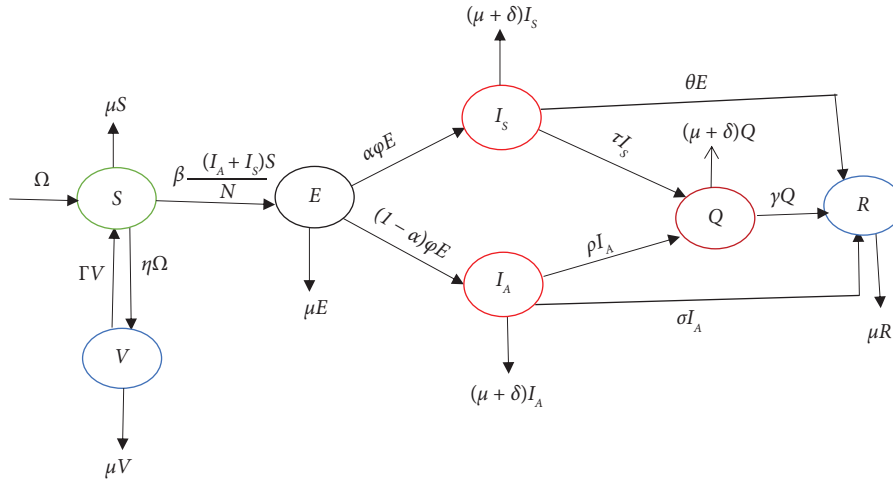


FIGURE 1: Flow chart of the COVID-19 fractional model.

$$\begin{aligned}
 {}_v^{ABC}D_t^\nu S &= (1 - \eta^\nu)\Omega^\nu + \Gamma^\nu V - \beta^\nu S \left(\frac{I_A + I_S}{N} \right) - \mu^\nu S, \\
 {}_v^{ABC}D_t^\nu E &= \beta^\nu S \left(\frac{I_A + I_S}{N} \right) - (\phi^\nu + \mu^\nu)E, \\
 {}_v^{ABC}D_t^\nu I_A &= (1 - \alpha)\phi^\nu E - (\delta^\nu + \rho^\nu + \mu^\nu + \sigma^\nu)I_A, \\
 {}_v^{ABC}D_t^\nu I_S &= \alpha\phi^\nu E - (\theta^\nu + \tau^\nu + \delta^\nu + \mu^\nu)I_S, \\
 {}_v^{ABC}D_t^\nu Q &= \rho^\nu I_A + \tau^\nu I_S - (\gamma^\nu + \mu^\nu + \delta^\nu)Q, \\
 {}_v^{ABC}D_t^\nu V &= \eta^\nu \Omega^\nu - (\Gamma^\nu + \mu^\nu)V, \\
 {}_v^{ABC}D_t^\nu R &= \theta^\nu I_S + \sigma^\nu I_A + \gamma^\nu Q - \mu^\nu R,
 \end{aligned}
 \tag{1}$$

with initial conditions $S(0) \geq 0, E(0) \geq 0, I_A(0) \geq 0, I_S(0) \geq 0, Q(0) \geq 0, V(0) \geq 0$ and $R(0) \geq 0$.

2.1. Preliminaries. We go over the definitions of the key terms used in this work and those specified in [10, 28] in this part.

Definition 1. Liouville and Caputo (LC) describe the fractional derivative of the order ν as in [10, 29] as

$${}_v^C D_t^\nu h(t) = \frac{1}{\Gamma(1 - \nu)} \int_0^t (t - p)^{-\nu} h(p) dp, 0 < \nu < 1. \tag{2}$$

Definition 2. We provide the Liouville–Caputo sense definition of the Atangana–Baleanu fractional derivative [10, 28]:

$${}_v^{ABC} D_t^\nu h(t) = \frac{B(\nu)}{(1 - \nu)} \int_0^t E_\nu \left(-\nu \left(\frac{t - p}{1 - \nu} \right) \right) \dot{h}(p) dp, \tag{3}$$

where $B(\nu) = 1 - \nu + \nu/\Gamma(\nu)$ is the normalized function.

Definition 3. The Atangana–Baleanu–Caputo derivative’s pertinent fractional integral is given by the definition in [10, 28]

$${}_v^{ABC} D_t^\nu h(t) = \frac{(1 - \nu)}{B(\nu)} h(t) + \frac{\nu}{B(\nu)\Gamma(\nu)} \int_0^t (t - p)^{\nu-1} \dot{h}(p) dp. \tag{4}$$

They calculated both derivatives’ Laplace transforms and discovered the following:

$$L\{ {}_0^{ABC} D_{0,t}^\nu h(t) \} = \frac{B(\nu)H(q)q^\nu - q^{\nu-1}h(0)}{(1 - \nu)(q^\nu + \nu/1 - \nu)}. \tag{5}$$

Theorem 1. :For a function $h \in C[a, b]$, the following results hold [10, 30]:

$$\| {}_v^{ABC} D_t^\nu r(t) \| < \frac{B(\nu)}{(1 - \nu)} \| h(t) \|, \text{ where } \| h(t) \| = \max_{a \leq t \leq b} |h(t)|. \tag{6}$$

Additionally, the derivatives of Atangana, Baleanu, and Caputo satisfy the Lipschitz criterion [10, 30].

$$\| {}_v^{ABC} D_t^\nu h_1(t) - {}_v^{ABC} D_t^\nu h_2(t) \| < \omega \| h_1(t) - h_2(t) \|. \tag{7}$$

2.2. Existence and Uniqueness. This section establishes the existence and distinctiveness of the solutions to the system (1).

We denote a Banach space by $D(G)$ with $G = [0, b]$, containing real-valued continuous function with sup norm $W = D(G) \times D(G) \times D(G) \times D(G) \times D(G) \times D(G) \times D(G)$ and the given norm $(S, E, I_A, I_S, Q, V, R) = S + E + I_A + I_S + Q + V + R$, where $S = \text{Sup}_{t \in G} |S|, E = \text{Sup}_{t \in G} |E|, I_A = \text{Sup}_{t \in G} |I_A|, I_S = \text{Sup}_{t \in G} |I_S|, Q = \text{Sup}_{t \in G} |Q|, V = \text{Sup}_{t \in G} |V|, R = \text{Sup}_{t \in G} |R|$. Using the ABC integral operator on the system (1), we have

$$\left\{ \begin{array}{l}
 S(t) - S(0) = {}^{\nu}ABC D_t^{\nu} S(t) \left\{ (1 - \eta^{\nu}) \Omega^{\nu} + \Gamma^{\nu} V - \beta^{\nu} \left(\frac{I_A(t) + I_S(t)}{N(t)} \right) S(t) - \mu^{\nu} S(t) \right\}, \\
 E(t) - E(0) = {}^{\nu}ABC D_t^{\nu} E(t) \left\{ \beta^{\nu} \left(\frac{I_A(t) + I_S(t)}{N(t)} \right) S(t) - (\phi^{\nu} + \mu^{\nu}) E(t) \right\}, \\
 I_A(t) - I_A(0) = {}^{\nu}ABC D_t^{\nu} I_A(t) \{ (1 - \alpha) \phi^{\nu} E - (\delta^{\nu} + \rho^{\nu} + \mu^{\nu} + \sigma^{\nu}) I_A(t) \}, \\
 I_S(t) - I_S(0) = {}^{\nu}ABC D_t^{\nu} I_S(t) \{ \alpha \phi^{\nu} E(t) - (\delta^{\nu} + \mu^{\nu} + \theta^{\nu} + \tau^{\nu}) I_S(t) \}, \\
 Q(t) - Q(0) = {}^{\nu}ABC D_t^{\nu} Q(t) \{ \rho^{\nu} I_A + \tau^{\nu} I_S - (\delta^{\nu} + \mu^{\nu} + \gamma^{\nu}) Q(t) \}, \\
 V(t) - V(0) = {}^{\nu}ABC D_t^{\nu} V(t) \{ \eta^{\nu} \Omega - (\Gamma^{\nu} + \mu^{\nu}) V(t) \}, \\
 R(t) - R(0) = {}^{\nu}ABC D_t^{\nu} R(t) \{ \gamma^{\nu} Q(t) + \theta^{\nu} I_S(t) + \sigma^{\nu} I_A(t) - \mu^{\nu} R(t) \}.
 \end{array} \right. \quad (8)$$

Now, from Definition 1, we have

$$\left\{ \begin{array}{l}
 S(t) - S(0) = \frac{1 - \nu}{B(\nu)} \Phi_1(\nu, t, S(t)) + \frac{\nu}{B(\nu)\Gamma(\nu)} \times \int_0^t (t - \tau)^{\nu-1} \Phi_1(\nu, \tau, S(\tau)) d\tau, \\
 E(t) - E(0) = \frac{1 - \nu}{B(\nu)} \Phi_2(\nu, t, E(t)) + \frac{\nu}{B(\nu)\Gamma(\nu)} \times \int_0^t (t - \tau)^{\nu-1} \Phi_2(\nu, \tau, E(\tau)) d\tau, \\
 I_A(t) - I_A(0) = \frac{1 - \nu}{B(\nu)} \Phi_3(\nu, t, I_A(t)) + \frac{\nu}{B(\nu)\Gamma(\nu)} \times \int_0^t (t - \tau)^{\nu-1} \Phi_3(\nu, \tau, I_A(\tau)) d\tau, \\
 I_S(t) - I_S(0) = \frac{1 - \nu}{B(\nu)} \Phi_4(\nu, t, I_S(t)) + \frac{\nu}{B(\nu)\Gamma(\nu)} \times \int_0^t (t - \tau)^{\nu-1} \Phi_4(\nu, \tau, I_S(\tau)) d\tau, \\
 Q(t) - Q(0) = \frac{1 - \nu}{B(\nu)} \Phi_5(\nu, t, Q(t)) + \frac{\nu}{B(\nu)\Gamma(\nu)} \times \int_0^t (t - \tau)^{\nu-1} \Phi_5(\nu, \tau, Q(\tau)) d\tau, \\
 V(t) - V(0) = \frac{1 - \nu}{B(\nu)} \Phi_6(\nu, t, V(t)) + \frac{\nu}{B(\nu)\Gamma(\nu)} \times \int_0^t (t - \tau)^{\nu-1} \Phi_6(\nu, \tau, V(\tau)) d\tau, \\
 R(t) - R(0) = \frac{1 - \nu}{B(\nu)} \Phi_7(\nu, t, R(t)) + \frac{\nu}{B(\nu)\Gamma(\nu)} \times \int_0^t (t - \tau)^{\nu-1} \Phi_7(\nu, \tau, R(\tau)) d\tau,
 \end{array} \right. \quad (9)$$

where

$$\left\{ \begin{aligned} \Phi_1(v, \tau, S(t)) &= (1 - \eta^v)\Omega^v + \Gamma^v V - \beta^v \left(\frac{I_A(t) + I_S(t)}{N(t)} \right) S(t) - \mu^v S(t), \\ \Phi_2(v, \tau, E(t)) &= \beta^v \left(\frac{I_A(t) + I_S(t)}{N(t)} \right) S(t) - (\phi^v + \mu^v) E(t), \\ \Phi_3(v, \tau, I_A(t)) &= (1 - \alpha)\phi^v E - (\delta^v + \rho^v + \mu^v + \sigma^v) I_A(t), \\ \Phi_4(v, \tau, I_S(t)) &= \alpha\phi^v E(t) - (\delta^v + \mu^v + \theta^v + \tau^v) I_S(t), \\ \Phi_5(v, \tau, Q(t)) &= \rho^v I_A + \tau^v I_S - (\delta^v + \mu^v + \gamma^v) Q(t), \\ \Phi_6(v, \tau, V(t)) &= \eta^v \Omega - (\Gamma^v + \mu^v) V(t), \\ \Phi_7(v, \tau, R(t)) &= \gamma^v Q(t) + \theta^v I_S(t) + \sigma^v I_A(t) - \mu^v R(t). \end{aligned} \right. \tag{10}$$

Furthermore, the Atangana–Baleanu–Caputo derivatives fulfill the Lipschitz condition [10, 30] only if $S(t), E(t), I_A(t), I_S(t), Q(t), V(t)$ and $R(t)$ possess an upper bound. We suppose that $S(t)$ and $S^*(t)$ are couple functions, then

$$\begin{aligned} &\|\Phi_1(v, t, S(t)) - \Phi_1(v, t, S^*(t))\| \\ &= \left\| - \left[\beta^v \left(\frac{I_A(t) + I_S(t)}{N(t)} \right) - \mu^v \right] (S(t) - S^*(t)) \right\|. \end{aligned} \tag{11}$$

Considering

$$d_1 = \left\| - \left(\beta^v \left(\frac{I_A(t) + I_S(t)}{N(t)} \right) - \mu^v \right) \right\|, \tag{12}$$

equation (11) simplifies to

$$\|\Phi_1(v, t, S(t)) - \Phi_1(v, t, S^*(t))\| \leq d_1 \| (S(t) - S^*(t)) \|. \tag{13}$$

Similarly,

$$\begin{aligned} &\|\Phi_2(v, t, E(t)) - \Phi_2(v, t, E^*(t))\| \leq d_2 \| (E(t) - E^*(t)) \|, \\ &\|\Phi_3(v, t, I_A(t)) - \Phi_3(v, t, I_A^*(t))\| \leq d_3 \| (I_A(t) - I_A^*(t)) \|, \\ &\|\Phi_4(v, t, I_S(t)) - \Phi_4(v, t, I_S^*(t))\| \leq d_4 \| (I_S(t) - I_S^*(t)) \|, \\ &\|\Phi_5(v, t, Q(t)) - \Phi_5(v, t, Q^*(t))\| \leq d_5 \| (Q(t) - Q^*(t)) \|, \\ &\|\Phi_6(v, t, V(t)) - \Phi_6(v, t, V^*(t))\| \leq d_6 \| (V(t) - V^*(t)) \|, \\ &\|\Phi_7(v, t, R(t)) - \Phi_7(v, t, R^*(t))\| \leq d_7 \| (R(t) - R^*(t)) \|, \end{aligned} \tag{14}$$

where

$$\begin{aligned} d_2 &= \| -(\phi^v + \mu^v) \|, \\ d_3 &= \| -(\alpha\phi^v + \mu^v + \rho^v + \delta^v + \sigma^v) \|, \\ d_4 &= \| -(\delta^v + \mu^v + \tau^v + \theta^v) \|, \\ d_5 &= \| -(\delta^v + \mu^v + \gamma^v) \|, \\ d_6 &= \| -(\Gamma^v + \mu^v) \|, \\ d_7 &= \| -\mu^v \|. \end{aligned} \tag{15}$$

Hence, the Lipschitz condition holds. Now, taking system (9) in a reiterative manner gives

$$\left\{ \begin{aligned}
 S_n(t) - S(0) &= \frac{1-\nu}{B(\nu)}\Phi_1(\nu, t, S_{n-1}(t)) + \frac{\nu}{B(\nu)\Gamma(\nu)} \times \int_0^t (t-\vartheta)^{\nu-1}\Phi_1(\nu, \vartheta, S_{n-1}(\vartheta))d\vartheta, \\
 E_n(t) - E(0) &= \frac{1-\nu}{B(\nu)}\Phi_2(\nu, t, E_{n-1}(t)) + \frac{\nu}{B(\nu)\Gamma(\nu)} \times \int_0^t (t-\vartheta)^{\nu-1}\Phi_2(\nu, \vartheta, E_{n-1}(\vartheta))d\vartheta, \\
 I_{A_n}(t) - I_A(0) &= \frac{1-\nu}{B(\nu)}\Phi_3(\nu, t, I_{A_{n-1}}(t)) + \frac{\nu}{B(\nu)\Gamma(\nu)} \times \int_0^t (t-\vartheta)^{\nu-1}\Phi_3(\nu, \vartheta, I_{A_{n-1}}(\vartheta))d\vartheta, \\
 I_{S_n}(t) - I_S(0) &= \frac{1-\nu}{B(\nu)}\Phi_4(\nu, t, I_{S_{n-1}}(t)) + \frac{\nu}{B(\nu)\Gamma(\nu)} \times \int_0^t (t-\vartheta)^{\nu-1}\Phi_4(\nu, \vartheta, I_{S_{n-1}}(\vartheta))d\vartheta, \\
 Q_n(t) - Q(0) &= \frac{1-\nu}{B(\nu)}\Phi_5(\nu, t, Q_{n-1}(t)) + \frac{\nu}{B(\nu)\Gamma(\nu)} \times \int_0^t (t-\vartheta)^{\nu-1}\Phi_5(\nu, \tau, Q_{n-1}(\vartheta))d\vartheta, \\
 V_n(t) - V(0) &= \frac{1-\nu}{B(\nu)}\Phi_6(\nu, t, V_{n-1}(t)) + \frac{\nu}{B(\nu)\Gamma(\nu)} \times \int_0^t (t-\vartheta)^{\nu-1}\Phi_5(\nu, \tau, V_{n-1}(\vartheta))d\vartheta, \\
 R_n(t) - R(0) &= \frac{1-\nu}{B(\nu)}\Phi_7(\nu, t, R_{n-1}(t)) + \frac{\nu}{B(\nu)\Gamma(\nu)} \times \int_0^t (t-\vartheta)^{\nu-1}\Phi_7(\nu, \vartheta, R_{n-1}(\vartheta))d\vartheta.
 \end{aligned} \right. \quad (16)$$

Difference of consecutive terms yields

$$\left\{ \begin{aligned}
 \Xi_{S_n}(t) &= S_n(t) - S_{n-1}(t) = \frac{1-\nu}{B(\nu)} (\Phi_1(\nu, t, S_{n-1}(t)) - \Phi_1(\nu, t, S_{n-2}(t))) \\
 &+ \frac{\nu}{B(\nu)\Gamma(\nu)} \int_0^t (t-\vartheta)^{\nu-1} (\Phi_1(\nu, \vartheta, S_{n-1}(\vartheta)) - \Phi_1(\nu, \tau, S_{n-2}(\vartheta))) d\vartheta \\
 \Xi_{E_n}(t) &= E_n(t) - E_{n-1}(t) = \frac{1-\nu}{B(\nu)} (\Phi_2(\nu, t, E_{n-1}(t)) - \Phi_2(\nu, t, E_{n-2}(t))) \\
 &+ \frac{\nu}{B(\nu)\Gamma(\nu)} \int_0^t (t-\vartheta)^{\nu-1} (\Phi_2(\nu, \vartheta, E_{n-1}(\vartheta)) - \Phi_2(\nu, \tau, E_{n-2}(\vartheta))) d\vartheta \\
 \Xi_{I_{A_n}}(t) &= I_{A_n}(t) - I_{A_{n-1}}(t) = \frac{1-\nu}{B(\nu)} (\Phi_3(\nu, t, I_{A_{(n-1)}}(t)) - \Phi_3(\nu, t, I_{A_{(n-2)}}(t))) \\
 &+ \frac{\nu}{B(\nu)\Gamma(\nu)} \int_0^t (t-\vartheta)^{\nu-1} (\Phi_3(\nu, \vartheta, I_{A_{(n-1)}}(\vartheta)) - \Phi_3(\nu, \tau, I_{A_{(n-2)}}(\vartheta))) d\vartheta \\
 \Xi_{I_{S_n}}(t) &= I_{S_n}(t) - I_{S_{(n-1)}}(t) = \frac{1-\nu}{B(\nu)} (\Phi_4(\nu, t, I_{S_{(n-1)}}(t)) - \Phi_4(\nu, t, I_{S_{(n-2)}}(t))) \\
 &+ \frac{\nu}{B(\nu)\Gamma(\nu)} \int_0^t (t-\vartheta)^{\nu-1} (\Phi_4(\nu, \vartheta, I_{S_{(n-1)}}(\vartheta)) - \Phi_4(\nu, \tau, I_{S_{(n-2)}}(\vartheta))) d\vartheta \\
 \Xi_{Q_n}(t) &= Q_n(t) - Q_{n-1}(t) = \frac{1-\nu}{B(\nu)} (\Phi_5(\nu, t, Q_{n-1}(t)) - \Phi_5(\nu, t, Q_{n-2}(t))) \\
 &+ \frac{\nu}{B(\nu)\Gamma(\nu)} \int_0^t (t-\vartheta)^{\nu-1} (\Phi_5(\nu, \vartheta, Q_{n-1}(\vartheta)) - \Phi_5(\nu, \tau, Q_{n-2}(\vartheta))) d\vartheta \\
 \Xi_{V_n}(t) &= V_n(t) - V_{n-1}(t) = \frac{1-\nu}{B(\nu)} (\Phi_6(\nu, t, V_{n-1}(t)) - \Phi_6(\nu, t, V_{n-2}(t))) \\
 &+ \frac{\nu}{B(\nu)\Gamma(\nu)} \int_0^t (t-\vartheta)^{\nu-1} (\Phi_6(\nu, \vartheta, V_{n-1}(\vartheta)) - \Phi_6(\nu, \tau, V_{n-2}(\vartheta))) d\vartheta \\
 \Xi_{R_n}(t) &= R_n(t) - R_{n-1}(t) = \frac{1-\nu}{B(\nu)} (\Phi_7(\nu, t, R_{n-1}(t)) - \Phi_7(\nu, t, R_{n-2}(t))) \\
 &+ \frac{\nu}{B(\nu)\Gamma(\nu)} \int_0^t (t-\vartheta)^{\nu-1} (\Phi_7(\nu, \vartheta, R_{n-1}(\vartheta)) - \Phi_7(\nu, \tau, R_{n-2}(\vartheta))) d\vartheta
 \end{aligned} \right. , \tag{17}$$

where $S_n(t) = \sum_{i=0}^n \Xi_{S_n}(t)$, $E_n(t) = \sum_{i=0}^n \Xi_{E_n}(t)$, $I_{A_n}(t) = \sum_{i=0}^n \Xi_{I_{A_n}}(t)$, $I_{S_n}(t) = \sum_{i=0}^n \Xi_{I_{S_n}}(t)$, $Q_n(t) = \sum_{i=0}^n \Xi_{Q_n}(t)$, $V_n(t) = \sum_{i=0}^n \Xi_{V_n}(t)$, $R_n(t) = \sum_{i=0}^n \Xi_{R_n}(t)$. Taking into

consideration equations (12) -(13) and considering $\Xi_{S_{n-1}}(t) = S_{n-1}(t) - S_{n-2}(t)$, $\Xi_{E_{n-1}}(t) = E_{n-1}(t) - E_{n-2}(t)$, $\Xi_{I_{A_{(n-1)}}}(t) = I_{A_{(n-1)}}(t) - I_{A_{(n-2)}}(t)$, $\Xi_{I_{S_{(n-1)}}}(t) = I_{S_{(n-1)}}(t) -$

$$I_{S(n-2)}(t), \Xi_{V_{n-1}}(t) = V_{n-1}(t) - V_{n-2}(t), \Xi_{R_{n-1}}(t) = R_{n-1}(t) - R_{n-2}(t),$$

$$\left\{ \begin{array}{l} \|\Xi_{S_n}(t)\| \leq \frac{1-\nu}{B(\nu)} d_1 \|\Xi_{S_{n-1}}(t)\| \frac{\nu}{B(\nu)\Gamma(\nu)} d_1 \times \int_0^t (t-\vartheta)^{\nu-1} \|\Xi_{S_{n-1}}(\vartheta)\| d\vartheta, \\ \|\Xi_{E_n}(t)\| \leq \frac{1-\nu}{B(\nu)} d_2 \|\Xi_{E_{n-1}}(t)\| \frac{\nu}{B(\nu)\Gamma(\nu)} d_2 \times \int_0^t (t-\vartheta)^{\nu-1} \|\Xi_{E_{n-1}}(\vartheta)\| d\vartheta, \\ \|\Xi_{I_{A_n}}(t)\| \leq \frac{1-\nu}{B(\nu)} d_3 \|\Xi_{I_{A_{n-1}}}(t)\| \frac{\nu}{B(\nu)\Gamma(\nu)} d_3 \times \int_0^t (t-\vartheta)^{\nu-1} \|\Xi_{I_{A_{n-1}}}(\vartheta)\| d\vartheta, \\ \|\Xi_{I_{S_n}}(t)\| \leq \frac{1-\nu}{B(\nu)} d_4 \|\Xi_{I_{S_{n-1}}}(t)\| \frac{\nu}{B(\nu)\Gamma(\nu)} d_4 \times \int_0^t (t-\vartheta)^{\nu-1} \|\Xi_{I_{S_{n-1}}}(\vartheta)\| d\vartheta, \\ \|\Xi_{Q_n}(t)\| \leq \frac{1-\nu}{B(\nu)} d_5 \|\Xi_{Q_{n-1}}(t)\| \frac{\nu}{B(\nu)\Gamma(\nu)} d_5 \times \int_0^t (t-\vartheta)^{\nu-1} \|\Xi_{Q_{n-1}}(\vartheta)\| d\vartheta, \\ \|\Xi_{V_n}(t)\| \leq \frac{1-\nu}{B(\nu)} d_6 \|\Xi_{V_{n-1}}(t)\| \frac{\nu}{B(\nu)\Gamma(\nu)} d_6 \times \int_0^t (t-\vartheta)^{\nu-1} \|\Xi_{V_{n-1}}(\vartheta)\| d\vartheta, \\ \|\Xi_{R_n}(t)\| \leq \frac{1-\nu}{B(\nu)} d_7 \|\Xi_{R_{n-1}}(t)\| \frac{\nu}{B(\nu)\Gamma(\nu)} d_7 \times \int_0^t (t-\vartheta)^{\nu-1} \|\Xi_{R_{n-1}}(\vartheta)\| d\vartheta. \end{array} \right. \quad (18)$$

Theorem 2. System (1) has a unique solution for $t \in [0, b]$ subject to the condition $1 - \nu/B(\nu)d_i + \nu/B(\nu)\Gamma(\nu)b^\nu n_i < 1, i = 1, 2, 3, \dots, 7$ hold [27].

Proof. Since $S(t), E(t), I_A(t), I_S(t), Q(t), V(t)$ and $R(t)$ are bounded functions, equations (12) and (13) hold. In a recurring manner, (16) reaches

$$\left\{ \begin{aligned}
 \|\Xi_{S_n}(t)\| &\leq \|S_o(t)\| \left(\frac{1-\nu}{B(\nu)}d_1 + \frac{\nu b^\nu}{B(\nu)\Gamma(\nu)}d_1 \right)^n, \\
 \|\Xi_{E_n}(t)\| &\leq \|E_o(t)\| \left(\frac{1-\nu}{B(\nu)}d_2 + \frac{\nu b^\nu}{B(\nu)\Gamma(\nu)}d_2 \right)^n, \\
 \|\Xi_{I_{An}}(t)\| &\leq \|I_{Ao}(t)\| \left(\frac{1-\nu}{B(\nu)}d_3 + \frac{\nu b^\nu}{B(\nu)\Gamma(\nu)}d_3 \right)^n, \\
 \|\Xi_{I_{Sn}}(t)\| &\leq \|I_{So}(t)\| \left(\frac{1-\nu}{B(\nu)}d_4 + \frac{\nu b^\nu}{B(\nu)\Gamma(\nu)}d_4 \right)^n, \\
 \|\Xi_{Q_n}(t)\| &\leq \|Q_o(t)\| \left(\frac{1-\nu}{B(\nu)}d_5 + \frac{\nu b^\nu}{B(\nu)\Gamma(\nu)}d_5 \right)^n, \\
 \|\Xi_{V_n}(t)\| &\leq \|V_o(t)\| \left(\frac{1-\nu}{B(\nu)}d_6 + \frac{\nu b^\nu}{B(\nu)\Gamma(\nu)}d_6 \right)^n, \\
 \|\Xi_{R_n}(t)\| &\leq \|R_o(t)\| \left(\frac{1-\nu}{B(\nu)}d_7 + \frac{\nu b^\nu}{B(\nu)\Gamma(\nu)}d_7 \right)^n,
 \end{aligned} \right. \quad (19)$$

$$\left\{ \begin{aligned}
 \|S_{n+j}(t) - S_n(t)\| &\leq \sum_{i=n+1}^{n+j} T_1^j = \frac{T_1^{n+1} - T_1^{n+k+1}}{1 - T_1}, \\
 \|E_{n+j}(t) - E_n(t)\| &\leq \sum_{i=n+1}^{n+j} T_2^j = \frac{T_2^{n+1} - T_2^{n+k+1}}{1 - T_2}, \\
 \|I_{A(n+j)}(t) - I_{An}(t)\| &\leq \sum_{i=n+1}^{n+j} T_3^j = \frac{T_3^{n+1} - T_3^{n+k+1}}{1 - T_3}, \\
 \|I_{S(n+j)}(t) - I_{Sn}(t)\| &\leq \sum_{i=n+1}^{n+j} T_4^j = \frac{T_4^{n+1} - T_4^{n+k+1}}{1 - T_4}, \\
 \|Q_{n+j}(t) - Q_n(t)\| &\leq \sum_{i=n+1}^{n+j} T_5^j = \frac{T_5^{n+1} - T_5^{n+k+1}}{1 - T_5}, \\
 \|V_{n+j}(t) - V_n(t)\| &\leq \sum_{i=n+1}^{n+j} T_6^j = \frac{T_6^{n+1} - T_6^{n+k+1}}{1 - T_6}, \\
 \|R_{n+j}(t) - R_n(t)\| &\leq \sum_{i=n+1}^{n+j} T_7^j = \frac{T_7^{n+1} - T_7^{n+k+1}}{1 - T_7}.
 \end{aligned} \right. \quad (20)$$

where $T_i = 1 - \nu/B(\nu)d_i + \nu/B(\nu)\Gamma(\nu)b^\nu d_i < 1$. Hence, there exists a unique solution for system (1) \square

and $\|\Xi_{S_n}(t)\| \rightarrow 0, \|\Xi_{E_n}(t)\| \rightarrow 0, \|\Xi_{I_{An}}(t)\| \rightarrow 0, \|\Xi_{I_{Sn}}(t)\| \rightarrow 0, \|\Xi_{Q_n}(t)\| \rightarrow 0, \|\Xi_{V_n}(t)\| \rightarrow 0, \|\Xi_{R_n}(t)\| \rightarrow 0$ as $n \rightarrow \infty$. Incorporating the triangular inequality and for any j , system (17) yields

3. Model Analyses

The disease-free equilibrium (E_0) is the steady state solution where there is no infection in the population. This is given as

$$E_0 = (S^0, E^0, I_A^0, I_S^0, Q^0, V^0, R^0) = \left(\frac{\Omega^\nu (\Gamma^\nu + \mu^\nu (1 - \eta^\nu))}{\mu^\nu (\mu^\nu + \Gamma^\nu)}, 0, 0, 0, 0, \frac{\eta^\nu \Omega^\nu}{(\Gamma^\nu + \mu^\nu)}, 0 \right). \quad (21)$$

The endemic equilibrium (E_1) of system (1) is represented by $E_1 = (S^*, E^*, V^*, I_A^*, I_S^*, Q^*, R^*)$, where

$$\left\{ \begin{aligned}
 S^* &= \frac{(1-\eta^\nu)\Omega^\nu + \Gamma^\nu V^*}{\beta^\nu (I_A^* + I_S^*) + \mu^\nu}, E^* = \frac{\beta^\nu S^* (I_A^* + I_S^*)}{\phi^\nu + \mu^\nu}, I_A^* = \frac{(1-\alpha)\phi^\nu E^*}{\rho^\nu + \sigma^\nu + \mu^\nu + \delta^\nu}, \\
 I_S^* &= \frac{\alpha\phi^\nu E^*}{\rho^\nu + \sigma^\nu + \mu^\nu + \delta^\nu}, Q^* = \frac{\rho^\nu I_A^* + \tau^\nu I_S^*}{\gamma^\nu + \mu^\nu + \delta^\nu}, V^* = \frac{\eta^\nu \Omega^\nu}{\Gamma^\nu + \mu^\nu}, R^* = \frac{\theta^\nu I_S^* + \sigma^\nu I_A^* + \gamma^\nu Q^*}{\mu^\nu}.
 \end{aligned} \right. \quad (22)$$

We now ascertain the basic reproduction number (R_0) of system (1). The total number of secondary instances that one sick person can bring about over the life of the infection in a society that is entirely susceptible is the basic

reproduction number [31]. Using the next generation operator technique, by denoting F and V as matrices representing the newly produced diseases and the transition terms, we discover, respectively,

$$\left. \begin{aligned}
 F &= \begin{bmatrix} 0 & \beta^v S^0 & \beta^v S^0 & 0 \\ (1-\alpha)\phi^v & 0 & 0 & 0 \\ \alpha\phi^v & 0 & 0 & 0 \\ 0 & \rho^v & \tau^v & 0 \end{bmatrix}, \\
 V &= \begin{bmatrix} \phi^v + \mu^v & 0 & 0 & 0 \\ 0 & \rho^v + \sigma^v + \mu^v + \delta^v & 0 & 0 \\ 0 & 0 & \theta^v + \tau^v + \mu^v + \delta^v & 0 \\ 0 & 0 & 0 & \gamma^v + \mu^v + \delta^v \end{bmatrix}.
 \end{aligned} \right\} \tag{23}$$

Now, the basic reproductive number is given as the spectrum radius of the matrix FV^{-1} .

$$\begin{aligned}
 R_1 &= \frac{\beta^v \Omega^v (\Gamma^v + \mu^v (1 - \eta^v))}{\mu^v (\mu^v + \Gamma^v) (\rho^v + \sigma^v + \mu^v + \delta^v)} \text{ and} \\
 R_2 &= \frac{\beta^v \Omega^v (\Gamma^v + \mu^v (1 - \eta^v))}{\mu^v (\mu^v + \Gamma^v) (\theta^v + \tau^v + \mu^v + \delta^v)},
 \end{aligned} \tag{24}$$

represents the reproduction number for system (1)

The necessary conditions for the local stability of the endemic equilibrium are established in Theorem 2.

Theorem 3. *The disease-free equilibrium is locally asymptotically stable if $R_0 < 1$ and unstable for $R_0 > 1$.*

Proof. The Jacobian matrix of system (1) is given as

$$J = \begin{pmatrix} -\mu^v & 0 & -\beta^v S & -\beta^v S & 0 & \Gamma^v & 0 \\ \beta^v (I_A + I_S) & -(\phi^v + \mu^v) & \beta^v S & \beta^v S & 0 & 0 & 0 \\ 0 & (1-\alpha)\phi^v & -(\rho^v + \sigma^v + \mu^v + \delta^v) & 0 & 0 & 0 & 0 \\ 0 & \alpha\phi^v & 0 & -(\theta^v + \tau^v + \mu^v + \delta^v) & 0 & 0 & 0 \\ 0 & 0 & \rho^v & \tau^v & -(\gamma^v + \mu^v + \delta^v) & 0 & 0 \\ 0 & 0 & 0 & 0 & 0 & -(\Gamma^v + \mu^v) & 0 \\ 0 & 0 & \sigma^v & \theta^v & \gamma^v & 0 & -\mu^v \end{pmatrix}. \tag{25}$$

The Jacobian matrix evaluated at the disease-free equilibrium point is given as

$$J_{E^0} = \begin{pmatrix} -\mu^v & 0 & -\beta^v S^0 & -\beta^v S^0 & 0 & \Gamma^v & 0 \\ 0 & -(\phi^v + \mu^v) & \beta^v S^0 & \beta^v S^0 & 0 & 0 & 0 \\ 0 & (1-\alpha)\phi^v & -(\rho^v + \sigma^v + \mu^v + \delta^v) & 0 & 0 & 0 & 0 \\ 0 & \alpha\phi^v & 0 & -(\theta^v + \tau^v + \mu^v + \delta^v) & 0 & 0 & 0 \\ 0 & 0 & \rho^v & \tau^v & -(\gamma^v + \mu^v + \delta^v) & 0 & 0 \\ 0 & 0 & 0 & 0 & 0 & -(\Gamma^v + \mu^v) & 0 \\ 0 & 0 & \sigma^v & \theta^v & \gamma^v & 0 & -\mu^v \end{pmatrix}. \tag{26}$$

We need to show that all eigenvalues of system (23) are negative. The first four eigenvalues are $-\mu^v$, $-(\gamma^v + \mu^v + \delta^v)$, $-(\Gamma^v + \mu^v)$, and $-\mu^v$. The others are obtained from the submatrix in system (24) formed by excluding the first, fifth, sixth, and seventh rows and columns of system (23). Hence, we have

$$J_{E^0} = \begin{pmatrix} -(\phi^v + \mu^v) & \beta^v S^0 & \beta^v S^0 \\ (1-\alpha)\phi^v & -(\rho^v + \sigma^v + \mu^v + \delta^v) & 0 \\ \alpha\phi^v & 0 & -(\theta^v + \tau^v + \mu^v + \delta^v) \end{pmatrix}. \tag{27}$$

The characteristic equation of system (24) is

$$\lambda^3 + A_1\lambda^2 + A_2\lambda + A_3 = 0, \tag{28} \quad \text{where}$$

$$\begin{aligned} A_1 &= (\phi^v + \mu^v) + (\rho^v + \sigma^v + \mu^v + \delta^v) + A, \\ A_2 &= (\phi^v + \mu^v)[(\rho^v + \sigma^v + \mu^v + \delta^v) + A] + (\rho^v + \sigma^v + \mu^v + \delta^v)[(A - \mu^v\phi^v(\mu^v + \Gamma^v)R_0)], \\ A_3 &= (\rho^v + \sigma^v + \mu^v + \delta^v)[(\phi^v + \mu^v)A + \alpha^v\phi^v\beta^vS^0] + (1 - \alpha)\phi^vA\beta^vS^0, \\ A &= (\theta^v + \tau^v + \mu^v + \delta^v). \end{aligned} \tag{29}$$

From the Routh–Hurwitz stability criterion, if the conditions $A_1 > 0, A_3 > 0$ and $A_1A_2 - A_3 > 0$ are satisfied, then all the roots of the characteristic equation have a negative real part which means stable equilibrium. \square

4. Fractional Optimal Control Problem

We add two control functions u_1 and u_2 into the system (1), where control u_1 and u_2 are social distancing and vaccination, respectively. We include the time-dependent controls into system (1), and we have

$$\left\{ \begin{aligned} {}^vABC D_t^v S &= (1 - \eta^v)\Omega^v + \Gamma^vV - (1 - u_1)\beta^v\frac{S(I_A + I_S)}{N} - \mu^vS - u_2S, \\ {}^vABC D_t^v E &= (1 - u_1)\beta^v\frac{S(I_A + I_S)}{N} - (\phi^v + \mu^v)E, \\ {}^vABC D_t^v I_A &= (1 - \alpha)\phi^vE - (\rho^v + \sigma^v + \mu^v + \delta^v)I_A, \\ {}^vABC D_t^v I_S &= \alpha\phi^vE - (\theta^v + \tau^v + \mu^v + \delta^v)I_S, \\ {}^vABC D_t^v Q &= \rho^vI_A + \tau^vI_S - (\gamma^v + \mu^v + \delta^v)Q, \\ {}^vABC D_t^v V &= \eta^v\Omega^v - (\Gamma^v + \mu^v)V + u_2S, \\ {}^vABC D_{0,t}^v [R(t)] &= \theta^vI_S + \sigma^vI_A + \gamma^vQ - \mu^vR. \end{aligned} \right. \tag{30}$$

The objective function for a fixed time t_f is given as

$$J(u_1, u_2) = \int_0^{t_f} \left[G_1S(t) + G_2E(t) + G_3I_A(t) + G_4I_S(t) + G_5Q(t) + \frac{1}{2}(T_1u_1^2 + T_2u_2^2) \right] dt, \tag{31}$$

where T_1 and T_2 are the measures of the relative cost of interventions associated with the controls u_1 and u_2 . We find optimal controls u_1 and u_2 that minimize the cost function

$$J(u_1, u_2) = \int_0^{t_f} \varsigma(S, E, I_A, I_S, Q, V, R) dt, \tag{32}$$

subject to the constraint

$$\begin{aligned} {}^v ABC D_t^v S(t) &= \varsigma_{1,v} {}^v ABC D_t^v E(t) = \varsigma_{2,v} {}^v ABC D_t^v I_A(t) = \varsigma_{3,v} {}^v ABC D_t^v I_S(t) = \varsigma_{4,v} {}^v ABC D_t^v Q(t) = \varsigma_5 \\ {}^v ABC D_t^v V(t) &= \varsigma_{6,v} {}^v ABC D_t^v R(t) = \varsigma_7, \end{aligned} \tag{33}$$

where $\varsigma_i = \varsigma(S, E, I_A, I_S, Q, V, R)$, $i = 1, 2, 3, \dots, 7$, $\Phi = (u_1, u_2) | u_i$ is a Lebesgue measurable on $[0, 1]$ such that $0 \leq (u_1, u_2) \leq 1, \forall t \in [0, t_f]$, where t_f is the final time and

with initial conditions $S(0) = S_o, E(0) = E_o, I_A(0) = I_{Ao}, I_S(0) = I_{so}, Q(0) = Q_o, V(0) = V_o, R(0) = R_o$.

To define the fractional optimal control, we consider the following modified cost function [10]:

$$J = \int_0^{t_f} \left[H_v(S, E, I_A, I_S, Q, V, R, u_j, t) - \sum_{i=1}^7 \lambda_i \varsigma_i(S, E, I_A, I_S, Q, V, R, u_j, t) \right] dt, \tag{34}$$

where $i = 1, \dots, 7$ and $j = 1, 2, 3$.

For the fractional optimal control, the Hamiltonian is

$$H_v(S, E, I_A, I_S, Q, V, R, u_j, t) = \nu(S, E, I_A, I_S, Q, V, R, u_j, t) + \sum_{i=1}^7 \lambda_i \varsigma_i(S, E, I_A, I_S, Q, V, R, u_j, t), \tag{35}$$

where $i = 1, \dots, 7$ and $j = 1, 2, 3$. The following are essential for the formulation of the fractional optimal control [10, 27]:

$${}^v ABC D_t^v \Lambda_S = \frac{\partial H_v}{\partial S}, {}^v ABC D_t^v \Lambda_E = \frac{\partial H_v}{\partial E}, {}^v ABC D_t^v \Lambda_{I_A} = \frac{\partial H_v}{\partial I_A}, {}^v ABC D_t^v \Lambda_{I_S} = \frac{\partial H_v}{\partial I_S}, {}^v ABC D_t^v \Lambda_Q = \frac{\partial H_v}{\partial Q}, \tag{36}$$

$${}^v ABC D_t^v \Lambda_V = \frac{\partial H_v}{\partial V}, {}^v ABC D_t^v \Lambda_R = \frac{\partial H_v}{\partial R},$$

$$0 = \frac{\partial H_v}{\partial u_i},$$

$${}^v ABC D_t^v S = \frac{\partial H_v}{\partial \Lambda_S}, {}^v ABC D_t^v E = \frac{\partial H_v}{\partial \Lambda_E}, {}^v ABC D_t^v I_A = \frac{\partial H_v}{\partial \Lambda_{I_A}}, {}^v ABC D_t^v I_S = \frac{\partial H_v}{\partial \Lambda_{I_S}}, {}^v ABC D_t^v Q = \frac{\partial H_v}{\partial \Lambda_Q}, \tag{37}$$

$${}^v ABC D_t^v V = \frac{\partial H_v}{\partial \Lambda_V}, {}^v ABC D_t^v R = \frac{\partial H_v}{\partial \Lambda_R}.$$

Moreover,

$$\begin{aligned} \Lambda_S(t_f) &= \Lambda_E(t_f) = \Lambda_{I_A}(t_f) = \Lambda_{I_S}(t_f) = \Lambda_Q(t_f) \\ &= \Lambda_V(t_f) = \Lambda_R(t_f) = 0, \end{aligned} \tag{38}$$

are the Lagrange multipliers. Equations (31) and (32) provide the necessary conditions for the fractional optimal control in terms of the Hamiltonian for the optimal control problem defined previously. The Hamiltonian, H , is defined by

$$\begin{aligned}
 H = & k_1 S^* + k_2 E^* + k_3 I_A^* + k_4 I_S^* + k_5 Q^* + \frac{1}{2}(T_1 u_1^2 + T_2 u_2^2) \\
 & + {}^v ABC D_t^\nu \Lambda_S + {}^v ABC D_t^\nu \Lambda_E + {}^v ABC D_t^\nu \Lambda_{I_A} + {}^v ABC D_t^\nu \Lambda_{I_S} + {}^v ABC D_t^\nu \Lambda_Q + {}^v ABC D_t^\nu \Lambda_V + {}^v ABC D_t^\nu \Lambda_R.
 \end{aligned} \tag{39}$$

Theorem 4. Given an optimal control (u_1^*, u_2^*) and corresponding solution $S^*, E^*, I_A^*, I_S^*, Q^*, V^*, R^*$ of the system (26)-(27) that minimizes $J(u)$ over U , there exist adjoint variables $\Lambda_S, \Lambda_E, \Lambda_{I_A}, \Lambda_{I_S}, \Lambda_Q, \Lambda_V,$ and Λ_R , satisfying [27]

$$\frac{d\Lambda_i}{dt} = \frac{\partial H}{\partial i}, \tag{40}$$

where $i = S, E, I_A, I_S, Q, V, R$ with the transversality conditions:

$$\begin{aligned}
 \Lambda_S(t_f) = \Lambda_E(t_f) = \Lambda_{I_A}(t_f) = \Lambda_{I_S}(t_f) = \Lambda_Q(t_f) \\
 = \Lambda_V(t_f) = \Lambda_R(t_f) = 0.
 \end{aligned} \tag{41}$$

Proof. The differential equations characterized by the adjoint variables are obtained by considering the right-hand side differentiation of system (34) determined by the optimal control. The adjoint equations derived are given as

$$\begin{aligned}
 {}^v ABC D_t^\nu \Lambda_S &= \beta^\nu (I_A - I_S)(1 - u_1)[\Lambda_S - \Lambda_E] + (\mu^\nu + u_2)\Lambda_S + u_2\Lambda_V, \\
 {}^v ABC D_t^\nu \Lambda_E &= (\phi^\nu + \mu^\nu)\Lambda_E - (1 - \alpha)\phi^\nu \Lambda_{I_A} - \alpha\phi^\nu \Lambda_{I_S}, \\
 {}^v ABC D_t^\nu \Lambda_{I_A} &= (\rho^\nu + \sigma^\nu + \mu^\nu + \delta^\nu)\Lambda_{I_A} + (1 - u_1)\beta^\nu S\Lambda_S - \rho^\nu \Lambda_Q - \sigma^\nu \Lambda_R, \\
 {}^v ABC D_t^\nu \Lambda_{I_S} &= (\theta^\nu + \tau^\nu + \mu^\nu + \delta^\nu)\Lambda_{I_S} + (1 - u_1)\beta^\nu S\Lambda_S - \tau^\nu \Lambda_Q - \theta^\nu \Lambda_R, \\
 {}^v ABC D_t^\nu \Lambda_Q &= (\gamma^\nu + \mu^\nu + \delta^\nu)\Lambda_Q - \gamma^\nu \Lambda_R, \\
 {}^v ABC D_t^\nu \Lambda_V &= -\Gamma^\nu \Lambda_S + (\Gamma^\nu + \mu^\nu)\Lambda_V, \\
 {}^v ABC D_t^\nu \Lambda_R &= \mu^\nu \Lambda_R.
 \end{aligned} \tag{42}$$

By obtaining the solution for u_1^* and u_2^* subject to the constraints, we have

$$0 = \frac{\partial H}{\partial u_1} = -T_1 u_1 + \beta^\nu S(I_A + I_S)[\Lambda_E - \Lambda_S], \tag{43}$$

$$0 = \frac{\partial H}{\partial u_2} = -T_2 u_2 + S[\Lambda_S - \Lambda_V].$$

This gives

$$u_1^* = \min\left(1, \max\left(0, \frac{\beta^\nu S(I_A + I_S)[\Lambda_E - \Lambda_S]}{T_1}\right)\right), \tag{44}$$

$$u_2^* = \min\left(1, \max\left(0, \frac{S[\Lambda_S - \Lambda_V]}{T_2}\right)\right).$$

□

5. Numerical Scheme of the Fractional Derivative

We apply the scheme in [10] to system (1). Let us consider the first equation of system (1).

$${}^v ABC D_t^\nu [S(t)] = h(t, S(t)), S(0) = S_o. \tag{45}$$

Applying the fundamental theorem of fractional calculus to equation (40), we obtain

$$\begin{aligned}
 S(t) - S(0) &= \frac{1 - \nu}{B(\nu)} h(t, S(t)) \\
 &+ \frac{\nu}{\Gamma(\nu)B(\nu)} \int_0^t g(\tau, S(\tau))(t - \tau)^{\nu-1} d\tau,
 \end{aligned} \tag{46}$$

where $B(\nu) = 1 - \nu + \nu\Gamma(\nu)$ is a normalized function and at $t_{\epsilon+1}$, we have

$$\begin{aligned}
 S_{\epsilon+1} &= S_o + \frac{(1 - \nu)\Gamma(\nu)}{(1 - \nu)\Gamma(\nu) + \nu} h(t_\epsilon, S(t_\epsilon)) \\
 &+ \frac{\nu}{\Gamma(\nu) + \nu(1 - \Gamma(\nu))} \sum_{\partial=0}^{\epsilon} \int_{t_\partial}^{t_\epsilon} h \times (t_{\epsilon+1} - \vartheta)^{\nu-1}.
 \end{aligned} \tag{47}$$

Implementing two-step Lagrange's interpolation polynomial on the interval $[t_\epsilon, t_{\epsilon+1}]$ [10, 32], we have

$$Y = \frac{h(t_\epsilon, S_\partial)}{g} (\vartheta - t_{\partial-1}) - \frac{h(t_{\partial-1}, S_{\partial-1})}{g} (\vartheta - t_\partial). \tag{48}$$

Equation (43) is replaced with equation (42), and by performing the steps given in [10, 32], we obtain

$$\begin{aligned}
 S(t_{\varepsilon+1}) &= S(t_0) + \frac{\Gamma(\nu)(1-\nu)}{\Gamma(\nu)(1-\nu)+\nu} h(t_\varepsilon, S(t_\varepsilon)) + \frac{1}{(\nu+1)\Gamma(\nu)+\nu} \sum_{\partial=0}^n g^\nu h(t_\partial, S(t_\partial)) (\varepsilon+1-\partial)^\nu \\
 &\quad \times (\varepsilon-\partial+2+\nu) - (\varepsilon-\partial)^\nu (\varepsilon-\partial+2+2\nu) - g^\nu h(t_{\partial-1}, S(t_{\partial-1})) (\varepsilon+1-\partial)^{\nu+1} (\varepsilon-\partial+2+\nu) \\
 &\quad - (\varepsilon-\partial)^\nu (\varepsilon-\partial+1+\nu).
 \end{aligned} \tag{49}$$

To obtain high stability, we replace the step-size g in equation (44) with $\vartheta(g)$ such that $\vartheta(g) = g + O(g^2)$, $0 < \vartheta(g) \leq 1$ [10, 31].

The new scheme which is called the nonstandard two-step Lagrange interpolation method (NS2LIM) is given as follows:

$$\begin{aligned}
 S(t_{\varepsilon+1}) &= S(t_0) + \frac{\Gamma(\nu)(1-\nu)}{\Gamma(\nu)(1-\nu)+\nu} h(t_\varepsilon, S(t_\varepsilon)) + \frac{1}{(\nu+1)(1-\nu)\Gamma(\nu)+\nu} \sum_{\partial=0}^{\varepsilon} \vartheta(g)^\nu h(t_\partial, S(t_\partial)) (\varepsilon+1-\partial)^\nu \\
 &\quad \times (\varepsilon-\partial+2+\nu) - (\varepsilon-\partial)^\nu (\varepsilon-\partial+2+2\nu) - \vartheta(g)^\nu h(t_{\partial-1}, S(t_{\partial-1})) (\varepsilon+1-\partial)^{\nu+1} (\varepsilon-\partial+2+\nu) \\
 &\quad - (\varepsilon-\partial)^\nu (\varepsilon-\partial+1+\nu).
 \end{aligned} \tag{50}$$

Similarly,

$$\begin{aligned}
 E(t_{\varepsilon+1}) &= E(t_0) + \frac{\Gamma(\nu)(1-\nu)}{\Gamma(\nu)(1-\nu)+\nu} h(t_\varepsilon, E(t_\varepsilon)) + \frac{1}{(\nu+1)(1-\nu)\Gamma(\nu)+\nu} \sum_{\partial=0}^{\varepsilon} \vartheta(g)^\nu h(t_\partial, E(t_\partial)) (\varepsilon+1-\partial)^\nu \\
 &\quad \times (\varepsilon-\partial+2+\nu) - (\varepsilon-\partial)^\nu (\varepsilon-\partial+2+2\nu) - \vartheta(g)^\nu h(t_{\partial-1}, E(t_{\partial-1})) (\varepsilon+1-\partial)^{\nu+1} (\varepsilon-\partial+2+\nu) \\
 &\quad - (\varepsilon-\partial)^\nu (\varepsilon-\partial+1+\nu), \\
 I_A(t_{\varepsilon+1}) &= I_A(t_0) + \frac{\Gamma(\nu)(1-\nu)}{\Gamma(\nu)(1-\nu)+\nu} h(t_\varepsilon, I_A(t_\varepsilon)) + \frac{1}{(\nu+1)(1-\nu)\Gamma(\nu)+\nu} \sum_{\partial=0}^{\varepsilon} \vartheta(g)^\nu h(t_\partial, I_A(t_\partial)) (\varepsilon+1-\partial)^\nu \\
 &\quad \times (\varepsilon-\partial+2+\nu) - (\varepsilon-\partial)^\nu (\varepsilon-\partial+2+2\nu) - \vartheta(g)^\nu h(t_{\partial-1}, I_A(t_{\partial-1})) (\varepsilon+1-\partial)^{\nu+1} (\varepsilon-\partial+2+\nu) \\
 &\quad - (\varepsilon-\partial)^\nu (\varepsilon-\partial+1+\nu), \\
 I_S(t_{\varepsilon+1}) &= I_S(t_0) + \frac{\Gamma(\nu)(1-\nu)}{\Gamma(\nu)(1-\nu)+\nu} h(t_\varepsilon, I_S(t_\varepsilon)) + \frac{1}{(\nu+1)(1-\nu)\Gamma(\nu)+\nu} \sum_{\partial=0}^{\varepsilon} \vartheta(g)^\nu h(t_\partial, I_S(t_\partial)) (\varepsilon+1-\partial)^\nu \\
 &\quad \times (\varepsilon-\partial+2+\nu) - (\varepsilon-\partial)^\nu (\varepsilon-\partial+2+2\nu) - \vartheta(g)^\nu h(t_{\partial-1}, I_S(t_{\partial-1})) (\varepsilon+1-\partial)^{\nu+1} (\varepsilon-\partial+2+\nu) \\
 &\quad - (\varepsilon-\partial)^\nu (\varepsilon-\partial+1+\nu),
 \end{aligned}$$

$$\begin{aligned}
Q(t_{\varepsilon+1}) &= Q(t_0) + \frac{\Gamma(\nu)(1-\nu)}{\Gamma(\nu)(1-\nu)+\nu} h(t_\varepsilon, Q(t_\varepsilon)) + \frac{1}{(\nu+1)(1-\nu)\Gamma(\nu)+\nu} \sum_{\partial=0}^{\varepsilon} \vartheta(g)^\nu h(t_\partial, Q(t_\partial)) (\varepsilon+1-\partial)^\nu \\
&\quad \times (\varepsilon-\partial+2+\nu) - (\varepsilon-\partial)^\nu (\varepsilon-\partial+2+2\nu) - \vartheta(g)^\nu h(t_{\partial-1}, Q(t_{\partial-1})) (\varepsilon+1-\partial)^{\nu+1} (\varepsilon-\partial+2+\nu) \\
&\quad - (\varepsilon-\partial)^\nu (\varepsilon-\partial+1+\nu), \\
V(t_{\varepsilon+1}) &= V(t_0) + \frac{\Gamma(\nu)(1-\nu)}{\Gamma(\nu)(1-\nu)+\nu} h(t_\varepsilon, V(t_\varepsilon)) + \frac{1}{(\nu+1)(1-\nu)\Gamma(\nu)+\nu} \sum_{\partial=0}^{\varepsilon} \vartheta(g)^\nu h(t_\partial, V(t_\partial)) (\varepsilon+1-\partial)^\nu \\
&\quad \times (\varepsilon-\partial+2+\nu) - (\varepsilon-\partial)^\nu (\varepsilon-\partial+2+2\nu) - \vartheta(g)^\nu h(t_{\partial-1}, V(t_{\partial-1})) (\varepsilon+1-\partial)^{\nu+1} (\varepsilon-\partial+2+\nu) \\
&\quad - (\varepsilon-\partial)^\nu (\varepsilon-\partial+1+\nu), \\
R(t_{\varepsilon+1}) &= R(t_0) + \frac{\Gamma(\nu)(1-\nu)}{\Gamma(\nu)(1-\nu)+\nu} h(t_\varepsilon, R(t_\varepsilon)) + \frac{1}{(\nu+1)(1-\nu)\Gamma(\nu)+\nu} \sum_{\partial=0}^{\varepsilon} \vartheta(g)^\nu h(t_\partial, R(t_\partial)) (\varepsilon+1-\partial)^\nu \\
&\quad \times (\varepsilon-\partial+2+\nu) - (\varepsilon-\partial)^\nu (\varepsilon-\partial+2+2\nu) - \vartheta(g)^\nu h(t_{\partial-1}, R(t_{\partial-1})) (\varepsilon+1-\partial)^{\nu+1} (\varepsilon-\partial+2+\nu) \\
&\quad - (\varepsilon-\partial)^\nu (\varepsilon-\partial+1+\nu).
\end{aligned} \tag{51}$$

6. Numerical Simulation

In this section, we validate the model using the parameter values given in [20] and use the numerical scheme in [10]. The parameter values are given in Table 1.

Using the initial conditions given in [20], $S(0) = 30800000$, $E(0) = 0$, $I_A(0) = 2$, $I_S(0) = 0$, $Q(0) = 0$, $V(0) = 0$, $R(0) = 0$, and setting the fractional operator $\nu \in [0.6, 1.0]$ at a step-size of 0.1, the simulations performed are displayed in Figures 2–8. The figures depict the behaviour of all compartments for the first 400 days since the outbreak.

Figures 2–8 depict the behaviour of susceptible, exposed, asymptomatic, symptomatic, quarantine, vaccinated, and recovered individuals, respectively, for different values of the fractional operator ν for the period of 400 days. In Figure 2, the population of susceptible decreases as the value of the fractional operator ν reduces. The exposed, asymptomatic, symptomatic, and quarantine population is extinct when the fractional operator is 0.6 and below (Figures 3–6). Again, exposed, asymptomatic, symptomatic, and quarantine population is seen to reach an early peak when the fractional operator value is reduced from 1. The number of exposed, asymptomatic, symptomatic, and quarantine individuals decays faster at the noninteger values. However, the number of immune individuals increases as ν reduces from 1.0 to 0.6 (Figure 7). On the other hand, the recovered population is seen to become extinct at $\nu = 0.6$. This is so because the infections in the population have also become extinct at the same value of the fractional operator (Figure 8).

7. Numerical Simulation of the Fractional Optimal Control

In this section, we analyze the numerical behavior of the fractional optimal control model using the parameter values given in Table 1 and the same initial conditions $S(0) = 30800000$, $E(0) = 0$, $I_A(0) = 2$, $I_S(0) = 0$, $Q(0) = 0$, $V(0) = 0$, $R(0) = 0$. Using MATLAB OD45 Ruge–Kutta method, the results of the simulations are displayed in Figures 9–20.

Figures 9–15 depict the behaviour of the susceptible, exposed, asymptomatic, symptomatic, quarantine, immune, and recovered individuals, respectively, when the optimal control u_1 is fully optimized while setting $u_2 = 0$ for the entire period of 400 days. With the social distancing control, it takes a longer period of 350 days before a significant decline in the susceptible population is observed as compared to a situation without optimal control which is 250 days (Figure 9). In Figure 10, there is a drastic decline in the number of individuals that get exposed to the disease when social distancing is observed. This leads to a corresponding decline in the number of asymptomatic, symptomatic, and quarantine individuals (Figures 11–13). The social distancing measures have no effect on the immune individuals as the population remains constant with or without the optimal control (Figure 14). With a drastic fall in the number of infections in the case of an optimal control, the recovered population is also seen to decline when there is an optimal control (Figure 15). Figures 16–22 describe the dynamics of each compartment when the vaccination control is implemented.

TABLE 1: Parameter values and description.

Parameters	Description	Values	Sources
Ω	Recruitment rate	29.08	[20, 33]
β	Transmission rate	0.9	[20, 27]
ϕ	The rate at which exposed individuals become infectious	0.25	[20, 27, 34]
μ	Natural death rate	0.4252912×10^{-4}	[20, 27]
δ	Disease-induced death rate	1.6728×10^{-5}	[20, 35]
θ	Recovery rate of symptomatic individuals	1/14	[36]
Γ	Rate at which vaccinated individuals lose their immunity	1.52×10^{-7}	[20]
σ	Recovery rate of asymptomatic individuals	1/14	[20, 27]
γ	Recovery rate of quarantine individuals	1/14	[20]
τ	Rate at which symptomatic individuals move to the quarantine class	0.01	[36]
ρ	Rate at which asymptomatic individuals move to the quarantine class	1.026×10^{-7}	Assumed
η	Rate at which susceptible individuals are vaccinated	0.01624	[20]

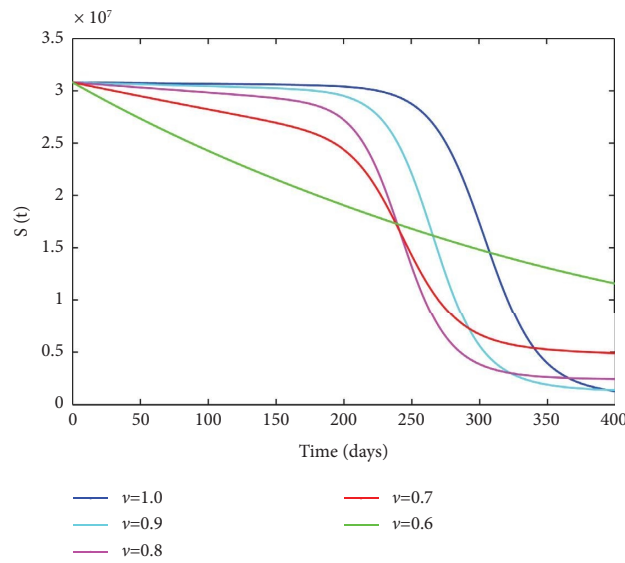


FIGURE 2: Behaviour of the susceptible individuals at different values of v .

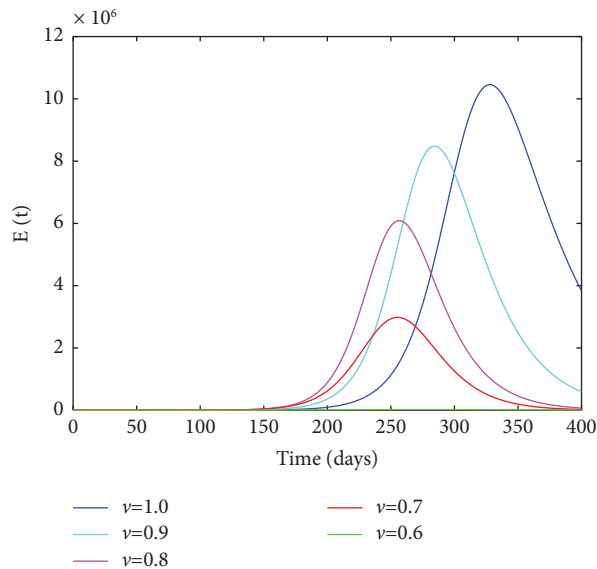


FIGURE 3: Behaviour of the exposed individuals at different values of v .

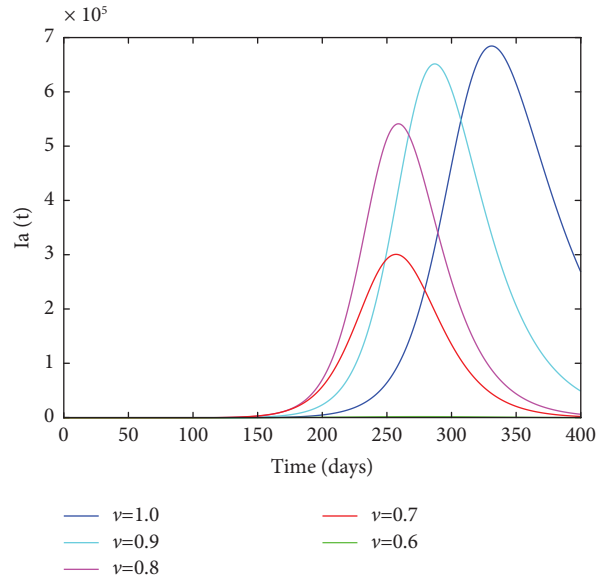


FIGURE 4: Behaviour of the asymptomatic individuals at different values of ν .

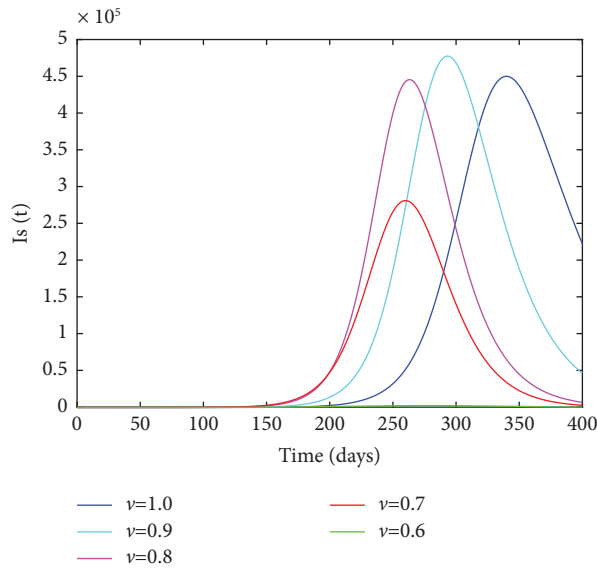


FIGURE 5: Behaviour of the symptomatic individuals at different values of ν .

Figures 16–22 show the behaviour of the susceptible, exposed, asymptomatic, symptomatic, quarantine, recovered, and immune individuals, respectively, when the vaccination control u_2 is fully optimized while setting $u_1 = 0$ for the entire period of 400 days. With the vaccination control, a significant decline in the number of susceptible individuals is observed for the first 300 days. However, after the 300 days, there is a slow decline in the number when

compared with a situation without optimal control. The vaccination reduces the number of individuals susceptible to the disease for the first 300 days (Figure 16). Vaccinating the susceptible individuals leads to a decline in the number of exposed, asymptomatic, symptomatic, and quarantine individuals as compared with a situation without the optimal control (Figures 17–20). The decline in infections leads to a decline in the recovered population (Figure 21). There are

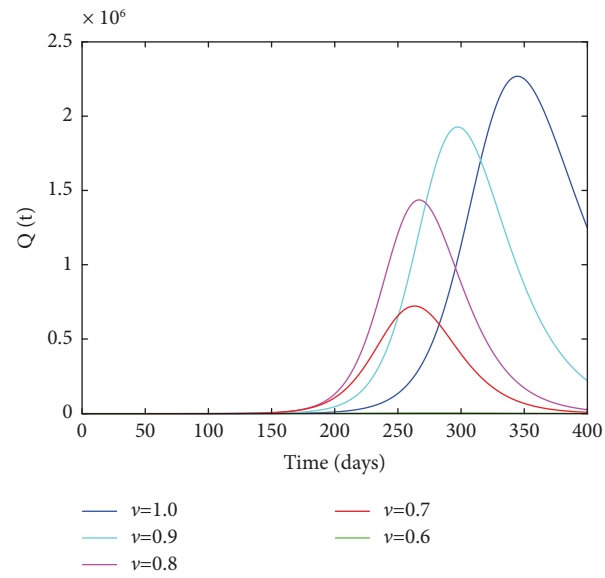


FIGURE 6: Behaviour of the quarantine individuals at different values of ν .

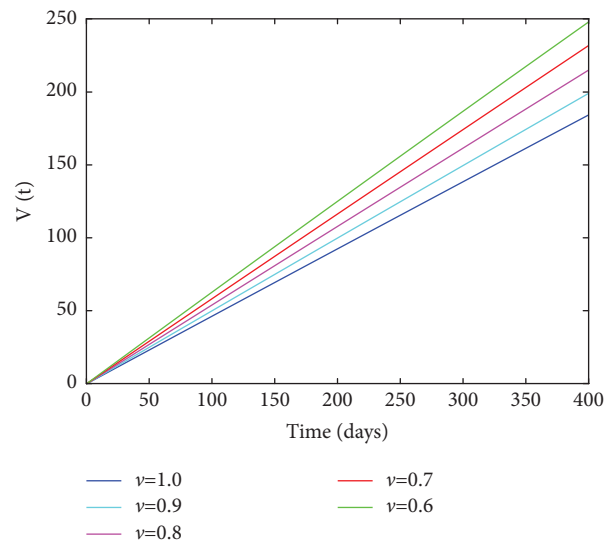


FIGURE 7: Behaviour of the vaccinated individuals at different values of ν .

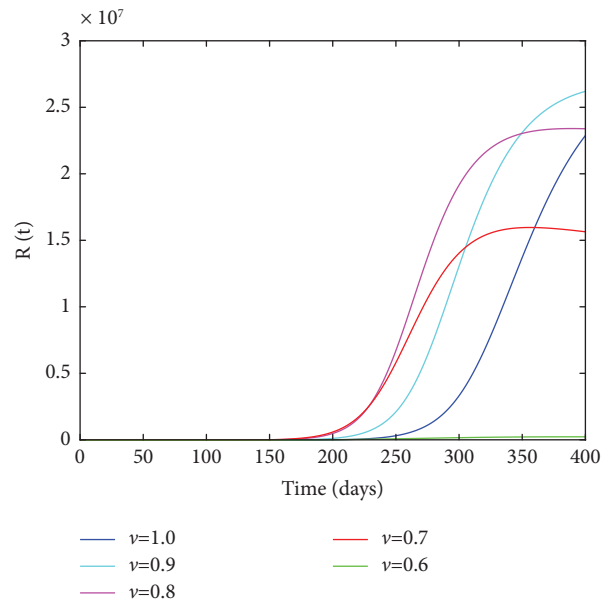


FIGURE 8: Behaviour of the recovered individuals at different values of ν .

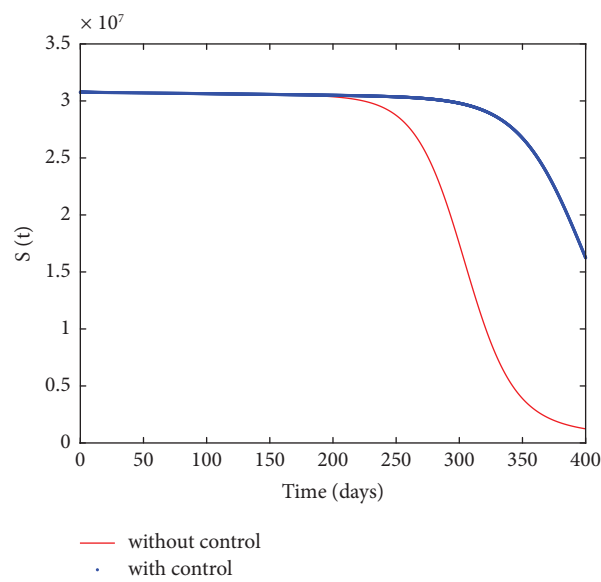


FIGURE 9: Behaviour of the susceptible individuals with and without the control.

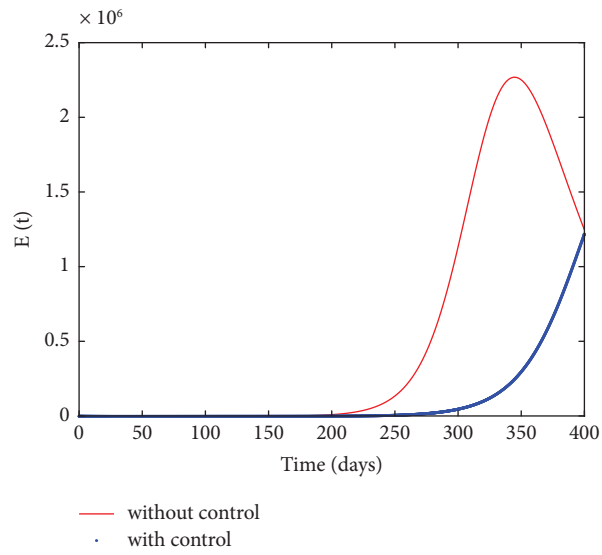


FIGURE 10: Behaviour of the exposed individuals with and without the optimal control.

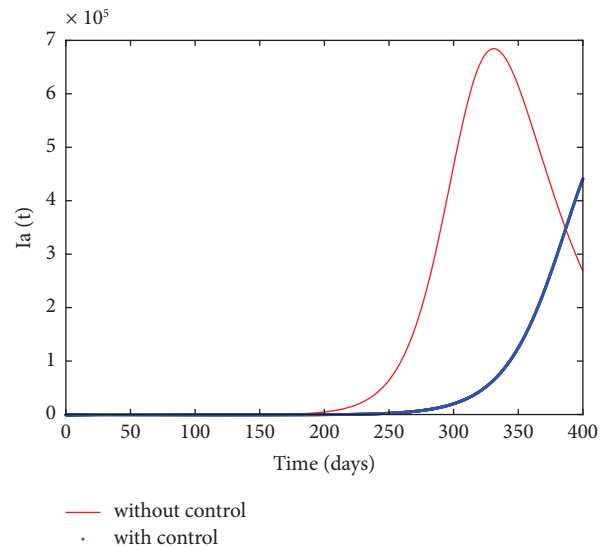


FIGURE 11: Behaviour of the asymptomatic individuals with and without the control.

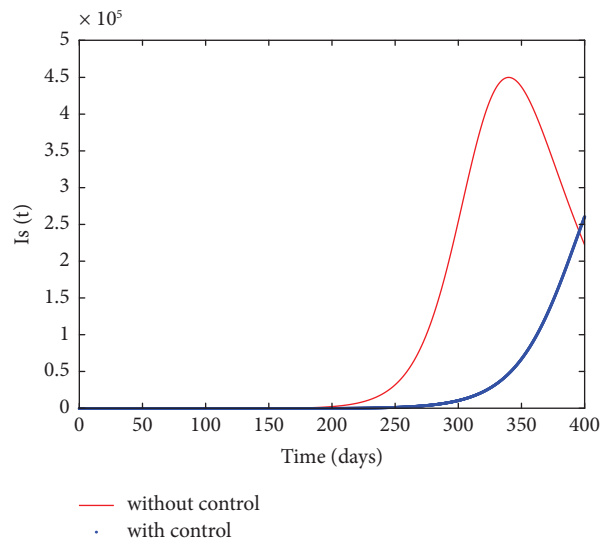


FIGURE 12: Behaviour of the symptomatic individuals with and without the control.

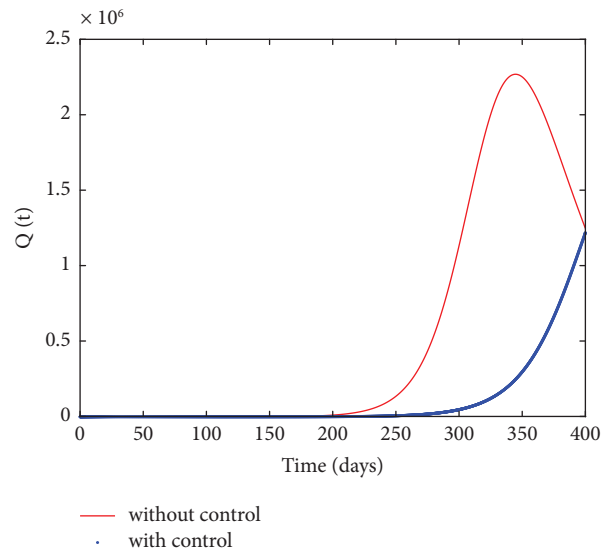


FIGURE 13: Behaviour of the quarantine individuals with and without the control.

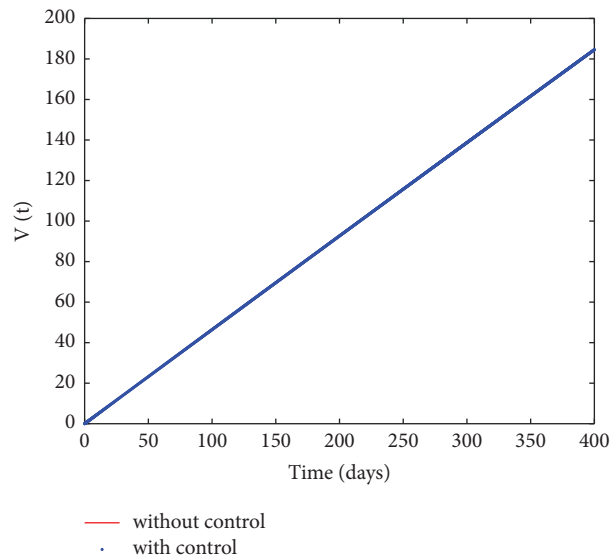


FIGURE 14: Behaviour of the immune individuals with and without the control.

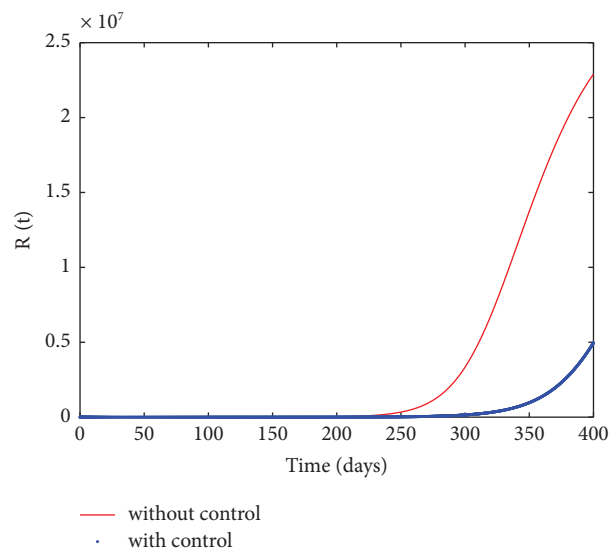


FIGURE 15: Behaviour of the recovered individuals with and without the control.

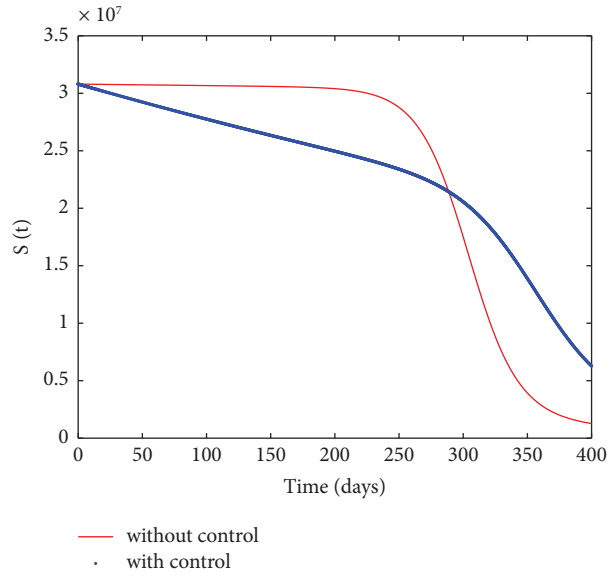


FIGURE 16: Behaviour of the susceptible individuals with and without the vaccination control.

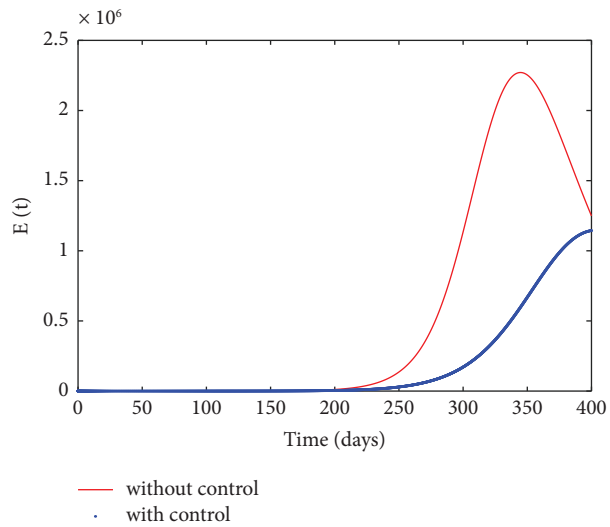


FIGURE 17: Behaviour of the exposed individuals with and without the vaccination control.

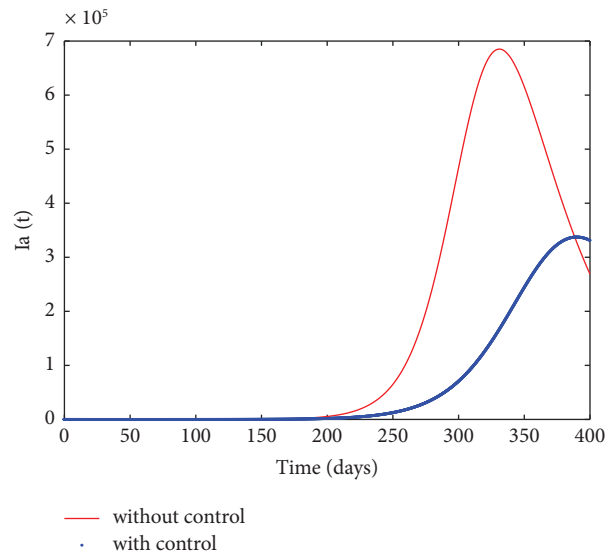


FIGURE 18: Behaviour of the asymptomatic individuals with and without the vaccination control.

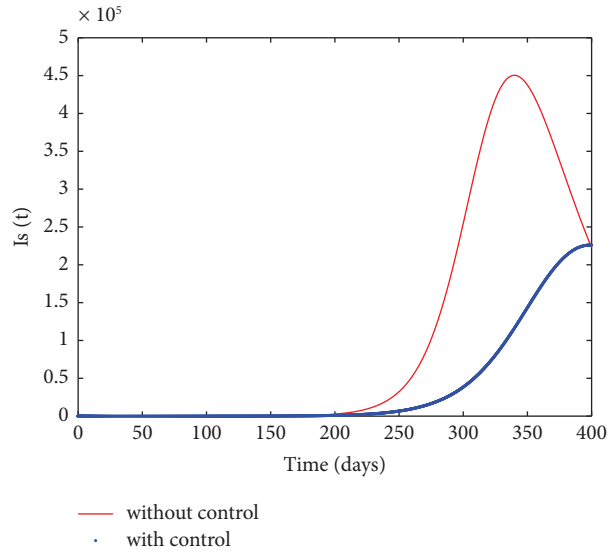


FIGURE 19: Behaviour of the symptomatic individuals with and without the control.

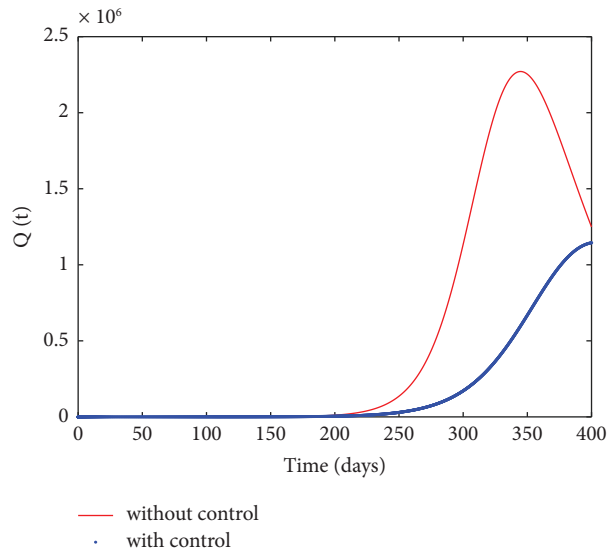


FIGURE 20: Behaviour of the quarantine individuals with and without the vaccination control.

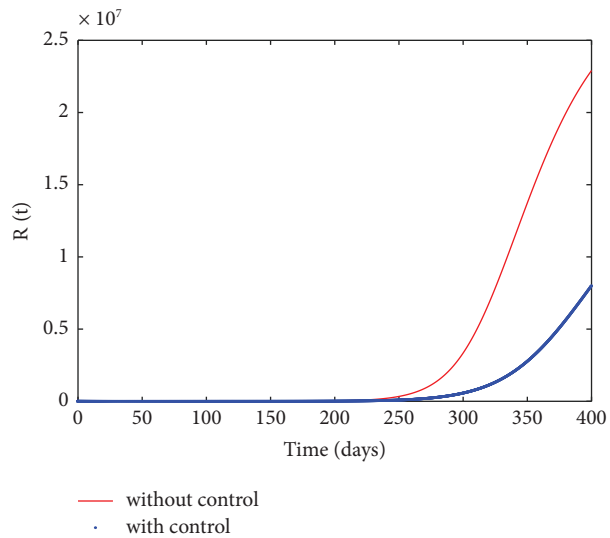


FIGURE 21: Behaviour of the recovered individuals with and without the vaccination control.

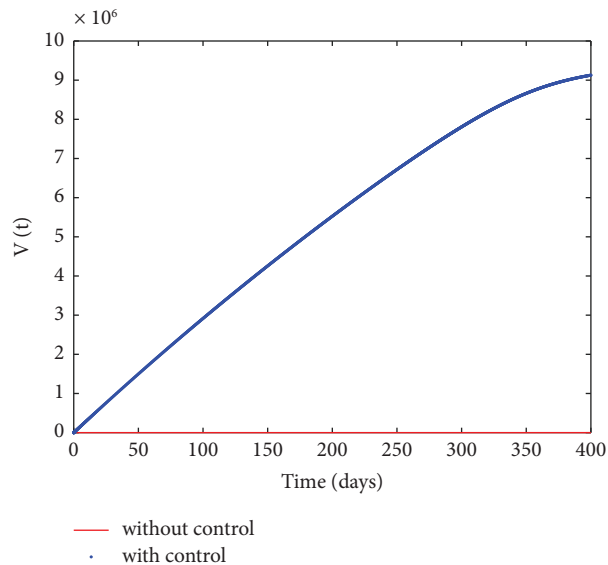


FIGURE 22: Behaviour of the immune individuals with and without the vaccination control.

a high number of individuals that develop immunity to the disease due to the vaccination of susceptible individuals (Figure 22).

8. Conclusion

In this study, the model in [20] has been modified and formulated using the fractional-order derivative defined in the Atangana–Baleanu–Caputo sense. The basic properties such as the equilibrium points, basic reproduction number, and uniqueness of the solutions have been explored. Fractional optimal controls were incorporated into the model to determine appropriate intervention strategies in curbing the spread of the disease. The model was validated using the parameter values given in [20] for a period of 400 days. The MATLAB software fourth-order Runge–Kutta method was used for the simulations. Results of the numerical simulation show that there is a significant number of individuals who become exposed, asymptomatic, symptomatic, quarantine, and recovered when the fractional operator ν is above 0.6. The number of immune individuals increases with a reduction in the fractional operator value from 1 to 0.6. Contrary to the number of immune individuals, the number of susceptible individuals declines as the fractional operator value decreases. The numerical simulation of the optimal control model demonstrates that vaccination and social isolation are both very successful strategies for preventing the spread of the disease. Social isolation had no impact on the immune population, while vaccination controls produced a sizable proportion of disease-immune individuals.

Data Availability

The data supporting the formulation of the mathematical model in this paper are from the Ghana Health Service website: <https://www.ghs.gov.gh/covid19/> which has been referenced in the article.

Disclosure

Previous versions of the work are also available as a preprint on <https://arxiv.org/ftp/arxiv/papers/2201/2201.08689.pdf> [38] and <https://arxiv.org/ftp/arxiv/papers/2201/2201.11659.pdf> [15].

Conflicts of Interest

The authors declare that there are no conflicts of interest.

Acknowledgments

This work was submitted as part of a student thesis at the Kwame Nkrumah University of Science and Technology, Ghana.

References

- [1] World Health Organization (WHO), “Coronavirus disease (COVID-19),” WHO, Geneva, Switzerland, 2021, <https://www.who.int/westernpacific/health-topics/detail/coronavirus>.
- [2] J. Duncan, “Two cases of coronavirus confirmed in Ghana,” 2022, <https://citinewsroom.com/2020/03/two-cases-of-coronavirus-confirmed-in-ghana/>.
- [3] European Centre for Disease Prevention and Control, “Transmission of COVID-19,” 2020, <https://www.ecdc.europa.eu/en/covid-19/latest-evidence/transmission>.
- [4] A. A. Agyeman, K. L. Chin, C. B. Landersdorfer, D. Liew, and R. Ofori-Asenso, “Smell and taste dysfunction in patients with COVID-19: a systematic review and meta – analysis,” *Mayo Clinic Proceedings*, vol. 95, no. 8, pp. 1621–1631, 2020.
- [5] J. Saniasiaya, M. A. Islam, and B. Abdullah, “Prevalence and characteristics of taste disorders in cases of COVID-19: a meta-analysis of 29,349 Patients,” *Otolaryngology - Head and Neck Surgery*, vol. 165, no. 1, pp. 33–42, 2021.
- [6] World Health Organization, “Q&A on coronaviruses (COVID-19),” 2020, <https://www.who.int/emergencies/diseases/novel-coronavirus-2019/question-and-answers-hub/q-a-detail/q-a-coronaviruses>.

- [7] Worldometer, "COVID-19 coronavirus pandemic," 2021, <http://www.worldometers.info/coronavirus>.
- [8] A. Khan, R. Zarin, U. W. Humphries, A. Akgül, A. Saeed, and T. Gul, "Fractional optimal control of COVID-19 pandemic model with generalized Mittag-Leffler function," *Advances in Difference Equations*, vol. 2021, no. 1, p. 387, 2021.
- [9] C. M. A. Pinto and J. A. Tenreiro Machado, "Fractional model for malaria transmission under control strategies," *Computers & Mathematics with Applications*, vol. 66, no. 5, pp. 908–916, 2013.
- [10] N. H. Sweilam, S. M. Al-Mekhlafi, and D. Baleanu, "Optimal control for a fractional tuberculosis infection model including the impact of diabetes and resistant strains," *Journal of Advanced Research*, vol. 17, pp. 125–137, 2019.
- [11] S. Ullah, M. Altaf Khan, M. Farooq, Z. Hammouch, and D. Baleanu, "A fractional model for the dynamics of tuberculosis infection using Caputo-Fabrizio derivative," *Discrete & Continuous Dynamical Systems - S*, vol. 13, no. 3, pp. 975–993, 2020.
- [12] E. Bonyah, W. Chukwu, M. Juga, and F. Fatmawati, "Modeling fractional-order dynamics of Syphilis via Mittag-Leffler law," *AIMS Mathematics*, vol. 6, no. 8, pp. 8367–8389, 2021.
- [13] S. Qureshi and A. Yusuf, "Modeling chickenpox disease with fractional derivatives: from caputo to atangana-baleanu," *Chaos, Solitons & Fractals*, vol. 122, pp. 111–118, 2019.
- [14] I. Owusu-Mensah, L. Akinyemi, B. Oduro, and O. S. Iyiola, "A fractional order approach to modeling and simulations of the novel COVID-19," *Advances in Difference Equations*, vol. 2020, no. 1, p. 683, 2020.
- [15] S. Okyere, J. A. Prah, E. Bonyah, and M. O. Fokuo, "A model of covid-19 with underlying health condition using fraction order derivative," 2020, <https://arxiv.org/ftp/arxiv/papers/2201/2201.11659.pdf>.
- [16] M. A. Bahloul, A. Chahid, and T.-M. Laleg-Kirati, "Fractional-order SEIQRDP model for simulating the dynamics of COVID-19 epidemic," *IEEE Open Journal of Engineering in Medicine and Biology*, vol. 1, pp. 249–256, 2020.
- [17] P. Kumar, V. S. Erturk, and M. Murillo-Arcila, "A new fractional mathematical modelling of COVID-19 with the availability of vaccine," *Results in Physics*, vol. 24, Article ID 104213, 2021.
- [18] A. Mouaouine, A. Boukhouima, K. Hattaf, and N. Yousfi, "A fractional order SIR epidemic model with nonlinear incidence rate," *Advances in Difference Equations*, vol. 2018, no. 1, p. 160, 2018.
- [19] M. A. Khan and A. Atangana, "Modeling the dynamics of novel coronavirus (2019-nCov) with fractional derivative," *Alexandria Engineering Journal*, vol. 59, no. 4, pp. 2379–2389, 2020.
- [20] S. Okyere and J. Ackora-Prah, "An optimal control model of the transmission dynamics of sars - cov - 2 (covid-19) in ghana," 2022, <https://arxiv.org/ftp/arxiv/papers/2201/2201.08224.pdf>.
- [21] B. A. Baba and B. Bilgehan, "Optimal control of a fractional order model for the COVID - 19 pandemic," *Chaos, Solitons & Fractals*, vol. 144, Article ID 110678, 2021.
- [22] K. N. Nabi, P. Kumar, and V. S. Erturk, "Projections and fractional dynamics of COVID-19 with optimal control strategies," *Chaos, Solitons & Fractals*, vol. 145, Article ID 110689, 2021.
- [23] B. Khajji, A. Kouidere, M. Elhia, O. Balatif, and M. Rachik, "Fractional optimal control problem for an age-structured model of COVID-19 transmission," *Chaos, Solitons & Fractals*, vol. 143, Article ID 110625, 2021.
- [24] M. Das and G. P. Samanta, "Optimal control of fractional order COVID-19 epidemic spreading in Japan and India," *Biophysical Reviews and Letters*, vol. 15, no. 4, pp. 207–236, 2020.
- [25] E. Bonyah, A. K. Sagoe, D. Kumar, and S. Deniz, "Fractional optimal control dynamics of coronavirus model with Mittag-Leffler law," *Ecological Complexity*, vol. 45, pp. 100880–945X, 2021.
- [26] N. H. Sweilam, S. M. Al-Mekhlafi, and D. Baleanu, "A hybrid fractional optimal control for a novel Coronavirus (2019-nCov) mathematical model," *Journal of Advanced Research*, vol. 32, pp. 149–160, 2021.
- [27] S. Okyere and J. Ackora-Prah, "A mathematical model of transmission dynamics of SARS-CoV-2 (COVID-19) with an underlying condition of diabetes," *International Journal of Mathematics and Mathematical Sciences*, vol. 2022, Article ID 7984818, 15 pages, 2022.
- [28] A. Atangana and D. Baleanu, "New fractional derivatives with nonlocal and non-singular kernel: t ," *Thermal Science*, vol. 20, no. 2, pp. 763–769, 2016.
- [29] B. P. Moghaddam, S. Yaghoobi, and J. T. Machado, "An extended predictor-corrector algorithm for variable-order fractional delay differential equations," *Journal of Computational and Nonlinear Dynamics*, vol. 1, pp. 1–11, 2016.
- [30] C. Coll, A. Herrero, E. Sanchez, and N. Thome, "A dynamic model for a study of diabetes," *Mathematical and Computer Modelling*, vol. 50, no. 5–6, pp. 713–716, 2009.
- [31] K. C. Patidar, "Nonstandard finite difference methods: recent trends and further developments," *Journal of Difference Equations and Applications*, vol. 22, no. 6, pp. 817–849, 2016.
- [32] J. E. Solís-Pérez, J. F. Gómez-Aguilar, and A. Atangana, "Novel numerical method for solving variable-order fractional differential equations with power, exponential and Mittag-Leffler laws," *Chaos, Solitons & Fractals*, vol. 114, pp. 175–185, 2018.
- [33] Indexmundi, "Ghana birth rate," 2021, <http://www.indexmundi.com>.
- [34] F. Ndaïrou, I. Area, J. J. Nieto, and D. F. M. Torres, "Mathematical modeling of COVID-19 transmission dynamics with a case study of Wuhan," *Chaos, Solitons & Fractals*, vol. 135, Article ID 109846, 2020.
- [35] I. Ahmed, G. U. Modu, A. Yusuf, P. Kumam, and I. Yusuf, "A mathematical model of coronavirus disease (COVID-19) containing asymptomatic and symptomatic classes," *Results in Physics*, vol. 21, Article ID 103776, 2021, <https://www.ncbi.nlm.nih.gov/pmc/articles/PMC7787076/>.
- [36] N. Anggriani, M. Z. Ndi, R. Amelia, W. Suryaningrat, and M. A. Pratama, "A mathematical COVID-19 model considering asymptomatic and symptomatic classes with waning immunity," *Alexandria Engineering Journal*, vol. 61, no. 1, pp. 113–124, 2022.
- [37] Ghana Health Service, "Covid-19 cases," 2021, <https://www.ghs.gov.gh/covid19/>.
- [38] S. Okyere, E. Bonyah, and J. Ackora-Prah, "A fractional differential equation modeling of sars-cov-2 (covid-19) in Ghana," 2022, <https://arxiv.org/abs/2201.08689>.

Research Article

Analytical and Approximate Solutions of the Nonlinear Gas Dynamic Equation Using a Hybrid Approach

Muhammad Nadeem ¹ and Mouad M. H. Ali ²

¹*School of Mathematics and Statistics, Qujing Normal University, Qujing 655011, China*

²*Department of Computer Science and Engineering, Hodeidah University, Al-Hudaydah, Yemen*

Correspondence should be addressed to Muhammad Nadeem; nadeem@mail.qjnu.edu.cn and Mouad M. H. Ali; mouad198080@hoduniv.net.ye

Received 24 August 2022; Revised 24 September 2022; Accepted 28 September 2022; Published 6 April 2023

Academic Editor: Arzu Akbulut

Copyright © 2023 Muhammad Nadeem and Mouad M. H. Ali. This is an open access article distributed under the Creative Commons Attribution License, which permits unrestricted use, distribution, and reproduction in any medium, provided the original work is properly cited.

This paper presents the study of a numerical scheme for the analytical solution of nonlinear gas dynamic equation. We use the idea of Laplace–Carson transform and associate it with the homotopy perturbation method (HPM) for obtaining the series solution of the equation. We show that this hybrid approach is excellent in agreement and converges to the exact solution very smoothly. Further, HPM combined with He’s polynomial is utilized to minimize the numerical simulations in nonlinear conditions that make it easy for the implementation of Laplace–Carson transform. We also exhibit a few graphical solutions to indicate that this approach is extremely reliable and convenient for linear and nonlinear challenges.

1. Introduction

The gas dynamic equation is mathematically modeled by various physical laws such as energy, mass and momentum conservation. Gas is a collection of numerous elements in continuous chaotic motion such as molecules, atoms, ions, etc. The nonlinear gas dynamics equation is used in shock waves, centered rarified waves, contact flows, and connection discontinuities. The study of gas motion and its impact on structures using the principles of fluid dynamics and fluid mechanics is known as “gas dynamic,” and it belongs to the discipline of fluid dynamics [1, 2]. Numerous researchers has studied the gas dynamic equation with different analysis [3, 4]. Srivastava and Saad [5] studied the theory of gas dynamic equation and extended it with different models. Various approaches have been introduced to solve the gas dynamics problems such as fractional reduced transform method [6], Elzaki transform homotopy perturbation approach [7], q -homotopy analysis [8], Adomian decomposition strategy [9], variational iteration method [10, 11], fractional homotopy analysis transform approach [12], homotopy perturbation

method using Laplace transform [13], Homotopy analysis transform method [14] and natural decomposition method [15].

He [16–18] demonstrated the strategy HPM for the solution of nonlinear problems arising in complex models and showed that this approach has an excellent performance in obtaining the series solutions. Some scientists [19, 20] modified this study and coupled it with Laplace transform to achieve the series solution of nonlinear differential problems. Aggarwal and Kumar [21] applied Laplace–Carson to Volterra integro-differential problem of first kind. After that, Kumar and Qureshi [22] received the results of initial value problems with the Caputo derivative in the shape of series and showed the authenticity of this scheme. Thange and Gade [23] studied a few definitions of Laplace–Carson with fractional order and used the convolution theorem which was very complicated to obtain the iterations.

In this article, we study a novel scheme Laplace–Carson homotopy perturbation method (\mathcal{L}_c -PTM) which is constructed on the basis of Laplace–Carson and HPM. We point out that the present scheme is very convenient to use and reveals the results in the shape of a series. This approach is an independent

convolution theorem that may face complications during the calculation of iterations. This article is designed as In Section 2, we present the definition of Laplace–Carson transform with basic propositions. In Section 3, we study the fundamental concept of HPM which is used to split the nonlinear elements. In Section 4, we present the numerical applications to show the ability of \mathcal{L}_c -PTM, and finally, we discuss the obtained results and conclusion in Sections 5 and 6 respectively.

2. Laplace and Laplace–Carson Transform

Definition 1. Consider $f(t)$ be a function with $t \geq 0$, so

$$\mathcal{L}\{f(t)\} = F(s) = \theta \int_0^\infty f(t)e^{-st} dt, \quad (1)$$

$$\mathcal{L}_c^{-1}\{R(\theta)\} = g(t), \quad \mathcal{L}_c^{-1} \text{ is said to be inverse Laplace – Carson transform.} \quad (3)$$

Definition 3. If $g(t) = t^m$, then Laplace–Carson transform is utilized as

$$\mathcal{L}_c\{g(t)\} = R(\theta) = \frac{m!}{\theta^m}. \quad (4)$$

Properties 1. If $\mathcal{L}_c\{g(t)\} = R(\theta)$, then it has the following differential properties [21, 23].

- (a) $\mathcal{L}_c\{g'(t)\} = \theta R(\theta) - \theta G(0)$,
- (b) $\mathcal{L}_c\{g''(t)\} = \theta^2 R(\theta) - \theta^2 G(0) - \theta G'(0)$,
- (c) $\mathcal{L}_c\{g^m(t)\} = \theta^m R(\theta) - \theta^m G(0) - \theta^{m-1} G'(0) - \dots - \theta G^{m-1}(0)$.

3. Fundamental Concept of HPM

This segment presents the concept of HPM with the consideration of a nonlinear functional equation [24, 25]. Consider

$$T(\vartheta) - g(h) = 0, \quad h \in \Omega. \quad (5)$$

With conditions

$$S\left(\vartheta, \frac{\partial \vartheta}{\partial n}\right) = 0, \quad h \in \Gamma. \quad (6)$$

Here T and S are identified as general functional and boundary operator respectively, $g(h)$ is source term with Γ as a interval of the domain Ω . We can now split T such that T_1 is said to be a linear and T_2 be a nonlinear operator. Thus, we can write equation (5) as

is said to Laplace transform and s is transform function of θ .

Definition 2. Aggarwal and Kumar [21] studied a theory such that

$$\mathcal{L}_c\{g(t)\} = R(\theta) = \theta \int_0^\infty g(t)e^{-\theta t} dt, \quad k_1 \leq \theta \leq k_2. \quad (2)$$

Here k_1 and k_2 are arbitrary constants and \mathcal{L}_c is termed as Laplace–Carson transform. Now, if $R(\theta)$ is the Laplace–Carson transform of a function $g(t)$ then $g(t)$ is the inverse of $R(\theta)$ so that,

$$T_1(\vartheta) + T_2(\vartheta) - g(h) = 0. \quad (7)$$

Consider $\vartheta(h, \theta): \Omega \times [0, 1] \rightarrow \mathbb{H}$ such that it is suitable for

$$H(\vartheta, \theta) = (1 - \theta)[T_1(\vartheta) - T_1(\vartheta_0)] + \theta[T_1(\vartheta) - T_2(\vartheta) - g(h)], \quad (8)$$

or

$$H(\vartheta, \theta) = T_1(\vartheta) - T_1(\vartheta_0) + \theta[T_2(\vartheta) - g(h)] = 0. \quad (9)$$

Here $\theta \in [0, 1]$ is homotopy element and ϑ_0 is an initial approximation of equation (5), which is appropriate for the boundary conditions. The study of HPM declares that θ is assumed as a minimal variable and the result of equation (5) can be expressed in the shape of θ .

$$\vartheta = \vartheta_0 + \theta\vartheta_1 + \theta^2\vartheta_2 + \theta^3\vartheta_3 + \dots = \sum_{i=0}^\infty \theta^i \vartheta_i. \quad (10)$$

Consider $\theta = 1$, we get particular of equation (10) as

$$\vartheta = \lim_{\theta \rightarrow 1} \vartheta = \vartheta_0 + \vartheta_1 + \vartheta_2 + \vartheta_3 + \dots = \sum_{i=0}^\infty \vartheta_i. \quad (11)$$

The nonlinear terms are obtained as

$$T_2\vartheta(x, t) = \sum_{n=0}^\infty \theta^n H_n(\vartheta), \quad (12)$$

where $H_n(\vartheta)$ is defined as

$$H_n(\vartheta_0 + \vartheta_1 + \dots + \vartheta_n) = \frac{1}{n!} \frac{\partial^n}{\partial \theta^n} \left(T_2 \left(\sum_{i=0}^\infty \theta^i \vartheta_i \right) \right)_{\theta=0}, \quad n = 0, 1, 2, \dots \quad (13)$$

This result in equation (12) generally converges as the rate of convergence depends on the nonlinear operator T_2 .

4. Numerical Applications

In this segment, we apply the scheme of \mathcal{L}_c -PTM to obtain the analytical results of nonlinear gas dynamic equation. We express that this approach generates the series solution only after iterations with excellent accuracy.

4.1. Example 1. Consider the homogenous and nonlinear gas dynamic equation

$$\frac{\partial \vartheta}{\partial t} + \vartheta \frac{\partial \vartheta}{\partial x} - \vartheta(1 - \vartheta) = 0. \tag{14}$$

With initial condition

$$\vartheta(x, 0) = e^{-x}. \tag{15}$$

Using the Laplace–Carson transform to equation (14), we get

$$\begin{aligned} \mathcal{L}_c \left[\frac{\partial \vartheta}{\partial t} + \vartheta \frac{\partial \vartheta}{\partial x} - \vartheta(1 - \vartheta) \right] &= 0, \\ \mathcal{L}_c \left[\frac{\partial \vartheta}{\partial t} \right] &= -\mathcal{L}_c \left[\vartheta \frac{\partial \vartheta}{\partial x} - \vartheta(1 - \vartheta) \right] = 0. \end{aligned} \tag{16}$$

Employing the definition of Laplace–Carson transform, we get

$$\theta \vartheta(x, \theta) - \theta \vartheta(x, 0) = -\mathcal{L}_c \left[\vartheta \frac{\partial \vartheta}{\partial x} - \vartheta(1 - \vartheta) \right]. \tag{17}$$

Which may be solved further as,

$$\vartheta(x, \theta) = \vartheta(x, 0) - \frac{1}{\theta} \mathcal{L}_c \left\{ \vartheta \frac{\partial \vartheta}{\partial x} - \vartheta + \vartheta^2 \right\}. \tag{18}$$

Applying inverse Laplace–Carson transform, we get

$$\vartheta(x, t) = \vartheta(x, 0) - \mathcal{L}_c^{-1} \left[\frac{1}{\theta} \mathcal{L}_c \left\{ \vartheta \frac{\partial \vartheta}{\partial x} - \vartheta + \vartheta^2 \right\} \right]. \tag{19}$$

Utilizing HPM on equation (19), we get

$$\sum_{n=0}^{\infty} p^n \vartheta_n(x, t) = \vartheta(x, 0) - p \mathcal{L}_c^{-1} \left[\frac{1}{\theta} \mathcal{L}_c \left\{ \sum_{n=0}^{\infty} p^n \vartheta_n(x, t) \frac{\partial}{\partial x} \sum_{n=0}^{\infty} p^n \vartheta_n(x, t) - \sum_{n=0}^{\infty} p^n \vartheta_n(x, t) + \sum_{n=0}^{\infty} p^n \vartheta_n^2(x, t) \right\} \right]. \tag{20}$$

On comparing, the following iterations can be obtained,

$$\begin{aligned} p^0: \vartheta_0(x, t) &= e^{-x}, \\ p^1: \vartheta_1(x, t) &= \mathcal{L}_c^{-1} \left[\frac{1}{\theta} \mathcal{L}_c \left\{ \vartheta_0 \frac{\partial \vartheta_0}{\partial x} - \vartheta_0 + \vartheta_0^2 \right\} \right] = e^{-x} \frac{t^2}{2!}, \\ p^2: \vartheta_2(x, t) &= \mathcal{L}_c^{-1} \left[\frac{1}{\theta} \mathcal{L}_c \left\{ \vartheta_0 \frac{\partial \vartheta_1}{\partial x} + \vartheta_1 \frac{\partial \vartheta_0}{\partial x} - \vartheta_1 + 2\vartheta_0 \vartheta_1 \right\} \right] = e^{-x} \frac{t^3}{3!}, \\ p^3: \vartheta_3(x, t) &= \mathcal{L}_c^{-1} \left[\frac{1}{\theta} \mathcal{L}_c \left\{ \vartheta_0 \frac{\partial \vartheta_2}{\partial x} + \vartheta_1 \frac{\partial \vartheta_1}{\partial x} + \vartheta_2 \frac{\partial \vartheta_0}{\partial x} - \vartheta_2 + \vartheta_1^2 + 2\vartheta_0 \vartheta_2 \right\} \right] = e^{-x} \frac{t^4}{4!}, \\ &\vdots \end{aligned} \tag{21}$$

Hence the solution can be expressed as

$$\begin{aligned} \vartheta(x, t) &= \vartheta_0(x, t) + \vartheta_1(x, t) + \vartheta_2(x, t) + \vartheta_3(x, t) + \dots, \\ \vartheta(x, t) &= e^{-x} + e^{-x} \frac{t^2}{2!} + e^{-x} \frac{t^3}{3!} + e^{-x} \frac{t^4}{4!} + \dots, \\ \vartheta(x, t) &= e^{t-x}. \end{aligned} \tag{22}$$

4.2. *Example 2.* Consider the non-homogenous and non-linear gas dynamic equation

$$\frac{\partial \vartheta}{\partial t} + \vartheta \frac{\partial \vartheta}{\partial x} - \vartheta(1 - \vartheta) = -e^{t-x}. \quad (23)$$

With initial condition

$$\vartheta(x, 0) = 1 - e^{-x}. \quad (24)$$

Using the Laplace–Carson transform to equation (23), we get

$$\begin{aligned} \mathcal{L}_c \left[\frac{\partial \vartheta}{\partial t} + \vartheta \frac{\partial \vartheta}{\partial x} - \vartheta(1 - \vartheta) \right] &= -\mathcal{L}_c [e^{t-x}], \\ \mathcal{L}_c \left[\frac{\partial \vartheta}{\partial t} \right] &= -\mathcal{L}_c [e^{t-x}] - \mathcal{L}_c \left[\vartheta \frac{\partial \vartheta}{\partial x} - \vartheta(1 - \vartheta) \right]. \end{aligned} \quad (25)$$

Employing the definition of Laplace–Carson transform, we get

$$\theta \vartheta(x, 0) - \theta \vartheta(x, 0) = -\frac{e^{-x}}{\theta - 1} - \mathcal{L}_c \left[\vartheta \frac{\partial \vartheta}{\partial x} - \vartheta(1 - \vartheta) \right]. \quad (26)$$

Which may be solved further as,

$$\vartheta(x, \theta) = \vartheta(x, 0) - \frac{e^{-x}}{\theta - 1} - \frac{1}{\theta} \mathcal{L}_c \left\{ \vartheta \frac{\partial \vartheta}{\partial x} - \vartheta + \vartheta^2 \right\}. \quad (27)$$

Applying inverse Laplace–Carson transform, we get

$$\begin{aligned} \vartheta(x, t) &= \vartheta(x, 0) - e^{-x} \mathcal{L}_c^{-1} \left[\frac{1}{\theta - 1} \right] - \mathcal{L}_c^{-1} \left[\frac{1}{\theta} \mathcal{L}_c \left\{ \vartheta \frac{\partial \vartheta}{\partial x} - \vartheta + \vartheta^2 \right\} \right], \\ \vartheta(x, t) &= \vartheta(x, 0) - e^{t-x} + e^{-x} - \mathcal{L}_c^{-1} \left[\frac{1}{\theta} \mathcal{L}_c \left\{ \vartheta \frac{\partial \vartheta}{\partial x} - \vartheta + \vartheta^2 \right\} \right], \\ \vartheta(x, t) &= 1 - e^{-x} - e^{t-x} + e^{-x} - \mathcal{L}_c^{-1} \left[\frac{1}{\theta} \mathcal{L}_c \left\{ \vartheta \frac{\partial \vartheta}{\partial x} - \vartheta + \vartheta^2 \right\} \right], \\ \vartheta(x, t) &= 1 - e^{t-x} - \mathcal{L}_c^{-1} \left[\frac{1}{\theta} \mathcal{L}_c \left\{ \vartheta \frac{\partial \vartheta}{\partial x} - \vartheta + \vartheta^2 \right\} \right]. \end{aligned} \quad (28)$$

Utilizing HPM on equation (28), we get

$$\sum_{n=0}^{\infty} p^n \vartheta_n(x, t) = 1 - e^{t-x} - p \mathcal{L}_c^{-1} \left[\frac{1}{\theta} \mathcal{L}_c \left\{ \sum_{n=0}^{\infty} p^n \vartheta_n(x, t) \frac{\partial}{\partial x} \sum_{n=0}^{\infty} p^n \vartheta_n(x, t) - \sum_{n=0}^{\infty} p^n \vartheta_n(x, t) + \sum_{n=0}^{\infty} p^n \vartheta_n^2(x, t) \right\} \right]. \quad (29)$$

On comparing, the following iterations can be obtained,

$$\begin{aligned} p^0: \vartheta_0(x, t) &= 1 - e^{t-x}, \\ p^1: \vartheta_1(x, t) &= \mathcal{L}_c^{-1} \left[\frac{1}{\theta} \mathcal{L}_c \left\{ \vartheta_0 \frac{\partial \vartheta_0}{\partial x} - \vartheta_0 + \vartheta_0^2 \right\} \right] = 0, \\ p^2: \vartheta_2(x, t) &= \mathcal{L}_c^{-1} \left[\frac{1}{\theta} \mathcal{L}_c \left\{ \vartheta_0 \frac{\partial \vartheta_1}{\partial x} + \vartheta_1 \frac{\partial \vartheta_0}{\partial x} - \vartheta_1 + 2\vartheta_0 \vartheta_1 \right\} \right] = 0, \\ p^3: \vartheta_3(x, t) &= \mathcal{L}_c^{-1} \left[\frac{1}{\theta} \mathcal{L}_c \left\{ \vartheta_0 \frac{\partial \vartheta_2}{\partial x} + \vartheta_1 \frac{\partial \vartheta_1}{\partial x} + \vartheta_2 \frac{\partial \vartheta_0}{\partial x} - \vartheta_2 + \vartheta_1^2 + 2\vartheta_0 \vartheta_2 \right\} \right] = 0, \\ &\vdots \end{aligned} \quad (30)$$

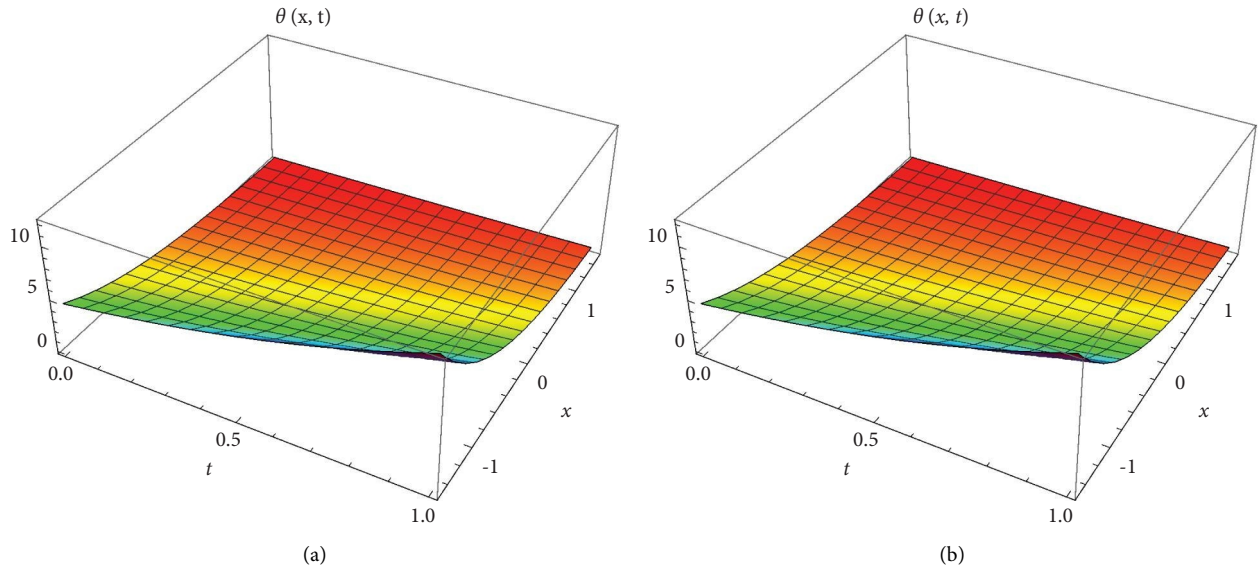


FIGURE 1: The surfaces solution of gas dynamic equation. (a) The approximate surface solution of $\vartheta(x, t)$. (b) The exact surface solution of $\vartheta(x, t)$.

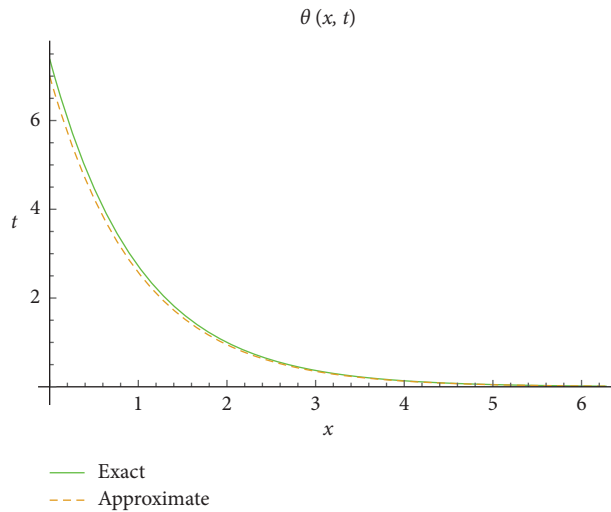


FIGURE 2: 2D plot for $\vartheta(x, t)$ with various parameter of t .

Hence the solution can be expressed as

$$\begin{aligned} \vartheta(x, t) &= \vartheta_0(x, t) + \vartheta_1(x, t) + \vartheta_2(x, t) + \vartheta_3(x, t) + \dots, \\ \vartheta(x, t) &= 1 - e^{t-x} + 0 + 0 + \dots, \\ \vartheta(x, t) &= 1 - e^{t-x}. \end{aligned} \tag{31}$$

5. Results and Discussion

In this portion, we demonstrate the graphical representation of nonlinear gas dynamic equation. Figure 1(a)

represents the the approximate solution obtained by \mathcal{L}_c -PTM and Figure 1(b) represents the exact solution of the nonlinear gas dynamic equation. In Figure 1, we compare these graphical illustrations at $-1.5 \leq x \leq 1.5$ and $0 \leq t \leq 1$

TABLE 1: Absolute error among the approximate and exact solution at $t = 0.5$ and 1 .

x	Approximate values at $t = 0.5$	Approximate values at $t = 1$	Exact values at $t = 1$	Absolute error at $t = 1$
0.1	1.49157	2.4506	2.4596	0.0464
0.2	1.34963	2.1274	2.22554	0.00814
0.3	1.22119	2.00638	2.01375	0.00737
0.4	1.10498	1.81545	1.82212	0.00667
0.5	0.999828	1.64269	1.64872	0.00603
0.6	0.904682	1.48636	1.49182	0.00546
0.7	0.81859	1.34492	1.34986	0.00494
0.8	0.740691	1.21693	1.2214	0.00447
0.9	0.670205	1.10113	1.10517	0.00404
1.0	0.606426	0.99634	1	0.00366

and observe that both surface solutions are in full agreement. Figure 2 represents the graphical error between the solutions obtained by \mathcal{L}_c -PTM and the exact solutions at $0 \leq x \leq \pi$. Table 1 presents the analysis of the absolute error at different times t and shows that the obtained values become closer to the exact solution with the increase of time. Finally, the figures and table demonstrate that our approach has high authenticity of performance and provides fast convergence results towards the exact solution.

6. Conclusion

In this article, we have successfully applied a new scheme \mathcal{L}_c -PTM to determine the approximate results of gas dynamic equation. We obtained these results in the shape of series instead of discretization, linearization, or assumptions. We observe that when HPM is used with Laplace–Carson transform, we can obtain a rapid convergent series solution with less computation. We compute these iterations with the help of Mathematica Software 11.0.1. We also compare the approximate and the exact solution results and provide the absolute error to examine the efficiency of our suggested approach. 2D plot and 3D surface solutions show that we have strong agreement with the results of gas dynamic equation. Therefore, we can say that \mathcal{L}_c -PTM is more efficient and appropriate than other schemes. This approach is also applicable to other nonlinear problems such as fractional partial differential equations and can be expanded in a variety of scientific and engineering applications in the future.

Data Availability

This article contains all the data.

Conflicts of Interest

This article have no conflict of interest.

References

- [1] J. Bonazebi Yindoula, S. Mikamona Mayembo, and G. Bissanga, “Application of Laplace variation iteration method to solving the nonlinear gas dynamics equation,” *American Journal of Mathematical and Computer Modelling*, vol. 5, no. 4, pp. 127–133, 2020.
- [2] R. Shah, A. Saad Alshehry, and W. Weera, “A semi-analytical method to investigate fractional-order gas dynamics equations by Shehu transform,” *Symmetry*, vol. 14, no. 7, p. 1458, 2022.
- [3] S. Kumar, H. Kocak, and A. Yildirim, “A fractional model of gas dynamics equations and its analytical approximate solution using Laplace transform,” *Zeitschrift für Naturforschung A*, vol. 67, no. 6-7, pp. 389–396, 2012.
- [4] K. M. Saad, Al, M. S. Mohamed, and X.-J. Yang, “Optimal q-homotopy analysis method for time-space fractional gas dynamics equation,” *The European Physical Journal Plus*, vol. 132, no. 1, pp. 23–11, 2017.
- [5] H. M. Srivastava and K. M. Saad, “Some new models of the time-fractional gas dynamics equation,” *Advanced Mathematical Models and Applications*, vol. 3, no. 1, pp. 5–17, 2018.
- [6] M. Tamsir and V. K. Srivastava, “Revisiting the approximate analytical solution of fractional-order gas dynamics equation,” *Alexandria Engineering Journal*, vol. 55, no. 2, pp. 867–874, 2016.
- [7] Bhadane and V. Pradhan, “Elzaki transform homotopy perturbation method for solving gas dynamics equation,” *International Journal of Renewable Energy Technology*, vol. 02, no. 12, pp. 260–264, 2013.
- [8] O. S. Iyiola, “On the solutions of non-linear time-fractional gas dynamic equations: an analytical approach,” *International Journal of Pure and Applied Mathematics*, vol. 98, no. 4, pp. 491–502, 2015.
- [9] D. J. Evans and H. Bulut, “A new approach to the gas dynamics equation: an application of the decomposition method,” *International Journal of Computer Mathematics*, vol. 79, no. 7, pp. 817–822, 2002.
- [10] A. Nikkar, “A new approach for solving gas dynamic equation,” *Acta Technica Corviniensis - Bulletin of Engineering*, vol. 5, no. 4, p. 113, 2012.
- [11] H. Jafari, H. Hosseinzadeh, and E. Salehpour, “A new approach to the gas dynamics equation: an application of the variational iteration method,” *Applied Mathematical Sciences*, vol. 2, no. 48, pp. 2397–2400, 2008.
- [12] S. Kumar and M. M. Rashidi, “New analytical method for gas dynamics equation arising in shock fronts,” *Computer Physics Communications*, vol. 185, no. 7, pp. 1947–1954, 2014.
- [13] J. Singh and D. Kumar, “Homotopy perturbation algorithm using Laplace transform for gas dynamics equation,” *Journal of Applied Mathematics, Statistics and Informatics*, vol. 8, no. 1, pp. 55–61, 2012.
- [14] M. S. Mohamed, F. Al-Malki, and M. Al-Humyani, “Homotopy analysis transform method for timespace

- fractional gas dynamics equation,” *General Mathematics Notes*, vol. 24, no. 1, pp. 1–16, 2014.
- [15] S. Maitama and S. M. Kurawa, “An efficient technique for solving gas dynamics equation using the natural decomposition method,” *International Mathematical Forum*, vol. 9, pp. 1177–1190, 2014.
- [16] J.-H. He, “Homotopy perturbation method: a new nonlinear analytical technique,” *Applied Mathematics and Computation*, vol. 135, no. 1, pp. 73–79, 2003.
- [17] J.-H. He, “Addendum: new interpretation of homotopy perturbation method,” *International Journal of Modern Physics B*, vol. 20, no. 18, pp. 2561–2568, 2006.
- [18] J.-H. He, “An elementary introduction to the homotopy perturbation method,” *Computers & Mathematics with Applications*, vol. 57, no. 3, pp. 410–412, 2009.
- [19] S. Gupta, D. Kumar, and J. Singh, “Analytical solutions of convection–diffusion problems by combining laplace transform method and homotopy perturbation method,” *Alexandria Engineering Journal*, vol. 54, no. 3, pp. 645–651, 2015.
- [20] S. A. Khuri and A. Sayfy, “A Laplace variational iteration strategy for the solution of differential equations,” *Applied Mathematics Letters*, vol. 25, no. 12, pp. 2298–2305, 2012.
- [21] S. Aggarwal and S. Kumar, “Laplace-carson transform for the primitive of convolution type volterra integro-differential equation of first kind,” *International Journal of Research and Innovation in Applied Science*, vol. 8, no. 6, pp. 2454–6194, 2020.
- [22] P. Kumar and S. Qureshi, “Laplace-carson integral transform for exact solutions of non-integer order initial value problems with caputo operator,” *Journal of Applied Mathematics and Computational Mechanics*, vol. 19, no. 1, pp. 57–66, 2020.
- [23] T. Thange and A. Gade, “Laplace-carson transform of fractional order,” *Malaya Journal of Matematik*, vol. 8, no. 4, pp. 2253–2258, 2020.
- [24] K. Wang, “He’s frequency formulation for fractal nonlinear oscillator arising in a microgravity space,” *Numerical Methods for Partial Differential Equations*, vol. 37, no. 2, pp. 1374–1384, 2021.
- [25] M. Nadeem and F. Li, “He–Laplace method for nonlinear vibration systems and nonlinear wave equations,” *Journal of Low Frequency Noise, Vibration and Active Control*, vol. 38, no. 3-4, pp. 1060–1074, 2019.

Research Article

Obtaining the Soliton Type Solutions of the Conformable Time-Fractional Complex Ginzburg–Landau Equation with Kerr Law Nonlinearity by Using Two Kinds of Kudryashov Methods

Arzu Akbulut 

Bursa Uludag University, Faculty of Arts and Science, Department of Mathematics, Bursa, Turkey

Correspondence should be addressed to Arzu Akbulut; ayakut1987@hotmail.com

Received 6 September 2022; Revised 26 October 2022; Accepted 24 November 2022; Published 4 February 2023

Academic Editor: Gaetano Luciano

Copyright © 2023 Arzu Akbulut. This is an open access article distributed under the Creative Commons Attribution License, which permits unrestricted use, distribution, and reproduction in any medium, provided the original work is properly cited.

The main idea of this study is to obtain the soliton-type solutions of the conformable time-fractional complex Ginzburg–Landau equation with Kerr law nonlinearity. For this aim, the generalized and modified Kudryashov methods are applied to the given model. The reason for using a conformable derivative is that the chain rule can be applied to this derivative. Thus, using the suitable wave transform, the given equation is converted into an ordinary differential equation. Then, the proposed methods are applied to the reduced equation. According to our results, both of the used methods are effective and powerful. Finally, 3D and contour plots are given for some results with suitable variables. Our findings in this paper are critical for explaining a wide range of scientific and physical applications. According to our knowledge, our results are new in the literature.

1. Introduction

The exact solutions of the nonlinear partial differential equations (NLPDEs) have an important place in different fields of science, such as fluid mechanics, plasma physics, solid-state physics, and optical fibers. This being the case, many methods were discovered to solve nonlinear partial differential equations, for example, the method of undetermined coefficients [1], the Riccati equation mapping approach [2], the trial equation method [3], the finite

element method [4], the extended trial approach [5], the Petrov–Galerkin method [6], the unified and \exp_a function methods [7], the modified extended tanh expansion method [8], the modified simple procedure [9], the exponential rational function procedure [10], the Kudryashov method [11], the ansatz method [12], and so on.

In this study, the following equation, called the conformable time-fractional complex Ginzburg–Landau equation, will be considered [13]:

$$i q_t^\delta + \epsilon q_{xx} + \lambda F(|q|^2)q - (|q|^2 q^*)^{-1} \left[\rho |q|^2 (|q|^2)_{xx} - \sigma [(|q|^2)_x]^2 \right] - \epsilon q = 0, \quad (1)$$

where $\delta \in (0, 1]$ represents the conformable derivative, $q(x, t)$ is a complex-valued function, the spatial coordinate is represented by x and the temporal coordinate is represented by t . The group velocity dispersions are represented by ϵ and λ , the perturbation effects are represented by ρ , σ , and ϵ . $F(|q|^2)$ is

a function of $|q|^2$ and F is a real-valued algebraic function that must have the smoothness of the function $F(|q|^2)q: \mathbb{C} \rightarrow \mathbb{C}$. When the complex plane \mathbb{C} is assumed as 2D linear space \mathbb{R}^2 , the $F(|q|^2)q$ is k times continuously differentiable, namely, $F(|q|^2)q \in \cup_{a,b=1}^{\infty} \mathbb{C}^k(-b, b) \times (-a, a; \mathbb{R}^2)$.

In literature, lots of researchers obtained the exact solutions of the given model with the different types of nonlinearity. Some researchers obtained the exact solutions of the generalized derivative of the given model for example Kudryashov applied the first integral method to the equation in [14], Das et al. applied the F-expansion to the model in [15], the modified (G'/G) -expansion method is applied to the model by Wang et al. in [16], the modified Jacobi elliptic expansion method is applied by Hosseini et al. in [17], Hosseini et al. implemented Kudryashov and exponential methods to the model including the parabolic nonlinearity in [18]. Some researchers obtained the exact solutions of equation (1) with different kinds of fractional derivatives, for example, Tozar obtained the analytical solutions of the conformable time-fractional complex Ginzburg–Landau equation with the help of the $(1/G')$ method in [19], optical solutions were discovered with the help of the generalized exponential rational function method in [20], Sulaiman et al. explored the optical solitons with the help of the extended sinh-Gordon equation expansion method in [21], the form of the space-time conformable fractional complex Ginzburg–Landau equation is handled in [22], Sadaf et al. applied the $(w(\xi)/2)$ method to the model with the different types of senses as the conformable, beta, truncated derivatives in [23].

1.1. The Conformable Derivative. In literature, fractional derivatives have an essential role, so many definitions of fractional derivatives are discovered, for example, Riemann–Liouville, Grunwald–Letnikov, the Caputo, Atangana–Baleanu, and modified Riemann–Liouville derivatives [24, 25]. In this study, the conformable derivative will be used, which is developed by Khalil et al. [26]. An important feature of this derivative is that we can apply the chain rule so we can reduce nonlinear differential equations to ordinary differential equations with the help of wave transforms. Basic definitions of the conformable derivative are given as follows:

When $\psi: (0, \infty) \rightarrow \mathbb{R}$, the conformable derivative of ψ of order $\delta, 0 < \delta < 1$, is defined as follows [27, 28]:

$$T_\delta(\psi)(t) = \lim_{\epsilon \rightarrow 0} \frac{\psi(t + \epsilon t^{1-\delta}) - \psi(t)}{\epsilon}, \quad (2)$$

for all $t > 0$. The basic properties of the conformable derivative are given as follows [29–31]:

- (1) $T_\delta(a\psi + b\varphi) = aT_\delta(\psi) + bT_\delta(\varphi)$, for all $a, b \in \mathbb{R}$
- (2) $T_\delta(t^\alpha) = \alpha t^{\alpha-\delta}$, for all $\alpha \in \mathbb{R}$
- (3) $T_\delta(\psi\varphi) = \psi T_\delta(\varphi) + \varphi T_\delta(\psi)$
- (4) $T_\delta(\psi/\varphi) = (\varphi T_\delta(\psi) - \psi T_\delta(\varphi))/\varphi^2$
- (5) If ψ is differentiable, then $T_\delta(\psi)(t) = t^{1-\delta} d\psi/dt$
- (6) $\psi(t) = \lambda$, $T_\delta(\lambda) = 0$, for all constant functions
- (7) Chain rule: Let $\psi, \varphi: (0, \infty) \rightarrow \mathbb{R}$ be a differentiable and δ -differentiable function then the chain rule is given by the following:

$$T_\delta(\psi \circ \varphi)(t) = t^{1-\alpha} \varphi'(t) \psi'(\varphi(t)). \quad (3)$$

In this paper, the conformable time-fractional complex Ginzburg–Landau equation with Kerr law was solved by two procedures, namely, the generalized Kudryashov and the modified Kudryashov procedures. For this aim, the main ideas of generalized Kudryashov and the modified Kudryashov procedures were in Section 2. Then, these procedures were applied to the given model, and 3D and contour plots of obtained solutions were given in Section 3. Finally, conclusions were given.

2. The Procedures

In this section, the used procedures will be given. We take into consideration a general nonlinear differential equation in the following form:

$$\Phi\left(q, \frac{\partial^\delta q}{\partial t^\delta}, \frac{\partial q}{\partial x}, \frac{\partial^{2\delta} q}{\partial t^{2\delta}}, \frac{\partial^2 u}{\partial x^2}, \dots\right) = 0, \quad (4)$$

where $q = q(x, t)$ is a complex-valued function and δ represents a conformable derivative. If we apply the following wave transformation to equation (4):

$$q(x, t) = u(\zeta) e^{i\varphi}, \quad (5)$$

where $\zeta = x - vt^\delta/\delta$ and $\varphi = -\kappa x + \omega t^\delta/\delta + \eta$, the following ordinary differential equation (ODE) is obtained:

$$\phi(u, u', u'', \dots) = 0, \quad (6)$$

here prime represents the differentiation of u with respect to ζ .

2.1. The Generalized Kudryashov Procedure. According to the method, we assume $u(\zeta)$ as follows (32, 33):

$$u(\zeta) = \frac{\sum_{n=0}^N a_n \Psi^n(\zeta)}{\sum_{m=0}^M b_m \Psi^m(\zeta)}, \quad (7)$$

where a_n, b_m ($n = 0, 1, \dots, N, m = 0, 1, \dots, M$) are constants and they should be $a_N \neq 0, b_M \neq 0$ and the following ODE is satisfied by $\psi(\zeta)$:

$$\frac{d\psi}{d\zeta} = \psi^2(\zeta) - \psi(\zeta), \quad (8)$$

and $\psi(\zeta)$ is given as follows:

$$\psi(\xi) = \frac{1}{1 + \chi e^\xi}, \quad \chi \text{ is integration constant}, \quad (9)$$

N and M are calculated by the homogeneous balance principle at (6). We can calculate a polynomial of ψ by substituting equation (7) into equation (6) without ignoring equation (8). Then, all the coefficients of the polynomial ψ are set to zero. If the obtained system is solved, the values of the $a_n, b_m, \kappa, v, \omega$ are obtained. Finally, the soliton-type solutions of the given model are obtained.

2.2. *The Modified Kudryashov Procedure.* According to the method, the solutions of equation (6) are assumed as follows [34–36]:

$$u(\zeta) = \sum_{m=0}^M \omega_m (\psi(\zeta))^m, \quad \omega_M \neq 0, \quad (10)$$

where $\omega_m (m = 0, 1, \dots, M)$ are constants that will be determined later, M is calculated by the homogeneous balance principle, and the function $\psi(\zeta)$ is given by the following:

$$\psi(\zeta) = \frac{1}{1 + \chi a^\zeta}, \quad (11)$$

where (11) satisfies the following ODE:

$$\psi'(\zeta) = (\psi^2(\zeta) - \psi(\zeta)) \ln a. \quad (12)$$

Substituting equation (10) into equation (6) without ignoring equation (12), a set of algebraic equations is obtained for $\omega_m, a, \chi, \kappa, \nu$ and ω . Finally, solving this obtained system, the exact solutions of equation (2) are calculated.

3. The Applications

In this section, the used procedures will be applied to the given model. For this aim, the given model will be reduced to the nonlinear differential equation by the wave transformation. If we implement the wave transformation, namely, equation (5) to equation (1) then separate the real and imaginary parts, we get the following ODE:

$$-\omega u + \epsilon(u'' - \kappa^2 u) + \lambda F(u^2)u - 2(\rho - 2\sigma) \frac{(u')^2}{u} - 2\rho u'' - \epsilon u = 0, \quad (13)$$

$$\nu = -2\epsilon\kappa. \quad (14)$$

If we take $\rho = 2\sigma$, equation (13) reduces to the following ODE:

$$(\epsilon - 4\sigma)u'' - (\omega + \epsilon\kappa^2 + \epsilon)u + \lambda F(u^2)u = 0. \quad (15)$$

If we take $F(u^2) = u$ for the Kerr law nonlinearity, equation (15) reduces to the following ODE:

$$(\epsilon - 4\sigma)u'' - (\omega + \epsilon\kappa^2 + \epsilon)u + \lambda u^3 = 0. \quad (16)$$

If we balance u'' and u^3 in equation (16), the balance number is obtained as 1.

3.1. *First Method.* In this subsection, the generalized Kudryashov procedure will be applied to the equation (16). According to the method, we assume

$$u = \frac{a_0 + a_1\psi + a_2\psi^2}{b_0 + b_1\psi}. \quad (17)$$

If we substitute the solution (17) without ignoring the (8) in equation (16), we obtain an overdetermining equation

system. If the obtained system is solved, four solution families are obtained as follows.

3.1.1. *First Family.* The values of the arbitrary constants are obtained as follows:

$$\begin{aligned} a_0 &= 0, \\ a_1 &= \pm b_1 \sqrt{\frac{\epsilon - 4\sigma}{2\lambda}}, \\ a_2 &= \pm \frac{b_1(\epsilon - 4\sigma)}{\lambda\sqrt{-\epsilon - 4\sigma/2\lambda}}, \\ b_0 &= 0, \\ b_1 &= b_1, \\ \omega &= -\epsilon\kappa^2 - \frac{\epsilon}{2} + 2\sigma - \epsilon. \end{aligned} \quad (18)$$

Then, the solutions of the given model are obtained as follows:

$$q_{1,2}(x, t) = \left(\mp \frac{(\chi e^{(x-\nu(t^\delta/\delta))} - 1)(\epsilon - 4\sigma)}{\sqrt{-2\epsilon + 8\sigma/\lambda} (1 + \chi e^{(x-\nu t^\delta/\delta)})\lambda} \right) e^{i(-\kappa x + \omega t^\delta/\delta + \eta)}. \quad (19)$$

3.1.2. *Second Family.* The values of the arbitrary constants are obtained as follows:

$$\begin{aligned} a_0 &= 0, \\ a_1 &= \pm b_0 \sqrt{\frac{8\epsilon - 32\sigma}{\lambda}}, \\ a_2 &= \mp b_0 \sqrt{\frac{8\epsilon - 32\sigma}{\lambda}}, \\ b_0 &= b_0, \\ b_1 &= -2b_0, \\ \omega &= -\epsilon\kappa^2 + \epsilon - 4\sigma - \epsilon, \end{aligned} \quad (20)$$

and the solutions are given by the following:

$$q_{3,4}(x, t) = \left(\pm \frac{2\chi e^{(x-\nu t^\delta/\delta)} \sqrt{-2\epsilon + 8\sigma/\lambda}}{(\chi^2 e^{2(x-\nu t^\delta/\delta)} - 1)} \right) e^{i(-\kappa x + \omega t^\delta/\delta + \eta)}. \quad (21)$$

3.1.3. *Third Family.* The values of the arbitrary constants are obtained as follows:

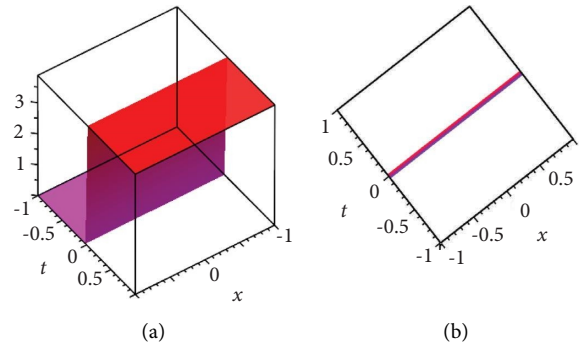


FIGURE 1: The plot of the |(25)| for $\epsilon = 1, \lambda = 2, \sigma = 4, \kappa = -2, \eta = 1, \epsilon = 2, \chi = 2, \delta = 0.1$: (a) 3D plot and (b) contour plot.

$$\begin{aligned}
 a_0 &= \pm \frac{b_0(\epsilon - 4\sigma)}{\lambda\sqrt{-2\epsilon - 8\sigma/\lambda}}, \\
 a_1 &= \mp \frac{(2b_0 - b_1)(\epsilon - 4\sigma)}{\lambda\sqrt{-2\epsilon - 8\sigma/\lambda}}, \\
 a_2 &= \pm b_1 \sqrt{\frac{2\epsilon - 8\sigma}{\lambda}}, \\
 b_0 &= b_0, \\
 b_1 &= b_1, \\
 \omega &= -\epsilon\kappa^2 - \frac{\epsilon}{2} + 2\sigma - \epsilon,
 \end{aligned} \tag{22}$$

and the solutions are given as follows:

$$q_{5,6}(x, t) = \left(\pm \frac{(\epsilon - 4\sigma)(\chi e^{(x - vt^\delta/\delta)} - 1)}{\lambda(1 + \chi e^{(x - vt^\delta/\delta)})\sqrt{-2\epsilon - 8\sigma/\lambda}} \right) e^{i(-\kappa x + \omega t^\delta/\delta + \eta)}. \tag{23}$$

3.1.4. *Fourth Family.* The values of the arbitrary constants are obtained as follows:

$$\begin{aligned}
 a_0 &= \mp \frac{b_1(\epsilon - 4\sigma)}{\lambda\sqrt{-2\epsilon - 8\sigma/\lambda}}, \\
 a_1 &= \pm \frac{2b_1(\epsilon - 4\sigma)}{\lambda\sqrt{-2\epsilon - 8\sigma/\lambda}}, \\
 a_2 &= \pm b_1 \sqrt{-2\epsilon - 8\sigma/\lambda}, \\
 b_0 &= \frac{b_1}{2}, \\
 b_1 &= b_1, \\
 \omega &= -\epsilon\kappa^2 - 2\epsilon + 8\sigma - \epsilon,
 \end{aligned} \tag{24}$$

and the solutions are given as follows:

$$q_{7,8}(x, t) = \left(\pm \frac{2(\epsilon - 4\sigma)(\chi^2 e^{2(x - vt^\delta/\delta)} + 1)}{\lambda(\chi^2 e^{2(x - vt^\delta/\delta)} - 1)\sqrt{-2\epsilon - 8\sigma/\lambda}} \right) e^{i(-\kappa x + \omega t^\delta/\delta + \eta)}. \tag{25}$$

The 3D and contour plots were given for (25) in Figure 1.

3.2. *Second Method.* In this subsection, the modified Kudryashov procedure will be applied to the equation (16). According to the method, we assume

$$u(\zeta) = \omega_0 + \omega_1 \psi(\zeta). \tag{26}$$

If we substitute the solution (26) without ignoring the (12) in equation (16) and collect the polynomial of $\psi(\zeta)$, we get an overdetermining equation system as follows:

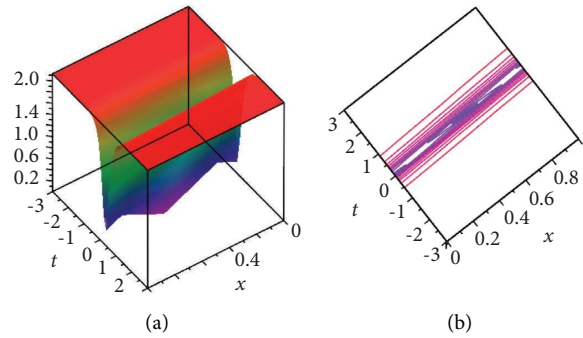


FIGURE 2: The plot of the $|q_{9,10}|$ for $\epsilon = 1, \lambda = 2, \sigma = 4, \kappa = -2, \eta = 1, \varepsilon = 2, \chi = 2, \delta = 0.9, a = 3$: (a) 3D plot and (b) contour plot.

$$\begin{aligned}
 \psi^3: & 2(\ln(a))^2 \omega_1 \epsilon - 8 \ln(a)^2 \omega_1 \sigma + \omega_1^3 \lambda, \\
 \psi^2: & -3(\ln(a))^2 \omega_1 \epsilon + 12(\ln(a))^2 \omega_1 \sigma + 3\omega_0 \omega_1^2 \lambda, \\
 \psi^1: & (\ln(a))^2 \omega_1 \epsilon - 4(\ln(a))^2 \omega_1 \sigma + 3\omega_0^2 \omega_1 \lambda - \omega_1 \epsilon \kappa^2 - \omega_1 \epsilon - \omega_1 \omega, \\
 \psi^0: & \lambda \omega_0^3 - \omega_0 \epsilon \kappa^2 - \omega_0 \epsilon - \omega_0 \omega.
 \end{aligned}
 \tag{27}$$

If the above system is solved, the values of the arbitrary constants are obtained as follows:

$$\begin{aligned}
 \omega_0 &= \pm \ln(a) \sqrt{\frac{\epsilon - 4\sigma}{2\lambda}}, \\
 \omega_1 &= \pm \frac{\ln(a)(\epsilon - 4\sigma)}{\lambda \sqrt{-\epsilon - 4\sigma/2\lambda}}, \\
 \omega &= -\frac{(\ln(a))^2 \epsilon}{2} + 2(\ln(a))^2 \sigma - \kappa^2 \epsilon - \epsilon.
 \end{aligned}
 \tag{28}$$

Then, the exact solutions are given by

$$q_{9,10}(x, t) = \pm \frac{(4\sigma - \epsilon) \ln(a) \left(\chi a^{(x - vt^\delta/\delta)} - 1 \right)}{\lambda \sqrt{-2\epsilon + 8\sigma/\lambda} \left(1 + \chi a^{(x - vt^\delta/\delta)} \right)}.
 \tag{29}$$

The 3D and contour plots were given for (29) in Figure 2.

4. Conclusions

In this study, the new soliton-type solutions of the conformable time-fractional complex Ginzburg–Landau equation with Kerr law nonlinearity were obtained with the help of generalized and modified Kudryashov methods. Firstly, the given model was reduced to the nonlinear differential equation with the help of the wave transformation. Then, the balance number was calculated by the balance method. We calculate the balance number for the generalized Kudryashov method in a different way than usual. The generalized Kudryashov method was applied to the given model. Four solution families were obtained. The 3D and contour plots were plotted for the latest family. Then, another method was applied to the given model. Also, the results of the modified Kudryashov method include the logarithmic solutions. The 3D and contour plots were given the obtain solutions. The Maple software program was used for all obtained results

and figures. According to our knowledge, our results are new in the literature. If we can calculate the balance number, the given methods provide soliton solutions for the nonlinear partial differential equations. All obtained results were checked by Maple and they are different from each other. Our findings in this paper are critical for explaining a wide range of scientific and physical applications. Thanks to this implementation, we contributed to the physical motions of the waves and other related areas. The proposed methods are effective and powerful for finding the soliton solutions of the nonlinear differential equations.

In new studies, the given equation can be solved with a different kind of derivative and compared with our results, or the used methods can be applied to the different nonlinear partial differential equations.

Data Availability

All data generated or analyzed during this study are included in this manuscript.

Conflicts of Interest

The authors declare that they have no conflicts of interest.

References

- [1] A. Biswas, H. Triki, Q. Zhou, S. P. Moshokoa, M. Z. Ullah, and M. Belic, “Cubic–quartic optical solitons in Kerr and power law media,” *Optik*, vol. 144, pp. 357–362, 2017.
- [2] Q. Zhou, L. Liu, H. Zhang et al., “Dark and singular optical solitons with competing nonlocal nonlinearities,” *Optica Applicata*, vol. 46, no. 1, pp. 79–86, 2016.
- [3] A. Biswas, Y. Yildirim, E. Yasar et al., “Optical soliton perturbation for Radhakrishnan–Kundu–Lakshmanan equation with a couple of integration schemes,” *Optik*, vol. 163, pp. 126–136, 2018.

- [4] S. B. G. Karakoc, T. Geyikli, and A. Bashan, "A numerical solution of the Modified Regularized Long Wave MRLW equation using quartic B splines," *TWMS Journal of Applied and Engineering Mathematics*, vol. 3, no. 2, pp. 231–244, 2013.
- [5] N. Raza, M. R. Aslam, and H. Rezazadeh, "Analytical study of resonant optical solitons with variable coefficients in Kerr and non-Kerr law media," *Optical and Quantum Electronics*, vol. 51, no. 2, p. 59, 2019.
- [6] S. K. Bhowmik and S. B. G. Karakoc, "Numerical approximation of the generalized regularized long wave equation using Petrov Galerkin finite element method," *Numerical Methods for Partial Differential Equations*, vol. 35, no. 6, pp. 2236–2257, 2019.
- [7] K. Hosseini, M. S. Osman, M. Mirzazadeh, and F. Rabiei, "Investigation of different wave structures to the generalized third-order nonlinear Schrödinger equation," *Optik*, vol. 206, Article ID 164259, 2020.
- [8] A. Zafar, M. Raheel, and A. Bekir, "Exploring the dark and singular soliton solutions of Biswas-Arshed model with full nonlinear form," *Optik*, vol. 204, Article ID 164133, 2020.
- [9] M. Kaplan, A. Akbulut, and A. Bekir, "Solving space-time fractional differential equations by using modified simple equation method," *Communications in Theoretical Physics*, vol. 65, no. 5, pp. 563–568, 2016.
- [10] M. Kaplan and A. Akbulut, "A mathematical analysis of a model involving an integrable equation for wave packet envelope," *Journal of Mathematics*, vol. 2022, Article ID 3486780, 10 pages, 2022.
- [11] K. K. Ali, S. B. G. Karakoc, and H. Rezazadeh, "Optical soliton solutions of the fractional perturbed nonlinear Schrödinger equation," *TWMS Journal of Applied and Engineering Mathematics*, vol. 10, no. 4, pp. 930–939, 2020.
- [12] S. B. G. Karakoc and K. K. Ali, "New exact solutions and numerical approximations of the generalized KdV equation," *Computational Methods for Differential Equations*, vol. 9, no. 3, pp. 670–691, 2021.
- [13] S. Arshed, "Soliton solutions of fractional complex Ginzburg-Landau equation with Kerr law and non-Kerr law media," *Optik*, vol. 160, pp. 322–332, 2018.
- [14] N. A. Kudryashov, "First integrals and general solution of the complex Ginzburg-Landau equation," *Applied Mathematics and Computation*, vol. 386, Article ID 125407, 2020.
- [15] A. Das, A. Biswas, M. Ekici, Q. Zhou, A. S. Alshomrani, and M. R. Belic, "Optical solitons with complex Ginzburg-Landau equation for two nonlinear forms using F-expansion," *Chinese Journal of Physics*, vol. 61, pp. 255–261, 2019.
- [16] H. Wang, M. Nur Alam, O. A. Ilhan, G. Singh, and J. Manafian, "New complex wave structures to the complex Ginzburg-Landau model," *AIMS Mathematics*, vol. 6, no. 8, pp. 8883–8894, 2021.
- [17] K. Hosseini, M. Mirzazadeh, M. S. Osman, M. Al Qurashi, and D. Baleanu, "Solitons and Jacobi elliptic function solutions to the complex ginzburg-landau equation," *Frontiers in Physics*, vol. 8, p. 225, 2020.
- [18] K. Hosseini, M. Mirzazadeh, L. Akinyemi, D. Baleanu, and S. Salahshour, "Optical solitons to the Ginzburg-Landau equation including the parabolic nonlinearity," *Optical and Quantum Electronics*, vol. 54, no. 10, p. 631, 2022.
- [19] A. Tozar, "New analytical solutions of fractional complex ginzburg-landau equation," *Universal Journal of Mathematics and Applications*, vol. 3, no. 3, pp. 129–132, 2020.
- [20] B. Ghanbari and F. Gomez, "Optical soliton solutions of the Ginzburg-Landau equation with conformable derivative and Kerr law nonlinearity," *Revista Mexicana de Física*, vol. 65, no. 1, pp. 73–81, 2018.
- [21] T. A. Sulaiman, H. M. Baskonus, and H. Bulut, "Optical solitons and other solutions to the conformable space-time fractional complex Ginzburg-Landau equation under Kerr law nonlinearity," *Pramana*, vol. 91, no. 4, p. 58, 2018.
- [22] C. Huang and Z. Li, "New exact solutions of the fractional complex ginzburg-landau equation," *Mathematical Problems in Engineering*, vol. 2021, Article ID 6640086, 8 pages, 2021.
- [23] M. Sadaf, G. Akram, and M. Dawood, "An investigation of fractional complex Ginzburg-Landau equation with Kerr law nonlinearity in the sense of conformable, beta and M-truncated derivatives," *Optical and Quantum Electronics*, vol. 54, no. 4, p. 248, 2022.
- [24] G. Samko, A. A. Kilbas, and O. I. Marichev, *Fractional Integrals and Derivatives: Theory and Applications*, Gordon and Breach, Philadelphia, PA, USA, 1993.
- [25] A. Kilbas, M. H. Srivastava, and J. J. Trujillo, "Theory and application of fractional differential equations," in *North Holland Mathematics Studies*, vol. 204, Elsevier, Amsterdam, Netherlands, 2006.
- [26] R. Khalil, M. Al Horani, A. Yousef, and M. Sababheh, "A new definition of fractional derivative," *Journal of Computational and Applied Mathematics*, vol. 264, pp. 65–70, 2014.
- [27] T. Abdeljawad, "On conformable fractional calculus," *Journal of Computational and Applied Mathematics*, vol. 279, pp. 57–66, 2015.
- [28] N. Benkhetto, S. Hassani, and D. F. M. Torres, "A conformable fractional calculus on arbitrary time scales," *Journal of King Saud University Science*, vol. 28, no. 1, pp. 93–98, 2016.
- [29] W. S. Chung, "Fractional Newton mechanics with conformable fractional derivative," *Journal of Computational and Applied Mathematics*, vol. 290, pp. 150–158, 2015.
- [30] H. A. Ghany, A. S. O. E. Bab, A. M. Zabel, and A. A. Hyder, "The fractional coupled KdV equations: exact solutions and white noise functional approach," *Chinese Physics B*, vol. 22, no. 8, Article ID 080501, 2013.
- [31] H. A. Ghany and A. A. Hyder, "Abundant solutions of Wick-type stochastic fractional 2D KdV equations," *Chinese Physics B*, vol. 23, no. 6, Article ID 060503, 2014.
- [32] N. A. Kudryashov, "One method for finding exact solutions of nonlinear differential equations," *Communications in Nonlinear Science and Numerical Simulation*, vol. 17, no. 6, pp. 2248–2253, 2012.
- [33] M. Kaplan and A. Akbulut, "The analysis of the soliton-type solutions of conformable equations by using generalized Kudryashov method," *Optical and Quantum Electronics*, vol. 53, no. 9, p. 498, 2021.
- [34] K. Hosseini and R. Ansari, "New exact solutions of nonlinear conformable time-fractional Boussinesq equations using the modified Kudryashov method," *Waves in Random and Complex Media*, vol. 27, no. 4, pp. 628–636, 2017.
- [35] A. Akbulut, A. H. Arnous, M. S. Hashemi, and M. Mirzazadeh, "Solitary waves for the generalized nonlinear wave equation in (3+1) dimensions with gas bubbles using the Nucci's reduction, enhanced and modified Kudryashov algorithms," *Journal of Ocean Engineering and Science*, 2022.
- [36] S. B. G. Karakoc and K. K. Ali, "Theoretical and computational structures on solitary wave solutions of Benjamin Bona Mahony-Burgers equation," *Tbilisi Mathematical Journal*, vol. 14, no. 2, pp. 33–50, 2021.

Research Article

A New Efficient Method for Solving System of Weakly Singular Fractional Integro-Differential Equations by Shifted Sixth-Kind Chebyshev Polynomials

S. Yaghoubi,¹ H. Aminikhah ^{1,2} and K. Sadri ³

¹Department of Applied Mathematics and Computer Science, Faculty of Mathematical Sciences, University of Guilan, P.O. Box 41938-19141, Rasht, Iran

²Center of Excellence for Mathematical Modelling, Optimization and Combinational Computing (MMOCC), University of Guilan, P.O. Box 41938-19141, Rasht, Iran

³Department of Mechanical Engineering, Faculty of Engineering, Ahrar Institute of Technology and Higher Education, P.O.Box 41931-63591, Rasht, Iran

Correspondence should be addressed to H. Aminikhah; aminikhah@guilan.ac.ir

Received 18 July 2022; Accepted 17 September 2022; Published 17 October 2022

Academic Editor: Arzu Akbulut

Copyright © 2022 S. Yaghoubi et al. This is an open access article distributed under the Creative Commons Attribution License, which permits unrestricted use, distribution, and reproduction in any medium, provided the original work is properly cited.

In this paper, a new approach for solving the system of fractional integro-differential equation with weakly singular kernels is introduced. The method is based on a class of symmetric orthogonal polynomials called shifted sixth-kind Chebyshev polynomials. First, the operational matrices are constructed, and after that, the method is described. This method reduces a system of weakly singular fractional integro-differential equations (WSFIDEs) by the collocation method into a system of algebraic equations. Thereupon, an upper error bound for the proposed method is determined. Finally, some numerical examples are prepared to test the accuracy and efficiency of the presented method.

1. Introduction

The study of fractional calculus has applications and popularity in various and wide fields of biology, physics, and fluid mechanics. Fractional calculus is actually integration and differentiation of arbitrary orders [1–4]. In various problems of physics and engineering, the fractional differential equations have been proved to be valuable tools in modeling of many phenomena [5, 6]. As we know, many mathematical models of real phenomena (arising in engineering and physics) are described as linear or nonlinear systems. It is worth mentioning that with the development of fractional calculus, the behavior of many systems can be described using the fractional differential and fractional integro-differential system [7, 8]. In recent years, systems of the fractional differential and integral equations are the subjects of extensive study due to their frequent appearance in many engineering and scientific disciplines [9–11]. However, most of the fractional-order equations and integral equations do not have analytic solutions or are hard to find. So, it is essen-

tial to find numerical methods to get approximate or exact solutions of a system of integro-differential equations. So far, researchers have utilized diverse numerical methods for solving a system of fractional integro-differential equations. In [12], the homotopy perturbation method was proposed for solving linear and nonlinear systems of fractional integro-differential equations. Heydari et al. have used the Chebyshev wavelet method for solving a class of systems of nonlinear fractional singular Volterra integro-differential equation in [13]. In the next year, for the first time, the hybrid functions composed of the Block-pulse functions and Bernoulli polynomials were applied for problems with fractional-order differential equations in [14]. Also, a novel technique based on iterative refinement was presented to analytically approximate a system of linear fractional integro-differential equations [15]. In 2018, Hesameddini and Shahbazi developed the concept of [14] and used it to solve the FDIE system in [16]. Also, Xie and Yi presented the simple and fast method based on the Block-pulse function to solve a nonlinear system of fractional

Volterra-Fredholm integro-differential equations in the same year [17]. In [18], the authors implemented the new Jacobi operational matrices to reduce the complexity of calculations to solve WSFDIEs. Next, the Haar wavelet method was employed to solve a coupled system of FIDEs, and the Muntz-Legendre wavelets were introduced to solve FIDVFEs in [19, 20]. Also, the other authors applied the Chebyshev Pseudo spectral method for solving fractional-order nonlinear system of Volterra integro-differential equations and a least square collocation Chebyshev technique for solving a system of linear fractional integro-differential equations [21, 22]. In this paper, we consider the following system of weakly singular integro-differential equations:

$$\begin{aligned} \mathcal{D}^{\nu_i} u_i(x) &= \mathcal{F}_i(x, u_1(x), u_2(x), \dots, u_m(x)) \\ &+ \sum_{j=1}^m \theta_{ij} \int_0^x \frac{K_{ij}(x, z) G_{ij}(z, u_j(z))}{(x-z)^{\alpha_{ij}}} dz \\ &+ f_i(x), i = 1, \dots, m, u_i^{(k)}(0^+) = u_{0i}^{(k)}, k = 0, 1, \\ &\dots, r-1, r-1 < \nu_i \leq r, \end{aligned} \tag{1}$$

where $u_i(x) \in C^r[0, 1], i = 1, \dots, m$, are the unknown functions, $\mathcal{F}_i : [0, 1] \times (C^r[0, 1])^m \rightarrow \mathbb{R}, G_{ij} : [0, 1] \times C^r[0, 1] \rightarrow \mathbb{R}$, and $K_{ij}(x, z) : [0, 1]^2 \rightarrow \mathbb{R}$ are continuous operators and functions that satisfy Lipschitz conditions, and \mathcal{D}^{ν_i} is the Caputo fractional derivative operator where $\nu_i \in (0, 1]$. The parameters $\theta_{ij}, \alpha_{ij} \in \mathbb{R}$ such that $|\theta_{ij}| \leq 1, 0 < \alpha_{ij} < 1$, and $i, j = 1, 2, \dots, m$. Moreover, $f_i(x), i = 1, \dots, m$, are known and sufficiently smooth functions.

As usual, a way for solving functional equations is to express the solution as a linear combination of the so-called basis functions. In most researches, various polynomials such as the Legendre, Chebyshev, Taylor, Hermit, and Bernstein are used as basis functions. Among all of them, the Chebyshev polynomials are the most important in the analysis and numerical analysis. Chebyshev polynomials are orthogonal on the interval $[-1, 1]$ and have good properties that are used widely in the approximation of the functions. For this reason, many studies are done based on the different kinds of Chebyshev polynomials. In [23], Masjed-Jamei introduced two half-trigonometric orthogonal Chebyshev polynomials, and he named them as the Chebyshev polynomials of the fifth and sixth kinds. The basic formulas and properties of this class of polynomials are displayed in [24, 25]. Up to now, many researchers have used various kinds of Chebyshev polynomials for the fractional-order differential and integro-differential equations (see [26, 27]). However, there are only a few works that have used the sixth-kind Chebyshev polynomials. The main aim of this work is to introduce these polynomials as a new basis function for solving WSFDIEs. In the current paper, we apply the orthogonal shifted sixth-kind Chebyshev polynomials together with the collocation method for solving a system of weakly singular integro-differential equations with fractional derivatives that, to the best of our knowledge, is proposed here for the first time. For solving these equations, we derive the fractional operational matrices

of fractional and integer orders and the product operational matrix, as well. Also, we introduce an operational matrix to approximate the integral term that has the weakly singular kernel in Equation (1). As far as we can tell, this operational matrix is presented for the first time. By substituting appropriate approximations in Equation (1), the original equations convert into algebraic equations that each of the equations of algebraic systems is collocated at $N + 1$ roots of the $(N + 1)$ th shifted sixth-kind Chebyshev polynomials (SSKCPs). By solving these algebraic systems, the approximate solutions of the original system are obtained. Although the calculation of the operational matrices may be complicated, we show that the obtained results are equal to other methods or are even more accurate. Implementing these matrices leads to a decrease in the number of required computations, and therefore, the computation time will be reduced.

The rest of the paper is organized as follows. In section 2, some essential preliminaries are mentioned briefly. Section 3 is devoted to constructing the operational matrices of SSKCPs. The proposed numerical procedure is described in Section 4. The error analysis of the proposed method is discussed in Section 5. Some numerical applications are indicated in Section 6, and conclusions are presented in Section 7.

2. Preliminaries and Notations

In this section, we recall some definitions and properties of fractional integral and derivative operators which will be used later. After that, some necessary definitions and fundamental properties of the shifted sixth-kind Chebyshev polynomials are reviewed briefly.

2.1. Some Essentials of the Fractional Calculus

Definition 1. The Riemann-Liouville fractional integral operator J^α of order α is given by [2]

$$J^\alpha f(x) = \frac{1}{\Gamma(\alpha)} \int_0^x (x-z)^{\alpha-1} f(z) dz, \alpha > 0, x > 0. \tag{2}$$

Definition 2. Let $\alpha \in \mathbb{R}, n - 1 < \alpha \leq n, n \in \mathbb{N}$, and $f(x)$ be a real-valued continuous function defined on $[0, \infty)$. Then, the Caputo fractional derivative of order $\alpha > 0$ is defined by [2]

$$\begin{cases} {}_0\mathcal{D}_x^\alpha f(x) = \frac{1}{\Gamma(n-\alpha)} \int_0^x \frac{f^n(z)}{(x-z)^{\alpha+1-n}} dz, \\ f^{(n)}(z), \alpha = n, \end{cases} \tag{3}$$

where $\Gamma(x)$ is the Gamma function as

$$\Gamma(x) = \int_0^\infty e^{-z} z^{x-1} dz, \text{Re}(z) > 0,$$

$$\Gamma(x+1) = x\Gamma(x),$$

$$B(u, v) = \int_0^1 z^{u-1} (1-z)^{v-1} dz = \frac{\Gamma(u)\Gamma(v)}{\Gamma(u+v)}, \text{Re}(u) > 0, \text{Re}(v) > 0. \tag{4}$$

The last integral is often called the Beta integral. For $\alpha_1, \alpha_2 > 0$, the Riemann-Liouville integral and Caputo fractional derivative operators satisfy the following properties:

- (1) $J^{\alpha_1}(J^{\alpha_2}f(x)) = J^{\alpha_2}(J^{\alpha_1}f(x)) = J^{\alpha_1+\alpha_2}f(x)$
- (2) $J^\alpha(\lambda_1f(x) + \lambda_2g(x)) = \lambda_1J^\alpha f(x) + \lambda_2J^\alpha g(x)$
- (3) $J^\alpha(\mathcal{D}^\alpha f(x)) = f(x) - \sum_{i=0}^{n-1} f^i(0)(x^i/i!), n - 1 < \alpha \leq n, x > 0$
- (4) $\mathcal{D}^\alpha x^\gamma = \begin{cases} 0, & \alpha > \gamma, \\ (\Gamma(\gamma + 1)/\Gamma(\gamma - \alpha + 1))x^{\gamma-\alpha}, & \text{otherwise} \end{cases}$
- (5) $J^\alpha x^\nu = ((\Gamma(\nu + 1))/(\Gamma(\nu + \alpha + 1)))x^{\nu+\alpha}, \nu > -1$

2.2. Shifted Sixth-Kind Chebyshev Polynomials and Their Properties (SSKCPs)

Definition 3. The sixth-kind Chebyshev polynomials are orthogonal functions on the interval $[-1, 1]$ and can be determined with the following recursive formula [23, 24]:

$$S_j(x) = xS_{j-1}(x) - \frac{j(j+1) + (-1)^j(2j+1) + 1}{4j(j+1)}S_{j-2}(x), j \geq 2,$$

$$S_0(x) = 1,$$

$$S_1(x) = x. \tag{5}$$

Definition 4. The shifted sixth-kind Chebyshev polynomials on $[0, 1]$ is defined by [23, 24]

$$S_j^*(x) = S_j(2x - 1), j = 0, 1, 2, \dots. \tag{6}$$

These polynomials have the following explicit analytic form:

$$S_j^*(x) = \sum_{k=0}^j \rho_{kj} x^k, \tag{7}$$

where

$$\rho_{kj} = \begin{cases} \frac{2^{2k-j}}{(2k+1)!} \sum_{i=\lfloor (k+1)/2 \rfloor}^{j/2} \frac{(-1)^{(j/2)+ik} (2i+k+1)!}{(2i-k)!}, & j \text{ even,} \\ \frac{2^{2k-j+1}}{(2k+1)!(j+1)} \sum_{i=\lfloor k/2 \rfloor}^{j-1/2} \frac{(-1)^{((j+1)/2)+ik} (i+1)(2i+k+2)!}{(2i-k+1)!}, & j \text{ odd.} \end{cases} \tag{8}$$

Moreover, the shifted polynomials $S_j^*(x)$ are orthogonal on $[0, 1]$ with respect to the weight function $V(x) = (2x - 1)^2 \sqrt{x - x^2}$ in the sense that

$$\int_0^1 S_i^*(x) S_j^*(x) V(x) dx = \lambda_i \delta_{ij}, \tag{9}$$

$$\lambda_i = \begin{cases} \frac{\pi}{2^{2i+5}}, & i \text{ even,} \\ \frac{\pi(i+3)}{2^{2i+5}(i+1)}, & i \text{ odd.} \end{cases} \tag{10}$$

Now, let $h(x) \in L^2[0, 1]$; then, $h(x)$ can be approximated in terms of $S_j^*(x)$ as

$$h(x) \approx \sum_{j=0}^N \mathbf{q}_j S_j^*(x) = F^T S(x) = S^T(x) F, \tag{11}$$

where

$$S(x) = [S_0^*(x), S_1^*(x), \dots, S_N^*(x)]^T, F = [\mathbf{q}_0, \mathbf{q}_1, \dots, \mathbf{q}_N]^T, \tag{12}$$

where the coefficients \mathbf{q}_j are given by

$$\mathbf{q}_j = \frac{1}{\lambda_j} \int_0^1 h(x) S_j^*(x) V(x) dx, \tag{13}$$

and λ_j is defined in Equation (10). Similarly, any continuous two-variable function, $\mathcal{F}(x, z)$, defined on $[0, 1] \times [0, 1]$ can be approximated by means of the double-shifted sixth-kind Chebyshev polynomials as

$$\mathcal{F}(x, z) \approx \sum_{j=0}^N \sum_{i=0}^N \mathcal{F}_{ij} S_i^*(x) S_j^*(z) = S^T(x) \mathcal{F} S(z), \tag{14}$$

where \mathcal{F} is a $(N + 1) \times (N + 1)$ matrix, and its entries are given by

$$\mathcal{F}_{ij} = \frac{1}{\lambda_i \lambda_j} \int_0^1 \int_0^1 \mathcal{F}(x, z) S_i^*(x) S_j^*(z) V(x) V(z) dx dz. \tag{15}$$

3. Operational Matrices of SSKCPs

In this section, the formulas of operational matrices with the fractional order will be derived for the sixth-kind Chebyshev polynomials. The following are the required lemmas.

Lemma 5. If $r \geq l, l \in \mathbb{N}$, then we have

$$\int_0^1 x^r S_l^*(x) V(x) dx = \sum_{m=0}^l \frac{\rho_{ml} \sqrt{\pi} \Gamma(r+m+(3/2))}{2\Gamma(r+m+5)} (m^2 + m + r^2 + 2rm + 3 + r). \tag{16}$$

Proof. From the properties of the orthogonal polynomials, if $r \leq l$, we have

$$\int_0^1 x^r S_l^*(x) V(x) dx = 0. \tag{17}$$

Hence, we suppose $r \geq l$. The lemma can be easily proved by the integration of the analytic form of SSKCPs in Equation (7). \square

Theorem 6. Let $S(x)$ be the SSKCP vector given by Equation (12) and $\mu \in \mathbb{R}$; then,

$$J^\mu S(x) \approx \mathcal{P}^{(\mu)} S(x), \tag{18}$$

where $\mathcal{P}^{(\mu)}$ is the $(N + 1) \times (N + 1)$ operational matrix of the fractional integration of the order μ in the Riemann-Liouville sense which is defined by

$$\mathcal{P}^{(\mu)} = \begin{bmatrix} \tilde{a}_{00} & \tilde{a}_{01} & \cdots & \tilde{a}_{0N} \\ \tilde{a}_{10} & \tilde{a}_{11} & \cdots & \tilde{a}_{1N} \\ \vdots & \vdots & \ddots & \vdots \\ \tilde{a}_{N0} & \tilde{a}_{N1} & \cdots & \tilde{a}_{NN} \end{bmatrix}, \tag{19}$$

$$\tilde{a}_{ij} = \sum_{l=0}^i \omega_{ijl}, \quad i = 0 \cdots N, j = 0 \cdots N. \tag{20}$$

ω_{ijl} are given by

$$\omega_{ijl} = \rho_{li} \frac{\Gamma(l+1)}{\lambda_j \Gamma(l+\mu+1)} \sum_{k=0}^j \rho_{kj} \frac{\sqrt{\pi} \Gamma(k+\mu+l+(3/2))}{2\Gamma(k+\mu+l+5)} \times ((k+\mu)^2 + (2l+1)(k+\mu) + l(l+1) + 3), \quad i = 0 \cdots N, j = 0 \cdots N. \tag{21}$$

Proof. By applying the Riemann-Liouville integral operator to the SSKCPs' analytic form, we have

$$J^\mu (S_i^*(x)) = \sum_{l=0}^i \rho_{li} \frac{\Gamma(l+1)}{\Gamma(l+\mu+1)} x^{\mu+l}. \tag{22}$$

Now, we can express $x^{\mu+l}$ in terms of the shifted sixth-kind Chebyshev polynomials as follows:

$$x^{\mu+l} \approx \sum_{j=0}^N \tilde{C}_{lj} S_j^*(x), \tag{23}$$

where the coefficients \tilde{C}_{lj} are given by

$$\tilde{C}_{lj} = \frac{1}{\lambda_j} \int_0^1 x^{\mu+l} S_j^*(x) V(x) dx. \tag{24}$$

According to Lemma 5, we can rewrite Equation (22) as

$$J^\mu S_j^{(*)}(x) \approx \sum_{j=0}^N \left\{ \sum_{l=0}^i \rho_{li} \frac{\Gamma(l+1)}{\lambda_j \Gamma(l+\mu+1)} \times \sum_{k=0}^j \rho_{kj} \frac{\sqrt{\pi} \Gamma(k+\mu+l+(3/2))}{2\Gamma(k+\mu+l+5)} ((k+\mu)^2 + (2l+1)(k+\mu) + l(l+1) + 3) \right\} S_j^*(x) = \sum_{j=0}^N \tilde{a}_{ij} S_j^*(x), \tag{25}$$

where \tilde{a}_{ij} is given in Equation (20). Rewriting the last relation in the vector form gives

$$J^\mu S^*(x) = [\tilde{a}_{i0}, \tilde{a}_{i1}, \dots, \tilde{a}_{iN}] S_j^*(x), \quad i = 0, 1, \dots, N. \tag{26}$$

This leads to the desired result. □

In the following, some useful and applicable lemmas are presented to get the Chebyshev operational matrix of product.

Lemma 7. If $S_j^*(x)$ and $S_i^*(x)$ are j th and i th shifted sixth-kind Chebyshev polynomials, respectively, then we can write the product of $S_j^*(x)$ and $S_i^*(x)$ as

$$Q_{i+j}(x) = S_i^*(x) S_j^*(x) = \sum_{k=0}^{i+j} \chi_k^{(i,j)} x^k. \tag{27}$$

Proof. See [18]. □

Lemma 8. If $S_i^*(x)$, $S_j^*(x)$, and $S_k^*(x)$ are i th, j th, and k th shifted sixth-kind Chebyshev polynomials, then

$$\begin{aligned} d_{ijk} &= \int_0^1 S_i^*(x) S_j^*(x) S_k^*(x) V(x) dx \\ &= \sum_{r=0}^{j+k} \sum_{l=0}^i \frac{\sqrt{\pi} \rho_{li} \chi_k^{(i,j)} \Gamma(r+l+(3/2))}{2\Gamma(r+l+5)} ((l+r)(l+r+1) + 3), \end{aligned} \tag{28}$$

where $\chi_k^{(i,j)}$ is obtained by Lemma 7.

Proof. According to Lemma 7, we can write

$$Q_{j+k}(x) = S_j^*(x) S_k^*(x) = \sum_{r=0}^{j+k} \chi_r^{(j,k)} x^r. \tag{29}$$

Then,

$$d_{ijk} = \int_0^1 S_i^*(x) \sum_{r=0}^{j+k} \chi_r^{(j,k)} x^r V(x) dx = \sum_{r=0}^{j+k} \chi_r^{(j,k)} \int_0^1 S_i^*(x) x^r V(x) dx. \tag{30}$$

The value of the last integral is obtained by Lemma 5. □

Assuming that E is a $(N + 1) \times 1$ vector, we have

$$S(x)S^T(x)E \approx \tilde{E}S(x), \tag{31}$$

where \tilde{E} is a $(N + 1) \times (N + 1)$ matrix called the product operational matrix. The next theorem presents a general form for entries of the matrix \tilde{E} .

Theorem 9. *The entries of the matrix \tilde{E} in Equation (31) are as follows:*

$$\tilde{E}_{jk} = \frac{1}{\lambda_k} \sum_{i=0}^N E_i d_{ijk}, j, k = 0, 1, \dots, N, \tag{32}$$

where d_{ijk} is obtained by Lemma 8 and E_i is the element of the vector E .

Proof. See [18]. □

In the following, we get an approximation for the integral part with the singular kernel in Equation (1). Before that, we present a theorem.

Theorem 10. *The following relation is determined for $0 < \kappa < 1$:*

$$\int_0^x \frac{z^r}{(x-z)^\kappa} dz = \frac{\Gamma(r+1)\Gamma(1-\kappa)}{\Gamma(r-\kappa+2)} x^{r-\kappa+1}, r = 0, 1, 2, \dots \tag{33}$$

Proof. By performing Equation (33) and the substitution of $z = \xi x$ into Equation (33) and then using the definition of the Beta function, we obtain

$$x^{r-\kappa+1} \int_0^1 (1-\xi)^{-\kappa} \xi^r d\xi = \frac{\Gamma(1-\kappa)\Gamma(r+1)}{\Gamma(r-\kappa+2)} x^{r-\kappa+1}, r = 0, 1, 2, \dots \tag{34}$$

□

$$\int_0^x \frac{S^T(z)}{(x-z)^\kappa} dz = \left[\sum_{j=0}^0 \rho_{j0} \int_0^x \frac{z^j}{(x-z)^\kappa} dz, \dots, \sum_{l=0}^N \rho_{lN} \int_0^x \frac{z^l}{(x-z)^\kappa} dz \right] = \left[\sum_{l=0}^0 \rho_{l0} \frac{\Gamma(l+1)\Gamma(1-\kappa)}{\Gamma(l-\kappa+2)} x^{l-\kappa+1}, \dots, \sum_{l=0}^N \rho_{lN} \frac{\Gamma(l+1)\Gamma(1-\kappa)}{\Gamma(l-\kappa+2)} x^{l-\kappa+1} \right]. \tag{39}$$

Now, we approximate $x^{l-\kappa+1}$ in terms of SSKCPs as follows:

$$x^{l-\kappa+1} \approx \sum_{j=0}^N \bar{C}_{j(l-\kappa+1)} S_j^*(x), \tag{40}$$

$$\bar{C}_{j(l-\kappa+1)} = \frac{1}{\lambda_j} \int_0^1 x^{l-\kappa+1} S_j^*(x) V(x) dx, j = 0, 1, \dots, N,$$

Now, we present an approximation for the integral part with a weakly singular kernel. For this purpose, see the following theorem.

Theorem 11. *Suppose that $u(x)$ is a continuous function on the interval $[0, 1]$ and $\kappa \in (0, 1)$ and $u(x) \approx S^T(x)F = F^T S(x)$ where $S(x)$ and F are defined by Equation (12), then we have*

$$\int_0^x \frac{u(z)}{(x-z)^\kappa} dz \approx F^T \mathfrak{F}^{(\kappa)} S(x), \tag{35}$$

where $\mathfrak{F}^{(\kappa)}$ is a $(N + 1) \times (N + 1)$ matrix as follows:

$$\mathfrak{F}^{(\kappa)} = \begin{bmatrix} \sigma_{00} & \sigma_{01} & \dots & \sigma_{0N} \\ \sigma_{10} & \sigma_{11} & \dots & \sigma_{1N} \\ \vdots & \vdots & \ddots & \vdots \\ \sigma_{N0} & \tilde{a}_{N1} & \dots & \sigma_{NN} \end{bmatrix}, \tag{36}$$

and its entries are determined as follows:

$$\mathfrak{F}_{ij}^{(\kappa)} = \sigma_{ij} = \sum_{l=0}^i \rho_{li} \frac{\Gamma(l+1)\Gamma(1-\kappa)}{\Gamma(l-\kappa+2)} \bar{C}_{j(l-\kappa+1)}, i, j = 0, 1, \dots, N, \tag{37}$$

where the quantities ρ_{li} and $\bar{C}_{j(l-\kappa+1)}$ are introduced by relation (8) and Lemma 5.

Proof. By the definition of vector $S(x)$ and Lemma 5, we can write

$$S^T(x) = [S_0^*(x), S_1^*(x), \dots, S_N^*(x)] = \left[\sum_{l=0}^0 \rho_{l0} x^l, \dots, \sum_{l=0}^N \rho_{lN} x^l \right]. \tag{38}$$

By applying Theorem 10, we have

where $\bar{C}_{j(l-\kappa+1)}$ is obtained by applying Lemma 5. Thus,

$$\begin{aligned} & \sum_{l=0}^i \rho_{li} \frac{\Gamma(l+1)\Gamma(1-\kappa)}{\Gamma(l-\kappa+2)} x^{l-\kappa+1} \\ & \approx \sum_{j=0}^N \left\{ \sum_{l=0}^i \frac{\rho_{li} \Gamma(l+1)\Gamma(1-\kappa) \bar{C}_{j(l-\kappa+1)}}{\Gamma(l-\kappa+2)} \right\} S_j^*(x) \\ & = \sum_{j=0}^N \sigma_{ij} S_j^*(x), i = 0, 1, \dots, N. \end{aligned} \tag{41}$$

Equation (39) is then represented as follows:

$$\int_0^x \frac{S^T(z)}{(z-x)^\kappa} dz \approx \begin{bmatrix} \sigma_{00} & \sigma_{01} & \cdots & \sigma_{0N} \\ \sigma_{10} & \sigma_{11} & \cdots & \sigma_{1N} \\ \vdots & \vdots & \ddots & \vdots \\ \sigma_{N0} & \tilde{a}_{N1} & \cdots & \sigma_{NN} \end{bmatrix} \begin{bmatrix} S_0^*(x) \\ S_1^*(x) \\ \vdots \\ S_N^*(x) \end{bmatrix} = \mathfrak{S}^{(\kappa)} S(x). \tag{42}$$

□

4. Numerical Procedure

We consider the system of fractional integro-differential equation with weakly singular kernels described in Equation (1). To solve the system, we approximate the function $\mathcal{D}^{v_i} u$ in a matrix form

$$\mathcal{D}^{v_i} u_i(x) \approx S^T(x) F_i, F_i = [\mathcal{Q}_0^i, \mathcal{Q}_1^i, \dots, \mathcal{Q}_N^i]^T, i = 1, 2, \dots, m. \tag{43}$$

Then, according to the initial conditions of the problem, we can approximate the known function $\mathcal{H}_i(x) = \sum_{k=0}^{r-1} (u_{0i}^{(k)} x^k / \Gamma(k+1))$, $k = \lceil v_i \rceil$ as follows:

$$\mathcal{H}_i(x) \approx S^T(x) \mathcal{C}_i, i = 1, 2, \dots, m. \tag{44}$$

Using Equations (43) and (44), we compute an approximate for $u_i(x)$:

$$u_i(x) \approx S^T(x) \mathcal{P}^{(v_i)} F_i + S^T(x) \mathcal{C}_i = S^T(x) U_i, i = 1, 2, \dots, m, \tag{45}$$

where $\mathcal{P}^{(v_i)}$ is the integral operational matrix presented in Theorem 6. We have the following approximations for the rest of the system:

$$\begin{aligned} \mathcal{F}_i(x, u_1(x), u_2(x), \dots, u_m(x)) &\approx \mathcal{X}_i^T S(x), \\ G_{ij}(x, u_j(x)) &\approx S^T(x) \mathcal{V}_{ij}, \quad i, j = 1, 2, \dots, m, \\ K_{ij}(x, z) &\approx S^T(x) K_{ij} S(z). \end{aligned} \tag{46}$$

Using Theorems 9 and 11, we have

$$\begin{aligned} &\int_0^x \frac{K_{ij}(x, z) G_{ij}(z, y_j(z))}{(x-z)^{\alpha_{ij}}} dz \\ &\approx \int_0^x \frac{S^T(x) K_{ij} S(z) S^T(z) \mathcal{V}_{ij}}{(x-z)^{\alpha_{ij}}} dz \\ &\approx S^T(x) K_{ij} \tilde{\mathcal{V}}_{ij} \int_0^x \frac{S(z)}{(x-z)^{\alpha_{ij}}} dz \approx S^T(x) K_{ij} \tilde{\mathcal{V}}_{ij} \mathfrak{S}^{(\alpha_{ij})} S(x). \end{aligned} \tag{47}$$

Now, by substituting Equations (43)-(47) into Equation

(1), we obtain

$$\begin{aligned} S^T(x) F_i - \mathcal{X}_i^T S(x) - \sum_{j=0}^m \theta_{ij} S^T(x) K_{ij} \tilde{\mathcal{V}}_{ij} \mathfrak{S}^{(\alpha_{ij})} S(x) \\ - f_i(x) \approx 0, i = 1, 2, \dots, m. \end{aligned} \tag{48}$$

Each equation of algebraic system (48) is collocated at $N + 1$ roots of the $(N + 1)$ th shifted sixth-kind Chebyshev polynomials. Thus, an algebraic system, including $m(N + 1)$ equations, is acquired. By solving the resultant algebraic system, we can obtain an approximation for unknown vectors $F_i, i = 1, 2, \dots, m$, and by substituting the vector F_i into Equation (45), we obtain an approximation for $u_i(x), i = 1, 2, \dots, m$.

5. Error Analysis

In this section, we prove some theorems. Then, we obtain an upper error bound for the approximation error. For this aim, we need the following norms:

$$\begin{aligned} \|f\|_{L^2(I)} &= \left(\int_I |f(x)|^2 V(x) dx \right)^{1/2}, \\ \|X\|_1 &= \sum_{i=0}^n |x_i|, \end{aligned} \tag{49}$$

where $f \in L^2(I)$ is a square integrable function on the interval $I = [0, 1]$ and $X = [x_0, x_1, \dots, x_n]^T$ is a vector.

Theorem 12. Suppose that $Y_N(x) = \sum_{i=0}^N \mathcal{E}_i S_i^*(x)$ is an approximation in SSKCPs to the continuous function $Y(x)$ on the interval $[0, 1]$. Then, the coefficients \mathcal{E}_i , for $i = 0, 1, \dots, N$, are bounded as

$$|\mathcal{E}_i| \leq \frac{\mathcal{M}_Y}{\lambda_i} \sum_{m=0}^i \rho_{mi} \frac{\sqrt{\pi} \Gamma(m + (3/2))}{2\Gamma(m + 5)} (m^2 + m + 3), \tag{50}$$

where \mathcal{M}_Y denotes the maximum value of $|Y(x)|$ on the interval $[0, 1]$.

Proof. Using Equations (7) and (9) for $i = 0, 1, \dots, N$, we have

$$\begin{aligned} \mathcal{E}_i &= \frac{1}{\lambda_i} \int_0^1 Y(x) S_i^*(x) V(x) dx = \frac{1}{\lambda_i} \int_0^1 Y(x) \sum_{m=0}^i \rho_{mi} x^m V(x) dx \\ &= \frac{1}{\lambda_i} \sum_{m=0}^i \rho_{mi} \int_0^1 Y(x) x^m V(x) dx. \end{aligned} \tag{51}$$

Since $Y(x)$ is a continuous function on the interval $[0, 1]$, so it is bounded and there is a constant \mathcal{M}_Y such that

$$\forall x \in [0, 1], |Y(x)| \leq \mathcal{M}_Y. \tag{52}$$

Using Equations (51) and (52), inequality (50) is deduced. \square

Theorem 13. Suppose that $Y(x)$ is a continuous function and $Y_N(x)$ is an approximation to $Y(x)$ in terms of SSKCPs. Then, the error bound can be achieved as follows:

$$\|Y(x) - Y_N(x)\|_{L^2} \leq \left(\sum_{i=N+1}^{\infty} \Omega_i \right)^{1/2} = \Omega_N, \quad (53)$$

where

$$\Omega_i = \frac{\mathcal{M}_Y^2}{\lambda_i} \sum_{m=0}^i \left(\rho_{mi} \frac{\sqrt{\pi} \Gamma(m + (3/2))}{2\Gamma(m + 5)} (m^2 + m + 3) \right)^2. \quad (54)$$

Proof. Assume $Y(x)$ is an arbitrary function. So, $Y(x)$ and $Y_N(x)$ have the following forms using SSKCP series:

$$\begin{aligned} Y(x) &= \sum_{i=0}^{\infty} \mathcal{E}_i S_i^*(x), \\ Y_N(x) &= \sum_{i=0}^N \mathcal{E}_i S_i^*(x), \end{aligned} \quad (55)$$

so,

$$Y(x) - Y_N(x) = \sum_{i=N+1}^{\infty} \mathcal{E}_i S_i^*(x). \quad (56)$$

Using Equations (9) and (56) and Theorem 12, we have

$$\begin{aligned} \|Y(x) - Y_N(x)\|_{L^2}^2 &= \int_0^1 |Y(x) - Y_N(x)|^2 V(x) dx \\ &= \int_0^1 \left(\sum_{i=N+1}^{\infty} \mathcal{E}_i S_i^*(x) \right)^2 V(x) dx \\ &= \int_0^1 \sum_{j=N+1}^{\infty} \sum_{i=N+1}^{\infty} \mathcal{E}_i \mathcal{E}_j S_i^*(x) S_j^*(x) V(x) dx \\ &= \sum_{i=N+1}^{\infty} \mathcal{E}_i^2 \lambda_i \leq \sum_{i=N+1}^{\infty} \Omega_i. \end{aligned} \quad (57)$$

\square

Theorem 14. Suppose that the continuous two-variable function $\mathcal{H}(x, y)$ is approximated on the interval $[0, 1] \times [0, 1]$ in terms of SSKCPs as $\mathcal{H}_N(x, y) = \sum_{i=0}^N \sum_{j=0}^N \mathcal{H}_{ij} S_i^*(x) S_j^*(y)$; then, the coefficients \mathcal{H}_{ij} , for $i, j = 0, 1, \dots, N$, can be bounded

as follows:

$$\begin{aligned} |\mathcal{H}_{ij}| &\leq \frac{\mathcal{M}_{\mathcal{H}} \pi}{4\lambda_i \lambda_j} \sum_{m=0}^i \frac{\rho_{mi} \Gamma(m + (3/2))}{\Gamma(m + 5)} (m^2 + m + 3) \\ &\quad \sum_{r=0}^j \frac{\rho_{rj} \Gamma(r + (3/2))}{\Gamma(r + 5)} (r^2 + r + 3), \end{aligned} \quad (58)$$

where $\mathcal{M}_{\mathcal{H}}$ denotes the maximum value of $|\mathcal{H}(x, y)|$ on the interval $[0, 1] \times [0, 1]$.

Proof. Using Equations (7) and (15), we have

$$\begin{aligned} \mathcal{H}_{ij} &= \frac{1}{\lambda_i \lambda_j} \int_0^1 \int_0^1 \mathcal{H}(x, y) S_i^*(x) S_j^*(y) V(x) V(y) dx dy \\ &= \frac{1}{\lambda_i \lambda_j} \int_0^1 \sum_{m=0}^i \rho_{mi} x^m V(x) \left(\int_0^1 \mathcal{H}(x, y) \sum_{r=0}^j \rho_{rj} y^r V(y) dy \right) dx \\ &= \frac{1}{\lambda_i \lambda_j} \sum_{m=0}^i \rho_{mi} \sum_{r=0}^j \rho_{rj} \int_0^1 \int_0^1 x^m \mathcal{H}(x, y) y^r V(x) V(y) dx dy. \end{aligned} \quad (59)$$

Since $\mathcal{H}(x, y)$ is a bounded and continuous function on the interval $[0, 1] \times [0, 1]$, so there is a constant $\mathcal{M}_{\mathcal{H}}$ such that

$$\forall (x, y) \in [0, 1] \times [0, 1], |\mathcal{H}(x, y)| \leq \mathcal{M}_{\mathcal{H}}. \quad (60)$$

Using Equations (59) and (60), Theorem 14 is proved. \square

Theorem 15. Suppose that $\mathcal{H}(x, y)$ is a continuous function with two variables and $\mathcal{H}_N(x, y)$ is the approximation to $\mathcal{H}(x, y)$ using SSKCPs. Then, the error bound can be obtained as

$$\begin{aligned} \|\mathcal{H}(x, y) - \mathcal{H}_N(x, y)\|_{L^2} &\leq \left(\sum_{i=0}^N \sum_{j=N+1}^{\infty} \zeta_{ij}^2 \lambda_i \lambda_j \right)^{1/2} \\ &\quad + \left(\sum_{i=N+1}^{\infty} \sum_{j=0}^N \zeta_{ij}^2 \lambda_i \lambda_j \right)^{1/2} = \Lambda_{\mathcal{H}}, \end{aligned} \quad (61)$$

where

$$\begin{aligned} \zeta_{ij} &= \frac{\mathcal{M}_{\mathcal{H}} \pi}{4\lambda_i \lambda_j} \sum_{m=0}^i \rho_{mi} \frac{\Gamma(m + (3/2))}{\Gamma(m + 5)} (m^2 + m + 3) \\ &\quad \sum_{r=0}^j \rho_{rj} \frac{\Gamma(r + (3/2))}{\Gamma(r + 5)} (r^2 + r + 3). \end{aligned} \quad (62)$$

Proof. Suppose that $\mathcal{H}(x, y)$ is an arbitrary function. SSKCP series of $\mathcal{H}(x, y)$ and its approximation in terms of SSKCPs

have the following form:

$$\mathcal{H}(x, y) = \sum_{i=0}^{\infty} \sum_{j=0}^{\infty} \mathcal{H}_{ij} S_i^*(x) S_j^*(y), \mathcal{H}_N(x, y) = \sum_{i=0}^N \sum_{j=0}^N \mathcal{H}_{ij} S_i^*(x) S_j^*(y). \tag{63}$$

□

Thus,

$$\mathcal{H}(x, y) - \mathcal{H}_N(x, y) = \sum_{i=0}^N \sum_{j=N+1}^{\infty} \mathcal{H}_{ij} S_i^*(x) S_j^*(y) + \sum_{i=N+1}^{\infty} \sum_{j=0}^{\infty} \mathcal{H}_{ij} S_i^*(x) S_j^*(y). \tag{64}$$

Using Equations (9) and (64) and Theorem 14, we conclude

$$\begin{aligned} \|\mathcal{H}(x, y)(x) - \mathcal{H}_N(x, y)\|_{L^2} &\leq \left\| \sum_{i=0}^N \sum_{j=N+1}^{\infty} \mathcal{H}_{ij} S_i^*(x) S_j^*(y) \right\|_{L^2} + \left\| \sum_{i=N+1}^{\infty} \sum_{j=0}^{\infty} \mathcal{H}_{ij} S_i^*(x) S_j^*(y) \right\|_{L^2} \\ &= \left(\int_0^1 \int_0^1 \left(\sum_{i=0}^N \sum_{j=N+1}^{\infty} \mathcal{H}_{ij} S_i^*(x) S_j^*(y) \right)^2 V(x) V(y) dy dx \right)^{1/2} \\ &\quad + \left(\int_0^1 \int_0^1 \left(\sum_{i=N+1}^{\infty} \sum_{j=0}^{\infty} \mathcal{H}_{ij} S_i^*(x) S_j^*(y) \right)^2 V(x) V(y) dy dx \right)^{1/2} = \left(\sum_{i=0}^N \sum_{j=N+1}^{\infty} \mathcal{H}_{ij}^2 \lambda_i \lambda_j \right)^{1/2} \\ &\quad + \left(\sum_{i=N+1}^{\infty} \sum_{j=0}^{\infty} \mathcal{H}_{ij}^2 \lambda_i \lambda_j \right)^{1/2} \leq \left(\sum_{i=0}^N \sum_{j=N+1}^{\infty} c_{ij}^2 \lambda_i \lambda_j \right)^{1/2} + \left(\sum_{i=N+1}^{\infty} \sum_{j=0}^{\infty} c_{ij}^2 \lambda_i \lambda_j \right)^{1/2}. \end{aligned} \tag{65}$$

In the following theorem, we obtain an upper error bound of the proposed method. First, suppose that for the $u_i(x), y_i(x) \in C^r[0, 1], i = 1, 2, \dots, m$, there exist positive constants $\xi_r^i, \eta_j^i > 0$ such that the following Lipschitz conditions hold.

- (1) $\| \mathcal{F}_i(x, u_1(x), u_2(x), \dots, u_m(x)) - \mathcal{F}_i(x, y_1(x), y_2(x), \dots, y_m(x)) \|_{L^2} \leq \xi_1^i \|u_1(x) - y_1(x)\|_{L^2} + \xi_2^i \|u_2(x) - y_2(x)\|_{L^2} + \dots + \xi_m^i \|u_m(x) - y_m(x)\|_{L^2}, i = 1, 2, \dots, m$
- (2) $\|G_{ij}(z, u_j(z)) - G_{ij}(z, y_j(z))\|_{L^2} \leq \eta_j^i \|u_j(z) - y_j(z)\|_{L^2}, i, j = 1, 2, \dots, m$

Theorem 16. Suppose that $\tilde{U}(x) = (\tilde{u}_1(x), \tilde{u}_2(x), \dots, \tilde{u}_m(x))$ is a set of approximate solutions obtained from the SSKCP collocation method, $U(x) = (u_1(x), u_2(x), \dots, u_m(x))$ is the set of exact solutions of system (1), $E = (\|u_1(x) - \tilde{u}_1(x)\|_{L^2}, \dots, \|u_m(x) - \tilde{u}_m(x)\|_{L^2})$ is the error vector of approximate solutions, and also $r_i(x), i = 1, 2, \dots, m$ denote the residual functions associated to the approximate solutions that are named perturbation terms. Assume that Hypotheses (1) and (2) are satisfied; then, a bound for the method error can be achieved as

$$\|E\|_1 \leq \frac{\Gamma_N^* + \sum_{i=1}^m \sum_{j=1}^m \gamma_j^i}{1 - \Delta_N^*}, 0 < \Delta_N^* < 1. \tag{66}$$

Proof. First, we apply the Riemann-Liouville integral operator on Equation (1) and obtain the following equation:

$$\begin{aligned} u_i(x) &= g_i(x) + \frac{1}{\Gamma(\nu_i)} \int_0^x (x-z)^{\nu_i-1} \mathcal{F}_i(z, u_1(z), u_2(z), \dots, u_m(z)) dz \\ &\quad + \sum_{j=1}^m \theta_{ij} \frac{\Gamma(1-\alpha_{ij})}{\Gamma(\nu_i - \alpha_{ij} + 1)} \int_0^x (x-z)^{\nu_i-\alpha_{ij}} K_{ij}(x, z) G_{ij}(z, u_j(z)) dz, \end{aligned} \tag{67}$$

where

$$g_i(x) = \sum_{k=0}^{r-1} \frac{u_{0i}^{(k)}}{\Gamma(k+1)} x^k + \frac{1}{\Gamma(\nu_i)} \int_0^x (x-z)^{\nu_i-1} f_i(z) dz. \tag{68}$$

We can write the approximate equation of Equation (67) as follows:

$$\begin{aligned} \tilde{u}_i(x) &= g_i(x) + \frac{1}{\Gamma(\nu_i)} \int_0^x (x-z)^{\nu_i-1} \mathcal{F}_i(z, \tilde{u}_1(z), \tilde{u}_2(z), \dots, \tilde{u}_m(z)) dz \\ &\quad + \sum_{j=1}^m \theta_{ij} \frac{\Gamma(1-\alpha_{ij})}{\Gamma(\nu_i - \alpha_{ij} + 1)} \int_0^x (x-z)^{\nu_i-\alpha_{ij}} \tilde{K}_{ij}(x, z) G_{ij}(z, \tilde{u}_j(z)) dz \\ &\quad + r_i(x), \end{aligned} \tag{69}$$

where $r_i(x)$ is the perturbation term. We subtract Equation (69) from Equation (67) and obtain the following result:

$$\begin{aligned} r_i(x) &= u_i(x) - \tilde{u}_i(x) + \frac{1}{\Gamma(\nu_i)} \int_0^x (x-z)^{\nu_i-1} (\mathcal{F}_i(z, u_1(z), u_2(z), \dots, u_m(z)) - \mathcal{F}_i(z, \tilde{u}_1(z), \tilde{u}_2(z), \dots, \tilde{u}_m(z))) dz \\ &\quad + \sum_{j=1}^m \theta_{ij} \frac{\Gamma(1-\alpha_{ij})}{\Gamma(\nu_i - \alpha_{ij} + 1)} \int_0^x (x-z)^{\nu_i-\alpha_{ij}} (K_{ij}(x, z) G_{ij}(z, u_j(z)) - \tilde{K}_{ij}(x, z) G_{ij}(z, \tilde{u}_j(z))) dz. \end{aligned} \tag{70}$$

First, we obtain a bound for the perturbation term, so by taking the L^2 -norm on Equation (70), we get the following inequality:

$$\begin{aligned} \|r_i(x)\|_{L^2} \leq & \|u_i(x) - \tilde{u}_i(x)\|_{L^2} + \frac{1}{\Gamma(\nu_i)} \left\| \int_0^x (x-z)^{\nu_i-1} (\mathcal{F}_i(z, u_1(z), \dots, u_m(z)) - \mathcal{F}_i(z, \tilde{u}_1(z), \dots, \tilde{u}_m(z))) dz \right\|_{L^2} \\ & + \sum_{j=1}^m \theta_{ij} \frac{\Gamma(1-\alpha_{ij})}{\Gamma(\nu_i-\alpha_{ij}+1)} \times \left\| \int_0^x (x-z)^{\nu_i-\alpha_{ij}} (K_{ij}(x, z)G_{ij}(z, u_j(z)) - \tilde{K}_{ij}(x, z)G_{ij}(z, \tilde{u}_j(z))) dz \right\|_{L^2}. \end{aligned} \tag{71}$$

Using Hypothesis 1 and Theorem 13, we have

$$\frac{1}{\Gamma(\nu_i)} \left\| \int_0^x (x-z)^{\nu_i-1} (\mathcal{F}_i(z, u_1(z), u_2(z), \dots, u_m(z)) - \mathcal{F}_i(z, \tilde{u}_1(z), \tilde{u}_2(z), \dots, \tilde{u}_m(z))) dz \right\|_{L^2} \leq \Psi_{\nu_i} \sum_{j=1}^m \xi_j^i \|u_j(z) - \tilde{u}_j(z)\|_{L^2} \leq \Psi_{\nu_i} \sum_{j=1}^m \xi_j^i \Omega_N^j, \tag{72}$$

where

$$\Psi_{\nu_i} = \frac{1}{\Gamma(\nu_i)} \left(\frac{4\Gamma(7/2)\Gamma(2\nu_i - (1/2))}{\Gamma(2\nu_i + 3)} - \frac{4\Gamma(5/2)\Gamma(2\nu_i - (1/2))}{\Gamma(2\nu_i + 2)} + \frac{\Gamma(3/2)\Gamma(2\nu_i - (1/2))}{\Gamma(2\nu_i + 1)} \right)^{1/2}. \tag{73}$$

Noting that $K_{ij}(x, z)$ and $G_{ij}(z, u_j(z))$ are continuous and known functions, thus, there are constants $M_{K_{ij}}$ and $N_{G_{ij}}$ such that

$$\|K_{ij}(x, z)\|_{L^2} \leq M_{K_{ij}}, \|G_{ij}(z, u_j(z))\|_{L^2} \leq N_{G_{ij}}. \tag{74}$$

From Hypothesis 2, Theorem 13, Theorem 15, and Equation (74), the following inequality is obtained:

$$\begin{aligned} \sum_{j=1}^m \theta_{ij} \frac{\Gamma(1-\alpha_{ij})}{\Gamma(\nu_i-\alpha_{ij}+1)} \left\| \int_0^x (x-z)^{\nu_i-\alpha_{ij}} (K_{ij}(x, z)G_{ij}(z, u_j(z)) - \tilde{K}_{ij}(x, z)G_{ij}(z, \tilde{u}_j(z))) dz \right\|_{L^2} \leq \\ \sum_{j=1}^m \theta_{ij} \Psi_{\nu_i-\alpha_{ij}} \left(M_{K_{ij}} \eta_j^i \|u_j(z) - \tilde{u}_j(z)\|_{L^2} + N_{G_{ij}} \Lambda_{K_{ij}} \right) \leq \sum_{j=1}^m \theta_{ij} \Psi_{\nu_i-\alpha_{ij}} \left(M_{K_{ij}} \eta_j^i \Omega_N^j + N_{G_{ij}} \Lambda_{K_{ij}} \right), \end{aligned} \tag{75}$$

where

$$\Psi_{\nu_i-\alpha_{ij}} = \frac{\Gamma(1-\alpha_{ij})}{\Gamma(\nu_i-\alpha_{ij}+1)} \times \left(\frac{4\Gamma(7/2)\Gamma(2(\nu_i-\alpha_{ij})+(3/2))}{\Gamma(2(\nu_i-\alpha_{ij})+5)} - \frac{4\Gamma(5/2)\Gamma(2(\nu_i-\alpha_{ij})+(3/2))}{\Gamma(2(\nu_i-\alpha_{ij})+4)} + \frac{\Gamma(3/2)\Gamma(2(\nu_i-\alpha_{ij})+(3/2))}{\Gamma(2(\nu_i-\alpha_{ij})+3)} \right)^{1/2}. \tag{76}$$

Here, Δ_j^i and γ_j^i can be introduced as below:

$$\Delta_j^i = \Psi_{v_i} \xi_j^i + \Psi_{v_i - \alpha_{ij}} \theta_{ij} M_{K_{ij}} \eta_j^i, \tag{77}$$

$$\gamma_j^i = \Psi_{v_i - \alpha_{ij}} \theta_{ij} N_{G_{ij}} \Lambda_{K_{ij}}. \tag{78}$$

From Equations (72)-(78), we can get the following upper bound for $r_i(x)$:

$$\|r_i(x)\|_{L^2} \leq \Omega_N^i + \sum_{j=1}^m \Delta_j^i \Omega_N^j + \sum_{j=1}^m \gamma_j^i, i = 1, 2, \dots, m. \tag{79}$$

By adding the above m inequalities, we have

$$\sum_{i=1}^m \|r_i(x)\|_{L^2} \leq \sum_{i=1}^m \Omega_N^i + \sum_{i=1}^m \sum_{j=1}^m \Delta_j^i \Omega_N^j + \sum_{i=1}^m \sum_{j=1}^m \gamma_j^i = \Gamma_N^*. \tag{80}$$

We define the vector R as

$$R = [\|r_1\|_{L^2}, \|r_2\|_{L^2}, \dots, \|r_m\|_{L^2}]^T. \tag{81}$$

Thus, we have

$$\|R\|_1 = \sum_{i=1}^m \|r_i\|_{L^2} \leq \Gamma_N^*. \tag{82}$$

Again, we consider Equation (70). So we have

$$\begin{aligned} \|u_i(x) - \tilde{u}_i(x)\|_{L^2} &\leq \|r_i(x)\|_{L^2} + \sum_{j=1}^m \Delta_j^i \|u_i(x) - \tilde{u}_i(x)\|_{L^2} \\ &\quad + \sum_{j=1}^m \gamma_j^i, i = 1, 2, \dots, m. \end{aligned} \tag{83}$$

Adding the above m inequalities leads to the following inequality:

$$\begin{aligned} &\sum_{i=1}^m \|u_i(x) - \tilde{u}_i(x)\|_{L^2} \\ &\leq \sum_{i=1}^m \|r_i(x)\|_{L^2} + \sum_{i=1}^m \sum_{j=1}^m \Delta_j^i \|u_i(x) - \tilde{u}_i(x)\|_{L^2} + \sum_{i=1}^m \sum_{j=1}^m \gamma_j^i \\ &= \|R\|_1 + (\Delta_1^1 \|u_1(x) - \tilde{u}_1(x)\|_{L^2} + \dots + \Delta_m^1 \|u_m(x) - \tilde{u}_m(x)\|_{L^2}) \\ &\quad + (\Delta_1^2 \|u_1(x) - \tilde{u}_1(x)\|_{L^2} + \dots + \Delta_m^2 \|u_m(x) - \tilde{u}_m(x)\|_{L^2}) \\ &\quad + \dots + (\Delta_1^m \|u_1(x) - \tilde{u}_1(x)\|_{L^2} + \dots + \Delta_m^m \|u_m(x) - \tilde{u}_m(x)\|_{L^2}) \\ &\quad + \sum_{i=1}^m \sum_{j=1}^m \gamma_j^i \\ &= \|R\|_1 + (\Delta_1^1 + \Delta_1^2 + \dots + \Delta_1^m) \|u_1(x) - \tilde{u}_1(x)\|_{L^2} \\ &\quad + \dots + (\Delta_m^1 + \Delta_m^2 + \dots + \Delta_m^m) \|u_m(x) - \tilde{u}_m(x)\|_{L^2} + \sum_{i=1}^m \sum_{j=1}^m \gamma_j^i. \end{aligned} \tag{84}$$

By defining the following quantities

$$\Delta_N^* = \text{Max} \left\{ \sum_{i=1}^m \Delta_j^i, j = 1, \dots, m \right\},$$

$$E = [\|u_1(x) - \tilde{u}_1(x)\|_{L^2}, \|u_2(x) - \tilde{u}_2(x)\|_{L^2}, \dots, \|u_m(x) - \tilde{u}_m(x)\|_{L^2}]^T, \tag{85}$$

we obtain the following upper bound for the method error:

$$\begin{aligned} \sum_{i=1}^m \|u_i(x) - \tilde{u}_i(x)\|_{L^2} &\leq \|R\|_1 + \Delta_N^* \sum_{i=1}^m \|u_i(x) - \tilde{u}_i(x)\|_{L^2} + \sum_{i=1}^m \sum_{j=1}^m \gamma_j^i \\ \|E\|_1 &\leq \frac{\Gamma_N^* + \sum_{i=1}^m \sum_{j=1}^m \gamma_j^i}{1 - \Delta_N^*}, 0 < \Delta_N^* < 1. \end{aligned} \tag{86}$$

□

6. Numerical Applications

In this section, three linear and nonlinear examples are presented to illustrate the practical implementation of our numerical method. Also, the comparison of results obtained from the proposed method with those of the other methods is shown. All calculations are done with mathematical software Maple 18.

Example 1. Let us consider the following linear system of WSFIDE:

$$\begin{cases} \mathcal{D}^{v_1} u_1(x) + u_1(x) + \int_0^x \frac{u_1(z)}{(x-z)^{1/2}} dz - \frac{1}{2} \int_0^x \frac{xu_2(z)}{(x-z)^{1/2}} dz = f_1(x), \\ \mathcal{D}^{v_2} u_2(x) + u_2(x) + \frac{1}{3} \int_0^x \frac{x^2 u_1(z)}{(x-z)^{1/2}} dz + \frac{1}{3} \int_0^x \frac{u_2(z)}{(x-z)^{1/2}} dz = f_2(x), \end{cases} \tag{87}$$

where

$$\begin{aligned} f_1(x) &= 2x + x^2 + \frac{2}{5} x^{5/2}, \\ f_2(x) &= 1 + x + \frac{32}{105} x^{1/2} + \frac{4}{9} x^{3/2}, \end{aligned} \tag{88}$$

and $0 < v_i \leq 1, i = 1, 2$, and the initial conditions are $u_1(0) = u_2(0) = 0$. The exact solutions are $u_1(x) = x^2$ and $u_2(x) = x$ if $v_1 = v_2 = 1$. According to the procedure presented in Section 4, we reach the following approximations:

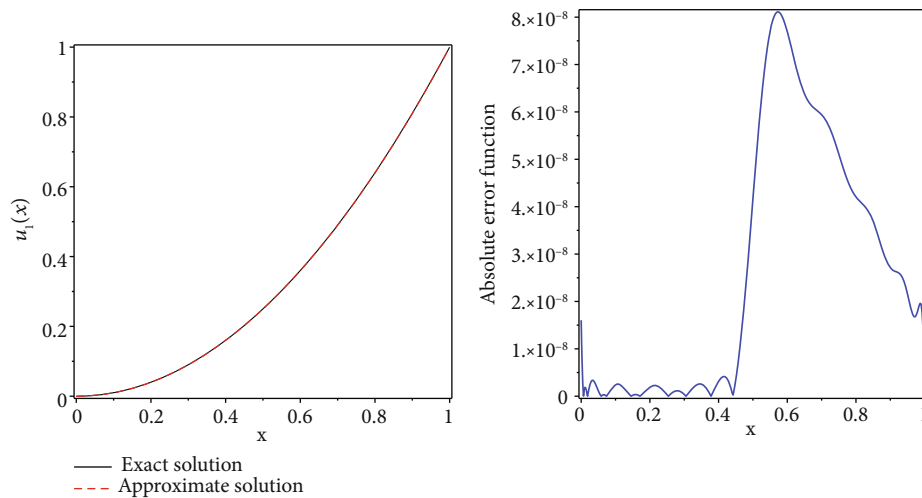


FIGURE 1: The graphs of the exact and approximate solutions and the absolute error function of $\tilde{u}_1(x)$ for $N = 20$ and $\nu_1 = \nu_2 = 1$ of Example 1.

$$\begin{aligned}
 \mathcal{D}^{\nu_1} u_1(x) &\approx S^T(x)F_1, & u_1(x) &\approx S^T(x)\mathcal{P}^{(\nu_1)T}F_1 = S^T(x)U_1, \\
 \mathcal{D}^{\nu_2} u_2(x) &\approx S^T(x)F_2, & u_2(x) &\approx S^T(x)\mathcal{P}^{(\nu_2)T}F_2 = S^T(x)U_2, \\
 x &\approx S^T(x)K_{12}S(z), & x^2 z &\approx S^T(x)K_{21}S(z), \\
 \int_0^x \frac{u_1(z)}{(x-z)^{1/2}} dz &\approx \int_0^x \frac{U_1^T S(z)}{(x-z)^{1/2}} dz = U_1^T \int_0^x \frac{S(z)}{(x-z)^{1/2}} dz \approx U_1^T \mathfrak{F}^{(1/2)} S(x), \\
 \int_0^x \frac{xu_2(z)}{(x-z)^{1/2}} dz &\approx \int_0^x \frac{S^T(x)K_{12}S(z)S^T(z)U_2}{(x-z)^{1/2}} dz = S^T(x)K_{12} \int_0^x \frac{S(z)S^T(z)U_2}{(x-z)^{1/2}} dz \approx S^T(x)K_{12}\tilde{U}_2 \int_0^x \frac{S(z)}{(x-z)^{1/2}} dz \approx S^T(x)K_{12}\tilde{U}_2 \mathfrak{F}^{(1/2)} S(x), \\
 \int_0^x \frac{x^2 zu_1(z)}{(x-z)^{1/2}} dz &\approx \int_0^x \frac{S^T(x)K_{21}S(z)S^T(z)U_1}{(x-z)^{1/2}} dz = S^T(x)K_{21} \int_0^x \frac{S(z)S^T(z)U_1}{(x-z)^{1/2}} dz = S^T(x)K_{21}\tilde{U}_1 \int_0^x \frac{S(z)}{(x-z)^{1/2}} dz \approx S^T(x)K_{21}\tilde{U}_1 \mathfrak{F}^{(1/2)} S(x), \\
 \int_0^x \frac{u_2(z)}{(x-z)^{1/2}} dz &\approx \int_0^x \frac{U_2^T S(z)}{(x-z)^{1/2}} dz \approx U_2^T \int_0^x \frac{S(z)}{(x-z)^{1/2}} dz \approx U_2^T \mathfrak{F}^{(1/2)} S(x),
 \end{aligned} \tag{89}$$

where \tilde{U}_1 and \tilde{U}_2 are the operational matrices of the product, corresponding to the vectors U_1 and U_2 , respectively.

Setting above approximations in system (87) leads to the following linear algebraic system.

$$\begin{cases} S^T(x)F_1 + S^T(x)U_1 + U_1^T \mathfrak{F}^{(1/2)} S(x) - \frac{1}{2} S^T(x)K_{12}\tilde{U}_2 \mathfrak{F}^{(1/2)} S(x) - f_1(x) \approx 0, \\ S^T(x)F_2 + S^T(x)U_2 + \frac{1}{3} S^T(x)K_{21}\tilde{U}_1 \mathfrak{F}^{(1/2)} S(x) + \frac{1}{3} U_2^T \mathfrak{F}^{(1/2)} S(x) - f_2(x) \approx 0. \end{cases} \tag{90}$$

Figures 1 and 2 show a comparison between the exact and numerical solutions and absolute error functions for $\nu_1 = \nu_2 = 1$ and $N = 20$. The maximum absolute errors are listed in Table 1 in versus of N . It can be seen that our proposed method shows good consistency between the numerical results and analytic solutions and also this method can achieve a higher convergence result when N increases. Figure 3 shows

the behavior of the numerical solutions for $N = 20$ and $\nu_i = 0.8, 0.9, 1, i = 1, 2$. As seen from Figure 3, as $\nu_i \rightarrow 1$, the approximate solutions are $\tilde{u}_i(x) \rightarrow u_i(x)$ for $i = 1, 2$.

Here, we calculate a numerical error bound for the first example. This result could confirm the correctness of the analytical error bound. This validation could be accomplished similarly for the other cases, but the calculations

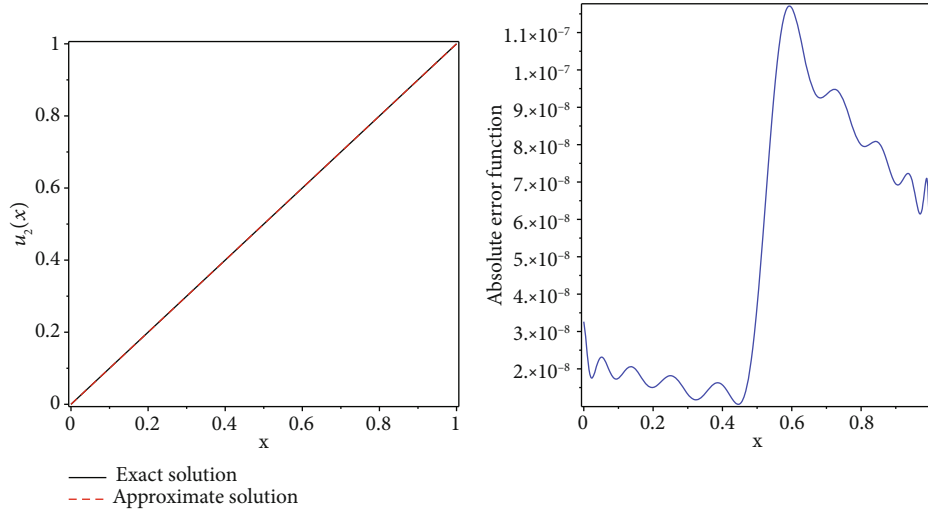


FIGURE 2: The graphs of the exact and approximate solutions and the absolute error function of $\tilde{u}_2(x)$ for $N = 20$ and $\nu_1 = \nu_2 = 1$ of Example 1.

are long.

$$\begin{aligned} \|u_1(x) - \tilde{u}_1(x)\|_{L^2} &= 8.93650018 \times 10^{-9}, \\ \|u_2(x) - \tilde{u}_2(x)\|_{L^2} &= 1.81941246 \times 10^{-8}, \\ E &= [8.93650018 \times 10^{-9}, 1.81941246 \times 10^{-8}]^T, \\ \|E\|_1 &= 2.71305687 \times 10^{-8}, \\ \xi_1^1 &= 0.4, \\ \xi_2^1 &= 0.3, \\ \xi_1^2 &= 0.8, \\ \xi_2^2 &= 0.62, \\ \eta_1^1 = \eta_1^2 = \eta_2^1 = \eta_2^2 &= 1, \\ \Psi_{\nu_1} = \Psi_{\nu_2} &= 0.31332853, \\ \Psi_{\nu_1 - \alpha_{11}} = \Psi_{\nu_1 - \alpha_{12}} &= 0.31332834, \\ \Psi_{\nu_2 - \alpha_{21}} = \Psi_{\nu_2 - \alpha_{22}} &= 0.31332834, \\ \Delta_1^1 &= 0.43865995, \\ \Delta_1^2 &= 0.25392268, \\ \Delta_2^1 &= 0.12405832, \\ \Delta_2^2 &= 0.29870654, \\ \Delta_N^* &= \text{Max} \left\{ \sum_{i=1}^2 \Delta_j^i, j = 1, 2 \right\} = 0.69258263, \\ \Lambda_{K_{11}} = \Lambda_{K_{12}} = \Lambda_{K_{21}} = \Lambda_{K_{22}} &= 14.31641021, \\ \gamma_1^1 &= 0.72969033, \\ \gamma_2^1 &= -0.43034788, \\ \gamma_1^2 &= 0.24323011, \\ \gamma_2^2 &= 0.28689859, \\ \Gamma_N^* &= 2.71305877 \times 10^{-8}, \\ \frac{\Gamma_N^* + \sum_{i=1}^m \sum_{j=1}^m \gamma_j^i}{1 - \Delta_N^*} &= 2.69819226, \\ \|E\|_1 &= 2.71305687 \times 10^{-8} \leq 2.69819226. \end{aligned}$$

TABLE 1: Maximum absolute errors for different values of N for Example 1.

N	$u_1(x)$	$u_2(x)$	CPU time
3	2.7867×10^{-5}	3.0371×10^{-5}	3.010
8	3.7450×10^{-6}	4.7250×10^{-6}	8.642
11	2.3054×10^{-7}	7.7804×10^{-7}	18.330
16	2.1369×10^{-7}	3.0206×10^{-7}	68.048
20	8.0541×10^{-8}	1.1680×10^{-7}	166.843

Example 2. In this example, consider the following system of linear WSFIDEs [13, 18]:

$$\begin{aligned} \mathcal{D}^{\nu_1} u_1(x) - u_3(x) - \int_0^x \frac{xzu_1(z)}{(x-z)^{1/2}} dz - \int_0^x \frac{u_2(z)}{(x-z)^{1/2}} dz &= f_1(x), \\ \mathcal{D}^{\nu_2} u_2(x) - u_1(x) - \int_0^x \frac{u_2(z)}{(x-z)^{1/3}} dz - \int_0^x \frac{u_3(z)}{(x-z)^{1/3}} dz &= f_2(x), \\ \mathcal{D}^{\nu_3} u_3(x) - u_3(x) - \int_0^x \frac{u_1(z)}{(x-z)^{1/4}} dz - \int_0^x \frac{x^2 zu_2(z)}{(x-z)^{1/4}} dz &= f_3(x), \end{aligned} \tag{92}$$

where $0 \leq x \leq 1$ and

$$\begin{aligned} f_1(x) &= 2x - 1 - x^3 + \frac{16}{15}x^{7/2} - \frac{16}{15}x^{5/2} - \frac{32}{35}x^{9/2}, \\ f_2(x) &= 2x - x(x-1) - \frac{27}{40}x^{8/3} - \frac{243}{440}x^{11/3}, \\ f_3(x) &= 3x^2 - x^3 + \frac{16}{21}x^{7/4} - \frac{128}{231}x^{11/4} - \frac{512}{1155}x^{23/4}, \end{aligned} \tag{93}$$

and $0 < \nu_i \leq 1, i = 1, 2, 3$, the initial conditions are $u_1(0) = u_2(0) = u_3(0) = 0$. The exact solutions are $u_1(x) = x(x-1)$,

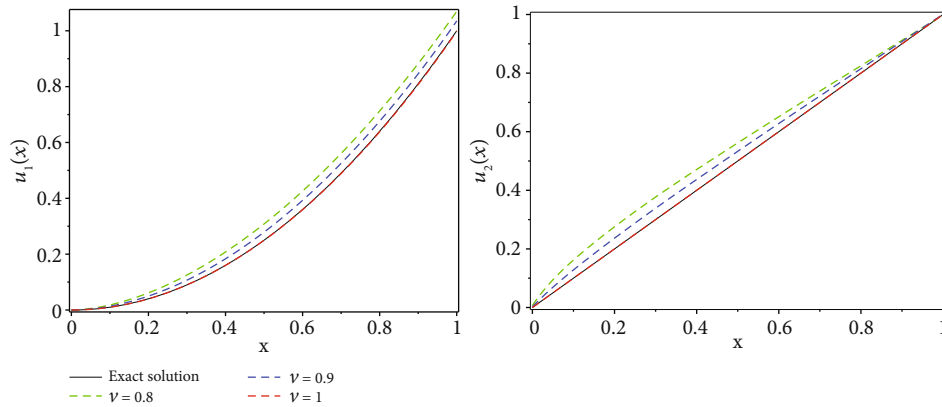


FIGURE 3: Some illustrations for the exact and approximate solutions using different values of ν_i ; $\nu_i = 0.8, 0.9, 1, i = 1, 2$ in Example 1.

TABLE 2: Maximum absolute errors for different values of N for Example 2.

N	$u_1(x)$	$u_2(x)$	$u_3(x)$	CPU time
4	8.1514×10^{-5}	6.7763×10^{-5}	1.0743×10^{-4}	5.382
9	2.3334×10^{-6}	1.8107×10^{-6}	3.3112×10^{-6}	17.457
12	6.8859×10^{-7}	5.4537×10^{-7}	1.1140×10^{-6}	36.941
17	1.2296×10^{-7}	9.5306×10^{-8}	2.0253×10^{-7}	115.316
20	5.9278×10^{-8}	4.6454×10^{-8}	1.0049×10^{-7}	216.638

TABLE 3: Maximum absolute errors obtained by SSKCP collocation and Jacobi collocation methods for $N = 9, \alpha = -1/2,$ and $\beta = 1/2$ in Example 2.

Method	$u_1(x)$	$u_2(x)$	$u_3(x)$
SSKCP collocation	2.3334×10^{-6}	1.8107×10^{-6}	3.3112×10^{-6}
Jacobi collocation [18]	2.0034×10^{-6}	1.8376×10^{-6}	2.0763×10^{-6}

$u_2(x) = x^2, u_3(x) = x^3$ if $\nu_1 = \nu_2 = \nu_3 = 1$. By assuming that $\mathcal{D}^{\nu_1} u_1(x) \approx S^T(x)F_1, \mathcal{D}^{\nu_2} u_2(x) \approx S^T(x)F_2,$ and $\mathcal{D}^{\nu_3} u_3(x) \approx S^T(x)F_3$ and using proper operational matrices, the following approximations are obtained:

$$\begin{aligned}
 u_1(x) &\approx S^T(x)\mathcal{D}^{(\nu_1)T}F_1 = S^T(x)U_1, \\
 u_2(x) &\approx S^T(x)\mathcal{D}^{(\nu_2)T}F_2 = S^T(x)U_2, \\
 u_3(x) &\approx S^T(x)\mathcal{D}^{(\nu_3)T}F_3 = S^T(x)U_3, \\
 xz &\approx S^T(x)K_{11}S(z), x^2z \approx S^T(x)K_{32}S(z), \\
 \int_0^x \frac{xzu_1(z)}{(x-z)^{1/2}} dz + \int_0^x \frac{u_2(z)}{(x-z)^{1/2}} dz &\approx S^T(x)K_{11}\tilde{U}_1\mathfrak{F}^{(1/2)}S(x) + U_2^T\mathfrak{F}^{(1/2)}S(x), \\
 \int_0^x \frac{u_2(z)}{(x-z)^{1/3}} dz + \int_0^x \frac{u_3(z)}{(x-z)^{1/3}} dz &\approx U_2^T\mathfrak{F}^{(1/3)}S(x) + U_3^T\mathfrak{F}^{(1/3)}S(x), \\
 \int_0^x \frac{u_1(z)}{(x-z)^{1/4}} dz + \int_0^x \frac{x^2zu_2(z)}{(x-z)^{1/4}} dz &\approx U_1^T\mathfrak{F}^{(1/4)}S(x) + S^T(x)K_{32}\tilde{U}_2\mathfrak{F}^{(1/4)}S(x),
 \end{aligned}
 \tag{94}$$

where \tilde{U}_1 and \tilde{U}_2 are the operational matrices of product, corresponding to the vectors U_1 and U_2 , respectively. By

substituting the above approximations into Equation (92), we achieve the following algebraic system

$$\begin{aligned}
 S^T(x)F_1 - S^T(x)U_3 - S^T(x)K_{11}\tilde{U}_1\mathfrak{F}^{(1/2)}S(x) - U_2^T\mathfrak{F}^{(1/2)}S(x) - f_1(x) &\approx 0, \\
 S^T(x)F_2 - S^T(x)U_1 - U_2^T\mathfrak{F}^{(1/3)}S(x) - U_3^T\mathfrak{F}^{(1/3)}S(x) - f_2(x) &\approx 0, \\
 S^T(x)F_3 - S^T(x)U_3 - U_1^T\mathfrak{F}^{(1/4)}S(x) - S^T(x)K_{32}\tilde{U}_2\mathfrak{F}^{(1/4)}S(x) - f_3(x) &\approx 0.
 \end{aligned}
 \tag{95}$$

Solving the above system by the collocation method for $N = 9$, we can determine the unknown vectors $F_i, i = 1, 2, 3$. Table 2 displays the maximum absolute errors for various N . The data in this table show that the numerical solutions get close to the analytical solutions with the increase of values of N . Table 3 shows a comparison between the SSKCP collocation and Jacobi collocation methods. This table shows that the results are approximately the same as reported by [18]. Figures 4–6 display a graphical comparison between approximate solutions and exact solutions and also absolute error functions for $N = 9$. Figure 7 shows the behavior of the numerical solutions for $N = 9$ and $\nu_i = 0.85, 0.90, 0.95, 1, i = 1, 2, 3$. From Figure 7, it can be seen that as $\nu_i \rightarrow 1$, the approximate solutions are $\tilde{u}_i(x) \rightarrow u_i(x), i = 1, 2, 3$.

Example 3. Consider the following nonlinear system of WSFIDEs [13, 18]:

$$\begin{aligned}
 \mathcal{D}^{3/4}u_1(x) - u_2(x) - \int_0^x \frac{u_1(z)}{(x-z)^{1/2}} dz - \int_0^x \frac{u_2^2(z)}{(x-z)^{1/2}} dz &= f_1(x), \\
 \mathcal{D}^{1/2}u_2(x) - u_1^3(x) - \int_0^x \frac{u_1(z)}{(x-z)^{2/3}} dz - \int_0^x \frac{u_2(z)}{(x-z)^{2/3}} dz &= f_2(x),
 \end{aligned}
 \tag{96}$$

where $0 \leq x \leq 1$ and

$$\begin{aligned}
 f_1(x) &= \frac{2}{\Gamma(9/4)}x^{5/4} - x^3 - \frac{\Gamma(3)\Gamma(1/2)}{\Gamma(7/2)}x^{5/2} - \frac{\Gamma(7)\Gamma(1/2)}{\Gamma(5/2)}x^{13/2}, \\
 f_2(x) &= \frac{\Gamma(4)}{\Gamma(7/2)}x^{5/2} - x^6 - \frac{\Gamma(3)\Gamma(1/3)}{\Gamma(10/3)}x^{7/3} - \frac{\Gamma(4)\Gamma(1/3)}{\Gamma(13/3)}x^{10/3}.
 \end{aligned}
 \tag{97}$$

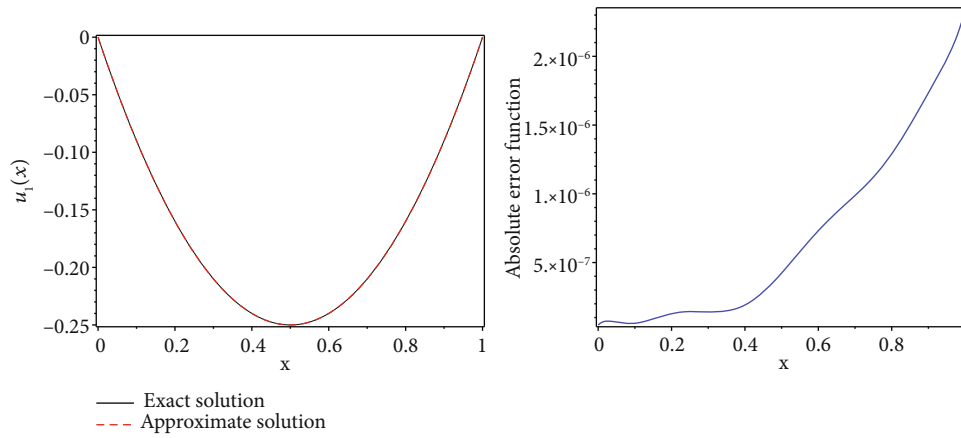


FIGURE 4: The graphs of the exact and approximate solutions and the absolute error function of $\tilde{u}_1(x)$ for $N=9$ and $\nu_1 = \nu_2 = \nu_3 = 1$ of Example 2.

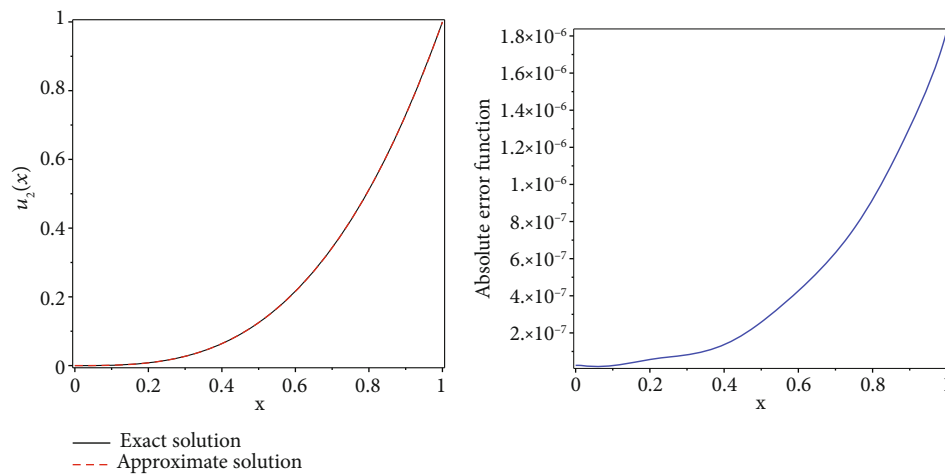


FIGURE 5: The graphs of the exact and approximate solutions and the absolute error function of $\tilde{u}_2(x)$ for $N=9$ and $\nu_1 = \nu_2 = \nu_3 = 1$ of Example 2.

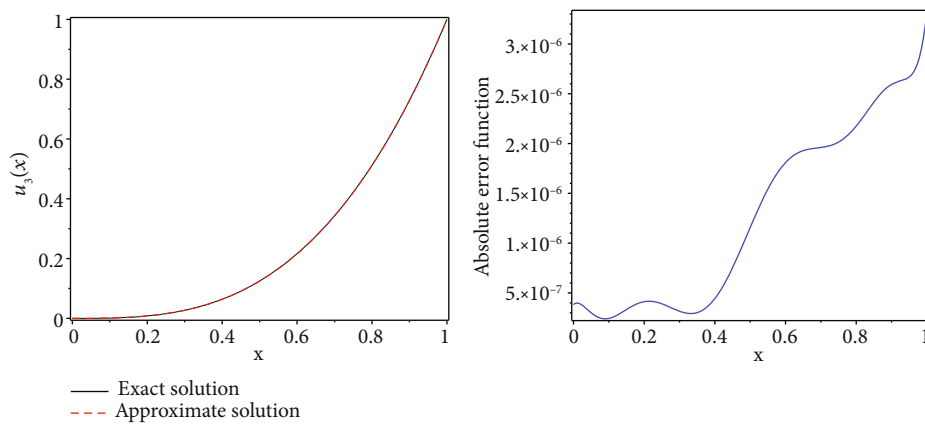


FIGURE 6: The graphs of the exact and approximate solutions and the absolute error function of $\tilde{u}_3(x)$ for $N=9$ and $\nu_1 = \nu_2 = \nu_3 = 1$ of Example 2.

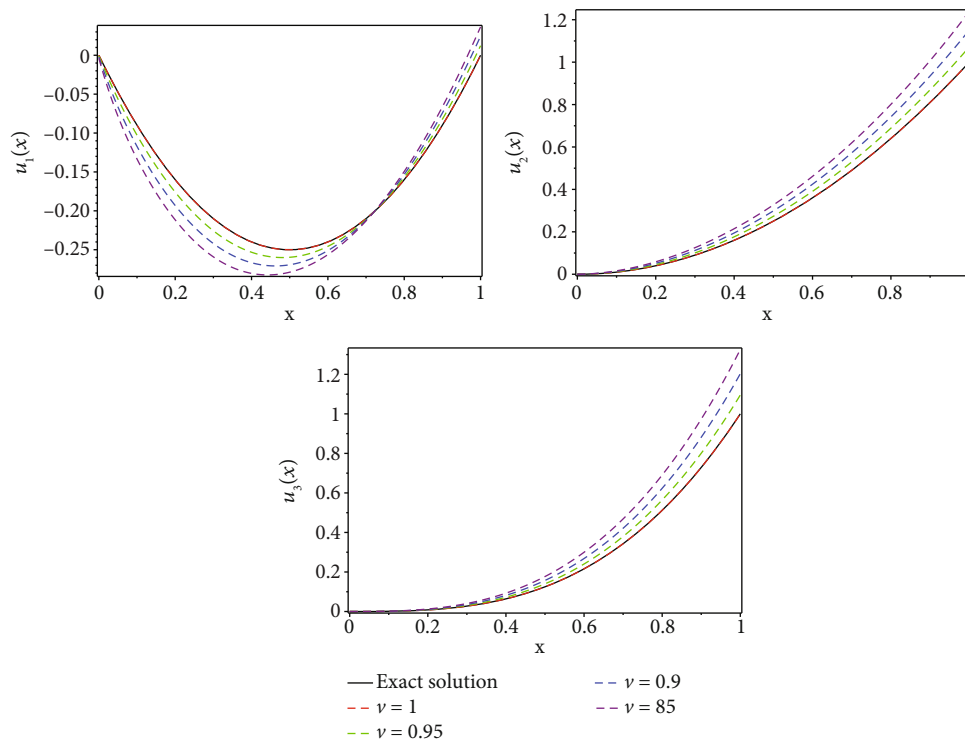


FIGURE 7: Some illustrations for the exact and approximate solutions using different values of ν_i : $\nu_i = 0.85, 0.90, 0.95, 1$, $i = 1, 2, 3$ for $N = 9$ in Example 2.

TABLE 4: Comparison between absolute errors of SSKCP collocation and Jacobi collocation methods at equally spaced points for $N = 12$ in Example 3.

x_i	SSKCP collocation method		Jacobi collocation method [18]	
	Error (u_1)	Error (u_2)	Error (u_1)	Error (u_2)
0.0	1.7182×10^{-5}	9.8329×10^{-7}	9.2840×10^{-6}	6.2830×10^{-7}
0.1	5.5657×10^{-6}	3.3268×10^{-6}	1.5202×10^{-6}	1.6472×10^{-7}
0.2	5.5935×10^{-6}	6.9555×10^{-6}	7.0504×10^{-7}	9.8923×10^{-8}
0.3	8.1095×10^{-6}	1.2777×10^{-5}	8.7678×10^{-7}	2.9284×10^{-7}
0.4	1.1355×10^{-5}	2.2448×10^{-5}	4.8193×10^{-7}	4.5120×10^{-7}
0.5	2.0566×10^{-5}	3.9797×10^{-5}	8.8367×10^{-7}	7.7271×10^{-7}
0.6	3.2387×10^{-5}	7.0527×10^{-5}	3.7500×10^{-7}	1.3807×10^{-6}
0.7	5.7063×10^{-5}	1.2877×10^{-4}	1.0664×10^{-6}	2.4661×10^{-6}
0.8	1.1121×10^{-4}	2.5191×10^{-4}	2.2537×10^{-6}	4.8902×10^{-6}
0.9	2.3722×10^{-4}	5.4688×10^{-4}	4.7116×10^{-6}	1.0475×10^{-5}
1.0	5.7984×10^{-4}	1.3758×10^{-3}	1.2704×10^{-5}	2.6197×10^{-5}

TABLE 5: Maximum absolute errors obtained by SSKCP collocation method for different values of N in Example 3.

N	Error (u_1)	Error (u_2)	CPU time
8	2.8334×10^{-3}	6.7948×10^{-3}	5.772
12	5.7819×10^{-4}	1.3597×10^{-3}	23.587
16	1.8841×10^{-4}	4.4719×10^{-4}	97.048
20	7.8006×10^{-5}	1.8536×10^{-4}	164.409
25	2.9931×10^{-5}	6.1196×10^{-5}	483.681

TABLE 6: Values of absolute errors at equally spaced points for $N = 25$ in Example 3.

x_i	Error (u_1)	Error (u_2)
0.0	1.3659×10^{-6}	3.2865×10^{-8}
0.1	2.6535×10^{-7}	1.7914×10^{-7}
0.2	3.1410×10^{-7}	3.8266×10^{-7}
0.3	4.3165×10^{-7}	7.0524×10^{-7}
0.4	6.3587×10^{-7}	1.2387×10^{-6}
0.5	9.6524×10^{-7}	2.1315×10^{-6}
0.6	1.5052×10^{-6}	3.6310×10^{-6}
0.7	2.8039×10^{-6}	6.5226×10^{-6}
0.8	5.5119×10^{-6}	1.2576×10^{-6}
0.9	1.1848×10^{-5}	2.7085×10^{-5}
1.0	2.8779×10^{-5}	6.9756×10^{-5}

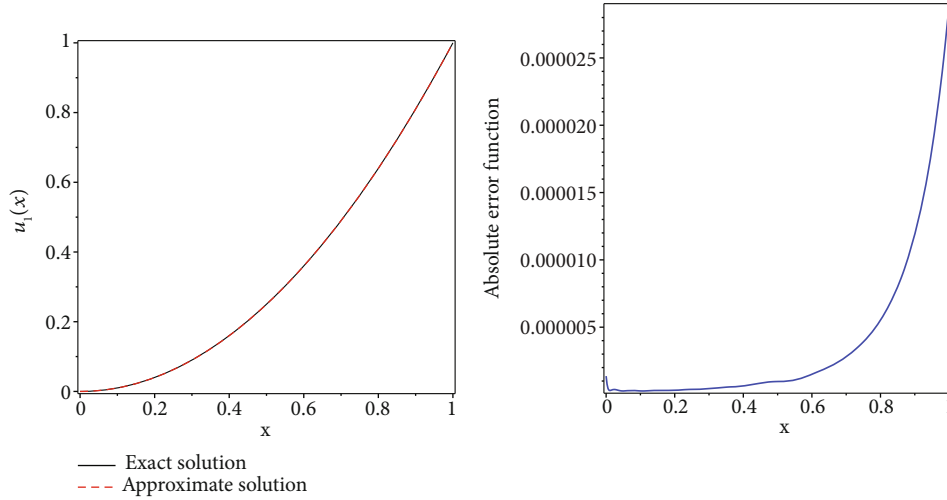


FIGURE 8: The graphs of the exact and approximate solutions and the absolute error function of $\tilde{u}_1(x)$ for $N = 25$ of Example 3.

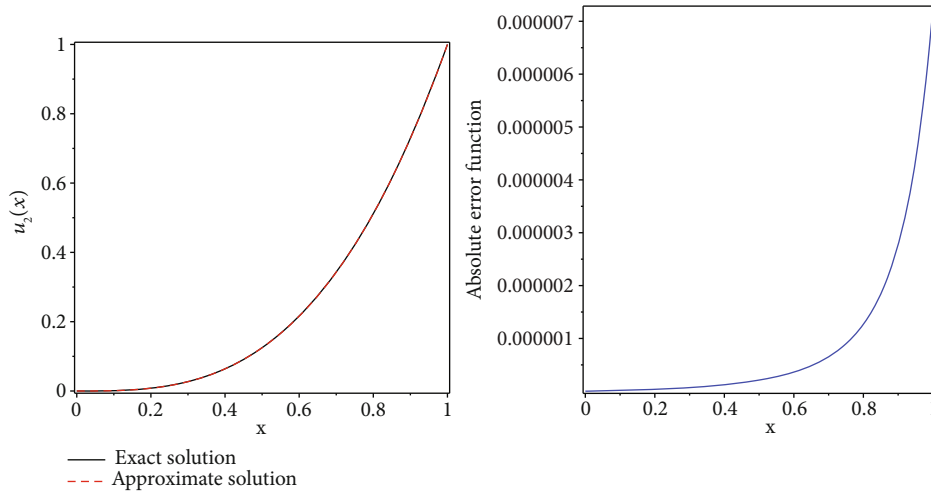


FIGURE 9: The graphs of the exact and approximate solutions and the absolute error function of $\tilde{u}_2(x)$ for $N = 25$ of Example 3.

The initial conditions are $u_1(0) = u_2(0) = 0$ and the exact solutions for this example are $u_1(x) = x^2$ and $u_2(x) = x^3$. We use the following approximations and convert the system (96) into an algebraic system, which will be described below:

$$\begin{aligned}
 \mathcal{D}^{3/4}u_1(x) &\approx S^T(x)F_1, & u_1(x) &\approx S^T(x)\mathcal{P}^{(3/4)T}F_1 = S^T(x)U_1, \\
 \mathcal{D}^{1/2}u_2(x) &\approx S^T(x)F_2, & u_2(x) &\approx S^T(x)\mathcal{P}^{(1/2)T}F_2 = S^T(x)U_2, \\
 u_1^3(x) &\approx S^T(x)U_3, & U_3 &\approx (\tilde{U}_1^2)^T U_1, \\
 u_2^2(x) &\approx S^T(x)U_4, & U_4 &\approx \tilde{U}_2^T U_2, \\
 \int_0^x \frac{u_1(z)}{(x-z)^{1/2}} dz + \int_0^x \frac{u_2^2(z)}{(x-z)^{1/2}} dz &\approx U_1^T \mathfrak{F}^{(1/2)} S(x) + U_4^T \mathfrak{F}^{(1/2)} S(x), \\
 \int_0^x \frac{u_1(z)}{(x-z)^{2/3}} dz + \int_0^x \frac{u_2(z)}{(x-z)^{2/3}} dz &\approx U_1^T \mathfrak{F}^{(2/3)} S(x) + U_2^T \mathfrak{F}^{(2/3)} S(x),
 \end{aligned}
 \tag{98}$$

where \tilde{U}_1 and \tilde{U}_2 are operational matrices of the product,

corresponding to the vectors U_1 and U_2 , respectively. So we have

$$\begin{cases}
 S^T(x)F_1 - S^T(x)U_2 - U_1^T \mathfrak{F}^{(1/2)} S(x) - U_4^T \mathfrak{F}^{(1/2)} S(x) - f_1(x) \approx 0, \\
 S^T(x)F_2 - S^T(x)U_3 - U_1^T \mathfrak{F}^{(2/3)} S(x) - U_2^T \mathfrak{F}^{(2/3)} S(x) - f_2(x) \approx 0.
 \end{cases}
 \tag{99}$$

Table 4 shows a comparison between the absolute errors of the SSKCP collocation method and the Jacobi collocation method at equally spaced points $x_i = 0.1i, i = 0, 1, \dots, 10$ for $N = 12$, which shows that the absolute errors of the Jacobi collocation method are less than the presented method, but with increasing N , the errors of the proposed method decrease. Maximum absolute errors for different values of N and numerical results for $N = 25$ reported in Tables 5 and 6 confirm that the results are close to those reported by [18]. Figures 8 and 9 show the comparison between the numerical results and the exact solutions and also the absolute error functions of $u_1(x), u_2(x)$ for $N = 25$, respectively.

7. Conclusion

In this paper, the shifted sixth-kind Chebyshev polynomials together with the collocation method were used to solve a class of the system of fractional integro-differential equations with weakly singular kernels. For this purpose, the integral and product operational matrices were calculated, and using the obtained approximations, the original system of equations was transformed into a corresponding linear and nonlinear system of algebraic equations that are easier for solving. Choosing an appropriate value of N , each of algebraic equations was collocated in the roots of $S_{N+1}^*(x)$, and finally, for obtaining the unknown vectors F_i , $i = 1, 2, \dots, m$, an algebraic system involving $m(N + 1)$ algebraic equations was solved. To eliminate the singularity of the kernels of the equations under study, an operational matrix was derived. Also, an error bound was determined for the proposed method. To show the ability and efficiency of the proposed method, three examples were presented and the maximum absolute errors were calculated for different N , and graphs of the absolute error functions and numerical solutions were plotted and numerical results showed a good agreement between the approximate and exact solutions. When the order of the fractional derivative ν was uncertain, the numerical solutions for the various values of ν , $0 < \nu \leq 1$, were approached to the exact solutions as $\nu \rightarrow 1$. The comparison of the proposed method with the Jacobi collocation method [18] showed good implementation of SSKCP collocation method for solving a system of linear fractional integro-differential equations with weakly singular kernels and for a system of nonlinear WSFIDEs; the error decreased with increasing N . CPU times were computed for all examples. According to the numerical results which were obtained in the relevant instances and compared with exact solutions and those obtained from the Jacobi collocation method, it can be concluded that the SSKCP collocation method is very helpful to look for approximate solutions of a system of WSFIDEs. This method can be applied to the linear and nonlinear systems of fractional-order Volterra-Fredholm integro-differential equations with weakly singular kernels, but additional operational matrices are required.

Data Availability

All results have been obtained by conducting the numerical procedure, and the ideas can be shared for the researchers.

Conflicts of Interest

The authors declare that they have no conflicts of interest.

References

- [1] D. A. Miller, *Fractional Calculus, Minor Thesis Part of PHD*, West Virginia University, 2004.
- [2] I. Podlubny, *Fractional Differential Equations*, Elsevier, 1998.
- [3] N. Sweilam, M. Khader, and R. Al-Bar, "Numerical studies for a multi-order fractional differential equation," *Physics Letters A*, vol. 371, no. 1-2, pp. 26-33, 2007.
- [4] D. Baleanu, A. Jajarmi, S. Sajjadi, and D. Mozyrska, "A new fractional model and optimal control of a tumor-immune surveillance with non-singular derivative operator," *Journal of Nonlinear Science*, vol. 29, no. 8, article 083127, 2019.
- [5] Ş. Yüzbaşı, "A numerical approximation for Volterra's population growth model with fractional order," *Applied Mathematical Modelling*, vol. 37, no. 5, pp. 3216-3227, 2013.
- [6] H. Sadeghian, H. Salarieh, A. Alasty, and A. Meghdari, "On the fractional-order extended Kalman filter and its application to chaotic cryptography in noisy environment," *Applied Mathematical Modelling*, vol. 38, no. 3, pp. 961-973, 2014.
- [7] S. Kumar, "A new fractional modeling arising in engineering sciences and its analytical approximate solution," *Alexandria Engineering Journal*, vol. 52, no. 4, pp. 813-819, 2013.
- [8] L. Tabharit and Z. Dahmani, "Integro-differential equations of arbitrary orders involving convergent series," *Journal of Interdisciplinary Mathematics*, vol. 23, no. 5, pp. 935-953, 2020.
- [9] E. Adams and H. Spreuer, "Uniqueness and stability for boundary value problems with weakly coupled systems of nonlinear integro-differential equations and application to chemical reactions," *Journal of Mathematical Analysis and Applications*, vol. 49, no. 2, pp. 393-410, 1975.
- [10] A. Kyselka, "Properties of systems of integro-differential equations in the statistics of polymer chains," *Polymer Science USSR*, vol. 19, no. 11, pp. 2852-2858, 1977.
- [11] K. Holmåker, "Global asymptotic stability for a stationary solution of a system of integro-differential equations describing the formation of liver zones," *SIAM Journal on Mathematical Analysis*, vol. 24, no. 1, pp. 116-128, 1993.
- [12] N. Sweilam, M. Khader, and R. Al-Bar, "Homotopy perturbation method for linear and nonlinear system of fractional integro-differential equations," *International Journal of Computational Mathematics and Numerical Simulation*, vol. 1, no. 1, pp. 73-87, 2008.
- [13] M. Heydari, M. Hooshmandasl, F. Mohammadi, and C. Cattani, "Wavelets method for solving systems of nonlinear singular fractional Volterra integro-differential equations," *Communications in Nonlinear Science and Numerical Simulation*, vol. 19, no. 1, pp. 37-48, 2014.
- [14] S. Mashayekhi and M. Razzaghi, "Numerical solution of nonlinear fractional integro-differential equations by hybrid functions," *Engineering Analysis with Boundary Elements*, vol. 56, pp. 81-89, 2015.
- [15] S. A. Deif and S. R. Grace, "Iterative refinement for a system of linear integro-differential equations of fractional type," *Journal of Computational and Applied Mathematics*, vol. 294, pp. 138-150, 2016.
- [16] E. Hesameddini and M. Shahbazi, "Hybrid Bernstein block-pulse functions for solving system of fractional integro-differential equations," *International Journal of Computer Mathematics*, vol. 95, no. 11, pp. 2287-2307, 2018.
- [17] J. Xie and M. Yi, "Numerical research of nonlinear system of fractional Volterra-Fredholm integral-differential equations via block-pulse functions and error analysis," *Journal of Computational and Applied Mathematics*, vol. 345, pp. 159-167, 2019.
- [18] J. Biazar and K. Sadri, "Solution of weakly singular fractional integro-differential equations by using a new operational approach," *Journal of Computational and Applied Mathematics*, vol. 352, pp. 453-477, 2019.
- [19] J. Xie, T. Wang, Z. Ren, J. Zhang, and L. Quan, "Haar wavelet method for approximating the solution of a coupled system of

- fractional-order integral-differential equations,” *Mathematics and Computers in Simulation*, vol. 163, pp. 80–89, 2019.
- [20] F. Saemi, H. Ebrahimi, and M. Shafiee, “An effective scheme for solving system of fractional Volterra-Fredholm integro-differential equations based on the Muntz-Legendre wavelets,” *Journal of Computational and Applied Mathematics*, vol. 374, article 112773, 2020.
- [21] P. Sunthrayuth, R. Ullah, A. Khan et al., “Numerical analysis of the fractional-order nonlinear system of Volterra integro-differential equations,” *Journal of Function Spaces*, vol. 2021, Article ID 1537958, 10 pages, 2021.
- [22] O. Taiye, T. O. Adebayo, A. A. James, I. A. Adam, and A. A. Muhammed, “Numerical solution of system of linear fractional integro-differential equations by least squares collocation Chebyshev technique,” *Mathematics and Computational Sciences*, vol. 3, no. 2, pp. 10–21, 2022.
- [23] M. Masjed-Jamei, *Some New Classes of Orthogonal Polynomials and Special Functions: A Symmetric Generalization of Sturm-Liouville Problems and Its Consequences*, Department of Mathematics, University of Kassel, 2006.
- [24] M. Masjed-Jamei, “A basic class of symmetric orthogonal polynomials using the extended Sturm-Liouville theorem for symmetric functions,” *Journal of Mathematical Analysis and Applications*, vol. 325, no. 2, pp. 753–775, 2007.
- [25] W. Abd-Elhameed and Y. Youssri, “Sixth-kind Chebyshev spectral approach for solving fractional differential equations,” *International Journal of Nonlinear Sciences and Numerical Simulation*, vol. 20, no. 2, pp. 191–203, 2019.
- [26] M. Khader and N. Sweilam, “On the approximate solutions for system of fractional integro-differential equations using Chebyshev pseudo-spectral method,” *Applied Mathematical Modelling*, vol. 37, no. 24, pp. 9819–9828, 2013.
- [27] E. Bargamadi, L. Torkzadeh, K. Nouri, and A. Jajarmi, “Solving a system of fractional-order Volterra-Fredholm integro-differential equations with weakly singular kernels via the second Chebyshev wavelets method,” *Fractal and Fractional*, vol. 5, no. 3, p. 70, 2021.

Research Article

Two Computational Strategies for the Approximate Solution of the Nonlinear Gas Dynamic Equations

Muhammad Nadeem ¹ and Mouad M. H. Ali ²

¹*School of Mathematics and Statistics, Qujing Normal University, 655011 Qujing, China*

²*Department of Computer Science and Engineering, Hodeidah University, Al-Hudaydah, Yemen*

Correspondence should be addressed to Mouad M. H. Ali; mouad198080@hoduniv.net.ye

Received 14 August 2022; Revised 25 September 2022; Accepted 30 September 2022; Published 13 October 2022

Academic Editor: Arzu Akbulut

Copyright © 2022 Muhammad Nadeem and Mouad M. H. Ali. This is an open access article distributed under the Creative Commons Attribution License, which permits unrestricted use, distribution, and reproduction in any medium, provided the original work is properly cited.

In this article, we propose an idea of Sawi homotopy perturbation transform method (SHPTM) to derive the analytical results of nonlinear gas dynamic (GD) equations. The implementation of this numerical scheme is straightforward and produces the results directly without any assumptions and hypothesis in the recurrence relation. Sawi transform (ST) has an advantage of reducing the computational work and the error of estimated results towards the precise solution. The results obtained with this approach are in the shape of an iteration that converges to the precise solution very gradually. We provide the validity and accuracy of this scheme with the help of illustrated examples and their graphical results. This scheme has shown to be the simplest approach for achieving the analytical results of nonlinear problems in science and engineering.

1. Introduction

In recent decades, nonlinear models are particularly describing various physical phenomena in engineering, physics, chemistry, and other sciences. Numerous analytical and numerical schemes have been broadly applied to these nonlinear problems. The procedure of obtaining the precise results for the nonlinear problems is very complicated, and it is still a challenging issue to solve these nonlinear PDEs in most of the cases; besides this, there are various strategies for their solution. As a result, various researchers and scientists have studied multiple novel methods for getting the analytical solution that are reasonably close to the precise solutions such as the Jacobi elliptic function method [1], Exp $(-\Phi(\eta))$ -expansion method [2], new Kudryashov's method [3], rank upgrading technique [4], modified exponential rational method [5], Hermite-Ritz method [6], residual power series (RPS) method [7], and Adomian decomposition method [8, 9].

He [10, 11] developed an idea of homotopy perturbation method (HPM) to obtain the analytical solution of differential problems. Later, Khuri and Sayfy [12] combined Laplace

transform with HPM for the analytical results of differential problems. Nadeem and Li [13] presented a combined approach of Laplace transform with HPM for dealing the analytical work of nonlinear vibration systems and nonlinear wave problems. HPM provides the significant results to solve linear and nonlinear equations of reaction-diffusion equations [14], heat transfer model [15], delay differential equations [16], integro-differential equation [17], and Schrödinger equations [18].

Gas dynamic equations are mathematically modeled by various physical laws such as energy, mass, and momentum conservation. The study of gas motion and its impact on structures using the principles of fluid dynamics and fluid mechanics is known as “gas dynamic,” and it belongs to the discipline of fluid dynamics [19–21]. Jafari [22] presented the idea of variational iteration method (VIM) on the basis of Lagrange multipliers to investigate the analytical solution of nonlinear gas dynamic equation and Stefan equation. Later, Matinfar et al. [23] used a simple procedure using He's polynomials to obtain the analytical results of GD equation and provided the efficient results to show that the suggested algorithm is quite suitable for such problems.

Kumar and Rashidi [24] formulated a scheme based on Laplace transform and the homotopy analysis scheme for handling the time-fractional GD equations. Singh et al. [25] provided the approximate solution of GD equation and showed that HPM presents the excellent performance in various nonlinear problems. Singh and Aggarwal [26] introduced Sawi transform for population growth and decay problems. Many authors provided that this transform has an excellent performance in various differential problems [27–29].

In this article, we combined Sawi transform and HPM to formulate the idea of SHPTM and obtain the analytical results of GD equations. HPM is used to handle nonlinear components. Sawi transform has an advantage of reducing the computational work and minimizing the error of the estimated results towards the precise results. We observe that HPM is very efficient technique in solving the nonlinear phenomena. Results show that this strategy is very unique and easy to implement than other approaches. This article is presented as follows: in Section 2, we report the concept of Sawi transform with some property functions. In Section 3, a basic idea of HPM is revealed to overcome the nonlinear components. Section 4 demonstrates the basic idea of SHPTM to handle the nonlinear problems. We illustrate two numerical examples to show the performance of SHPTM and present the conclusion in Sections 5 and 6, respectively.

2. Sawi Transform

Definition 1. Consider $f(t)$ be a function with $t \geq 0$, so

$$\mathcal{L}\{f(t)\} = F(s) = \theta \int_0^\infty f(t)e^{-st} dt \quad (1)$$

is said to be Laplace transform.

Definition 2. Sawi transform is represented by $S(\cdot)$ for a function $\vartheta(\theta)$

$$S[\vartheta(t)] = R(\theta) = \frac{1}{\theta^2} \int_0^\infty \vartheta(t)e^{-t\theta} dt, t \geq 0, k_1 \leq \theta \leq k_2. \quad (2)$$

Here, S is termed as Sawi transform and if $R(\theta)$ is the Sawi transform of a function $\vartheta(t)$. then $\vartheta(t)$ is the inverse of $R(\theta)$ so that $S^{-1}[R(\theta)] = \vartheta(t)$, S^{-1} is said to be inverse Sawi transform.

Properties. If $S\{g(t)\} = R(\theta)$, the following differential properties yield [26, 28]:

- (a) $S\{g'(t)\} = (R(\theta)/\theta) - (G(0)/\theta^2)$
- (b) $S\{g''(t)\} = (R(\theta)/\theta^2) - (G(0)/\theta^3) - (G'(0)/\theta^2)$
- (c) $S\{g^m(t)\} = (R(\theta)/\theta^m) - (G(0)/\theta^{m+1}) - (G'(0)/\theta^m) - \dots - (G^{m-1}(0)/\theta^2)$

3. Fundamental Concept of HPM

This sector presents the strategy of HPM with the consideration of a nonlinear functional equation [13]. Consider

$$T(\vartheta) - g(h) = 0, h \in \Omega, \quad (3)$$

with conditions

$$S\left(\vartheta, \frac{\partial \vartheta}{\partial n}\right) = 0, h \in \Gamma. \quad (4)$$

Here, T is a general function and S is the boundary operator, and $g(h)$ is source term. We can now split T such that T_1 is said to be a linear and T_2 be a nonlinear operator. Thus, we can write Equation (3) as

$$T_1(\vartheta) + T_2(\vartheta) - g(h) = 0. \quad (5)$$

Consider $\vartheta(h, \theta): \Omega \times [0, 1] \rightarrow \mathbb{H}$ such that it is suitable for

$$H(\vartheta, \theta) = (1 - \theta)[T_1(\vartheta) - T_1(\vartheta_0)] + \theta[T_1(\vartheta) - T_2(\vartheta) - g(h)], \quad (6)$$

or

$$H(\vartheta, \theta) = T_1(\vartheta) - T_1(\vartheta_0) + qL(\vartheta_0) + \theta[T_2(\vartheta) - g(h)] = 0. \quad (7)$$

Here, $\theta \in [0, 1]$ is homotopy element and ϑ_0 is the starting approximation of Equation (3). The study of HPM declares that θ is assumed as a minimal factor and the result of Equation (3) can be expressed in the shape of θ .

$$\vartheta = \vartheta_0 + \theta\vartheta_1 + \theta^2\vartheta_2 + \theta^3\vartheta_3 + \dots = \sum_{i=0}^\infty \theta^i \vartheta_i. \quad (8)$$

Considering $\theta = 1$, we get particular of Equation (3) as

$$\vartheta = \lim_{\theta \rightarrow 1} \vartheta = \vartheta_0 + \vartheta_1 + \vartheta_2 + \vartheta_3 + \dots = \sum_{i=0}^\infty \vartheta_i. \quad (9)$$

The nonlinear terms are obtained as

$$T_2\vartheta(x, t) = \sum_{n=0}^\infty \theta^n H_n(\vartheta), \quad (10)$$

where $H_n(\vartheta)$ is defined as

$$H_n(\vartheta_0 + \vartheta_1 + \dots + \vartheta_n) = \frac{1}{n!} \frac{\partial^n}{\partial \theta^n} \left(T_2 \left(\sum_{i=0}^\infty \theta^i \vartheta_i \right) \right)_{\theta=0}, n = 0, 1, 2, \dots \quad (11)$$

This result in Equation (10) generally converges as the rate of convergence depends on the nonlinear operator T_2 .

4. Formulation of SHPTM

This section reveals the construction of SHPTM for achieving the analytical results GD equation. Consider a nonlinear differential problem such as

$$\vartheta'(x, t) + \vartheta(x, t) + g(\vartheta) = g(x, t), \quad (12)$$

with initial condition

$$\vartheta(x, 0) = a, \quad (13)$$

where ϑ is a function in time domain t , $g(\vartheta)$ represents nonlinear component, $g(x, t)$ is known, and a is the constant. Now, Equation (12) can reconsider as

$$\vartheta'(x, t) = -\vartheta(x, t) - g(\vartheta) + g(x, t). \quad (14)$$

Operating ST on Equation (14), we get

$$S[\vartheta'(x, t)] = S[-\vartheta(x, t) - g(\vartheta) + g(x, t)]. \quad (15)$$

Implementing the properties of ST, it yields

$$\frac{R(\theta)}{\theta} - \frac{G(0)}{\theta^2} = -S[\vartheta(x, t) + g(\vartheta) - g(x, t)]. \quad (16)$$

Thus, $R(\theta)$ is found from Equation (16) as

$$R[\theta] = \frac{G(0)}{\theta} - \theta S[\vartheta(x, t) + g(\vartheta) - g(x, t)]. \quad (17)$$

Applying inverse ST on Equation (17), it yields

$$\vartheta(x, t) = G(x, t) - S^{-1}[\theta S[\vartheta(x, t) + g(\vartheta)]], \quad (18)$$

Equation (18) is called the recurrence relation of Equation (12) where

$$G(x, t) = S^{-1}\left[\frac{G(0)}{\theta} + \theta g(x, t)\right]. \quad (19)$$

According to the strategy of HPM, consider

$$\vartheta(t) = \sum_{i=0}^{\infty} p^i \vartheta_i(n) = \vartheta_0 + p^1 \vartheta_1 + p^2 \vartheta_2 + \dots, \quad (20)$$

and nonlinear terms $g(\vartheta)$ can be determined using an algorithm

$$g(\vartheta) = \sum_{i=0}^{\infty} p^i H_i(\vartheta) = H_0 + p^1 H_1 + p^2 H_2 + \dots, \quad (21)$$

where H_n 's is He's polynomial, and we calculate them by

using the following procedure.

$$H_n(\vartheta_0 + \vartheta_1 + \dots + \vartheta_n) = \frac{1}{n!} \frac{\partial^n}{\partial p^n} \left(g \left(\sum_{i=0}^{\infty} p^i \vartheta_i \right) \right), \quad n = 0, 1, 2, \dots \quad (22)$$

Putting Equations (20), (21), and (22) in Equation (18) and equating the same components of p , we obtain the following iterations

$$\begin{aligned} p^0 : \vartheta_0(x, t) &= G(x, t), \\ p^1 : \vartheta_1(x, t) &= -S^{-1}[\theta S\{\vartheta_0(x, t) + H_0(\vartheta)\}], \\ p^2 : \vartheta_2(x, t) &= -S^{-1}[\theta S\{\vartheta_1(x, t) + H_1(\vartheta)\}], \\ p^3 : \vartheta_3(x, t) &= -S^{-1}[\theta S\{\vartheta_2(x, t) + H_2(\vartheta)\}], \\ &\vdots \end{aligned} \quad (23)$$

By repeating the same manner, we can sum up this series to obtain the analytical results such that

$$\vartheta(x, t) = \vartheta_0 + \vartheta_1 + \vartheta_2 + \dots = \sum_{i=0}^{\infty} \vartheta_i. \quad (24)$$

Thus, Equation (24) yields as an analytical result of differential problem of Equation (12).

5. Numerical Applications

In this portion, we implement the idea of SHPTM in order to obtain the analytical solution of nonlinear GD equations. The solution series converges to the exact solution with few iterations which shows the significance of this approach.

5.1. Example 1. Consider the homogenous and nonlinear GD equation

$$\frac{\partial \vartheta}{\partial t} + \vartheta \frac{\partial \vartheta}{\partial x} - \vartheta(1 - \vartheta) = 0, \quad (25)$$

with initial condition

$$\vartheta(x, 0) = e^{-x}. \quad (26)$$

Taking the Sawi transform of Equation (25), we get

$$\begin{aligned} S\left[\frac{\partial \vartheta}{\partial t} + \vartheta \frac{\partial \vartheta}{\partial x} - \vartheta(1 - \vartheta)\right] &= 0, \\ S\left[\frac{\partial \vartheta}{\partial t}\right] &= -S\left[\vartheta \frac{\partial \vartheta}{\partial x} - \vartheta(1 - \vartheta)\right] = 0. \end{aligned} \quad (27)$$

Employing the properties of Sawi transform, we get

$$\frac{\vartheta(x, \theta)}{\theta} - \frac{\vartheta(x, 0)}{\theta^2} = -S\left[\vartheta \frac{\partial \vartheta}{\partial x} - \vartheta(1 - \vartheta)\right], \quad (28)$$

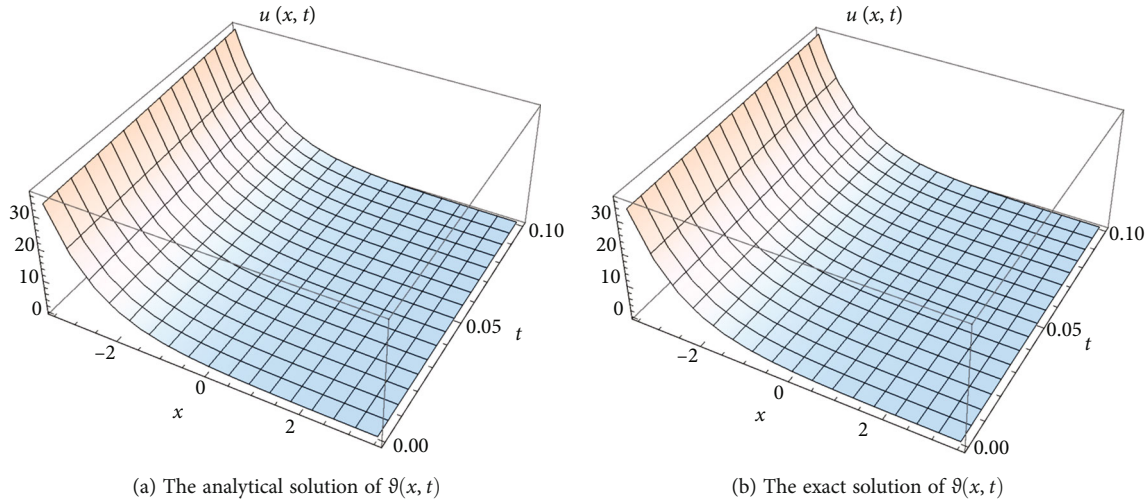


FIGURE 1: The surface solution of GD equation for Example 1.

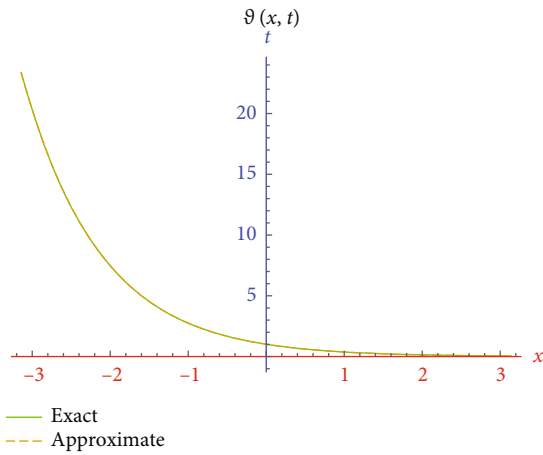


FIGURE 2: 2D plot for $\vartheta(x, t)$ with various parameter of t .

which may be solved further as

$$\vartheta(x, \theta) = \frac{\vartheta(x, 0)}{\theta} - \theta S \left\{ \vartheta \frac{\partial \vartheta}{\partial x} - \vartheta + \vartheta^2 \right\}. \quad (29)$$

Applying inverse Sawi transform, we get

$$\vartheta(x, t) = \vartheta(x, 0) - S^{-1} \left[\theta S \left\{ \vartheta \frac{\partial \vartheta}{\partial x} - \vartheta + \vartheta^2 \right\} \right]. \quad (30)$$

Utilizing HPM on Equation (30), we get

$$\sum_{n=0}^{\infty} p^n \vartheta_n(x, t) = \vartheta(x, 0) - p S^{-1} \left[\theta S \left\{ \sum_{n=0}^{\infty} p^n \vartheta_n(x, t) \frac{\partial}{\partial x} \sum_{n=0}^{\infty} p^n \vartheta_n(x, t) - \sum_{n=0}^{\infty} p^n \vartheta_n(x, t) + \sum_{n=0}^{\infty} p^n \vartheta_n^2(x, t) \right\} \right]. \quad (31)$$

In comparing, the following iterations can be obtained:

$$\begin{aligned} p^0 : \vartheta_0(x, t) &= e^{-x}, \\ p^1 : \vartheta_1(x, t) &= -S^{-1} \left[\theta S \left\{ \vartheta_0 \frac{\partial \vartheta_0}{\partial x} - \vartheta_0 + \vartheta_0^2 \right\} \right] = e^{-x} t, \\ p^2 : \vartheta_2(x, t) &= -S^{-1} \left[\theta S \left\{ \vartheta_0 \frac{\partial \vartheta_2}{\partial x} + \vartheta_1 \frac{\partial \vartheta_1}{\partial x} - \vartheta_1 + 2\vartheta_0 \vartheta_1 \right\} \right] = e^{-x} \frac{t^2}{2!}, \\ p^3 : \vartheta_3(x, t) &= -S^{-1} \left[\theta S \left\{ \vartheta_0 \frac{\partial \vartheta_3}{\partial x} + \vartheta_1 \frac{\partial \vartheta_2}{\partial x} + \vartheta_2 \frac{\partial \vartheta_1}{\partial x} - \vartheta_2 + \vartheta_1^2 + 2\vartheta_0 \vartheta_2 \right\} \right] = e^{-x} \frac{t^3}{3!}, \\ &\vdots \end{aligned} \quad (32)$$

Hence, the solution can be expressed as

$$\begin{aligned} \vartheta(x, t) &= \vartheta_0(x, t) + \vartheta_1(x, t) + \vartheta_2(x, t) + \vartheta_3(x, t) + \dots, \\ \vartheta(x, t) &= e^{-x} + e^{-x} t + e^{-x} \frac{t^2}{2!} + e^{-x} \frac{t^3}{3!} + \dots, \\ \vartheta(x, t) &= e^{t-x}. \end{aligned} \quad (33)$$

In Figure 1, we show the analytical and exact solution graphs of Problem 1 at $-3.5 \leq x \leq 3.5$ and $0 \leq t \leq 0.1$. The graphical results show that the analytical solution and the exact solutions are very close to each other. In addition, Figure 2 presents the graphical error with $-\pi \leq x \leq \pi$ at $t = 0.01$, and it seems that the suggested approach is very efficient and authentic for finding the analytical solution of nonlinear GD equations.

5.2. Example 2. Consider the nonhomogenous and nonlinear GD equation

$$\frac{\partial \vartheta}{\partial t} + \vartheta \frac{\partial \vartheta}{\partial x} - \vartheta(1 - \vartheta) = -e^{t-x}, \quad (34)$$

with initial condition

$$\vartheta(x, 0) = 1 - e^{-x}. \quad (35)$$

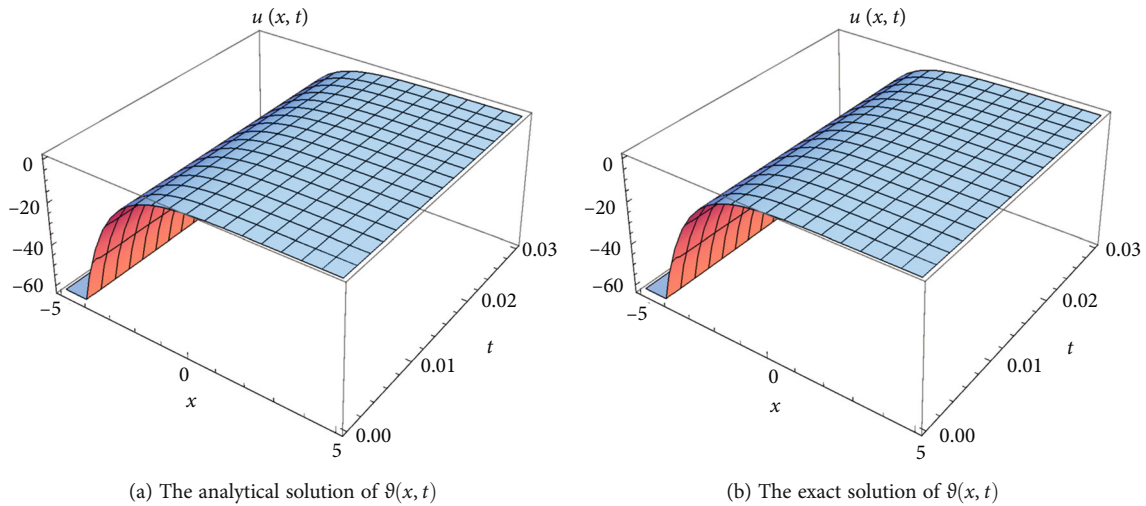


FIGURE 3: The surface solution of GD equation for Example 2.

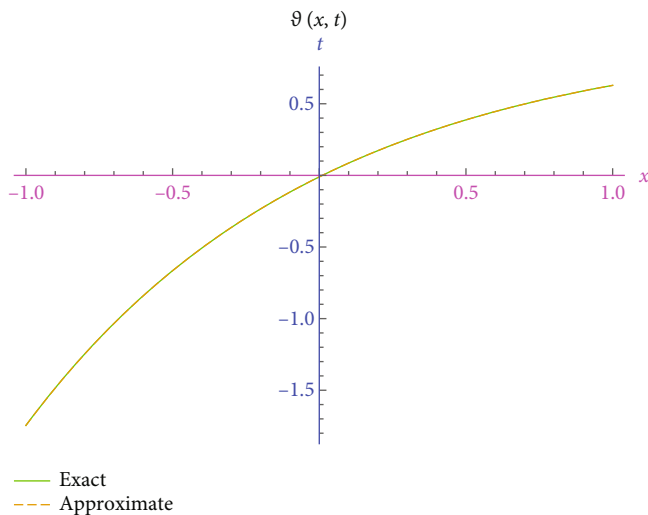


FIGURE 4: 2D plot for $\vartheta(x, t)$ with various parameter of t .

Taking the Sawi transform of Equation (34), we get

$$\begin{aligned}
 S\left[\frac{\partial \vartheta}{\partial t} + \vartheta \frac{\partial \vartheta}{\partial x} - \vartheta(1 - \vartheta)\right] &= -S[e^{t-x}], \\
 S\left[\frac{\partial \vartheta}{\partial t}\right] &= -S[e^{t-x}] - S\left[\vartheta \frac{\partial \vartheta}{\partial x} - \vartheta(1 - \vartheta)\right].
 \end{aligned}
 \tag{36}$$

Employing the properties of Sawi transform, we get

$$\frac{\vartheta(x, \theta)}{\theta} - \frac{\vartheta(x, 0)}{\theta^2} = -\frac{e^{-x}}{\theta(1-\theta)} - S\left[\vartheta \frac{\partial \vartheta}{\partial x} - \vartheta(1 - \vartheta)\right], \tag{37}$$

which may be solved further as

$$\vartheta(x, \theta) = \frac{\vartheta(x, 0)}{\theta} - \frac{e^{-x}}{1-\theta} - \theta S\left\{\vartheta \frac{\partial \vartheta}{\partial x} - \vartheta + \vartheta^2\right\}. \tag{38}$$

Applying inverse Sawi transform, we get

$$\vartheta(x, t) = \vartheta(x, 0) - e^{-x} S^{-1}\left[\frac{1}{1-\theta}\right] - S^{-1}\left[\theta S\left\{\vartheta \frac{\partial \vartheta}{\partial x} - \vartheta + \vartheta^2\right\}\right]. \tag{39}$$

Utilizing HPM on Equation (39), we get

$$\begin{aligned}
 \sum_{n=0}^{\infty} p^n \vartheta_n(x, t) &= 1 - e^{-x} - p S^{-1} \\
 &\left[\theta S\left\{\sum_{n=0}^{\infty} p^n \vartheta_n(x, t) \frac{\partial}{\partial x} \sum_{n=0}^{\infty} p^n \vartheta_n(x, t) - \sum_{n=0}^{\infty} p^n \vartheta_n(x, t) + \sum_{n=0}^{\infty} p^n \vartheta_n^2(x, t)\right\}\right].
 \end{aligned}
 \tag{40}$$

In comparing, the following iterations can be obtained:

$$\begin{aligned}
 p^0 : \vartheta_0(x, t) &= 1 - e^{-x}, \\
 p^1 : \vartheta_1(x, t) &= S^{-1}\left[\theta S\left\{\vartheta_0 \frac{\partial \vartheta_0}{\partial x} - \vartheta_0 + \vartheta_0^2\right\}\right] = 0 \\
 p^2 : \vartheta_2(x, t) &= S^{-1}\left[\theta S\left\{\vartheta_0 \frac{\partial \vartheta_1}{\partial x} + \vartheta_1 \frac{\partial \vartheta_0}{\partial x} - \vartheta_1 + 2\vartheta_0 \vartheta_1\right\}\right] = 0, \\
 p^3 : \vartheta_3(x, t) &= S^{-1}\left[\theta S\left\{\vartheta_0 \frac{\partial \vartheta_2}{\partial x} + \vartheta_1 \frac{\partial \vartheta_1}{\partial x} + \vartheta_2 \frac{\partial \vartheta_0}{\partial x} - \vartheta_2 + \vartheta_1^2 + 2\vartheta_0 \vartheta_2\right\}\right] = 0, \\
 &\vdots
 \end{aligned}
 \tag{41}$$

Hence, the solution can be expressed as

$$\begin{aligned}
 \vartheta(x, t) &= \vartheta_0(x, t) + \vartheta_1(x, t) + \vartheta_2(x, t) + \vartheta_3(x, t) + \dots, \\
 \vartheta(x, t) &= 1 - e^{-x} + 0 + 0 + \dots, \\
 \vartheta(x, t) &= 1 - e^{-x}.
 \end{aligned}
 \tag{42}$$

In Figure 3, we show the analytical and exact solution graphs of Problem 1 at $-5 \leq x \leq 5$ and $0 \leq t \leq 0.03$. The graphical results show that the analytical solution and the exact solutions are very close to each other. In addition, Figure 4 presents the graphical error with $-1 \leq x \leq 1$ at $t =$

0.01, and it seems that the suggested approach is very efficient and authentic for finding the analytical solution of nonlinear GD equations.

6. Conclusion

In this paper, we constructed a SHPTM to obtain the analytical solution of nonlinear GD equations. The conservation characteristics of the numerical scheme are demonstrated by theoretical analysis. Additionally, we determined the error estimates to show that the obtained results are in quick convergence. One observation is that if Sawi transform is used with HPM, we do not need to digitize the GD equations which leads to a high number of restrictions and assumptions. This is because Sawi transform is independent of restrictive variable and considered as a direct approach for the conservation law in both linear and nonlinear problems. We use Mathematica software 11.0.1 for the numerical analysis and computation of the iterations of series solutions. One can use this scheme for other nonlinear numerical problems to obtain the excellent results that are stable and accurate. However, our work can easily be modified to study the theory of fractional calculus in science and engineering.

Data Availability

This article contains all the data.

Conflicts of Interest

This article has no conflicts of interest.

References

- [1] K. A. Gepreel, T. A. Nofal, and A. A. Al-Thobaiti, "The modified rational Jacobi elliptic functions method for nonlinear differential difference equations," *Journal of Applied Mathematics*, vol. 2012, Article ID 427479, 30 pages, 2012.
- [2] R. Islam, M. N. Alam, A. Hossain, H. Roshid, and M. Akbar, "Traveling wave solutions of nonlinear evolution equations via $\exp(-\phi(n))$ expansion method," *Global Journal of Science Frontier Research*, vol. 13, no. 11, pp. 63–71, 2013.
- [3] H. Rezaadeh, N. Ullah, L. Akinyemi et al., "Optical soliton solutions of the generalized non-autonomous nonlinear Schrodinger equations by the new Kudryashov's method," *Results in Physics*, vol. 24, article 104179, 2021.
- [4] Y. O. El-Dib R. Matoog et al., "The rank upgrading technique for a harmonic restoring force of nonlinear oscillators," *Journal of Applied and Computational Mechanics*, vol. 7, no. 2, pp. 782–789, 2021.
- [5] A. Althobaiti, S. Althobaiti, K. El-Rashidy, and A. R. Seadawy, "Exact solutions for the nonlinear extended KdV equation in a stratified shear flow using modified exponential rational method," *Results in Physics*, vol. 29, article 104723, 2021.
- [6] S. K. Jena, S. Chakraverty, M. Malikan, and H. Sedighi, "Implementation of Hermite–Ritz method and Naviers technique for vibration of functionally graded porous nanobeam embedded in Winkler–Pasternak elastic foundation using bi-Helmholtz nonlocal elasticity," *Journal of Mechanics of Materials and Structures*, vol. 15, no. 3, pp. 405–434, 2020.
- [7] M. Alaroud, M. Al-Smadi, R. Rozita Ahmad, and U. K. Salma Din, "An analytical numerical method for solving fuzzy fractional Volterra integro-differential equations," *Symmetry*, vol. 11, no. 2, p. 205, 2019.
- [8] J.-S. Duan, R. Rach, and A.-M. Wazwaz, "Higher order numeric solutions of the Lane–Emden-type equations derived from the multi-stage modified Adomian decomposition method," *International Journal of Computer Mathematics*, vol. 94, no. 1, pp. 197–215, 2017.
- [9] H. M. Sedighi and K. H. Shirazi, "Asymptotic approach for nonlinear vibrating beams with saturation type boundary condition," *Proceedings of the Institution of Mechanical Engineers, Part C: Journal of Mechanical Engineering Science*, vol. 227, no. 11, pp. 2479–2486, 2013.
- [10] J.-H. He, "Homotopy perturbation technique," *Computer Methods in Applied Mechanics and Engineering*, vol. 178, no. 3–4, pp. 257–262, 1999.
- [11] J.-H. He, "Homotopy perturbation method: a new nonlinear analytical technique," *Applied Mathematics and Computation*, vol. 135, no. 1, pp. 73–79, 2003.
- [12] S. A. Khuri and A. Sayfy, "A Laplace variational iteration strategy for the solution of differential equations," *Applied Mathematics Letters*, vol. 25, no. 12, pp. 2298–2305, 2012.
- [13] M. Nadeem and F. Li, "He–Laplace method for nonlinear vibration systems and nonlinear wave equations," *Journal of Low Frequency Noise, Vibration and Active Control*, vol. 38, no. 3–4, pp. 1060–1074, 2019.
- [14] D. Ganji and A. Sadighi, "Application of He's homotopy-perturbation method to nonlinear coupled systems of reaction-diffusion equations," *International Journal of Nonlinear Sciences and Numerical Simulation*, vol. 7, no. 4, pp. 411–418, 2006.
- [15] V. Marinca and N. Herişanu, "Application of optimal homotopy asymptotic method for solving nonlinear equations arising in heat transfer," *International Communications in Heat and Mass Transfer*, vol. 35, no. 6, pp. 710–715, 2008.
- [16] F. Shakeri and M. Dehghan, "Solution of delay differential equations via a homotopy perturbation method," *Mathematical and Computer Modelling*, vol. 48, no. 3–4, pp. 486–498, 2008.
- [17] M. Dehghan and F. Shakeri, "Solution of an integro-differential equation arising in oscillating magnetic fields using He's homotopy perturbation method," *Progress In Electromagnetics Research*, vol. 78, pp. 361–376, 2008.
- [18] J. Biazar and H. Ghazvini, "Exact solutions for non-linear Schrodinger equations by He's homotopy perturbation method," *Physics Letters A*, vol. 366, no. 1–2, pp. 79–84, 2007.
- [19] H. Jafari, H. Hosseinzadeh, and E. Salehpour, "A new approach to the gas dynamics equation: an application of the variational iteration method," *Applied Mathematical Sciences*, vol. 2, no. 48, pp. 2397–2400, 2008.
- [20] J. B. Yindoula, S. M. Mayembo, and G. Bissanga, "Application of Laplace variation iteration method to solving the nonlinear gas dynamics equation," *American Journal of Mathematical and Computer Modelling*, vol. 5, no. 4, pp. 127–133, 2020.
- [21] S. Maitama and S. M. Kurawa, "An efficient technique for solving gas dynamics equation using the natural decomposition method," in *International Mathematical Forum*, vol. 9, pp. 1177–1190, Hikari, Ltd., 2014.
- [22] E. S. H. Jafari, "Variational iteration method: a tools for solving partial differential equations," *The Journal of Mathematics and Computer Science*, vol. 2, no. 2, pp. 388–393, 2011.

- [23] M. Matinfar, M. Saeidy, M. Mahdavi, and M. Rezaei, "Variational iteration method for exact solution of gas dynamic equation using Hes polynomials," *Bulletin of Mathematical Analysis and Applications*, vol. 3, no. 3, pp. 50–55, 2011.
- [24] S. Kumar and M. M. Rashidi, "New analytical method for gas dynamics equation arising in shock fronts," *Computer Physics Communications*, vol. 185, no. 7, pp. 1947–1954, 2014.
- [25] J. Singh, D. Kumar, and Sushila, "Homotopy perturbation algorithm using Laplace transform for gas dynamics equation," *Journal of Applied Mathematics, Statistics and Informatics*, vol. 8, no. 1, pp. 55–61, 2012.
- [26] G. P. Singh and S. Aggarwal, "Sawi transform for population growth and decay problems," *International Journal of Latest Technology in Engineering, Management & Applied Science*, vol. 8, no. 8, pp. 157–162, 2019.
- [27] M. Higazy, S. Aggarwal, and T. A. Nofal, "Sawi decomposition method for Volterra integral equation with application," *Journal of Mathematics*, vol. 2020, Article ID 6687134, 13 pages, 2020.
- [28] M. Higazy and S. Aggarwal, "Sawi transformation for system of ordinary differential equations with application," *Ain Shams Engineering Journal*, vol. 12, no. 3, pp. 3173–3182, 2021.
- [29] A. Georgieva and A. Pavlova, "Fuzzy Sawi decomposition method for solving nonlinear partial fuzzy differential equations," *Symmetry*, vol. 13, no. 9, p. 1580, 2021.

Research Article

Mathematical Modeling of Coronavirus Dynamics with Conformable Derivative in Liouville–Caputo Sense

Ebenezer Bonyah ¹, Zakia Hammouch ^{2,3,4} and Mehmet Emir Koksal ^{5,6}

¹Department of Mathematics Education, University of Skills Training and Entrepreneurial Development, Kumasi, Ghana

²Division of Applied Mathematics, Thu Dau Mot University, Binh Duong Province, Vietnam

³Department of Medical Research China Medical University Hospital, Taichung, Taiwan

⁴Department of Sciences, Ecole Normale Supérieure, Moulay Ismail University of Meknes, Meknes, Morocco

⁵Department of Mathematics, Ondokuz Mayıs University, Atakum 55139, Samsun, Turkey

⁶Department of Applied Mathematics, University of Twente, P.O. Box 217, 7500 AE Enschede, Netherlands

Correspondence should be addressed to Mehmet Emir Koksal; emirkoksal@gmail.com

Received 15 May 2022; Accepted 1 July 2022; Published 3 October 2022

Academic Editor: Arzu Akbulut

Copyright © 2022 Ebenezer Bonyah et al. This is an open access article distributed under the Creative Commons Attribution License, which permits unrestricted use, distribution, and reproduction in any medium, provided the original work is properly cited.

Coronavirus has become a serious global phenomenon in recent times and has negative effects on the entire world economy. In this study, a fractional mathematical model formulated in fractional conformable derivative is studied. The model hinges on the concept of mammal hosts and humans. The basic properties of the coronavirus model are investigated. The stability analysis is carried out as well as sensitivity analysis based on the reproduction number. Numerical simulation is undertaken to give impetus to the analytical results which indicate that both fractional conformable order derivative and fractional-order derivative have serious consequences in numerical result outcomes.

1. Introduction

The world has not been free of diseases since creation, and mankind has not also done well in the immediate environment. Technology and science have brought fast changes, making lives easy and more comfortable [1, 2]. The natural environment is undergoing serious degradation in almost all parts of the world. Humans' advancement through science and technology has brought a dramatic shift in many natural certain, including marital principles, modernized agriculture, transportation, education, culture and many more. Currently, through technology, man has been able to develop some genetically modified foods [3–5]. Some of these advancements have serious consequences in human endeavor. Many plants and animals are going into extinction because of man's overexploitation of the natural environment. Why does society, therefore, blame the occurrence of epidemics and pandemic in the world? Are we not the creation of our own problems? There have been several

pandemics in the past including the recent Ebola menace which killed many people and totally destroyed many countries' economy [6, 7].

The coronavirus is not an exception and would not probably the last one man would ever encounter. The outbreak of the current pandemic begun at Wuhan in the province of Hubei in the Republic of China. The association of the pandemic has to do with a seafood market centre which dealt with live animals. It is believed that the virus was associated with a host animal that humans infected [8]. Subsequently, human-to-human infection began. Due to migration, as people are now very mobile, the disease has spread to almost all parts of the continents. Notably, countries that have suffered severely are Italy, United Kingdom, United States of America, France, South Korea, and so on [1, 5]. Sub-Saharan Africa is not spared with this menace. South Africa is the leading country, and most countries have recorded the coronavirus infection. They have fragile economies with poor health infrastructure and

would have serious effect on patients if care is not taken [1, 4, 5].

The symptoms of the disease include the following: severe headache, respiratory infection, and high temperature. The latent period of the disease is fourteen days, and during this period, the person can infect others. Currently, there is no cure for the disease; however, the WHO suggests preventive mechanisms such as social distancing, frequent washing of hands with running water, and application of hand sanitizer [5]. Several research studies are currently underway in the hope of obtaining drugs and vaccines to prevent the spread and mortality of the disease. It is important that quantitative and qualitative information on etiology be studied. It has been found that mathematical modeling is capable of providing qualitative information on many important parameters that are important for decision making by health professionals. There have been number of mathematical models on many epidemics both current and past [9, 10].

In recent times, non-integer models have gained tremendous advancement due to their ability to predict complex models or phenomena in light of engineering, technology, economics, etc. Fractional derivatives and integrals possess the past memory and the present state of phenomenon which helps in the accurate predictions of models. There are many fractional operators including Liouville–Caputo, Grunwald–Letnikov, Atangana–Gomez, Caputo–Fabrizio, Atangana–Baleanu, and others which are commonly used by researchers [11–14].

The recently introduced operator by Khalil et al. [15] has attracted several researchers because of its applicability and wide usefulness in many scientific problems. The operator boasts of some interesting properties such as conformable vectors, conformable partial derivatives, Taylor series expansion, Laplace transform, and others [16]. Thus, conformable fractional derivative is just local derivative in Riemann–Liouville and Caputo sense whose purpose is to give rise to non-local fractional derivative. Qureshi [17] investigated the effects of vaccination on measles dynamics under fractional conformable derivative with Liouville–Caputo operator and obtained a threshold in conformable derivative form that reduces infection. Khan and Aguilar [18] explored the dynamics of tuberculosis (TB) model and presented results that prove superiority of the

conformable operator. This study is motivated by the effective and efficient results obtained by the previous authors with the fractional conformable order derivative. Harir et al. [19] employed conformable fractional-order derivative to examine SIR epidemic model and obtained a result that provided a qualitative information in 2021. In the same year, Hosseini et al. [20] utilized conformable derivative to demonstrate the effectiveness of numerical scheme result by comparing it with the analytical solutions in a heat transfer problem. Then, Allahamou et al. [21] also used conformable approach to study co-infection model of Hantavirus and validated the model using European moles in 2021.

The analytical and numerical results based on conformable derivative meet all the standard derivative criteria and are easy to compute which makes the results more efficient and reliable for predicting the model. The aim of this paper is to employ the fractional conformable derivative in Liouville–Caputo sense to examine the dynamics of the coronavirus model and also to present some qualitative information on coronavirus menace.

The rest of the paper is arranged as follows. In Section 2, mathematical preliminaries in both analysis and numerical simulations of our model are presented. Section 3 is solely devoted to the formulation of mathematical modeling. In the next section, the existence of bounded solutions in a biologically feasible region is presented. Section 5 contains the disease-free equilibrium and its stability, and Section 6 deals with the sensitivity analysis for the threshold quantity R_0 . Sections 7 and 8 present numerical algorithms and simulation results, respectively. MATLAB 2016a has been used to obtain numerical solutions. Finally, the study ends up with a conclusion.

2. Preliminaries

Some of the basic results needed in the qualitative analysis and numerical simulations of the proposed coronavirus model (7) are presented.

Definition 1. The definition of fractional derivative presented by Riemann and Liouville of order α (RL^α) in terms of the power law type kernel $(x - \xi)^{p-\alpha-1}$ with convolution of a function $z(\xi)$ [16] is as follows:

$${}_{RL^\alpha} \mathfrak{D}_{a_1, x}^\alpha z(x) = \frac{1}{\Gamma(p - \alpha)} \frac{d^p}{dx^p} \int_{a_1}^x (x - \xi)^{p-\alpha-1} z(\xi) d\xi, \quad \alpha \in (p - 1, p]. \quad (1)$$

Definition 2. The definition of fractional derivative presented by Liouville and Caputo of order β (LC^β) in terms of

the power law type kernel $(x - \xi)^{p-\beta-1}$ with convolution of the local derivative of a function $z(\xi)$ is as follows:

$${}_{LC^\beta} \mathfrak{D}_{a_1, x}^\beta z(x) = \frac{1}{\Gamma(p - \beta)} \int_{a_1}^x (x - \xi)^{p-\beta-1} \frac{d^\beta}{d\xi^\beta} z(\xi) d\xi, \quad \beta \in (p - 1, p]. \quad (2)$$

Definition 3. The conformable fractional derivative of order α (CFD^α) is defined as

$${}_{CFD^\alpha} \mathfrak{D}_{a_1, x}^\alpha z(x) = \lim_{\zeta \rightarrow 0} \frac{z(x + \zeta x^{1-\alpha}) - z(x)}{\zeta}, \quad t, \alpha > 0. \quad (3)$$

Remark 1. The relation between CFD^α and local ordinary derivative is

$${}_{CFD^\alpha} \mathfrak{D}_{a_1, x}^\alpha z(x) = (x - a_1)^{1-\alpha} \frac{d}{dx} z(x). \quad (4)$$

Definition 4. The CFD^α in the sense of LC^β is defined as

$$\begin{aligned} {}_C^\beta \mathfrak{D}_{a_1, x}^\alpha z(x) &= \frac{1}{\Gamma(p - \beta)} \int_{a_1}^x \left[\frac{(x - a_1)^\alpha - (\xi - a_1)^\alpha}{\alpha} \right]^{p - \beta - 1} \\ &\quad \cdot \frac{{}_{CFD^\alpha} \mathfrak{D}_{a_1, \xi}^\alpha z(\xi)}{(\xi - a_1)^{1-\alpha}} d\xi, \\ {}_C^\beta \mathfrak{D}_{a_1, x}^\alpha z x &= {}_{CFD}^{p-\beta} \mathbb{I}_{a_1, x}^\alpha \left({}_{CFD^\alpha} \mathfrak{D}_{a_1, x}^\alpha z(x) \right), \end{aligned} \quad (5)$$

where $z(x) \in C_{\alpha, a_1}^p([a_1, a_2])$, $\text{Re}(\beta) \geq 0$, and $p = \lceil \text{Re}(\beta) \rceil + 1$.

3. Mathematical Model Formulation

This section presents a coronavirus model of fractional conformable derivative version by Bonyah et al. [22] in which the total host mammal population N_a is apportioned into susceptible mammal class S_a , latent mammal class L_a , infected mammal class I_a , and recovered mammal class R_a . Hence, total host mammal population is denoted by $N_a = S_a + L_a + I_a + R_a$. Human total population is also subdivided into susceptible human class S_b , latent human class L_b , infected human class I_b , and recovered human class R_b . Mammal and human recruitment rates are Λ_a and Λ_b , respectively. Natural mortality rate for humans and mammals is μ_a and μ_b in that order. Effective contact rate between infected mammals and susceptible mammals is given by β_1 . The effective contact rate between infected mammals and susceptible human is denoted by β_2, β_3 . The waning rate of recovered human losses immunity to be part of the susceptible class is γ . The recovery rate of human and mammal is τ_b and τ_a , respectively. The rate human and mammal move into infected classes is denoted by θ_b and θ_a while human disease induced mortality rate is ω . With initial conditions $S_m^0 = S_a(0), L_a^0 = L_a(0), I_a^0 = I_a(0), R_a^0 = R_a(0), S_b^0 = S_b(0), L_b^0 = L_b(0), I_b^0 = I_b(0), R_b^0 = R_b(0)$, the following non-linear differential equations represent the interactions among the various compartments:

$$\begin{aligned} \frac{dS_a}{dt} &= \Lambda_a - \beta_1 S_a I_a - \mu_a S_a, \\ \frac{dL_a}{dt} &= \beta_1 S_a I_a - (\mu_a + \theta_a) L_a, \\ \frac{dI_a}{dt} &= \theta_a L_a - (\tau_a + \mu_a) I_a, \\ \frac{dR_a}{dt} &= \tau_a I_a - \mu_a R_a, \\ \frac{dS_b}{dt} &= \Lambda_b - \beta_2 S_b I_a - \beta_3 S_b I_b + \gamma R_b - \mu_b S_b, \\ \frac{dL_b}{dt} &= \beta_2 S_b I_a + \beta_3 S_b I_b - (\mu_b + \theta_b) L_b, \\ \frac{dI_b}{dt} &= \theta_b L_b - (\tau_b + \mu_b + \omega) I_b, \\ \frac{dR_b}{dt} &= \tau_b I_b - (\mu_b + \gamma) R_b. \end{aligned} \quad (6)$$

Now, replacing the integer-order derivatives in coronavirus system (6) with CFD^α in the sense of LC^β , we obtain the following system:

$$\begin{aligned} {}_C^\beta D_{0,t}^\alpha S_a &= \Lambda_a - \beta_1 S_a I_a - \mu_a S_a, \\ {}_C^\beta D_{0,t}^\alpha L_a &= \beta_1 S_a I_a - (\mu_a + \theta_a) L_a, \\ {}_C^\beta D_{0,t}^\alpha I_a &= \theta_a L_a - (\tau_a + \mu_a) I_a, \\ {}_C^\beta D_{0,t}^\alpha R_a &= \tau_a I_a - \mu_a R_a, \\ {}_C^\beta D_{0,t}^\alpha S_b &= \Lambda_b - \beta_2 S_b I_a - \beta_3 S_b I_b + \gamma R_b - \mu_b S_b, \\ {}_C^\beta D_{0,t}^\alpha L_b &= \beta_2 S_b I_a + \beta_3 S_b I_b - (\mu_b + \theta_b) L_b, \\ {}_C^\beta D_{0,t}^\alpha I_b &= \theta_b L_b - (\tau_b + \mu_b + \omega) I_b, \\ {}_C^\beta D_{0,t}^\alpha R_b &= \tau_b I_b - (\mu_b + \gamma) R_b. \end{aligned} \quad (7)$$

4. Existence of Bounded Solutions in a Biologically Feasible Region

Here, we will study the boundedness of the solution of model (7) in a positively invariant region.

Lemma 1. *The region $\Omega = \{(S_a(t), L_a(t), I_a(t), R_a(t), S_b(t), L_b(t), I_b(t), R_b(t)) \in \mathbb{R}_+^8 : N_a(t) \leq \Lambda_a / \mu_a, N_b(t) \leq \Lambda_b / \mu_b\}$ is positively invariant for coronavirus model (7) with CFD^α in the sense of LC^β and initial conditions in \mathbb{R}_+^8 .*

Proof 1. Adding all the equations of the host mammal population, we get

$${}_C^\beta D_{0,t}^\alpha N_a(t) = \Lambda_a - \mu_a N_a(t). \quad (8)$$

By separating variables and integrating, we get

$$N_a(t) = \frac{1}{\mu_a} \left(\Lambda_a - \exp\left(-\frac{\mu_a t^\alpha}{\alpha}\right) \right). \quad (9)$$

Thus, it is deduced that

$$\lim_{t \rightarrow \infty} \sup N_a(t) \leq \frac{\Lambda_a}{\mu_a}. \tag{10}$$

Now, similarly adding all the equations of the human population, we obtain

$$\lim_{t \rightarrow \infty} \sup N_b(t) \leq \frac{\Lambda_b}{\mu_b}. \tag{11}$$

These results show that the solutions are bounded for time and model (7) possesses the positively invariant region Ω . \square

5. Disease-Free Equilibrium (DFE) and Its Stability

Solving model (7) under no infection condition, we obtain the following disease-free steady state (DFSS) D_0 :

$$D_0 = (S_a^0, L_a^0, I_a^0, R_a^0, S_b^0, L_b^0, I_b^0, R_b^0), \tag{12}$$

$$D_0 = \left(\frac{\Lambda_a}{\mu_a}, 0, 0, 0, \frac{\Lambda_b}{\mu_b}, 0, 0, 0 \right).$$

For the next generation method [23], we have

$$F = \begin{pmatrix} 0 & \frac{\beta_1 \Lambda_a}{\mu} & 0 & 0 \\ 0 & 0 & 0 & 0 \\ 0 & \frac{\beta_2 \Lambda_b}{\mu_b} & 0 & \frac{\beta_3 \Lambda_b}{\mu_b} \\ 0 & 0 & 0 & 0 \end{pmatrix}, \tag{13}$$

$$V = \begin{pmatrix} \mu_a + \theta_a & 0 & 0 & 0 \\ -\theta_a & \tau_a + \mu_a & 0 & 0 \\ 0 & 0 & \mu_b + \theta_b & 0 \\ 0 & 0 & -\theta_b & \tau_b + \mu_b + \omega \end{pmatrix}. \tag{14}$$

Therefore, the reproduction number is $\mathcal{R}_0 = \mathcal{R}_1 + \mathcal{R}_2$, where $\mathcal{R}_1 = \beta_1 \theta_a \Lambda_a / \mu_a (\theta_a + \mu_a) (\mu_a + \tau_a)$ and $\mathcal{R}_2 = \beta_3 \theta_b \Lambda_b / \mu_b (\theta_b + \mu_b) (\omega + \mu_b + \tau_b)$.

Theorem 1. *If $\mathcal{R}_0 < 1$, then D_0 of coronavirus model (7) satisfies $Re(\lambda_j) < 0$, for $j = 1(1)8$, and D_0 is locally asymptotically stable (LAS), where $Re(\lambda)$ represents the real part of an eigenvalue of the corresponding Jacobian matrix of coronavirus model (7) at D_0 .*

Proof 2. For the required result, the corresponding Jacobian matrix calculated at D_0 is

$$J_{D_0} = \begin{pmatrix} -\mu_a & 0 & \frac{\beta_1 \Lambda_a}{\mu_a} & 0 & 0 & 0 & 0 & 0 \\ 0 & -\theta_a - \mu_a & \frac{\beta_1 \Lambda_a}{\mu_a} & 0 & 0 & 0 & 0 & 0 \\ 0 & \theta_a & -\mu_a - \tau_a & 0 & 0 & 0 & 0 & 0 \\ 0 & 0 & \tau_a & -\mu_a & 0 & 0 & 0 & 0 \\ 0 & 0 & \frac{\beta_2 \Lambda_b}{\mu_b} & 0 & -\mu_b & 0 & \frac{\beta_3 \Lambda_b}{\mu_b} & \gamma \\ 0 & 0 & \frac{\beta_2 \Lambda_b}{\mu_b} & 0 & 0 & -\theta_b - \mu_b & \frac{\beta_3 \Lambda_b}{\mu_b} & 0 \\ 0 & 0 & 0 & 0 & 0 & \theta_b & -\omega - \mu_b - \tau_b & 0 \\ 0 & 0 & 0 & 0 & 0 & 0 & \tau_b & -\gamma - \mu_b \end{pmatrix}. \tag{15}$$

Its corresponding characteristic equation is given by

$$(\lambda + \mu_b)(\lambda + \mu_b + \gamma)(\lambda + \mu_a)^2(\lambda^4 + D_1\lambda^3 + D_2\lambda^2 + D_3\lambda + D_4) = 0, \tag{16}$$

where the coefficients D_j for $j = 1, 2, 3, 4$ are given by

$$\begin{aligned}
 D_1 &= \omega + \theta_b + \tau_b + 2\mu_b + \theta_a + \tau_a + 2\mu_a, \\
 D_2 &= (\omega + \theta_b + \tau_b + 2\mu_b)(\theta_a + \tau_a + 2\mu_a) + (\theta_a + \mu_a)(\mu_a + \tau_a)(1 - \mathcal{R}_1) \\
 &\quad + (\theta_b + \mu_b)(\omega + \tau_b + \mu_b)(1 - \mathcal{R}_2), \\
 D_3 &= (\omega + \theta_b + \tau_b + 2\mu_b)(\theta_a + \mu_a)(\mu_a + \tau_a)(1 - \mathcal{R}_1) \\
 &\quad + (\theta_a + \tau_a + 2\mu_a)(\theta_b + \mu_b)(\omega + \tau_b + \mu_b)(1 - \mathcal{R}_2), \\
 D_4 &= (\theta_b + \mu_b)(\omega + \tau_b + \mu_b)(\theta_a + \mu_a)(\mu_a + \tau_a)(1 - \mathcal{R}_1)(1 - \mathcal{R}_2).
 \end{aligned}
 \tag{17}$$

Since the eigenvalues $-\mu_b, -\mu_b, -\mu_a,$ and $-(\mu_a + \gamma)$ are negative, all the other coefficients D_j for $j = 1(1)4$ of the characteristic polynomial are positive if $R_0 < 1$. The Routh–Hurwitz [24] criteria $D_j > 0$ for $j = 1(1)4$ and $D_1 D_2 D_3 > D_1^2 D_4 + D_3^2$ can be satisfied easily. So, the DFSS D_0 of coronavirus model (7) is LAS if $R_0 < 1$. \square

Theorem 2. *The DFSS D_0 of coronavirus model (7) is globally asymptotically stable (GAS) for $R_0 < 1$ and unstable for $R_0 > 1$.*

Proof 3. For the proof, let us construct a Lyapunov function at DFSS D_0 :

$$\begin{aligned}
 {}^{\beta}_C \mathfrak{D}_{a_1, t}^{\alpha} \mathcal{L}(t) &= \mathcal{E}_1 \{ \beta_1 S_m^0 I_a - (\mu_a + \theta_a) L_a \} + \mathcal{E}_2 \{ \theta_a L_a - (\tau_a + \mu_a) I_a \} \\
 &\quad + \mathcal{E}_3 \{ \beta_2 S_b^0 I_a + \beta_3 S_b^0 I_b - (\mu_b + \theta_b) L_b \} + \mathcal{E}_4 \{ \theta_b L_b - (\tau_b + \mu_b + \omega) I_b \}, \\
 &= \{ \beta_1 S_a^0 \mathcal{E}_1 - (\tau_a + \mu_a) \mathcal{E}_2 + \beta_2 S_b^0 \mathcal{E}_3 \} I_a + \{ -(\theta_a + \mu_a) \mathcal{E}_1 + \theta_a \mathcal{E}_2 \} L_a \\
 &\quad + \{ -(\theta_b + \mu_b) \mathcal{E}_3 + \theta_b \mathcal{E}_4 \} L_b + \{ \beta_3 S_b^0 \mathcal{E}_3 - (\tau_b + \mu_b + \omega) \mathcal{E}_4 \} I_b.
 \end{aligned}
 \tag{20}$$

Now, choose $C_1 = \theta_a,$ $C_2 = \mu_a + \theta_a,$ $C_3 = \{ (\mu_a + \tau_a) (\mu_a + \theta_a) - \beta_1 \Lambda_a \theta_b / \mu_a \} \mu_b / \beta_2 \Lambda_b \theta_b,$ and $C_4 = (\theta_b + \mu_b)$

$$\mathcal{L}(t) = \mathcal{E}_1 L_a(t) + \mathcal{E}_2 I_a(t) + \mathcal{E}_3 L_b(t) + \mathcal{E}_4 I_b(t), \tag{18}$$

where the constants $C_j > 0,$ for $j = 1, 2, 3, 4$ and they are chosen later. Calculating the CFD^{α} in the sense of $LC^{\beta},$ we get

$$\begin{aligned}
 {}^{\beta}_C \mathfrak{D}_{a_1, x}^{\alpha} \mathcal{L}(t) &= \mathcal{E}_1 {}^{\beta}_C D_{0, t}^{\alpha} L_a(t) + \mathcal{E}_2 {}^{\beta}_C D_{0, t}^{\alpha} I_a(t) \\
 &\quad + \mathcal{E}_3 {}^{\beta}_C D_{0, t}^{\alpha} L_b(t) + \mathcal{E}_4 {}^{\beta}_C D_{0, t}^{\alpha} I_b(t).
 \end{aligned}
 \tag{19}$$

Using the proposed coronavirus model (7), we obtain

$\{ (\mu_a + \tau_a) (\mu_a + \theta_a) - \beta_1 \Lambda_a \theta_b / \mu_a \} \mu_b / \beta_2 \Lambda_b \theta_b.$ After simplification, we obtain

$${}^{\beta}_C D_{0, t}^{\alpha} \mathcal{L}(t) = \frac{\mu_b}{\beta_2 \Lambda_b \theta_b} (\mu_a + \tau_a) (\mu_a + \theta_a) (\theta_b + \mu_b) (\mu_b + \tau_b + \omega) (1 - \mathcal{R}_1) (\mathcal{R}_2 - 1). \tag{21}$$

Clearly, if $R_0 < 1,$ then the derivative presented in equation (21) is negative. \square

6. Sensitivity Analysis for the Threshold Quantity \mathcal{R}_0

In mathematical models of infectious diseases, \mathcal{R}_0 has a very vital role in the prediction of an infectious disease that either the infection will die out or remain in the population. In this

regard, it is good to know which parameter has more influence on the value of threshold quantity $\mathcal{R}_0,$ for which we use sensitivity indices for \mathcal{R}_0 known as forward sensitivity indices [16] with the help of

$$\prod_{\rho}^{\mathcal{R}_0} = \frac{\partial \mathcal{R}_0}{\partial \rho} \times \frac{\rho}{\mathcal{R}_0}, \tag{22}$$

where ρ represents the biological parameters used in the proposed coronavirus model (7). Using definition (22), we obtain

$$\begin{aligned} \prod_{\beta_1}^{\mathcal{R}_1} &= 1, \prod_{\Lambda_a}^{\mathcal{R}_1} = 1, \prod_{\theta_a}^{\mathcal{R}_1} = \frac{\mu_a}{\theta_a + \mu_a}, \prod_{\mu_a}^{\mathcal{R}_1} = -\left\{1 + \frac{\mu_a}{\theta_a + \mu_a} + \frac{\mu_a}{\tau_a + \mu_a}\right\}, \\ \prod_{\tau_a}^{\mathcal{R}_1} &= -\frac{\tau_a}{\tau_a + \mu_a}, \prod_{\beta_3}^{\mathcal{R}_2} = 1, \prod_{\Lambda_h}^{\mathcal{R}_2} = 1, \prod_{\theta_h}^{\mathcal{R}_2} = \frac{\mu_b}{\theta_b + \mu_b}, \\ \prod_{\mu_b}^{\mathcal{R}_2} &= -1 - \frac{\mu_b}{\theta_b + \mu_b} - \frac{\mu_b}{\tau_b + \mu_b + \omega}, \prod_{\tau_b}^{\mathcal{R}_2} = -\frac{\tau_b}{\tau_b + \mu_b + \omega}, \prod_{\omega}^{\mathcal{R}_2} = -\frac{\omega}{\tau_b + \mu_b + \omega}. \end{aligned} \tag{23}$$

7. Numerical Algorithms and Results

Here, we derive the numerical schemes for coronavirus model (7) with CFD^α in the LC^β sense. An Adams–Moulton iterative (AMI) technique [17] will be implemented for the numerical approximations of state variables $(S_a, L_a, I_a, R_a, S_b, L_b, I_b, R_b)$ used in the proposed coronavirus model (7).

Consider a Cauchy initial value problem with the operator LC^β

$$\begin{aligned} {}_{LC^\beta}^{\beta} \mathfrak{D}_{0,t} z(t) &= h(t, z(t)), \quad \beta > 0, t \in [0, T], \\ z^{(q)}(0) &= z_0^{(q)}, \end{aligned} \tag{24}$$

where $q = 0, 1, \dots, [\beta] - 1$. The Volterra integral equation of the second kind can be obtained from the above-mentioned Cauchy problem as follows:

$$z(t) = \sum_{q=0}^{p-1} z_0^{(q)} \frac{t^q}{q!} + \frac{1}{\Gamma(\beta)} \int_0^t (t-\tau)^{\beta-1} h(\tau, z(\tau)) d\tau, \quad \beta \in (p-1, p]. \tag{25}$$

Discretize the interval $[0, T]$ such that $b = T - 0/P$, $t_k = kb$, $k = 0, 1, \dots, P$ with the CFD^α . We obtain the following AMI scheme for the CFD^α in the sense of LC^β :

$$z(t_{p+1}) = z(0) + \frac{b^\beta}{\beta \Gamma(\beta)} \sum_{k=0}^p \left[(p+1-k)^\beta - (p-k)^\beta \right] {}_{CFD^\alpha} \mathfrak{D}_{0,t}^\alpha h(t_k, z(t_k)), \quad k \in [0, p], \tag{26}$$

where

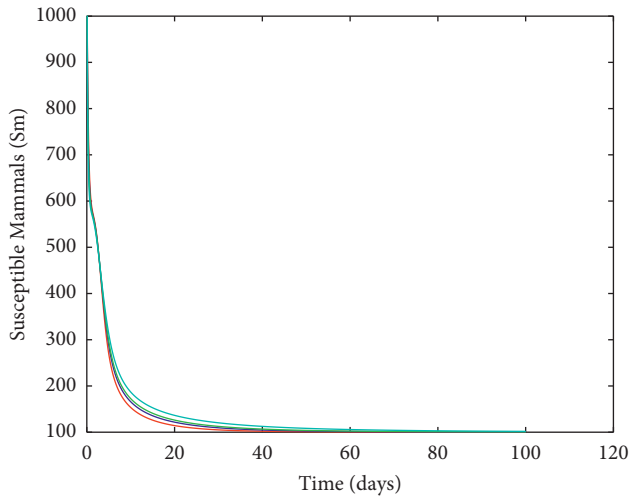
$${}_{CFD^\alpha} \mathfrak{D}_{0,t}^\alpha h(t_k, z(t_k)) = \frac{1}{t_k^{\alpha-1}} \frac{d}{dt} h(t_k, z(t_k)), \quad \alpha > 0. \tag{27}$$

Now, take $X(t_k) = (S_a(t_k), L_a(t_k), I_a(t_k), R_a(t_k), S_b(t_k), L_b(t_k), I_b(t_k), R_b(t_k))$ and using (25) and (26), we obtain the following iterative schemes for the proposed coronavirus model (7) with CFD^α in the LC^β sense:

$$\begin{aligned}
 S_a(t_{p+1}) &= S_a(0) + \frac{b^\beta}{\beta\Gamma(\beta)} \sum_{k=0}^p [(p+1-k)^\beta - (p-k)^\beta] h_1(X(t_k)), \\
 L_a(t_{p+1}) &= L_a(0) + \frac{b^\beta}{\beta\Gamma(\beta)} \sum_{k=0}^p [(p+1-k)^\beta - (p-k)^\beta] h_2(X(t_k)), \\
 I_a(t_{p+1}) &= I_a(0) + \frac{b^\beta}{\beta\Gamma(\beta)} \sum_{k=0}^p [(p+1-k)^\beta - (p-k)^\beta] h_3(X(t_k)), \\
 R_a(t_{p+1}) &= R_a(0) + \frac{b^\beta}{\beta\Gamma(\beta)} \sum_{k=0}^p [(p+1-k)^\beta - (p-k)^\beta] h_4(X(t_k)), \\
 S_b(t_{p+1}) &= S_b(0) + \frac{b^\beta}{\beta\Gamma(\beta)} \sum_{k=0}^p [(p+1-k)^\beta - (p-k)^\beta] h_5(X(t_k)), \\
 L_b(t_{p+1}) &= L_b(0) + \frac{b^\beta}{\beta\Gamma(\beta)} \sum_{k=0}^p [(p+1-k)^\beta - (p-k)^\beta] h_6(X(t_k)), \\
 I_b(t_{p+1}) &= I_b(0) + \frac{b^\beta}{\beta\Gamma(\beta)} \sum_{k=0}^p [(p+1-k)^\beta - (p-k)^\beta] h_7(X(t_k)), \\
 R_b(t_{p+1}) &= R_b(0) + \frac{b^\beta}{\beta\Gamma(\beta)} \sum_{k=0}^p [(p+1-k)^\beta - (p-k)^\beta] h_8(X(t_k)),
 \end{aligned}
 \tag{28}$$

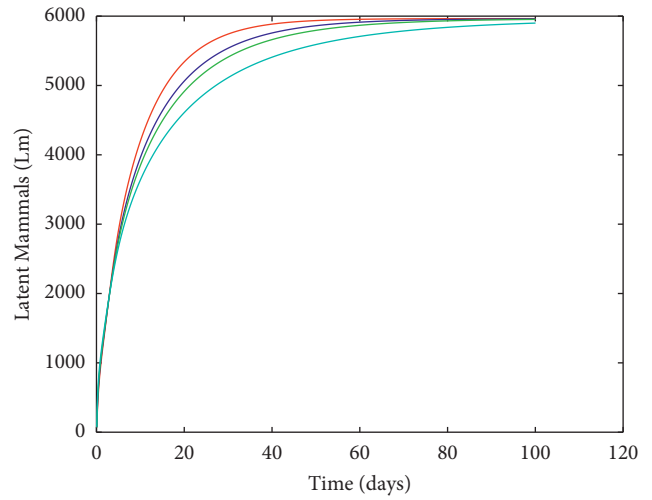
where

$$\begin{aligned}
 h_1(X(t_k)) &= \frac{1}{t_k^{1-\alpha}} (\Lambda_a - \beta_1 S_a(t_k) I_a(t_k) - \mu_a S_a(t_k)), \\
 h_2(X(t_k)) &= \frac{1}{t_k^{1-\alpha}} (\beta_1 S_a(t_k) I_a(t_k) - (\mu_a + \theta_a) L_a(t_k)), \\
 h_3(X(t_k)) &= \frac{1}{t_k^{1-\alpha}} (\theta_a L_a(t_k) - (\tau_a + \mu_a) I_a(t_k)), \\
 h_4(X(t_k)) &= \frac{1}{t_k^{1-\alpha}} (\tau_a I_a(t_k) - \mu_a R_a(t_k)), \\
 h_5(X(t_k)) &= \frac{1}{t_k^{1-\alpha}} (\Lambda_b - \beta_2 S_b(t_k) I_a(t_k) - \beta_3 S_b(t_k) I_b(t_k) + \gamma R_b(t_k) - \mu_b S_b(t_k)), \\
 h_6(X(t_k)) &= \frac{1}{t_k^{1-\alpha}} (\beta_2 S_b(t_k) I_a(t_k) + \beta_3 S_b(t_k) I_b(t_k) - (\mu_b + \theta_b) L_b(t_k)), \\
 h_7(X(t_k)) &= \frac{1}{t_k^{1-\alpha}} (\theta_b L_b(t_k) - (\tau_b + \mu_b + \omega) I_b(t_k)), \\
 h_8(X(t_k)) &= \frac{1}{t_k^{1-\alpha}} (\tau_b I_b(t_k) - (\mu_b + \gamma) R_b(t_k)).
 \end{aligned}
 \tag{29}$$



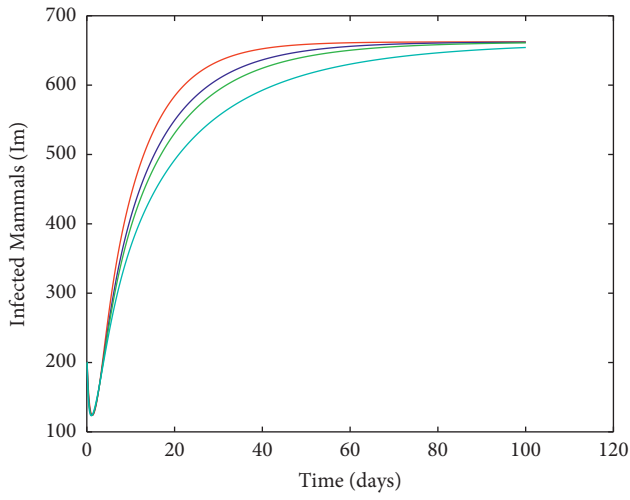
$\beta=1, \alpha=1$ $\beta=0.85, \alpha=1$
 $\beta=0.90, \alpha=1$ $\beta=0.75, \alpha=1$

(a)



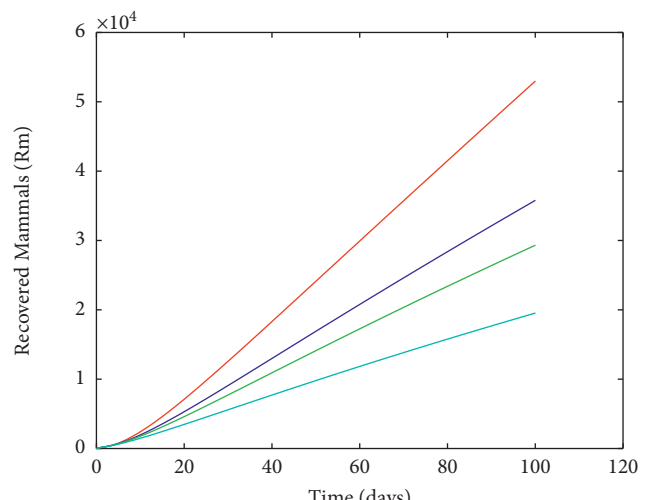
$\beta=1, \alpha=1$ $\beta=0.85, \alpha=1$
 $\beta=0.90, \alpha=1$ $\beta=0.75, \alpha=1$

(b)



$\beta=1, \alpha=1$ $\beta=0.85, \alpha=1$
 $\beta=0.90, \alpha=1$ $\beta=0.75, \alpha=1$

(c)



$\beta=1, \alpha=1$ $\beta=0.85, \alpha=1$
 $\beta=0.90, \alpha=1$ $\beta=0.75, \alpha=1$

(d)

FIGURE 1: Continued.

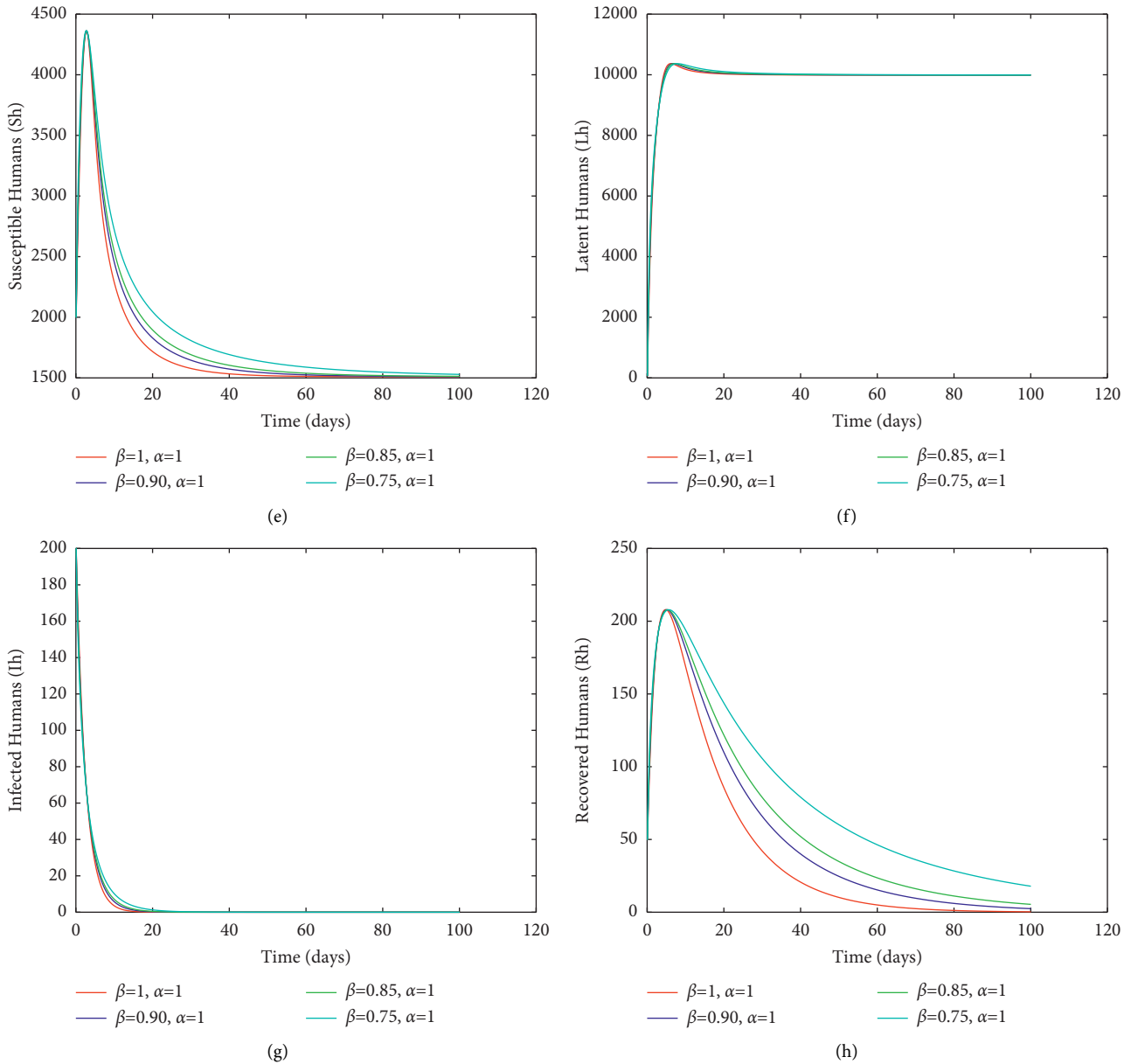


FIGURE 1: Simulation of fractional conformable model (7), when $\beta = 1, \beta = 0.90, \beta = 0.85, \beta = 0.75$, and $\alpha = 1$.

8. Numerical Simulation Results

The step size used for this work is 10^{-2} and the time interval considered is $[0, 30]$ with the following initial conditions: $(1000, 80, 200, 3, 2000, 80, 200, 50)$. The parameter values employed for the numerical simulation were obtained in [25] as follows: $\Lambda_a = 600, \Lambda_b = 9000, \beta_1 = 0.009, \mu_a = 0.000474, \theta_a = 0.1, \tau_a = 0.9, \beta_2 = 0.009, \beta_3 = 0.009, \gamma = 0.07, \mu_b = 0.0009, \theta_b = 0.9, \omega = 0.8, \tau_b = 0.5$. In this work, β represents the fractional conformable derivative order and α depicts the Liouville–Caputo operator order in equation (7). In Figures 1(a)–1(h), the fractional conformable derivative order β is varied while the fractional order α derivative in Liouville–Caputo is kept constant. The number of mammals in Figure 1(a) decreases as the conformable fractional order β increases from 0.75 to 1

which implies that more mammals are getting infected with the virus. In Figures 1(b)–1(d), the number of mammals in these classes increases as the fractional conformable order β increases from 0.75 to 1. Figure 1(f) indicates that the number of latent humans increases as fractional conformable order β increases from 0.75 towards 1. For Figures 1(e), 1(g), and 1(h), the number of humans in these classes reduces as the fractional conformable order β approaches 1 as the number of individuals reduces. Figures 2(a)–2(h) represent the numerical simulation based on equation (7) with constant fractional conformable derivative and a varied fractional order α in sense of Liouville–Caputo. Figure 2(a) shows that as the fractional order increases towards 1, the number of susceptible mammals increases gradually. In Figures 2(b)–2(d), the number of mammals in the

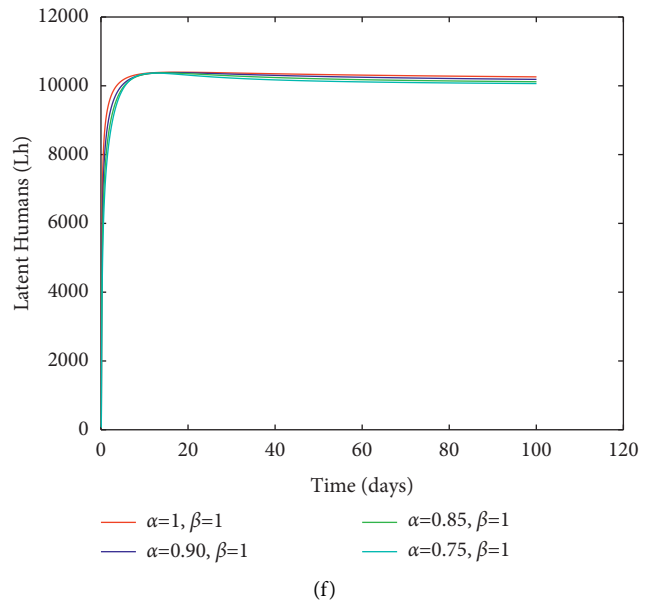
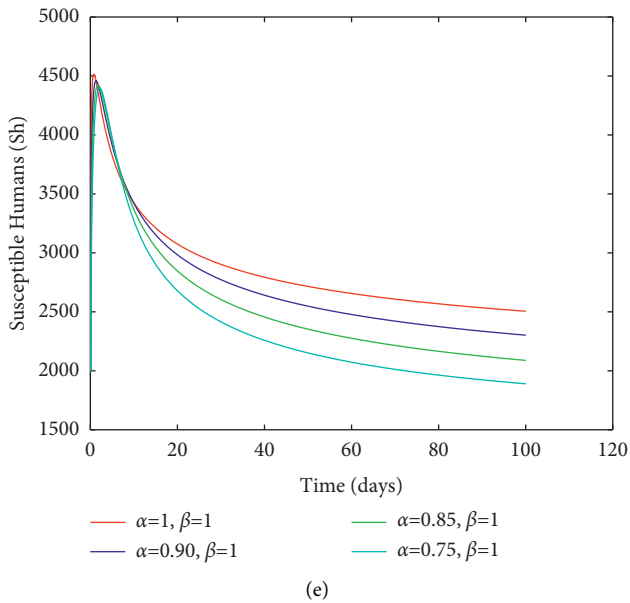
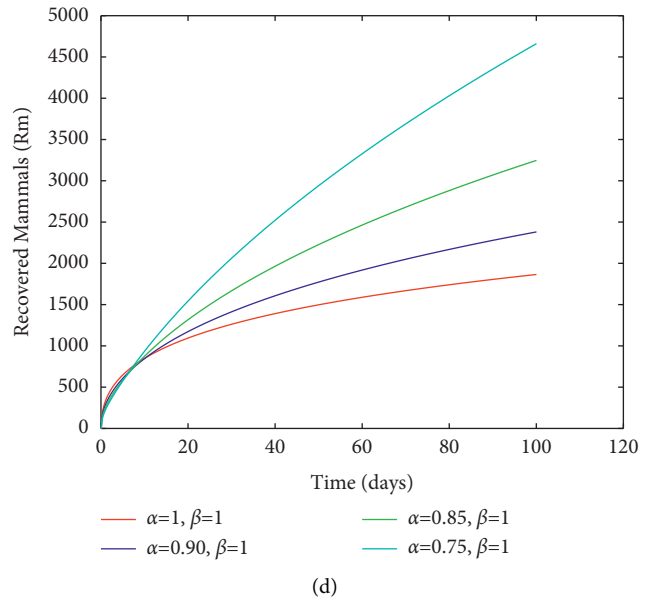
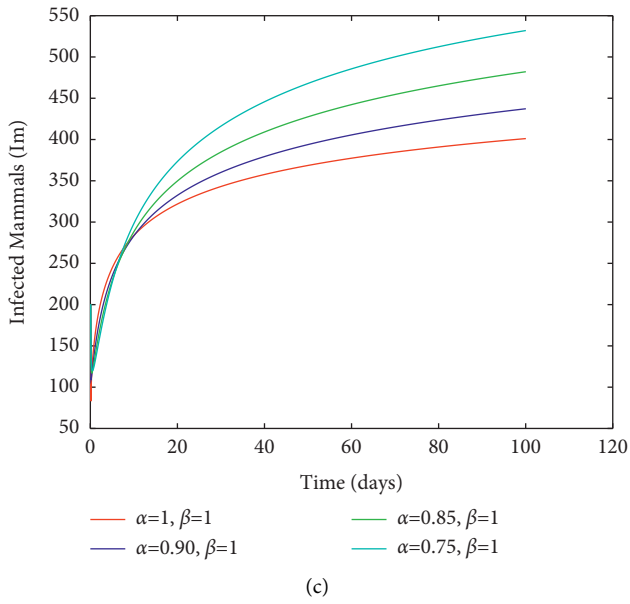
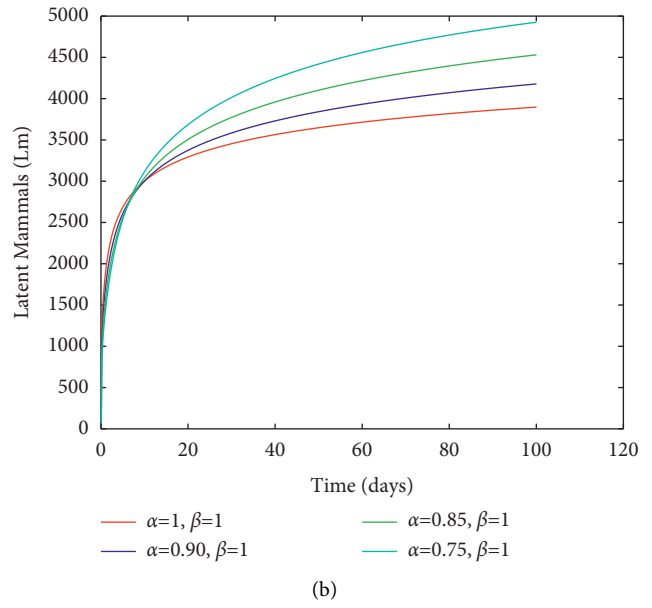
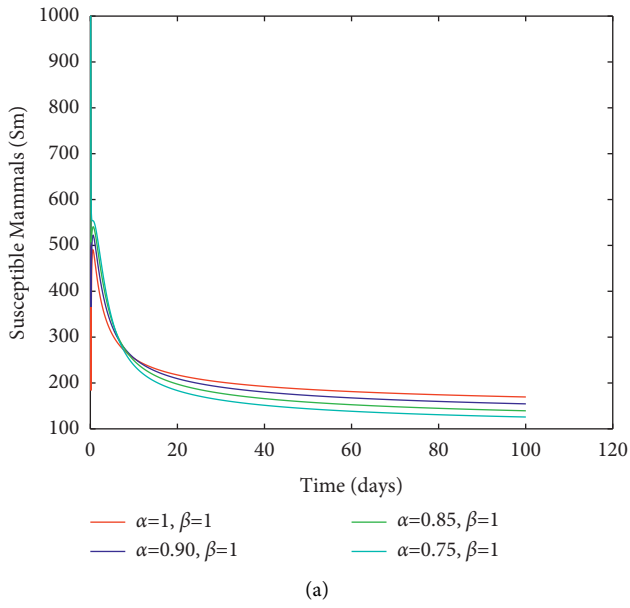


FIGURE 2: Continued.

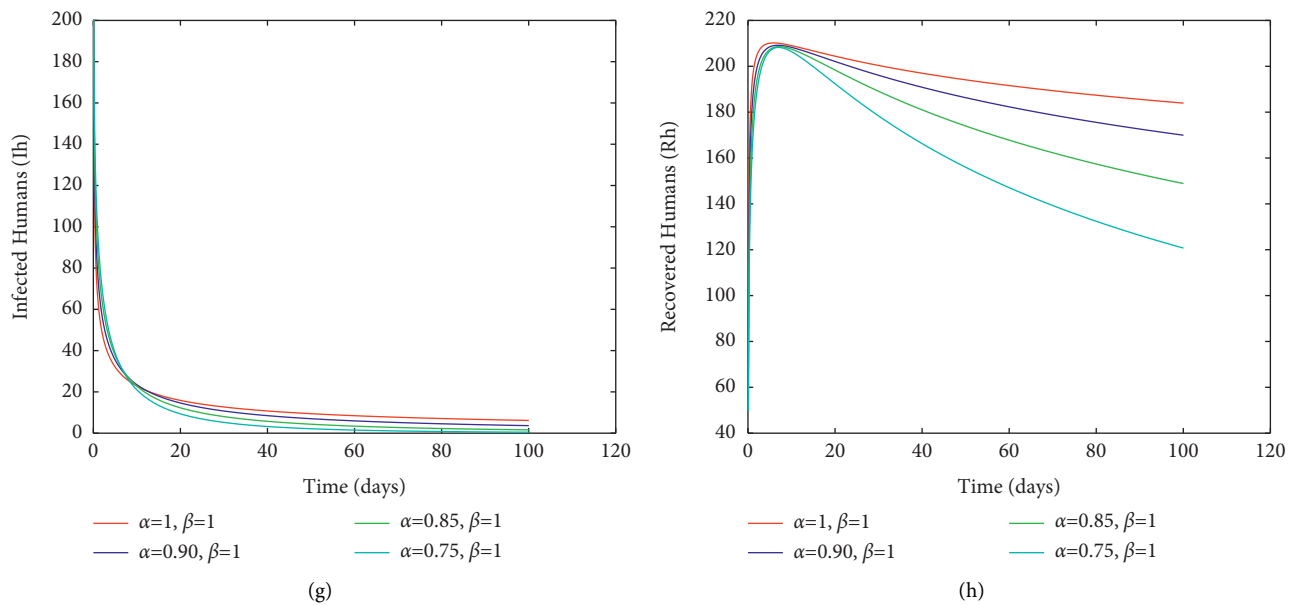


FIGURE 2: Simulation of fractional conformable model (7), when $\alpha = 1, \alpha = 0.90, \alpha = 0.85, \alpha = 0.75$, and $\beta = 1$.

respective classes eventually reduces as the fractional order α increases towards 1. Figure 2(e) indicates that the number of susceptible humans increase as the fractional order α decreases and a similar situation can be seen in Figure 2(g) for the infected humans class. The case is not different from Figures 2(f) and 2(h). As the fractional order α increases, the number of humans in these classes also increases, respectively.

9. Conclusions

In this work, a coronavirus model in the context of fractional conformable derivative in light of Liouville–Caputo sense was formulated. The basic property of model boundedness was investigated. The asymptotic stability of the steady states of the model has been studied. Sensitivity analysis was undertaken to have some basic idea about the parameter values involving the basic reproduction number. Numerical analysis based on the Adams–Moulton scheme was carried out, and the results indicated both fractional order conformable derivative order have an effect on the dynamics of coronavirus. It is, therefore, suggested that this derivative can be applied to other complex physical phenomena. In the future, similar models can be investigated using the fractional conformal approach because it conforms to the principles of derivatives and is easy to use. Other related models can be studied using the fractional conformal stochastic modeling approach. This could also be employed in financial and economic models since it is easy to utilize.

Data Availability

No data were used to support this study.

Conflicts of Interest

The authors declare that they have no conflicts of interest.

References

- [1] Wuhan, China Population 1950-2020.
- [2] China Virus Death Toll Rises to 41, More than 1,300 Infected Worldwide. CNBC. 24 January 2020. Archived from the Original on 26 January 2020.
- [3] Is the World Ready for the Coronavirus? Editorial. The New York Times. 29 January 2020.
- [4] Y. Yin and R. G. Wunderink, “Mers, sars and other coronaviruses as causes of pneumonia,” *Respirology*, vol. 23, no. 2, pp. 130–137, 2018.
- [5] World Health Organization (Who), 2019-2020 CoV Situation Report-22 on 12 February, 2020.
- [6] P. C. Y. Woo, Y. Huang, S. K. P. Lau, and K.-Y. Yuen, “Coronavirus genomics and bioinformatics analysis,” *Viruses*, vol. 2, no. 8, pp. 1804–1820, 2010.
- [7] A. M. Zaki, S. Van Boheemen, T. M. Bestebroer, A. D. Osterhaus, and R. A. Fouchier, “Isolation of a novel coronavirus from a man with pneumonia in Saudi Arabia,” *New England Journal of Medicine*, vol. 367, no. 19, pp. 1814–1820, 2012.
- [8] Z. Chen, W. Zhang, Y. Lu et al., “From sars-cov to wuhan 2019-COVID outbreak: similarity of early epidemic and prediction of future trends,” 2020.
- [9] E. Bonyah, G. Twagirumukiza, and P. P. Gambrah, “Mathematical analysis of diarrhoea model with saturated incidence rate,” 2019.
- [10] A. Akgul and E. Bonyah, “Reproducing kernel hilbert space method for the solutions of generalized kuramotosivashinsky equation,” *Journal of Taibah University for Science*, vol. 13, no. 1, pp. 661–669, 2019.
- [11] E. Bonyah, A. Atangana, and M. Chand, “Analysis of 3d is-lm macroeconomic system model within the scope of fractional

- calculus, Chaos,” *Solitons & Fractals: X*, vol. 2, Article ID 100007, 2019.
- [12] O. Kolebaje, E. Bonyah, and L. Mustapha, “The first integral method for two fractional non-linear biological models,” *Discrete & Continuous Dynamical Systems-S*, vol. 12, no. 3, pp. 487–502, 2019.
- [13] B. Ghanbari and A. Atangana, “A new application of fractional Atangana-Baleanu derivatives: designing abc-fractional masks in image processing,” *Physica A: Statistical Mechanics and Its Applications*, vol. 542, Article ID 123516, 2020.
- [14] K. M. Owolabi and A. Shikongo, “Fractional operator method on a multi-mutation and intrinsic resistance model,” *Alexandria Engineering Journal*, vol. 59, no. 4, pp. 1999–2013, 2020.
- [15] R. Khalil, M. Al Horani, A. Yousef, and M. Sababheh, “A new definition of fractional derivative,” *Journal of Computational and Applied Mathematics*, vol. 264, pp. 65–70, 2014.
- [16] A. Atangana, D. Baleanu, and A. Alsaedi, “New properties of conformable derivative,” *Open Mathematics*, vol. 13, no. 1, 2015.
- [17] S. Qureshi, “Effects of vaccination on measles dynamics under fractional conformable derivative with Liouville- Caputo operator,” *The European Physical Journal Plus*, vol. 135, no. 1, p. 63, 2020.
- [18] M. A. Khan and F. Gomez-Aguilar, “Tuberculosis model with relapse via fractional conformable derivative with power law,” *Mathematical Methods in the Applied Sciences*, vol. 42, no. 18, pp. 7113–7125, 2019.
- [19] A. Harir, S. Malliani, and L. S. Chandli, “Solutions of conformable fractional-order SIR epidemic model,” *International Journal of Differential Equations*, vol. 2021, Article ID 6636686, 7 pages, 2021.
- [20] K. Hosseini, K. Sadri, M. Mirzazadeh, A. Ahmadian, Y. Chu, and S. Salahshour, “Reliable methods to look for analytical and numerical solutions of a nonlinear differential equation arising in heat transfer with the conformable derivative,” *Mathematical Methods in the Applied Sciences*, vol. 25, 2021.
- [21] A. Allahamou, E. Azroul, Z. Hammouch, and A. L. Alaoui, “Modeling and numerical investigation of a conformable co-infection model for describing Hantavirus of the European moles,” *Mathematical Methods in the Applied Sciences*, vol. 45, no. 5, pp. 2736–2759, 2021.
- [22] E. Bonyah, A. K. Sagoe, D. Kumar, and S. Deniz, “Fractional optimal control dynamics of coronavirus model with mittagleffler law,” *Ecological Complexity*, vol. 45, Article ID 100880, 2021.
- [23] F. Agosto and M. Khan, “Optimal control strategies for dengue transmission in Pakistan,” *Mathematical Biosciences*, vol. 305, pp. 102–121, 2018.
- [24] E. Bonyah, M. A. Khan, K. O. Okosun, and S. Islam, “A theoretical model for zika virus transmission,” *PLoS One*, vol. 12, no. 10, Article ID e0185540, 2017.
- [25] M. A. Khan and A. Atangana, “Modeling the dynamics of novel coronavirus (2019-nCov) with fractional derivative,” *Alexandria Engineering Journal*, vol. 59, no. 4, pp. 2379–2389, 2020.

Research Article

Modeling Drug Concentration Level in Blood Using Fractional Differential Equation Based on Psi-Caputo Derivative

Muath Awadalla ¹, Yves Yannick Yameni Noupoue,² Kinda Abu Asbeh ¹,
and Nouredine Ghiloufi ^{1,3}

¹Department of Mathematics and Statistics, College of Science, King Faisal University, Hafuf, Al Ahsa 31982, Saudi Arabia

²Université Catholique de Louvain, Louvain, La-Neuve, Belgium

³University of Gabes, Faculty of Sciences of Gabes, LR17ES11 Mathematics and Applications, 6072 Gabes, Tunisia

Correspondence should be addressed to Muath Awadalla; mawadalla@kfu.edu.sa

Received 5 August 2022; Revised 1 September 2022; Accepted 5 September 2022; Published 28 September 2022

Academic Editor: Arzu Akbulut

Copyright © 2022 Muath Awadalla et al. This is an open access article distributed under the Creative Commons Attribution License, which permits unrestricted use, distribution, and reproduction in any medium, provided the original work is properly cited.

This article studies a pharmacokinetics problem, which is the mathematical modeling of a drug concentration variation in human blood, starting from the injection time. Theories and applications of fractional calculus are the main tools through which we establish main results. The psi-Caputo fractional derivative plays a substantial role in the study. We prove the existence and uniqueness of the solution to the problem using the psi-Caputo fractional derivative. The application of the theoretical results on two data sets shows the following results. For the first data set, a psi-Caputo with the kernel $\psi = x + 1$ is the best approach as it yields a mean square error (MSE) of 0.04065. The second best is the simple fractional method whose MSE is 0.05814; finally, the classical approach is in the third position with an MSE of 0.07299. For the second data set, a psi-Caputo with the kernel $\psi = x + 1$ is the best approach as it yields an MSE of 0.03482. The second best is the simple fractional method whose MSE is 0.04116 and, finally, the classical approach with an MSE of 0.048640.

1. Introduction

To treat an infection from a human being or even from an animal, a suitable dose of medicine is substantial. Owing to the amount of the drug in the blood plasma decreasing with time, medicine must be given in multiple doses.

In phase I of clinical development, the time to achievement of steady state of a new regimen is routinely evaluated. The time to the achievability of the steady state is the time needed until the drug concentration is stable in the blood, i.e., does not display an increasing tendency by drug accumulation. If a drug is given at orderly dosing intervals, drug sediment from preceding doses is accumulated. Stabilization of the concentration occurs when the quantity of drug discarded during the dosing interval equals the amount that was given. In order to evaluate the time to achieve steady state, blood is sampled at a certain time point within each dosing interval see [1].

Following the drug concentrations at these time points [2] Jordan et al. proposed a model for the achievement of the steady state of the drug concentration in plasma. Authors of [3] proposed a model for the prediction of the “unbound brain-to-plasma” drug concentration ratio. Zhang et al. [4] studied the ratio of the drug concentration between tissues and plasma.

A simple and novel sensor was developed for the analysis of clinical doxorubicin (DOX) concentration based on the screen-printed electrode by evaluating the DOX concentration, see [5]. In [6] the authors evaluated the drug concentrations in postmortem blood samples where the value of concentrations slightly differs depending on the sample site. For more works on drug concentration in the blood, we refer the reader to the references [7–11].

Fractional calculus (F.C) helps to describe models and natural phenomena problems. Many researches have dedicated their work in this branch (see, e.g., previous studies [12–19]). The results obtained were significantly positive in

different fields of Medicine and Biology. The foundation of fractional calculus is laid on fractional integrals and derivatives. The efficiency of the fractional order model over the integer order is investigated by Bagley and Torvik [20]. Through fractional calculus, Djordjevic et al. [21] developed a rheological model of airway smooth muscle cells, which came as an alternative to the least square data fitting technique often used for this purpose. Recently, an application of fractional calculus to nanotechnology was proposed in [22]. These are just a few out of plenty examples of research works in which fractional calculus has proven its efficiency compared to existing classical approach.

This research article contributes to showing the power of mathematical modeling using fractional calculus. In particular, a class of fractional derivatives called ψ -Caputo, introduced by Almeida [23], has proven its efficiency in various applications including a recent study by Awadalla et al. [24]. A preliminary investigation on the topic of this study was carried out by us. The results of the said investigation are provided in this reference [25]. The main contribution of this work to the literature is the reduction or further minimization of the MSE in modeling the drug's concentration kinetics. The article starts with an introduction; then, some preliminaries of fractional calculus are covered. Elements of pharmacokinetics and the mathematical model of drug concentration in the blood are discussed in the third section. Main theoretical results are established in the fourth section followed by application examples in the fifth section. Finally, the last section provides concluding remarks on the overall study.

More generally, realization of this work was motivated by the aim to reduce modeling error in pharmacokinetics.

2. Preliminaries

This section is dedicated to preliminary tools that will enable a smooth study in upcoming sections. Indeed, F.C theories are built thanks to theorems, definitions, and lemmas. Similar to classical calculus, integrals and derivatives taken in the fractional sense are the foundation of F.C. Concerning the abovementioned sentences, selected definitions, theorems, and notations are discussed in this section. They play important roles in the rest of the paper.

Definition 1 (see [9]). The fractional integral of order $\xi > 0$ of a function $\mathcal{H} : [a, b] \rightarrow \mathcal{R}_e$ taken in the Riemann-Liouville sense is defined as

$$\left({}_{\mathcal{R}\mathcal{L}}\mathcal{I}_0^\xi \mathcal{H} \right) (\varrho) = \frac{1}{\Gamma(\xi)} \int_0^\varrho (\varrho - \vartheta)^{\xi-1} \mathcal{H}(\vartheta) d\vartheta. \quad (1)$$

Equation (1) holds only if the right-hand side of the given integral is point-wise defined on $]0, +\infty[$. Note that the function Γ is the commonly-known gamma function, which is defined as follows: $\Gamma(u) = \int_0^{+\infty} \varrho^{u-1} e^{-\varrho} d\varrho, \forall u > 0$.

Definition 2 (see [9]). The Caputo derivative of order $\xi > 0$ of a function $\mathcal{H} : [a, b] \rightarrow \mathcal{R}_e$ is defined as

$$\left({}_C\mathcal{D}_0^{\xi, \psi} \mathcal{H} \right) (\varrho) = \begin{cases} \frac{1}{\Gamma(n-\xi)} \int_0^\varrho (\varrho - \vartheta)^{n-\xi-1} \mathcal{H}^{(n)}(\vartheta) d\vartheta, & n-1 < \xi < n, \xi \in \mathcal{R}_e, \\ \mathcal{H}^{(n)}(\varrho), & \xi \in \mathbb{N}, \end{cases} \quad (2)$$

where $n = \lfloor \xi \rfloor + 1, \lfloor \xi \rfloor$ is the integer part of ξ .

Definition 3 (see [2]). Let $\xi > 0, \mathcal{H} \in \mathcal{L}^1[a, b]$ and $\psi \in \mathcal{C}^1[a, b]$ is selected to be an increasing function with $\psi'(x) \neq 0, \forall x \in [a, b]$; then, the notation $\mathcal{I}_0^{\xi, \psi} \mathcal{H}(\varrho)$ represents the fractional integral of \mathcal{H} with respect to another function ψ , and it is defined by

$$\mathcal{I}_0^{\xi, \psi} \mathcal{H}(\varrho) = \frac{1}{\Gamma(\xi)} \int_0^\varrho \psi'(\vartheta) (\psi(\varrho) - \psi(\vartheta))^{\xi-1} \mathcal{H}(\vartheta) d\vartheta. \quad (3)$$

The idea of integrating a function definition is known as ψ -Caputo integral of the fractional integral is taken in the Caputo sense. This is used in the sequel for formulating the solution to the ψ -Caputo fractional model.

Definition 4 (see [2]). Let $\xi > 0$ and $\mathcal{H}, \psi \in \mathcal{C}^n[a, b]$ where ψ is an increasing function and $\psi'(x) \neq 0, \forall x \in [a, b]$. Then, $\left({}_C\mathcal{D}_0^{\xi, \psi} \mathcal{H} \right) (\varrho)$ denotes the fractional derivative of \mathcal{H} with respect to ψ . ψ -Caputo if the fractional derivative is taken in the Caputo sense, and it is given by

$${}_C\mathcal{D}_0^{\xi, \psi} \mathcal{H}(\varrho) = \frac{1}{\Gamma(n-\xi)} \int_0^\varrho \psi'(\vartheta) (\psi(\varrho) - \psi(\vartheta))^{n-\xi-1} \left(\frac{1}{\psi'(\vartheta)} \frac{d}{d\varrho} \right)^n \mathcal{H}(\vartheta) d\vartheta. \quad (4)$$

Lemma 5 (see [2]). Let $\xi > 0$ and n be a positive integer such that $\xi \in]n-1, n[$. For every $\mathcal{H}, \psi \in \mathcal{C}^n[a, b]$, we have

$$\mathcal{I}_0^{\xi, \psi} \left({}_C\mathcal{D}_0^{\xi, \psi} \mathcal{H} \right) (\varrho) = \mathcal{H}(\varrho) - \sum_{p=0}^{n-1} \frac{1}{p!} \left(\frac{1}{\psi'(\vartheta)} \frac{d}{d\varrho} \right)^p \mathcal{H}(0) (\psi(\varrho) - \psi(0))^p. \quad (5)$$

3. Pharmacokinetics and Drug Concentration Model

A brief definition and overview of pharmacokinetics are proposed in this section. To treat an infection from a human body, a suitable dose of medicine is substantial. Once a drug is administrated to an individual through intravenous injection, it has an initial concentration that decreases over time. The decrement appears as a result of metabolism and excretion. Pharmacokinetics is a branch of medicine that studies the dynamic (kinetics of drugs in a living body). Owing to the amount of the drug in the human body decreasing with time medicine must be given in multiple doses.

Two main streams of study exist in pharmacokinetics, the theoretical approach and the experimental approach.

The former approach focuses on the development of a pharmacokinetics (mathematical) model that predicts drug concentration levels in the blood over time. The latter method involves empirical development based on a biological sample, during which analytical methods for drugs and their metabolites are measured. In this case, it is required to have an adequate experimental setting for data collection and handling. This article focuses in the sequel on the development of a mathematical pharmacokinetics model. The entire process of absorption, distribution, metabolism, and elimination (ADME) of a drug is illustrated in the next figure as described in [26, 27].

Figure 1 represents the ADME process of a drug after it has been administrated to a human. The process is governed by a change in concentration over time. The change rate can be denoted by $\pm d(\text{concentration})/dQ$. More generally, let us denote by \mathcal{Y} the drug concentration in the body; then, the mathematical model describing the rate change is given by

$$\frac{d\mathcal{Y}}{dQ} = -k\mathcal{Y}, \tag{6}$$

where k is a constant to be experimentally determined for each drug. If a patient is given an initial drug dose, \mathcal{Y}_0 , then, the drug level in his body at any time is the solution of the differential equation defined by Eq. (6), that is,

$$\mathcal{Y}(Q) = \mathcal{Y}_0 e^{-kQ}. \tag{7}$$

The objective of this work is to prove the advantages of modeling drug concentration kinetics using fractional differential equations. Indeed, we will show empirically that modeling results using F.C are better than those obtained from classical calculus. The starting point is to build a fractional counterpart of Eq. (6). The said equation is built as follows

$${}_C \mathcal{D}_{0^+}^{\xi, \psi} \mathcal{Y}(Q) = -k\mathcal{Y}(Q), \quad \xi \in]0, 1[, \mathcal{Y}(0) = \mathcal{Y}_0. \tag{8}$$

or simply

$${}_C \mathcal{D}_{0^+}^{\xi, \psi} \mathcal{Y}(Q) = \mathcal{Q}(Q, \mathcal{Y}(Q)), \quad \xi \in]0, 1[, \mathcal{Y}(0) = \mathcal{Y}_0. \tag{9}$$

The Lemma below is defined to introduce a general form of the solution to Eq. (9) representing drug concentration kinetics with initial condition.

Lemma 6. *Let us consider \mathcal{Q} , with the assumption that it is an integrable function, which is defined over $[0, \mathcal{T}]$. It follows that the solution of the fractional differential equation given by Eq. (9) has a general form which can be expressed by the following integral equation*

$$\mathcal{Y}(Q) = \mathcal{Y}_0 + \frac{1}{\Gamma(\xi)} \int_0^Q \psi'(\vartheta) (\psi(Q) - \psi(\vartheta))^{\xi-1} \mathcal{Q}(\vartheta, \mathcal{Y}(\vartheta)) d\vartheta. \tag{10}$$

It is worth to highlight in Eq. (10) from Lemma 6 the presence of ψ -Caputo fractional integral.

Proof. Let us apply the operator $\mathcal{I}_{0^+}^{\xi, \psi}$ to both sides of Eq. (9) leads to $\mathcal{Y}(Q) - \mathcal{Y}_0 = \mathcal{I}_{0^+}^{\xi, \psi} \mathcal{Q}(Q, \mathcal{Y}(Q))$. \square

Equation (10) can be rewritten in the following form

$$\mathcal{Y}(Q) = \mathcal{Y}_0 E_{\xi} \left[-k(\psi(Q) - \psi(0))^{\xi} \right]. \tag{11}$$

where $E_{\xi}(Q) = \sum_{n=0}^{+\infty} (Q^n / \Gamma(n\xi + 1))$, $Q \in \mathcal{R}_e$ is the Mittag-Leffler function.

In the application, Kernel functions are selected under the data distribution. There is not a steady rule for that. However, a linear kernel works well in many cases. Other commonly used kernel includes but is not limited to \sqrt{u} , $\log u$.

4. Main Result of Psi-Caputo Drug Concentration Model

This section aims to investigate theoretical study around Eq. (9). The final goal is to build prove of the existence and the uniqueness of a solution to Eq. (9).

Let $\mathcal{E}[0, \mathcal{T}]$ be the space of real valued functions that are continuous on $[0, \mathcal{T}]$ endowed with the norm of the uniform convergence: $\|\mathcal{Y}\|_{\infty} = \sup_{Q \in [0, \mathcal{T}]} |\mathcal{Y}(Q)|$ for every $\mathcal{Y} \in \mathcal{E}[0, \mathcal{T}]$. Then, $\Phi := (\mathcal{E}[0, \mathcal{T}], \|\cdot\|_{\infty})$ is a Banach space.

An operator $\mathfrak{I} : \Phi \rightarrow \Phi$ defined and attached to the problem introduced by Eq. (9) can be built as

$$\mathfrak{I}\mathcal{Y}(Q) = \mathcal{Y}_0 + \frac{1}{\Gamma(\xi)} \int_0^Q \psi'(\vartheta) (\psi(Q) - \psi(\vartheta))^{\xi-1} \mathcal{Q}(\vartheta, \mathcal{Y}(\vartheta)) d\vartheta. \tag{12}$$

In what follows, the existence of a solution to Eq. (10) is proved followed by a proof of the uniqueness of the said solution. Before establishing the proof of the main results, let us first establish the following statements. Indeed, the statements are mathematical hypotheses that are used in sections dedicated to proofs.

$$(A_1) \text{ | The function } \mathcal{Q} : [0, \mathcal{T}] \times \mathcal{R}_e \rightarrow \mathcal{R}_e \text{ is continuous,} \tag{13}$$

$$(A_2) \text{ | There exists } \mathcal{L}_{\mathcal{Q}} > 0 \text{ such that,} \\ \left| \mathcal{Q}(Q, \mathcal{Y}_1) - \mathcal{Q}(Q, \mathcal{Y}_2) \right| \leq \mathcal{L}_{\mathcal{Q}} |\mathcal{Y}_1 - \mathcal{Y}_2|, \quad \forall Q \in [0, \mathcal{T}], \tag{14}$$

$$(A_3) \text{ | There exists a function } \mathcal{H} \in \mathcal{E}([0, \mathcal{T}], \mathcal{R}_e^+) \text{ and a nondecreasing function,} \\ \chi : \mathcal{R}_e^+ \rightarrow \mathcal{R}_e^+ \text{ such that } |\mathcal{Q}(Q, \mathcal{Y})| \leq \mathcal{H}(Q) \chi(|\mathcal{Y}|), \quad \forall (Q, \mathcal{Y}) \in [0, \mathcal{T}] \times \mathcal{R}_e. \tag{15}$$

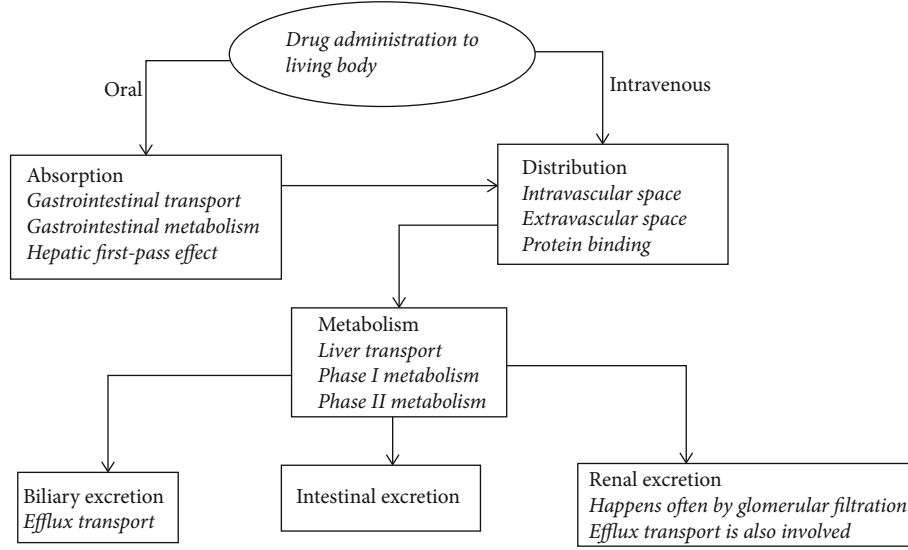


FIGURE 1: ADME process.

$$(A_4) \left| \frac{\text{There exists a constant } W > 0 \text{ such that,}}{W} \right| > 1. \quad (16)$$

$$\frac{W}{|\mathcal{Y}_0| + \|\mathcal{H}\|_{\infty} \chi(\lambda) \left((1/\Gamma(\xi + 1)) (\psi(\mathcal{T}) - \psi(0))^{\xi} \right)}$$

Existence of at least one solution to the problem Eq. (9) is proved in the theorem below

Theorem 7. *Let us assume that the three conditions (A_1) , (A_3) , and (A_4) hold. Then, there exists at least one solution to Eq. (9). The said solution is in the interval $[0, \mathcal{T}]$.*

Proof. The proof of theorem 7 will be divided into several steps. The first step consists of showing that the operator $\mathfrak{T} : \Phi \rightarrow \Phi$ maps bounded sets of Φ into bounded sets of Φ . Let $\mathfrak{B}_{\lambda} := \{\mathcal{Y} \in \Phi; \|\mathcal{Y}\|_{\infty} \leq \lambda\}$ be a bounded set of Φ . Then

$$\begin{aligned} |\mathfrak{T}\mathcal{Y}(\varrho)| &\leq |\mathcal{Y}_0| + \frac{1}{\Gamma(\xi)} \int_0^{\varrho} \psi'(\vartheta) (\psi(\varrho) - \psi(\vartheta))^{\xi-1} |\mathcal{Q}(\vartheta, \mathcal{Y}(\vartheta))| d\vartheta \\ &\leq |\mathcal{Y}_0| + \frac{1}{\Gamma(\xi)} \int_0^{\varrho} \psi'(\vartheta) (\psi(\varrho) - \psi(\vartheta))^{\xi-1} \mathcal{H}(\vartheta) \chi(\|\mathcal{Y}\|_{\infty}) d\vartheta \\ &\leq |\mathcal{Y}_0| + \|\mathcal{H}\|_{\infty} \chi(\|\mathcal{Y}\|_{\infty}) \frac{1}{\Gamma(\xi+1)} (\psi(\varrho) - \psi(0))^{\xi}. \end{aligned} \quad (17)$$

□

Applying the supremum on t on both sides of Eq. (17) leads to

$$\|\mathfrak{T}\mathcal{Y}\|_{\infty} \leq |\mathcal{Y}_0| + \|\mathcal{H}\|_{\infty} \chi(\lambda) \frac{1}{\Gamma(\xi+1)} (\psi(\mathcal{T}) - \psi(0))^{\xi}. \quad (18)$$

The second step of this proof is to show that the operator

$\mathfrak{T} : \Phi \rightarrow \Phi$ maps bounded sets of Φ into equi-continuous sets of Φ .

Let $\varrho_1, \varrho_2 \in [0, \mathcal{T}]$ with $\varrho_1 < \varrho_2$ and $\mathcal{Y} \in \mathfrak{B}_{\lambda}$. The relation below holds as results of the assumptions $(A1)$ - $(A4)$

$$\begin{aligned} |\mathfrak{T}\mathcal{Y}(\varrho_2) - \mathfrak{T}\mathcal{Y}(\varrho_1)| &\leq \chi(\|\mathcal{Y}\|_{\infty}) \left| \frac{1}{\Gamma(\xi)} \int_0^{\varrho_1} \psi'(\vartheta) [(\psi(\varrho_2) - \psi(\vartheta))^{\xi-1} \right. \\ &\quad \left. - (\psi(\varrho_1) - \psi(\vartheta))^{\xi-1}] \mathcal{H}(\vartheta) d\vartheta \right. \\ &\quad \left. + \frac{1}{\Gamma(\xi)} \int_{\varrho_1}^{\varrho_2} \psi'(\vartheta) (\psi(\varrho_2) - \psi(\vartheta))^{\xi-1} \mathcal{H}(\vartheta) d\vartheta \right|. \end{aligned} \quad (19)$$

The right-hand side of Eq. (19) tends to zero as $\varrho_1 \rightarrow \varrho_2$. That is $|\mathfrak{T}\mathcal{Y}(\varrho_2) - \mathfrak{T}\mathcal{Y}(\varrho_1)| \rightarrow 0$ as $\varrho_1 \rightarrow \varrho_2$.

It is worth observing that the right hand part of Eq. (19) does not depend on $\mathcal{Y} \in \mathfrak{B}_{\lambda}$, this implies by Arzela-Ascoli theorem that $\mathfrak{T}(\mathfrak{B}_{\lambda})$ is completely continuous.

The third step of the proof requires a last intermediate step to complete the assumptions of the Leray-Schauder nonlinear alternative theorem. This consists of showing the boundedness of the set of all solutions to equation $\mathcal{Y} = \delta \mathfrak{T}(\mathcal{Y})$. Assume that \mathcal{Y} is a solution Eq. (9), then, it follows from Eq. (10) that

$$\begin{aligned} |\mathcal{Y}(\varrho)| &= |\delta \mathfrak{T}(\mathcal{Y})(\varrho)| \leq \delta \left(|\mathcal{Y}_0| + \|\mathcal{H}\|_{\infty} \chi(\lambda) \frac{1}{\Gamma(\xi+1)} (\psi(\mathcal{T}) - \psi(0))^{\xi} \right) \\ &\leq |\mathcal{Y}_0| + \|\mathcal{H}\|_{\infty} \chi(\lambda) \frac{1}{\Gamma(\xi+1)} (\psi(\mathcal{T}) - \psi(0))^{\xi}. \end{aligned} \quad (20)$$

Inverting both sides of Eq. (20) and dividing them by R.H.S of Eq. (20) leads to the following relation

$$\frac{\|\mathcal{Y}\|_{\infty}}{|\mathcal{Y}_0| + \|\mathcal{H}\|_{\infty} \chi(\lambda) (1/\Gamma(\xi+1)) (\psi(\mathcal{T}) - \psi(0))^{\xi}} \leq 1. \quad (21)$$

Recalling (A_4) , there exists a constant $W > 0$, which is indeed such that $W \neq \mathcal{Y}$. Moreover, let us construct the set $\Omega = \{\mathcal{Y} \in \Phi; \|\mathcal{Y}\|_\infty < W\}$. It is obvious that the operator $\mathfrak{Z} : \Omega \rightarrow \Phi$ is continuous and completely continuous. Based on the constructed Ω , there exists $\mathcal{Y} \in \partial\Omega$ such that $\mathcal{Y} \delta \mathfrak{Z}(\mathcal{Y})$ for some $\delta \in]0, 1[$. Consequently, by the nonlinear alternative of Leray-Schauder type, we deduce that \mathfrak{Z} has a fixed point $\mathcal{Y} \in \bar{\Omega}$ which is a solution to the problem defined by Eq. (10).

Theorem 8. *Let us assume that conditions (A_1) and (A_2) hold. Moreover, if the condition*

$$\frac{\mathcal{L}_{\mathcal{Y}}}{\Gamma(\xi + 1)} (\psi(\mathcal{T}) - \psi(0))^\xi < 1, \tag{22}$$

holds; then, the problem defined by Eq. (9) has a solution which is unique. The said solution belongs to the interval $[0, \mathcal{T}]$.

Proof. Let us consider the operator \mathfrak{Z} defined in Eq. (12). Let us also define a ball

$$\mathfrak{B}_\lambda = \{\mathcal{Y} \in \Phi; \|\mathcal{Y}\|_\infty \leq \varepsilon\} \text{ with } \varepsilon \geq \frac{|\mathcal{Y}_0| + (\mathcal{M}_Q/\Gamma(\xi + 1))(\psi(\mathcal{T}) - \psi(0))^\xi}{1 - (\mathcal{L}_{\mathcal{Y}}/\Gamma(\xi + 1))(\psi(\mathcal{T}) - \psi(0))^\xi}, \tag{23}$$

where $\mathcal{M}_Q := \sup_{0 \leq \vartheta \leq \mathcal{T}} |\mathcal{Q}(\vartheta, 0)|$. □

First, let us show that $\mathfrak{Z}\mathfrak{B}_\varepsilon \subset \mathfrak{B}_\varepsilon$. For any $\mathcal{Y} \in \mathfrak{B}_\varepsilon, \rho \in [0, \mathcal{T}]$, and using Eq. (12), we have the following relation

$$|\mathfrak{Z}\mathcal{Y}(\varrho)| \leq |\mathcal{Y}_0| + \frac{1}{\Gamma(\xi)} \int_0^\varrho \psi'(\vartheta) (\psi(\varrho) - \psi(\vartheta))^{\xi-1} |\mathcal{Q}(\vartheta, \mathcal{Y}(\vartheta))| d\vartheta. \tag{24}$$

On the other hand,

$$\begin{aligned} |\mathcal{Q}(\vartheta, \mathcal{Y}(\vartheta))| &\leq |\mathcal{Q}(\vartheta, \mathcal{Y}(\vartheta)) - \mathcal{Q}(\vartheta, 0)| + |\mathcal{Q}(\vartheta, 0)| \\ &\leq \mathcal{L}_Q \|\mathcal{Y}\|_\infty + \mathcal{M}_Q \leq \mathcal{L}_Q \varepsilon + \mathcal{M}_Q. \end{aligned} \tag{25}$$

Substituting the appropriate fragment of equation in Eq. (24) by Eq. (25) implies a new relation which is given by

$$\|\mathfrak{Z}\mathcal{Y}\|_\infty \leq |\mathcal{Y}_0| + \frac{1}{\Gamma(\xi + 1)} (\psi(\mathcal{T}) - \psi(0))^\xi (\mathcal{L}_Q \varepsilon + \mathcal{M}_Q) \leq \varepsilon. \tag{26}$$

Equation (26) is sufficient to conclude that $\mathfrak{Z}\mathfrak{B}_\varepsilon \subset \mathfrak{B}_\varepsilon$.

The second step of the proof is to show that the considered operator is a contraction mapping. For every $\mathcal{Y}_1, \mathcal{Y}_2$

$\in \Phi$, the following relation holds.

$$\begin{aligned} |\mathfrak{Z}\mathcal{Y}_1(\varrho) - \mathfrak{Z}\mathcal{Y}_2(\varrho)| &\leq \frac{1}{\Gamma(\xi)} \int_0^\varrho \psi'(\vartheta) (\psi(\varrho) - \psi(\vartheta))^{\xi-1} |\mathcal{Q}(\vartheta, \mathcal{Y}_1(\vartheta)) \\ &\quad - \mathcal{Q}(\vartheta, \mathcal{Y}_2(\vartheta))| d\vartheta \\ &\leq \left(\frac{1}{\Gamma(\xi)} \int_0^\varrho \psi'(\vartheta) (\psi(\varrho) - \psi(\vartheta))^{\xi-1} d\vartheta \right) \mathcal{L}_Q \|\mathcal{Y}_1 - \mathcal{Y}_2\|_\infty \\ &\leq \left(\frac{\mathcal{L}_Q}{\Gamma(\xi + 1)} (\psi(\mathcal{T}) - \psi(0))^\xi \right) \|\mathcal{Y}_1 - \mathcal{Y}_2\|_\infty. \end{aligned} \tag{27}$$

From Eq. (27), we deduce that \mathfrak{Z} is a contraction. By the Banach contraction mapping theorem, the problem defined by Eq. (9) has a unique solution. The said solution belongs to the interval $[0, \mathcal{T}]$.

5. Application Example

In this section, application examples are provided to support the theoretical work developed above. Data set obtained from real-life experiment were used. The classical method, simple fractional method, and kernel fractional method were used to fit the data set. Finally, a comparison of results is done to support theoretical findings.

5.1. First Experimental Data Set. This data set was retrieved from [28]. The author carried out an experiment in which he measured a drug concentration in (mg/L) over 6 hours of an antibiotic. A single dose of the said antibiotic was administered intravenously to a 50-kilogram woman. The dose level was 20 mg/kg. A scatter plot of the concentration data over time shows a decay. Three deterministic approaches were used to fit the data set. The first approach is what is referred to as the classical approach, in which the general solution is defined by Eq. (7). The second and third approaches are fractional differential method and kernel fractional differential method, respectively, which general solutions are given by Eq. (11), respectively, with $\psi(x) = x$, trivial kernel, and $\psi(x) \neq x$, pure kernel. The selected pure kernel here is linear $\psi(x) = x + 1$. It was observed empirically that using any linear kernel $\psi(x) = x + a$, with $a \neq 0$, would produce a similar result to the case where $\psi(x) = x + 1$ is used.

Table 1 summarises one hand best estimates of the parameters for both classical and fractional approaches. On the other hand, it displays the MSE of each method. It is observed that the fractional kernel method with $\psi(x) = x + 1$ performed the best, followed by the fractional method with $\psi(x) = x$ and lastly the classical method. It is worth highlighting consistency in the results. Indeed, the solution to the classical approach is a first order differential equation; therefore, one would expect the solution to its fractional counterparts to be such that $\xi \in (0, 1) \cup (1, 2)$.

Figure 2 is the graph of the original data set, the fitted line is obtained from the classical model, and the fitted line is obtained from the fractional method with $\psi(x) = x$. Both fitted lines overlap over each other at the beginning of the plot but show a difference toward the end. The fractional

TABLE 1: Results of the first experiment.

parameter	k	ξ	MSE
Method			
Classical method	0.53355		0.07299
Fractional with $\psi(x) = x$	0.51749	1.13327	0.05814
Fractional with $\psi(x) = x + 1$	0.49621	1.11080	0.04065

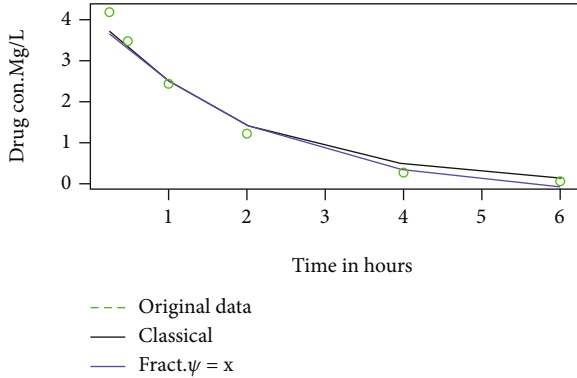


FIGURE 2: Original, classical, and fractional. $\psi(x) = x$.

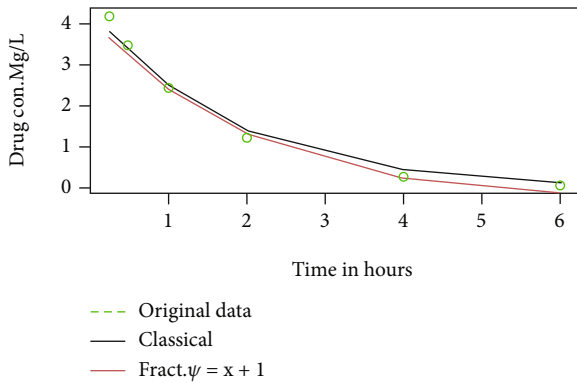


FIGURE 3: Original, classical, and fractional. $\psi(x) = x + 1$.

TABLE 2: Results of the second experiment.

parameter	k	ξ	MSE
Method			
Classical method	0.34785		0.048640
Fractional with $\psi(x) = x$	0.34714	1.00456	0.04116
Fractional with $\psi(x) = x + 1$	0.34590	1.00360	0.03482

method with $\psi(x) = x$ seems to be closer to the true data. MSE in Table 1 is an evidence.

Figure 3 is the graph of the original data set, the fitted line is obtained from the classical model, and the fitted line is obtained from the fractional method with $\psi(x) = x + 1$. Similar to Figure 2, a close look at the figure reveals that the fractional method with $\psi(x) = x + 1$ does the job better than the classical method. Moreover, recalling Figures 2

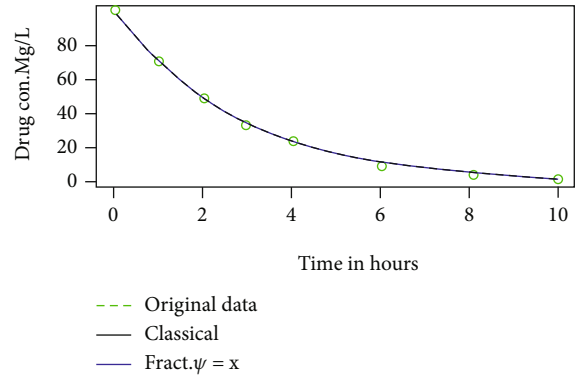


FIGURE 4: Original, classical, and fract. $\psi(x) = x$.

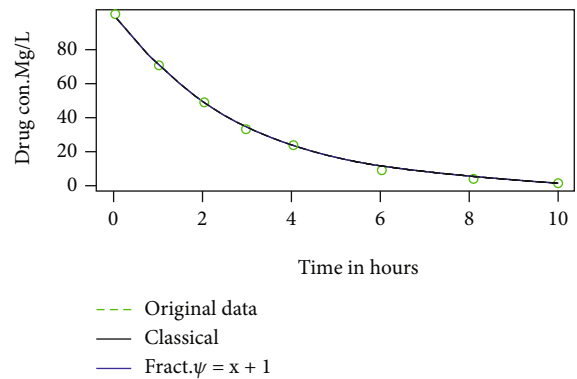


FIGURE 5: Original, classical, and fract. $\psi(x) = x + 1$.

and 3 as well as Table 1, the ordinal classification (first : fractional method with $\psi(x) = x + 1$; second : fractional method with $\psi(x) = x$; and third : classical method) of the three methods used in this work becomes explicit.

5.2. *Second Experimental Data Set.* In this experiment, a newly developed drug was administrated to a patient. The administration was done through an IV injection. A sample of blood was taken regularly, and the drug plasma concentration was determined. The data set was retrieved from [29].

Similar experimental procedures to those from the first example are used. The best values of parameters as well as MSE of each method are consigned in the table below.

Table 2 summarises and displays the results of the second experiment. It is observed that the fractional kernel method with $\psi(x) = x + 1$ performed the best, followed by the fractional method with $\psi(x) = x$ and lastly the classical method. Moreover, the fractional order of derivatives is always such that $\xi \in (0, 1) \cup (1, 2)$, proving that the results are in line with the first-order differential equation. Hence, the results are consistent.

Figure 4 displays the original data, the classical solution, and the fractional with the kernel $\psi(x) = x$. The results in Table 2 are reflected by the fact that the fractional approach fits the original data points better than the classical approach does.

Figure 5 is the graph of the original data set, the fitted line is obtained from the classical model, and the fitted line is obtained from the fractional method with $\psi(x) = x + 1$. A close check of the figure reveals that the fractional method with $\psi(x) = x + 1$ does the job better than the classical method.

6. Conclusion and Future Work

In this work, we studied the ψ -Caputo type of fractional differential equation. This derivative is the fractional analog of the so-called (fog)' derivative in classical calculus. The existence and uniqueness of the proposed method were discussed before the application examples. Experiment results show that the ψ -Caputo method which uses a pure kernel function performed the best, followed by a simple fractional approach and finally the classical method. The fractional order of derivative that allows to best fit the data is always such that $\xi \in (0, 1) \cup (1, 2)$, which is in line with the setup of the studied problem since the classical approach solution is a first-order differential equation. The experimental section has revealed the following results:

For the first data set, a psi-Caputo with the kernel $\psi = x + 1$ is the best approach as it yields a mean square error (MSE) of 0.04065. The second best is the simple fractional method whose MSE is 0.05814; finally, the classical approach is in the third position with an MSE of 0.07299.

For the second data set, a psi-Caputo with the kernel $\psi = x + 1$ is the best approach as it yields an MSE of 0.03482. The second best is the simple fractional method whose MSE is 0.04116 and, finally, the classical approach with an MSE of 0.048640.

In future works, we aim to investigate if the obtained results hold for all or most of existing fractional derivatives. We may also study properties that can help in the selection of a suitable kernel function. In the current study, the selection ψ function was done randomly, on a try and error basis, until we found out that a family of linear functions could well do the job.

Data Availability

The data set used in application section is available through the url provided in [27].

Conflicts of Interest

The authors declare that they have no competing interests.

Authors' Contributions

Each of the authors, M.A, Y.Y.Y, K.A, and N.G., contributed to each part of this work equally and read and approved the final version of the manuscript.

Acknowledgments

This article was funded by the Deanship of Scientific Research, King Faisal University (KFU), Ahsa, Saudi Arabia.

The authors, therefore, acknowledge technical and financial support under NASHER track with a grant number (NA00080) of DSR at KFU.

References

- [1] M. Rowland and T. N. Tozer, *Clinical Pharmacokinetics: Concepts and Applications*, Williams and Wilkins, Baltimore, 1995.
- [2] P. Jordan, H. Brunschwig, and E. Luedin, "Modeling attainment of steady state of drug concentration in plasma by means of a Bayesian approach using MCMC methods," *Pharmaceutical Statistics*, vol. 7, no. 1, pp. 36–41, 2008.
- [3] S. Varadharajan, S. Winiwarter, L. Carlsson et al., "Exploring _in silico_ prediction of the unbound brain-to-plasma drug concentration ratio: model validation, renewal, and interpretation," *Journal of Pharmaceutical Sciences*, vol. 104, no. 3, pp. 1197–1206, 2015.
- [4] D. Zhang, C. E. C. A. Hop, G. Patilea-Vrana et al., "Drug concentration asymmetry in tissues and plasma for small molecule-related therapeutic modalities," *Drug Metabolism and Disposition*, vol. 47, no. 10, pp. 1122–1135, 2019.
- [5] A. Peng, H. Xu, C. Luo, and H. Ding, "Application of a disposable doxorubicin sensor for direct determination of clinical drug concentration in patient blood," *International Journal of Electrochemical Science*, vol. 11, pp. 6266–6278, 2016.
- [6] B. Zilg, G. Thelander, B. Giebe, and H. Druid, "Postmortem blood sampling—comparison of drug concentrations at different sample sites," *Forensic Science International*, vol. 278, pp. 296–303, 2017.
- [7] M. Gibaldi, R. Nagashima, and G. Levy, "Relationship between drug concentration in plasma or serum and amount of drug in the body," *Journal of Pharmaceutical Sciences*, vol. 58, no. 2, pp. 193–197, 1969.
- [8] P. J. McNamara, G. Levy, and M. Gibaldi, "Effect of plasma protein and tissue binding on the time course of drug concentration in plasma," *Journal of Pharmacokinetics and Biopharmaceutics*, vol. 7, no. 2, pp. 195–206, 1979.
- [9] R. E. Bullingham, H. J. McQuay, E. J. Porter, M. C. Allen, and R. A. Moore, "Sublingual buprenorphine used postoperatively: ten hour plasma drug concentration analysis," *British Journal of Clinical Pharmacology*, vol. 13, no. 5, pp. 665–673, 1982.
- [10] T. Uchimura, M. Kato, T. Saito, and H. Kinoshita, "Prediction of human blood-to-plasma drug concentration ratio," *Biopharmaceutics & Drug Disposition*, vol. 31, no. 5-6, pp. 286–297, 2010.
- [11] S. Notari, C. Mancone, M. Sergi et al., "Determination of anti-tuberculosis drug concentration in human plasma by MALDI-TOF/TOF," *IUBMB Life*, vol. 62, no. 5, pp. 387–393, 2010.
- [12] T. K. H. Vu, D. T. Hung, V. I. Wheaton, and S. R. Coughlin, "Molecular cloning of a functional thrombin receptor reveals a novel proteolytic mechanism of receptor activation," *Cell*, vol. 64, no. 6, pp. 1057–1068, 1991.
- [13] D. Baleanu, Z. B. Güvenç, and J. T. Machado, *New Trends in Nanotechnology and Fractional Calculus Applications*, Springer, New York, 2010.
- [14] A. A. Kilbas, H. M. Srivastava, and J. J. Trujillo, *Theory and Applications of Fractional Differential Equations (Vol. 204)*, Elsevier, 2006.
- [15] A. Atangana and B. S. T. Alkahtani, "Analysis of the Keller-Segel model with a fractional derivative without singular kernel," *Entropy*, vol. 17, no. 12, pp. 4439–4453, 2015.

- [16] Z. J. Fu, W. Chen, and H. T. Yang, "Boundary particle method for Laplace transformed time fractional diffusion equations," *Journal of Computational Physics*, vol. 235, pp. 52–66, 2013.
- [17] R. I. T. U. Agarwal, S. O. N. A. L. Jain, and R. P. Agarwal, "Mathematical modeling and analysis of dynamics of cytosolic calcium ion in astrocytes using fractional calculus," *Journal of Fractional Calculus and Applications*, vol. 9, no. 2, pp. 1–12, 2018.
- [18] T. F. Wiesner, B. C. Berk, and R. M. Nerem, "A mathematical model of cytosolic calcium dynamics in human umbilical vein endothelial cells," *American Journal of Physiology-Cell Physiology*, vol. 270, no. 5, pp. C1556–C1569, 1996.
- [19] L. Lenoci, M. Duvernay, S. Satchell, E. DiBenedetto, and H. E. Hamm, "Mathematical model of PARI-mediated activation of human platelets," *Molecular BioSystems*, vol. 7, no. 4, pp. 1129–1137, 2011.
- [20] R. L. Bagley and P. J. Torvik, "A theoretical basis for the application of fractional calculus to viscoelasticity," *Journal of Rheology*, vol. 27, no. 3, pp. 201–210, 1983.
- [21] V. D. Djordjević, J. Jarić, B. Fabry, J. J. Fredberg, and D. Stamenović, "Fractional derivatives embody essential features of cell rheological behavior," *Annals of Biomedical Engineering*, vol. 31, no. 6, pp. 692–699, 2003.
- [22] D. Kumar, J. Singh, and D. Baleanu, "Numerical computation of a fractional model of differential-difference equation," *Journal of Computational and Nonlinear Dynamics*, vol. 11, no. 6, 2016.
- [23] R. Almeida, "A Caputo fractional derivative of a function with respect to another function," *Communications in Nonlinear Science and Numerical Simulation*, vol. 44, pp. 460–481, 2017.
- [24] M. Awadalla, Y. Y. Yameni Noupoue, and K. Abuasbeh, "Psi-Caputo logistic population growth model," *Journal of Mathematics*, vol. 2021, Article ID 8634280, 9 pages, 2021.
- [25] M. Awadalla, Y. Y. Yameni Noupoue, K. Abuasbeh, and G. Noureddine, "A fractional model approach for drug concentration in blood," Retrieved September 06, 2022, from https://assets.researchsquare.com/files/rs-1412567/v1_covered.pdf?c=1647012038.
- [26] S. D. Undevia, G. Gomez-Abuin, and M. J. Ratain, "Pharmacokinetic variability of anticancer agents," *Nature Reviews Cancer*, vol. 5, no. 6, pp. 447–458, 2005.
- [27] L.-E. Peyret, "Characteristics of anti-cancer drug adme - overview," OncologyPRO. (2015, July 16). Retrieved November 24, 2021, from <https://oncologypro.esmo.org/oncology-in-practice/anti-cancer-agents-and-biological-therapy/drug-drug-interactions-with-kinase-inhibitors/general-introduction/characteristics-of-anti-cancer-drug-adme-overview>.
- [28] A. Tarek, "Ahmed pharmacokinetics of drugs following IV bolus, IV infusion, and oral administration," <https://www.intechopen.com/chapters/49459>.
- [29] Chapter 2, "Chapter 2 - Page 8. (n.d.)," Retrieved May 21, 2022, from <https://www.boomer.org/c/p4/c02/c0208.php>.

Research Article

Impact of Multiplicative Noise on the Exact Solutions of the Fractional-Stochastic Boussinesq-Burger System

Wael W. Mohammed ^{1,2}, Farah M. Al-Askar,³ and M. El-Morshedy ^{4,5}

¹Department of Mathematics, Faculty of Science, University of Ha'il, Ha'il 2440, Saudi Arabia

²Department of Mathematics, Faculty of Science, Mansoura University, Mansoura 35516, Egypt

³Department of Mathematical Science, Collage of Science, Princess Nourah Bint Abdulrahman University, P.O. Box 84428, Riyadh 11671, Saudi Arabia

⁴Department of Mathematics, College of Science and Humanities in Al-Kharj, Prince Sattam Bin Abdulaziz University, Al-Kharj 11942, Saudi Arabia

⁵Department of Statistics and Computer Science, Faculty of Science, Mansoura University, Mansoura 35516, Egypt

Correspondence should be addressed to Wael W. Mohammed; wael.mohammed@mans.edu.eg

Received 24 May 2022; Revised 26 August 2022; Accepted 7 September 2022; Published 22 September 2022

Academic Editor: Arzu Akbulut

Copyright © 2022 Wael W. Mohammed et al. This is an open access article distributed under the Creative Commons Attribution License, which permits unrestricted use, distribution, and reproduction in any medium, provided the original work is properly cited.

In this paper, we consider the fractional-stochastic Boussinesq-Burger system (FSBBS) generated by the multiplicative Brownian motion. The Jacobi elliptic function techniques are used to create creative elliptic, hyperbolic, and rational fractional-stochastic solutions for FSBBS. Furthermore, we draw 2D and 3D graphs by using the MATLAB Package for some obtained solutions of FSBBS to discuss the influence of the Brownian motion on these solutions. Finally, we indicate that the Brownian motion stabilizes the solutions of FSBBS around zero.

1. Introduction

Nonlinear partial differential equations (NLPDEs) have grown in popularity in the area of nonlinear science, owing to their large variety of uses in economics [1], engineering [2], civil engineering [3], soil mechanics [4], physics [5], quantum mechanics [6], statistical mechanics [7], solid-state physics [8], population ecology [9], etc. Solitons are among the most common in the setting of NLPDE solutions, and they are essential for understanding nonlinear physical phenomena. Solitons are utilized to understand the properties of nonlinear media in various areas including quantum electronics, plasma physics, nonlinear optics, and fluid dynamics [10–13]. Recently, the searching of exact soliton solutions to NLPDEs has become an enthralling research topic in engineering and applied sciences. Many techniques have been used to determine exact solutions for NLPDE including tanh-sech [14, 15], Darboux transformation [16], sine-cosine [17, 18], $\exp(-\phi(\zeta))$ -expansion [19], (G'/G) -expansion

[20–22], Lie symmetry analysis method [23], improved F-expansion method [24, 25], Hirota's function [26], the Jacobi elliptic function [27, 28], and perturbation [29, 30].

The fractional differential equation is extensively used in fluid mechanics, solid state physics, optical fibers, neural physics, quantum field theory, mathematical biology, plasma physics, and other areas [31–34]. Researchers recommend fractional-order derivative over ordinary order derivative because integer-order derivative is essentially a local operator, but fractional-order derivative is so much more. Also, they explain physical phenomena such as quantum mechanics, diffusion, gravity, heat, elasticity, fluid dynamics, electrodynamics, electrostatics, and sound. Recently, the exact solutions with conformable derivative have been obtained in many papers for instance [35–40].

On the other hand, a wide variety of complex nonlinear physical phenomena can be represented using stochastic partial differential equations (SPDEs). These kind of equations can be found in many fields, such as physics and finance.

On the other side, stochastic partial differential equations (SPDEs) can be used to represent a wide range of complicated nonlinear physical processes. These kind of equations appear in a variety of areas including engineering, geophysical, biology, climate dynamics, finance, and physics [41–43].

To realize a higher level of qualitative accord, we take the following fractional-stochastic Boussinesq-Burger system (FSBBS) perturbed in the itô sense by multiplicative noise:

$$d\Phi + \left[2\Phi \mathbb{D}_x^\alpha \Phi - \frac{1}{2} \mathbb{D}_x^{3\alpha} \Phi \right] dt = \sigma \Phi d\mathbb{B}, \quad (1)$$

$$d\Psi + \left[2\mathbb{D}_x^\alpha (\Phi \Psi) - \frac{1}{2} \mathbb{D}_x^{3\alpha} \Phi \right] dt = \sigma \Psi d\mathbb{B}, \quad (2)$$

where $\Phi(x, t)$ denotes the horizontal velocity field. \mathbb{D}^α is the conformable derivative (CD) [44]. $\Psi(x, t)$ is the height of the water surface above the bottom horizontal level. $\mathbb{B}(t)$ is a Brownian motion (BM) and σ is the noise strength.

The Boussinesq-Burgers system (BBS), with $\alpha = 1$ and $\sigma = 0$, appears in fluid flow research and explains how shallow water waves spread. Due to the importance of BBS, many researchers have created its exact solutions by using various methods such as Hirota method [45], Lie symmetry method [46], sine-Gordon expansion method [47], Jacobi elliptic function method [48], extended homogeneous balance [49], Darboux transformation [50], The modified $\exp(-\phi(\zeta))$ -expansion function method [51], and Exp-function method [52]. On the other side, many techniques have been documented for fractional BBS, including a domain decomposition method [53] and generalized Kudryashov method [54]. The exact solutions of the FSBBS (1-2) have not yet been studied.

Our novelty of this paper is to find the exact fractional stochastic solutions of FSBBS (1-2). In the presence of a stochastic term and the fractional space, this study is the first to obtain analytical solutions to the FSBBS (1-2). Numerous solutions, including those involving elliptic, trigonometric, rational, and hyperbolic functions, can be obtained using the Jacobi elliptic function technique. Moreover, we utilize MATLAB to build 2D and 3D figures for some of the obtained solutions in this study to display how the BM influences on the solutions of FSBBS (1-2).

The layout of the document is as follows: in Sec. 2, we define and give some properties of the CD and BM. In Sec. 3, we use an effective wave transformation to establish the FSBBS (1-2) wave equation. In Sec.4, we use the Jacobi elliptic function method to generate the analytic of FSBBS (1-2). While, in Sec.5, the effect of the BM on the solutions obtained is studied. In Sec. 6, the document's conclusion is shown.

2. Preliminaries

In this section, we define and clarify some characteristics of the BM and CD. In the following, we define BM $\mathbb{B}(t)$ as:

Definition 1 (see [55]). Stochastic process $\{\mathbb{B}(t)\}_{t \geq 0}$ is said a BM if the following conditions satisfy: $B(t)$ is continuous function of $t \geq 0$; $B(0) = 0$; for $\tau_1 < \tau_2$, $B(\tau_2) - B(\tau_1)$ is independent; and $B(\tau_2) - B(\tau_1)$ has a Gaussian distribution $\mathcal{N}(0, \tau_2 - \tau_1)$.

Lemma 2 (see [55]). $\mathbb{E}(e^{\sigma \mathbb{B}(t)}) = e^{((1/2)\sigma^2 t)}$ for $\sigma \geq 0$.

Definition 3 (see [44]). Let $\phi : (0, \infty) \rightarrow \mathbb{R}$, then the CD of ϕ of order $\alpha \in (0, 1]$ is defined as

$$\mathbb{D}_x^\alpha \phi(x) = \lim_{\kappa \rightarrow 0} \frac{\phi(x + \kappa x^{1-\alpha}) - \phi(x)}{\kappa}. \quad (3)$$

Let us go through some of the CD's features. If a, b are constant, then

- (1) $\mathbb{D}_x^\alpha [a] = 0$,
- (2) $\mathbb{D}_x^\alpha [x^b] = b x^{b-\alpha}$,
- (3) $\mathbb{D}_x^\alpha [a\Theta_1(x) + b\Theta_2(x)] = a\mathbb{D}_x^\alpha \Theta_1(x) + b\mathbb{D}_x^\alpha \Theta_2(x)$,
- (4) $\mathbb{D}_x^\alpha \Theta(x) = x^{1-\alpha} (d\Theta/dx)$,
- (5) $\mathbb{D}_x^\alpha (\Theta_1 \circ \Theta_2)(x) = x^{1-\alpha} \Theta_2'(x) \Theta_1'(\Theta_2(x))$.

3. Wave Equation of FSBBS

The next wave transformation is used

$$\begin{aligned} \Phi(x, t) &= \varphi(\xi) e^{(\sigma \mathbb{B}(t) - ((1/2)\sigma^2 t))}, \Psi(x, t) \\ &= \psi(\xi) e^{(\sigma \mathbb{B}(t) - ((1/2)\sigma^2 t))}, \xi = \frac{1}{\alpha} x^\alpha + \omega t, \end{aligned} \quad (4)$$

in order to attain the wave equation of FSBBS (1-2). Where ω is a constant, φ and ψ are deterministic functions. Plugging Equation (4) into Equations (1) and (2) and utilizing

$$\begin{aligned} d\Phi &= \left[\omega \varphi' dt + \sigma \varphi d\mathbb{B} \right] e^{(\sigma \mathbb{B}(t) - ((1/2)\sigma^2 t))}, \\ d\Psi &= \left[\omega \psi' dt + \sigma \psi d\mathbb{B} \right] e^{(\sigma \mathbb{B}(t) - ((1/2)\sigma^2 t))}, \\ \mathbb{D}_x^\alpha \Phi &= \varphi' e^{(\sigma \mathbb{B}(t) - ((1/2)\sigma^2 t))}, \mathbb{D}_x^\alpha \Psi = \psi' e^{(\sigma \mathbb{B}(t) - ((1/2)\sigma^2 t))}, \\ \mathbb{D}_x^{3\alpha} \Phi &= \varphi''' e^{(\sigma \mathbb{B}(t) - ((1/2)\sigma^2 t))}, \mathbb{D}_x^{3\alpha} \Psi = \psi''' e^{(\sigma \mathbb{B}(t) - ((1/2)\sigma^2 t))}, \end{aligned} \quad (5)$$

we get

$$\omega \varphi' + 2\omega \varphi' e^{(\sigma \mathbb{B}(t) - ((1/2)\sigma^2 t))} - \frac{1}{2} \psi' = 0, \quad (6)$$

$$\omega \psi' + 2(\varphi \psi)' e^{(\sigma \mathbb{B}(t) - ((1/2)\sigma^2 t))} - \frac{1}{2} \varphi''' = 0. \quad (7)$$

Taking expectation $\mathbb{E}(\cdot)$ for Equations (6) and (7), we

attain

$$\omega\varphi' + 2\varphi\varphi' e^{-((1/2)\sigma^2 t)} \mathbb{E}\left(e^{\sigma\mathbb{B}(t)}\right) - \frac{1}{2}\psi' = 0, \quad (8)$$

$$\omega\psi' + 2(\varphi\psi)' e^{-((1/2)\sigma^2 t)} \mathbb{E}\left(e^{\sigma\mathbb{B}(t)}\right) - \frac{1}{2}\varphi''' = 0. \quad (9)$$

Since $\mathbb{B}(t)$ is a Gaussian distribution, then $\mathbb{E}(e^{\sigma\mathbb{B}(t)}) = e^{((\sigma^2/2)t)}$. Now Equations (8) and (9) become

$$\omega\varphi' + 2\varphi\varphi' - \frac{1}{2}\psi' = 0, \quad (10)$$

$$\omega\psi' + (\varphi\psi)' - \frac{1}{2}\varphi''' = 0. \quad (11)$$

Integrating Equations (10) and (11) and putting the constants of integration equal zero, we have

$$\psi = 2\omega\varphi + 2\varphi^2, \quad (12)$$

$$\omega\psi + 2(\varphi\psi) - \frac{1}{2}\varphi'' = 0. \quad (13)$$

Plugging Equation (12) into (13), we attain

$$\varphi'' - 8\varphi^3 - 12\omega\varphi^2 - 4\omega^2\varphi = 0. \quad (14)$$

4. Exact Solutions of FSBBS

We use the Jacobi elliptic functions approach described by Peng [56] to find the solutions of Equation (14). Consequently, we can therefore derive the exact solutions of FSBBS (1-2).

4.1. *Jacobi Elliptic Functions Method.* First, we suppose the solutions of Equation (14) are

$$\varphi(\xi) = \sum_{i=1}^N a_i \chi^i, \quad (15)$$

where χ is the solution of

$$\chi' = \sqrt{\frac{1}{2}p\chi^4 + q\chi^2 + r}, \quad (16)$$

where r, q and p are real parameters.

We note from the next Table 1 that Equation (16) has different types of solutions relying on r, q and p :

Where $dn(\xi, m) = dn(\xi, m)$, $cn(\xi) = cn(\xi, m)$, $sn(\xi) = sn(\xi, m)$, for $0 < m < 1$ are the Jacobi elliptic functions (JEFs). If $m \rightarrow 1$, then JEFs are converted into the hyperbolic functions as follows:

$$\begin{aligned} dn(\xi) &\longrightarrow \operatorname{sech}(\xi)sn(\xi) \longrightarrow \tanh(\xi), \quad cn(\xi) \longrightarrow \operatorname{sech}(\xi), \\ cs(\xi) &\longrightarrow \operatorname{csch}(\xi), \quad ds \longrightarrow \operatorname{csch}(\xi). \end{aligned} \quad (17)$$

TABLE 1: All possible solutions for Equation (16).

Case	p	q	r	$\chi(\xi)$
1	$2m^2$	$-(1+m^2)$	1	$sn(\xi)$
2	2	$2m^2-1$	$-m^2(1-m^2)$	$ds(\xi)$
3	2	$2-m^2$	$(1-m^2)$	$cs(\xi)$
4	$-2m^2$	$2m^2-1$	$(1-m^2)$	$cn(\xi)$
5	-2	$2-m^2$	(m^2-1)	$dn(\xi)$
6	$\frac{m^2}{2}$	$\frac{(m^2-2)}{2}$	$\frac{1}{4}$	$\frac{sn(\xi)}{1 \pm dn(\xi)}$
7	$\frac{m^2}{2}$	$\frac{(m^2-2)}{2}$	$\frac{m^2}{4}$	$\frac{sn(\xi)}{1 \pm dn(\xi)}$
8	$\frac{-1}{2}$	$\frac{(m^2+1)}{2}$	$\frac{-(1-m^2)^2}{4}$	$m cn(\xi) \pm dn(\xi)$
9	$\frac{m^2-1}{2}$	$\frac{(m^2+1)}{2}$	$\frac{(m^2-1)}{4}$	$\frac{dn(\xi)}{1 \pm sn(\xi)}$
10	$\frac{1-m^2}{2}$	$\frac{(1-m^2)}{2}$	$\frac{(1-m^2)}{4}$	$\frac{cn(\xi)}{1 \pm sn(\xi)}$
11	$\frac{(1-m^2)^2}{2}$	$\frac{(1-m^2)^2}{2}$	$\frac{1}{4}$	$\frac{sn(\xi)}{dn \pm cn(\xi)}$
12	2	0	0	$\frac{c}{\xi}$
13	0	1	0	ce^{ξ}

4.2. *Solutions of FSBBS.* By balancing φ'' with φ^3 in Equation (14), we can calculate the parameter N as

$$N + 2 = 3N \Rightarrow N = 1. \quad (18)$$

Hence, Equation (15) with $N = 1$ becomes

$$\varphi = a_0 + a_1\chi. \quad (19)$$

Differentiating Equation (19) twice, we have, by using (16),

$$\varphi'' = a_1q\chi + a_1p\chi^3. \quad (20)$$

Substituting Equation (19) and Equation (20) into Equation (14) we obtain

$$\begin{aligned} (a_1p - 8a_1^3)\chi^3 - (24a_0a_1^2 + 12\omega a_1^2)\chi^2 \\ + (a_1q - 24a_0^2a_1 - 24\omega a_0a_1 - 4\omega^2a_1)\chi \\ - (8a_0^3 + 12\omega a_0^2 + 4\omega^2a_0) = 0. \end{aligned} \quad (21)$$

Equating each coefficient of χ^k , for $k = 0, 1, 2, 3$, to zero,

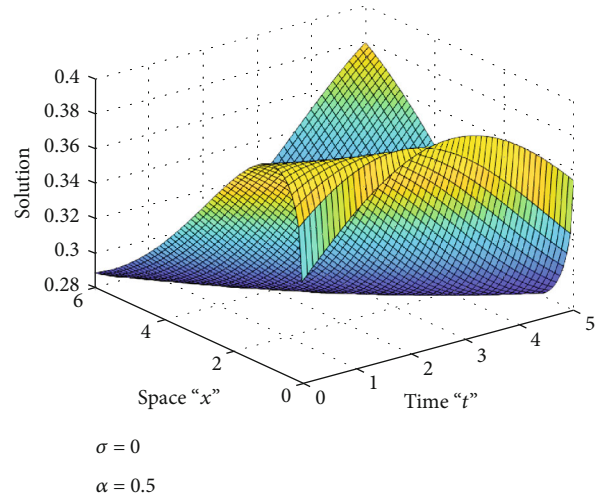
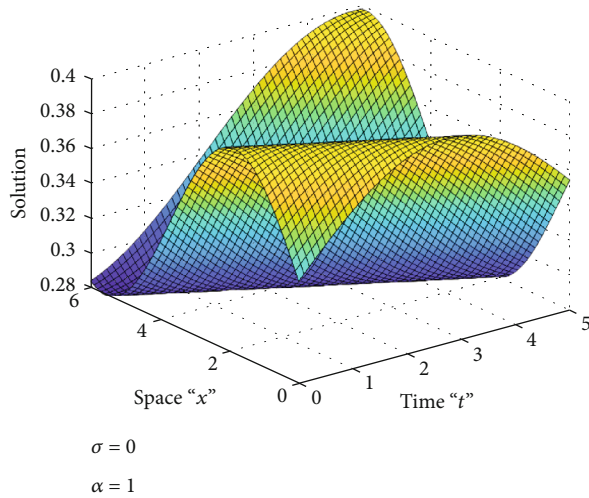


FIGURE 1: 3D-graph of Equation (33) with $\sigma = 0$ and various values of $\alpha = 1, 0.5$.

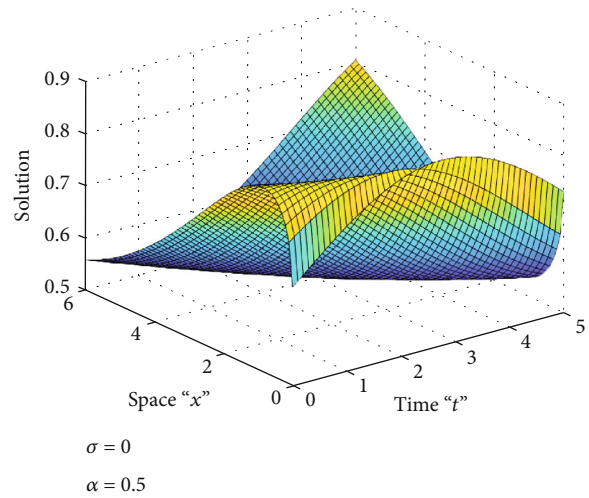
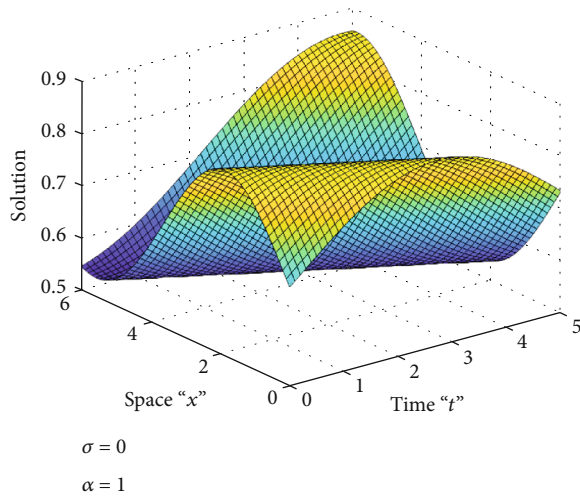


FIGURE 2: 3D-graph of Equation (34) with $\sigma = 0$ and various values of $\alpha = 1, 0.5$.

we have

$$\begin{aligned} a_1 p - 8a_1^3 &= 0, \\ 24a_0 a_1^2 + 12\omega a_1^2 &= 0, \\ a_1 q - 24a_0^2 a_1 - 24\omega a_0 a_1 - 4\omega^2 a_1 &= 0, \end{aligned} \tag{22}$$

and

$$8a_0^3 + 12\omega a_0^2 + 4\omega^2 a_0 = 0. \tag{23}$$

We get by solving these equations:

$$a_0 = \frac{1}{2} \sqrt{-\frac{1}{2}q}, a_1 = \pm \sqrt{\frac{p}{8}}, \omega = \pm \sqrt{-\frac{1}{2}q}, \tag{24}$$

for $p > 0$ and $q \leq 0$. Then, the Equation (14) has the

solutions:

$$\varphi(\xi) = \sqrt{-\frac{1}{8}q} \pm \sqrt{\frac{p}{8}\chi(\xi)}. \tag{25}$$

Therefore, by utilizing (4) and (12), the solution of the FSBBS (2-1) are

$$\begin{aligned} \Phi(x, t) &= \left[\sqrt{-\frac{1}{8}q} + \sqrt{\frac{p}{8}\chi(\xi)} \right] e^{(\sigma \mathbb{B}(t) - ((1/2)\sigma^2 t))}, \\ \Psi(x, t) &= \left[-\frac{3q}{4} + \sqrt{-pq}\chi(\xi) + \frac{p}{4}\chi^2 \right] e^{(\sigma \mathbb{B}(t) - ((1/2)\sigma^2 t))}. \end{aligned} \tag{26}$$

There are numerous cases, by using the previous Table 1, for $q \leq 0, p > 0$ and r as follows:

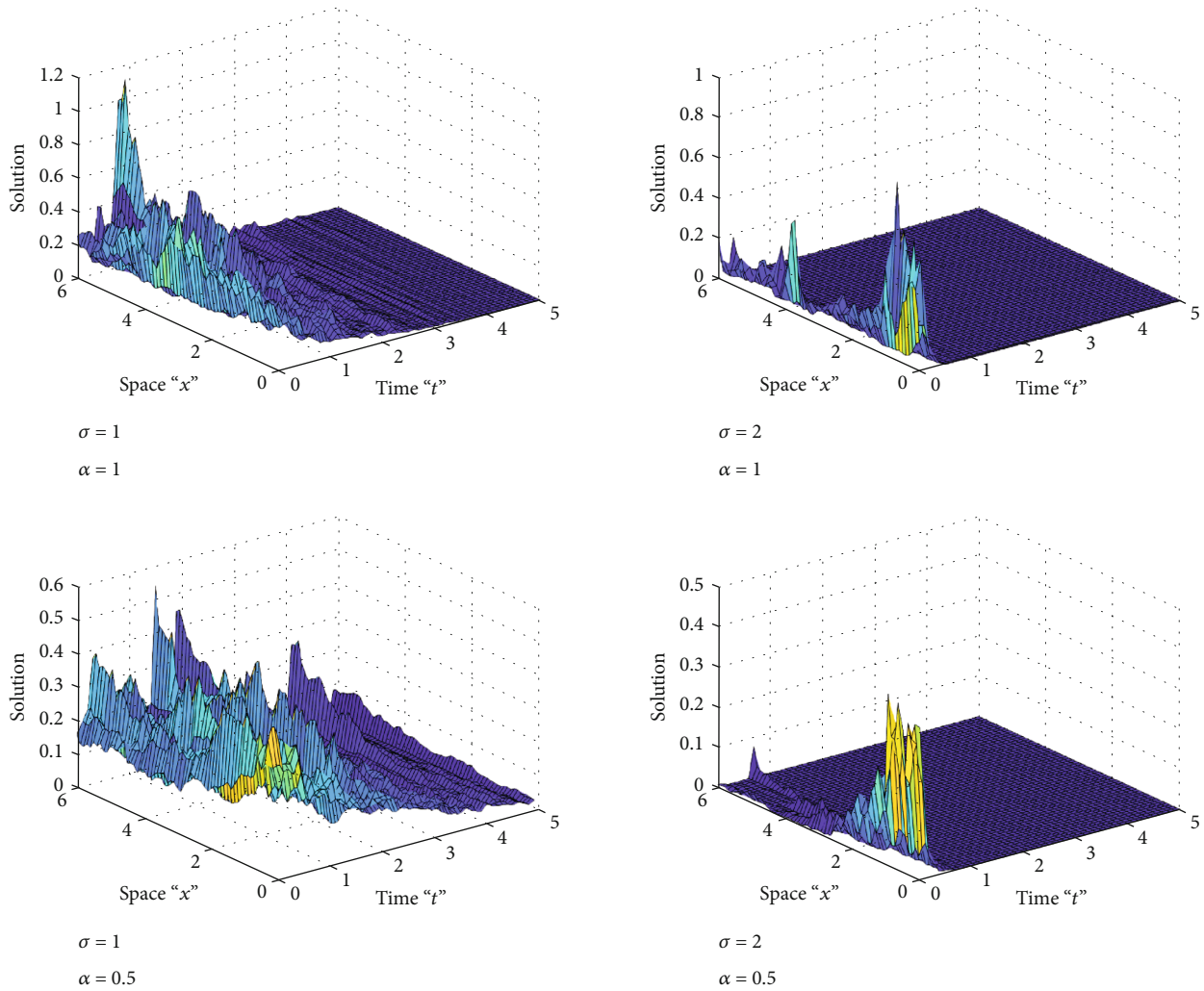


FIGURE 3: 3D-graph of Equation (33) with $\sigma = 1, 2$ and $\alpha = 1, 0.5$.

Case 1. If $q = -(1 + m^2), p = 2m^2$ and $r = 1$, then $\chi(\xi) = sn(\xi)$.
Therefore, the FSBBS (1-2) has the solution

$$\Phi(x, t) = \left[\sqrt{-\frac{1}{8}q} + \sqrt{\frac{p}{8}} sn \left(\frac{1}{\alpha} x^\alpha + \sqrt{\frac{-q}{2}} t \right) \right] e^{(\sigma B(t) - ((1/2)\sigma^2 t))}, \tag{27}$$

$$\Psi(x, t) = \left[-\frac{3q}{4} + \sqrt{-pq} sn \left(\frac{x^\alpha}{\alpha} + \sqrt{\frac{-q}{2}} t \right) + \frac{p}{4} sn^2 \left(\frac{x^\alpha}{\alpha} + \sqrt{\frac{-q}{2}} t \right) \right] e^{(\sigma B(t) - ((1/2)\sigma^2 t))}. \tag{28}$$

If $m \rightarrow 1$, then Equations (27) and (28) degenerates to

$$\Phi(x, t) = \left[\sqrt{-\frac{1}{8}q} + \sqrt{\frac{p}{8}} \tanh \left(\frac{1}{\alpha} x^\alpha + \sqrt{\frac{-q}{2}} t \right) \right] e^{(\sigma B(t) - ((1/2)\sigma^2 t))},$$

$$\Psi(x, t) = \left[-\frac{3q}{4} + \sqrt{-pq} \tanh \left(\frac{1}{\alpha} x^\alpha + \sqrt{\frac{-q}{2}} t \right) + \frac{p}{4} \tanh^2 \left(\frac{1}{\alpha} x^\alpha + \sqrt{\frac{-q}{2}} t \right) \right] e^{(\sigma B(t) - ((1/2)\sigma^2 t))}. \tag{29}$$

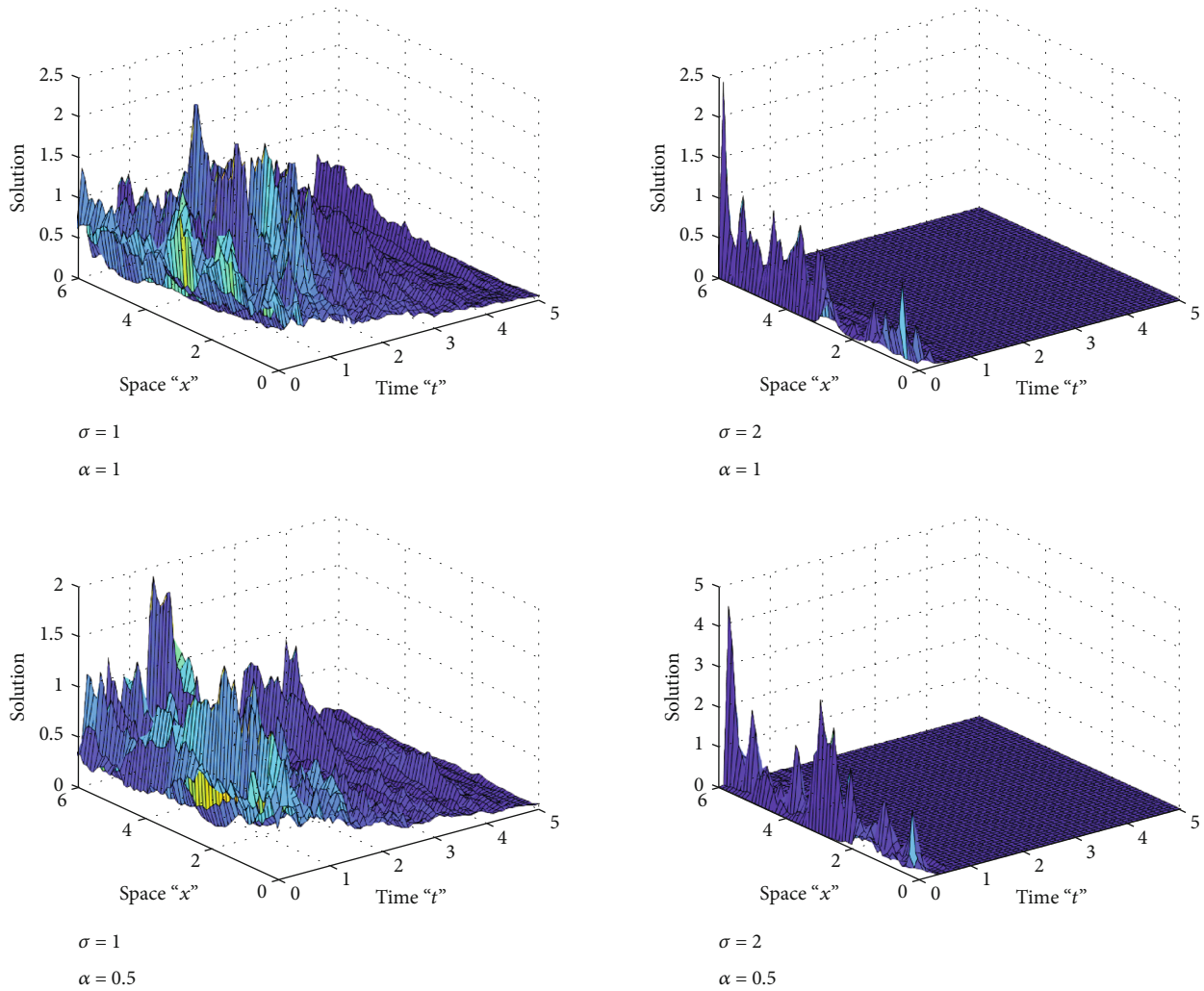


FIGURE 4: 3D-graph of Equation (34) with $\sigma = 1, 2$ and $\alpha = 1, 0.5$.

Case 2. If $q = 2m^2 - 1$ for $m \leq (1/\sqrt{2})$, $p = 2$ and $r = -m^2(1 - m^2)$, then $\chi(\xi) = ds(\xi)$. So, the FSBBS (1-2) has the solution:

$$\Phi(x, t) = \left[\sqrt{-\frac{1}{8}q} + \sqrt{\frac{p}{8}} ds \left(\frac{1}{\alpha} x^\alpha + \sqrt{\frac{-q}{2}} t \right) \right] e^{(\sigma B(t) - ((1/2)\sigma^2 t))}, \tag{30}$$

$$\Psi(x, t) = \left[-\frac{3q}{4} + \sqrt{-pq} ds \left(\frac{x^\alpha}{\alpha} + \sqrt{\frac{-q}{2}} t \right) + \frac{p}{4} ds^2 \cdot \left(\frac{x^\alpha}{\alpha} + \sqrt{\frac{-q}{2}} t \right) \right] e^{(\sigma B(t) - ((1/2)\sigma^2 t))}. \tag{31}$$

If $m \rightarrow 1$, then Equations (30) and (31) degenerates to

$$\Phi(x, t) = \left[\sqrt{-\frac{1}{8}q} + \sqrt{\frac{p}{8}} \operatorname{csch} \left(\frac{x^\alpha}{\alpha} + \sqrt{\frac{-q}{2}} t \right) \right] e^{(\sigma B(t) - ((1/2)\sigma^2 t))},$$

$$\Psi(x, t) = \left[-\frac{3q}{4} + \sqrt{-pq} \operatorname{csch} \left(\frac{x^\alpha}{\alpha} + \sqrt{\frac{-q}{2}} t \right) + \frac{p}{4} \operatorname{csch}^2 \left(\frac{x^\alpha}{\alpha} + \sqrt{\frac{-q}{2}} t \right) \right] e^{(\sigma B(t) - ((1/2)\sigma^2 t))}. \tag{32}$$

Case 3. If $q = ((m^2 - 2)/2), p = (m^2/2)$ and $r = (1/4)$ (or $r = (m^2/4)$), then $\chi(\xi) = ((sn(\xi))/(1 \pm dn(\xi)))$. Therefore, the FSBBS (1-2) has the solution:

$$\Phi(x, t) = \left[\sqrt{-\frac{1}{8}q} + \sqrt{\frac{p}{8}} \frac{\left(\operatorname{sn} \left(\left(\frac{1}{\alpha} \right) x^\alpha + \sqrt{-q/2} t \right) \right)}{\left(1 \pm \operatorname{dn} \left(\left(\frac{1}{\alpha} \right) x^\alpha + \sqrt{-q/2} t \right) \right)} \right] e^{(\sigma \mathbb{B}(t) - ((1/2)\sigma^2 t))}, \tag{33}$$

$$\Psi(x, t) = \left[-\frac{3q}{4} + \sqrt{-pq} \frac{\left(\operatorname{sn} \left(\left(\frac{1}{\alpha} \right) x^\alpha + \sqrt{-q/2} t \right) \right)}{\left(1 \pm \operatorname{dn} \left(\left(\frac{1}{\alpha} \right) x^\alpha + \sqrt{-q/2} t \right) \right)} + \frac{p}{4} \frac{\left(\operatorname{sn}^2 \left(\left(\frac{1}{\alpha} \right) x^\alpha + \sqrt{-q/2} t \right) \right)}{\left(1 \pm \operatorname{dn} \left(\left(\frac{1}{\alpha} \right) x^\alpha + \sqrt{-q/2} t \right) \right)^2} \right] e^{(\sigma \mathbb{B}(t) - ((1/2)\sigma^2 t))}. \tag{34}$$

If $m \rightarrow 1$, then Equations (33) and (34) degenerates to

$$\Phi(x, t) = \left[\sqrt{-\frac{1}{8}q} + \sqrt{\frac{p}{8}} \frac{\left(\tanh \left(\left(\frac{1}{\alpha} \right) x^\alpha + \sqrt{-q/2} t \right) \right)}{\left(1 \pm \operatorname{sech} \left(\left(\frac{1}{\alpha} \right) x^\alpha + \sqrt{-q/2} t \right) \right)} \right] e^{(\sigma \mathbb{B}(t) - ((1/2)\sigma^2 t))}, \tag{35}$$

$$\Psi(x, t) = \left[-\frac{3q}{4} + \sqrt{-pq} \frac{\left(\tanh \left(\left(\frac{1}{\alpha} \right) x^\alpha + \sqrt{-q/2} t \right) \right)}{\left(1 \pm \operatorname{sech} \left(\left(\frac{1}{\alpha} \right) x^\alpha + \sqrt{-q/2} t \right) \right)} + \frac{p}{4} \frac{\left(\tanh^2 \left(\left(\frac{1}{\alpha} \right) x^\alpha + \sqrt{-q/2} t \right) \right)}{\left(1 \pm \operatorname{sech} \left(\left(\frac{1}{\alpha} \right) x^\alpha + \sqrt{-q/2} t \right) \right)^2} \right] e^{(\sigma \mathbb{B}(t) - ((1/2)\sigma^2 t))}. \tag{36}$$

Case 4. If $q = 0, p = 2$ and $r = 0$, then $\chi(\xi) = (C/\xi)$. Hence, the FSBBS (1-2) has the solution:

$$\begin{aligned} \Phi(x, t) &= \left[\frac{\alpha C}{2} x^{-\alpha} \right] e^{(\sigma \mathbb{B}(t) - ((1/2)\sigma^2 t))}, \\ \Psi(x, t) &= \left[\frac{\alpha C}{2} x^{-2\alpha} \right] e^{(\sigma \mathbb{B}(t) - ((1/2)\sigma^2 t))}. \end{aligned} \tag{37}$$

Remark 4. If we set $\sigma = 0$ and $\alpha = 1$ in Equations (27) and (36), then we get the same results as reported in [48].

5. The Influence of Fractional Derivative and Noise

Here, the influence of noise on the achieved solutions of FSBBS (1-2) is explained. For various values of α (the fractional derivative order) and σ (noise strength), some graphs are provided using the MATLAB tools.

Firstly the Fractional Derivative Influence. In Figures 1 and 2, if $\sigma = 0$ and $m = 0.4$, we can observe that the surface shrinks when α is decreasing:

Secondly the Noise Influence. In Figures 3 and 4, when noise is introduced, the surface flattens significantly if its strength is increased $\sigma = 1, 2$

In Figure 5, we introduce 2D-graph of the $\Phi(x, t)$ in (33) with $\alpha = 1$ and with $\sigma = 0, 0.5, 1, 2$, which highlights the previous outcomes:

We may deduct from Figures 1–5 that:

- (1) When the fractional-order α increases, the surface expands,
- (2) The multiplicative noise stabilizes the solutions of FSBBS at zero.

This results show that it is important to add the stochastic term into the Boussinesq-Burger equation in order to obtain accurate solutions.

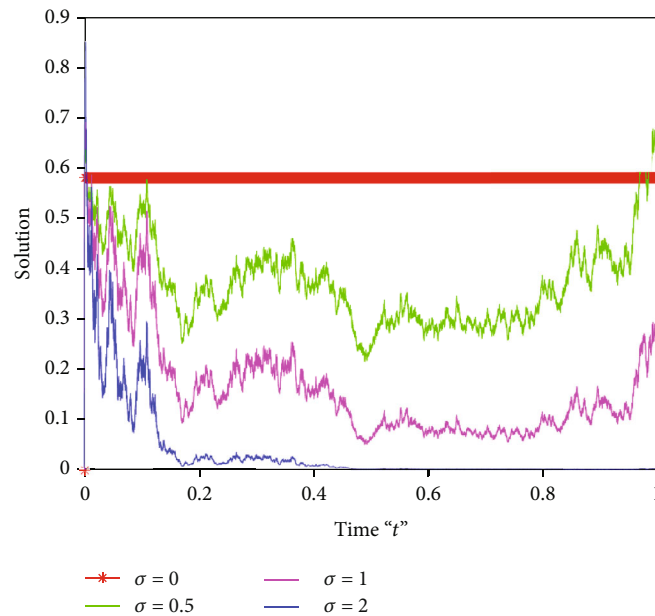


FIGURE 5: 2D graph of Equation (33)

6. Conclusions

In this article, the exact fractional-stochastic solutions of the fractional-stochastic Boussinesq-Burger system (1-2) driven by multiplicative noise were successfully obtained by using the Jacobi elliptic function method. Numerous analytical solutions for FSBBS (1-2) including elliptic, trigonometric, rational, and hyperbolic functions can be determined using the Jacobi elliptic function method. Because of the importance of FSBBS in fluid flow research and in explaining the propagation of shallow water waves, the acquired solutions are far more beneficial and efficient in understanding several critical complicated physical phenomena. In addition, we utilized the MATLAB package to demonstrate how multiplicative noise and fractional derivative influenced the solutions of FSBBS. As a result, we concluded that the stabilization of the solutions of the FSBBS (1-2) is affected by the multiplicative noise.

Data Availability

All data are available in this paper

Conflicts of Interest

The authors declare that they have no competing interests.

Authors' Contributions

All authors contributed equally to the writing of this paper. All authors read and approved the final manuscript.

Acknowledgments

This work was supported by the Princess Nourah Bint Abdulrahman University Researchers Supporting Project

(No. PNURSP2022R273) of Princess Nourah Bint Abdulrahman University, Riyadh, Saudi Arabia.

References

- [1] E. Scalas, R. Gorenflo, and F. Mainardi, "Fractional calculus and continuous-time finance," *Physica A*, vol. 284, no. 1-4, pp. 376-384, 2000.
- [2] J. Sabatier, O. P. Agrawal, and J. A. T. Machado, *Advances in Fractional Calculus*, Springer, Dordrecht, 2007.
- [3] L. Baudouin, A. Rondepierre, and S. Neild, "Robust control of a cable from a hyperbolic partial differential equation model," *IEEE Transactions on Control Systems Technology*, vol. 27, no. 3, pp. 1343-1351, 2019.
- [4] L. Shao, X. Guo, S. Liu, and G. Zheng, *Effective Stress and Equilibrium Equation for Soil Mechanics*, CRC Press, Boca Raton, FL, USA, 2017.
- [5] F. M. Al-Askar, W. W. Mohammed, and M. Alshammari, "Impact of Brownian motion on the analytical solutions of the space-fractional stochastic approximate long water wave equation," *Symmetry*, vol. 14, no. 4, p. 740, 2022.
- [6] N. Laskin, "Nonlocal quantum mechanics: fractional calculus approach," in *Volume 5 Applications in Physics, Part B*, pp. 207-236, Walter de Gruyter, 2019.
- [7] E. Barkai, R. Metzler, and J. Klafter, "From continuous time random walks to the fractional Fokker-Planck equation," *Physical Review E*, vol. 61, no. 1, pp. 132-138, 2000.
- [8] Z. He, Z. Han, J. Yuan et al., "Quantum plasmonic control of trions in a picocavity with monolayer WS₂," *Science Advances*, vol. 5, no. 10, article eaau8763, 2019.
- [9] Y. Lin and J. Gao, "Research on diffusion effect of ecological population model based on delay differential equation," *Caribbean Journal of Science*, vol. 52, pp. 333-335, 2019.
- [10] A. Biswas and D. Milovic, "Bright and dark solitons of the generalized nonlinear Schrödinger's equation," *Communications in Nonlinear Science and Numerical Simulation*, vol. 15, no. 6, pp. 1473-1484, 2010.

- [11] A. M. Wazwaz, "Bright and dark optical solitons for (2+1)-dimensional Schrodinger (NLS) equations in the anomalous dispersion regimes and the normal dispersive regimes," *Optik*, vol. 192, article 162948, 2019.
- [12] H. Rezazadeh, A. Korkmaz, A. E. Achab, W. Adel, and A. Bekir, "New travelling wave solution-based new Riccati equation for solving KdV and modified KdV equations," *Applied Mathematics and Nonlinear Sciences*, vol. 6, no. 1, pp. 447–458, 2021.
- [13] H. U. Rehman, M. Bibi, M. S. Saleem, H. Rezazadeh, and W. Adel, "New optical soliton solutions of the Chen Lee Liu equation," *International Journal of Modern Physics B*, vol. 35, no. 18, p. 2150184, 2021.
- [14] A. M. Wazwaz, "The tanh method: exact solutions of the sine-Gordon and the sinh-Gordon equations," *Applied Mathematics and Computation*, vol. 167, no. 2, pp. 1196–1210, 2005.
- [15] W. Malfliet and W. Hereman, "The tanh method. I. Exact solutions of nonlinear evolution and wave equations," *Physica Scripta*, vol. 54, no. 6, pp. 563–568, 1996.
- [16] M. Wen-Xiu and B. Sumayah, "A binary darbox transformation for multicomponent NLS equations and their reductions," *Analysis and Mathematical Physics*, vol. 11, no. 2, p. 44, 2021.
- [17] A. M. Wazwaz, "A sine-cosine method for handling nonlinear wave equations," *Mathematical and Computer Modelling*, vol. 40, no. 5-6, pp. 499–508, 2004.
- [18] C. Yan, "A simple transformation for nonlinear waves," *Physics Letters A*, vol. 224, no. 1-2, pp. 77–84, 1996.
- [19] K. Khan and M. A. Akbar, "The $\exp(-\Phi(\zeta))$ -expansion method for finding travelling wave solutions of Vakhnenko-Parkes equation," *International Journal of Dynamical Systems and Differential Equations*, vol. 5, no. 1, pp. 72–83, 2014.
- [20] M. L. Wang, X. Z. Li, and J. L. Zhang, "The (G'G)-expansion method and travelling wave solutions of nonlinear evolution equations in mathematical physics," *Physics Letters A*, vol. 372, no. 4, pp. 417–423, 2008.
- [21] H. Zhang, "New application of the G'G-expansion method," *Communications in Nonlinear Science and Numerical Simulation*, vol. 14, no. 8, pp. 3220–3225, 2009.
- [22] W. W. Mohammed, M. Alesemi, S. Albosaily, N. Iqbal, and M. El-Morshedy, "The exact solutions of stochastic fractional-space Kuramoto-Sivashinsky equation by using (G'G)-Expansion Method," *Mathematics*, vol. 9, no. 21, p. 2712, 2021.
- [23] M. S. Hashemi, A. Haji-Badali, and P. Vafadar, "Group invariant solutions and conservation laws of the Fornberg-Whitham equation," *Zeitschrift für Naturforschung A*, vol. 69, no. 8-9, pp. 489–496, 2014.
- [24] A. Akbulut, M. S. Hashemi, and H. Rezazadeh, "New conservation laws and exact solutions of coupled burgers' equation," *Waves in Random and Complex Media*, pp. 1–20, 2021.
- [25] A. Akbulut and S. M. R. Islam, "Study on the Biswas-Arshed equation with the Beta time derivative," *International Journal of Applied and Computational Mathematics*, vol. 8, no. 4, p. 167, 2022.
- [26] R. Hirota, "Exact solution of the Korteweg-de Vries equation for multiple collisions of solitons," *Physical Review Letters*, vol. 27, no. 18, pp. 1192–1194, 1971.
- [27] Z. L. Yan, "Abundant families of Jacobi elliptic function solutions of the (2+1)-dimensional integrable Davey-Stewartson-type equation via a new method," *Chaos, Solitons and Fractals*, vol. 18, no. 2, pp. 299–309, 2003.
- [28] F. M. Al-Askar and W. W. Mohammed, "The analytical solutions of the stochastic fractional RKL equation via Jacobi elliptic function method," *Advances in Mathematical Physics*, vol. 2022, Article ID 1534067, 8 pages, 2022.
- [29] W. W. Mohammed, "Stochastic amplitude equation for the stochastic generalized Swift-Hohenberg equation," *Journal of the Egyptian Mathematical Society*, vol. 23, no. 3, pp. 482–489, 2015.
- [30] W. W. Mohammed, "Amplitude equation with quintic nonlinearities for the generalized Swift-Hohenberg equation with additive degenerate noise," *Advances in Difference Equations*, vol. 2016, no. 1, Article ID 84, 2016.
- [31] S. B. Yuste, L. Acedo, and K. Lindenberg, "Reaction front in an $A+B \rightarrow C$ reaction-subdiffusion process," *Physical Review E*, vol. 69, no. 3, article 036126, 2004.
- [32] W. W. Mohammed, O. Bazighifan, M. M. Al-Sawalha, A. O. Almatroud, and E. S. Aly, "The influence of noise on the exact solutions of the stochastic fractional-space chiral nonlinear Schrödinger equation," *Fractal and Fractional*, vol. 5, no. 4, p. 262, 2021.
- [33] D. A. Benson, S. W. Wheatcraft, and M. M. Meerschaert, "The fractional-order governing equation of Lévy motion," *Water Resources Research*, vol. 36, no. 6, pp. 1413–1423, 2000.
- [34] N. Iqbal, R. Wu, and W. W. Mohammed, "Pattern formation induced by fractional cross-diffusion in a 3-species food chain model with harvesting," *Mathematics and Computers in Simulation*, vol. 188, pp. 102–119, 2021.
- [35] H. Tajadodi, Z. A. Khan, A. R. Irshad, J. F. Gómez-Aguilare, A. Khan, and H. Khan, "Exact solutions of conformable fractional differential equations," *Results in Physics*, vol. 22, article 103916, 2021.
- [36] H. Bulut, T. A. Sulaiman, and H. M. Baskonus, "Dark, bright optical and other solitons with conformable space-time fractional second-order spatiotemporal dispersion," *Optik*, vol. 163, pp. 1–7, 2018.
- [37] H. Rezazadeh, H. Tariq, M. Mirzazadeh, and Q. Zhou, "New exact solutions of nonlinear conformable time-fractional Phi-4 equation," *Chinese Journal of Physics*, vol. 56, no. 6, pp. 2805–2816, 2018.
- [38] S. W. Yao, T. Rasool, R. Hussain, H. Rezazadeh, and M. Inc, "Exact soliton solutions of conformable fractional coupled Burger's equation using hyperbolic function approach," *Results in Physics*, vol. 30, article 104776, 2021.
- [39] M. A. Shallal, K. K. Ali, K. R. Raslan, H. Rezazadeh, and A. Bekir, "Exact solutions of the conformable fractional EW and MEW equations by a new generalized expansion method," *Journal of Ocean Engineering and Science*, vol. 5, no. 3, pp. 223–229, 2020.
- [40] A. Zafar, M. Raheel, A. Bekir, and W. Razaq, "The conformable space-time fractional Fokas-Lenells equation and its optical soliton solutions based on three analytical schemes," *International Journal of Modern Physics B*, vol. 35, no. 1, p. 2150004, 2021.
- [41] L. Arnold, *Random Dynamical Systems*, Springer-Verlag, 1998.
- [42] P. Imkeller and A. H. Monahan, "Conceptual stochastic climate models," *Stochastics and Dynamics*, vol. 2, no. 3, pp. 311–326, 2002.
- [43] W. W. Mohammed and D. Blömker, "Fast-diffusion limit with large noise for systems of stochastic reaction-diffusion equations," *Stochastic Analysis and Applications*, vol. 34, no. 6, pp. 961–978, 2016.

- [44] R. Khalil, M. Al Horani, A. Yousef, and M. Sababheh, "A new definition of fractional derivative," *Journal of Computational and Applied Mathematics*, vol. 264, pp. 65–70, 2014.
- [45] P. Wang, B. Tian, W. Liu, X. Lü, and Y. Jiang, "Lax pair, Bäcklund transformation and multi-soliton solutions for the Boussinesq–Burgers equations from shallow water waves," *Applied Mathematics and Computation*, vol. 218, no. 5, pp. 1726–1734, 2011.
- [46] I. E. Mhlanga and C. M. Khalique, "Exact solutions of generalized Boussinesq-Burgers equations and (2+1)-dimensional Davey-Stewartson equations," *Journal of Applied Mathematics*, vol. 2012, Article ID 389017, 8 pages, 2012.
- [47] K. K. Ali, R. Yilmazer, and H. Bulut, "Analytical Solutions to the Coupled Boussinesq–Burgers Equations via Sine-Gordon Expansion Method," in *4th International Conference on Computational Mathematics and Engineering Sciences (CMES-2019)*, pp. 233–240, Springer, 2020.
- [48] A. A. Rady and M. Khalfallah, "On soliton solutions for Boussinesq-Burgers equations," *Communications in Nonlinear Science and Numerical Simulation*, vol. 15, no. 4, pp. 886–894, 2010.
- [49] K. Mohammed, "Exact traveling wave solutions of the Boussinesq-Burgers equation," *Mathematical and Computer Modelling*, vol. 49, no. 3-4, pp. 666–671, 2009.
- [50] X. Li and A. Chen, "Darboux transformation and multi-soliton solutions of Boussinesq-Burgers equation," *Physics Letters A*, vol. 342, no. 5-6, pp. 413–420, 2005.
- [51] T. A. Sulaiman, H. Bulut, A. Yokus, and H. M. Baskonus, "On the exact and numerical solutions to the coupled Boussinesq equation arising in ocean engineering," *Indian Journal of Physics*, vol. 93, no. 5, pp. 647–656, 2019.
- [52] L. K. Ravi, S. S. Ray, and S. Sahoo, "New exact solutions of coupled Boussinesq–Burgers equations by Exp-function method," *Journal of Ocean Engineering and Science*, vol. 2, no. 1, pp. 34–46, 2017.
- [53] L. Meenatchi and M. Kaliyappan, "Solving time-fractional nonlinear coupled Boussinesq-Burgers equations arise in propagation of shallow water waves using adomian decomposition method," *AIP Conference Proceedings*, vol. 2095, article 030015, 2019.
- [54] M. M. A. Khater and D. Kumar, "New exact solutions for the time fractional coupled Boussinesq–Burger equation and approximate long water wave equation in shallow water," *Journal of Ocean Engineering and Science*, vol. 2, no. 3, pp. 223–228, 2017.
- [55] O. Calin, *An informal introduction to stochastic calculus with applications*, World Scientific Publishing Co. Pte. Ltd, 2015.
- [56] Y. Z. Peng, "Exact solutions for some nonlinear partial differential equations," *Physics Letters A*, vol. 314, no. 5-6, pp. 401–408, 2003.

Research Article

Solution of Space-Time Fractional Differential Equations Using Aboodh Transform Iterative Method

Michael A. Awuya ¹, Gbenga O. Ojo ², and Nazim I. Mahmudov ¹

¹Department of Mathematics, Faculty of Arts and Sciences, Eastern Mediterranean University, Famagusta, T.R. North Cyprus via Mersin 10, Turkey

²Department of Information System Engineering, Faculty of Engineering Cyprus West University, Famagusta, T.R. North Cyprus via Mersin 10, Turkey

Correspondence should be addressed to Nazim I. Mahmudov; nazim.mahmudov@emu.edu.tr

Received 8 June 2022; Accepted 18 July 2022; Published 22 September 2022

Academic Editor: Arzu Akbulut

Copyright © 2022 Michael A. Awuya et al. This is an open access article distributed under the Creative Commons Attribution License, which permits unrestricted use, distribution, and reproduction in any medium, provided the original work is properly cited.

A relatively new and efficient approach based on a new iterative method and the Aboodh transform called the Aboodh transform iterative method is proposed to solve space-time fractional differential equations, the fractional order is considered in the Caputo sense. This method is a combination of the Aboodh transform and the new iterative method and gives the solution in series form with easily computable components. The nonlinear term is easily handled by the new iterative method, to affirm the simplicity and performance of the proposed method, five examples were considered, and the solution plots were presented to show the effect of the fractional order. The outcome reveals that the approach is accurate and easy to implement.

1. Introduction

Fractional Calculus can be described as the field of mathematics that consists of ordinary and partial derivatives of positive noninteger order. It is the generalization of classical integral and differential equations [1, 2]. One major attractive property of fractional calculus is the nonlocal property.

Recently, various problems in Biology and Physics has been modeled with fractional order derivative, an analytical solution of the Fornberg–Whithan equation was presented in [3], fractional model of the Rosenau–Hyman equation which is a KdV-like equation was considered in [4], for application of fractional derivative to Biology population model see [5], the numerical study of HIV-1 infection of CD4+ T-cell was presented in [6], Caputo–Fabrizio fractional model of photocatalytic degradation of dyes was studied in [7], a wavelet based numerical scheme for fractional order SEIR epidemic of measles by using Genocchi polynomials was presented in [8], and the investigation of fractional order susceptible-infected-recovered epidemic

model of childhood disease was presented in [9]. Therefore, it is extremely important to find an effective method of solving fractional differential equations, as only the solutions can give a better comprehension of the underlying problems. Many researchers have presented different methods for solving fractional differential equations such as reproducing kernel discretization method [10], Chebyshev wavelet collocation method, [11] Tichonov regularization method [12], Chebyshev collocation method, [13] q-homotopy analysis Shehu transform method [14], Fractional differential transform, [15] Fractional variational iterational method [16], and iterative Laplace transform method [17].

In 2016, the new iterative method was presented by Daftardar–Gejji and Jafari to solve functional equations [18], but now the iterative method has been used to solve many integral and fractional order differential equations. [5, 19, 20] But most of these methods considered a single term time-fractional order differential equations.

In this paper, the main objective is to extend the Aboodh transform iterative method to solve space-time fractional differential equations with more than a single term fractional

derivative. The fractional derivative is considered in Caputo sense both for time and space, when $\alpha = \beta = 1$, the space-time fractional differential equations becomes the classical differential equations. The rest of this paper is arranged as follows: in Section 2, we gave some definitions and a preliminary concept of Aboodh transform. In Section 3, we described briefly the Aboodh transform iterative method for space-time fractional derivative while in Section 4, a few examples were considered to describe the efficiency of the method. Finally, we concluded in Section 5.

2. Definitions and Preliminaries

In this section, we give some definitions and notions about Aboodh transform.

Definition 1. Caputo time-fractional derivative of order $\alpha > 0$ for the function $Q(x, t)$ is defined as follows [1, 2]:

$$D_t^\alpha Q(x, t) = \frac{1}{\Gamma(n - \alpha)} \int_0^t (t - \tau)^{n - \alpha - 1} Q^{(n)}(x, \tau) d\tau, \quad (1)$$

$$n - 1 < \alpha \leq n.$$

Similarly, the Caputo space fractional derivative of order $\beta > 0$ for the function $Q(x, t)$ is defined as follows:

$$D_x^\beta Q(x, t) = \frac{1}{\Gamma(n - \beta)} \int_0^x (x - t)^{n - \beta - 1} Q^{(n)}(x, t) dt, \quad (2)$$

$$n - 1 < \beta \leq n.$$

Remark 1. $D_t^\alpha Q(x, t) = D_x^\beta Q(x, t) = 0$, whenever $Q(x, t)$ is a constant.

Remark 2. $D_t^\alpha t^b = \{ (\Gamma(b + 1)/\Gamma(b - \alpha + 1)) t^{b - \alpha}$, if $n - 1 < \alpha \leq n, b > \alpha - 1, 0, n - 1 < \alpha \leq n, b \leq \alpha - 1$.

Definition 2. One parameter Mittag-Leffler function is given as follows [5]:

$$E_\alpha(z) = \sum_{k=0}^{\infty} \frac{z^k}{\Gamma(1 + k\alpha)}, \quad \alpha, z \in C \text{Re}(\alpha) \geq 0. \quad (3)$$

Definition 3. The Aboodh transform of $Q(t)$ is defined as follows [5]:

$$\mathcal{A}[Q(t)] = \frac{1}{v} \int_0^{\infty} Q(t) e^{-vt} dt = A(v), \quad t \geq 0. \quad (4)$$

The inverse Aboodh transform of function $Q(t)$ if $\mathcal{A}[Q(t)] = A(v)$ is defined as follows:

$$Q(t) = \mathcal{A}^{-1}[A(v)]. \quad (5)$$

Remark 3. The Aboodh transform of the function $Q(t)$ satisfy the linearity property [5].

Definition 4. The Aboodh transform for Caputo time-fractional derivative of order β is given as follows [5]:

$$\mathcal{A}[D_t^\beta Q(x, t); v] = v^\beta \mathcal{A}[Q(x, t)] - \sum_{k=0}^{m-1} \frac{Q^{(k)}(x, 0)}{v^{2-\beta+k}}, \quad (6)$$

$$m - 1 < \beta \leq m.$$

3. Basic Idea of the Proposed Method

Consider the space-time fractional partial differential equation of the form.

$$D_t^\alpha Q(x, t) = \Phi(Q(x, t), D_x^\beta Q(x, t), D_x^{2\beta} Q(x, t), D_x^{3\beta} Q(x, t)), \quad (7)$$

$$0 < \alpha, \beta \leq 1,$$

with the initial conditions

$$Q^{(k)}(x, 0) = h_k, \quad k = 0, 1, \dots, m - 1, \quad (8)$$

$Q(x, t)$ is the unknown function to be determine and $\Phi(Q(x, t), D_x^\beta Q(x, t), D_x^{2\beta} Q(x, t), D_x^{3\beta} Q(x, t))$ can be linear or nonlinear operator of $Q(x, t), D_x^\beta Q(x, t), D_x^{2\beta} Q(x, t)$, and $D_x^{3\beta} Q(x, t)$ For convenience we represent $Q(x, t)$ with Q , so by applying the Aboodh transform to both sides of equation (7) we have the following equation:

$$\mathcal{A}[Q(x, t)] = \frac{1}{v^\alpha} \left(\sum_{k=0}^{m-1} \frac{Q^{(k)}(x, 0)}{v^{2-\alpha+k}} + \mathcal{A}[\Phi(Q, D_x^\beta Q, D_x^{2\beta} Q, D_x^{3\beta} Q)] \right), \quad (9)$$

taking the inverse Aboodh transform, we get the following equation:

$$Q(x, t) = \mathcal{A}^{-1} \left[\frac{1}{v^\alpha} \left(\sum_{k=0}^{m-1} \frac{Q^{(k)}(x, 0)}{v^{2-\alpha+k}} + \mathcal{A}[\Phi(Q, D_x^\beta Q, D_x^{2\beta} Q, D_x^{3\beta} Q)] \right) \right]. \quad (10)$$

The Aboodh transform iterative method gives the solution in form of an infinite series.

$$Q(x, t) = \sum_{i=0}^{\infty} Q_i. \quad (11)$$

Since $\Phi(Q, D_x^\beta Q, D_x^{2\beta} Q, D_x^{3\beta} Q)$ is either a linear or nonlinear operator which can be decomposed as follows:

$$\begin{aligned} \Phi(Q, D_x^\beta Q, D_x^{2\beta} Q, D_x^{3\beta} Q) &= \Phi(Q_0, D_x^\beta Q_0, D_x^{2\beta} Q_0, D_x^{3\beta} Q_0) \\ &+ \sum_{i=0}^{\infty} \left\{ \Phi \left(\sum_{k=0}^i (Q_k, D_x^\beta Q_k, D_x^{2\beta} Q_k, D_x^{3\beta} Q_k) \right) - \Phi \left(\sum_{k=1}^{i-1} (Q_k, D_x^\beta Q_k, D_x^{2\beta} Q_k, D_x^{3\beta} Q_k) \right) \right\}. \end{aligned} \tag{12}$$

Substituting equations (12) and (11) into equation (10) we obtain the following equation:

$$\begin{aligned} \sum_{i=0}^{\infty} Q_i(x, t) &= \mathcal{A}^{-1} \left[\frac{1}{v^\alpha} \left(\sum_{k=0}^{m-1} \frac{Q^{(k)}(x, 0)}{v^{2-\alpha+k}} + \mathcal{A} [\Phi(Q_0, D_x^\beta Q_0, D_x^{2\beta} Q_0, D_x^{3\beta} Q_0)] \right) \right] \\ &+ \mathcal{A}^{-1} \left[\frac{1}{v^\alpha} \left(\mathcal{A} \left[\sum_{i=0}^{\infty} \left\{ \Phi \left(\sum_{k=0}^i (Q_k, D_x^\beta Q_k, D_x^{2\beta} Q_k, D_x^{3\beta} Q_k) \right) \right\} \right] \right) \right] \\ &- \mathcal{A}^{-1} \left[\frac{1}{v^\alpha} \left(\mathcal{A} \left[\left\{ \Phi \left(\sum_{k=1}^{i-1} (Q_k, D_x^\beta Q_k, D_x^{2\beta} Q_k, D_x^{3\beta} Q_k) \right) \right\} \right] \right) \right]. \end{aligned} \tag{13}$$

Now, recursively, we compute the terms.

$$\begin{aligned} Q_0(x, t) &= \mathcal{A}^{-1} \left[\frac{1}{v^\alpha} \sum_{k=0}^{m-1} \frac{Q^{(k)}(x, 0)}{v^{2-\alpha+k}} \right], \\ Q_1(x, t) &= \mathcal{A}^{-1} \left[\frac{1}{v^\alpha} \left(\mathcal{A} [\Phi(Q_0, D_x^\beta Q_0, D_x^{2\beta} Q_0, D_x^{3\beta} Q_0)] \right) \right], \\ &\vdots \\ Q_{m+1}(x, t) &= \mathcal{A}^{-1} \left[\frac{1}{v^\alpha} \left(\mathcal{A} \left[\sum_{i=0}^{\infty} \left\{ \Phi \left(\sum_{k=0}^i (Q_k, D_x^\beta Q_k, D_x^{2\beta} Q_k, D_x^{3\beta} Q_k) \right) \right\} \right] \right) \right] \\ &- \mathcal{A}^{-1} \left[\frac{1}{v^\alpha} \left(\mathcal{A} \left[\sum_{i=0}^{\infty} \left\{ \Phi \left(\sum_{k=1}^{i-1} (Q_k, D_x^\beta Q_k, D_x^{2\beta} Q_k, D_x^{3\beta} Q_k) \right) \right\} \right] \right) \right], \quad m = 1, 2, \dots \end{aligned} \tag{14}$$

The series converges rapidly, for convergence see [18, 21]. So the m-term analytically approximate solution of equation (7) is given by the following equation:

$$Q(x, t) \approx \sum_{i=0}^{m-1} Q_i. \tag{15}$$

4. Application

Here, the Aboodh transform iterative method is applied to solve five distinct space-time fractional differential equations with suitable initial conditions.

Example 1. Consider the fractional Airy's-like equation with an additional term [22].

$$D_t^\alpha Q(x, t) = D_x^\beta Q + Q, \quad 0 < \alpha, \beta \leq 1. \tag{16}$$

With the initial condition,

$$Q(x, 0) = x^3. \tag{17}$$

Applying the Aboodh transform on both sides of equation (16), we obtain the following equation:

$$\mathcal{A}[Q(x, t)] = \frac{1}{v^\alpha} \left(\sum_{k=0}^{m-1} \frac{Q^{(k)}(x, 0)}{v^{2-\alpha+k}} + \mathcal{A}[D_x^\beta Q + Q] \right), \tag{18}$$

taking the inverse Aboodh transform on equation (18), we have the following equation:

$$Q(x, t) = \mathcal{A}^{-1} \left[\frac{1}{v^\alpha} \left(\sum_{k=0}^{m-1} \frac{Q^{(k)}(x, 0)}{v^{2-\alpha+k}} + \mathcal{A}[D_x^\beta Q + Q] \right) \right]. \tag{19}$$

Using the Aboodh transform iterative procedure, we obtain the following equation:

$$\begin{aligned}
 Q_0(x, t) &= \mathcal{A}^{-1} \left[\frac{1}{v^\alpha} \left(\sum_{k=0}^{m-1} \frac{Q^{(k)}(x, 0)}{v^{2-\alpha+k}} \right) \right] \\
 &= \mathcal{A}^{-1} \left[\frac{Q(x, 0)}{v^2} \right] \\
 &= x^3, \\
 Q_1(x, t) &= \mathcal{A}^{-1} \left[\frac{1}{v^\alpha} (\mathcal{A} [D_x^\beta Q_0 + Q_0]) \right] \\
 &= \mathcal{A}^{-1} \left[\frac{\Gamma(4)x^{3-\beta}}{v^{2+\alpha}\Gamma(4-\beta)} + \frac{x^3}{v^{2+\alpha}} \right] \\
 &= \frac{\Gamma(4)x^{3-\beta}t^\alpha}{\Gamma(\alpha+1)\Gamma(4-\beta)} + \frac{x^3t^\alpha}{\Gamma(\alpha+1)}, \\
 Q_2(x, t) &= \mathcal{A}^{-1} \left[\frac{1}{v^\alpha} (\mathcal{A} [D_x^\beta (Q_0 + Q_1) + (Q_0 + Q_1)]) \right] - \mathcal{A}^{-1} \left[\frac{1}{v^\alpha} (\mathcal{A} [D_x^\beta Q_0 + Q_0]) \right] \\
 &= \mathcal{A}^{-1} \left[\frac{\Gamma(4)x^{3-\beta}}{v^{2+\alpha}\Gamma(4-\beta)} + \frac{\Gamma(4)x^{3-2\beta}}{v^{2+2\alpha}\Gamma(4-2\beta)} + \frac{2\Gamma(4)x^{3-\beta}}{v^{2+2\alpha}\Gamma(4-\beta)} + \frac{x^3}{v^{2+\alpha}} + \frac{x^3}{v^{2+2\alpha}} \right] - \mathcal{A}^{-1} \left[\frac{\Gamma(4)x^{3-\beta}}{v^{2+\alpha}\Gamma(4-\beta)} + \frac{x^3}{v^{2+\alpha}} \right] \\
 &= \frac{\Gamma(4)x^{3-2\beta}t^{2\alpha}}{\Gamma(2\alpha+1)\Gamma(4-2\beta)} + \frac{2\Gamma(4)x^{3-\beta}t^{2\alpha}}{\Gamma(4-\beta)\Gamma(2\alpha+1)} + \frac{x^3t^{2\alpha}}{\Gamma(2\alpha+1)}, \\
 &\vdots
 \end{aligned}
 \tag{20}$$

and so on. The series solution is given by the following equation:

$$Q(x, t) = Q_0 + Q_1 + Q_2 + \dots \tag{21}$$

Figure 1 represent the solution plots of equation (16) when $\alpha = \beta = .02, .04, .06, .08, 2, .4, .6, .8$ at $x = 1$ and $t = 1$, respectively. While the remaining are the surface plots.

Example 2. Consider the nonlinear space-time fractional Fokker-Planck equation [23].

$$D_t^\alpha Q(x, t) = D_x^\beta \left(\frac{xQ}{3} \right) - \left(\frac{4}{x} Q^2 \right)_x + (Q^2)_{xx}, \quad 0 < \alpha, \beta \leq 1. \tag{22}$$

With the initial condition,

$$Q(x, 0) = x^2. \tag{23}$$

Applying the Aboodh transform on equation (22), we obtain the following equation:

$$\mathcal{A}[Q(x, t)] = \frac{1}{v^\alpha} \left(\sum_{k=0}^{m-1} \frac{Q^{(k)}(x, 0)}{v^{2-\alpha+k}} + \mathcal{A} \left[D_x^\beta \left(\frac{x}{3} Q \right) - \left(\frac{4}{x} Q^2 \right)_x + (Q^2)_{xx} \right] \right), \tag{24}$$

taking the inverse Aboodh transform, we have the following equation:

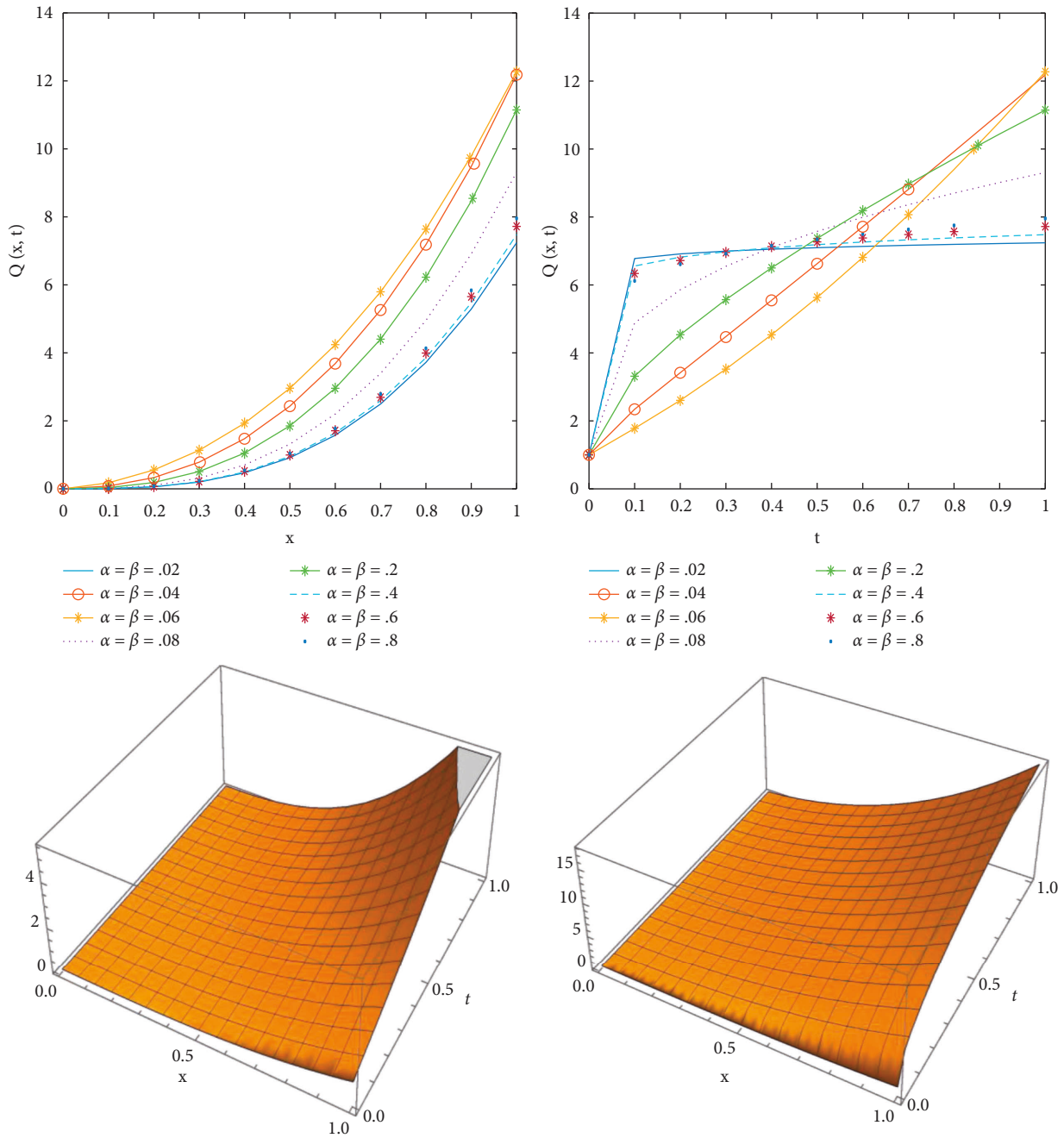


FIGURE 1: Comparison of the solution at various values of alpha and beta.

$$Q(x, t) = \mathcal{A}^{-1} \left[\frac{1}{v^\alpha} \left(\sum_{k=0}^{m-1} \frac{Q^{(k)}(x, 0)}{v^{2-\alpha+k}} + \mathcal{A} \left[D_x^\beta \left(\frac{x}{3} Q \right) - \left(\frac{4}{x} Q^2 \right)_x + (Q^2)_{xx} \right] \right) \right]. \tag{25}$$

Using the Aboodh transform iterative method procedure, we obtain the following equation:

$$\begin{aligned}
 Q_0(x, t) &= \mathcal{A}^{-1} \left[\frac{1}{v^\alpha} \left(\sum_{k=0}^{m-1} \frac{Q^{(k)}(x, 0)}{v^{2-\alpha+k}} \right) \right] \\
 &= \mathcal{A}^{-1} \left[\frac{Q(x, 0)}{v^2} \right] \\
 &= x^2, \\
 Q_1(x, t) &= \mathcal{A}^{-1} \left[\frac{1}{v^\alpha} \left(\mathcal{A} \left[D_x^\beta \left(\frac{x}{3} Q_0 \right) - \left(\frac{4}{x} Q_0^2 \right)_x + (Q_0^2)_{xx} \right] \right) \right] \\
 &= \mathcal{A}^{-1} \left[\frac{2x^{3-\beta}}{\Gamma(4-\beta)v^{2+\alpha}} \right] \\
 &= \frac{2x^{3-\beta}t^\alpha}{\Gamma(4-\beta)\Gamma(\alpha+1)}, \\
 Q_2(x, t) &= \mathcal{A}^{-1} \left[\frac{1}{v^\alpha} \left(\mathcal{A} \left[D_x^\beta \left(\frac{x}{3} (Q_0 + Q_1) \right) - \left(\frac{4}{x} (Q_0 + Q_1)^2 \right)_x + (Q_0 + Q_1)_{xx}^2 \right] \right) \right. \\
 &\quad \left. - \mathcal{A}^{-1} \left[\frac{1}{v^\alpha} \left(\mathcal{A} \left[D_x^\beta \left(\frac{x}{3} Q_0 \right) - \left(\frac{4}{x} Q_0^2 \right)_x + (Q_0^2)_{xx} \right] \right) \right] \right] \\
 &= \mathcal{A}^{-1} \left[\frac{2x^{3-\beta}}{\Gamma(4-\beta)v^{2+\alpha}} + \frac{2\Gamma(3-\beta)x^{4-2\beta}}{3\Gamma(4-\beta)\Gamma(3-2\beta)v^{2+2\alpha}} - \frac{(4-\beta)16x^{3-\beta}}{\Gamma(4-\beta)v^{2+2\alpha}} \right] \\
 &\quad - \mathcal{A}^{-1} \left[\frac{(5-2\beta)16x^{4-2\beta}}{[\Gamma(4-\beta)\Gamma(\alpha+1)]^2v^{2+3\alpha}} + \frac{4(5-\beta)(4-\beta)x^{3-\beta}}{\Gamma(4-\beta)v^{2+2\alpha}} \right] \\
 &\quad + \mathcal{A}^{-1} \left[\frac{4(6-2\beta)(5-2\beta)\Gamma(2\alpha+1)x^{4-2\beta}}{[\Gamma(4-\beta)\Gamma(\alpha+1)]^2v^{2+3\alpha}} - \frac{2x^{3-\beta}}{\Gamma(4-\beta)v^{2+\alpha}} \right] \\
 &= \frac{2\Gamma(5-\beta)x^{4-2\beta}t^{2\alpha}}{3\Gamma(4-\beta)\Gamma(5-2\beta)\Gamma(2\alpha+1)} + \frac{(4-4\beta)(4-\beta)x^{3-\beta}t^{2\alpha}}{\Gamma(4-\beta)\Gamma(2\alpha+1)} + \frac{(8-8\beta)(5-2\beta)\Gamma(2\alpha+1)x^{4-2\beta}t^{3\alpha}}{[\Gamma(4-\beta)\Gamma(\alpha+1)]^2\Gamma(3\alpha+1)}, \\
 &\vdots
 \end{aligned} \tag{26}$$

and so on. The series solution is obtained as follows:

$$\begin{aligned}
 Q(x, t) &= Q_0 + Q_1 + Q_2 + \dots \\
 &= x^2 + \frac{2x^{3-\beta}t^\alpha}{\Gamma(4-\beta)\Gamma(\alpha+1)} \\
 &\quad + \frac{2\Gamma(5-\beta)x^{4-2\beta}t^{2\alpha}}{3\Gamma(4-\beta)\Gamma(5-2\beta)\Gamma(2\alpha+1)} \\
 &\quad + \frac{(4-4\beta)(4-\beta)x^{3-\beta}t^{2\alpha}}{\Gamma(4-\beta)\Gamma(2\alpha+1)} \\
 &\quad + \frac{(8-8\beta)(5-2\beta)\Gamma(2\alpha+1)x^{4-2\beta}t^{3\alpha}}{[\Gamma(4-\beta)\Gamma(\alpha+1)]^2\Gamma(3\alpha+1)} + \dots
 \end{aligned} \tag{27}$$

Setting $\beta = 1$ in equation (27), we obtain the following equation:

$$\begin{aligned}
 Q(x, t) &= x^2 \left(1 + \frac{t^\alpha}{\Gamma(\alpha+1)} + \frac{t^{2\alpha}}{\Gamma(2\alpha+1)} + \dots \right) \\
 &= x^2 \sum_{i=0}^{\infty} \frac{t^{i\alpha}}{\Gamma(i\alpha+1)}.
 \end{aligned} \tag{28}$$

The solution obtained in equation (28) converges to the exact solution in a closed form as $i \rightarrow \infty$,

$$\begin{aligned}
 Q(x, t) &= x^2 \lim_{i \rightarrow \infty} \sum_{i=0}^{\infty} \frac{t^{i\alpha}}{\Gamma(i\alpha+1)} \\
 &= x^2 E_\alpha(t^\alpha).
 \end{aligned} \tag{29}$$

So, by setting $\alpha = 1$, we obtain the following equation:

$$Q(x, t) = x^2 e^t. \tag{30}$$

Which is the same solution obtained in [23]. Figure 2 represents the solution plots of equation (22) when $\alpha = \beta = .02, .04, .06, .08, .2, .6, .8$ at $x = 1$ and $t = 1$ respectively. While the remaining are the surface plots.

Example 3. Consider the one-dimensional space-time diffusion equation [24].

$$D_t^\alpha = D_x^{2\beta} Q + D_x^\beta (xQ), \quad 0 < \alpha, \beta \leq 1. \tag{31}$$

With the initial condition,

$$Q(x, 0) = 1. \tag{32}$$

Applying the Aboodh transform on equation (31), we obtain the following equation:

$$\mathcal{A}[Q(x, t)] = \frac{1}{v^\alpha} \left(\sum_{k=0}^{m-1} \frac{Q^{(k)}(x, 0)}{v^{2-\alpha+k}} + \mathcal{A}[D_x^{2\beta} Q + D_x^\beta (xQ)] \right). \tag{33}$$

Taking the Aboodh transform inverse of equation (33), we obtain the following equation:

$$Q(x, t) = \mathcal{A}^{-1} \left[\frac{1}{v^\alpha} \left(\sum_{k=0}^{m-1} \frac{Q^{(k)}(x, 0)}{v^{2-\alpha+k}} + \mathcal{A}[D_x^{2\beta} Q + D_x^\beta (xQ)] \right) \right]. \tag{34}$$

Using the Aboodh transform iterative procedure, we obtain the following equation:

$$\begin{aligned} Q_0(x, t) &= \mathcal{A}^{-1} \left[\frac{1}{v^\alpha} \left(\sum_{k=0}^{m-1} \frac{Q^{(k)}(x, 0)}{v^{2-\alpha+k}} \right) \right] \\ &= \mathcal{A}^{-1} \left[\frac{Q(x, 0)}{v^2} \right] \\ &= 1, \\ Q_1(x, t) &= \mathcal{A}^{-1} \left[\frac{1}{v^\alpha} \left(\mathcal{A}[D_x^{2\beta} Q_0 + D_x^\beta (xQ_0)] \right) \right] \\ &= \mathcal{A}^{-1} \left[\frac{x^{1-\beta}}{v^{2+\alpha} \Gamma(2-\beta)} \right] \\ &= \frac{x^{1-\beta} t^\alpha}{\Gamma(\alpha+1) \Gamma(2-\beta)}, \\ Q_2(x, t) &= \mathcal{A}^{-1} \left[\frac{1}{v^\alpha} \left(\mathcal{A}[D_x^{2\beta} (Q_0 + Q_1) + D_x^\beta (x(Q_0 + Q_1))] \right) \right] - \mathcal{A}^{-1} \left[\frac{1}{v^\alpha} \left(\mathcal{A}[D_x^{2\beta} Q_0 + D_x^\beta (xQ_0)] \right) \right] \\ &= \mathcal{A}^{-1} \left[\frac{x^{1-\beta}}{\Gamma(2-\beta)v^{2+\alpha}} + \frac{\Gamma(3-\beta)x^{2-2\beta}}{\Gamma(3-2\beta)\Gamma(2-\beta)v^{2+2\alpha}} \right] - \mathcal{A}^{-1} \left[\frac{x^{1-\beta}}{\Gamma(2-\beta)v^{2+\alpha}} \right] \\ &= \frac{(2-\beta)x^{2-2\beta} t^{2\alpha}}{\Gamma(3-2\beta)\Gamma(2\alpha+1)}. \end{aligned} \tag{35}$$

The series solution is obtained as follows:

$$\begin{aligned} Q(x, t) &= Q_0 + Q_1 + Q_2 + \dots \\ &= 1 + \frac{x^{1-\beta} t^\alpha}{\Gamma(2-\beta)\Gamma(\alpha+1)} \\ &\quad + \frac{(2-\beta)x^{2-2\beta} t^{2\alpha}}{\Gamma(3-2\beta)\Gamma(2\alpha+1)} + \dots \end{aligned} \tag{36}$$

Setting $\beta = 1$ in equation (36), we obtain the following equation:

$$\begin{aligned} Q(x, t) &= 1 + \frac{t^\alpha}{\Gamma(\alpha+1)} + \frac{t^{2\alpha}}{\Gamma(2\alpha+1)} + \dots \\ &= \sum_{i=0}^{\infty} \frac{t^{i\alpha}}{\Gamma(i\alpha+1)}. \end{aligned} \tag{37}$$

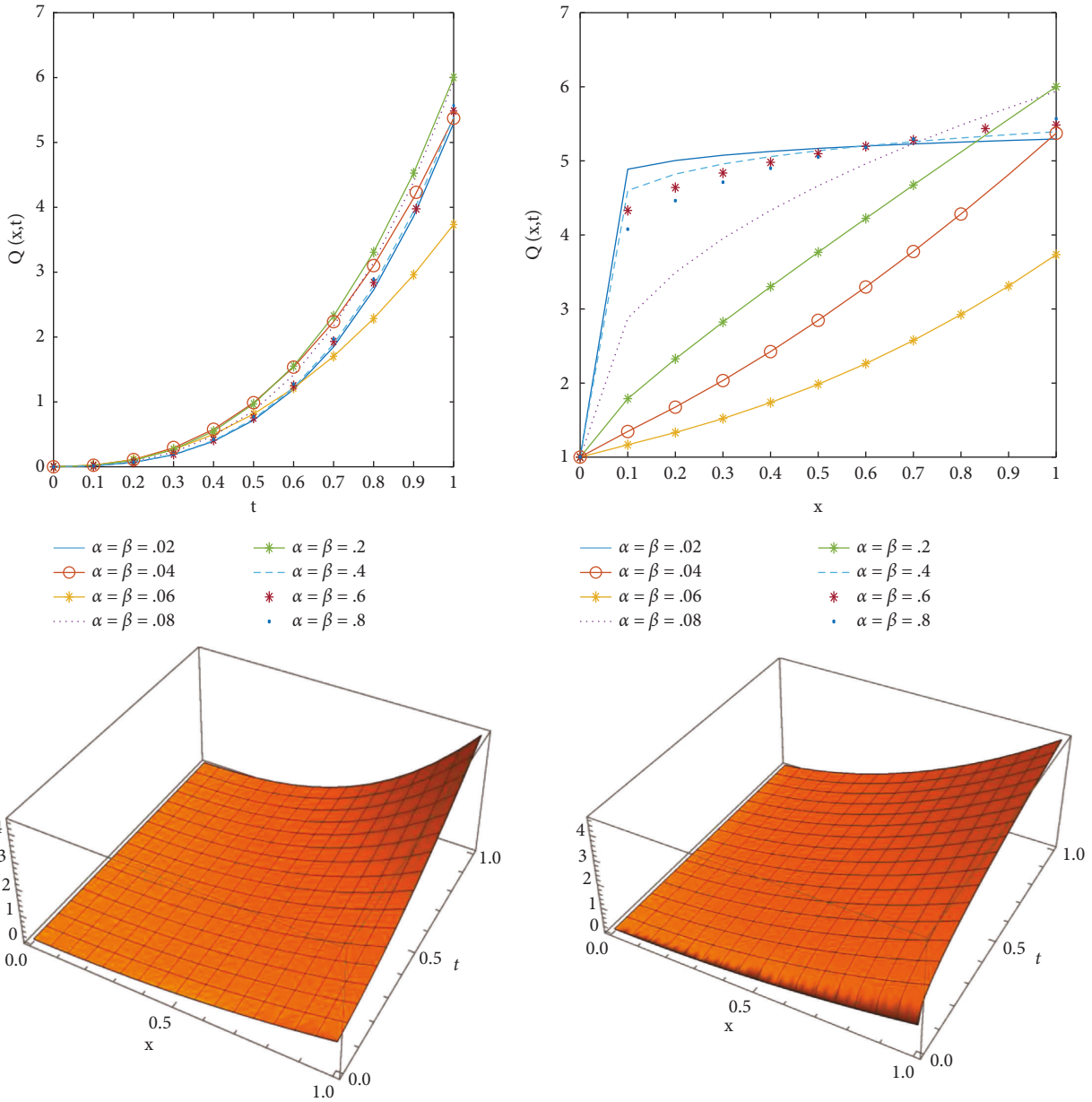


FIGURE 2: Comparison of the solution at various values of alpha and beta.

The solution obtained in equation (37) converges to the exact solution in a closed form as $i \rightarrow \infty$,

$$Q(x, t) = \lim_{i \rightarrow \infty} \sum_{i=0}^{\infty} \frac{t^{i\alpha}}{\Gamma(i\alpha + 1)} \quad (38)$$

$$= E_{\alpha}(t^{\alpha}).$$

So, by setting $\alpha = (1/2)$, we obtain the following equation:

$$Q(x, t) = E_{(1/2)}(t^{(1/2)}). \quad (39)$$

Which is the solution obtained in [24] using the natural transform method. Figure 3 represents the solution plots of equation (31) when $\alpha = \beta = .02, .04, .06, .08, .2, .4, .6, .8$ at

$x = 1$ and $t = 1$, respectively. While the remaining are the surface plots.

Example 4. Consider the space-time fractional Airy's partial differential equations [22].

$$D_t^{\alpha} Q(x, t) = D_x^{3\beta} Q, \quad 0 < \alpha, \beta \leq 1. \quad (40)$$

With the initial condition,

$$Q(x, 0) = \frac{1}{6}x^3. \quad (41)$$

Applying the Aboodh transform on equation (40), we get the following equation:

$$\mathcal{A}[Q(x, t)] = \frac{1}{v^\alpha} \left(\sum_{k=0}^{m-1} \frac{Q^{(k)}(x, 0)}{v^{2-\alpha+k}} + \mathcal{A}[D_x^{3\beta} Q] \right), \quad (42)$$

taking the inverse Aboodh transform of equation (42), we get the following equation:

$$Q(x, t) = \mathcal{A}^{-1} \left[\frac{1}{v^\alpha} \left(\sum_{k=0}^{m-1} \frac{Q^{(k)}(x, 0)}{v^{2-\alpha+k}} + \mathcal{A}[D_x^{3\beta} Q] \right) \right]. \quad (43)$$

Using the Aboodh transform iterative method procedure, we obtain the following equation:

$$\begin{aligned} Q_0(x, t) &= \mathcal{A}^{-1} \left[\frac{1}{v^\alpha} \left(\sum_{k=0}^{m-1} \frac{Q^{(k)}(x, 0)}{v^{2-\alpha+k}} \right) \right] \\ &= \mathcal{A}^{-1} \left[\frac{Q(x, 0)}{v^2} \right] \\ &= \frac{1}{6} x^3, \\ Q_1(x, t) &= \mathcal{A}^{-1} \left[\frac{1}{v^\alpha} (\mathcal{A}[D_x^{3\beta} Q_0]) \right] \\ &= \mathcal{A}^{-1} \left[\frac{x^{3-3\beta}}{\Gamma(4-3\beta)v^{2+\alpha}} \right] \\ &= \frac{x^{3-3\beta} t^\alpha}{\Gamma(4-3\beta)\Gamma(\alpha+1)}, \\ Q_2(x, t) &= \mathcal{A}^{-1} \left[\frac{1}{v^\alpha} (\mathcal{A}[D_x^{3\beta} (Q_1 + Q_0)]) \right] - \mathcal{A}^{-1} \left[\frac{1}{v^\alpha} (\mathcal{A}[D_x^{3\beta} Q_0]) \right] \\ &= \mathcal{A}^{-1} \left[\frac{\Gamma(4)x^{3-3\beta}}{6\Gamma(4-3\beta)v^{2+\alpha}} \right] - \mathcal{A}^{-1} \left[\frac{x^{3-3\beta}}{\Gamma(4-3\beta)v^{2+\alpha}} \right] \\ &= 0, \\ &\vdots \end{aligned} \quad (44)$$

and so on. The series solution is obtained as follows:

$$\begin{aligned} Q(x, t) &= Q_0 + Q_1 + Q_2 + \dots \\ &= \frac{1}{6} x^3 + \frac{x^{3-3\beta} t^\alpha}{\Gamma(4-3\beta)\Gamma(\alpha+1)} + 0 + \dots, \end{aligned} \quad (45)$$

for all $i > 1$, $Q_i(x, t) = 0$. Setting $\beta = 1$ in equation (45), we obtain the following equation:

$$\begin{aligned} Q(x, t) &= \frac{1}{6} x^3 + \frac{t^\alpha}{\Gamma(\alpha+1)} + 0 + 0 + \dots \\ &= \frac{1}{6} x^3 + \frac{t^\alpha}{\Gamma(\alpha+1)}. \end{aligned} \quad (46)$$

We obtain the exact solution when $\alpha = 1$,

$$Q(x, t) = \frac{1}{6} x^3 + t, \quad (47)$$

which is the solution obtained in [22]. Figure 4 represents the solution plots of equation (40) when $\alpha = \beta = .02, .04, .06, .08, .2, .4, .6, .8$ at $x = 1$ and $t = 1$ respectively. While Figure 5 is the surface plots.

Example 5. Consider the nonlinear space-time fractional Fokker-Planck equation which consists of a single term time-fractional order and three terms of space fractional order [23].

$$D_t^\alpha Q(x, t) = D_x^\beta \left(\frac{xQ}{3} \right) - D_x^\beta \left(\frac{4Q^2}{x} \right) + D_x^{2\beta} (Q^2), \quad 0 < \alpha, \beta \leq 1. \quad (48)$$

Subject to the initial condition,

$$Q(x, 0) = x^2. \quad (49)$$

Applying the Aboodh transform on equation (48), we obtain the following equation:

$$\mathcal{A}[Q(x, t)] = \frac{1}{v^\alpha} \left(\sum_{k=0}^{m-1} \frac{Q^{(k)}(x, 0)}{v^{2-\alpha+k}} + \mathcal{A} \left[D_x^\beta \left(\frac{xQ}{3} \right) - D_x^\beta \left(\frac{4Q^2}{x} \right) + D_x^{2\beta} (Q^2) \right] \right), \quad (50)$$

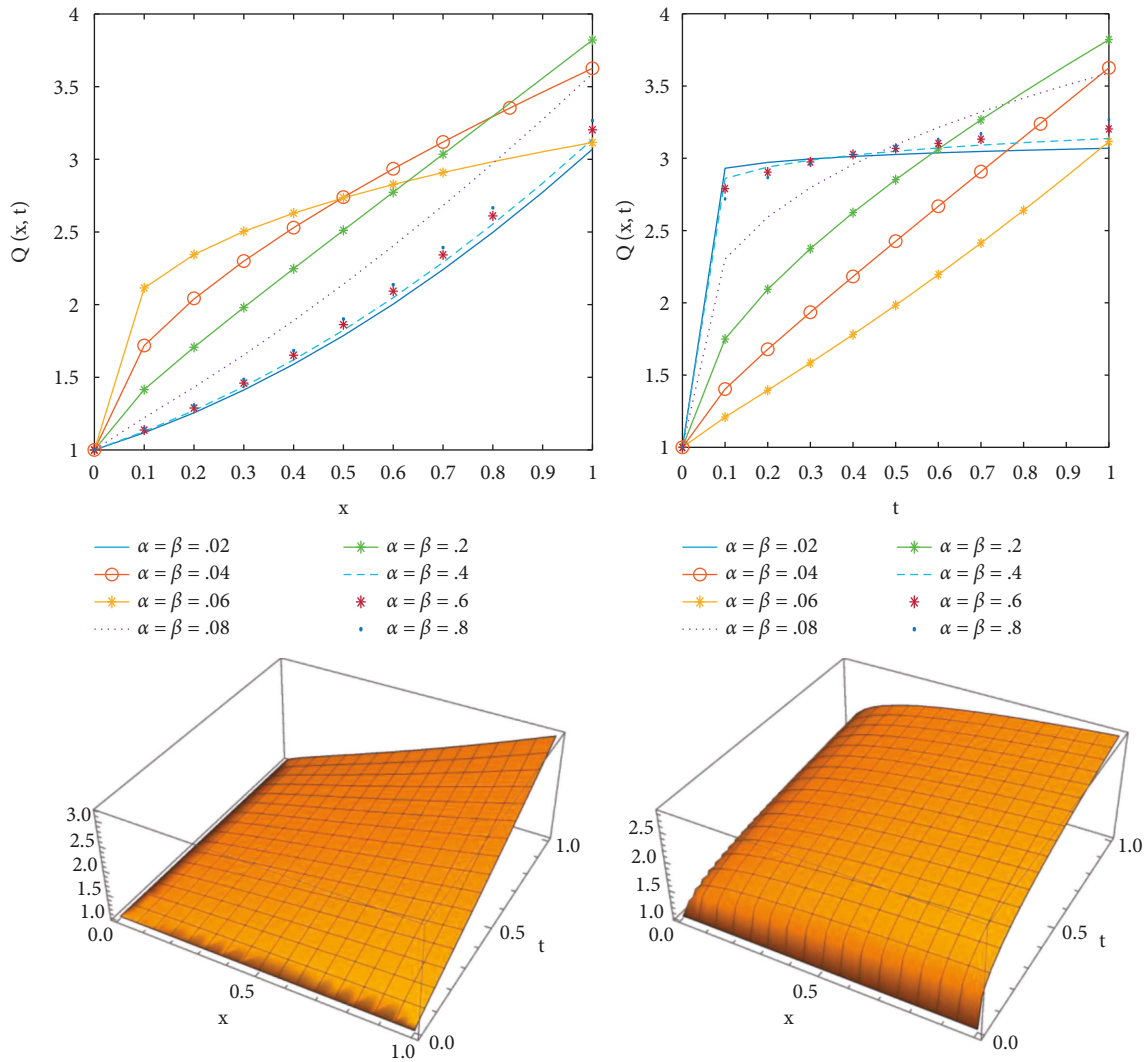


FIGURE 3: Comparison of the solution at various values of alpha and beta.

taking the inverse Aboodh transform, we get the following equation:

$$Q(x, t) = \mathcal{A}^{-1} \left[\frac{1}{v^\alpha} \left(\sum_{k=0}^{m-1} \frac{Q^{(k)}(x, 0)}{v^{2-\alpha+k}} + \mathcal{A} \left[D_x^\beta \left(\frac{xQ}{3} \right) - D_x^\beta \left(\frac{4Q^2}{x} \right) + D_x^{2\beta} (Q^2) \right] \right) \right]. \tag{51}$$

Using Aboodh transform iterative procedure, we get the following equation:

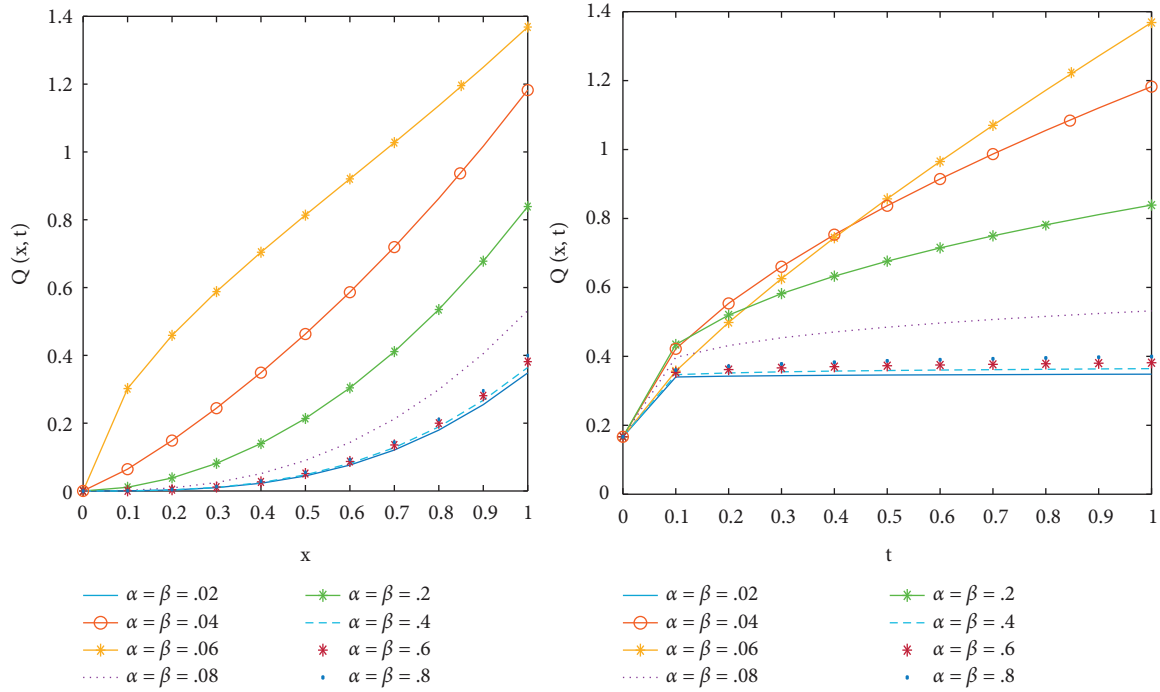


FIGURE 4: Comparison of the solution at various values of alpha and beta.

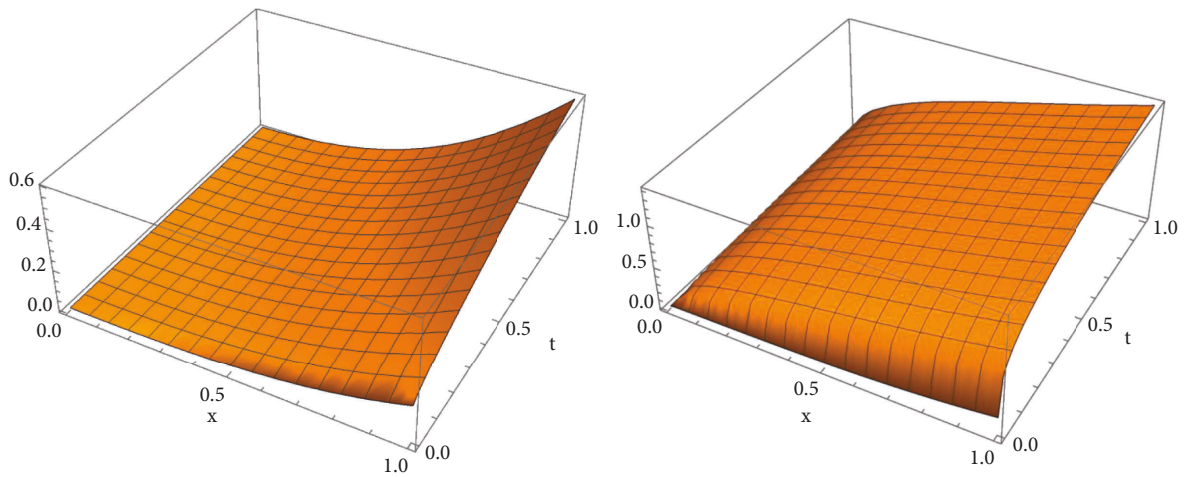


FIGURE 5: Comparison of the solution at various values of alpha and beta. (a) Early strength. (b) Early strength loss rate.

$$\begin{aligned}
 Q_0(x, t) &= \mathcal{A}^{-1} \left[\frac{1}{v^\alpha} \left(\sum_{k=0}^{m-1} \frac{Q^{(k)}(x, 0)}{v^{-\alpha+k}} \right) \right] \\
 &= \mathcal{A}^{-1} \left[\frac{Q(x, 0)}{v^2} \right] \\
 &= x^2, \\
 Q_1(x, t) &= \mathcal{A}^{-1} \left[\frac{1}{v^\alpha} \left(\mathcal{A} \left[D_x^\beta \left(\frac{xQ_0}{3} \right) - D_x^\beta \left(\frac{4Q_0^2}{x} \right) + D_x^{2\beta} (Q_0^2) \right] \right) \right] \\
 &= \mathcal{A}^{-1} \left[\frac{24x^{4-2\beta}}{\Gamma(5-2\beta)v^{2+\alpha}} - \frac{22x^{3-\beta}}{\Gamma(4-\beta)v^{2+\alpha}} \right] \\
 &= \frac{24x^{4-2\beta}t^\alpha}{\Gamma(5-2\beta)\Gamma(\alpha+1)} - \frac{22x^{3-\beta}t^\alpha}{\Gamma(4-\beta)\Gamma(\alpha+1)}, \\
 Q_2(x, t) &= \mathcal{A}^{-1} \left[\frac{1}{v^\alpha} \left(\mathcal{A} \left[D_x^\beta \left(\frac{x(Q_0+Q_1)}{3} \right) - D_x^\beta \left(\frac{4(Q_0+Q_1)^2}{x} \right) + D_x^{2\beta} (Q_0+Q_1)^2 \right] \right) \right] \\
 &\quad - \mathcal{A}^{-1} \left[\frac{1}{v^\alpha} \left(\mathcal{A} \left[D_x^\beta \left(\frac{xQ_0}{3} \right) - D_x^\beta \left(\frac{4Q_0^2}{x} \right) + D_x^{2\beta} (Q_0^2) \right] \right) \right] \\
 &= \mathcal{A}^{-1} \left[\frac{8\Gamma(6-2\beta)x^{5-3\beta}}{\Gamma(5-2\beta)\Gamma(6-3\beta)v^{2+2\alpha}} - \frac{22\Gamma(5-\beta)x^{4-2\beta}}{3\Gamma(4-\beta)\Gamma(5-2\beta)v^{2+2\alpha}} + \frac{\Gamma(4)x^{3-\beta}}{3\Gamma(4-\beta)v^{2+2\alpha}} \right] \\
 &\quad + \mathcal{A}^{-1} \left[\frac{-1152\Gamma(8-4\beta)\Gamma(2\alpha+1)x^{7-5\beta}}{[\Gamma(5-2\beta)\Gamma(\alpha+1)]^2\Gamma(8-5\beta)v^{2+3\alpha}} - \frac{192\Gamma(6-2\beta)x^{5-3\beta}}{\Gamma(5-2\beta)\Gamma(6-3\beta)v^{2+2\alpha}} \right] \\
 &\quad + \mathcal{A}^{-1} \left[\frac{-1936\Gamma(6-2\beta)\Gamma(2\alpha+1)x^{5-3\beta}}{[\Gamma(4-\beta)\Gamma(\alpha+1)]^2\Gamma(6-3\beta)v^{2+3\alpha}} + \frac{4,224\Gamma(7-3\beta)\Gamma(2\alpha+1)x^{6-4\beta}}{\Gamma(5-2\beta)\Gamma(\alpha+1)^2\Gamma(4-\beta)\Gamma(7-4\beta)v^{2+3\alpha}} \right] \\
 &\quad + \mathcal{A}^{-1} \left[\frac{176\Gamma(5-\beta)x^{4-2\beta}}{\Gamma(4-\beta)\Gamma(5-2\beta)v^{2+2\alpha}} - \frac{4\Gamma(4)x^{3-\beta}}{\Gamma(4-\beta)v^{2+\alpha}} + \frac{576\Gamma(9-4\beta)\Gamma(2\alpha+1)x^{8-6\beta}}{[\Gamma(5-2\beta)\Gamma(\alpha+1)]^2\Gamma(9-6\beta)v^{2+3\alpha}} \right] \\
 &\quad + \mathcal{A}^{-1} \left[\frac{-1056\Gamma(8-3\beta)\Gamma(2\alpha+1)x^{7-5\beta}}{[\Gamma(5-2\beta)\Gamma(\alpha+1)]^2\Gamma(4-\beta)\Gamma(8-5\beta)v^{2+3\alpha}} + \frac{48\Gamma(7-2\beta)x^{6-4\beta}}{\Gamma(5-2\beta)\Gamma(7-4\beta)v^{2+2\alpha}} \right] \\
 &\quad + \mathcal{A}^{-1} \left[\frac{484\Gamma(7-2\beta)\Gamma(2\alpha+1)x^{6-4\beta}}{[\Gamma(4-\beta)\Gamma(\alpha+1)]^2\Gamma(7-4\beta)v^{2+3\alpha}} + \frac{44\Gamma(6-\beta)x^{5-3\beta}}{\Gamma(4-\beta)\Gamma(6-3\beta)v^{2+2\alpha}} + \frac{24x^{4-2\beta}}{\Gamma(5-2\beta)v^{2+\alpha}} \right] \\
 &\quad - \mathcal{A}^{-1} \left[\frac{24x^{4-2\beta}}{\Gamma(5-2\beta)v^{2+\alpha}} - \frac{22x^{3-\beta}}{\Gamma(4-\beta)v^{2+\alpha}} \right] \\
 &= \frac{8\Gamma(6-2\beta)x^{5-3\beta}t^{2\alpha}}{\Gamma(5-2\beta)\Gamma(6-3\beta)\Gamma(2\alpha+1)} - \frac{1152\Gamma(8-4\beta)\Gamma(2\alpha+1)x^{7-5\beta}t^{3\alpha}}{[\Gamma(5-2\beta)\Gamma(\alpha+1)]^2\Gamma(8-5\beta)\Gamma(3\alpha+1)} \\
 &\quad - \frac{22\Gamma(5-\beta)x^{4-2\beta}t^{2\alpha}}{3\Gamma(4-\beta)\Gamma(5-2\beta)\Gamma(2\alpha+1)} + \frac{4224\Gamma(7-3\beta)\Gamma(2\alpha+1)x^{6-4\beta}t^{3\alpha}}{\Gamma(5-2\beta)\Gamma(\alpha+1)^2\Gamma(4-\beta)\Gamma(7-4\beta)\Gamma(3\alpha+1)} \\
 &\quad - \frac{1436\Gamma(6-2\beta)\Gamma(2\alpha+1)x^{5-3\beta}t^{3\alpha}}{[\Gamma(4-\beta)\Gamma(\alpha+1)]^2\Gamma(6-3\beta)\Gamma(3\alpha+1)} - \frac{192\Gamma(6-2\beta)x^{5-3\beta}t^{2\alpha}}{\Gamma(5-2\beta)\Gamma(6-3\beta)\Gamma(2\alpha+1)} \\
 &\quad + \frac{176\Gamma(5-\beta)x^{4-2\beta}x^{4-2\beta}t^{2\alpha}}{\Gamma(4-\beta)\Gamma(5-2\beta)\Gamma(2\alpha+1)} + \frac{576\Gamma(9-4\beta)\Gamma(2\alpha+1)x^{8-6\beta}t^{3\alpha}}{[\Gamma(5-2\beta)\Gamma(\alpha+1)]^2\Gamma(9-6\beta)\Gamma(3\alpha+1)} \\
 &\quad - \frac{1056\Gamma(8-3\beta)\Gamma(2\alpha+1)x^{7-5\beta}t^{3\alpha}}{[\Gamma(5-2\beta)\Gamma(\alpha+1)]^2\Gamma(4-\beta)\Gamma(8-5\beta)\Gamma(3\alpha+1)} + \frac{48\Gamma(7-2\beta)x^{6-4\beta}t^{2\alpha}}{\Gamma(5-2\beta)\Gamma(7-4\beta)\Gamma(2\alpha+1)} \\
 &\quad + \frac{484\Gamma(7-2\beta)\Gamma(2\alpha+1)x^{6-4\beta}t^{3\alpha}}{[\Gamma(4-\beta)\Gamma(\alpha+1)]^2\Gamma(7-4\beta)\Gamma(3\alpha+1)} + \frac{44\Gamma(6-\beta)x^{5-3\beta}t^{2\alpha}}{\Gamma(4-\beta)\Gamma(6-3\beta)\Gamma(2\alpha+1)}, \\
 &\quad \vdots
 \end{aligned}
 \tag{52}$$

and so on. The series solution is obtained as follows:

$$Q(x, t) = Q_0 + Q_1 + Q_2 + \dots \quad (53)$$

Setting $\alpha = \beta = 1$ we get the following equation:

$$\begin{aligned} Q(x, t) &= x^2 + x^2 t + \frac{x^2 t^2}{2} + \dots \\ &= x^2 \left(1 + t + \frac{t^2}{2} + \dots \right). \end{aligned} \quad (54)$$

Hence,

$$\begin{aligned} Q(x, t) &= x^2 \sum_{i=0}^{\infty} \frac{t^i}{i!} \\ &= x^2 e^t, \end{aligned} \quad (55)$$

which agrees with the exact solution obtained in [23], also it is similar to the solution obtained in Example 2. The reason being that in Example 2, only one space fractional derivative term was considered while here three terms of space fractional derivative was considered.

5. Conclusion and Future Work

We proposed the Aboodh transform iterative method for the solution of space-time fractional differential equation with fractional order derivative in more than one term. The proposed method is efficient and effective, the method combined the Aboodh transform which is a modification of the Laplace transform with the new iterative method. To the best of our knowledge, no attempt has been recorded regarding the approximate analytical solution of space-time fractional differential equations using the Aboodh transform iterative method which is the novelty of this study.

The new iterative method decomposes the linear and nonlinear term. Some examples were considered, if $\alpha = \beta = 1$ the fractional differential equations becomes the classical differential equations. Aboodh transforms iterative method yields closed form solutions in this study and exact solutions in some cases. Also, the effect of the fractional orders α and β are displayed in Figures 1 to 5, this is left for the readers in different fields of study to transcribe for different applications.

In the future, we hope to extend the Aboodh transform iterative method to solve boundary value problems with consideration for other fractional order differential equations which till date have not been solved either analytically or numerically.

Data Availability

No data were used to support this study.

Conflicts of Interest

The authors declare that there are no conflicts of interest.

Authors' Contributions

N.I.M. did the conceptualization of the idea; G.O.O. did the formal analysis; M.A.A. did the formal analysis.

References

- [1] I. Podlubny, *Fractional Differential Equations: An Introduction to Fractional Derivatives, Fractional Differential Equations, to Methods of Their Solution and Some of Their Applications*, Elsevier, Amsterdam, The Netherlands, 1998.
- [2] K. Oldham and J. Spanier, *The Fractional Calculus Theory and Applications of Differentiation and Integration to Arbitrary Order*, Academic Press, New York, NY, USA, 1974.
- [3] O. S. Iyiola and G. O. Ojo, "On the analytical solution of fornerberg-whitham equation with the new fractional derivative," *Pramana*, vol. 85, no. 4, pp. 567–575, 2015.
- [4] O. S. Iyiola, G. O. Ojo, and O. Mmaduabuchi, "The fractional rosenau-hyman model and its approximate solution," *Alexandria Engineering Journal*, vol. 55, no. 2, pp. 1655–1659, 2016.
- [5] G. O. Ojo and N. I. Mahmudov, "Aboodh transform iterative method for spatial diffusion of a biological population with fractional-order," *Mathematics*, vol. 9, no. 2, p. 155, 2021.
- [6] K. K. Ali, M. S. Osman, H. M. Baskonus, N. S. Elazabb, and E. Ilhan, "Analytical and numerical study of the HIV-1 infection of CD4+ T-cells conformable fractional mathematical model that causes acquired immunodeficiency syndrome with the effect of antiviral drug therapy," *Mathematical Methods in the Applied Sciences*, vol. 2020, pp. 1–17, 2020.
- [7] S. Dave, A. M. Khan, S. D. Purohit, and D. L. Suthar, "Application of green synthesized metal nanoparticles in the photocatalytic degradation of dyes and its mathematical modelling using the Caputo-Fabrizio fractional derivative without the singular kernel," *Journal of Mathematics*, vol. 2021, pp. 1–8, 2021.
- [8] S. Kumar, R. Kumar, M. S. Osman, and B. Samet, "A wavelet based numerical scheme for fractional order SEIR epidemic of measles by using genocchi polynomials," *Numerical Methods for Partial Differential Equations*, vol. 37, no. 2, pp. 1250–1268, 2021.
- [9] P. Veerasha, E. Ilhan, D. G. Prakasha, H. M. Baskonus, and W. Gao, "A new numerical investigation of fractional order susceptible-infected-recovered epidemic model of childhood disease," *Alexandria Engineering Journal*, vol. 61, no. 2, pp. 1747–1756, 2022.
- [10] O. A. Arqub, M. S. Osman, A. H. Abdel-Aty, A. B. A. Mohamed, and S. Momani, "A numerical algorithm for the solutions of ABC singular lane-Emden type models arising in astrophysics using reproducing kernel discretization method," *Mathematics*, vol. 8, no. 6, p. 923, 2020.
- [11] S. Dhawan, J. A. T. Machado, D. W. Brzezinski, and M. S. Osman, "A Chebyshev wavelet collocation method for some types of differential problems," *Symmetry*, vol. 13, no. 4, p. 536, 2021.
- [12] S. Djennadi, N. Shawagfeh, and O. Abu Arqub, "A fractional Tikhonov regularization method for an inverse backward and source problems in the time-space fractional diffusion equations," *Chaos, Solitons & Fractals*, vol. 150, Article ID 111127, 2021.
- [13] K. K. Ali, M. A. Abd El Salam, E. M. H. Mohamed, B. Samet, S. Kumar, and M. S. Osman, "Numerical solution for generalized nonlinear fractional integro-differential equations with linear functional arguments using Chebyshev series,"

- Advances in Difference Equations*, vol. 2020, no. 1, pp. 494–523, 2020.
- [14] L. K. Yadav, G. Agarwal, D. L. Suthar, and S. D. Purohit, “Time-fractional partial differential equations: a novel technique for analytical and numerical solutions,” *Arab Journal of Basic and Applied Sciences*, vol. 29, no. 1, pp. 86–98, 2022.
- [15] V. S. Erturk and S. Momani, “Solving systems of fractional differential equations using differential transform method,” *Journal of Computational and Applied Mathematics*, vol. 215, no. 1, pp. 142–151, 2008.
- [16] S. Das, “Analytical solution of a fractional diffusion equation by variational iteration method,” *Computers & Mathematics with Applications*, vol. 57, no. 3, pp. 483–487, 2009.
- [17] L. Yan, “Merical solutions of fractional fokker-planck equations using iterative laplace transform method,” *Abstract and Applied Analysis*, 2013.
- [18] H. Jafari, *Iterative Methods for solving system of fractional differential equations*, Ph.D. thesis, Pune University, Pune, India, 2006.
- [19] L. Akinyemi and O. S. Iyiola, “Exact and approximate solutions of time-fractional models arising from physics via shehu transform,” *Mathematical Methods in the Applied Sciences*, vol. 43, no. 12, pp. 7442–7464, 2020.
- [20] S. C. Sharma and R. K. Bairwa, “Iterative laplace transform method for solving fractional heat and wavelike equations,” *Research Journal of Mathematical and Statistical Sciences*, vol. 2320, p. 6047, 2015.
- [21] V. Daftardar-Gejji and H. Jafari, “An iterative method for solving nonlinear functional equations,” *Journal of Mathematical Analysis and Applications*, vol. 316, no. 2, pp. 753–763, 2006.
- [22] D. M. Gusu, D. Wegi, G. Gemechu, and D. Gemechu, “Fractional order airy’s type differential equations of its models using RDTM,” *Mathematical Problems in Engineering*, vol. 2021, 21 pages, 2021.
- [23] L. Riabi, K. Belghaba, M. H. Cherif, and D. Ziane, “Homotopy perturbation method combined with ZZ transform to solve some nonlinear fractional differential equations,” *International Journal of Analysis and Applications*, vol. 17, no. 3, pp. 406–419, 2019.
- [24] K. Shah, H. Khalil, and R. A. Khan, “Analytical solutions of fractional order diffusion equations by natural transform method,” *Iranian Journal of Science and Technology Transaction A-Science*, vol. 42, no. 3, pp. 1479–1490, 2018.

Research Article

Bivariate Chebyshev Polynomials to Solve Time-Fractional Linear and Nonlinear KdV Equations

Azam Zahrani , Mashaallah Matinfar , and Mostafa Eslami 

Department of Mathematics, Faculty of Mathematical Science, University of Mazandaran, Babolsar, Iran

Correspondence should be addressed to Azam Zahrani; a.zahrani@stu.umz.ac.ir

Received 5 July 2022; Accepted 3 September 2022; Published 19 September 2022

Academic Editor: Arzu Akbulut

Copyright © 2022 Azam Zahrani et al. This is an open access article distributed under the Creative Commons Attribution License, which permits unrestricted use, distribution, and reproduction in any medium, provided the original work is properly cited.

This work concerns the numerical solutions of a category of nonlinear and linear time-fractional partial differential equations (TFPDEs) that are called time-fractional inhomogeneous KdV and nonlinear time-fractional KdV equations, respectively. The fractional derivative operators are of the Caputo type. Two-variable second-kind Chebyshev wavelets (SKCWs) are constructed using one-variable ones; then, utilizing corresponding integral operational matrices leads to an approximate solution to the problem under study. Also, it is found that the perturbation term tends to zero even if a finite number of the basis functions is adopted. To exhibit the applicability and efficiency of the proposed scheme, two models of the KdV equations are given.

1. Introduction

Many scientists and researchers are interested in fractional integral and derivative operators as mathematical tools for modeling diverse physical, chemical, and biological phenomena [1–5]. Fractional operators have the memory property, and this characteristic converts them into a powerful tool for studying real-world problems [6–8]. Different fractional derivative operators have been introduced by researchers for successfully and effectively modeling scientific phenomena. For example, the fractional pseudohyperbolic telegraph partial differential equation employing the Caputo fractional derivative was solved in [9] utilizing the explicit finite difference method. Generalized Caputo and Caputo fractional derivatives were studied in [10], and the nonlinear heat equation in the sense of the generalized Caputo derivative was solved by fractional Green's functions, the generalized Laplace transform, and generalized Mellin transform. A type of the fractional diffusion equation in the sense of the Grunwald–Letnikov derivative was solved by Gorenflo and Abdel-Rehim in [11] using a difference scheme. The $(2+1)$ -dimensional fractional Ablowitz–Kanup–Newell–Segur equation in the sense of the conformable derivative was studied to extract general analytical wave solutions in [12] implementing the $\exp(-\phi(\xi))$ -expansion

method. A modified definition of the conformable fractional derivative was presented in [13], and then, the exact solutions of linear and nonlinear time- and space-fractional mixed partial differential equations involving a new fractional derivative were obtained applying the invariant subspace method. Abu-Shady and Kaabar proposed the generalized fractional derivative (GFD) and showed that this operator coincides with the Caputo and Riemann–Liouville fractional derivatives [14, 15]. Therefore, this computational tool can be used to model different scientific phenomena. Nonlinear fractional partial differential equations (FPDEs) have attracted wide attention for describing many phenomena in engineering, physics, material science, and acoustics [7, 16–19]. Korteweg and de Vries introduced a class of nonlinear evolution equations, namely, KdV equations, for the first time in 1895, to describe the nonlinear shallow-water waves [20]. The KdV equations emerge in diverse phenomena of physics like the one-dimensional waves in shallow-water waves; the Fermi–Pastor–Ulam problem in the continuum limit; the evolution of long, ion-acoustic waves in a plasma, and so on. Time-fractional KdV equations are obtained by replacing the first-order time derivatives with fractional ones of the arbitrary orders. Many works have been done on the KdV and generalized KdV equations. For example, Bagheri and Khani used rational functions,

trigonometric functions, and hyperbolic functions, to reach the exact solutions of a fractional model of the KdV equation [21]. A balance method was given to obtain some closed forms of solutions of the KdV equation in [22]. Authors in [23] applied the q -homotopy analysis transform method to study the modified coupled KdV equations. An extended tanh-function method was used in [24] to achieve soliton solutions of modified coupled KdV and generalized Hirota–Satsuma coupled KdV equations. Sahoo and Saha applied the (G'/G) -expansion method to solve the time-fractional KdV equation [25]. Kaya et al. applied radial basis functions to KdV and mKdV equations [26]. Momani et al. [27] utilized the variational iteration method for time-fractional KdV. The analytical traveling wave solutions of the nonlinear fractional KdV equation are obtained by introducing an approximate-analytical method in [28]. Authors in [29] dealt with obtaining exact solutions to the fractional KdV equation. In [30–34], the new iteration method, Adomian decomposition method, variational iteration method, and homotopy perturbation method were utilized to derive approximate solutions to different forms of the KdV equations.

The target of the current work is to achieve approximate solutions for two models of the KdV by means of the second-kind Chebyshev wavelets. From a viewpoint of comparison, the proposed method has a less computational size compared to some existing methods. The orthogonal second-kind Chebyshev polynomials are utilized as basis functions in diverse methods to obtain approximate solutions of integrodifferential equations [35], integral equations [36, 37], ordinary differential equations [38, 39], and partial differential equations [40, 41]. In the present paper, an approach based on the second-kind Chebyshev polynomials is presented to work out time-fractional inhomogeneous KdV and nonlinear time-fractional KdV equations. Finding analytic solutions to linear and especially nonlinear equations is hard; hence, presenting or modifying computational methods to find an approximate solution to these problems is noteworthy.

The main goal of this paper is to assess the numerical solutions of the linear inhomogeneous fractional KdV equation and nonlinear time-fractional KdV equations. An orthogonal collocation scheme is proposed based upon the SKCW functions. Two-dimensional integral operational matrices of fractional and integer orders are derived utilizing one-dimensional ones. Resultant matrices accompanied by the collocation method convert the main problem into an algebraic equation by collocating this algebraic equation at tensor points $\{(\theta_i, \vartheta_j)\}$, $i = 0, 1, \dots, M_1, j = 0, 1, \dots, M_2$ leading to a linear or nonlinear algebraic system. θ_i and ϑ_j are roots of the second-kind Chebyshev polynomials of degrees M_1 and M_2 , respectively. By solving the resulted system, an approximate solution is achieved.

The organization of this paper is as follows: the fractional operators, one- and two-variable second-kind Chebyshev wavelets are introduced, and then, operational matrices of the integral are derived in Section 2. In Section 3, two models of the equations under study are presented. Then, it can be seen how using appropriate approximations results

in a residual function. In Section 4, some error bounds of the resulted approximations are computed. The established approach is utilized for two equations in Section 5, and a conclusion is provided in the last section.

2. Fractional Operators and SKCWs

This section presented some definitions of the fractional calculus, the SKCWs are introduced, and their integral operational matrices of integer and fractional orders are gained.

2.1. Fractional Operators

Definition 1. The Caputo fractional derivative operator of $\mathbf{g}(\theta, \vartheta) \in C^n(\Omega)$ with the order $\mu \in \mathbb{R}$ is given as the following [42]:

$${}_0^C \mathcal{D}_\vartheta^\mu \mathbf{g}(\theta, \vartheta) = \begin{cases} \frac{1}{\Gamma(n-\mu)} \int_0^\vartheta (\vartheta-\eta)^{n-\mu-1} \frac{\partial^n \mathbf{g}(\theta, \eta)}{\partial \eta^n} d\eta, & n-1 < \mu < n, n \in \mathbb{N}, \\ \frac{\partial^n \mathbf{g}(\theta, \vartheta)}{\partial \vartheta^n}, & \mu = n \in \mathbb{N}. \end{cases} \tag{1}$$

Definition 2. The Riemann-Liouville fractional integral operator of $\mathbf{g}(\theta, \vartheta) \in C(\Omega)$ with the order $\mu \in \mathbb{R}$ is given as [42]

$${}_0^{RL} \mathcal{I}_\vartheta^\mu \mathbf{g}(\theta, \vartheta) = \begin{cases} \frac{1}{\Gamma(\mu)} \int_0^\vartheta (\vartheta-\eta)^{\mu-1} \mathbf{g}(\theta, \eta) d\eta, & \mu > 0, \\ {}_0^{RL} \mathcal{I}_\vartheta^0 \mathbf{g}(\theta, \vartheta) = \mathbf{g}(\theta, \vartheta). \end{cases} \tag{2}$$

Some features of the above-mentioned operators are as follows:

$$\begin{aligned} {}_0^{RL} \mathcal{I}_\vartheta^{\mu_1} {}_0^{RL} \mathcal{I}_\vartheta^{\mu_2} \mathbf{g}(\theta, \vartheta) &= {}_0^{RL} \mathcal{I}_\vartheta^{\mu_2} {}_0^{RL} \mathcal{I}_\vartheta^{\mu_1} \mathbf{g}(\theta, \vartheta) = {}_0^{RL} \mathcal{I}_\vartheta^{\mu_1+\mu_2} \mathbf{g}(\theta, \vartheta), \\ {}_0^{RL} \mathcal{I}_\vartheta^\mu \vartheta^\sigma &= \frac{\Gamma(\sigma+1)}{\Gamma(\sigma+\mu+1)} \vartheta^{\sigma+\mu}, \quad \sigma > -1, \\ {}_0^C \mathcal{D}_\vartheta^\mu \vartheta^\sigma &= \begin{cases} 0, & \mu > \lfloor \sigma \rfloor, \\ \frac{\Gamma(\sigma+1)}{\Gamma(\sigma-\mu+1)} \vartheta^{\sigma-\mu}, & \lfloor \sigma \rfloor \geq \mu, \end{cases} \\ {}_0^C \mathcal{D}_\vartheta^\mu \left({}_0^{RL} \mathcal{I}_\vartheta^\mu \mathbf{g}(\theta, \vartheta) \right) &= \mathbf{g}(\theta, \vartheta), \\ {}_0^{RL} \mathcal{I}_\vartheta^\mu \left({}_0^C \mathcal{D}_\vartheta^\mu \mathbf{g}(\theta, \vartheta) \right) &= \mathbf{g}(\theta, \vartheta) - \mathbf{g}(\theta, 0), \quad 0 < \mu \leq 1. \end{aligned} \tag{3}$$

2.2. SKCWs. The one-variable second-kind Chebyshev wavelet $\psi_{nm}(\vartheta)$ is defined on the interval $J = [0, 1)$ as

$$\psi_{nm}(\vartheta) = \begin{cases} 2^{\frac{\ell}{2}} \tilde{U}_m \left(2^\ell \vartheta - 2n + 1 \right), & \frac{n-1}{2^{\ell-1}} < \vartheta < \frac{n}{2^{\ell-1}}, \\ 0, & \text{otherwise,} \end{cases} \tag{4}$$

where $\tilde{U}_m(\vartheta) = \sqrt{2/\pi}U_m(\vartheta)$, $m = 0, 1, \dots, \mathcal{M} - 1$. $U_m(\vartheta)$, $m = 0, 1, \dots, \mathcal{M} - 1$, are the Chebyshev polynomials of the second kind which are orthogonal with respect to the weight function $\omega(\vartheta) = (1 - \vartheta^2)^{1/2}$ on the interval $[-1, 1]$; on the other hand,

$$\int_{-1}^1 U_m(\vartheta)U_f(\vartheta)\omega(\vartheta)d\vartheta = \begin{cases} \frac{\pi}{2}, & m = f, \\ 0, & m \neq f. \end{cases} \quad (5)$$

These polynomials are obtained from the following formula:

$$\begin{aligned} U_{m+1}(\vartheta) &= 2\vartheta U_m(\vartheta) - U_{m-1}(\vartheta), \quad m = 1, 2, \dots, \\ U_0(\vartheta) &= 1, U_1(\vartheta) = 2\vartheta. \end{aligned} \quad (6)$$

From (4), $\psi_{nm}(\vartheta)$ involves four arguments, $n = 1, \dots, 2^{\mathfrak{k}-1}$, $\mathfrak{k} \in \mathbb{N}$, m is the degree of the second-kind Chebyshev polynomials, and ϑ is the time variable. The SKCWs are orthogonal with respect to the weight functions $\omega_n(\vartheta) = \omega(\vartheta)$

$2^{\mathfrak{k}}\vartheta - 2n + 1$, $n = 1, 2, \dots, 2^{\mathfrak{k}-1}$, over the interval $J_n = [(n - 1)/2^{\mathfrak{k}-1}, n/2^{\mathfrak{k}-1}]$.

Every function $g \in L^2_{\omega_n}(J_n)$ can be expanded as

$$g(\vartheta) = \sum_{n=1}^{\infty} \sum_{m=0}^{\infty} G_{nm} \psi_{nm}(\vartheta), \quad (7)$$

where

$$G_{nm} = \int_0^1 g(\vartheta)\psi_{nm}(\vartheta)\omega_n(\vartheta)d\vartheta. \quad (8)$$

Using a truncated form of the series in (7), an approximation to $g(\vartheta)$ is gained as follows:

$$g(\vartheta) \approx g_m(\vartheta) = \sum_{n=1}^{2^{\mathfrak{k}-1}} \sum_{m=0}^{M-1} G_{nm} \psi_{nm}(\vartheta) = \bar{G}^T \bar{\Psi}(\vartheta), \quad (9)$$

where \bar{G} and $\bar{\Psi}(\vartheta)$ are $(2^{\mathfrak{k}-1}\mathcal{M})$ -order vectors as follows:

$$\bar{G} = [G_{10}, G_{11}, \dots, G_{1(\mathcal{M}-1)}, G_{20}, G_{21}, \dots, G_{2(\mathcal{M}-1)}, \dots, G_{2^{\mathfrak{k}-1}0}, G_{2^{\mathfrak{k}-1}1}, \dots, G_{2^{\mathfrak{k}-1}(\mathcal{M}-1)}]^T, \quad (10)$$

$$\bar{\Psi}(\vartheta) = [\psi_{10}(\vartheta), \psi_{11}(\vartheta), \dots, \psi_{1(\mathcal{M}-1)}(\vartheta), \psi_{20}(\vartheta), \psi_{21}(\vartheta), \dots, \psi_{2(\mathcal{M}-1)}(\vartheta), \dots, \psi_{2^{\mathfrak{k}-1}0}(\vartheta), \psi_{2^{\mathfrak{k}-1}1}(\vartheta), \dots, \psi_{2^{\mathfrak{k}-1}(\mathcal{M}-1)}(\vartheta)]^T.$$

The two-variable SKCWs can be defined on the interval $\mathbf{J} = [0, 1) \times [0, 1)$ using (4) as follows:

$$\psi_{n_1 m_1 n_2 m_2}(\theta, \vartheta) = \begin{cases} 2^{(\mathfrak{k}_1 + \mathfrak{k}_2)/2} \tilde{U}_{m_1}(2^{\mathfrak{k}_1}\theta - 2n_1 + 1) \tilde{U}_{m_2}(2^{\mathfrak{k}_2}\vartheta - 2n_2 + 1), & \frac{n_1 - 1}{2^{\mathfrak{k}_1 - 1}} < \theta < \frac{n_1}{2^{\mathfrak{k}_1 - 1}}, \frac{n_2 - 1}{2^{\mathfrak{k}_2 - 1}} < \vartheta < \frac{n_2}{2^{\mathfrak{k}_2 - 1}}, \\ 0, & \text{otherwise,} \end{cases} \quad (11)$$

where $n_i = 1, \dots, 2^{\mathfrak{k}_i - 1}$, $m_i = 0, 1, \dots, M_i - 1$, $\mathfrak{k}_i \in \mathbb{N}$, $i = 1, 2$. It is clear that $\psi_{n_1 m_1 n_2 m_2}(\theta, \vartheta) = \psi_{n_1 m_1}(\theta)\psi_{n_2 m_2}(\vartheta)$. Every two-variable $g \in L^2_{W_{n_1 n_2}}(\mathbf{J})$ can be written as follows:

$$g(\theta, \vartheta) = \sum_{n_1=1}^{\infty} \sum_{m_1=0}^{\infty} \sum_{n_2=1}^{\infty} \sum_{m_2=0}^{\infty} G_{n_1 m_1 n_2 m_2} \psi_{n_1 m_1 n_2 m_2}(\theta, \vartheta), \quad (12)$$

where the coefficients $G_{n_1 m_1 n_2 m_2}$ are computed as

$$G_{n_1 m_1 n_2 m_2} = \int_0^1 \int_0^1 g(\theta, \vartheta) \psi_{n_1 m_1 n_2 m_2}(\theta, \vartheta) W_{n_1 n_2}(\theta, \vartheta) d\theta d\vartheta, \quad (13)$$

and $W_{n_1 n_2}(\theta, \vartheta) = \omega_{n_1}(\theta)\omega_{n_2}(\vartheta)$. By considering the trun-

cated series of the infinite series in (12), one gets the following approximation to $g(\theta, \vartheta)$:

$$\begin{aligned} g(\theta, \vartheta) &\approx g_{\mathcal{M}_1, \mathcal{M}_2}(\theta, \vartheta) = \sum_{n_1=1}^{2^{\mathfrak{k}_1-1}} \sum_{m_1=0}^{\mathcal{M}_1-1} \sum_{n_2=1}^{2^{\mathfrak{k}_2-1}} \sum_{m_2=0}^{\mathcal{M}_2-1} G_{n_1 m_1 n_2 m_2} \psi_{n_1 m_1 n_2 m_2}(\theta, \vartheta) \\ &= \mathbf{G}^T \Delta(\theta, \vartheta) = \mathbf{G}^T (\Psi(\theta) \otimes \Psi(\vartheta)), \end{aligned} \quad (14)$$

where \mathbf{G} and Δ are $(2^{\mathfrak{k}_1-1}\mathcal{M}_1)(2^{\mathfrak{k}_2-1}\mathcal{M}_2) \times 1$ vectors and \otimes denotes the Kronecker product.

2.3. Operational Matrices of the Integration. The integration of the one-variable basis in (10) can be approximated as

$$\int_0^{\vartheta} \bar{\Psi}(\eta) d\eta \approx \mathcal{P}^1 \bar{\Psi}(\vartheta), \quad (15)$$

where \mathcal{P}^1 is the operational matrix of the integration, and its entries are calculated as

$$\mathcal{P}^1[i, j] := \left\langle \int_0^\vartheta \bar{\Psi}_i(\eta) d\eta, \bar{\Psi}_j(\vartheta) \right\rangle_{\omega_n}, \quad i, j = 1, 2, \dots, 2^{\ell-1} \mathcal{M}. \tag{16}$$

If ${}^{RL}_0 \mathcal{I}_\vartheta^\mu$ is the fractional integral of order $\mu > 0$ [7], then the operational matrix of the integration of the fractional order μ , $\mathcal{P}^{(\mu)}$, is given as

$${}^{RL}_0 \mathcal{I}_\vartheta^\mu \bar{\Psi}(\vartheta) \approx \mathcal{P}^{(\mu)} \bar{\Psi}(\vartheta), \tag{17}$$

where

$$\begin{aligned} {}^{RL}_0 \mathcal{I}_\vartheta^\mu \bar{\Psi}(\vartheta) &= \left[{}^{RL}_0 \mathcal{I}_\vartheta^\mu \psi_{10}(\vartheta), \dots, {}^{RL}_0 \mathcal{I}_\vartheta^\mu \psi_{1(\mathcal{M}-1)}(\vartheta), \dots, {}^{RL}_0 \mathcal{I}_\vartheta^\mu \psi_{2^{\ell-1}0}(\vartheta), \dots, {}^{RL}_0 \mathcal{I}_\vartheta^\mu \psi_{2^{\ell-1}(\mathcal{M}-1)}(\vartheta) \right]^T, \\ {}^{RL}_0 \mathcal{I}_\vartheta^\mu \psi_{mn}(\vartheta) &= \begin{cases} 2^{\ell/2} {}^{RL}_0 \mathcal{I}_\vartheta^\mu \tilde{U}_m(2^\ell \vartheta - 2n + 1), & \frac{n-1}{2^{\ell-1}} < \vartheta < \frac{n}{2^{\ell-1}}, \\ 0, & \text{otherwise.} \end{cases} \end{aligned} \tag{18}$$

Now, the two-dimensional operational matrices of the integration are constructed using \mathcal{P}^1 and $\mathcal{P}^{(\mu)}$:

$$\begin{aligned} \int_0^\vartheta \Delta(\xi, \vartheta) d\xi &\approx \mathbf{P}_\theta \Delta(\theta, \vartheta) = (\mathcal{P}^1 \otimes I) \Delta(\theta, \vartheta), \\ \int_0^\vartheta \Delta(\theta, \eta) d\eta &\approx \mathbf{P}_\vartheta \Delta(\theta, \vartheta) = (I \otimes \mathcal{P}^1) \Delta(\theta, \vartheta), \end{aligned} \tag{19}$$

$${}^{RL}_0 \mathcal{I}_\vartheta^\mu \Delta(\theta, \eta) \approx \mathbf{P}_\vartheta^{(\mu)} \Delta(\theta, \vartheta) = (I \otimes \mathcal{P}^{(\mu)}) \Delta(\theta, \vartheta),$$

where \mathbf{P}_θ , \mathbf{P}_ϑ , and $\mathbf{P}_\vartheta^{(\mu)}$ are two-dimensional operational matrices regarding the classic and fractional integral operators, respectively, and I is the $(\mathcal{M} \times \mathcal{M})$ identity matrix.

3. Methodology

To show the applicability of the proposed scheme, the time-fractional inhomogeneous KdV equation and nonlinear time-fractional KdV equation are considered.

3.1. Time-Fractional Inhomogeneous KdV Equation. A form of this model is given as follows [27]:

$${}^c_0 \mathcal{D}_\vartheta^\mu \mathbf{u}(\theta, \vartheta) + p(\theta, \vartheta) \frac{\partial \mathbf{u}(\theta, \vartheta)}{\partial \theta} + q(\theta, \vartheta) \frac{\partial^3 \mathbf{u}(\theta, \vartheta)}{\partial \theta^3} = \mathbf{f}(\theta, \vartheta), \quad (\theta, \vartheta) \in \mathbf{J}, \mu \in (0, 1], \tag{20}$$

with

$$\mathbf{u}(\theta, 0) = \rho_1(\theta), \mathbf{u}(0, \vartheta) = \phi_1(\vartheta), \frac{\partial \mathbf{u}(0, \vartheta)}{\partial \theta} = \phi_2(\vartheta), \frac{\partial^2 \mathbf{u}(0, \vartheta)}{\partial \theta^2} = \phi_3(\vartheta), \tag{21}$$

where functions $\rho_1, \phi_1, \phi_2, \phi_3$ are known continuous ones. By considering the highest orders of derivative operators regarding θ and ϑ , the following approximation is given:

$$\frac{\partial^4 \mathbf{u}(\theta, \vartheta)}{\partial t \partial \theta^3} \approx \mathbf{C}^T \Delta(\theta, \vartheta). \tag{22}$$

Triple integrating (22) regarding θ and using conditions (21) lead to the following approximations:

$$\begin{aligned} \frac{\partial^3 \mathbf{u}(\theta, \vartheta)}{\partial \vartheta \partial \theta^2} &\approx \mathbf{C}^T \mathbf{P}_\theta \Delta(\theta, \vartheta) + \frac{\partial^3 \mathbf{u}(0, \vartheta)}{\partial \vartheta \partial \theta^2} = \mathbf{C}^T \mathbf{P}_\theta \Delta(\theta, \vartheta) \\ &+ \phi_3'(\vartheta) \approx \mathbf{C}^T \mathbf{P}_\theta \Delta(\theta, \vartheta) + F_1^T \Delta(\theta, \vartheta), \end{aligned} \tag{23}$$

$$\begin{aligned} \frac{\partial^2 \mathbf{u}(\theta, \vartheta)}{\partial \vartheta \partial \theta} &\approx \mathbf{C}^T (\mathbf{P}_\theta)^2 \Delta(\theta, \vartheta) + F_1^T \mathbf{P}_\vartheta \Delta(\theta, \vartheta) + \phi_2'(\vartheta) \\ &\approx \mathbf{C}^T (\mathbf{P}_\theta)^2 \Delta(\theta, \vartheta) + F_1^T \mathbf{P}_\vartheta \Delta(\theta, \vartheta) + F_2^T \Delta(\theta, \vartheta), \end{aligned} \tag{24}$$

$$\begin{aligned} \frac{\partial \mathbf{u}(\theta, \vartheta)}{\partial t} &\approx \mathbf{C}^T (\mathbf{P}_\theta)^3 \Delta(\theta, \vartheta) + F_1^T (\mathbf{P}_\theta)^2 \Delta(\theta, \vartheta) + F_2^T \mathbf{P}_\vartheta \Delta(\theta, \vartheta) \\ &+ \phi_1'(\vartheta) \approx \mathbf{C}^T (\mathbf{P}_\theta)^3 \Delta(\theta, \vartheta) + F_1^T (\mathbf{P}_\theta)^2 \Delta(\theta, \vartheta) \\ &+ F_2^T \mathbf{P}_\vartheta \Delta(\theta, \vartheta) + F_3^T \Delta(\theta, \vartheta). \end{aligned} \tag{25}$$

Now, by integrating (23) regarding ϑ , an approximation to $\mathbf{u}(\theta, \vartheta)$ is obtained:

$$\begin{aligned} \mathbf{u}(\theta, \vartheta) &\approx \mathbf{C}^T (\mathbf{P}_\theta)^3 \mathbf{P}_\vartheta \Delta(\theta, \vartheta) + F_1^T (\mathbf{P}_\theta)^2 \mathbf{P}_\vartheta \Delta(\theta, \vartheta) \\ &+ F_2^T \mathbf{P}_\theta \mathbf{P}_\vartheta \Delta(\theta, \vartheta) + F_3^T \mathbf{P}_\vartheta \Delta(\theta, \vartheta) + \rho_1(\theta) \\ &\approx \mathbf{C}^T (\mathbf{P}_\theta)^3 \mathbf{P}_\vartheta \Delta(\theta, \vartheta) + F_1^T (\mathbf{P}_\theta)^2 \mathbf{P}_\vartheta \Delta(\theta, \vartheta) \\ &+ F_2^T \mathbf{P}_\theta \mathbf{P}_\vartheta \Delta(\theta, \vartheta) + F_3^T \mathbf{P}_\vartheta \Delta(\theta, \vartheta) + F_4^T \Delta(\theta, \vartheta). \end{aligned} \tag{26}$$

Again, by integrating (22) regarding ϑ and θ , approximations to $\mathbf{u}_{\theta\theta}$ and \mathbf{u}_θ are obtained:

$$\frac{\partial^3 \mathbf{u}(\theta, \vartheta)}{\partial \theta^3} \approx \mathbf{C}^T \mathbf{P}_\vartheta \Delta(\theta, \vartheta) + \rho_1'''(\theta) \approx \mathbf{C}^T \mathbf{P}_\vartheta \Delta(\theta, \vartheta) + F_5^T \Delta(\theta, \vartheta), \tag{27}$$

$$\begin{aligned} \frac{\partial^2 \mathbf{u}(\theta, \vartheta)}{\partial \theta^2} &\approx \mathbf{C}^T \mathbf{P}_\vartheta \mathbf{P}_\theta \Delta(\theta, \vartheta) + F_5^T \mathbf{P}_\vartheta \Delta(\theta, \vartheta) + \phi_3(\vartheta) \\ &\approx \mathbf{C}^T \mathbf{P}_\vartheta \mathbf{P}_\theta \Delta(\theta, \vartheta) + F_5^T \mathbf{P}_\theta \Delta(\theta, \vartheta) + F_6^T \Delta(\theta, \vartheta), \end{aligned} \tag{28}$$

$$\begin{aligned} \frac{\partial \mathbf{u}(\theta, \vartheta)}{\partial \theta} &\approx \mathbf{C}^T \mathbf{P}_\vartheta (\mathbf{P}_\vartheta)^2 \Delta(\theta, \vartheta) + F_5^T (\mathbf{P}_\theta)^2 \Delta(\theta, \vartheta) \\ &\quad + F_6^T \mathbf{P}_\theta \Delta(\theta, \vartheta) + \phi_2(\vartheta) \approx \mathbf{C}^T \mathbf{P}_\vartheta (\mathbf{P}_\theta)^2 \Delta(\theta, \vartheta) \\ &\quad + F_5^T (\mathbf{P}_\theta)^2 \Delta(\theta, \vartheta) + F_6^T \mathbf{P}_\theta \Delta(\theta, \vartheta) + F_7^T \Delta(\theta, \vartheta). \end{aligned} \tag{29}$$

Now, an approximation to ${}^C_0 \mathcal{D}_\vartheta^\mu \mathbf{u}(\theta, \vartheta)$ is computed using (23):

$$\begin{aligned} {}^C_0 \mathcal{D}_\vartheta^\mu \mathbf{u}(\theta, \vartheta) &\stackrel{RL}{\approx} \mathcal{I}_\vartheta^{1-\mu} \left(\frac{\partial \mathbf{u}(\theta, \vartheta)}{\partial \vartheta} \right) \approx {}^{RL} \mathcal{I}_\vartheta^{1-\mu} (\mathbf{C}^T (\mathbf{P}_\theta)^3 \Delta(\theta, \vartheta) \\ &\quad + F_1^T (\mathbf{P}_\theta)^2 \Delta(\theta, \vartheta) + F_2^T \mathbf{P}_\theta \Delta(\theta, \vartheta) + F_3^T \Delta(\theta, \vartheta)) \\ &\approx \mathbf{C}^T (\mathbf{P}_\theta)^3 \mathbf{P}_\vartheta^{(1-\mu)} \Delta(\theta, \vartheta) + F_1^T (\mathbf{P}_\theta)^2 \mathbf{P}_\vartheta^{(1-\mu)} \Delta(\theta, \vartheta) \\ &\quad + F_2^T \mathbf{P}_\theta \mathbf{P}_\vartheta^{(1-\mu)} \Delta(\theta, \vartheta) + F_3^T \mathbf{P}_\vartheta^{(1-\mu)} \Delta(\theta, \vartheta). \end{aligned} \tag{30}$$

Substituting approximations (27)–(30) into (20) yields $\mathcal{R}(\theta, \vartheta)$ as the residual function as follows:

$$\begin{aligned} \mathcal{R}(\theta, \vartheta) &= \mathbf{C}^T (\mathbf{P}_\theta)^3 \mathbf{P}_\vartheta^{(1-\mu)} \Delta(\theta, \vartheta) + F_1^T (\mathbf{P}_\theta)^2 \mathbf{P}_\vartheta^{(1-\mu)} \Delta(\theta, \vartheta) \\ &\quad + F_2^T \mathbf{P}_\theta \mathbf{P}_\vartheta^{(1-\mu)} \Delta(\theta, \vartheta) + F_3^T \mathbf{P}_\vartheta^{(1-\mu)} \Delta(\theta, \vartheta) \\ &\quad + p(\theta, \vartheta) (\mathbf{C}^T \mathbf{P}_\vartheta (\mathbf{P}_\theta)^2 \Delta(\theta, \vartheta) + F_5^T (\mathbf{P}_\theta)^2 \Delta(\theta, \vartheta) \\ &\quad + F_6^T \mathbf{P}_\theta \Delta(\theta, \vartheta) + F_7^T \Delta(\theta, \vartheta)) + q(\theta, \vartheta) (\mathbf{C}^T \mathbf{P}_\vartheta \Delta(\theta, \vartheta) \\ &\quad + F_5^T \Delta(\theta, \vartheta)) - \check{f}(\theta, \vartheta). \end{aligned} \tag{31}$$

3.2. Time-Fractional Nonlinear KdV Equation. In this paper, the following class of time-fractional nonlinear KdV equations is studied:

$${}^C_0 \mathcal{D}_\vartheta^\mu \mathbf{u}(\theta, \vartheta) + 6\mathbf{u}(\theta, \vartheta) \frac{\partial \mathbf{u}(\theta, \vartheta)}{\partial \theta} + \frac{\partial^3 \mathbf{u}(\theta, \vartheta)}{\partial \theta^3} = 0, (\theta, \vartheta) \in \mathbf{J}, \mu \in (0, 1], \tag{32}$$

with the conditions in (21). Substituting approximations (26)–(30) into (32) yields the following residual function:

$$\begin{aligned} \mathcal{R}(\theta, \vartheta) &= \mathbf{C}^T (\mathbf{P}_\theta)^3 \mathbf{P}_\vartheta^{(1-\mu)} \Delta(\theta, \vartheta) + F_1^T (\mathbf{P}_\theta)^2 \mathbf{P}_\vartheta^{(1-\mu)} \Delta(\theta, \vartheta) \\ &\quad + F_2^T \mathbf{P}_\theta \mathbf{P}_\vartheta^{(1-\mu)} \Delta(\theta, \vartheta) + F_3^T \mathbf{P}_\vartheta^{(1-\mu)} \Delta(\theta, \vartheta) \\ &\quad + (\mathbf{C}^T (\mathbf{P}_\theta)^3 \mathbf{P}_\vartheta \Delta(\theta, \vartheta) + F_1^T (\mathbf{P}_\theta)^2 \mathbf{P}_\vartheta \Delta(\theta, \vartheta) \\ &\quad + F_2^T \mathbf{P}_\theta \mathbf{P}_\vartheta \Delta(\theta, \vartheta) + F_3^T \mathbf{P}_\theta \Delta(\theta, \vartheta) + F_4^T \Delta(\theta, \vartheta)) \\ &\quad \times (\mathbf{C}^T \mathbf{P}_\vartheta (\mathbf{P}_\theta)^2 \Delta(\theta, \vartheta) + F_5^T (\mathbf{P}_\theta)^2 \Delta(\theta, \vartheta) \\ &\quad + F_6^T \mathbf{P}_\theta \Delta(\theta, \vartheta) + F_7^T \Delta(\theta, \vartheta)) + \mathbf{C}^T \mathbf{P}_\vartheta \Delta(\theta, \vartheta) + F_5^T \Delta(\theta, \vartheta). \end{aligned} \tag{33}$$

Collocating residual functions (31) and (33) at points $\{(\theta_i, \vartheta_j)\}$, $i = 1, 2, \dots, 2^{\xi_1-1} \mathcal{M}_1, j = 1, 2, \dots, 2^{\xi_2-1} \mathcal{M}_2$ results in a system of algebraic equations, where θ_i and ϑ_j are roots of $\tilde{\mathcal{U}}_{2^{\xi_1-1} \mathcal{M}_1}(\theta)$ and $\tilde{\mathcal{U}}_{2^{\xi_2-1} \mathcal{M}_2}(\vartheta)$, respectively. This algebraic system can be handled by the Newton scheme. Therefore, an approximate solution is acquired from (26).

Two models were solved by the variational iteration method in [27], and some figures of approximate solutions were depicted. The nonlinear time-fractional KdV equation (32) was solved by El-Wakil et al. in [43] using He’s variational iteration method and presented a second-order solution including some parameters. Authors in [44] obtained an approximate solution utilizing the iteration method after spending many algebraic computational costs. Inc et al. acquired new numerical solutions of fractional-time KdV equation by a technique of fictitious time integration and group preserving [45]. Authors in [46–48] used algebraic computational methods such as the modified extended tanh method, Sardar-subequation method, and He’s semi-inverse variation method and the ansatz method to construct some soliton solutions of the nonlinear time-fractional KdV equation.

4. Error Bound

In this section, error bounds are derived for the residual functions/perturbation terms for two given models in Section 3. First, some error bounds are computed for approximation errors.

4.1. Time-Fractional Inhomogeneous KdV Equation. Consider Equation (20) and suppose that $\mathbf{u}_{\mathcal{M}_1, \mathcal{M}_2}(\theta, \vartheta)$ is its approximate solution obtained from the presented algorithm in Section 3. Thus, $\mathbf{u}_{\mathcal{M}_1, \mathcal{M}_2}(\theta, \vartheta)$ satisfies the following equations:

$$\begin{aligned} {}^C_0 \mathcal{D}_\vartheta^\mu \mathbf{u}_{\mathcal{M}_1, \mathcal{M}_2}(\theta, \vartheta) + p(\theta, \vartheta) \frac{\partial \mathbf{u}_{\mathcal{M}_1, \mathcal{M}_2}(\theta, \vartheta)}{\partial \theta} \\ + q(\theta, \vartheta) \frac{\partial^3 \mathbf{u}_{\mathcal{M}_1, \mathcal{M}_2}(\theta, \vartheta)}{\partial \theta^3} = \check{f}(\theta, \vartheta) - \mathcal{R}_{\mathcal{M}_1, \mathcal{M}_2}(\theta, \vartheta), \end{aligned} \tag{34}$$

where $\mathcal{R}_{\mathcal{M}_1, \mathcal{M}_2}(\theta, \vartheta)$ is called the residual function/perturbation term. By subtracting Equation (34) from Equation (20), one gets

$$\begin{aligned} \mathcal{R}_{\mathcal{M}_1, \mathcal{M}_2}(\theta, \vartheta) &= \left({}^C_0 \mathcal{D}_\vartheta^\mu \mathbf{u}(\theta, \vartheta) - {}^C_0 \mathcal{D}_\vartheta^\mu \mathbf{u}_{\mathcal{M}_1, \mathcal{M}_2}(\theta, \vartheta) \right) \\ &\quad + p(\theta, \vartheta) \left(\frac{\partial \mathbf{u}(\theta, \vartheta)}{\partial \theta} - \frac{\partial \mathbf{u}_{\mathcal{M}_1, \mathcal{M}_2}(\theta, \vartheta)}{\partial \theta} \right) \\ &\quad + q(\theta, \vartheta) \left(\frac{\partial^3 \mathbf{u}(\theta, \vartheta)}{\partial \theta^3} - \frac{\partial^3 \mathbf{u}_{\mathcal{M}_1, \mathcal{M}_2}(\theta, \vartheta)}{\partial \theta^3} \right). \end{aligned} \tag{35}$$

Suppose that $p(\theta, \vartheta), q(\theta, \vartheta)$ are continuous functions

over \mathbf{J} . By taking L^2 -norm on Equation (35), one has

$$\begin{aligned} \|\mathcal{R}_{\mathcal{M}_1, \mathcal{M}_2}\|_{L^2} &\leq \left\| {}_0^C \mathcal{D}_\vartheta^\mu \mathbf{u} - {}_0^C \mathcal{D}_\vartheta^\mu \mathbf{u}_{\mathcal{M}_1, \mathcal{M}_2} \right\|_{L^2} + \|p\|_{L^2} \left\| \frac{\partial \mathbf{u}}{\partial \theta} - \frac{\partial \mathbf{u}_{\mathcal{M}_1, \mathcal{M}_2}}{\partial \theta} \right\|_{L^2} \\ &\quad + \|q\|_{L^2} \left\| \frac{\partial^3 \mathbf{u}}{\partial \theta^3} - \frac{\partial^3 \mathbf{u}_{\mathcal{M}_1, \mathcal{M}_2}}{\partial \theta^3} \right\|_{L^2}. \end{aligned} \tag{36}$$

First, error bounds are calculated for terms on the right-hand side in (36). Assume that $\mathcal{T}_{\mathcal{M}_1, \mathcal{M}_2}(\theta, \vartheta)$ is the Taylor series expansion of $\mathbf{u}(\theta, \vartheta)$, $\Theta_1 = \max_{(\theta, \vartheta) \in \mathbf{J}} |\mathbf{u}^{(\mathcal{M}_1 + \mathcal{M}_2 - \mu)}(\theta, \vartheta)|$, and $\mathbf{J}_{n_1, n_2} = [(\mathbf{n}_1 - 1)/2^{\mathfrak{k}_1 - 1}, \mathbf{n}_1/2^{\mathfrak{k}_1 - 1}] \times [(\mathbf{n}_2 - 1)/2^{\mathfrak{k}_2 - 1}, \mathbf{n}_2/2^{\mathfrak{k}_2 - 1}]$. One has,

$$\begin{aligned} &\left\| {}_0^C \mathcal{D}_\vartheta^\mu \mathbf{u} - {}_0^C \mathcal{D}_\vartheta^\mu \mathbf{u}_{\mathcal{M}_1, \mathcal{M}_2} \right\|_{L^2}^2 = \int_0^1 \int_0^1 \left(\mathcal{D}_\vartheta^\mu \mathbf{u}(\theta, \vartheta) - {}_0^C \mathcal{D}_\vartheta^\mu \mathbf{u}_{\mathcal{M}_1, \mathcal{M}_2}(\theta, \vartheta) \right)^2 W(\theta, \vartheta) d\vartheta d\theta \\ &= \sum_{n_1=1}^{2^{\mathfrak{k}_1-1}} \sum_{n_2=1}^{2^{\mathfrak{k}_2-1}} \int_{(n_1-1)/2^{\mathfrak{k}_1-1}}^{n_1/2^{\mathfrak{k}_1-1}} \int_{(n_2-1)/2^{\mathfrak{k}_2-1}}^{n_2/2^{\mathfrak{k}_2-1}} \left(\mathcal{D}_\vartheta^\mu \mathbf{u}(\theta, \vartheta) - {}_0^C \mathcal{D}_\vartheta^\mu \mathbf{u}_{\mathcal{M}_1, \mathcal{M}_2}(\theta, \vartheta) \right)^2 W_{n_1, n_2}(\theta, \vartheta) d\vartheta d\theta \\ &\leq \sum_{n_1=1}^{2^{\mathfrak{k}_1-1}} \sum_{n_2=1}^{2^{\mathfrak{k}_2-1}} \int_{(n_1-1)/2^{\mathfrak{k}_1-1}}^{n_1/2^{\mathfrak{k}_1-1}} \int_{(n_2-1)/2^{\mathfrak{k}_2-1}}^{n_2/2^{\mathfrak{k}_2-1}} \left(\mathcal{D}_\vartheta^\mu \mathbf{u}(\theta, \vartheta) - {}_0^C \mathcal{D}_\vartheta^\mu \mathcal{T}_{\mathcal{M}_1, \mathcal{M}_2}(\theta, \vartheta) \right)^2 W_{n_1, n_2}(\theta, \vartheta) d\vartheta d\theta \\ &\leq \sum_{n_1=1}^{2^{\mathfrak{k}_1-1}} \sum_{n_2=1}^{2^{\mathfrak{k}_2-1}} \int_{(n_1-1)/2^{\mathfrak{k}_1-1}}^{n_1/2^{\mathfrak{k}_1-1}} \int_{(n_2-1)/2^{\mathfrak{k}_2-1}}^{n_2/2^{\mathfrak{k}_2-1}} \left(\frac{\max_{(\xi_{n_1}, \eta_{n_2}) \in \mathbf{J}_{n_1, n_2}} |\mathbf{u}^{(\mathcal{M}_1 + \mathcal{M}_2 - \mu)}(\xi_{n_1}, \eta_{n_2})|}{\mathcal{M}_1! (\mathcal{M}_2 - \mu)! 2^{\mathcal{M}_1(\mathfrak{k}_1 - 1)} 2^{\mathcal{M}_2(\mathfrak{k}_2 - 1)}} \right)^2 W_{n_1, n_2}(\theta, \vartheta) d\vartheta d\theta \\ &\leq \left(\frac{\Theta_1}{\mathcal{M}_1! (\mathcal{M}_2 - \mu)! 2^{\mathcal{M}_1(\mathfrak{k}_1 - 1)} 2^{\mathcal{M}_2(\mathfrak{k}_2 - 1)}} \right)^2 \underbrace{\int_0^1 \int_0^1 W(\theta, \vartheta) d\vartheta d\theta}_{\omega(\theta)\omega(\vartheta)} \\ &= \left(\frac{\Theta_1}{\mathcal{M}_1! (\mathcal{M}_2 - \mu)! 2^{\mathcal{M}_1(\mathfrak{k}_1 - 1)} 2^{\mathcal{M}_2(\mathfrak{k}_2 - 1)}} \right)^2 \int_0^1 \theta^{1/2} (1 - \theta)^{1/2} d\theta \int_0^1 \vartheta^{1/2} (1 - \vartheta)^{1/2} d\vartheta \\ &= \left(\frac{\Theta_1}{\mathcal{M}_1! (\mathcal{M}_2 - \mu)! 2^{\mathcal{M}_1(\mathfrak{k}_1 - 1)} 2^{\mathcal{M}_2(\mathfrak{k}_2 - 1)}} \right)^2 \left(\frac{\pi}{8} \right)^2. \end{aligned} \tag{37}$$

So, one gets

$$\left\| {}_0^C \mathcal{D}_\vartheta^\mu \mathbf{u} - {}_0^C \mathcal{D}_\vartheta^\mu \mathbf{u}_{\mathcal{M}_1, \mathcal{M}_2} \right\|_{L^2} \leq \frac{\pi \Theta_1}{\mathcal{M}_1! (\mathcal{M}_2 - \mu)! 2^{\mathcal{M}_1(\mathfrak{k}_1 - 1)} 2^{\mathcal{M}_2(\mathfrak{k}_2 - 1)} 2^3}. \tag{38}$$

In a similar way, if $\Theta_{2,l} = \max_{(\theta, \vartheta) \in \mathbf{J}} |\mathbf{u}^{(\mathcal{M}_1 + \mathcal{M}_2 - l)}(\theta, \vartheta)|$, $l = 0, 1, 2, 3$, one has

$$\begin{aligned} &\left\| \frac{\partial^l \mathbf{u}}{\partial \theta^l} - \frac{\partial^l \mathbf{u}_{\mathcal{M}_1, \mathcal{M}_2}}{\partial \theta^l} \right\|_{L^2}^2 = \int_0^1 \int_0^1 \left(\frac{\partial^l \mathbf{u}(\theta, \vartheta)}{\partial \theta^l} - \frac{\partial^l \mathbf{u}_{\mathcal{M}_1, \mathcal{M}_2}(\theta, \vartheta)}{\partial \theta^l} \right)^2 W(\theta, \vartheta) d\vartheta d\theta \\ &= \sum_{n_1=1}^{2^{\mathfrak{k}_1-1}} \sum_{n_2=1}^{2^{\mathfrak{k}_2-1}} \int_{(n_1-1)/2^{\mathfrak{k}_1-1}}^{n_1/2^{\mathfrak{k}_1-1}} \int_{(n_2-1)/2^{\mathfrak{k}_2-1}}^{n_2/2^{\mathfrak{k}_2-1}} \left(\frac{\partial^l \mathbf{u}(\theta, \vartheta)}{\partial \theta^l} - \frac{\partial^l \mathbf{u}_{\mathcal{M}_1, \mathcal{M}_2}(\theta, \vartheta)}{\partial \theta^l} \right)^2 W_{n_1, n_2}(\theta, \vartheta) d\vartheta d\theta \\ &\leq \sum_{n_1=1}^{2^{\mathfrak{k}_1-1}} \sum_{n_2=1}^{2^{\mathfrak{k}_2-1}} \int_{(n_1-1)/2^{\mathfrak{k}_1-1}}^{n_1/2^{\mathfrak{k}_1-1}} \int_{(n_2-1)/2^{\mathfrak{k}_2-1}}^{n_2/2^{\mathfrak{k}_2-1}} \left(\frac{\partial^l \mathbf{u}(\theta, \vartheta)}{\partial \theta^l} - \frac{\partial^l \mathcal{T}_{\mathcal{M}_1, \mathcal{M}_2}(\theta, \vartheta)}{\partial \theta^l} \right)^2 W_{n_1, n_2}(\theta, \vartheta) d\vartheta d\theta \\ &\leq \sum_{n_1=1}^{2^{\mathfrak{k}_1-1}} \sum_{n_2=1}^{2^{\mathfrak{k}_2-1}} \int_{(n_1-1)/2^{\mathfrak{k}_1-1}}^{n_1/2^{\mathfrak{k}_1-1}} \int_{(n_2-1)/2^{\mathfrak{k}_2-1}}^{n_2/2^{\mathfrak{k}_2-1}} \left(\frac{\max_{(\xi_{n_1}, \eta_{n_2}) \in \mathbf{J}_{n_1, n_2}} |\mathbf{u}^{(\mathcal{M}_1 + \mathcal{M}_2 - l)}(\xi_{n_1}, \eta_{n_2})|}{(\mathcal{M}_1 - l)! \mathcal{M}_2! 2^{\mathcal{M}_1(\mathfrak{k}_1 - 1)} 2^{\mathcal{M}_2(\mathfrak{k}_2 - 1)}} \right)^2 W_{n_1, n_2}(\theta, \vartheta) d\vartheta d\theta \\ &\leq \left(\frac{\Theta_{2,l}}{(\mathcal{M}_1 - l)! \mathcal{M}_2! 2^{\mathcal{M}_1(\mathfrak{k}_1 - 1)} 2^{\mathcal{M}_2(\mathfrak{k}_2 - 1)}} \right)^2 \left(\frac{\pi}{8} \right)^2. \end{aligned} \tag{39}$$

TABLE 1: Maximum absolute errors for $\mu = 1$ and different values of M_1, M_2 for Example 1.

$M_1 = M_2$	2	3	4	5
MAE	5.2885×10^{-3}	7.0306×10^{-4}	2.3882×10^{-5}	2.0614×10^{-6}

TABLE 2: Absolute errors for $k_1 = k_2 = 1, M_1 = M_2 = 4$ at equally spaced points for Example 1.

$\theta_i = \vartheta_i$	$\mu = 0.7$	$\mu = 0.8$	$\mu = 0.9$	$\mu = 1$
0	4.8935×10^{-7}	5.4663×10^{-7}	4.4250×10^{-7}	1.4522×10^{-11}
0.2	6.1889×10^{-7}	6.0321×10^{-7}	4.6254×10^{-7}	1.2627×10^{-7}
0.4	8.5473×10^{-7}	8.0229×10^{-7}	7.3242×10^{-7}	6.8164×10^{-7}
0.6	5.8306×10^{-6}	5.6182×10^{-6}	3.6174×10^{-6}	1.1872×10^{-6}
0.8	1.7757×10^{-5}	1.6597×10^{-5}	1.0738×10^{-5}	1.7657×10^{-6}
1	9.7134×10^{-5}	7.8075×10^{-5}	3.3765×10^{-5}	2.3881×10^{-5}

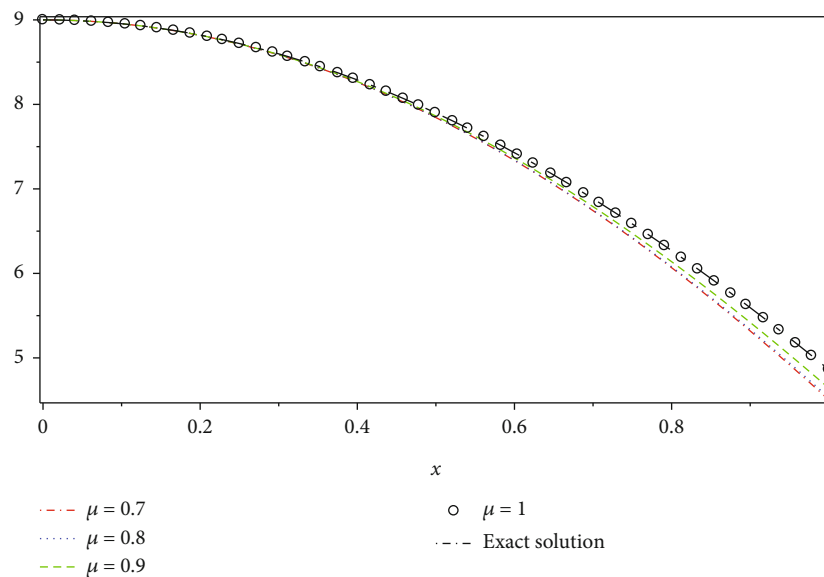


FIGURE 1: Exact and approximate solutions for $k_1 = k_2 = 1, M_1 = M_2 = 4$, and $\mu = 0.7, 0.8, 0.9, 1$ at time $\vartheta = 3$ for Example 1.

Thus, one gets

$$\left\| \frac{\partial^l \mathbf{u}}{\partial \theta^l} - \frac{\partial^l \mathbf{u}_{\mathcal{M}_1, \mathcal{M}_2}}{\partial \theta^l} \right\|_{L^2} \leq \frac{\pi \Theta_{2,l}}{(\mathcal{M}_1 - l)! \mathcal{M}_2! 2^{\mathcal{M}_1(\mathbb{k}_1 - 1)} 2^{\mathcal{M}_2(\mathbb{k}_2 - 1)} 2^3}, \quad l = 0, 1, 2, 3. \tag{40}$$

Therefore, a bound is obtained for inequality (36) using (37) and (39) as follows:

$$\begin{aligned} & \left\| \mathcal{R}_{\mathcal{M}_1, \mathcal{M}_2} \right\|_{L^2} \frac{\pi \Theta_{1,1}}{\mathcal{M}_1! (\mathcal{M}_2 - \mu)! 2^{\mathcal{M}_1(\mathbb{k}_1 - 1)} 2^{\mathcal{M}_2(\mathbb{k}_2 - 1)} 2^3} \\ & + \|p\|_{L^2} \frac{\pi \Theta_{2,1}}{(\mathcal{M}_1 - 1)! \mathcal{M}_2! 2^{\mathcal{M}_1(\mathbb{k}_1 - 1)} 2^{\mathcal{M}_2(\mathbb{k}_2 - 1)} 2^3} \\ & + \|q\|_{L^2} \frac{\pi \Theta_{2,3}}{(\mathcal{M}_1 - 3)! \mathcal{M}_2! 2^{\mathcal{M}_1(\mathbb{k}_1 - 1)} 2^{\mathcal{M}_2(\mathbb{k}_2 - 1)} 2^3}. \end{aligned} \tag{41}$$

It is evident from the right-hand side of (40) that $\left\| \mathcal{R}_{\mathcal{M}_1, \mathcal{M}_2} \right\|_{L^2} \rightarrow 0$ when $\mathcal{M}_1, \mathcal{M}_2 \rightarrow \infty$.

4.2. Time-Fractional Nonlinear KdV Equation. Consider Equation (32) and suppose that $\mathbf{u}_{\mathcal{M}_1, \mathcal{M}_2}(\theta, \vartheta)$ is its approximate solution obtained from the proposed method. Thus, $\mathbf{u}_{\mathcal{M}_1, \mathcal{M}_2}(\theta, \vartheta)$ satisfies the following equation:

$$\begin{aligned} {}_0^C \mathcal{D}_\theta^\mu \mathbf{u}_{\mathcal{M}_1, \mathcal{M}_2}(\theta, \vartheta) + 6\mathbf{u}_{\mathcal{M}_1, \mathcal{M}_2}(\theta, \vartheta) \frac{\partial \mathbf{u}_{\mathcal{M}_1, \mathcal{M}_2}(\theta, \vartheta)}{\partial \theta} \\ + \frac{\partial^3 \mathbf{u}_{\mathcal{M}_1, \mathcal{M}_2}(\theta, \vartheta)}{\partial \theta^3} = -\mathcal{R}_{\mathcal{M}_1, \mathcal{M}_2}(\theta, \vartheta). \end{aligned} \tag{42}$$

Subtracting Equation (41) from (32) leads to the

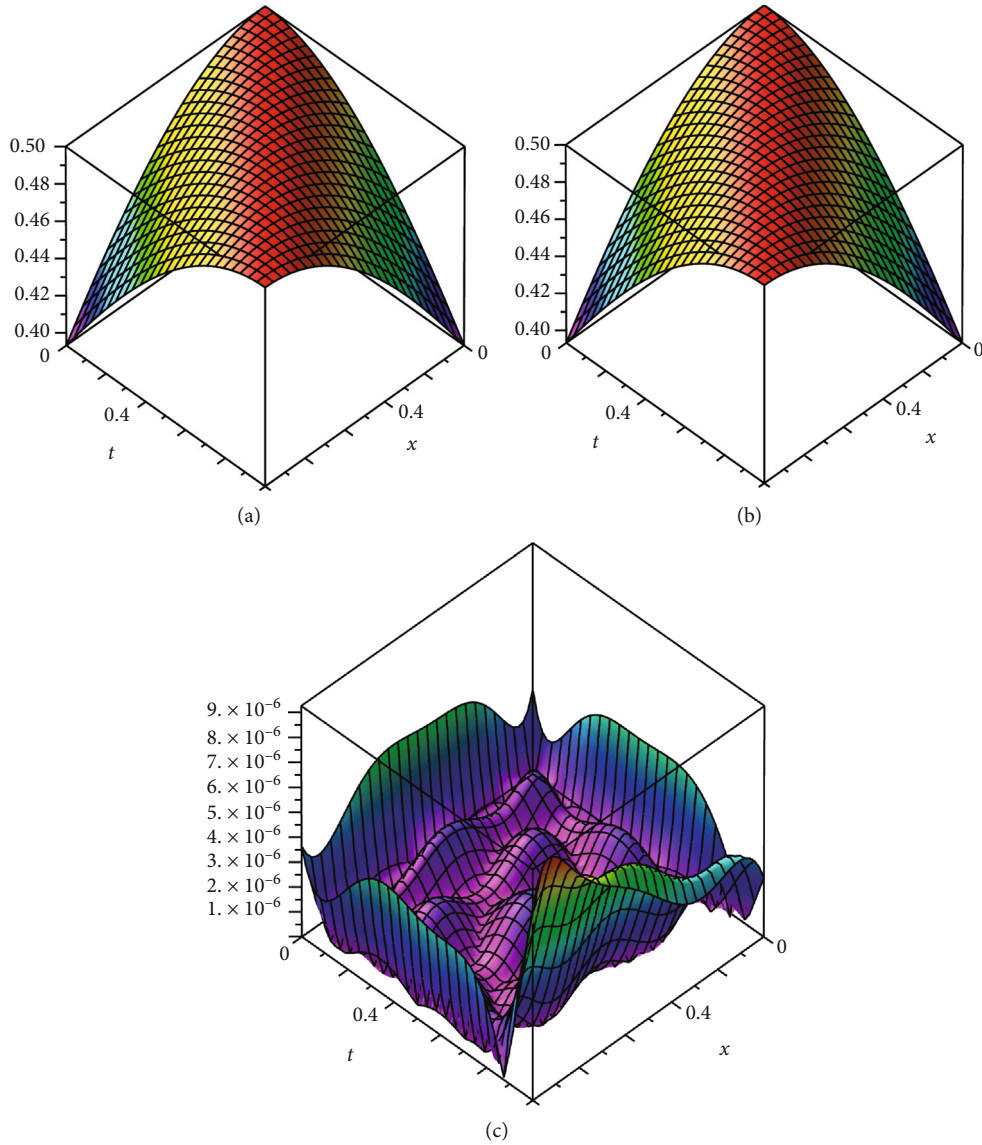


FIGURE 2: (a) Exact solution, (b) approximate solution, and (c) absolute error function for $k_1 = k_2 = 1, M_1 = M_2 = 5,$ and $\mu = 1$ for Example 2.

following equation:

$$\begin{aligned} \mathcal{R}_{\mathcal{M}_1, \mathcal{M}_2}(\theta, \vartheta) = & \left({}_0^C \mathcal{D}_\vartheta^\mu \mathbf{u}(\theta, \vartheta) - {}_0^C \mathcal{D}_\vartheta^\mu \mathbf{u}_{\mathcal{M}_1, \mathcal{M}_2}(\theta, \vartheta) \right) \\ & + 6 \left(\mathbf{u}(\theta, \vartheta) \frac{\partial \mathbf{u}(\theta, \vartheta)}{\partial \theta} - \mathbf{u}_{\mathcal{M}_1, \mathcal{M}_2}(\theta, \vartheta) \frac{\partial \mathbf{u}_{\mathcal{M}_1, \mathcal{M}_2}(\theta, \vartheta)}{\partial \theta} \right) \\ & + \left(\frac{\partial^3 \mathbf{u}(\theta, \vartheta)}{\partial \theta^3} - \frac{\partial^3 \mathbf{u}_{\mathcal{M}_1, \mathcal{M}_2}(\theta, \vartheta)}{\partial \theta^3} \right). \end{aligned} \quad (43)$$

The nonlinear term $\mathbf{u} \mathbf{u}_\theta - \mathbf{u}_{\mathcal{M}_1, \mathcal{M}_2} \mathbf{u}_{\theta, \mathcal{M}_1, \mathcal{M}_2}$ can be written as

$$\begin{aligned} \mathbf{u} \mathbf{u}_\theta - \mathbf{u}_{\mathcal{M}_1, \mathcal{M}_2} \mathbf{u}_{\theta, \mathcal{M}_1, \mathcal{M}_2} = & (\mathbf{u} - \mathbf{u}_{\mathcal{M}_1, \mathcal{M}_2}) \mathbf{u}_\theta \\ & + (\mathbf{u}_\theta - \mathbf{u}_{\theta, \mathcal{M}_1, \mathcal{M}_2}) \mathbf{u}_{\mathcal{M}_1, \mathcal{M}_2} = (\mathbf{u} - \mathbf{u}_{\mathcal{M}_1, \mathcal{M}_2}) (\mathbf{u}_\theta - \mathbf{u}_{\theta, \mathcal{M}_1, \mathcal{M}_2} + \mathbf{u}_{\theta, \mathcal{M}_1, \mathcal{M}_2}) \\ & + (\mathbf{u}_\theta - \mathbf{u}_{\theta, \mathcal{M}_1, \mathcal{M}_2}) \mathbf{u}_{\mathcal{M}_1, \mathcal{M}_2} = (\mathbf{u} - \mathbf{u}_{\mathcal{M}_1, \mathcal{M}_2}) (\mathbf{u}_\theta - \mathbf{u}_{\theta, \mathcal{M}_1, \mathcal{M}_2}) \\ & + (\mathbf{u} - \mathbf{u}_{\mathcal{M}_1, \mathcal{M}_2}) \mathbf{u}_{\theta, \mathcal{M}_1, \mathcal{M}_2} + (\mathbf{u}_\theta - \mathbf{u}_{\theta, \mathcal{M}_1, \mathcal{M}_2}) \mathbf{u}_{\mathcal{M}_1, \mathcal{M}_2}. \end{aligned} \quad (44)$$

Now, using bounds obtained in the previous section, an error bound of (42) can be calculated as follows:

$$\begin{aligned} \|\mathcal{R}_{\mathcal{M}_1, \mathcal{M}_2}\|_{L^2} \leq & \frac{\pi \Theta_1}{\mathcal{M}_1! (\mathcal{M}_2 - \mu)! 2^{\mathcal{M}_1(\mathfrak{k}_1 - 1)} 2^{\mathcal{M}_2(\mathfrak{k}_2 - 1)} 2^3} \\ & + 6 \left[\frac{\pi \Theta_{2,0}}{\mathcal{M}_1! \mathcal{M}_2! 2^{\mathcal{M}_1(\mathfrak{k}_1 - 1)} 2^{\mathcal{M}_2(\mathfrak{k}_2 - 1)} 2^3} \right. \\ & \times \left(\frac{\pi \Theta_{2,1}}{(\mathcal{M}_1 - 1)! \mathcal{M}_2! 2^{\mathcal{M}_1(\mathfrak{k}_1 - 1)} 2^{\mathcal{M}_2(\mathfrak{k}_2 - 1)} 2^3} + \|\mathbf{u}_{\theta, \mathcal{M}_1, \mathcal{M}_2}\|_{L^2} \right) \\ & \left. + \frac{\pi \Theta_{2,1} \|\mathbf{u}_{\mathcal{M}_1, \mathcal{M}_2}\|_{L^2}}{(\mathcal{M}_1 - 1)! \mathcal{M}_2! 2^{\mathcal{M}_1(\mathfrak{k}_1 - 1)} 2^{\mathcal{M}_2(\mathfrak{k}_2 - 1)} 2^3} \right] \\ & + \frac{\pi \Theta_{2,3} \|\mathbf{u}_{\mathcal{M}_1, \mathcal{M}_2}\|_{L^2}}{(\mathcal{M}_1 - 3)! \mathcal{M}_2! 2^{\mathcal{M}_1(\mathfrak{k}_1 - 1)} 2^{\mathcal{M}_2(\mathfrak{k}_2 - 1)} 2^3}. \end{aligned} \quad (45)$$

Obviously, the right-hand side of (44) tends to zero, when $\mathcal{M}_1, \mathcal{M}_2$ are sufficiently large.

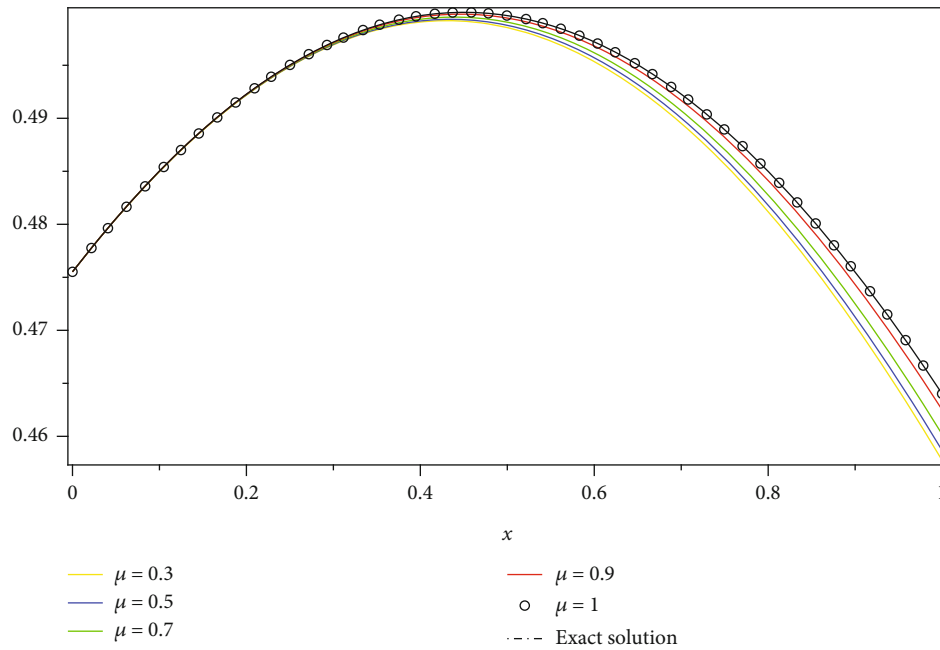


FIGURE 3: Exact and approximate solutions for $k_1 = k_2 = 1, M_1 = M_2 = 6$, and $\mu = 0.3, 0.5, 0.7, 0.9, 1$ at time $\vartheta = 0.45$ for Example 2.

TABLE 3: Absolute errors for $k_1 = k_2 = 1, M_1 = M_2 = 6$ at equally spaced points for Example 2.

$\theta_i = \vartheta_i$	$\mu = 0.3$	$\mu = 0.5$	$\mu = 0.7$	$\mu = 0.9$	$\mu = 1$
0	6.6378×10^{-8}	6.8466×10^{-8}	5.5505×10^{-8}	2.4525×10^{-8}	1.3170×10^{-9}
0.2	8.6724×10^{-5}	6.7852×10^{-5}	4.4262×10^{-5}	1.5860×10^{-5}	3.1335×10^{-9}
0.4	6.5214×10^{-4}	5.1748×10^{-4}	3.4307×10^{-4}	1.2522×10^{-4}	3.7353×10^{-10}
0.6	2.0195×10^{-3}	1.6274×10^{-3}	1.0975×10^{-3}	4.0827×10^{-4}	1.2169×10^{-8}
0.8	4.2767×10^{-3}	3.5051×10^{-3}	2.4073×10^{-3}	9.1284×10^{-4}	3.0611×10^{-8}
1	7.2448×10^{-3}	6.0506×10^{-3}	4.2372×10^{-3}	1.6379×10^{-3}	4.9306×10^{-8}

5. Numerical Examples

The two models given in Section 3 are considered to illustrate the accuracy and applicability of the proposed scheme. Maximum absolute errors are computed when the derivative order is an integer (classical case). The results are compared to the exact ones. Computations and simulations are handled by Maple 16.

Example 1. As a first example, the following linear inhomogeneous time-fractional KdV equation:

$${}_0^C \mathcal{D}_\vartheta^\mu \mathbf{u}(\theta, \vartheta) + \frac{\partial \mathbf{u}(\theta, \vartheta)}{\partial \theta} + \frac{\partial^3 \mathbf{u}(\theta, \vartheta)}{\partial \theta^3} = \frac{2\vartheta^{2-\mu}}{\Gamma(3-\mu)} \cos(\theta), (\theta, \vartheta) \in \mathbf{J}, \quad \mu \in (0, 1], \tag{46}$$

subject to the initial and boundary conditions:

$$\mathbf{u}(\theta, 0) = 0, \mathbf{u}(0, \vartheta) = 0, \frac{\partial \mathbf{u}(0, \vartheta)}{\partial \theta} = 0, \frac{\partial^2 \mathbf{u}(0, \vartheta)}{\partial \theta^2} = 0. \tag{47}$$

The exact solution is $\mathbf{u}(\theta, \vartheta) = \vartheta^2 \cos(\theta)$, if $\mu = 1$. Maximum absolute errors (MAE) are listed in Table 1 for $\mu = 1, \mathfrak{K}_1 = \mathfrak{K}_2 = 1, \mathcal{M}_1 = \mathcal{M}_2 = 2, 3, 4, 5$. As seen, the errors decrease when $\mathcal{M}_1, \mathcal{M}_2$ increase. Values of absolute errors of the exact and numerical solutions, at equally spaced points $\theta_i = \vartheta_j = 0.2i, i = 0, 1, \dots, 5$, are seen in Table 2 for $\mathfrak{K}_1 = \mathfrak{K}_2 = 1, \mathcal{M}_1 = \mathcal{M}_2 = 4, \mu = 0.7, 0.8, 0.9, 1$. The results have more accuracy as $\mu \rightarrow 1$. Plots of numerical solutions are depicted in Figure 1 for $\mathfrak{K}_1 = \mathfrak{K}_2 = 1, \mathcal{M}_1 = \mathcal{M}_2 = 4, \mu = 0.7, 0.8, 0.9, 1$, and $\vartheta = 3$. It can be found that the approximate solutions approach the exact one when $\mu \rightarrow 1$.

Example 2. Consider the time-fractional nonlinear KdV equation as follows:

$${}_0^C \mathcal{D}_\vartheta^\mu \mathbf{u}(\theta, \vartheta) + 6\mathbf{u}(\theta, \vartheta) \frac{\partial \mathbf{u}(\theta, \vartheta)}{\partial \theta} + \frac{\partial^3 \mathbf{u}(\theta, \vartheta)}{\partial \theta^3} = 0, (\theta, \vartheta) \in \mathbf{J}, \quad \mu \in (0, 1], \tag{48}$$

with

$$\begin{aligned} u(\theta, 0) &= \frac{1}{2} \sec h^2\left(\frac{\theta}{2}\right), u(0, \vartheta) = \frac{1}{2} \sec h^2\left(\frac{\vartheta}{2}\right), \frac{\partial u(0, \vartheta)}{\partial \theta} = \frac{1}{2} \sec h^2\left(\frac{\vartheta}{2}\right) \tanh\left(\frac{\vartheta}{2}\right), \\ \frac{\partial^2 u(0, \vartheta)}{\partial \theta^2} &= \frac{1}{2} \sec h^2\left(\frac{\vartheta}{2}\right) \tanh^2\left(\frac{\vartheta}{2}\right) + \frac{1}{2} \sec h^2\left(\frac{\vartheta}{2}\right) \left(-\frac{1}{2} + \frac{1}{2} \tanh^2\left(\frac{\vartheta}{2}\right)\right). \end{aligned} \quad (49)$$

The exact solution is $u(\theta, \vartheta) = (1/2) \sec h^2(\theta/2 - \vartheta/2)$, if $\mu = 1$. Plots of exact and approximate solutions and the absolute error function are depicted in Figure 2 for $\mathfrak{k}_1 = \mathfrak{k}_2 = 1$, $\mathcal{M}_1 = \mathcal{M}_2 = 5$, and $\mu = 1$. A graphical comparison between exact and approximate solutions is observed in Figure 3 for $\mathfrak{k}_1 = \mathfrak{k}_2 = 1$; $\mathcal{M}_1 = \mathcal{M}_2 = 4$; $\mu = 0.3, 0.5, 0.7, 0.9, 1$; and $\vartheta = 0.45$. It can be found that the approximate solutions approach the exact one when $\mu \rightarrow 1$. Values of absolute errors are listed in Table 3 for $\mathcal{M}_1 = \mathcal{M}_2 = 6$; $\mu = 0.3, 0.5, 0.7, 0.9, 1$; and $\theta_i = \vartheta_i = 0.2i, i = 0, 1, \dots, 5$. It can be seen from Figure 3 and Table 3 that the approximate solutions approach the exact one when $\mu \rightarrow 1$.

6. Conclusion

In this paper, the second-kind Chebyshev wavelets were employed to solve time-fractional inhomogeneous KdV and time-fractional nonlinear KdV equations. Using the presented scheme, the main problem was converted into a system of algebraic equations wherein obtaining its solution is easier than finding the solution of the problem under study. In comparison with the Adomian decomposition, homotopy analysis, and homotopy perturbation methods, the SKCW method possesses fewer computational costs. The few numbers of the basis functions lead to an approximate solution with appropriate accuracy. As seen from Table 1, by increasing values of $\mathcal{M}_i, i = 1, 2$, the maximum absolute errors decrease. In Tables 2 and 3, values of absolute errors at equally spaced points decrease as $\mu \rightarrow 1$; then, approximate solutions are getting close to exact ones. This can be seen in Figures 1 and 3. It was seen from illustrative examples that the method is an efficient numerical scheme to find an approximate solution for linear or nonlinear PDEs. The authors intend to test the proposed approach on other nonlinear fractional partial differential equations such as Newell–Whitehead–Segel and Phi-four.

Data Availability

Data are available on request.

Conflicts of Interest

The authors declare that they have no competing interests.

Acknowledgments

We would like to thank the reviewers for their thoughtful comments and efforts toward improving our manuscript.

References

- [1] J. M. Cruz-Duarte, J. R. Garcia, C. R. Correa-Cely, A. G. Perez, and J. G. Avina-Cervantes, "A closed form expression for the Gaussian-based Caputo-Fabrizio fractional derivative for signal processing applications," *Communications in Nonlinear Science and Numerical Simulation*, vol. 61, pp. 138–148, 2018.
- [2] A. Esen, T. A. Sulaiman, H. Bulut, and H. M. Baskonus, "Optical solitons to the space-time fractional (1+1)-dimensional coupled nonlinear Schrödinger equation," *Optik*, vol. 167, pp. 150–156, 2018.
- [3] N. H. Sweilam, M. M. A. Hasan, and D. Baleanu, "New studies for general fractional financial models of awareness and trial advertising decisions," *Chaos, Solitons and Fractals*, vol. 104, pp. 772–784, 2017.
- [4] D. Baleanu, G. C. Wu, and S. D. Zeng, "Chaos analysis and asymptotic stability of generalized Caputo fractional differential equations," *Chaos, Solitons and Fractals*, vol. 102, pp. 99–105, 2017.
- [5] P. Veerasha, D. G. Prakasha, and H. M. Baskonus, "New numerical surfaces to the mathematical model of cancer chemotherapy effect in Caputo fractional derivatives," *Chaos*, vol. 29, no. 1, article 013119, 2019.
- [6] K. S. Miller and B. Ross, *An Introduction to Fractional Calculus and Fractional Differential Equations*, Wiley, New York, NY, USA, 1993.
- [7] I. Podlubny, *Fractional Differential Equations*, Academic Press, New York, NY, USA, 1999.
- [8] A. A. Kilbas, H. M. Srivastava, and J. J. Trujillo, *Theory and Applications of Fractional Differential Equations*, Elsevier, Amsterdam, The Netherlands, 2006.
- [9] S. T. Abdulazeez and M. Modanli, "Solutions of fractional order pseudo-hyperbolic telegraph partial differential equations using finite difference method," *Alexandria Engineering Journal*, vol. 61, no. 12, pp. 12443–12451, 2022.
- [10] W. Sawangtong and P. Sawangtong, "An analytical solution for the Caputo type generalized fractional evolution equation," *Alexandria Engineering Journal*, vol. 61, no. 7, pp. 5475–5483, 2022.
- [11] R. Gorenflo and E. A. Abdel-Rehim, "Convergence of the Grunwald-Letnikov scheme for time-fractional diffusion," *Journal of computational and applied mathematics*, vol. 205, no. 2, pp. 871–881, 2007.
- [12] N. H. M. Shahen, M. H. Bashar, and M. S. Ali, "Dynamical analysis of long-wave phenomena for the nonlinear conformable space-time fractional (2 + 1)-dimensional AKNS equation in water wave mechanics," *Heliyon*, vol. 6, article e05276, 2020.
- [13] C. D. Vinodbhai and S. Dubey, "Investigation to analytic solutions of modified conformable time-space fractional mixed partial differential equations," *Partial Differential Equations in Applied Mathematics*, vol. 5, article 100294, 2022.
- [14] M. Abu-Shady and M. K. A. Kaabar, "A generalized definition of the fractional derivative with applications," *Mathematical Problems in Engineering*, vol. 2021, Article ID 9444803, 9 pages, 2021.
- [15] M. Abu-Shady and M. K. A. Kaabar, "A novel computational tool for the fractional-order special functions arising from modeling scientific phenomena via Abu-Shady–Kaabar fractional derivative," *Computational and Mathematical Methods in Medicine*, vol. 2022, Article ID 2138775, 5 pages, 2022.

- [16] K. S. Miller and B. Ross, *An Introduction to the Fractional Calculus and Fractional Differential Equations*, John Wiley and Sons, New York, 1993.
- [17] V. Lakshmikantham, S. Leela, and J. Vasundhara Devi, *Theory of Fractional Dynamic Systems*, Cambridge Academic, Cambridge, 2009.
- [18] B. West, M. Bologna, and P. Grigolini, *Physics of Fractal Operators*, Springer, New York, 2003.
- [19] S. G. Samko, A. A. Kilbas, and O. I. Marichev, *Fractional Integrals and Derivatives: Theory and Applications*, Gordon and Breach, Yverdon, 1993.
- [20] D. J. Korteweg and G. de Vries, "XLI. On the change of form of long waves advancing in a rectangular canal, and on a new type of long stationary waves," *Philosophical Magazine*, vol. 39, no. 240, pp. 422–443, 1895.
- [21] M. Bagheri and A. Khani, "Analytical method for solving the fractional order generalized KdV equation by a beta-fractional derivative," *Advances in Mathematical Physics*, vol. 2020, Article ID 8819183, 18 pages, 2020.
- [22] J. Liu, L. Yang, and K. Yang, "Jacobi elliptic function solutions of some nonlinear PDEs," *Physics Letters A*, vol. 325, no. 3-4, pp. 268–275, 2004.
- [23] L. Akinyemi and O. S. Iyiola, "A reliable technique to study nonlinear time-fractional coupled Korteweg–de Vries equations," *Advances in Difference equations*, vol. 2020, no. 1, Article ID 169, 2020.
- [24] Z. Z. Ganji, D. D. Ganji, and Y. Rostamiyan, "Solitary wave solutions for a time-fraction generalized Hirota–Satsuma coupled KdV equation by an analytical technique," *Applied Mathematical Modelling*, vol. 33, no. 7, pp. 3107–3113, 2009.
- [25] S. Sahoo and S. Saha Ray, "Solitary wave solutions for time fractional third order modified KdV equation using two reliable techniques (G'/G)-expansion method and improved (G'/G)-expansion method," *Physica A: Statistical Mechanics and its Applications*, vol. 448, pp. 265–282, 2016.
- [26] D. Kaya, S. Gülbahar, A. Yokuş, and M. Gülbahar, "Solutions of the fractional combined KdV–mKdV equation with collocation method using radial basis function and their geometrical obstructions," *Advances in Difference Equations*, vol. 2018, no. 1, Article ID 77, 6 pages, 2018.
- [27] S. Momani, Z. Odibat, and A. Alawneh, "Variational iteration method for solving the space- and time-fractional KdV equation," *Numerical Methods for Partial Differential Equations: An International Journal*, vol. 24, no. 1, pp. 262–271, 2008.
- [28] H. Thabet, S. Kendre, and J. Peters, "Traveling wave solutions for fractional Korteweg–de Vries equations via an approximate-analytical method," *AIMS Mathematics*, vol. 4, no. 4, 2019.
- [29] X. J. Yang, J. A. T. Machado, D. Baleanu, and C. Cattani, "On exact traveling-wave solutions for local fractional Korteweg–de Vries equation," *Chaos*, vol. 26, no. 8, 2016.
- [30] B. R. Sontakke, A. Shaikh, and K. S. Nisar, "Approximate solutions of a generalized Hirota–Satsuma coupled KdV and a coupled mKdV systems with time fractional derivatives," *Malaysian Journal of Mathematical Sciences*, vol. 12, no. 2, pp. 175–196, 2018.
- [31] D. D. Ganji and M. Rafei, "Solitary wave solutions for a generalized Hirota–Satsuma coupled KdV equation by homotopy perturbation method," *Physics Letters A*, vol. 356, no. 2, pp. 131–137, 2006.
- [32] S. Abbasbandy, "The application of homotopy analysis method to solve a generalized Hirota–Satsuma coupled KdV equation," *Physics Letters A*, vol. 361, no. 6, pp. 478–483, 2007.
- [33] Z. Guo-Zhong, Y. Xi-Jun, X. Yun, Z. Jiang, and W. Di, "Approximate analytic solutions for a generalized Hirota–Satsuma coupled KdV equation and a coupled mKdV equation," *Chinese Physics B*, vol. 19, no. 8, article 080204, 2010.
- [34] Q. Wang, "Homotopy perturbation method for fractional KdV equation," *Applied Mathematics and Computation*, vol. 190, no. 2, pp. 1795–1802, 2007.
- [35] S. Nemati, S. Sedaghat, and I. Mohammadi, "A fast numerical algorithm based on the second kind Chebyshev polynomials for fractional integro-differential equations with weakly singular kernels," *Journal of Computational and Applied Mathematics*, vol. 308, pp. 231–242, 2016.
- [36] K. Maleknejad, S. Sohrabi, and Y. Rostami, "Numerical solution of nonlinear Volterra integral equations of the second kind by using Chebyshev polynomials," *Applied Mathematics and Computation*, vol. 188, no. 1, pp. 123–128, 2007.
- [37] L. Zhu and Q. Fan, "Solving fractional nonlinear Fredholm integro-differential equations by the second kind Chebyshev wavelet," *Communications in nonlinear science and numerical simulation*, vol. 17, no. 6, pp. 2333–2341, 2012.
- [38] Y. Wang and Q. Fan, "The second kind Chebyshev wavelet method for solving fractional differential equations," *Applied Mathematics and Computation*, vol. 218, no. 17, pp. 8592–8601, 2012.
- [39] O. Baghani, "Second Chebyshev wavelets (SCWs) method for solving finite-time fractional linear quadratic optimal control problems," *Mathematics and Computers in Simulation*, vol. 190, pp. 343–361, 2021.
- [40] F. Zhou and X. Xu, "Numerical solution of the convection diffusion equations by the second kind Chebyshev wavelets," *Applied Mathematics and Computation*, vol. 247, pp. 353–367, 2014.
- [41] A. K. Gupta and S. Saha Ray, "Numerical treatment for the solution of fractional fifth-order Sawada–Kotera equation using second kind Chebyshev wavelet method," *Applied Mathematical Modelling*, vol. 39, no. 17, pp. 5121–5130, 2015.
- [42] J. Biazar and K. Sadri, "Two-variable Jacobi polynomials for solving some fractional partial differential equations," *Journal of Computational Mathematics*, vol. 38, no. 6, pp. 849–873, 2020.
- [43] S. A. El-Wakil, E. M. Abulwafa, M. A. Zahran, and A. A. Mahmoud, "Time-fractional KdV equation: formulation and solution using variational methods," *Nonlinear Dynamics*, vol. 65, no. 1-2, pp. 55–63, 2011.
- [44] S. A. El-Wakil, E. M. Abulwafa, E. K. El-Shewy, and A. A. Mahmoud, "Time-fractional KdV equation for plasma of two different temperature electrons and stationary ion," *Physics of Plasmas*, vol. 18, no. 9, article 092116, 2011.
- [45] M. Inc, M. Parto-Haghighi, M. A. Akinlar, and Y. M. Chu, "New numerical solutions of fractional-order Korteweg–de Vries equation," *Results in Physics*, vol. 19, article 103326, 2020.
- [46] A. Taqi, M. Shallal, and B. Jomaa, "Soliton solutions for space-time fractional Korteweg–de Vries equation," in *2019 International Conference on Computing and Information Science and Technology and Their Applications (ICCISTA)*, Kirkuk, Iraq, 2019.

- [47] H. U. Rehman, M. Inc, M. I. Asjad, and A. Habib, "New soliton solutions for the space-time fractional modified third order Korteweg–de Vries equation," *Journal of Ocean Engineering and Science*, 2022.
- [48] E. M. Ozkan and A. Ozkan, "Bright soliton solutions for time fractional Korteweg–de Vries equation," in *International Conference on Analysis and Applied Mathematics*, Mersin, Turkey, 2020.

Research Article

An Efficient Numerical Scheme for Solving Multiorder Tempered Fractional Differential Equations via Operational Matrix

Abiodun Ezekiel Owoyemi ^{1,2}, Chang Phang ¹, and Yoke Teng Toh ³

¹Department of Mathematics and Statistics, Universiti Tun Hussein Onn Malaysia, Johor, Malaysia

²Department of General Studies, Federal College of Agricultural Produce Technology, Kano, Nigeria

³Faculty of Civil Engineering and Built Environment, Universiti Tun Hussein Onn Malaysia, Johor, Malaysia

Correspondence should be addressed to Chang Phang; pchang@uthm.edu.my

Received 12 July 2022; Revised 22 August 2022; Accepted 29 August 2022; Published 19 September 2022

Academic Editor: Arzu Akbulut

Copyright © 2022 Abiodun Ezekiel Owoyemi et al. This is an open access article distributed under the Creative Commons Attribution License, which permits unrestricted use, distribution, and reproduction in any medium, provided the original work is properly cited.

In this paper, we extend the operational matrix method to solve the tempered fractional differential equation, via shifted Legendre polynomial. Although the operational matrix method is widely used in solving various fractional calculus problems, it is yet to apply in solving fractional differential equations defined in the tempered fractional derivatives. We first derive the analytical expression for tempered fractional derivative for x^p , hence, using it to derive the new operational matrix of fractional derivative. By using a few terms of shifted Legendre polynomial and via collocation scheme, we were able to obtain a good approximation for the solution of the multiorder tempered fractional differential equation. We illustrate it using some numerical examples.

1. Introduction

Tempered fractional calculus is a type of fractional derivative/integral operator which multiplies an exponential factor to its power law kernel. This type of exponential tempering had been received increasing attention from researchers as having both mathematical and practical advantages [1, 2]. Several phenomena were best described by using this tempered fractional derivative/integral operator such as tempered fractional Brownian motion [3], epidemic modelling [4], and diffusion-wave equation [5]. Besides that, the tempered fractional model also been proven superior to the standard mechanism-based models in an experiment for quantifying colloid fate and transport in complex soil-vegetation systems [6].

In this research direction, reliable numerical schemes are needed to obtain the approximation solution for tempered fractional differential equations. This is because normally there are no exact solution or the analytical solution for these tempered fractional differential equations is difficult to obtain. To date, limited researches are done to tackle this

problem, which include third-order semidiscretized schemes [7], two-dimensional Gegenbauer wavelets method [8], predictor-corrector scheme [9], and finite difference iterative method [10]. However, some of the established numerical schemes which already been successfully applied to solve fractional differential equations in the Caputo sense are still not been employed to solve these tempered fractional differential equations, which include the operational matrix method. Hence, in this paper, we aim to develop a reliable numerical scheme that involves an operational matrix via shifted Legendre polynomial to tackle this tempered fractional differential equation. The tempered fractional differential equations will be transformed into a system of algebraic equations; then, solving the system of algebraic equation will solve multiorder tempered fractional differential equations as follows:

$$\sum_{r=1}^l q_r^T D_x^{(\alpha_r, \beta_r)} f(x) = h(x), \quad (1)$$
$$f^{(i)}(0) = d_i, \quad i = 0, 1, \dots, m-1,$$

where $f(x)$ is the unknown solution, ${}^T D_x^{(\alpha_r, \beta_r)}$ is tempered fractional derivatives, $q_r \in \mathbb{R}, r = 1, \dots, l$ are constants, and $\alpha_r, \beta_r \geq 0$ are real derivative orders which β denotes the tempered coefficient, while $h(x)$ is the unhomogeneous terms.

To date, various numerical or analytical methods were derived to find the solution for different fractional calculus problems, such as [11–13]. On top of that, the operational matrix method via different types of the polynomial is one of the common numerical schemes which had been widely used in solving various types of fractional calculus problems, such as the poly-Bernoulli operational matrix for solving fractional delay differential equation [14], poly-Genocchi operational matrix for solving fractional differential equation [15], Jacobi wavelet operational matrix of fractional integration for solving fractional integro-differential equation [16], and Fibonacci wavelet operational matrix of integration for solving of non-linear Stratonovich Volterra integral equations [17]. Recently, the operational matrix method had been successfully extended to solve other fractional operator problems, such as solving Prabhakar fractional differential equation [18]. Although the operational matrix method is widely used in solving various fractional calculus problems, it is yet to apply in solving fractional differential equations defined in the tempered fractional derivatives. Hence, we hope it can fill in this research gap. The main advantages of using this operational matrix method over other existing methods are its simplicity of implementation and programmable easily in using any computer algebra system. Besides that, if the fractional differential equations are in multiorder or having variable coefficients, operational matrix method is also efficient in finding the numerical solution.

The rest of this paper is as follows. Section 2 discusses some important concepts for tempered fractional calculus. Section 3 presents the shifted Legendre operational matrix for tempered fractional derivative and is followed by the procedure of solving tempered fractional differential equation via collocation scheme using this new shifted Legendre operational matrix. Some numerical examples and conclusion are presented in Sections 4 and 5.

2. Some Concepts regarding Tempered Fractional Calculus

Definition 1 (see [19, 20]). For $\alpha \in [0, 1]$ and $\alpha, \beta \in \mathbb{C}$ where $\text{Re}(\alpha) > 0, \text{Re}(\beta) \geq 0$, the tempered fractional integral of order (α, β) for a function $f \in L^1[a, b]$ is given by

$$\begin{aligned}
 {}^T I_x^{(\alpha, \beta)} f(x) &= \frac{1}{\Gamma(\alpha)} \int_0^x (x-u)^{\alpha-1} e^{-\beta(x-u)} f(u) du \\
 &= \frac{e^{-\beta x}}{\Gamma(\alpha)} \int_0^x (x-u)^{\alpha-1} e^{\beta u} f(u) du, x \in [a, b].
 \end{aligned}
 \tag{2}$$

Definition 2 (see [20]). For $\alpha, \beta \in \mathbb{C}$ where $\text{Re}(\alpha) > 0, \text{Re}(\beta) \geq 0$, the Riemann-Liouville tempered fractional derivative of order (α, β) for a function $f \in L^1[a, b]$ is given by

$$\begin{aligned}
 {}^{RL} D_x^{(\alpha, \beta)} f(x) &= e^{-\beta x} \left({}^T D_x^{(\alpha)} e^{\beta x} f(x) \right) \\
 &= \frac{e^{-\beta x}}{\Gamma(n-\alpha)} \frac{d^n}{dx^n} \int_0^x (x-u)^{n-\alpha-1} e^{\beta(u)} f(u) du, x \in [a, b],
 \end{aligned}
 \tag{3}$$

where $n = [\alpha] + 1$ and $[\alpha]$ is integer part of α .

For Caputo type of tempered fractional derivative, we take the derivative of the function under the integral (3), and we obtain Definition 3.

Definition 3 (see [20]). For $\alpha, \beta \in \mathbb{C}$ where $\text{Re}(\alpha) > 0, \text{Re}(\beta) \geq 0$. The Caputo tempered fractional derivative of order (α, β) for a function $f \in L^1[a, b]$ is given by

$${}^{CT} D_x^{(\alpha, \beta)} f(x) = \frac{1}{\Gamma(n-\alpha)} \int_0^x (x-u)^{n-\alpha-1} \frac{d^n e^{\beta(u)} f(u)}{du^n} du, x \in [a, b],
 \tag{4}$$

where $n = [\alpha] + 1$ and $[\alpha]$ is integer part of α .

The relationship between the tempered fractional derivative and tempered fractional integral is given by

$${}^T D_x^{(\alpha, \beta)} f(x) = \left(\frac{d}{dx} + \beta \right)^n \left({}^T I_x^{(n-\alpha, \beta)} f(x) \right),
 \tag{5}$$

where $n = [\text{Re}(\alpha)] + 1$.

The tempered fractional derivative for function x^p , where p is integer positive, we obtain

$$\begin{aligned}
 {}^T D_x^{(\alpha, \beta)} x^p &= \frac{e^{-\beta x}}{\Gamma(n-\alpha)} \int_0^x (x-u)^{n-\alpha-1} \frac{d^n}{du^n} \left(e^{\beta u} u^p \right) du, x \in [a, b], \\
 &= \frac{e^{-\beta x}}{\Gamma(n-\alpha)} \int_0^x (x-u)^{n-\alpha-1} \frac{d^n}{du^n} \sum_{k=0}^{\infty} \frac{\beta^k u^{k+p}}{k!} du \\
 &= \frac{e^{-\beta x}}{\Gamma(n-\alpha)} \int_0^x (x-u)^{n-\alpha-1} \sum_{k=0}^{\infty} \frac{\beta^k \Gamma(k+p+1)}{k! \Gamma(k+p+1-n)} u^{k+p-n} du \\
 &= \frac{e^{-\beta x}}{\Gamma(n-\alpha)} \sum_{k=0}^{\infty} \frac{\beta^k}{k!} \frac{\Gamma(k+p+1)}{\Gamma(k+p+1-n)} \int_0^x (x-u)^{n-\alpha-1} u^{k+p-n} du.
 \end{aligned}
 \tag{6}$$

By using integration $\int_0^x (x-t)^{a-1} t^{b-1} dt = B(a, b) x^{a+b-1} = (\Gamma(a)\Gamma(b)/\Gamma(a+b)) x^{a+b-1}$ where $B(a, b)$ is beta function and $a, b > 0$, we obtain

$$\begin{aligned}
 {}^T D_x^{(\alpha, \beta)} x^p &= \frac{e^{-\beta x}}{\Gamma(n-\alpha)} \sum_{k=0}^{\infty} \frac{\beta^k}{k!} \frac{\Gamma(k+p+1)}{\Gamma(k+p-n+1)} \frac{\Gamma(n-\alpha)\Gamma(k+p-n+1)}{\Gamma(n-\alpha+k+p-n+1)} x^{n-\alpha+k+p-n} \\
 &= e^{-\beta x} \sum_{k=0}^{\infty} \frac{\beta^k}{k!} \frac{\Gamma(k+p+1)}{\Gamma(k+p-\alpha+1)} x^{k+p-\alpha}.
 \end{aligned}
 \tag{7}$$

For the function $f(x) = (x - a)^p$ with $\text{Re}(p) > -1$, we have [21],

$$T_a D_x^{(\alpha, \beta)} (x - a)^k = (x - a)^{k - \alpha} \frac{\Gamma(k + 1)}{\Gamma(k - \alpha + 1)} F_1(-\alpha; k - \alpha + 1; -\beta(x - a)). \tag{8}$$

Here, we take k as positive integer number. For $a = 0$, both expressions in (7) and (8) have the same result.

While using (8) to derive the operational matrix, we need the following results related to the hypergeometric function:

$${}_1F_1(a; c; x) = \sum_{k=0}^{\infty} \frac{\Gamma(a + k)}{\Gamma(a)} \frac{\Gamma(c)}{\Gamma(c + k)} \frac{x^k}{k!}, \tag{9}$$

$${}_2F_2(a, b; c, d; x) = \sum_{k=0}^{\infty} \frac{\Gamma(a + k)}{\Gamma(a)} \frac{\Gamma(b + k)}{\Gamma(b)} \frac{\Gamma(c)}{\Gamma(c + k)} \frac{\Gamma(d)}{\Gamma(d + k)} \frac{x^k}{k!}, \tag{10}$$

$$\int_0^1 F_1(a; c; x) dx = \frac{c - 1}{a - 1} F_1(a - 1; c - 1; x), \tag{11}$$

$$\int_0^1 x^l F_1(a; c; mx) dx = \frac{1}{l + 1} F_2(a, l + 1; c, l + 2; m). \tag{12}$$

In another aspect, the solution for single tempered fractional differential equation, i.e., ${}^T D_x^{\alpha, \beta} y(x) = \kappa y(x) + h(x)$ for $\alpha \in (0, 1]$, $\beta > 0$, and the initial condition is $y(0) = y_0$ can be expressed as follows [20]:

$$y(x) = y_0 e^{-\beta x} E_{\alpha, 1}(\kappa x^\alpha) + \int_0^x h(x - s) e^{-\beta s} s^{\alpha - 1} E_{\alpha, \alpha}(\kappa s^\alpha) ds. \tag{13}$$

where $E_{\alpha, b}(x) = \sum_{k=0}^{\infty} x^k / \Gamma(\alpha k + b)$. However, this type of solution may fail when there are involving multiorder tempered fractional differential equations. Hence, we proposed to solve these multiorder tempered fractional differential equations via collocation scheme using shifted Legendre operational matrix. Other types of polynomials can be used also to derive the new operational matrix to tackle the tempered fractional derivative.

3. Shifted Legendre Operational Matrix for Tempered Fractional Derivative

3.1. Shifted Legendre Polynomials. The Legendre polynomials is an orthogonal polynomial on the interval $[-1, 1]$. One of the ways to obtain Legendre polynomials is via recurrence relation as follows:

$$L_{i+1}(t) = \frac{2i + 1}{i + 1} t L_i(t) - \frac{i}{i + 1} L_{i-1}(t), i = 1, 2, \dots, \tag{14}$$

where $L_0(t) = 1$ and $L_1(t) = t$. The Legendre polynomials in domain $[-1, 1]$ can be transformed into the domain of $[0, 1]$ by using $t = 2x - 1$, which we get shifted Legendre polynomials, $\tilde{L}_i(x)$ as follows:

$$\tilde{L}_{i+1}(x) = \frac{(2i + 1)(2x - 1)}{i + 1} \tilde{L}_i(x) - \frac{i}{i + 1} \tilde{L}_{i-1}(x), i = 1, 2, \dots, \tag{15}$$

where $\tilde{L}_0(x) = 1$ and $\tilde{L}_1(x) = 2x - 1$. Besides that, the shifted Legendre polynomials $\tilde{L}_i(x)$ of degree i can be obtained via the analytical form:

$$\tilde{L}_i(x) = \sum_{k=0}^i (-1)^{i+k} \frac{(i + k)! x^k}{(i - k)! (k!)^2}, i = 0, 1, 2, \dots, \tag{16}$$

where $\tilde{L}_i(0) = (-1)^i$ and $\tilde{L}_i(1) = 1$. The orthogonality condition is

$$\int_0^1 \tilde{L}_i(x) \tilde{L}_j(x) dx = \begin{cases} \frac{1}{2i + 1}, & \text{for } i = j, \\ 0, & \text{for } i \neq j. \end{cases} \tag{17}$$

The shifted Legendre polynomials have a nice property that is useful for function approximation. In this case, a square integrable function $f(x) \in L^2[0, 1]$ can be expressed in terms of shifted Legendre polynomials as follows:

$$f(x) = \sum_{j=0}^{\infty} c_j \tilde{L}_j(x), \tag{18}$$

where the coefficients c_j are given by

$$c_j = (2j + 1) \int_0^1 f(x) \tilde{L}_j(x) dx, j = 0, 1, 2, \dots. \tag{19}$$

In order to use equation (18) to approximate the function, normally, we truncated after $(N + 1)$ terms shifted Legendre polynomials as follows:

$$f_N^*(x) = \sum_{j=0}^N c_j \tilde{L}_j(x) = C^T \Phi_L(x), \tag{20}$$

where the shifted Legendre coefficient vector, C is given by $C^T = [c_0, c_1, \dots, c_N]$ and the shifted Legendre vector, $\Phi_L(x)$ can be expressed as

$$\Phi_L(x) = [\tilde{L}_0(x), \tilde{L}_1(x), \dots, \tilde{L}_N(x)]^T. \tag{21}$$

3.2. Shifted Legendre Polynomial Operational Matrix. In this subsection, we derive the new shifted Legendre operational matrix for tackling tempered fractional derivative. We have the following theorem.

Theorem 4. Let $\Phi_{\tilde{L}}(x)$ be the shifted Legendre vector as shown in (20). For $n - 1 < \alpha < n, n \in \mathbb{N}$, then,

$${}^T_0 D_x^{(\alpha, \beta)} \Phi_{\tilde{L}}(x) = \mathbf{P}_{x; \tilde{L}}^{\alpha, \beta} \Phi(x), \quad (22)$$

where $\mathbf{P}_x^{\alpha, \beta}$ is the $N \times N$ operational matrix of tempered fractional derivative of order α, β defined as

$$\mathbf{P}_x^{\alpha, \beta} = \begin{bmatrix} 0 & 0 & \cdots & 0 \\ \vdots & \vdots & \cdots & \vdots \\ 0 & 0 & \cdots & 0 \\ \sum_{k=\lceil \alpha \rceil}^{\lceil \alpha \rceil} \xi_{\lceil \alpha \rceil, 0, k} & \sum_{k=\lceil \alpha \rceil}^{\lceil \alpha \rceil} \xi_{\lceil \alpha \rceil, 1, k} & \cdots & \sum_{k=\lceil \alpha \rceil}^{\lceil \alpha \rceil} \xi_{\lceil \alpha \rceil, N-1, k} \\ \vdots & \vdots & \cdots & \vdots \\ \sum_{k=\lceil \alpha \rceil}^i \xi_{i, 0, k} & \sum_{k=\lceil \alpha \rceil}^i \xi_{i, 1, k} & \cdots & \sum_{k=\lceil \alpha \rceil}^i \xi_{i, N-1, k} \\ \vdots & \vdots & \cdots & \vdots \\ \sum_{k=\lceil \alpha \rceil}^{N-1} \xi_{N-1, 0, k} & \sum_{k=\lceil \alpha \rceil}^{N-1} \xi_{N-1, 1, k} & \cdots & \sum_{k=\lceil \alpha \rceil}^{N-1} \xi_{N-1, N-1, k} \end{bmatrix}, \quad (23)$$

where $\xi_{i,j,k}$ is given by

$$\xi_{i,j,k} = (2j + 1) \frac{(-1)^{i+k} (i+k)!}{(i-k)! k! (k-\alpha)!} \sum_{l=0}^j \frac{(-1)^{j+l} (j+l)!}{(j-l)! l!^2 (1+k-\alpha+l)} \times {}_2F_2(-\alpha, 1+k-\alpha+l; k-\alpha+1, 2+k-\alpha+l; -\beta), \quad (24)$$

where $i = \lceil \alpha \rceil, \dots, N-1, j = 0, 1, 2, \dots, N-1$.

Proof. By using equation (8) and letting $a = 0$, the tempered fractional derivative for x^k is given as follows:

$${}^T_0 D_x^{(\alpha, \beta)} x^k = x^{k-\alpha} \frac{\Gamma(k+1)}{\Gamma(k-\alpha+1)_1} F_1(-\alpha; k-\alpha+1; -\beta x). \quad (25)$$

□

Using the expression as in (25), the explicit expression of tempered fractional derivative of the i -th degree shifted Legendre polynomials which is the $(i+1)$ -th element of $\Phi_{\tilde{L}}(x)$ is computed:

$$\begin{aligned} {}^T_0 D_x^{(\alpha, \beta)} \tilde{L}_i(x) &= \sum_{k=0}^i \frac{(-1)^{i+k} (i+k)!}{(i-k)! k!^2} \left({}^T_0 D_x^{(\alpha, \beta)} x^k \right), \quad i = 0, 1, 2, \dots \\ &= \sum_{k=\lceil \alpha \rceil}^i \frac{(-1)^{i+k} (i+k)!}{(i-k)! k!^2} \left[x^{k-\alpha} \frac{\Gamma(k+1)}{\Gamma(k-\alpha+1)_1} F_1(-\alpha; k-\alpha+1; -\beta x) \right] \\ &= \sum_{k=\lceil \alpha \rceil}^i \frac{(-1)^{i+k} (i+k)!}{(i-k)! k!} \left[\frac{x^{k-\alpha}}{\Gamma(k-\alpha+1)_1} F_1(-\alpha; k-\alpha+1; -\beta x) \right]. \end{aligned} \quad (26)$$

The elements $\rho_{i,j}$ of the operational matrix $\mathbf{P}_{x; \tilde{L}}^{\alpha, \beta}$ are computed by taking inner product for the tempered fractional derivative of shifted Legendre polynomials, ${}^T_0 D_x^{(\alpha, \beta)} \tilde{L}_i(x)$ with shifted Legendre polynomials, $\tilde{L}_j(x), j = 0, 1, \dots, N-1$:

$${}^T_0 D_x^{(\alpha, \beta)} \tilde{L}_i(x) = \sum_{j=0}^{N-1} \rho_{i,j} \tilde{L}_j(x), \quad (27)$$

$$\rho_{i,j} = \left\langle {}^T_0 D_x^{(\alpha, \beta)} \tilde{L}_i(x), \tilde{L}_j(x) \right\rangle = \sum_{k=\lceil \alpha \rceil}^i \frac{(-1)^{i+k} (i+k)!}{(i-k)! k!} \left[\frac{1}{\Gamma(k-\alpha+1)} \left\langle x^{k-\alpha} {}_1F_1(-\alpha; k-\alpha+1; -\beta x), \tilde{L}_j(x) \right\rangle \right], \quad (28)$$

where the inner product can be computed as follows

$$\begin{aligned} \left\langle x^{k-\alpha} {}_1F_1(-\alpha; k-\alpha+1; -\beta x), \tilde{L}_j(x) \right\rangle &= (2j+1) \int_0^1 x^{k-\alpha} {}_1F_1(-\alpha; k-\alpha+1; -\beta x) \sum_{l=0}^j \frac{(-1)^{j+l} (j+l)!}{(j-l)! l!^2} x^l dx \\ &= (2j+1) \sum_{l=0}^j \frac{(-1)^{j+l} (j+l)!}{(j-l)! l!^2} \int_0^1 x^{k-\alpha} {}_1F_1(-\alpha; k-\alpha+1; -\beta x) x^l dx \\ &= (2j+1) \sum_{l=0}^j \frac{(-1)^{j+l} (j+l)!}{(j-l)! l!^2} \left(\frac{{}_2F_2(-\alpha, 1+k-\alpha+l; k-\alpha+1, 2+k-\alpha+l; -\beta)}{1+k-\alpha+l} \right). \end{aligned} \quad (29)$$

The integration in (29) can be obtained via the formula in (10). Putting equation (29) into (28), we obtain

$$\begin{aligned} \rho_{i,j} &= \left\langle {}^T_0 D_x^{(\alpha, \beta)} \tilde{L}_i(x), \tilde{L}_j(x) \right\rangle \\ &= \sum_{k=\lceil \alpha \rceil}^i \frac{(-1)^{i+k} (i+k)!}{(i-k)! k!} \left[\frac{(2j+1)}{\Gamma(k-\alpha+1)} \right. \\ &\quad \times \left. \sum_{l=0}^j \frac{(-1)^{j+l} (j+l)!}{(j-l)! l!^2} \left(\frac{{}_2F_2(-\alpha, 1+k-\alpha+l; k-\alpha+1, 2+k-\alpha+l; -\beta)}{1+k-\alpha+l} \right) \right] \\ &= (2j+1) \sum_{k=\lceil \alpha \rceil}^i \frac{(-1)^{i+k} (i+k)!}{(i-k)! k! (k-\alpha)!} \sum_{l=0}^j \frac{(-1)^{j+l} (j+l)!}{(j-l)! l!^2 (1+k-\alpha+l)} \\ &\quad \times {}_2F_2(-\alpha, 1+k-\alpha+l; k-\alpha+1, 2+k-\alpha+l; -\beta). \end{aligned} \quad (30)$$

Setting $\rho_{i,j} = \sum_{k=\lceil \alpha \rceil}^i \xi_{i,j,k}$

$$\begin{aligned} \xi_{i,j,k} &= (2j+1) \frac{(-1)^{i+k} (i+k)!}{(i-k)! k! (k-\alpha)!} \sum_{l=0}^j \frac{(-1)^{j+l} (j+l)!}{(j-l)! l!^2 (1+k-\alpha+l)} \\ &\quad \times {}_2F_2(-\alpha, 1+k-\alpha+l; k-\alpha+1, 2+k-\alpha+l; -\beta). \end{aligned} \quad (31)$$

Hence, each element of shifted Legendre operational matrix for tempered fractional derivative is obtained.

To test the accuracy of the operational matrix derived in Theorem 4, we use it to approximate tempered fractional derivative for $\tilde{L}_2(x) = 6x^2 - 6x + 1$ and $\tilde{L}_3(x) = 20x^3 - 30x^2$

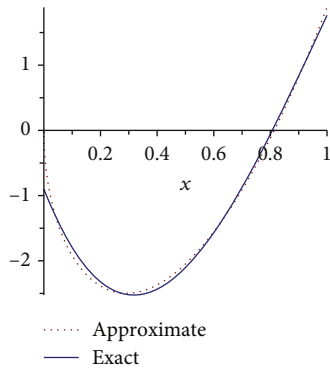


FIGURE 1: Comparison of the exact solution and approximation for $\tilde{L}_2(x)$.

+ 12x - 1. For $N = 4$, we obtain the following operational matrix $\mathbf{P}_x^{\alpha,\beta}$ when $\alpha = 1/2, \beta = 1$,

$$\begin{bmatrix} 0.0 & 0.0 & 0.0 & 0.0, \\ 1.786057010727 & 1.257808290370 & -0.157033776306 & 0.090092226619, \\ -1.257808290370 & 1.678966426855 & 1.690298665024 & -0.345920769399, \\ 1.629023234421 & -0.432490374653 & 2.103160984111 & 2.122192953652. \end{bmatrix} \quad (32)$$

Figures 1 and 2 show the comparison between the exact solution for tempered fractional derivative for $\tilde{L}_2(x)$ and $\tilde{L}_3(x)$ with the approximation using operational matrix as in (32). Accuracy of the approximate can be increased with increasing the N .

4. Solving Tempered Fractional Differential Equation Using Shifted Legendre Operational Matrix Method and Error Analysis

This section consists of an explanation for the proposed method that combines collocation scheme with shifted Legendre polynomials operational matrix of tempered fractional derivative to solve multiorder tempered fractional differential equations.

$$\sum_{r=1}^l q_r {}^T D_x^{(\alpha_r, \beta_r)} f(x) = h(x), \quad (33)$$

$$f^{(i)}(0) = d_i, \quad i = 0, 1, \dots, m - 1.$$

Here, we present the general procedure for solving multiorder tempered fractional differential equations as in equation (33) via shifted Legendre operational matrix.

Step 1. The unknown function, i.e., the solution, $f(x)$ is approximated by truncated shifted Legendre polynomials,

$$f(x) \approx f_N(x) \approx \mathbf{C}^T \tilde{\mathbf{L}}(x), \quad (34)$$

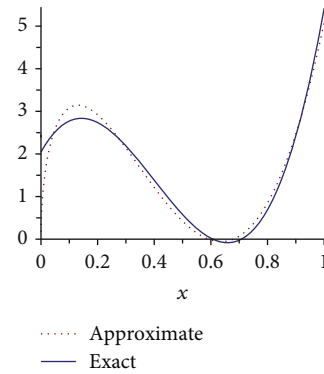


FIGURE 2: Comparison of the exact solution and approximation for $\tilde{L}_3(x)$.

where $\mathbf{C}^T = [c_0, c_1, c_2, \dots, c_N]$. The tempered fractional derivative of equation (33) is approximated using the shifted Legendre operational matrix of tempered fractional derivative as in equations (22)–(24).

$${}^T D_x^{(\alpha, \beta)} f(x) \approx \mathbf{C}^T \mathbf{P}_{x; \tilde{L}}^{(\alpha, \beta)} \Phi_{\tilde{L}}(x). \quad (35)$$

Remark 5. The function, $h(x)$ in the RHS of equation (33) can also approximated in term of truncated shifted Legendre polynomials as follows:

$$h(x) \approx \mathbf{H}^T \Phi_{\tilde{L}}(x), \quad (36)$$

where $\mathbf{H} = [h_i]^T$ and the coefficients h_i are computed using equation (19). However, to increase the accuracy of the method and also increase speed of its computer implementation, collocation scheme can be applied directly to these known functions.

Step 2. From Step 1, the following is obtained:

$$\sum_{r=1}^l q_r \Phi_{\tilde{L}}^T(x) \left(\mathbf{P}_{x; \tilde{L}}^{(\alpha_r, \beta_r)} \right)^T \mathbf{C} = h(x). \quad (37)$$

After some algebraic manipulations, we obtain $\Phi_{\tilde{L}}^T(x) \left(\sum_{r=1}^l q_r \left(\mathbf{P}_{x; \tilde{L}}^{(\alpha_r, \beta_r)} \right)^T \mathbf{C} \right) - h(x) = 0$. Thus, the residual is

$$\mathcal{R}(x) = \Phi_{\tilde{L}}^T(x) \left(\sum_{r=1}^l q_r \left(\mathbf{P}_{x; \tilde{L}}^{(\alpha_r, \beta_r)} \right)^T \mathbf{C} \right) - h(x) = 0. \quad (38)$$

Step 3. Due to the set of shifted Legendre polynomials basis, $\Phi_{\tilde{L}}^T(x) = [\tilde{L}_0(x)\tilde{L}_1(x) \dots \tilde{L}_N(x)]$ is linearly independent, we obtain

$$\Phi_{\tilde{L}}^T(x) \sum_{r=1}^l q_r \left(\mathbf{P}_{x; \tilde{L}}^{(\alpha_r, \beta_r)} \right)^T \mathbf{C} = h(x). \quad (39)$$

We obtain a system of $N + 1$ algebraic equations from equation (39). The initial condition in equation (33) is also approximated in term of shifted Legendre polynomials:

$$\begin{aligned} f^{(i)}(0) &= d_i, i = 0, \dots, m - 1, \\ \Phi_{\bar{L}}^T(0) \left(\mathbf{P}_{0+\bar{L}}^i \right)^T \mathbf{C} &= d_i. \end{aligned} \quad (40)$$

Step 4. Select $N - m$ equations from equation (39) and combine with initial conditions from equation (40), we obtain a system of N linear algebraic equations in term of \mathbf{C} . Hence, solve the system with using any suitable numerical methods. Then, the approximate solution can be computed by following equation:

$$f^*(x) = \mathbf{C}^T \Phi_{\bar{L}}(x). \quad (41)$$

4.1. Error Analysis. To discuss the error analysis for our method, we follow the approach done in [22] where the alternating Legendre polynomials are applied to derive the operational matrix to solve the fractional differential equations problem defined in the classical Caputo sense.

Lemma 6. Suppose that $f(x) \in C^{n+1}(\Theta)$ and $f(x) \approx f_N(x) \approx \mathbf{C}^T \tilde{\mathbf{L}}(x)$ be its expansion in terms of shifted Legendre polynomials, as described by equation (34). Then

$$\|f(x) - f_N(x)\|_2 \leq \frac{M}{(N+1)!2^{2N+1}}, \quad (42)$$

where M is a constant such that $|f^{(N+1)}(x)| \leq M$.

Proof. Assume that $s_n(x)$ is the interpolating polynomials to $f(x)$ at points x_j , where x_j be the roots of the shifted Chebyshev polynomials of degree $n + 1$, then

$$f(x) - s_n(x) = \frac{f^{(n+1)}(\zeta_x)}{(n+1)!} \prod_{j=0}^n (x - x_j), \zeta_x \in \Theta = [0, 1]. \quad (43)$$

As proof in [22], the above approximation has the bound as follows:

$$|f(x) - s_n(x)| \leq \frac{M}{(n+1)!2^{2n+1}}, \forall x \in \Theta. \quad (44)$$

Then, we have

$$\begin{aligned} \|f(x) - f_N(x)\|_2^2 &\leq \|f(x) - s_N(x)\|_2^2 \\ &= \int_0^1 \|f(x) - s_N(x)\|^2 dx = \int_0^1 \left(\frac{M}{(N+1)!2^{2N+1}} \right)^2 dx \\ &= \left(\frac{M}{(N+1)!2^{2N+1}} \right)^2. \end{aligned} \quad (45)$$

TABLE 1: Absolute errors obtained by proposed method with $N = 4, 6$ for Example 1.

x	Exact solution	Abs. error ($N = 4$)	Abs. error ($N = 6$)
0.1	0.402	1.61661E-02	2.72390E-03
0.2	0.816	1.87810E-02	6.74832E-03
0.3	1.254	1.25442E-02	6.06411E-03
0.4	1.728	2.15555E-02	1.63810E-03
0.5	2.250	7.68546E-02	2.20223E-03
0.6	2.832	1.22791E-02	1.38416E-03
0.7	3.486	6.92580E-03	4.29494E-03
0.8	4.224	1.30742E-02	7.55223E-03
0.9	5.058	5.24204E-02	9.99599E-03
1.0	6.000	1.15813E-02	8.14496E-02

Hence, take the square root of both sides, we obtain

$$\|f(x) - f_N(x)\|_2 \leq \frac{M}{(N+1)!2^{2N+1}}. \quad (46)$$

This completes the proof. \square

In order to perform the error estimation for this new numerical scheme, we apply residual correction procedure. From equation (39), i.e., $\mathcal{R}(x) = \Phi_{\bar{L}}^T(x) \left(\sum_{r=1}^l q_r \left(\mathbf{P}_{x;\bar{L}}^{(\alpha_r, \beta_r)} \right)^T \mathbf{C} \right) - h(x) = 0$, hence

$$\Phi_{\bar{L}}^T(x) \left(\sum_{r=1}^l q_r \left(\mathbf{P}_{x;\bar{L}}^{(\alpha_r, \beta_r)} \right)^T \mathbf{C} \right) - h(x) = 0. \quad (47)$$

If $N \rightarrow \infty$, using the operational matrix via shifted Legendre polynomials to approximate multiorder tempered fractional derivative and approximate $h(x)$ via shifted Legendre polynomials, we obtain

$$\left| \Phi_{\bar{L}}^T(x) \sum_{r=1}^l q_r \left(\mathbf{P}_{x;\bar{L}}^{(\alpha_r, \beta_r)} \right)^T_{(N \times N)} - \sum_{r=1}^l q_r {}^T D_x^{(\alpha_r, \beta_r)} f(x) \right| \approx 0, N \rightarrow \infty. \quad (48)$$

For our proposed method, N is finite. Hence, suppose m term of shifted Legendre polynomials had been used, then, small error, e_m , is inevitable.

$$\sum_{r=1}^l \left| D_x^{(\alpha_r, \beta_r)} f(x) - \mathbf{P}_{x;\bar{L}}^{(\alpha_r, \beta_r)} \right|_2 = e_m, N = m. \quad (49)$$

Let e_m^* is the approximation solution of equation (1) obtained by the shifted Legendre operational matrix method, if $\|e_m - e_m^*\| < \varepsilon$ is sufficiently small; then, the absolute errors e_m can be estimated by e_m^* . Hence, we obtain the optimal value m (i.e., N).

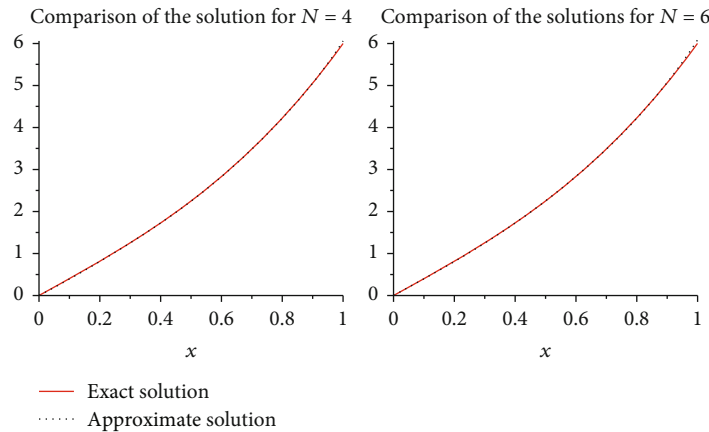


FIGURE 3: The comparison result of the approximate and exact solutions for Example 1 ($N = 4, 6$).

TABLE 2: Absolute errors obtained by proposed method with $N = 6, 8$ for Example 2.

x	Exact solution	Abs. error ($N = 6$)	Abs. error ($N = 8$)
0.1	0.00002	6.44679E-05	2.57668E-07
0.2	0.00064	2.17039E-05	4.92156E-07
0.3	0.00486	8.06877E-06	6.44773E-07
0.4	0.02048	3.64403E-06	5.63021E-07
0.5	0.06250	3.18313E-05	5.17865E-07
0.6	0.15552	3.62011E-05	3.12227E-07
0.7	0.33614	5.94866E-07	9.34225E-07
0.8	0.65536	3.47375E-05	2.46696E-07
0.9	1.18098	7.69841E-05	8.54648E-08
1.0	2.00000	6.15397E-04	4.12816E-05

5. Numerical Examples

In this section, we will apply the new operational matrix for tempered fractional derivative to solve the tempered fractional differential equations.

Example 1. Consider the multiorder tempered fractional differential equation as follows:

$$\begin{aligned}
 & {}_0^T D_x^{(1/2,1/2)} y(x) + {}_0^T D_x^{(1/2,1/4)} y(x) \\
 &= x^2 y(x) - 2x^5 - 4x^3 + \sqrt{2}(x^3 + 3x^2 - x \\
 &+ 5) \operatorname{erf}\left(\sqrt{\frac{x}{2}}\right) + \frac{2x}{\sqrt{\pi x}} e^{-x/2}(x^2 + 2x - 1) \\
 &+ (x^3 + 6x^2 - 10x + 28) \operatorname{erf}\left(\frac{\sqrt{x}}{2}\right) \\
 &+ \frac{2x}{\sqrt{\pi x}} e^{-x/4}(x^2 + 4x - 10),
 \end{aligned} \tag{50}$$

with initial condition $y(0) = 0$. The exact solution is known as $y(x) = 2x^3 + 4x$.

Solution: by using $N = 4, 6$, we have the following numerical result as shown in Table 1 and Figure 3. Only using few terms of shifted Legendre polynomials, we were able to obtain good result for this multiorder tempered fractional differential equation.

Example 2. Consider a simple tempered fractional differential equation as follows:

$$\begin{aligned}
 & {}_0^T D_x^{(1/2,3/4)} y(x) \\
 &= -2.0 x^{15/2} + 1.128379167 e^{-0.75x} x^5 + 3.009011112 e^{-0.75x} x^4 \\
 &+ 1.732050807 x^{11/2} \operatorname{erf}(0.8660254038 \sqrt{x}) \\
 &+ 5.773502692 x^{9/2} \operatorname{erf}(0.8660254038 \sqrt{x}) \\
 &- 6.018022225 e^{-0.75x} x^3 \\
 &- 7.698003593 x^{7/2} \operatorname{erf}(0.8660254038 \sqrt{x}) \\
 &+ 15.39600718 x^{5/2} \operatorname{erf}(0.8660254038 \sqrt{x}) \\
 &+ 13.37338272 e^{-0.75x} x^2 \\
 &- 25.66001197 x^{3/2} \operatorname{erf}(0.8660254038 \sqrt{x}) \\
 &+ 23.94934450 \operatorname{erf}(0.8660254038 \sqrt{x}) \\
 &\cdot \sqrt{x} - 23.40341976 e^{-0.75x} x,
 \end{aligned} \tag{51}$$

with initial condition $y(0) = 0$. The exact solution is known as $y(x) = 2x^5$.

Solution: by using $N = 6, 8$, we have the following numerical result as shown in Table 2 and Figure 4. Again, by only using few terms of shifted Legendre polynomials, we were able to obtain good result for this tempered fractional differential equation.

Example 3. Consider the tempered fractional differential equation taken from [23] as follows:

$${}_0^T D_x^{(\alpha,\beta)} y(x) = e^{-\beta x} \left(\frac{\Gamma(6)}{\Gamma(6-\alpha)} x^{5-\alpha} - e^{-\beta x} x^{10} + e^{\beta x} y^2(x) \right), 0 < \alpha < 1, \tag{52}$$

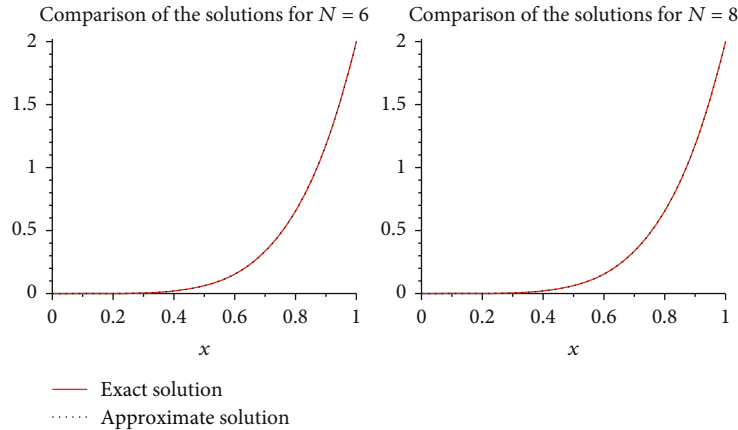


FIGURE 4: The comparison result of the approximate and exact solutions for Example 2 ($N = 6, 8$).

TABLE 3: Comparison of errors for proposed method with Jacobi-predictor-corrector algorithm [23] for Example 3 with $\alpha = 0.4$.

β	N	Max abs. error	Stepsize (iteration)	Error
0	6	1.06818E-04	1/10	2.4208E-04
0	8	4.10270E-06	1/20	4.9371E-06
0	10	3.37294E-07	1/40	1.0390E-07
3	6	2.43410E-04	1/10	7.4482E-07
3	8	8.27866E-06	1/20	6.8759E-08
3	10	4.77932E-07	1/40	3.1715E-09

TABLE 4: Relative absolute errors obtained by proposed method with $N = 6, 8, 10$ for Example 4.

x	Exact solution	RAE ($N = 6$)	RAE ($N = 8$)	RAE ($N = 10$)
0.2	0.0725173321	1.80058E-03	9.61065E-04	2.41946E-04
0.4	0.2620226201	1.09846E-04	6.15192E-05	9.17638E-06
0.6	0.5332522504	2.56602E-04	4.80993E-05	2.88812E-05
0.8	0.8586273304	7.19889E-04	7.26678E-05	2.39416E-06

with initial condition $dy(0)/dx = 0$. The exact solution is given as $y(x) = e^{-\beta x} x^5$. This can be verified by using the procedure as in equations (6) and (7), where ones should get

$${}_0^T D_x^{(\alpha, \beta)} e^{-\beta x} x^p = \frac{p+1}{\Gamma(p-\alpha+1)} e^{-\beta x} x^{p-\alpha}, \alpha > -1. \quad (53)$$

Solution: by using $N = 6, 8, 10$ and $\alpha = 0.4$, we have the following numerical result for $\beta = 0, 3$, as shown in Table 3. We compare our solution with Jacobi-predictor-corrector algorithm [23]. Again, only using few terms of shifted Legendre polynomials, we were able to obtain good results compare with Jacobi-predictor-corrector algorithm. More specifically, say if $N = 10$ has been used, the size of each subinterval is 0.1, which is equivalent to the iteration Jacobi-predictor-corrector algorithm with stepsize 1/10. For $\beta = 3$, our absolute error is 4.779320E-07, ($N = 10$), which is comparable with 7.4482E-07, stepsize = 1/10.

Example 4. Consider the multiorder tempered fractional differential equation as follows:

$${}_0^T D_x^{(0.5, 0.5)} y(x) + {}_0^T D_x^{(0.25, 0.5)} y(x) = \frac{16 e^{-x/2} x^{3/2}}{3 \sqrt{\pi}} + \frac{64 e^{-x/2} x^{7/4}}{21 \sqrt{3/4}}, \quad (54)$$

with initial condition $y(0) = 0$. The exact solution is given as $y(x) = 2e^{-x/2} x^2$.

Solution: by using $N = 6, 8, 10$, we have the following numerical result as shown in Table 4. Again, for the relative absolute errors presented, it is obvious that by only using few terms of shifted Legendre polynomials via its operational matrix, we able to obtain good results for this multiorder tempered fractional differential equations.

6. Conclusion

In this paper, we manage to derive a new operational matrix for tempered fractional derivatives. Hence, we use it to solve tempered fractional differential equations. The proposed method is easy to apply and yet able to give accurate results. The accuracy of the method can be improved by increasing the number of the term of shifted Legendre polynomials. The proposed method should extend to solve some other tempered fractional calculus problems, such as tempered fractional partial differential equations. Besides that, this operational matrix also can be extended to solve other kinds of fractional calculus problems such as those in [24–27].

Data Availability

No data were used to support this study.

Conflicts of Interest

There is no conflicts of interest.

References

- [1] N. A. Obeidat and D. E. Benti, "New theories and applications of tempered fractional differential equations," *Nonlinear Dynamics*, vol. 105, no. 2, pp. 1689–1702, 2021.
- [2] F. Sabzikar, M. M. Meerschaert, and J. Chen, "Tempered fractional calculus," *Journal of Computational Physics*, vol. 293, pp. 14–28, 2015.
- [3] M. M. Meerschaert and F. Sabzikar, "Tempered fractional Brownian motion," *Statistics & Probability Letters*, vol. 83, no. 10, pp. 2269–2275, 2013.
- [4] Y. Wang, L. Zhang, and Y. Yuan, "Tempered fractional order compartment models and applications in biology," *Discrete & Continuous Dynamical Systems-B*, vol. 27, no. 9, p. 5297, 2022.
- [5] P. Verma and M. Kumar, "Exact solution with existence and uniqueness conditions for multi-dimensional time-space tempered fractional diffusion-wave equation," *Engineering with Computers*, vol. 38, no. 1, pp. 271–281, 2022.
- [6] C. Yu, S. Wei, Y. Zhang et al., "Quantifying colloid fate and transport through dense vegetation and soil systems using a particle-plugging tempered fractional-derivative model," *Journal of Contaminant Hydrology*, vol. 224, article 103484, 2019.
- [7] L. Bu and C. W. Oosterlee, "On high-order schemes for tempered fractional partial differential equations," *Applied Numerical Mathematics*, vol. 165, pp. 459–481, 2021.
- [8] A. Rayal and S. R. Verma, "Two-dimensional Gegenbauer wavelets for the numerical solution of tempered fractional model of the nonlinear Klein-Gordon equation," *Applied Numerical Mathematics*, vol. 174, pp. 191–220, 2022.
- [9] M. Saedshoar Heris and M. Javidi, "A predictor-corrector scheme for the tempered fractional differential equations with uniform and non-uniform meshes," *The Journal of Supercomputing*, vol. 75, no. 12, pp. 8168–8206, 2019.
- [10] Z. Luo and H. Ren, "A reduced-order extrapolated finite difference iterative method for the Riemann-Liouville tempered fractional derivative equation," *Applied Numerical Mathematics*, vol. 157, pp. 307–314, 2020.
- [11] Y. T. Toh, C. Phang, and Y. X. Ng, "Temporal discretization for Caputo-Hadamard fractional derivative with incomplete gamma function via Whittaker function," *Computational and Applied Mathematics*, vol. 40, no. 8, 2021.
- [12] M. Naeem, H. Rezazadeh, A. A. Khammash, R. Shah, and S. Zaland, "Analysis of the fuzzy fractional-order solitary wave solutions for the KdV equation in the sense of Caputo-Fabrizio derivative," *Journal of Mathematics*, vol. 2022, Article ID 3688916, 12 pages, 2022.
- [13] N. H. Aljahdaly, R. Shah, M. Naeem, and M. A. Arefin, "A comparative analysis of fractional space-time advection-dispersion equation via semianalytical methods," *Journal of Function Spaces*, vol. 2022, Article ID 4856002, 11 pages, 2022.
- [14] C. Phang, Y. T. Toh, and F. S. Md Nasrudin, "An operational matrix method based on poly-Bernoulli polynomials for solving fractional delay differential equations," *Computation*, vol. 8, no. 3, p. 82, 2020.
- [15] C. Phang, A. Isah, and Y. T. Toh, "Poly-Genocchi polynomials and its applications," *AIMS Mathematics*, vol. 6, no. 8, pp. 8221–8238, 2021.
- [16] L. J. Rong and P. Chang, "Jacobi wavelet operational matrix of fractional integration for solving fractional integro-differential equation," *Journal of Physics: Conference Series*, vol. 693, article 012002, 2016.
- [17] S. Shiralashetti and L. Lamani, "Fibonacci wavelet based numerical method for the solution of nonlinear Stratonovich Volterra integral equations," *Scientific African*, vol. 10, article e00594, 2020.
- [18] F. S. Md Nasrudin and C. Phang, "Numerical solution via operational matrix for solving Prabhakar fractional differential equations," *Journal of Mathematics*, vol. 2022, Article ID 7220433, 7 pages, 2022.
- [19] C. Çelik and M. Duman, "Finite element method for a symmetric tempered fractional diffusion equation," *Applied Numerical Mathematics*, vol. 120, pp. 270–286, 2017.
- [20] B. P. Moghaddam, J. Machado, and A. Babaei, "A computationally efficient method for tempered fractional differential equations with application," *Computational and Applied Mathematics*, vol. 37, no. 3, pp. 3657–3671, 2018.
- [21] A. Fernandez and C. Ustaoglu, "On some analytic properties of tempered fractional calculus," *Journal of Computational and Applied Mathematics*, vol. 366, article 112400, 2020.
- [22] Z. Meng, M. Yi, J. Huang, and L. Song, "Numerical solutions of nonlinear fractional differential equations by alternative Legendre polynomials," *Applied Mathematics and Computation*, vol. 336, pp. 454–464, 2018.
- [23] C. Li, W. Deng, and L. Zhao, "Well-posedness and numerical algorithm for the tempered fractional ordinary differential equations," *Discrete and Continuous Dynamical System Series B*, vol. 24, no. 4, pp. 1989–2015, 2019.
- [24] J. R. Loh, C. Phang, and K. G. Tay, "New method for solving fractional partial integro-differential equations by combination of Laplace transform and resolvent kernel method," *Chinese Journal of Physics*, vol. 67, pp. 666–680, 2020.
- [25] X. Wang, X.-G. Yue, M. K. Kaabar, A. Akbulut, and M. Kaplan, "A unique computational investigation of the exact traveling wave solutions for the fractional-order Kaup-Boussinesq and generalized Hirota Satsuma coupled KdV systems arising from water waves and interaction of long waves," *Journal of Ocean Engineering and Science*, 2022.
- [26] E. Fendzi-Donfack, D. Kumar, E. Tala-Tebue, L. Nana, J. P. Nguenang, and A. Kenfack-Jiotsa, "Construction of exotical soliton-like for a fractional nonlinear electrical circuit equation using differential-difference Jacobi elliptic functions sub-equation method," *Results in Physics*, vol. 32, article 105086, 2022.
- [27] F. Mofarreh, A. Zidan, M. Naeem, R. Shah, R. Ullah, and K. Nonlaopon, "Analytical analysis of fractional-order physical models via a Caputo-Fabrizio operator," *Journal of Function Spaces*, vol. 2021, Article ID 7250308, 9 pages, 2021.

Research Article

The Fractional Series Solutions for the Conformable Time-Fractional Swift-Hohenberg Equation through the Conformable Shehu Daftardar-Jafari Approach with Comparative Analysis

Muhammad Imran Liaqat ¹ and Eric Okyere ²

¹National College of Business Administration & Economics, Lahore, Pakistan

²Department of Mathematics and Statistics, University of Energy and Natural Resources, Sunyani, Ghana

Correspondence should be addressed to Eric Okyere; eric.okyere@uenr.edu.gh

Received 10 August 2022; Revised 29 August 2022; Accepted 3 September 2022; Published 15 September 2022

Academic Editor: Arzu Akbulut

Copyright © 2022 Muhammad Imran Liaqat and Eric Okyere. This is an open access article distributed under the Creative Commons Attribution License, which permits unrestricted use, distribution, and reproduction in any medium, provided the original work is properly cited.

The major objective of this study is to derive fractional series solutions of the time-fractional Swift-Hohenberg equations (TFSHEs) in the sense of conformable derivative using the conformable Shehu transform (CST) and the Daftardar-Jafari approach (DJA). We call it the conformable Shehu Daftardar-Jafari approach (CSDJA). One of the universal equations used in the description of pattern formation in spatially extended dissipative systems is the Swift-Hohenberg equation. To assess the effectiveness and consistency of the suggested approach, the numerical results are compared with those obtained by the Elzaki decomposition method (EDM) in the sense of relative and absolute error functions, proving that the CSDJA is an effective substitute for techniques that use He's or Adomian polynomials to solve TFSHEs. The transition from the imprecise solution to the precise solution at various values of fractional-order derivatives is shown using the recurrence error function. Furthermore, the exact and approximative solutions are compared using 2D and 3D graphics and also numerically in the form of relative and absolute error functions. The results show that the procedure is quick, precise, and easy to implement, and it yields outstanding results. The recommended approach's strength, which gives it an advantage over the Adomian decomposition and homotopy perturbation methods, is its algorithm for dealing with nonlinear problems without the use of Adomian polynomials or He's polynomials. The advantage of this method is that it does not make any assumptions about physical parameters. As a result, it can be used to solve both weakly and strongly nonlinear problems and circumvent some of the drawbacks of perturbation techniques.

1. Introduction

A more than the 300-year-old extension of traditional calculus is fractional calculus (FC). Leibniz and L'Hospital started the FC as a result of a correspondence that lasted for several months in 1695. Leibniz addressed a letter to L'Hospital in that year, posing the following query [1].

Is it possible to generalize the definition of derivatives with integer orders to derivatives with noninteger orders? The preceding query piqued L'Hospital's interest, so it asked Leibniz another straightforward query in response: "What if the order is $1/2$?" In a letter dated September 30, 1695, Leib-

niz said, "It will lead to a paradox, from which one-day valuable conclusions will be deduced."

That date is regarded as the actual birthday of the FC. The fractional-order differential equations (FODEs), fractional dynamics, and other practical disciplines have all benefited greatly from the rapid development of the theory of FC since the 19th century. These days, FC is used in a wide variety of applications. It is safe to argue that nearly no field of contemporary engineering or research is unaffected by the methods and instruments of FC. For instance, mechanical engineering, electrical engineering, control theory, viscoelasticity, optics, rheology, chemistry, physics,

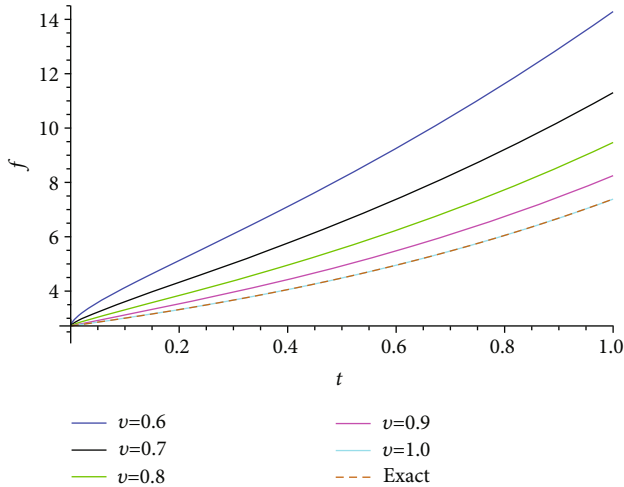


FIGURE 1: The 2D plot of the 5th-step approximate solution and exact solution of Example 3 for various quantities of ν in the interval $t \in [0, 1.0]$ when $x = 1.0$ is shown.

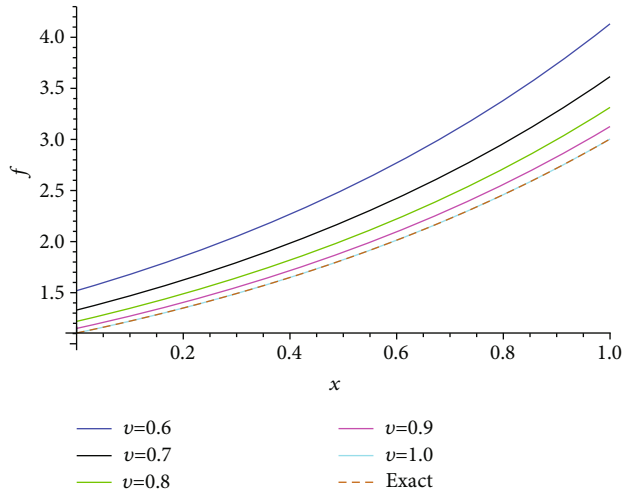


FIGURE 2: The 5th iteration's approximate and exact solutions for Example 3 are shown in a 2D graphic for various values of ν in the interval $x \in [0, 1.0]$ with $t = 0.1$.

statistics, robotics, and bioengineering are just a few fields with numerous and fruitful applications [2–5]. In fact, it may be argued that fractional-order systems in general characterize real-world processes. The success of FC applications is mostly due to the fact that these new fractional-order models are frequently more accurate than integer-order ones since they have more degrees of freedom than the corresponding classical ones. The fact that fractional derivatives are not a local number is one of the subject's interesting aspects. The nonlocal and distributed effects frequently observed in technical and natural phenomena can be modeled by all fractional operators since they consider the whole history of the activity under consideration. In order to describe the memory and hereditary characteristics of various materials and processes, FC is a great collection of tools.

Examples of fractional derivative definitions used in a range of natural phenomena and applications include Hada-

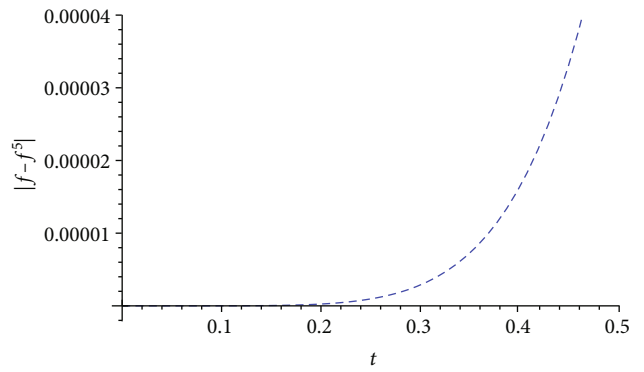


FIGURE 3: The 2D plot of the absolute error graph of $f(x, t)$ for the 5th iteration approximate solution in the interval $t \in [0, 0.5]$ when $\nu = 1.0$ and $x = 1.0$ in Example 3.

ward, Grunwald, Riemann-Liouville, Letnikov, Riesz, and Caputo derivatives [6–10]. In contrast to past formulations, the conformable derivative (CD), which Khalil et al. proposed [11], is a new formulation of the fractional operators that is far simpler to compute. The main benefits of CD are as follows [12–17]: in contrast to the previous fractional formulations, it satisfies all the concepts and guidelines of an ordinary derivative, including the chain, product, and quotient criteria. It is easily and quickly adaptable to solve exact and numerical FODEs and systems. It simplifies the well-known transforms, like the Sumudu and Laplace transforms, which are used as tools to explain some FODEs. Class conformable fractional operators, modified conformable fractional operators, fuzzy generalized conformable fractional operators, deformable fractional operators, M -conformable fractional operators, and Katugampola fractional operators are just a few examples of the new definitions that can be created and expanded upon. In a variety of applications, it produces new comparisons between CD and the earlier fractional definitions. Researchers have shown a great deal of interest in CD due to the numerous applications and phenomena that it may represent and the necessity to address them.

Various integral transforms are used with other analytical, numerical, or homotopy-based methods to handle FODEs. The Laplace transform (LT) [18], the Elzaki transform (ET) [19], the traveling wave transform (TWT) [20], the Yang transform (YT) [21], the Aboodh transform (AT) [22], the fractional complex transform (FCT) [23], and the natural transform (NT) [24] are all transformations that can be used to solve FODEs. The Shehu transform (ST), which has been used by numerous academics for the solutions of FODEs, has recently piqued the curiosity of many mathematicians [25–27].

The significant advantages of ST include the following:

- (i) The ET, SIT, and NT are all more challenging to understand than the ST
- (ii) When variable $n = 1$ is used, the ST becomes LT, and when variable $m = 1$ is used, it becomes YT

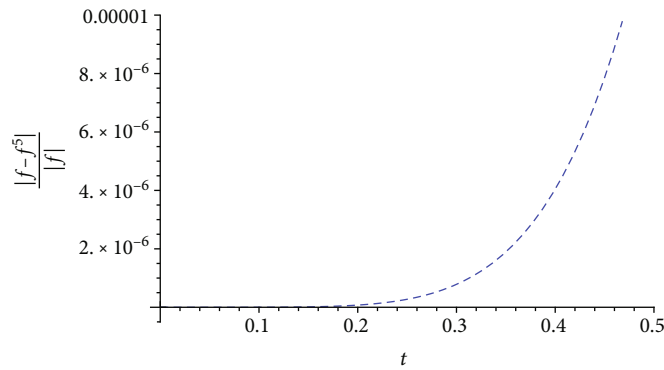


FIGURE 4: The 2D plot of the relative error graph of $f(x, t)$ for the 5th iteration approximate solution in the interval $t \in [0, 0.5]$ when $v = 1.0$ and $x = 1.0$ in Example 3.

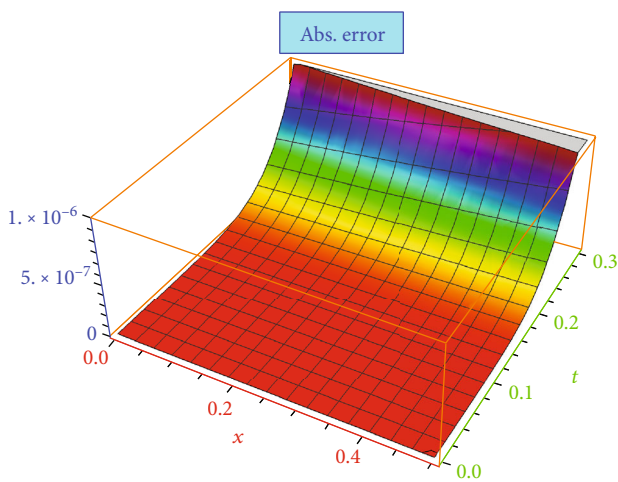


FIGURE 5: The 3D plot of the absolute error graph of $f(x, t)$ for the 5th iteration approximate solution when $v = 1.0$ with $x \in [0, 0.5]$ and $t \in [0, 0.3]$ in Example 3.

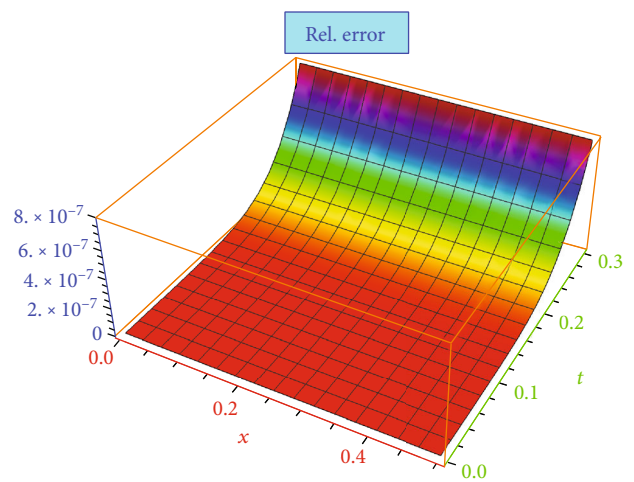


FIGURE 6: The 3D plot of the relative error graph of $f(x, t)$ for the 5th iteration approximate solution when $v = 1.0$ and $x \in [0, 0.5]$ and $t \in [0, 0.3]$ in Example 3.

- (iii) It is an extension of the LT and SIT
- (iv) It can be used efficiently to find exact and numerical solutions to FODEs

We understand that the majority of engineering issues are nonlinear and that addressing them analytically is challenging. Obtaining closed form or approximate solutions to nonlinear FODEs remains a fundamental topic in physics and mathematics, requiring innovative ways to locate exact or approximate solutions. As a result of the foregoing, researchers have devised a variety of numerical strategies for solving nonlinear FODEs. A few examples include the Elzaki residual power series method [28], the Haar Wavelet method [29], the operational Matrix Technique [30], the reduced differential transform method [31], the spectral Tau approach [32], the reproducing kernel technique [33], and the fractional power series technique [34].

Finding the solutions to TFSHEs is an interesting and important field for researchers [35–39]. Each of these tech-

niques has distinct restrictions and flaws. These techniques have long run times and enormous computational demands. In this study, we used CNDJM to acquire approximate and closed-form results of TFSHEs in the sense of CD. The recurrence, relative, and absolute error analyses among the exact solution and approximate solution of five linear-nonlinear problems have been used to demonstrate the accuracy and efficacy of the proposed method. The results obtained using the recommended method show excellent agreement with EDM [36], proving that the CSDJA is an acceptable substitute tool for the He’s or Adomian polynomial-based methods used to solve FODEs. The effectiveness of the CSDJA has been demonstrated by results in both graphs and numerically. The approximate solutions achieved using CSDJA are in perfect agreement with the corresponding precise solutions, as can be seen from the graphs and tables. The numerical evidence for the convergence of the approximative solution to the exact solution is presented in the tables. The absolute, relative, and recurrence error analyses have demonstrated a more accurate and faster convergence.

TABLE 1: Absolute and relative error in the 4th-step approximate solution of $f(x, t)$ when $\nu = 1.0$, $Y = 3$, and $\Theta = 2$ for Example 3.

(x, t)	$f^4(x, t)$	$f(x, t)$	Abs.error = $ f - f^4 $	Re l.error = $ f - f^4 / f $
(0.02, 0.02)	1.040810774165092	1.0408107741923882	$2.729616532803902 \times 10^{-11}$	$2.622586737653570 \times 10^{-11}$
(0.12, 0.12)	1.271248911766325	1.2712491503214047	$2.385550796901725 \times 10^{-7}$	$1.8765407208324160 \times 10^{-7}$
(0.22, 0.22)	1.552701664430785	1.5527072185113360	0.00000555408055080697	0.00000357703016034920
(0.32, 0.32)	1.896440220522181	1.8964808793049515	0.00004065878276993118	0.00002143906812539674
(0.42, 0.42)	2.316188883508124	2.3163669767810915	0.00017809327296758326	0.00007688474009203334
(0.52, 0.52)	2.828634231524732	2.8292170143515600	0.00058278282682744380	0.00020598731870733296
(0.62, 0.62)	3.454033558387693	3.4556134647626755	0.00157990637498217620	0.00045719997074113760
(0.72, 0.72)	4.216940784284310	4.2206958169965520	0.00375503271224175700	0.00088967148428948830
(0.82, 0.82)	5.303822828551244	5.1551695122346800	0.00809833753451094700	0.00157091585743035090
(0.92, 0.92)	6.280329876306269	6.2965382610266570	0.01620838472038777000	0.00257417394264272700

TABLE 2: Absolute and relative error in the 5th iteration approximate solution of $f(x, t)$ when $\nu = 1.0$, $Y = 3$, and $\Theta = 2$ for Example 3.

(x, t)	$f^5(x, t)$	$f(x, t)$	Abs.error = $ f - f^5 $	Re l.error = $ f - f^5 / f $
(0.02, 0.02)	1.0408107741922974	1.0408107741923882	$9.08162434143378 \times 10^{-14}$	$8.725528757598248 \times 10^{-14}$
(0.12, 0.12)	1.2712491455640722	1.2712491503214047	$4.757332527915992 \times 10^{-9}$	$3.742250310816896 \times 10^{-9}$
(0.22, 0.22)	1.5527070159482126	1.5527072185113360	$2.025631233859570 \times 10^{-7}$	$1.304580290289145 \times 10^{-7}$
(0.32, 0.32)	1.8592962781683804	1.8964808793049515	0.00000215149950033577	0.00000113446938685945
(0.42, 0.42)	2.3163546393670910	2.3163669767810915	0.00001233741400064047	0.00000532619145597775
(0.52, 0.52)	2.8291671596033580	2.8292170143515600	0.00004985474820173863	0.00001762139416978059
(0.62, 0.62)	3.4554527458972446	3.4556134647626755	0.00016071886543089775	0.00004650950318077187
(0.72, 0.72)	4.2202534168201780	4.2206958169965520	0.00044240017637431350	0.00010481688222894147
(0.82, 0.82)	5.1540858809814400	5.1551695122346800	0.00108363125324029140	0.00021020283633128398
(0.92, 0.92)	6.2941117674091895	6.2965382610266570	0.00242649361746760660	0.00038536947079107625

TABLE 3: The recurrence error for $f(x, t)$ at various values of ν for Example 3.

(x, t)	$\nu = 0.7$	$\nu = 0.8$	$\nu = 0.9$	$\nu = 1.0$
(0.03, 0.03)	$2.389361050347296 \times 10^{-7}$	$2.122670930232615 \times 10^{-8}$	$2.04023732018427 \times 10^{-9}$	$2.086670431255871 \times 10^{-10}$
(0.13, 0.13)	0.00004472893622536946	0.00000827180924889488	0.00000165504411671953	$3.523658391081241 \times 10^{-7}$
(0.23, 0.23)	0.00036413607844953396	0.00008957109715237295	0.00002383796620121089	0.000006750651136424606
(0.33, 0.33)	0.00142378535825781070	0.00041950945889177800	0.00013373223882468582	0.000045363403631587120
(0.43, 0.43)	0.00397388024822836750	0.00133656248951324060	0.00048636339807192120	0.000188324862522390530
(0.53, 0.53)	0.00912998728886662200	0.00340916776057963170	0.00137728461232044700	0.000592071528646969300
(0.63, 0.63)	0.01847676778128128800	0.00752205562040674600	0.00331317368190818600	0.001552841126987777000
(0.73, 0.73)	0.03419743526328207000	0.01498632791930036700	0.00710549027016691900	0.003584825550795332800
(0.83, 0.83)	0.05923335025813710600	0.02767869489816617700	0.01399336113675867500	0.007527896437711811000
(0.93, 0.93)	0.09747937634589607000	0.04821636669617927000	0.02580318662074363600	0.014693571306273750000

Many applications of the TFSHEs are found in engineering and science, including physics, biology, laser studies, fluids, and hydrodynamics. In fluid layers restricted between horizontal well-conducting barriers, the Swift-Hohenberg

(SH) equations play a significant role in pattern creation theory. There are numerous uses for this equation in the modeling of pattern generation and its many difficulties, such as pattern selection, noise effects on bifurcations, defect

TABLE 4: The absolute and relative error in various approaches for Example 3 at $\nu = 1.0$.

(x, t)	Abs.error (CSDJA)	Abs.error(EDM) [36]	Re l.error (CSDJA)	Re l.error(EDM) [36]
(0.06, 0.06)	$6.940115149234316 \times 10^{-11}$	$6.940115149234316 \times 10^{-11}$	$6.15532995902626 \times 10^{-11}$	$6.15532995902626 \times 10^{-11}$
(0.16, 0.16)	$2.798253562197317 \times 10^{-8}$	$2.798253562197317 \times 10^{-8}$	$2.031949129677607 \times 10^{-8}$	$2.031949129677607 \times 10^{-8}$
(0.26, 0.26)	$5.778071316964173 \times 10^{-7}$	$5.778071316964173 \times 10^{-7}$	$3.435182125572402 \times 10^{-7}$	$3.435182125572402 \times 10^{-7}$
(0.36, 0.36)	0.0000045667026689066	0.0000045667026689066	0.000002228528263887	0.000002228528263887
(0.46, 0.46)	0.0000222971843411023	0.0000222971843411023	0.0000088858525225007	0.0000088858525225007
(0.56, 0.56)	0.0000814362943066804	0.0000814362943066804	0.0000265710173812450	0.0000265710173812450
(0.66, 0.66)	0.0002449136020046261	0.0002449136020046261	0.0000654250690270498	0.0000654250690270498
(0.76, 0.76)	0.0006408613764907756	0.0006408613764907756	0.0001401640009270912	0.0001401640009270912
(0.86, 0.86)	0.0015103634891575624	0.0015103634891575624	0.0002704549719496070	0.0002704549719496070
(0.96, 0.96)	0.0032809722748394776	0.0032809722748394776	0.0004810133780481200	0.0004810133780481200

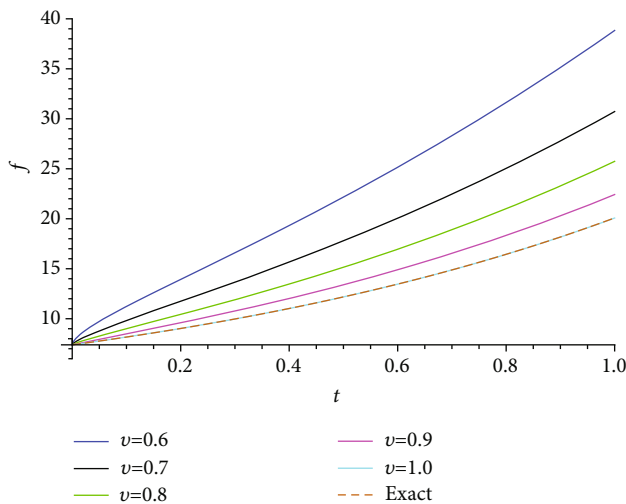


FIGURE 7: The 2D plot of the 5th step exact solution and approximate solution of Example 4 for various values of ν in the interval $t \in [0, 1.0]$, when $x = 2.0$ is shown.

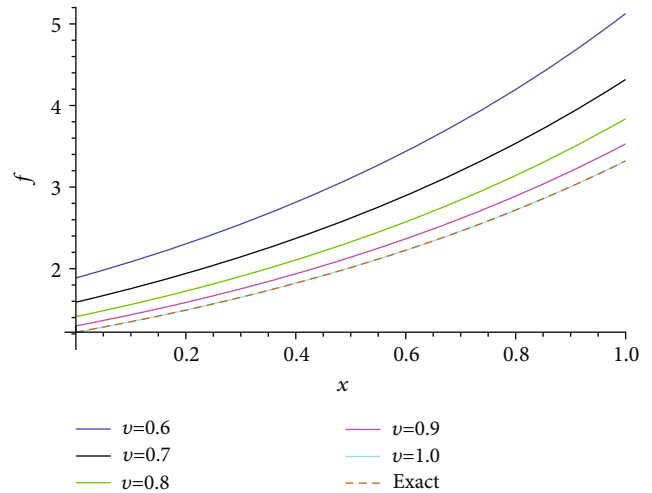


FIGURE 8: The 2D plot of the 5th iteration approximate and exact solutions of Example 4 for different values of ν in the interval $x \in [0, 1.0]$, with $t = 0.2$.

dynamics, and spatiotemporal chaos. The general form of the S-H equation is given by [40]

$$\frac{\partial}{\partial t} f(x, t) = \omega f(x, t) - (1 + \nabla^2)^2 f(x, t) - f^3(x, t), \quad (1)$$

where $x \in R, t > 0, \omega$ is bifurcation parameter, and $f(x, t)$ is a scalar function of x and t defined on the line or the plane.

The following is how this study is structured: first, in Section 2, we use crucial terminology and findings from FC theory. Next, in Section 3, we described how to solve TFSHEs using the CSDJA. In Section 4, to assess the efficiency of the CSDJA, we solved five numerical problems with a conclusion remark. Finally, we summarize our results in the conclusion.

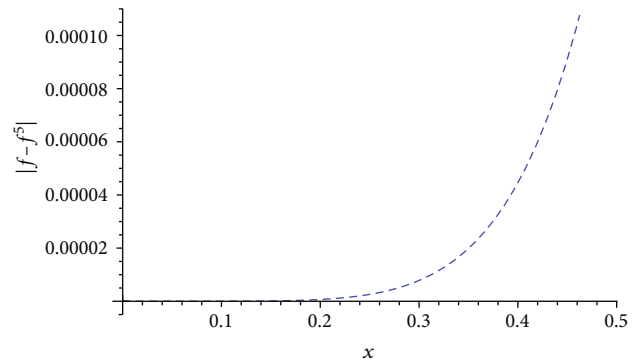


FIGURE 9: The 2D plot of the absolute error graph of $f(x, t)$ for the 5th iteration approximate solution in the interval $t \in [0, 0.5]$ when $\nu = 1.0$ and $x = 2.0$ in Example 4.

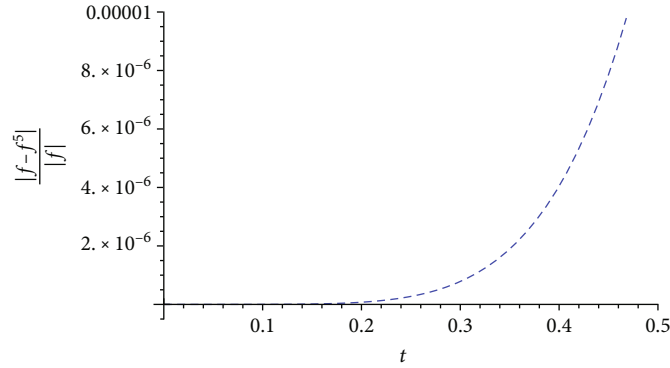


FIGURE 10: The 2D plot of the relative error graph of $f(x, t)$ for the 5th iteration approximate solutions in the interval $t \in [0, 0.5]$ when $\nu = 1.0$ and $x = 2.0$ in Example 4.

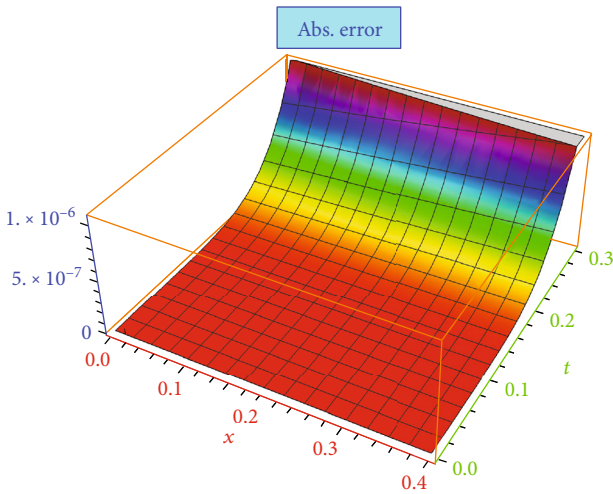


FIGURE 11: The 3D plot of the absolute error graph of $f = (x, t)$ for the 5th iteration approximate solutions when $\nu = 1.0$ with $x \in [0, 0.4]$ and $t \in [0, 0.3]$ in Example 4.

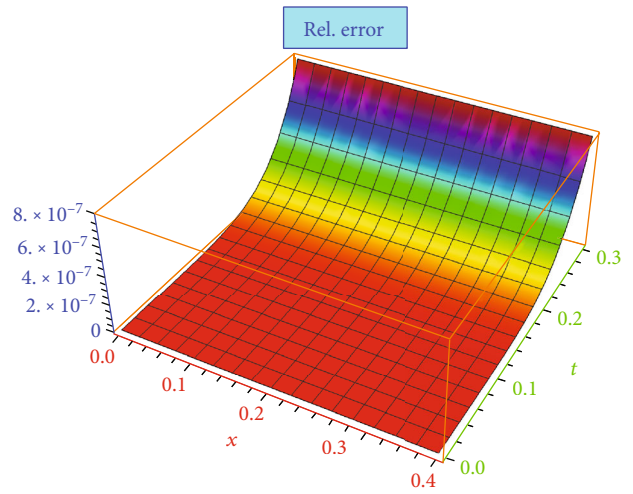


FIGURE 12: The 3D plot of the relative error graph of $f = (x, t)$ for the 5th iteration approximate solutions when $\nu = 1.0$ and $x \in [0, 0.4]$ and $t \in [0, 0.3]$ in Example 4.

2. Preliminaries

The definitions, theorems, and mathematical foundations of CD and CST that will be used in this work are reviewed in this part.

Definition 1. Assumed a function $f : [0, \infty) \rightarrow R$ as well the CD of f order ν is defined as follows [41]:

$$T_t^\nu f(t) = \lim_{\epsilon \rightarrow 0} \frac{f(t + \epsilon t^{1-\nu}) - f(t)}{\epsilon}, \quad (2)$$

for $t > 0$ and $\nu \in (0, 1]$. If f is ν -differentiable in some $(0, P), P > 0$, and $\lim_{t \rightarrow 0^+} (T_\nu f)(t)$, happen afterward, it is drawn as

$$(T_\nu f)(0) = \lim_{t \rightarrow 0^+} (T_\nu f)(t). \quad (3)$$

Theorem 2. Let f_1 and f_2 be ν -differentiable at a point $t > 0$. Then, for $\nu \in (0, 1]$, we take the following [42]:

$$(i) T_t^\nu(e_1 f_1 + e_2 f_2) = e_1 T_t^\nu(f_1) + e_2 T_t^\nu(f_2), \forall e_1, e_2 \in R$$

$$(ii) T_t^\nu(t^e) = e t^{e-\nu}, \forall e \in R T_t^\nu(e) = 0, \text{ where } e \in R$$

$$(iii) T_t^\nu(f_1 f_2) = f_1 T_t^\nu(f_2) + f_2 T_t^\nu(f_1)$$

$$(iv) T_t^\nu(f_1/f_2) = (f_2 T_t^\nu(f_1) - f_1 T_t^\nu(f_2))/(f_2)^2$$

Definition 3. Let $0 < \nu \leq 1$ and $f : [0, \infty) \rightarrow R$ be a real value function. Then, the CST of order ν is defined by [43]:

$$\mathfrak{F}_\nu[f(t)] = R_\nu(m, n) = \int_0^\infty e^{-(mt^\nu/m\nu)} f(t) t^{\nu-1} dt, \quad (4)$$

assuming the integral is present.

Theorem 4. Let $[0, \infty) \rightarrow R$ be differentiable function and $0 < \nu \leq 1$. Then, we have the following [44]:

$$\mathfrak{F}_\nu[T_t^\nu f(x, t)] = \frac{m}{n} \mathfrak{F}_\nu[f(x, t)] - f(x, 0). \quad (5)$$

TABLE 5: Relative and absolute error in the 4th-step approximate solution of $f(x, t)$ when $\nu = 1.0$, $Y = 3$, and $\Theta = 2$ for Example 4.

(x, t)	$f^4(x, t)$	$f(x, t)$	Re l.error = $ f - f^4 / f $	Abs.error = $ f - f^4 $
(0.03, 0.03)	1.0618365463356450	1.0618365465453596	$1.975018572683782 \times 10^{-10}$	$2.097146900581492 \times 10^{-10}$
(0.13, 0.13)	1.2969297265212163	1.2969300866657718	$2.776900306454735 \times 10^{-7}$	$3.601445555112548 \times 10^{-7}$
(0.23, 0.23)	1.5683052371426760	1.5840739849944818	0.00000443046196873528	0.00000701817954618100
(0.33, 0.33)	1.9347443533545630	1.9347923344020317	0.00002479906841452054	0.05280880783415465000
(0.43, 0.43)	2.3629579963630247	2.3631606937057947	0.00008577382964683130	0.00020269734277000850
(0.53, 0.53)	2.8857223796091587	2.8863709892679585	0.00022471458492741108	0.00064860965879987020
(0.63, 0.63)	3.5236896816699144	3.5254214873653824	0.00049123365863474670	0.00173180569546804720
(0.73, 0.73)	4.3018885509799105	4.3059595283452060	0.00094542861782547080	0.00407097736529582500
(0.83, 0.83)	5.2506040155785140	5.2593108444468980	0.00165550756095314270	0.00870682886838469700
(0.93, 0.93)	6.4064239349551840	6.4237367714291350	0.00269513479303095400	0.01731283647395098800

TABLE 6: Relative and absolute error in the 5th-step approximate solution of $f(x, t)$ when $\nu = 1.0$, $Y = 3$, and $\Theta = 2$ for Example 4.

(x, t)	$f^5(x, t)$	$f(x, t)$	Re l.error = $ f - f^5 / f $	Abs.error = $ f - f^5 $
(0.03, 0.03)	1.0618365465443120	1.0618365465453596	$9.865985960312264 \times 10^{-13}$	$1.047606446036297 \times 10^{-12}$
(0.13, 0.13)	1.2969300788870555	1.2969300866657718	$5.997791567719124 \times 10^{-9}$	$7.778716337725200 \times 10^{-9}$
(0.23, 0.23)	1.5840737174660720	1.5840739849944818	$1.688863098591869 \times 10^{-7}$	$2.675284098696551 \times 10^{-7}$
(0.33, 0.33)	1.9347897167581944	1.9347923344020317	0.00000135293271050344	0.00000261764383724383
(0.43, 0.43)	2.3631463212255475	2.3631606937057947	0.00000608188866950595	0.00001437248024727111
(0.53, 0.53)	2.8863144511378060	2.8863709892679585	0.00001958796369660575	0.00005653813015271680
(0.63, 0.63)	3.5252425227969020	3.5254214873653824	0.00005076402045020574	0.00017896456848021103
(0.73, 0.73)	4.3054733765307050	4.3059595283452060	0.00011290208635281496	0.00048615181450095690
(0.83, 0.83)	5.2581319120162260	5.2593108444468980	0.00022416100997668992	0.00117893243067257460
(0.93, 0.93)	6.4211175062614570	6.4237367714291350	0.00040774789828359850	0.00261926516767729820

Theorem 5. Let $e, a \in R$ and $0 < \nu \leq 1$. After that, we have the following [45]:

- (i) $\mathfrak{F}_\nu[e] = ne/m, m > 0$
- (ii) $\mathfrak{F}_\nu[e^{a(t^\nu/v)}] = 1/(n - am), m > an$
- (iii) $\mathfrak{F}_\nu[\sin(a(t^\nu/v))] = an/(m^2 + a^2n^2), m > 0$
- (iv) $\mathfrak{F}_\nu[\cos(a(t^\nu/v))] = m/(m^2 + a^2n^2), m > 0$
- (v) $\mathfrak{F}_\nu[\sinh(a(t^\nu/v))] = an/(m^2 - a^2n^2), m > |an|$
- (vi) $\mathfrak{F}_\nu[\cosh(a(t^\nu/v))] = m/(m^2 - a^2n^2), m > |an|$
- (vii) $\mathfrak{F}_\nu[t^e] = \nu^{(e/\nu)} \Gamma((e/\nu) + 1)(n/m)^{(e/\nu)+1}, m > 0$

In the succeeding part, we generate the foremost suggestion of the CSDJA to obtain the results for linear and nonlinear TFSHEs.

3. The Methodology of the CSDJA for the TFSHEs

To show a detailed understanding of the CSDJA for the TFSHEs, we consider the following problem in common operator systems with the preliminary condition [35, 40]:

$$\begin{cases} T_t^\nu f(x, t) + L(f(x, t)) + N(f(x, t)) = X(x, t), & 0 < \nu \leq 1, \\ f_0(x, t) = f(x, 0) = M(x), \end{cases} \tag{6}$$

where T_t^ν is the CD, $L(f(x, t))$ is a linear operator, $N(f(x, t))$ is nonlinear operator, $X(x, t)$ is a source operator, and $M(x)$ is a function of x .

Considering CST over both sides of Equation (6), we get the following:

$$\mathfrak{F}_\nu[T_t^\nu f(x, t) + L(f(x, t)) + N(f(x, t))] = \mathfrak{F}_\nu[X(x, t)]. \tag{7}$$

TABLE 7: The recurrence error for $f(x, t)$ at various values of ν for Example 4.

(x, t)	$\nu = 0.7$	$\nu = 0.8$	$\nu = 0.9$	$\nu = 1.0$
(0.04, 0.04)	$6.605570054968454 \times 10^{-7}$	$6.776111811148356 \times 10^{-8}$	$7.520521323907584 \times 10^{-9}$	$8.88158527310838 \times 10^{-10}$
(0.14, 0.14)	0.00005855687695655334	0.000011237823043034677	0.000002333369918901773	$5.155373796638246 \times 10^{-7}$
(0.24, 0.24)	0.00042687289116174175	0.000107261647058368440	0.000029159996674309360	0.000008435399161940688
(0.34, 0.34)	0.00159648516526208390	0.000477468374476977100	0.000154497500358521600	0.000053195324562529430
(0.44, 0.44)	0.00435013258370755200	0.001480025155353154600	0.000544794636100933600	0.000213388842878693700
(0.54, 0.54)	0.00984522698715773800	0.003710760102727795500	0.001513202834688249000	0.000656608610049396100
(0.64, 0.64)	0.01972000093709039600	0.008091651751701122000	0.003592233495567985300	0.001696942365438352200
(0.74, 0.74)	0.03622575866606469000	0.015983563638428833000	0.007630040833314809000	0.003875745658449868000
(0.84, 0.84)	0.06238977506975238000	0.029328734766364786000	0.014916617684664520000	0.008072769438923630000
(0.94, 0.94)	0.10221458141443295000	0.050829641468808535000	0.027347545964240397000	0.015656505501509240000

TABLE 8: The absolute and relative error in different methods for Example 4 at $\nu = 1.0$.

(x, t)	Abs.errors	Abs.errors(EDM) [36]	Re l.errors	Re l.errors(EDM) [36]
	(CSDJA)		(CSDJA)	
(0.07, 0.07)	$1.770170676707039 \times 10^{-10}$	$1.770170676707039 \times 10^{-10}$	$1.538912455856741 \times 10^{-10}$	$1.538912455856741 \times 10^{-10}$
(0.17, 0.17)	$4.072256909459781 \times 10^{-8}$	$4.072256909459781 \times 10^{-8}$	$2.898511614818456 \times 10^{-8}$	$2.898511614818456 \times 10^{-8}$
(0.27, 0.27)	$7.330046871700802 \times 10^{-7}$	$7.330046871700802 \times 10^{-7}$	$4.271572004303072 \times 10^{-7}$	$4.271572004303072 \times 10^{-7}$
(0.37, 0.37)	0.0000054448562791797	0.0000054448562791797	0.0000025978166988087	0.0000025978166988087
(0.47, 0.47)	0.0000256617119771540	0.0000256617119771540	0.0000100241790012295	0.0000100241790012295
(0.57, 0.57)	0.0000916097361671752	0.0000916097361671752	0.0000292985362098356	0.0000292985362098356
(0.67, 0.67)	0.0002711490539653027	0.0002711490539653027	0.0000709992053204676	0.0000709992053204676
(0.77, 0.77)	0.0007012039032332495	0.0007012039032332495	0.0001503248651000401	0.0001503248651000401
(0.87, 0.87)	0.0016376884224653665	0.0016376884224653665	0.0002874477279969388	0.0002874477279969388
(0.97, 0.97)	0.0035321427112258164	0.0035321427112258164	0.0005075828587816742	0.0005075828587816742

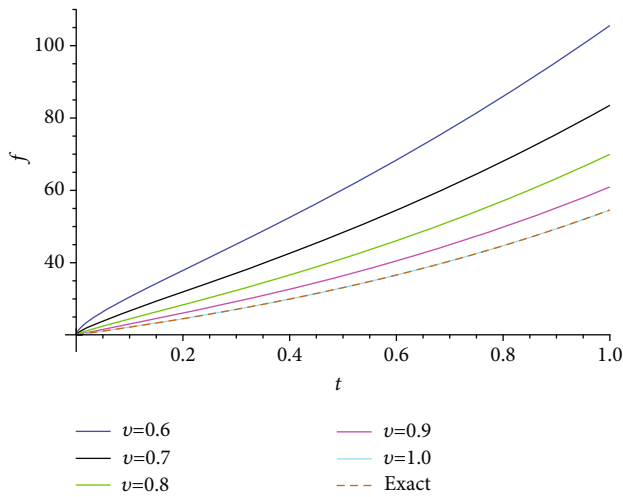


FIGURE 13: The 2D plot of the 5th iteration approximate and exact solutions of Example 5 for different values of ν in the interval $t \in [0, 1.0]$, when $x = 3.0$ is shown.

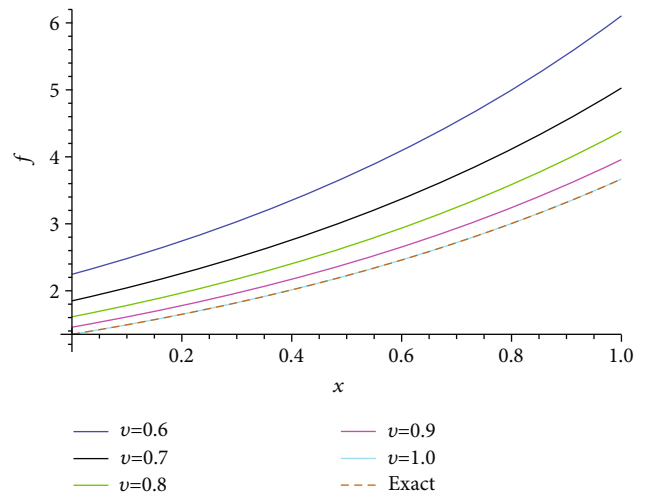


FIGURE 14: The 2D plot of the 5th iteration approximate and exact solutions of Example 5 for different values of ν in the interval $x \in [0, 1.0]$, with $t = 0.3$ is shown.

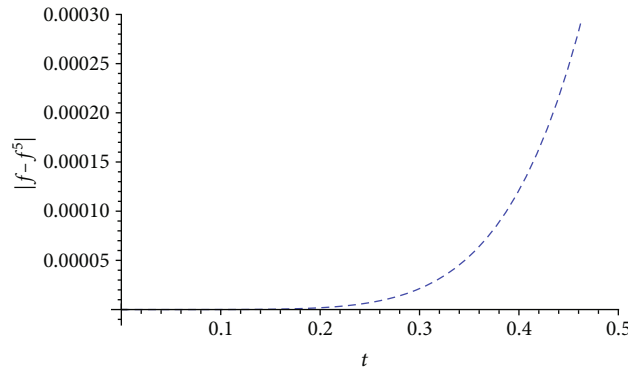


FIGURE 15: The 2D plot of the absolute error graph of $f(x, t)$ for the 5th iteration approximate solution in the intervals $t \in [0, 0.5]$ when $\nu = 1.0$ and $x = 3.0$ in Example 5.

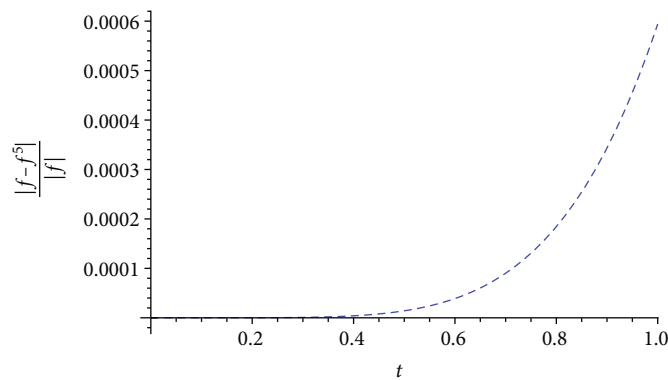


FIGURE 16: The 2D plot of the relative error graph of $f(x, t)$ for the 5th iteration approximate solution in the interval $t \in [0, 0.5]$ when $\nu = 1.0$ and $x = 3.0$ in Example 5.

We acquire the following by simplifying Equation (7).

$$\begin{aligned} \mathfrak{F}_\nu[f(x, t)] &= \frac{n}{m}f(x, 0) + \frac{n}{m}\mathfrak{F}_\nu[X(x, t)] - \frac{n}{m}\mathfrak{F}_\nu[L(f(x, t))] \\ &\quad - \frac{n}{m}\mathfrak{F}_\nu[N(f(x, t))]. \end{aligned} \tag{8}$$

We obtain the following when we use the inverse CST on both sides of Equation (8).

$$\begin{aligned} f(x, t) &= \mathfrak{F}_\nu^{-1}\left\{\frac{n}{m}f(x, 0) + \frac{n}{m}\mathfrak{F}_\nu[X(x, t)]\right\} - \mathfrak{F}_\nu^{-1}\left\{\frac{n}{m}\mathfrak{F}_\nu[L(f(x, t))]\right\} \\ &\quad - \mathfrak{F}_\nu^{-1}\left\{\frac{n}{m}\mathfrak{F}_\nu[Nf((x, t))]\right\}. \end{aligned} \tag{9}$$

Next, assume the following:

$$\begin{aligned} A(f(x, t)) &= \mathfrak{F}_\nu^{-1}\left\{\frac{n}{m}f(x, 0) + \frac{n}{m}\mathfrak{F}_\nu[X(x, t)]\right\}, \\ B(f(x, t)) &= \mathfrak{F}_\nu^{-1}\left\{\frac{n}{m}\mathfrak{F}_\nu[L(f(x, t))]\right\}, \\ C(f(x, t)) &= \mathfrak{F}_\nu^{-1}\left\{\frac{n}{m}\mathfrak{F}_\nu[N(f(x, t))]\right\}. \end{aligned} \tag{10}$$

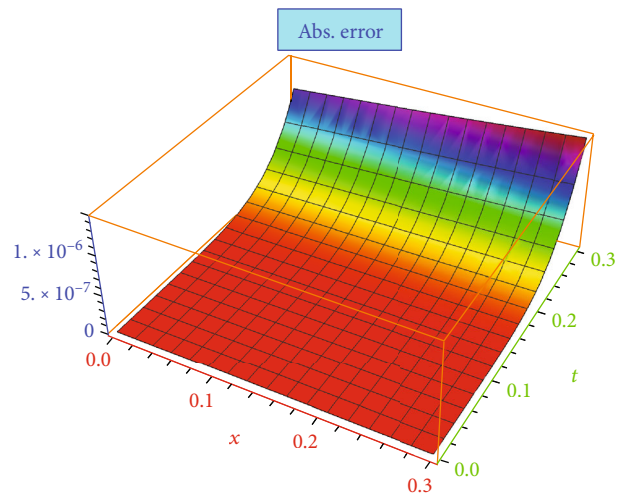


FIGURE 17: The 3D plot of the absolute error graph of $f = (x, t)$ for the 5th iteration approximate solution when $\nu = 1.0$ with $x \in [0, 0.3]$ and $t \in [0, 0.3]$ in Example 5.

As a result, Equation (9) can be written as

$$f(x, t) = A(f(x, t)) + B(f(x, t)) + C(f(x, t)), \tag{11}$$

where B and C are given as linear and nonlinear operators of

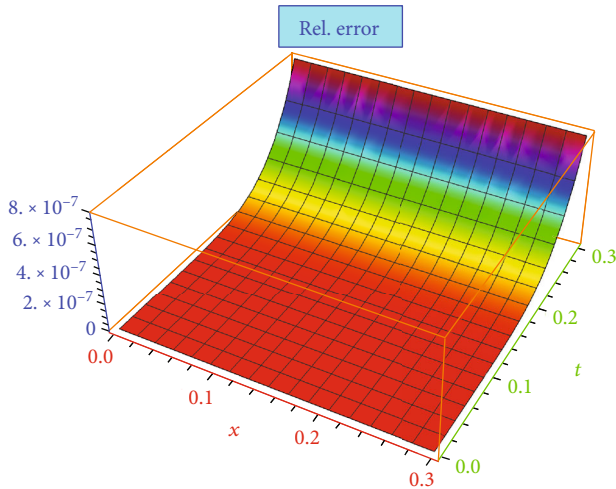


FIGURE 18: The 3D plot of the relative error graph of $f = (x, t)$ for the 5th iteration approximate solution when $\nu = 1.0$ and $x \in [0, 0.3]$ and $t \in [0, 0.3]$ in Example 5.

$f(x, t)$, respectively, where $A(f(x, t))$ is a known function. The solution to Equation (6) can be expressed in the following expansion form:

$$f(x, t) = \sum_{i=0}^{\infty} f_i(x, t). \tag{12}$$

Assume the following:

$$B\left(\sum_{i=0}^{\infty} f_i(x, t)\right) = \sum_{i=0}^{\infty} B(f_i(x, t)). \tag{13}$$

Decompose the nonlinear operator as [45]

$$C\left(\sum_{i=0}^{\infty} f_i(x, t)\right) = C(f_0(x, t)) + \sum_{i=0}^{\infty} \left\{ C\left(\sum_{k=0}^i f_k(x, t)\right) - C\left(\sum_{k=0}^{i-1} f_k(x, t)\right) \right\}. \tag{14}$$

As a result, Equation (6) can be considered the following arrangement.

$$\sum_{i=0}^{\infty} f_i(x, t) = A(f(x, t)) + \sum_{i=0}^{\infty} B(f_i(x, t)) + C(f_0(x, t)) + \sum_{i=0}^{\infty} \left\{ CC\left(\sum_{k=0}^{i-1} f_k(x, t)\right) \right\}. \tag{15}$$

Use Equation (15) to define the recurrence relation.

$$f_0(x, t) = A(f(x, t)),$$

$$f_1(x, t) = B(f_0(x, t)) + C(f_0(x, t)),$$

$$f_{j+1}(x, t) = B\left(f_k(x, t) + C\left(f_0(x, t) + f_1(x, t) + \dots + f_j(x, t)\right) - C\left(f_0(x, t) + f_1(x, t) + \dots + f_{j-1}(x, t)\right)\right). \tag{16}$$

As a result, we have the following:

$$\begin{aligned} & \left(f_1(x, t) + f_2(x, t) + \dots + f_{j+1}(x, t)\right) \\ &= B\left(f_0(x, t) + f_1(x, t) + \dots + f_j(x, t)\right) \\ &+ C\left(f_0(x, t) + f_1(x, t) + \dots + f_j(x, t)\right). \end{aligned} \tag{17}$$

Particularly,

$$\sum_{i=0}^{\infty} f_i(x, t) = A\left(\sum_{i=0}^{\infty} f_i(x, t)\right) + B\left(\sum_{i=0}^{\infty} f_i(x, t)\right) + C\left(\sum_{i=0}^{\infty} f_i(x, t)\right). \tag{18}$$

Equation (6) has j th approximate solution, which is given by

$$f_j(x, t) = f_0(x, t) + f_1(x, t) + \dots + f_{j-1}(x, t). \tag{19}$$

In the next section, we will assess the suitability of the suggested approach by solving numerical problems.

4. Numerical Examples and Concluding Remarks

In this section, five TFSHEs in the CD sense are solved in order to assess the effectiveness and suitability of the suggested approach.

Example 1. Take the following SH equation, which is linear and time-fractional [36]:

$$T_t^\nu f(x, t) + (1 - \Upsilon)f(x, t) + 2\frac{\partial^2 f(x, t)}{\partial x^2} + \frac{\partial^4 f(x, t)}{\partial x^4} = 0, \quad 0 < \nu \leq 1, \tag{20}$$

with the initial condition:

$$f(x, 0) = \sin x. \tag{21}$$

The results of applying CST to both sides of Equation (20) are as follows:

$$\mathfrak{S}_\nu \left[T_t^\nu f(x, t) + (1 - \Upsilon)f(x, t) + 2\frac{\partial^2 f(x, t)}{\partial x^2} + \frac{\partial^4 f(x, t)}{\partial x^4} \right] = 0. \tag{22}$$

By using the method described in Section 3, we achieve the following outcome:

$$\mathfrak{S}_\nu[f(x, t)] = \frac{n}{m} \sin x - \frac{n}{m} \mathfrak{S}_\nu[(1 - \Upsilon)f(x, t)] - \frac{n}{m} \mathfrak{S}_\nu \left[2\frac{\partial^2 f(x, t)}{\partial x^2} \right] - \frac{n}{m} \mathfrak{S}_\nu \left[\frac{\partial^4 f(x, t)}{\partial x^4} \right]. \tag{23}$$

TABLE 9: Absolute and relative error in the 4th-step approximate solution of $f(x, t)$ when $\nu = 1.0$ for Example 5.

(x, t)	$f^4(x, t)$	$f(x, t)$	Re l.error = $ f - f^4 / f $	Abs.error = $ f - f^4 $
(0.05, 0.05)	1.1051709153149847	1.1051709180756477	$2.497951209498041 \times 10^{-9}$	$2.760663031509125 \times 10^{-9}$
(0.15, 0.15)	1.3498580535708110	1.3498588075760032	$5.585807849316814 \times 10^{-7}$	$7.540051922827473 \times 10^{-7}$
(0.25, 0.25)	1.6487103698322902	1.6487212707001282	0.00000661171056119114	0.00001090086783794852
(0.35, 0.35)	2.0136867849099350	2.0137527074704766	0.00003273617475320743	0.00006592256054149814
(0.45, 0.45)	2.4593426274569340	2.4596031111569500	0.00010590476928346425	0.00026048370001596766
(0.55, 0.55)	3.0033668369534470	3.0041660239464334	0.00026602624043272600	0.00079918699298620060
(0.65, 0.65)	3.6672236017846527	3.6692966676192444	0.00056497634897884670	0.00207306583459176960
(0.75, 0.75)	4.4769175156003390	4.4816890703380645	0.00106467777278576500	0.00477155473772583600
(0.85, 0.85)	5.4639046334569470	5.4739473917272000	0.00183464647201958890	0.01004275827025313800
(0.95, 0.95)	6.6661756508830850	6.6858944422792685	0.00294931240186632400	0.01971879139618337700

TABLE 10: Absolute and relative error in the 5th-step approximate solution of $f(x, t)$ when $\nu = 1.0$ for Example 5.

(x, t)	$f^5(x, t)$	$f(x, t)$	Rel.error = $ f - f^5 / f $	Abs.error = $ f - f^5 $
(0.05, 0.05)	1.1051709180526696	1.1051709180756477	$2.079141200717798 \times 10^{-11}$	$2.297806389606194 \times 10^{-11}$
(0.15, 0.15)	1.3498587887940425	1.3498588075760032	$1.391401867217576 \times 10^{-8}$	$1.878196065341342 \times 10^{-8}$
(0.25, 0.25)	1.6487208192578820	1.6487212707001282	$2.738135634414047 \times 10^{-7}$	$4.514422462520429 \times 10^{-7}$
(0.35, 0.35)	2.0137488949836050	2.0137527074704766	0.00000189322495130197	0.00000381248687153501
(0.45, 0.45)	2.4595837922127695	2.4596031111569500	0.00000785449656196916	0.00001931894418039093
(0.55, 0.55)	3.0040937695882923	3.0041660239464334	0.00002405138649632585	0.00007225435814106618
(0.65, 0.65)	3.6690757551727438	3.6692966676192444	0.00006020566514836269	0.00022091244650068730
(0.75, 0.75)	4.4811039658285040	4.4816890703380645	0.00013055446292173030	0.00058510450956017480
(0.85, 0.85)	5.4725555812700595	5.4739473917272000	0.00025426083912386135	0.00139181045714043000
(0.95, 0.95)	6.6828487579188190	6.6858944422792685	0.00045553880438038890	0.00304568436044938550

TABLE 11: The recurrence error for $f(x, t)$ at various values of ν for Example 5.

(x, t)	$\nu = 0.7$	$\nu = 0.8$	$\nu = 0.9$	$\nu = 1.0$
(0.05, 0.05)	0.000001456928681921672	$1.6709504069900890 \times 10^{-7}$	$2.073413635883548 \times 10^{-8}$	$2.7376851468125640 \times 10^{-9}$
(0.15, 0.15)	0.000075299507010213980	0.000014958154942352114	0.000003214852447088009	$7.3522323172649170 \times 10^{-7}$
(0.25, 0.25)	0.000497384451313588700	0.000127556464740409500	0.000035392387988058570	0.000010449425591534353
(0.35, 0.35)	0.001784718714941603100	0.000541556864447976400	0.000177793334429172840	0.000062110073669809540
(0.45, 0.45)	0.004753405550388819000	0.001635503172715662700	0.000608828586232166100	0.000241164755835960970
(0.55, 0.55)	0.010603761039668216000	0.004033495177363797000	0.001659970134744652700	0.000726932634845213500
(0.65, 0.65)	0.021028907727128978000	0.008695882418547608000	0.003890520650822312500	0.001852153388091293700
(0.75, 0.75)	0.038349864797284756000	0.017034709587258750000	0.008186584586292290000	0.004186450228164713000
(0.85, 0.85)	0.065681808688387200000	0.031059526557876346000	0.015890650727901650000	0.008650947813112190000
(0.95, 0.95)	0.107137357433544080000	0.053560299636793150000	0.028969579299671387000	0.016673107035735170000

TABLE 12: The absolute and relative error in various approaches for Example 5 at $v = 1.0$.

(x, t)	Abs.errors	Abs.errors(EDM) [36]	Re l.errors	Re l.errors(EDM) [36]
	(CSDJA)		(CSDJA)	
(0.08, 0.08)	$3.989657493264076 \times 10^{-10}$	$3.989657493264076 \times 10^{-10}$	$3.399761852987486 \times 10^{-10}$	$3.399761852987486 \times 10^{-10}$
(0.18, 0.18)	$5.804326486114064 \times 10^{-8}$	$5.804326486114064 \times 10^{-8}$	$4.049541178148838 \times 10^{-8}$	$4.049541178148838 \times 10^{-8}$
(0.28, 0.28)	$9.222621923932195 \times 10^{-7}$	$9.222621923932195 \times 10^{-7}$	$5.268045235400865 \times 10^{-7}$	$5.268045235400865 \times 10^{-7}$
(0.38, 0.38)	0.0000064634844112454	0.0000064634844112454	0.0000030227546606414	0.0000030227546606414
(0.48, 0.48)	0.0000294538494971519	0.0000294538494971519	0.0000112776694370410	0.0000112776694370410
(0.58, 0.58)	0.0001028641032836397	0.0001028641032836397	0.0000322464748883020	0.0000322464748883020
(0.68, 0.68)	0.0002997943734013297	0.0002997943734013297	0.0000769454568034897	0.0000769454568034897
(0.78, 0.78)	0.0007664534267357581	0.0007664534267357581	0.0001610595118526153	0.0001610595118526153
(0.88, 0.88)	0.0017743428907426306	0.0017743428907426306	0.0003052665810132136	0.0003052665810132136
(0.98, 0.98)	0.0038001237563074497	0.0038001237563074497	0.0005352794316180174	0.0005352794316180174

Apply the inverse CST on both sides of Equation (23).

$$f(x, t) = \mathfrak{F}_v^{-1} \left\{ \frac{n}{m} \sin x \right\} - \mathfrak{F}_v^{-1} \left\{ \frac{n}{m} \mathfrak{F}_v [(1 - \Upsilon)f(x, t)] \right\} - \mathfrak{F}_v^{-1} \left\{ \frac{n}{m} \mathfrak{F}_v \left[2 \frac{\partial^2 f(x, t)}{\partial x^2} \right] \right\} - \mathfrak{F}_v^{-1} \left\{ \frac{n}{m} \mathfrak{F}_v \left[\frac{\partial^4 f(x, t)}{\partial x^4} \right] \right\}. \tag{24}$$

The procedure described in Section 3 leads to the following outcome:

$$B(f(x, t)) = -\mathfrak{F}_v^{-1} \left\{ \frac{n}{m} \mathfrak{F}_v [(1 - \Upsilon)f(x, t)] \right\} - \mathfrak{F}_v^{-1} \left\{ \frac{n}{m} \mathfrak{F}_v \left[2 \frac{\partial^2 f(x, t)}{\partial x^2} \right] \right\} - \mathfrak{F}_v^{-1} \left\{ \frac{n}{m} \mathfrak{F}_v \left[\frac{\partial^4 f(x, t)}{\partial x^4} \right] \right\}, \tag{25}$$

$$\sum_{i=0}^{\infty} f_i(x, t) = \mathfrak{F}_v^{-1} \left\{ \frac{n}{m} \sin x \right\} - \mathfrak{F}_v^{-1} \left\{ \frac{n}{m} \mathfrak{F}_v \left[(1 - \Upsilon) \sum_{i=0}^{\infty} f_i(x, t) \right] \right\} - \mathfrak{F}_v^{-1} \left\{ \frac{n}{m} \mathfrak{F}_v \left[2 \frac{\partial^2}{\partial x^2} \sum_{i=0}^{\infty} f_i(x, t) \right] \right\} - \mathfrak{F}_v^{-1} \left\{ \frac{n}{m} \mathfrak{F}_v \left[\frac{\partial^4}{\partial x^4} \sum_{i=0}^{\infty} f_i(x, t) \right] \right\}. \tag{26}$$

Here, we will discuss the following two cases.

Case 1. $\Upsilon \neq 0$.

Using the iteration process outlined in Section 3, the results from Equation (26) are as follows:

$$\begin{aligned} f_0(x, t) &= \sin x, \\ f_1(x, t) &= \sin x ((\Upsilon - 1) + 1) \frac{t^v}{1!v^1}, \\ f_2(x, t) &= \sin x ((\Upsilon - 1)^2 + (\Upsilon - 1) + 1) \frac{t^{2v}}{2!v^2}, \\ f_3(x, t) &= \sin x ((\Upsilon - 1)^3 + (\Upsilon - 1)^2 + (\Upsilon - 1) + 1) \frac{t^{3v}}{3!v^3}, \\ f_4(x, t) &= \sin x ((\Upsilon - 1)^4 + (\Upsilon - 1)^3 + (\Upsilon - 1)^2 + (\Upsilon - 1) + 1) \frac{t^{4v}}{4!v^4}, \\ f_5(x, t) &= \sin x ((\Upsilon - 1)^5 + (\Upsilon - 1)^4 + (\Upsilon - 1)^3 + (\Upsilon - 1)^2 + (\Upsilon - 1) + 1) \frac{t^{5v}}{5!v^5}. \end{aligned} \tag{27}$$

As a result, we get the 5th step approximate solution to Equations (20) and (21) obtained from the 5th iteration as follows:

$$\begin{aligned} f^{(5)}(x, t) &= \sin x + \sin x ((\Upsilon - 1) + 1) \frac{t^v}{1!v^1} + \sin x ((\Upsilon - 1)^2 + (\Upsilon - 1) + 1) \frac{t^{2v}}{2!v^2} + \sin x ((\Upsilon - 1)^3 + (\Upsilon - 1)^2 + (\Upsilon - 1) + 1) \frac{t^{3v}}{3!v^3} \\ &+ \sin x ((\Upsilon - 1)^4 + (\Upsilon - 1)^3 + (\Upsilon - 1)^2 + (\Upsilon - 1) + 1) \frac{t^{4v}}{4!v^4} + \sin x ((\Upsilon - 1)^5 + (\Upsilon - 1)^4 + (\Upsilon - 1)^3 + (\Upsilon - 1)^2 + (\Upsilon - 1) + 1) \frac{t^{5v}}{5!v^5}. \end{aligned} \tag{28}$$

We get the following exact solution to Equations (20) and (21):

$$f(x, t) = -\frac{1}{\Upsilon} \sin x \lim_{j \rightarrow \infty} \sum_{i=0}^j (1 - (\Upsilon - 1)^{i+1}) \frac{t^{iv}}{i!v^i}. \quad (29)$$

Case 2. $\Upsilon = 0$.

Using the iteration process outlined in Section 3, the results from Equation (26) are as follows.

$$\begin{aligned} f_0(x, t) &= \sin x, \\ f_1(x, t) &= 0, \\ f_2(x, t) &= 0, \\ f_i(x, t) &= 0, i = 3, 4, \dots \end{aligned} \quad (30)$$

Hence, the solution to Equations (20) and (21) is

$$f(x, t) = \sin x. \quad (31)$$

As a consequence, the solution of Equations (20) and (21) is

$$f(x, t) = \begin{cases} -\frac{1}{\Upsilon} \sin x \lim_{j \rightarrow \infty} \sum_{i=0}^j (1 - (\Upsilon - 1)^{i+1}) \frac{t^{iv}}{i!v^i}, & \Upsilon \neq 0, \\ \sin x & \Upsilon = 0. \end{cases} \quad (32)$$

Example 2. Take the following SH equation, which is linear and time-fractional [37]:

$$T_t^\nu f(x, t) + (1 - \Upsilon)f(x, t) + 2 \frac{\partial^2 f(x, t)}{\partial x^2} + \frac{\partial^4 f(x, t)}{\partial x^4} = 0, \quad 0 < \nu \leq 1, \quad (33)$$

subject to the initial condition:

$$f(x, 0) = \cos x. \quad (34)$$

When CST is applied to both sides of an equation (33), we get the following:

$$\mathfrak{F}_\nu \left[T_t^\nu f(x, t) + (1 - \Upsilon)f(x, t) + 2 \frac{\partial^2 f(x, t)}{\partial x^2} + \frac{\partial^4 f(x, t)}{\partial x^4} \right] = 0. \quad (35)$$

By using the method described in Section 3, we achieve

the following outcome:

$$\begin{aligned} \mathfrak{F}_\nu[f(x, t)] &= \frac{n}{m} \cos x - \frac{n}{m} \mathfrak{F}_\nu[(1 - \Upsilon)f(x, t)] \\ &\quad - \frac{n}{m} \mathfrak{F}_\nu \left[2 \frac{\partial^2 f(x, t)}{\partial x^2} \right] - \frac{n}{m} \mathfrak{F}_\nu \left[\frac{\partial^4 f(x, t)}{\partial x^4} \right]. \end{aligned} \quad (36)$$

Consider the inverse of CST on both sides of Equation (33).

$$\begin{aligned} f(x, t) &= \mathfrak{F}_\nu^{-1} \left\{ \frac{n}{m} \cos x \right\} - \mathfrak{F}_\nu^{-1} \left\{ \frac{n}{m} \mathfrak{F}_\nu[(1 - \Upsilon)f(x, t)] \right\} \\ &\quad - \mathfrak{F}_\nu^{-1} \left\{ \frac{n}{m} \mathfrak{F}_\nu \left[2 \frac{\partial^2 f(x, t)}{\partial x^2} \right] \right\} - \mathfrak{F}_\nu^{-1} \left\{ \frac{n}{m} \mathfrak{F}_\nu \left[\frac{\partial^4 f(x, t)}{\partial x^4} \right] \right\}. \end{aligned} \quad (37)$$

We obtain the following outcome by following the procedure described in Section 3:

$$\begin{aligned} B(f(x, t)) &= -\mathfrak{F}_\nu^{-1} \left\{ \frac{n}{m} \mathfrak{F}_\nu[(1 - \Upsilon)f(x, t)] \right\} \\ &\quad - \mathfrak{F}_\nu^{-1} \left\{ \frac{n}{m} \mathfrak{F}_\nu \left[2 \frac{\partial^2 f(x, t)}{\partial x^2} \right] \right\} \\ &\quad - \mathfrak{F}_\nu^{-1} \left\{ \frac{n}{m} \mathfrak{F}_\nu \left[\frac{\partial^4 f(x, t)}{\partial x^4} \right] \right\}. \end{aligned} \quad (38)$$

$$\begin{aligned} \sum_{i=0}^{\infty} f_i(x, t) &= \mathfrak{F}_\nu^{-1} \left\{ \frac{n}{m} \sin x \right\} - \mathfrak{F}_\nu^{-1} \left\{ \frac{n}{m} \mathfrak{F}_\nu \left[(1 - \Upsilon) \sum_{i=0}^{\infty} f_i(x, t) \right] \right\} \\ &\quad - \mathfrak{F}_\nu^{-1} \left\{ \frac{n}{m} \mathfrak{F}_\nu \left[2 \frac{\partial^2}{\partial x^2} \sum_{i=0}^{\infty} f_i(x, t) \right] \right\} \\ &\quad - \mathfrak{F}_\nu^{-1} \left\{ \frac{n}{m} \mathfrak{F}_\nu \left[\frac{\partial^4}{\partial x^4} \sum_{i=0}^{\infty} f_i(x, t) \right] \right\}. \end{aligned} \quad (39)$$

Here, we will deal with the following two situations:

Case 1. $\Upsilon \neq 0$.

The outcomes of Equation (39) are as follows when applying the iteration procedure described in Section 3:

$$f_0(x, t) = \cos x,$$

$$f_1(x, t) = \cos x((\Upsilon - 1) + 1) \frac{t^\nu}{1!v^1},$$

$$f_2(x, t) = \cos x((\Upsilon - 1)^2 + (\Upsilon - 1) + 1) \frac{t^{2\nu}}{2!v^2},$$

$$f_3(x, t) = \cos x((\Upsilon - 1)^3 + (\Upsilon - 1)^2 + (\Upsilon - 1) + 1) \frac{t^{3\nu}}{3!v^3},$$

$$f_4(x, t) = \cos x((\Upsilon - 1)^4 + (\Upsilon - 1)^3 + (\Upsilon - 1)^2 + (\Upsilon - 1) + 1) \frac{t^{4\nu}}{4!v^4},$$

$$f_5(x, t) = \cos x((Y - 1)^5 + (Y - 1)^4 + (Y - 1)^3 + (Y - 1)^2 + (Y - 1) + 1) \frac{t^{5\nu}}{5!v^5}. \tag{40}$$

As a result, we get the 5th step approximate solution to Equations (33) and (34) obtained from the 5th iteration as follows:

$$f^{(5)}(x, t) = \cos x + \cos x((Y - 1) + 1) \frac{t^\nu}{1!v^1} + \cos x((Y - 1)^2 + (Y - 1) + 1) \frac{t^{2\nu}}{2!v^2} + \cos x((Y - 1)^3 + (Y - 1)^2 + (Y - 1) + 1) \frac{t^{3\nu}}{3!v^3} + \cos x((Y - 1)^4 + (Y - 1)^3 + (Y - 1)^2 + (Y - 1) + 1) \frac{t^{4\nu}}{4!v^4} + \cos x((Y - 1)^5 + (Y - 1)^4 + (Y - 1)^3 + (Y - 1)^2 + (Y - 1) + 1) \frac{t^{5\nu}}{5!v^5}. \tag{41}$$

We get the following exact solution to Equations (33) and (34).

$$f(x, t) = -\frac{1}{Y} \cos x \lim_{j \rightarrow \infty} \sum_{i=0}^j (1 - (Y - 1)^{i+1}) \frac{t^{i\nu}}{i!v^i}. \tag{42}$$

Case 2. $Y = 0$.

Using the iteration process outlined in Section 3, the results from Equation (39) are as follows.

$$\begin{aligned} f_0(x, t) &= \cos x \\ f_1(x, t) &= 0, \\ f_2(x, t) &= 0, \\ f_i(x, t) &= 0, i = 3, 4, \dots \end{aligned} \tag{43}$$

Hence, the solution to Equations (33) and (34) is

$$f(x, t) = \cos x. \tag{44}$$

As a consequence, the solution of Equations (33) and (34) is

$$f(x, t) = \begin{cases} -\frac{1}{Y} \cos x \lim_{j \rightarrow \infty} \sum_{i=0}^j (1 - (Y - 1)^{i+1}) \frac{t^{i\nu}}{i!v^i}, & Y \neq 0, \\ \cos x, & Y = 0. \end{cases} \tag{45}$$

Example 3. Consider the following SH equation, which is linear and time-fractional [36]:

$$T_t^\nu f(x, t) + (1 - Y)f(x, t) + 2 \frac{\partial^2 f(x, t)}{\partial x^2} + \frac{\partial^4 f(x, t)}{\partial x^4} - \Theta \frac{\partial^3 f(x, t)}{\partial x^3} = 0, \quad 0 < \nu \leq 1, \tag{46}$$

with the initial condition:

$$f(x, 0) = e^x. \tag{47}$$

Using CST on both sides of Equation (46),

$$\mathfrak{F}_\nu \left[T_t^\nu f(x, t) + (1 - Y)f(x, t) + 2 \frac{\partial^2 f(x, t)}{\partial x^2} + \frac{\partial^4 f(x, t)}{\partial x^4} - \Theta \frac{\partial^3 f(x, t)}{\partial x^3} \right] = 0. \tag{48}$$

We obtain the following result from Equation (48) by carrying out the processes outlined in Section 3.

$$\begin{aligned} \mathfrak{F}_\nu[f(x, t)] &= \frac{n}{m} e^x - \frac{n}{m} \mathfrak{F}_\nu[(1 - Y)f(x, t)] - \frac{n}{m} \mathfrak{F}_\nu \left[2 \frac{\partial^2 f(x, t)}{\partial x^2} \right] \\ &\quad - \frac{n}{m} \mathfrak{F}_\nu \left[\frac{\partial^4 f(x, t)}{\partial x^4} \right] + \frac{n}{m} \mathfrak{F}_\nu \left[\Theta \frac{\partial^3 f(x, t)}{\partial x^3} \right]. \end{aligned} \tag{49}$$

Use inverse CST on both sides of Equation (49).

$$\begin{aligned} f(x, t) &= \mathfrak{F}_\nu^{-1} \left\{ \frac{n}{m} e^x \right\} - \mathfrak{F}_\nu^{-1} \left\{ \frac{n}{m} \mathfrak{F}_\nu[(1 - Y)f(x, t)] \right\} \\ &\quad - \mathfrak{F}_\nu^{-1} \left\{ \frac{n}{m} \mathfrak{F}_\nu \left[2 \frac{\partial^2 f(x, t)}{\partial x^2} \right] \right\} - \mathfrak{F}_\nu^{-1} \left\{ \frac{n}{m} \mathfrak{F}_\nu \left[\frac{\partial^4 f(x, t)}{\partial x^4} \right] \right\} \\ &\quad + \mathfrak{F}_\nu^{-1} \left\{ \frac{n}{m} \mathfrak{F}_\nu \left[\Theta \frac{\partial^3 f(x, t)}{\partial x^3} \right] \right\}. \end{aligned} \tag{50}$$

By following the steps indicated in Section 3, we obtain the following outcome:

$$A(f(x, t)) = \mathfrak{F}_\nu^{-1} \left\{ \frac{n}{m} e^x \right\}, \tag{51}$$

$$\begin{aligned} B(f(x, t)) &= -\mathfrak{F}_\nu^{-1} \left\{ \frac{n}{m} \mathfrak{F}_\nu[(1 - Y)f(x, t)] \right\} - \mathfrak{F}_\nu^{-1} \left\{ \frac{n}{m} \mathfrak{F}_\nu \left[2 \frac{\partial^2 f(x, t)}{\partial x^2} \right] \right\} \\ &\quad - \mathfrak{F}_\nu^{-1} \left\{ \frac{n}{m} \mathfrak{F}_\nu \left[\frac{\partial^4 f(x, t)}{\partial x^4} \right] \right\} + \mathfrak{F}_\nu^{-1} \left\{ \frac{n}{m} \mathfrak{F}_\nu \left[\Theta \frac{\partial^3 f(x, t)}{\partial x^3} \right] \right\}, \end{aligned} \tag{52}$$

$$\begin{aligned} \sum_{i=0}^{\infty} f_i(x, t) &= \mathfrak{F}_\nu^{-1} \left\{ \frac{n}{m} e^x \right\} - \mathfrak{F}_\nu^{-1} \left\{ \frac{n}{m} \mathfrak{F}_\nu \left[(1 - Y) \sum_{i=0}^{\infty} f_i(x, t) \right] \right\} \\ &\quad - \mathfrak{F}_\nu^{-1} \left\{ \frac{n}{m} \mathfrak{F}_\nu \left[2 \frac{\partial^2}{\partial x^2} \sum_{i=0}^{\infty} f_i(x, t) \right] \right\} \\ &\quad + \mathfrak{F}_\nu^{-1} \left\{ \frac{n}{m} \mathfrak{F}_\nu \left[\Theta \frac{\partial^3}{\partial x^3} \sum_{i=0}^{\infty} f_i(x, t) \right] \right\} \\ &\quad - \mathfrak{F}_\nu^{-1} \left\{ \frac{n}{m} \mathfrak{F}_\nu \left[\frac{\partial^4}{\partial x^4} \sum_{i=0}^{\infty} f_i(x, t) \right] \right\}. \end{aligned} \tag{53}$$

The findings from Equation (53) are as follows using the

iteration method described in Section 3:

$$\begin{aligned}
 f_0(x, t) &= e^x, \\
 f_1(x, t) &= e^x(Y - 4 + \Theta)^1 \frac{t^{1v}}{1!v^1}, \\
 f_2(x, t) &= e^x(Y - 4 + \Theta)^2 \frac{t^{2v}}{2!v^2}, \\
 f_3(x, t) &= e^x(Y - 4 + \Theta)^3 \frac{t^{3v}}{3!v^3}, \\
 f_4(x, t) &= e^x(Y - 4 + \Theta)^4 \frac{t^{4v}}{4!v^4}, \\
 f_5(x, t) &= e^x(Y - 4 + \Theta)^5 \frac{t^{5v}}{5!v^5}.
 \end{aligned}
 \tag{54}$$

As a result, we get the approximate solution to Equations (46) and (47) obtained from the 5th iteration as follows:

$$\begin{aligned}
 f^{(5)}(x, t) &= e^x + e^x(Y - 4 + \Theta)^1 \frac{t^{1v}}{1!v^1} + e^x(Y - 4 + \Theta)^2 \frac{t^{2v}}{2!v^2} \\
 &+ e^x(Y - 4 + \Theta)^3 \frac{t^{3v}}{3!v^3} + e^x(Y - 4 + \Theta)^4 \frac{t^{4v}}{4!v^4} \\
 &+ e^x(Y - 4 + \Theta)^5 \frac{t^{5v}}{5!v^5}.
 \end{aligned}
 \tag{55}$$

When $v = 1$ is employed in Equation (55), we get the following exact solution to Equations (46) and (47):

$$f(x, t) = e^{x+(\Theta+Y-4)t}.
 \tag{56}$$

We compare the numerical and graphical results of the exact and approximative solutions to the models presented in Examples 3–5. Error functions can be used to evaluate the numerical method’s accuracy and capabilities. It is important to provide the error of the analytical approximate solution that CSDJA offers in terms of an infinite fractional power series. We employed the recurrence, absolute, and relative error functions to show the accuracy and efficiency of CSDJA.

The 2D graph of the comparison between the exact solution and the approximation is shown in Figures 1 and 2 obtained by the proposed method in Example 3. Figure 1 represents the 2D graph of the exact solution and the 5th iteration approximate solution attained by CSDJA at $v = 0.6, 0.7, 0.8, 0.9$, and $v = 1.0$ with $x = 1.0, Y = 3$, and $\Theta = 2$ in the interval $t \in [0, 1.0]$ for Example 3. Figure 2 represents the 2D graph of the exact solution and 5th iteration approximate solution attained by CSDJA at $v = 0.6, 0.7, 0.8, 0.9$, and $v = 1.0$ with $t = 0.1, Y = 3$, and $\Theta = 2$ in the interval $x \in [0, 1.0]$ for Example 3. These graphs show how effective the approximative solution provided by the CSDJA is when $v \rightarrow 1.0$. The approximate solution corresponds with the precise solution at $v = 1.0$, which proves the suggested method’s effectiveness and precision.

Figures 3 and 4 show the 2D graph of the comparative study of the approximate solution obtained from the five

iterations and the exact solution obtained by the proposed method in the form of absolute and relative error with $v = 1.0$ at $x = 1.0, Y = 3$, and $\Theta = 2$ in the interval $t \in [0, 0.5]$ to Example 3, respectively. The comparison has shown that the suggested method’s fifth-step approximation and precise solution are extremely close. The relative and absolute error comparison of the approximate and exact solutions on a graph demonstrates the superior accuracy of CSDJA.

Figures 5 and 6 display the 3D graphs of the comparison research in terms of absolute and relative error for the approximate solution produced by the suggested method in the fifth stage and the exact solution at $v = 1.0, Y = 3$, and $\Theta = 2$ in the intervals $x \in [0, 0.5]$ and $t \in [0, 0.3]$ to Example 3, respectively. The comparison has proven that the suggested method’s fifth-step approximation solution is quite near to the precise solution, and this proves the effectiveness and precision of the suggested method.

Tables 1 and 2 show that the approximate solution for the fourth phase has very low relative and absolute error to Example 3. The relative and absolute error will be even smaller if we consider the fifth-step approximation. The relative and absolute error processes demonstrate the precision of our suggested strategy, and as a result, the approximation is quickly approaching the exact solution. We anticipate that our approach will be a key step in the management of several FODEs with engineering and applied mathematics fields of physical interest.

Recurrence error has been used to quantitatively demonstrate how the approximate solution for Example 3 converges to the exact solution for suitably specified grid locations in the intervals $x \in [0, 1.0]$ and $t \in [0, 1.0]$ when $Y = 3$ and $\Theta = 2$ as in Table 3. From Table 3, we see that the approximate solution obtained by the proposed method in the fifth step quickly approaches the exact solution as the order of the fractional-order derivative increases. The increased degree of accuracy and convergence rates have been proven by the recurrence error analysis. We conclude that the proposed method is a viable and efficient algorithm for solving particular classes of FODEs with minimal calculations and iterative phases.

Table 4 also compares the absolute and relative error of the approximation from the fifth iterations obtained by the CSDJA of Example 3 at plausible short-listed grid points in the range $x \in [0, 1.0]$ and $t \in [0, 1.0]$ when $Y = 3$ and $\Theta = 2$ with the absolute and relative error of the 5th-step approximation obtained by EDM [36]. The comparison has proven that the suggested procedure and EDM yield the same results. Because of the comparison, we concluded that CSDJA can be used as a substitute for method EDM to solve TFSHEs.

Example 4. Consider the following SH equation, which is nonlinear and time-fractional [36]:

$$\begin{aligned}
 T_t^\nu f(x, t) + (1 - Y)f(x, t) + 2 \frac{\partial^2 f(x, t)}{\partial x^2} + \frac{\partial^4 f(x, t)}{\partial x^4} - \Theta \frac{\partial^3 f(x, t)}{\partial x^3} \\
 - f^2(x, t) + \left(\frac{\partial f(x, t)}{\partial x} \right)^2 = 0, \quad 0 < \nu \leq 1,
 \end{aligned}
 \tag{57}$$

subject to the following initial conditions:

$$f(x, 0) = e^x. \tag{58}$$

Using CST on both sides of Equation (57),

$$\begin{aligned} \mathfrak{F}_v \left[T_t^\nu f(x, t) + (1 - \Upsilon)f(x, t) + 2 \frac{\partial^2 f(x, t)}{\partial x^2} + \frac{\partial^4 f(x, t)}{\partial x^4} \right. \\ \left. - \Theta \frac{\partial^3 f(x, t)}{\partial x^3} - f^2(x, t) + \left(\frac{\partial f(x, t)}{\partial x} \right)^2 \right] = 0. \end{aligned} \tag{59}$$

We obtain the following result from Equation (59) by carrying out the processes outlined in Section 3.

$$\begin{aligned} \mathfrak{F}_v[f(x, t)] = \frac{n}{m} e^x - \frac{n}{m} \mathfrak{F}_v[(1 - \Upsilon)f(x, t)] - \frac{n}{m} \mathfrak{F}_v \left[2 \frac{\partial^2 f(x, t)}{\partial x^2} \right] \\ - \frac{n}{m} \mathfrak{F}_v \left[\frac{\partial^4 f(x, t)}{\partial x^4} \right] + \frac{n}{m} \mathfrak{F}_v \left[\Theta \frac{\partial^3 f(x, t)}{\partial x^3} \right] \\ + \frac{n}{m} \mathfrak{F}_v[f^2(x, t)] - \frac{n}{m} \mathfrak{F}_v \left[\left(\frac{\partial f(x, t)}{\partial x} \right)^2 \right]. \end{aligned} \tag{60}$$

Use inverse CST on both sides of Equation (60).

$$\begin{aligned} f(x, t) = \mathfrak{F}_v^{-1} \left\{ \frac{n}{m} e^x \right\} - \mathfrak{F}_v^{-1} \left\{ \frac{n}{m} \mathfrak{F}_v[(1 - \Upsilon)f(x, t)] \right\} \\ - \mathfrak{F}_v^{-1} \left\{ \frac{n}{m} \mathfrak{F}_v \left[2 \frac{\partial^2 f(x, t)}{\partial x^2} \right] \right\} - \mathfrak{F}_v^{-1} \left\{ \frac{n}{m} \mathfrak{F}_v \left[\frac{\partial^4 f(x, t)}{\partial x^4} \right] \right\} \\ + \mathfrak{F}_v^{-1} \left\{ \frac{n}{m} \mathfrak{F}_v \left[\Theta \frac{\partial^3 f(x, t)}{\partial x^3} \right] \right\} + \mathfrak{F}_v^{-1} \left\{ \frac{n}{m} \mathfrak{F}_v[f^2(x, t)] \right\} \\ - \mathfrak{F}_v^{-1} \left\{ \frac{n}{m} \mathfrak{F}_v \left[\left(\frac{\partial f(x, t)}{\partial x} \right)^2 \right] \right\}. \end{aligned} \tag{61}$$

By following the steps indicated in Section 3, we obtain the following outcome:

$$\begin{aligned} B(f(x, t)) = -\mathfrak{F}_v^{-1} \left\{ \frac{n}{m} \mathfrak{F}_v[(1 - \Upsilon)f(x, t)] \right\} - \mathfrak{F}_v^{-1} \left\{ \frac{n}{m} \mathfrak{F}_v \left[2 \frac{\partial^2 f(x, t)}{\partial x^2} \right] \right\} \\ - \mathfrak{F}_v^{-1} \left\{ \frac{n}{m} \mathfrak{F}_v \left[\frac{\partial^4 f(x, t)}{\partial x^4} \right] \right\} + \mathfrak{F}_v^{-1} \left\{ \frac{n}{m} \mathfrak{F}_v \left[\Theta \frac{\partial^3 f(x, t)}{\partial x^3} \right] \right\}, \end{aligned} \tag{62}$$

$$C(f(x, t)) = \mathfrak{F}_v^{-1} \left\{ \frac{n}{m} \mathfrak{F}_v[f^2(x, t)] \right\} - \mathfrak{F}_v^{-1} \left\{ \frac{n}{m} \mathfrak{F}_v \left[\left(\frac{\partial f(x, t)}{\partial x} \right)^2 \right] \right\}, \tag{63}$$

$$\begin{aligned} \sum_{i=0}^{\infty} f_i(x, t) = \mathfrak{F}_v^{-1} \left\{ \frac{n}{m} e^x \right\} - \mathfrak{F}_v^{-1} \left\{ \frac{n}{m} \mathfrak{F}_v \left[(1 - \Upsilon) \sum_{i=0}^{\infty} f_i(x, t) \right] \right\} \\ - \mathfrak{F}_v^{-1} \left\{ \frac{n}{m} \mathfrak{F}_v \left[2 \frac{\partial^2 \sum_{i=0}^{\infty} f_i(x, t)}{\partial x^2} \right] \right\} \\ + \mathfrak{F}_v^{-1} \left\{ \frac{n}{m} \mathfrak{F}_v \left[\Theta \frac{\partial^3 \sum_{i=0}^{\infty} f_i(x, t)}{\partial x^3} \right] \right\} \\ + \mathfrak{F}_v^{-1} \left\{ \frac{n}{m} \mathfrak{F}_v \left[\frac{\partial^4 \sum_{i=0}^{\infty} f_i(x, t)}{\partial x^4} \right] \right\} \\ + \mathfrak{F}_v^{-1} \left\{ \frac{n}{m} \mathfrak{F}_v \left[\sum_{i=0}^{\infty} f_i(x, t) \right]^2 \right\} \\ - \mathfrak{F}_v^{-1} \left\{ \frac{n}{m} \mathfrak{F}_v \left[\left(\frac{\partial \sum_{i=0}^{\infty} f_i(x, t)}{\partial x} \right)^2 \right] \right\}. \end{aligned} \tag{64}$$

The findings from Equation (64) are as follows using the iteration method described in Section 3:

$$\begin{aligned} f_0(x, t) &= e^x, \\ f_1(x, t) &= e^x (\Upsilon - 4 + \Theta)^1 \frac{t^{1\nu}}{1!v^1}, \\ f_2(x, t) &= e^x (\Upsilon - 4 + \Theta)^2 \frac{t^{2\nu}}{2!v^2}, \\ f_3(x, t) &= e^x (\Upsilon - 4 + \Theta)^3 \frac{t^{3\nu}}{3!v^3}, \\ f_4(x, t) &= e^x (\Upsilon - 4 + \Theta)^4 \frac{t^{4\nu}}{4!v^4}, \\ f_5(x, t) &= e^x (\Upsilon - 4 + \Theta)^5 \frac{t^{5\nu}}{5!v^5}. \end{aligned} \tag{65}$$

As a result, we get the approximate solution to Equations (46) and (47) obtained from the 5th iteration as follows:

$$\begin{aligned} f^{(5)}(x, t) = e^x + e^x (\Upsilon - 4 + \Theta)^1 \frac{t^{1\nu}}{1!v^1} + e^x (\Upsilon - 4 + \Theta)^2 \frac{t^{2\nu}}{2!v^2} \\ + e^x (\Upsilon - 4 + \Theta)^3 \frac{t^{3\nu}}{3!v^3} + e^x (\Upsilon - 4 + \Theta)^4 \frac{t^{4\nu}}{4!v^4} \\ + e^x (\Upsilon - 4 + \Theta)^5 \frac{t^{5\nu}}{5!v^5}. \end{aligned} \tag{66}$$

When $\nu = 1$ is employed in Equation (66), we get the following exact solution to Equations (57) and (58):

$$f(x, t) = e^{x+(\Theta+\Upsilon-4)t}. \tag{67}$$

Figure 7 represents the 2D graph of the exact solution and 5th iteration approximate solution attained by CSDJA at $\nu = 0.6, 0.7, 0.8, 0.9,$ and $\nu = 1.0$ with $x = 2.0$ in the interval $t \in [0,1.0]$ for Example 4. Figure 8 represents the 2D graph of the 5th-step approximate and the exact solutions obtained by CSDJA at $\nu = 0.6, 0.7, 0.8, 0.9,$ and $\nu = 1.0$ with $t = 0.2,$

$Y = 3$, and $\Theta = 2$ in the interval $x \in [0, 1.0]$ for Example 4. These figures display that the approximate solution attained through CSDJA approach the exact solution when $\nu \rightarrow 1.0$. The approximate solution corresponds with the precise solution at $\nu = 1.0$, demonstrating the precision and effectiveness of the suggested approach.

Figures 9 and 10 show the 2D graph of the comparative study of the approximate solution obtained from the five iterations and exact solution obtained by the proposed method in the form of absolute and relative error with $\nu = 1.0$ at $x = 2.0, Y = 3$, and $\Theta = 2$ in the interval $t \in [0, 0.5]$ for Example 4, respectively. The comparison has proven that the suggested method's fifth-step approximation is quite near to the exact solution. Lastly, we draw the conclusion from the graphical results that the suggested method provides a solution in the form of a fractional series with high accuracy and few calculations.

Figures 11 and 12 display a 3D graph of the comparison research that compares the approximate solution and exact solution achieved in the fifth stage using the suggested method at $\nu = 1.0, Y = 3$, and $\Theta = 2$ in the intervals $x \in [0, 0.4]$ and $t \in [0, 0.3]$ to Example 4, respectively. The comparison has proven that the suggested method's fifth-step approximations are quite near to the precise solutions. As a result, the suggested approach is a methodical, potent, and useful tool for analytic approximations and precise solutions to FODEs.

Tables 5 and 6 demonstrate that Example 4's absolute and relative error for the fourth phase is quite small. If we consider the fifth-step approximation, the absolute and relative error will be even lower. The approximation is rapidly getting closer to the exact solution as a result of the accuracy of our suggested method being shown by the absolute and relative error processes. We anticipate that our approach will be a key step in obtaining solutions to numerous FODEs with a physical interest in the domains of applied mathematics and engineering.

Recurrence error has been used to numerically demonstrate the convergence of the approximate solution to the exact solution for Example 4 for appropriately set grid locations in the interval $x \in [0, 1.0]$ and $t \in [0, 1.0]$ when $Y = 3$, and $\Theta = 2$ as in Table 7. Table 6 demonstrates how the approximate solution found by the suggested method in the fifth step progressively approaches the exact solution as the order of the fractional-order derivative increases. Higher degrees of accuracy and convergence rates have been shown for the recurrent error analysis. We conclude that the suggested approach is a practical and efficient procedure for resolving specific classes of FODEs with a minimum number of calculations and iterations.

Table 8 also compares the absolute and relative error of the approximations from the fifth iterations obtained by the CSDJA of Example 4 at plausible short-listed grid points in the range $x \in [0, 1.0]$ and $t \in [0, 1.0]$ when $Y = 3$ and $\Theta = 2$ with the absolute and relative error of the 5th-step approximations obtained by EDM [36]. The comparison has shown that the suggested method and EDM have the same outcomes. The comparison led us to the conclusion that CSDJA can be used in place of EDM to solve TFSHEs.

Example 5. Consider the following SH equation, which is nonlinear and time-fractional [36]:

$$T_t^\nu f(x, t) + (1 - \Upsilon)f(x, t) + 2 \frac{\partial^2 f(x, t)}{\partial x^2} + \frac{\partial^4 f(x, t)}{\partial x^4} - f^2(x, t) + \left(\frac{\partial f(x, t)}{\partial x}\right)^2 = 0, \quad 0 < \nu \leq 1, \tag{68}$$

with the initial condition:

$$f(x, 0) = e^x. \tag{69}$$

Using CST on both sides of Equation (68),

$$\mathfrak{F}_\nu \left[T_t^\nu f(x, t) + (1 - \Upsilon)f(x, t) + 2 \frac{\partial^2 f(x, t)}{\partial x^2} + \frac{\partial^4 f(x, t)}{\partial x^4} - f^2(x, t) + \left(\frac{\partial f(x, t)}{\partial x}\right)^2 \right] = 0. \tag{70}$$

We get the following result from the Equation (70) by following the processes outlined in Section 3.

$$\mathfrak{F}_\nu [f(x, t)] = \frac{n}{m} e^x - \frac{n}{m} \mathfrak{F}_\nu [(1 - \Upsilon)f(x, t)] - \frac{n}{m} \mathfrak{F}_\nu \left[2 \frac{\partial^2 f(x, t)}{\partial x^2} \right] - \frac{n}{m} \mathfrak{F}_\nu \left[\frac{\partial^4 f(x, t)}{\partial x^4} \right] + \frac{n}{m} \mathfrak{F}_\nu [f^2(x, t)] - \frac{n}{m} \mathfrak{F}_\nu \left[\left(\frac{\partial f(x, t)}{\partial x}\right)^2 \right]. \tag{71}$$

Applying inverse CST to Equation (71),

$$f(x, t) = \mathfrak{F}_\nu^{-1} \left\{ \frac{n}{m} e^x \right\} - \mathfrak{F}_\nu^{-1} \left\{ \frac{n}{m} \mathfrak{F}_\nu [(1 - \Upsilon)f(x, t)] \right\} - \mathfrak{F}_\nu^{-1} \left\{ \frac{n}{m} \mathfrak{F}_\nu \left[2 \frac{\partial^2 f(x, t)}{\partial x^2} \right] \right\} - \mathfrak{F}_\nu^{-1} \left\{ \frac{n}{m} \mathfrak{F}_\nu \left[\frac{\partial^4 f(x, t)}{\partial x^4} \right] \right\} + \mathfrak{F}_\nu^{-1} \left\{ \frac{n}{m} \mathfrak{F}_\nu [f^2(x, t)] \right\} - \mathfrak{F}_\nu^{-1} \left\{ \frac{n}{m} \mathfrak{F}_\nu \left[\left(\frac{\partial f(x, t)}{\partial x}\right)^2 \right] \right\}. \tag{72}$$

Following the procedure given in Section 3 yields the following result:

$$B(f(x, t)) = -\mathfrak{F}_\nu^{-1} \left\{ \frac{n}{m} \mathfrak{F}_\nu [(1 - \Upsilon)f(x, t)] \right\} - \mathfrak{F}_\nu^{-1} \left\{ \frac{n}{m} \mathfrak{F}_\nu \left[2 \frac{\partial^2 f(x, t)}{\partial x^2} \right] \right\} - \mathfrak{F}_\nu^{-1} \left\{ \frac{n}{m} \mathfrak{F}_\nu \left[\frac{\partial^4 f(x, t)}{\partial x^4} \right] \right\}, \tag{73}$$

$$C(f(x, t)) = \mathfrak{F}_v^{-1} \left\{ \frac{n}{m} \mathfrak{F}_v [f^2(x, t)] \right\} - \mathfrak{F}_v^{-1} \left\{ \frac{n}{m} \mathfrak{F}_v \left[\left(\frac{\partial f(x, t)}{\partial x} \right)^2 \right] \right\}, \tag{74}$$

$$\begin{aligned} \sum_{i=0}^{\infty} f_i(x, t) &= \mathfrak{F}_v^{-1} \left\{ \frac{n}{m} e^x \right\} - \mathfrak{F}_v^{-1} \left\{ \frac{n}{m} \mathfrak{F}_v \left[(1 - \Upsilon) \sum_{i=0}^{\infty} f_i(x, t) \right] \right\} \\ &\quad - \mathfrak{F}_v^{-1} \left\{ \frac{n}{m} \mathfrak{F}_v \left[2 \frac{\partial^2}{\partial x^2} \sum_{i=0}^{\infty} f_i(x, t) \right] \right\} \\ &\quad - \mathfrak{F}_v^{-1} \left\{ \frac{n}{m} \mathfrak{F}_v \left[\frac{\partial^4}{\partial x^4} \sum_{i=0}^{\infty} f_i(x, t) \right] \right\} \\ &\quad + \mathfrak{F}_v^{-1} \left\{ \frac{n}{m} \mathfrak{F}_v \left[\sum_{i=0}^{\infty} f_i(x, t) \right]^2 \right\} \\ &\quad - \mathfrak{F}_v^{-1} \left\{ \frac{n}{m} \mathfrak{F}_v \left[\left(\frac{\partial}{\partial x} \sum_{i=0}^{\infty} f_i(x, t) \right)^2 \right] \right\}. \end{aligned} \tag{75}$$

Using the iteration process given in Section 3, the following results are obtained from Equation (75):

$$\begin{aligned} f_0(x, t) &= e^x, \\ f_1(x, t) &= e^x (\Upsilon - 4)^1 \frac{t^{1v}}{1!v^1}, \\ f_2(x, t) &= e^x (\Upsilon - 4)^2 \frac{t^{2v}}{2!v^2}, \\ f_3(x, t) &= e^x (\Upsilon - 4)^3 \frac{t^{3v}}{3!v^3}, \\ f_4(x, t) &= e^x (\Upsilon - 4)^4 \frac{t^{4v}}{4!v^4}, \\ f_5(x, t) &= e^x (\Upsilon - 4)^5 \frac{t^{5v}}{5!v^5}. \end{aligned} \tag{76}$$

As a result, we get the approximate solution to Equations (68) and (69) obtained from the 5th iteration as follows:

$$\begin{aligned} f^{(5)}(x, t) &= e^x + e^x (\Upsilon - 4)^1 \frac{t^v}{1!v^1} + e^x (\Upsilon - 4)^2 \frac{t^{2v}}{2!v^2} \\ &\quad + e^x (\Upsilon - 4)^3 \frac{t^{3v}}{3!v^3} + e^x (\Upsilon - 4)^4 \frac{t^{4v}}{4!v^4} \\ &\quad + e^x (\Upsilon - 4)^5 \frac{t^{5v}}{5!v^5}. \end{aligned} \tag{77}$$

When $v = 1$ is employed in Equation (77), we get the following precise solution to Equations (68) and (69):

$$f(x, t) = e^{x+(\Upsilon-4)t}. \tag{78}$$

Figure 13 represents the 2D graph of the 5th-step approximate and the exact solutions obtained by CSDJA at $v = 0.6, 0.7, 0.8, 0.9$, and $v = 1.0$ with $x = 3.0$ in the interval $t \in [0, 1.0]$ for Example 5. Figure 14 represents the 2D graph of the 5th-step approximate and the exact solutions obtained by CSDJA at $v = 0.6, 0.7, 0.8, 0.9$, and $v = 1.0$ with $Y = 5$

and $t = 0.3$ in the interval $x \in [0, 1.0]$ for Example 5. One can notice the identical conclusions described for Examples 3 and 4.

Figures 15 and 16 show the 2D graph of the comparative study of the approximate solution obtained from the five iterations and exact solution obtained by the proposed method in the form of absolute and relative error with $v = 1.0$ at $x = 3.0$ and $Y = 5$ in the interval $t \in [0, 0.5]$ to Example 5, respectively. One can notice the identical conclusions described for Examples 3 and 4.

The accuracy of the fifth step approximation obtained using the suggested method and the precise solution is shown in a 3D graph in Figures 17 and 18 together with the absolute and relative error at $v = 1.0$ and $Y = 5$ in the intervals $x \in [0, 0.3]$ and $t \in [0, 0.3]$, to Example 5, respectively. From Figures 17 and 18, we yield the same outcomes as in Examples 3 and 4.

From Tables 9 and 10, one can observe the corresponding findings portrayed for Examples 3 and 4.

Recurrence error has been used to quantitatively demonstrate how the approximate solution for Example 5 converges to the exact solution for suitably specified grid locations in the interval $x \in [0, 1.0]$ and $t \in [0, 1.0]$ as in Table 11. One can perceive the equivalent verdicts depicted for Examples 3 and 4.

Table 12 also compares the absolute and relative error of the approximations from the fifth iterations obtained by the CSDJA of Example 5 at plausible short-listed grid points in the range $x \in [0, 1.0]$ and $t \in [0, 1.0]$ with the absolute and relative error of the 5th-step approximations obtained by EDM [36]. One can notice the identical conclusions described for Examples 3 and 4.

Finally, the primary advantages of the CSDJA are as follows, as shown by the numerical and graphical results: the suggested approach is a methodical, potent, and useful tool for both precise and approximate analytical solutions to FODEs. The strength of the suggested method is its modest size of computation, which allows it to be more efficient than existing numerical methods with fewer computations. In the form of absolute and relative error, the numerical results acquired by CSDJA are also contrasted with the other results obtained by EDM. Because of the comparison's great agreement with this method, CSDJA can be used as a substitute for the method EDM to solve TFSHEs. The higher degrees of accuracy and convergence rates were confirmed by the error analysis, demonstrating the suggested method's efficacy and reliability.

5. Conclusion

In this study, we solved TFSHEs in the sense of CD using the CSDJA. We were able to successfully solve both linear and nonlinear TFSHEs using the aforementioned approach. Results in graphs and numerical information have been used to prove the CSDJA's efficacy. According to Table 2, the magnitude of absolute and relative error ranges from $9.08162434143378 \times 10^{-14}$ to 0.00242649361746760660 and from $8.72552875759824810^{-14}$ to 0.00038536947079107625 , respectively, in Example 3. According to Table 6, the

magnitude of absolute and relative error ranges from $1.047606446036297 \times 10^{-12}$ to 0.00261926516767729820 and from $9.865985960312264 \times 10^{-13}$ to 0.00040774789828359850 , respectively, in Example 4. According to Table 10, the magnitude of absolute and relative error ranges from $2.297806389606194 \times 10^{-11}$ to 0.00304568436044938550 and from $2.079141200717798 \times 10^{-11}$ to 0.00045553880438038890 , respectively, in Example 5.

The results of the CSDJA are also contrasted with the EDM in the sense of absolute and relative error. Moreover, the numerical evidence for the convergence of the approximative solution to the exact solution is presented numerically.

The following are the main advantages of the CSDJA, as illustrated by the results obtained using the proposed technique, which demonstrates excellent agreement with EDM. The CSDJA is a suitable replacement tool for the He or Adomian polynomial-based methods used to solve FODEs. The pattern between the coefficients of the series solution made it simple to find accurate solution to numerical problems, and we did so to achieve the exact solutions as indicated in the five applications. The greater degree of accuracy and convergence rates have been proven by the absolute, relative, and recurrence error analysis. Making any large or small physical parametric assumptions about the problem is not necessary. So, it applies to both weak and strongly nonlinear systems, overcoming some of the inherent limits of standard perturbation techniques. The CSDJA can solve nonlinear problems without the aid of He's or Adomian polynomials. The number of calculations needed to solve nonlinear TFSHEs is extremely low. As a result, it performs far better than homotopy analysis and Adomian decomposition methods. As a solution to problems, the CSDJA provides a quick and simple procedure for figuring out the values of the fractional power series. Finally, the CSDJA can generate expansion solutions for linear and nonlinear TFSHEs without the need for perturbation, linearization, or discretization, in contrast to traditional analytic approximation methods. The results led us to the conclusion that our technique is easy to use, accurate, flexible, and effective. We intend to use the CSDJA to address other FODE systems that develop in different contexts in the future.

Data Availability

The numerical data used to support the findings of this study is included in the article.

Conflicts of Interest

The authors declare that they have no conflicts of interest.

References

- [1] D. S. Sachan, S. Jaloree, and J. Choi, "Certain recurrence relations of two parametric Mittag-Leffler function and their application in fractional calculus," *Fractal and Fractional*, vol. 5, no. 4, p. 215, 2021.
- [2] D. Baleanu, A. Jajarmi, H. Mohammadi, and S. Rezapour, "A new study on the mathematical modelling of human liver with Caputo-Fabrizio fractional derivative," *Chaos, Solitons & Fractals*, vol. 134, article 109705, 2020.
- [3] R. Hilfer, P. L. Butzer, and U. Westphal, "An introduction to fractional calculus," in *Applications of Fractional Calculus in Physics*, pp. 1–85, World Scientific, 2010.
- [4] Z. E. A. Fellah, M. Fellah, E. Ogam, A. Berbiche, and C. Depollier, "Reflection and transmission of transient ultrasonic wave in fractal porous material: application of fractional calculus," *Wave Motion*, vol. 106, article 102804, 2021.
- [5] N. H. Tuan, H. Mohammadi, and S. Rezapour, "A mathematical model for COVID-19 transmission by using the Caputo fractional derivative," *Chaos, Solitons & Fractals*, vol. 140, article 110107, 2020.
- [6] J. T. Machado, "The bouncing ball and the Grünwald-Letnikov definition of fractional derivative," *Fractional Calculus and Applied Analysis*, vol. 24, no. 4, pp. 1003–1014, 2021.
- [7] X. Li, C. Han, and Y. Wang, "Novel patterns in fractional-in-space nonlinear coupled FitzHugh–Nagumo models with Riesz fractional derivative," *Fractal and Fractional*, vol. 6, no. 3, p. 136, 2022.
- [8] M. A. Herzallah, "Notes on some fractional calculus operators and their properties," *Journal of Fractional Calculus and Applications*, vol. 5, no. 19, pp. 1–10, 2014.
- [9] M. I. Liaqat, A. Khan, M. Alam, and M. K. Pandit, "A highly accurate technique to obtain exact solutions to time-fractional quantum mechanics problems with zero and non-zero trapping potential," *Journal of Mathematics*, vol. 2022, Article ID 9999070, 20 pages, 2022.
- [10] H. Mohammadi, S. Kumar, S. Rezapour, and S. Etemad, "A theoretical study of the Caputo-Fabrizio fractional modeling for hearing loss due to Mumps virus with optimal control," *Chaos, Solitons & Fractals*, vol. 144, article 110668, 2021.
- [11] R. Khalil, M. Al Horani, A. Yousef, and M. Sababheh, "A new definition of fractional derivative," *Journal of Computational and Applied Mathematics*, vol. 264, pp. 65–70, 2014.
- [12] A. Harir, S. Melliani, and L. S. Chadli, "Fuzzy Generalized Conformable Fractional Derivative," *Advances in fuzzy systems*, vol. 2020, Article ID 1954975, 7 pages, 2020.
- [13] A. El-Ajou, "A modification to the conformable fractional calculus with some applications," *Alexandria Engineering Journal*, vol. 59, no. 4, pp. 2239–2249, 2020.
- [14] D. R. Anderson and D. J. Ulness, "Properties of the Katugampola fractional derivative with potential application in quantum mechanics," *Journal of Mathematical Physics*, vol. 56, no. 6, article 063502, 2015.
- [15] C. Vanterler da, J. Sousa, and E. Capelas de Oliveira, "A new truncated M-fractional derivative type unifying some fractional derivative types with classical properties," *International Journal of Analysis and Applications*, vol. 16, no. 1, pp. 83–96, 2018.
- [16] P. Ahuja, F. Zulfqarr, and A. Ujlayan, "Deformable fractional derivative and its applications," *AIP Conference Proceedings*, vol. 1897, no. 1, article 020008, 2017.
- [17] D. R. Anderson and D. J. Ulness, "Newly defined conformable derivatives," *Advances in Dynamical Systems and Applications*, vol. 10, no. 2, pp. 109–137, 2015.
- [18] O. H. Mohammed and H. A. Salim, "Computational methods based Laplace decomposition for solving nonlinear system of fractional order differential equations," *Alexandria Engineering Journal*, vol. 57, no. 4, pp. 3549–3557, 2018.

- [19] A. Khan, M. I. Liaqat, M. Younis, and A. Alam, "Approximate and exact solutions to fractional order Cauchy reaction-diffusion equations by new combine techniques," *Journal of Mathematics*, vol. 2021, Article ID 5337255, 12 pages, 2021.
- [20] K. J. Wang, "On new abundant exact traveling wave solutions to the local fractional Gardner equation defined on cantor sets," *Mathematical Methods in the Applied Sciences*, vol. 45, no. 4, pp. 1904–1915, 2022.
- [21] T. A. J. Al-Griffi and A. S. J. Al-Saif, "Yang transform–homotopy perturbation method for solving a non-Newtonian viscoelastic fluid flow on the turbine disk," *ZAMM-Journal of Applied Mathematics and Mechanics*, vol. 102, no. 8, article e202100116, 2022.
- [22] M. I. Liaqat, S. Etemad, S. Rezapour, and C. Park, "A novel analytical Aboodh residual power series method for solving linear and nonlinear time-fractional partial differential equations with variable coefficients," *AIMS Mathematics*, vol. 7, no. 9, pp. 16917–16948, 2022.
- [23] Z. B. Li and J. H. He, "Fractional complex transform for fractional differential equations," *Mathematical and Computational Applications*, vol. 15, no. 5, pp. 970–973, 2010.
- [24] M. I. Liaqat and A. Akgül, "A novel approach for solving linear and nonlinear time-fractional Schrodinger equations," *Chaos, Solitons & Fractals*, vol. 162, article 112487, 2022.
- [25] R. Shah, A. Saad Alshehry, and W. Weera, "A semi-analytical method to investigate fractional-order gas dynamics equations by Shehu transform," *Symmetry*, vol. 14, no. 7, p. 1458, 2022.
- [26] P. Sunthrayuth, R. Shah, A. M. Zidan, S. Khan, and J. Kafle, "The analysis of fractional-order Navier-Stokes model arising in the unsteady flow of a viscous fluid via Shehu transform," *Journal of Function Spaces*, vol. 2021, Article ID 1029196, 15 pages, 2021.
- [27] S. Maitama and W. Zhao, "Homotopy perturbation Shehu transform method for solving fractional models arising in applied sciences," *Journal of Applied Mathematics and Computational Mechanics*, vol. 20, no. 1, pp. 71–82, 2021.
- [28] M. I. Liaqat, A. Khan, A. Akgül, and M. Ali, "A novel numerical technique for fractional ordinary differential equations with proportional delay," *Journal of Function Spaces*, vol. 2022, Article ID 6333084, 21 pages, 2022.
- [29] Ü. Lepik, "Numerical solution of evolution equations by the Haar wavelet method," *Applied Mathematics and Computation*, vol. 185, no. 1, pp. 695–704, 2007.
- [30] J. Liu, X. Li, and L. Wu, "An operational matrix technique for solving variable order fractional differential-integral equation based on the second kind of Chebyshev polynomials," *Advances in Mathematical Physics*, vol. 2016, Article ID 6345978, 9 pages, 2016.
- [31] Y. Keskin and G. Oturanc, "Reduced differential transform method for partial differential equations," *International Journal of Nonlinear Sciences and Numerical Simulation*, vol. 10, no. 6, pp. 741–750, 2009.
- [32] F. Ghoreishi and S. Yazdani, "An extension of the spectral tau method for numerical solution of multi-order fractional differential equations with convergence analysis," *Computers & Mathematics with Applications*, vol. 61, no. 1, pp. 30–43, 2011.
- [33] S. Hasan, A. El-Ajou, S. Hadid, M. Al-Smadi, and S. Momani, "Atangana-Baleanu fractional framework of reproducing kernel technique in solving fractional population dynamics system," *Chaos, Solitons & Fractals*, vol. 133, article 109624, 2020.
- [34] M. I. Liaqat, A. Khan, and A. Akgül, "Adaptation on power series method with conformable operator for solving fractional order systems of nonlinear partial differential equations," *Chaos, Solitons & Fractals*, vol. 157, article 111984, 2022.
- [35] W. K. Zahra, M. A. Nasr, and D. Baleanu, "Time-fractional nonlinear Swift-Hohenberg equation: analysis and numerical simulation," *Alexandria Engineering Journal*, vol. 59, no. 6, pp. 4491–4510, 2020.
- [36] K. Nonlaopon, A. M. Alsharif, A. M. Zidan, A. Khan, Y. S. Hamed, and R. Shah, "Numerical investigation of fractional-order Swift–Hohenberg equations via a novel transform," *Symmetry*, vol. 13, no. 7, p. 1263, 2021.
- [37] M. Alaroud, N. Tahat, S. Al-Omari, D. L. Suthar, and S. Gulyaz-Ozyurt, "An attractive approach associated with transform functions for solving certain fractional Swift-Hohenberg equation," *Journal of Function Spaces*, vol. 2021, Article ID 3230272, 14 pages, 2021.
- [38] D. G. Prakasha, P. Veeresha, and H. M. Baskonus, "Residual power series method for fractional Swift–Hohenberg equation," *Fractal and fractional*, vol. 3, no. 1, 2019.
- [39] W. K. Zahra, S. M. Elkholy, and M. Fahmy, "Rational spline-nonstandard finite difference scheme for the solution of time-fractional Swift-Hohenberg equation," *Applied Mathematics and Computation*, vol. 343, pp. 372–387, 2019.
- [40] T. Ban and R. Q. Cui, "He's homotopy perturbation method for solving time fractional Swift-Hohenberg equations," *Thermal Science*, vol. 22, no. 4, pp. 1601–1605, 2018.
- [41] E. Balcı, İ. Öztürk, and S. Kartal, "Dynamical behaviour of fractional order tumor model with Caputo and conformable fractional derivative," *Chaos, Solitons & Fractals*, vol. 123, pp. 43–51, 2019.
- [42] W. S. Chung, "Fractional Newton mechanics with conformable fractional derivative," *Journal of Computational and Applied Mathematics*, vol. 290, pp. 150–158, 2015.
- [43] M. I. Liaqat, A. Khan, M. Alam, M. K. Pandit, S. Etemad, and S. Rezapour, "Approximate and closed-form solutions of Newell-Whitehead-Segel equations via modified conformable Shehu transform decomposition method," *Mathematical Problems in Engineering*, vol. 2022, Article ID 6752455, 14 pages, 2022.
- [44] M. E. Benattia and K. Belghaba, "Shehu conformable fractional transform, theories and applications," *Cankaya University Journal of Science and Engineering*, vol. 18, no. 1, pp. 24–32, 2021.
- [45] S. Rezapour, M. I. Liaqat, and S. Etemad, "An effective new iterative method to solve conformable Cauchy reaction-diffusion equation via the Shehu transform," *Journal of Mathematics*, vol. 2022, Article ID 4172218, 12 pages, 2022.

Research Article

Computational Insights of Bioconvective Third Grade Nanofluid Flow past a Riga Plate with Triple Stratification and Swimming Microorganisms

Safak Kayikci 

Department of Computer Engineering, Bolu Abant Izzet Baysal University, Bolu, Turkey

Correspondence should be addressed to Safak Kayikci; safak.kayikci@ibu.edu.tr

Received 14 June 2022; Revised 14 July 2022; Accepted 16 July 2022; Published 31 August 2022

Academic Editor: Arzu Akbulut

Copyright © 2022 Safak Kayikci. This is an open access article distributed under the Creative Commons Attribution License, which permits unrestricted use, distribution, and reproduction in any medium, provided the original work is properly cited.

The goal of this study is to examine the heat-mass effects of a third grade nanofluid flow through a triply stratified medium containing nanoparticles and gyrostatic microorganisms swimming in the flow. The heat and mass fluxes are considered as a non-Fourier model. The governing models are constructed as a partial differential system. Using correct transformations, these systems are converted to an ordinary differential model. Ordinary systems are solved using convergent series solutions. The effects of physical parameters for fluid velocity, fluid temperature, nanoparticle volume percentage, motile microbe density, skin friction coefficients, local Nusselt number, and local Sherwood number are all illustrated in detail. When the values of the bioconvection Lewis number increase, the entropy rate also rises. The porosity parameter and modified Hartmann number show the opposite behaviour in the velocity profile.

1. Introduction

Researchers are interested in learning more about how to increase heat transmission because it is so important in design and business. Thermal transfer of convectional liquids such as ethylene glycol, water, and oil can be used in a variety of mechanical assemblies, electrical devices, and heat dissipates. Despite this, the thermal conductivity of these base fluids is weak. To counter this flaw, experts from several sectors are attempting to improve the heat conductivity of newly cited fluids by incorporating a unique type of nanosized particle into a new fluid known as “nanofluid,” see Choi [1]. Nanofluid flow on a flat surface was examined by Khan and Pop [2]. They see that the mass transfer gradient reduces for enhancing the thermophoresis parameter. Barnoon and Toghraie [3] analyze the impact of a non-Newtonian nanofluid on a porous medium. Natural convective flow of nanofluid past a heated porous plate was demonstrated by Ghaleb et al. [4], and they concluded that the fluid velocity ceases when increasing the thermophoresis parameter. Aziz and Khan [5] demonstrated the

characteristics of natural convective flow of nanofluids over a plate. They identified that heat transfer reduced by the impact of Brownian motion parameter. The nanofluid flow over a thin needle was addressed by Ahmad et al. [6]. They proved that the Brownian motion parameter leads to suppressing the nanofluid concentration. Prasannakumara et al. [7] addressed the consequences of multiple slips of MHD Jeffery nanofluid past a surface. They detected that the thermal boundary layer thickness thickens when enriching the thermophoresis parameter.

The bioconvection phenomenon is a fluid dynamic mechanism that occurs in macroscopic convective fluid flow generated by a fluid density gradient established by collective swimming of microorganisms. Because of their motility, these bacteria are classified as chemotactic, oxytactic, or gyrotactic. Near the top of the fluid layer, these self-propelled motile bacteria clump together, forming a dense upper surface that is unstable or unstabilized. Bioconvection is used in a variety of industrial applications, including microbial improved oil recovery, sustainable fuel cell technologies, water treatment facilities, polymer synthesis,

and so on. The 2D radiative flow of tangent hyperbolic nanofluid past a Riga plate with gyrotactic microorganisms was disclosed by Waqas et al. [8]. They noted that the density of motile microorganisms decays when enriching the bioconvection Lewis number. Uddin et al. [9] portrayed the consequences of Stefan blowing of bioconvective flow of nanofluid past a porous medium. They see that the density of motile microorganisms enriches when strengthening the wall suction parameter. MHD flow of cross nanofluids with gyrotactic motile microorganisms past wedge was scrutinized by Alshomrani et al. [10]. They noted that the motile microorganisms suppress when escalating the Peclet number. Muhammad et al. [11] developed the mathematical model for the unsteady MHD flow of Carreau nanofluids with bioconvection. They detected that the density of local motile number depresses when enhancing the Peclet parameter.

Due to its numerous industrial and engineering uses, such as cooling nuclear reactors, power generation, cooling of electronic equipment, energy production, and many others, the process of heat transfer has gotten a lot of attention from modern scholars. Fourier [12] was the first to present the heat transfer law. However, this law has the disadvantage of producing a parabolic energy equation. To address this flaw, Cattaneo [13] rewrote the Fourier equation by including the relaxation time heat flux component. In addition, Christov [14] tweaked the Cattaneo model by incorporating thermal relaxation time and used the Oldroyd upper convective model. The heat transport analysis of 2D flow cross nanofluid Cattaneo–Christov theory was investigated by Salahuddin et al. [15], and they proved that concentration relaxation leads to downfall of the nanofluid concentration. Farooq et al. [16] examined the impact of MHD flow of radiative nanofluids with Cattaneo–Christov theory. They revealed that the fluid temperature diminishes when raising the thermal relaxation parameter. Thermally radiative flow of hybrid nanoliquids with Cattaneo–Christov heat flux theory was implemented by Waqas et al. [17].

Despite the fact that nanofluids have been widely investigated, the third grade nanofluid flow over a stretching sheet with entropy optimization was examined by Loganathan et al. [18]. This study is extended with the effects of including the mixed convective flow of third grade nanofluids over a Riga plate with triple stratification and swimming microorganisms. The thermal radiative flow of third grade nanofluids containing microorganisms owing to the movement of the Riga plate is shown in this study to achieve this goal.

- (i) The modified Fourier’s law is used to frame energy and nanoparticle concentration equations
- (ii) The homotopy analysis method is used to compute the non-linear equations analytically
- (iii) The results of the simulations might have unique implications in the fields of thermal processes, heat transfer industry, energy systems, nuclear systems, and so on

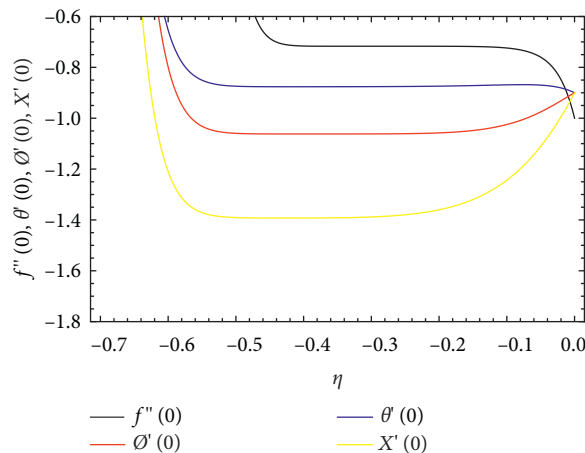


FIGURE 1: h -curves for $(h_f, h_\theta, h_\phi, \text{ and } h_\chi)$.

2. Problem Development

For an incompressible fluid model with body forces, the continuity and motion equations are

$$\begin{aligned} \operatorname{div} v^* &= 0, \\ \rho \frac{dv}{dt} &= \operatorname{div} T + \rho b + J + B, \end{aligned} \quad (1)$$

where ρ is the “fluid density,” v^* is the “velocity field,” b is the “body forces,” J is the “electric current,” and T is the “third-grade incompressible fluids Cauchy stress tensor” [19].

$$\begin{aligned} T &= -pI + \mu H_1 + A_1^* H_2 + A_2^* H_1^2 + \gamma_1 H_3 \\ &\quad + \gamma_2 (H_1, H_2 + H_2 H_1) + \gamma_3 (\operatorname{tr} H_1^2) H_1, \end{aligned} \quad (2)$$

where $\mu, (H_1, H_2, H_3)$ and A_1^*, γ_i – “viscosity coefficient”, “kinematics tensors” and “material modulus”

$$\begin{aligned} H_1 &= L + (L)^T, \\ H_n &= \frac{d}{dt} H_{n-1} + H_{n-1} L + (L)^T H_{n-1}, \quad n = 2, 3, \\ L &= \nabla v^*, \end{aligned} \quad (3)$$

d/dt is expressed as the material time derivative

$$\frac{d(\cdot)}{dt} = \frac{\partial(\cdot)}{\partial t} + v^* \cdot \nabla(\cdot). \quad (4)$$

The relationship between the Clausius–Duhem inequality and the thermodynamically compatible fluid is described by Fosdick and Rajagopal. [20].

$$\begin{aligned} \mu &\geq 0, \\ A_1^* &\geq 0, \\ \gamma_1 = \gamma_2 &= 0, \\ \gamma_3 &\geq 0, \\ |A_1^* + A_2^*| &\leq 2\sqrt{6\mu\gamma_3}, \\ T &= -pI + \mu H_1 + A_1^* H_2 + A_2^* H_1^2 + \gamma_3 (\operatorname{tr} H_1^2) H_1. \end{aligned} \quad (5)$$

Pakdemirli [21] took into consideration the Boussinesq and normal boundary layer approximations.

The representation of steady flow of third grade nano-fluids containing motile microorganisms is assumed. The surface is linearly stretched via velocity $u_w = ax$, in positive x direction in its own path. Moreover, the flow is considered along the sheet while v is perpendicular, and B_0 magnetic

field is taken vertical to the flow direction. The wall temperature T_w , wall concentration C_w , and motile microorganisms' wall concentration N_w are defined. Figure 1 portrays the flow geometry of the problem. The governing equations are extended from Loganathan et al. [18] as follows:

$$\begin{aligned} \frac{\partial u}{\partial x} + \frac{\partial v}{\partial y} &= 0, \\ u \frac{\partial u}{\partial x} + v \frac{\partial u}{\partial y} &= \nu \frac{\partial^2 u}{\partial y^2} + \frac{A_1^*}{\rho} \left(u \frac{\partial^3 u}{\partial y^2 \partial x} + v \frac{\partial^3 u}{\partial y^3} + \frac{\partial u}{\partial x} \frac{\partial^2 u}{\partial y^2} + 3 \frac{\partial u}{\partial y} \frac{\partial^2 u}{\partial x \partial y} \right) + 2 \frac{A_2^*}{\rho} \frac{\partial u}{\partial y} \frac{\partial^2 u}{\partial x \partial y} \\ &+ 6 \frac{\beta_1^*}{\rho} \left(\frac{\partial u}{\partial y} \right)^2 \frac{\partial^2 u}{\partial y^2} - \frac{\nu}{k_p} u - \frac{C_b}{x \sqrt{k_p}} u^2 + \frac{1}{\rho_f} (1 - C_\infty) \rho_f \beta g (T - T_\infty) \\ &- (\rho_p - \rho_f) g (C - C_\infty) - (N - N_\infty) g \gamma (\rho_m - \rho_f) + \frac{\pi J_0 M_0}{8\rho} \exp\left(-\frac{\pi}{a_1} y\right) \\ &\cdot u \frac{\partial T}{\partial x} + v \frac{\partial T}{\partial y} + \lambda_T \left(u^2 \frac{\partial^2 T}{\partial x^2} + v^2 \frac{\partial^2 T}{\partial y^2} + \left(u \frac{\partial u}{\partial x} \frac{\partial T}{\partial x} + v \frac{\partial u}{\partial y} \frac{\partial T}{\partial x} \right) + 2uv \frac{\partial T^2}{\partial x \partial y} \right) \\ &+ \left(u \frac{\partial v}{\partial x} \frac{\partial T}{\partial y} + v \frac{\partial v}{\partial y} \frac{\partial T}{\partial y} \right) = \frac{k}{\rho c_p} \frac{\partial^2 T}{\partial y^2} - \frac{1}{\rho c_p} \frac{16\sigma^*}{3k^*} \frac{\partial}{\partial y} \left(T^3 \frac{\partial T}{\partial y} \right) + \frac{Q_0}{\rho c_p} (T - T_\infty) + \tau \left[D_B \frac{\partial C}{\partial y} \frac{\partial T}{\partial y} + \frac{D_T}{T_\infty} \left(\frac{\partial T}{\partial y} \right)^2 \right], \\ u \frac{\partial C}{\partial x} + v \frac{\partial C}{\partial y} &= D_B \frac{\partial^2 C}{\partial y^2} + \frac{D_T}{T_\infty} \frac{\partial^2 T}{\partial y^2} + \lambda_C \left(u^2 \frac{\partial^2 C}{\partial x^2} + v^2 \frac{\partial^2 C}{\partial y^2} + \left(u \frac{\partial u}{\partial x} \frac{\partial C}{\partial x} + v \frac{\partial u}{\partial y} \frac{\partial C}{\partial x} \right) + 2uv \frac{\partial C^2}{\partial x \partial y} \right) \\ &+ \left(u \frac{\partial v}{\partial x} \frac{\partial C}{\partial y} + v \frac{\partial v}{\partial y} \frac{\partial C}{\partial y} \right) - k_c (C - C_\infty), \\ u \frac{\partial N}{\partial x} + v \frac{\partial N}{\partial y} - D_m \left(\frac{\partial^2 N}{\partial y^2} \right) &= -\frac{bW_c}{(C_w - C_\infty)} \left[\frac{\partial}{\partial y} \left(N \frac{\partial C}{\partial y} \right) \right]. \end{aligned} \quad (6)$$

With the boundary points

$$\begin{aligned} u &= u_w = ax, \\ v &= 0, \\ T &= T_w = T_0 + b_1 x, \\ C &= C_w = C_0 + d_1 x, \\ N &= N_w = N_0 + e_1 x \text{ at } y = 0, \\ u &\longrightarrow 0, \\ T &= T_\infty = T_0 + b_2 x, \\ C &= C_\infty \\ N &= N_\infty = N_0 + e_2 x \text{ as } y \longrightarrow \infty. \end{aligned} \quad (7)$$

Here, b_1, b_2, d_1, d_2, e_1 , and e_2 are the dimensional constants, and T_0 and C_0 are the "reference temperature and concentrations," respectively. u and v are the "velocity components" in x and y directions, ρ is the "fluid density," ν is the "fluid kinematics viscosity," k_p is the "permeability of the porous medium," C_b is the "drag coefficient," J_0 is the "current density applied to the electrodes," M_0 is the "magnetic property of the permanent magnets," a_1 is the "magnets positioned in the interval separating the electrodes," σ^* is the "Stefen-Boltzmann constant," C_p is the "specific heat capacity of the fluid," and k is the "thermal conductivity."

Transformations are declared as follows:

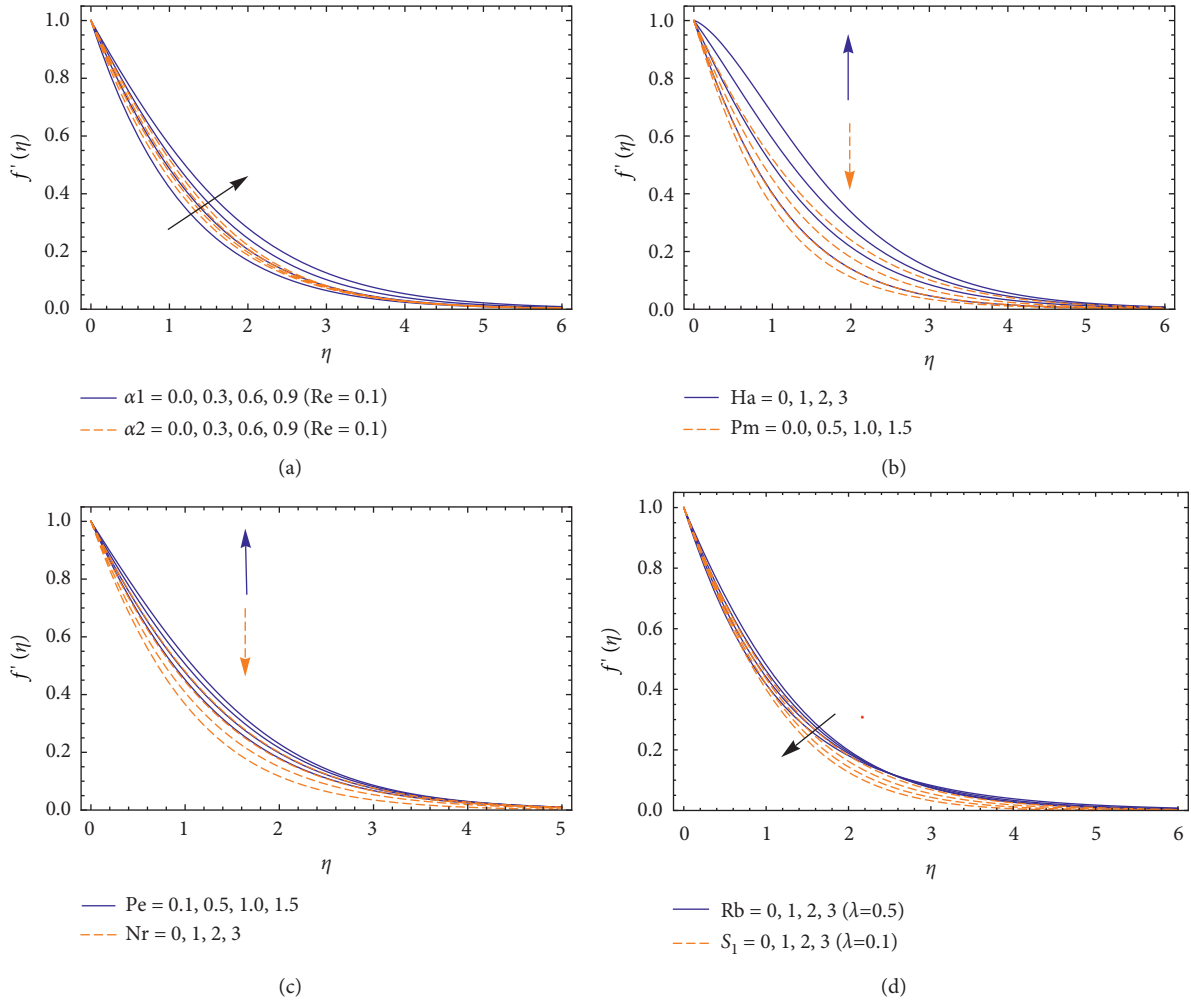


FIGURE 2: Velocity profile for different values of $\alpha_1, \alpha_2, Ha, P_m, Pe, Nr, Rb$, and S_1 .

$$\begin{aligned}
 \eta &= y \left(\frac{a}{\nu} \right)^{1/2}, \\
 \psi &= (a\nu)^{1/2} f(\eta), \\
 u &= \frac{\partial \psi}{\partial y}, \\
 v &= -\frac{\partial \psi}{\partial x}, \\
 u &= u_w f'(\eta), \\
 v &= -(u_w)^{1/2} f(\eta), \\
 \theta &= \frac{T - T_\infty}{T_w - T_0}, \\
 \phi(\eta) &= \frac{C - C_\infty}{C_w - C_0}, \\
 \chi(\eta) &= \frac{N - N_\infty}{N_w - N_0}.
 \end{aligned} \tag{8}$$

The nonlinear governing equations are

$$\begin{aligned}
 f''' + f f'' - f'^2 + \alpha_1 (2f' f''' - f f^{iv}) + (3\alpha_1 + 2\alpha_2) f'^2 \\
 + 6\beta \text{Re} f''' f'^2 - P_m f' - \text{Fr} f'^2 + Hm e^{-\delta \eta} \\
 + \lambda (\theta - N_r \phi - R_b \chi) = 0, \\
 \left(1 + \frac{4}{3} R d \right) \theta'' + \text{Pr} f \theta' - \text{Pr} S_1 f' \\
 - \text{Pr} \Gamma_1 \left[f'^2 \theta + S_1 f'^2 - f f' \theta' - f f'' \theta - S_1 f f'' + f^2 \theta'' \right] \\
 + \text{Pr} H g \theta + \text{Pr} N b \theta' \phi + \text{Pr} N t \theta'^2 = 0, \\
 \phi'' + L_e f \phi' - L_e S_2 f' \\
 - L_e \Gamma_2 \left[f'^2 \phi + S_2 f'^2 - f f' \phi' - f f'' \phi - S_2 f f'' + f^2 \phi'' \right] \\
 + \frac{N t}{N b} \theta'' - L_e C r \phi = 0, \\
 \chi'' + L_b \left[f \chi' - f' \chi \right] - L_b S_3 f' \\
 - P_e \left[\phi'' (\chi + \Omega) + \phi' \chi' \right] = 0.
 \end{aligned} \tag{9}$$

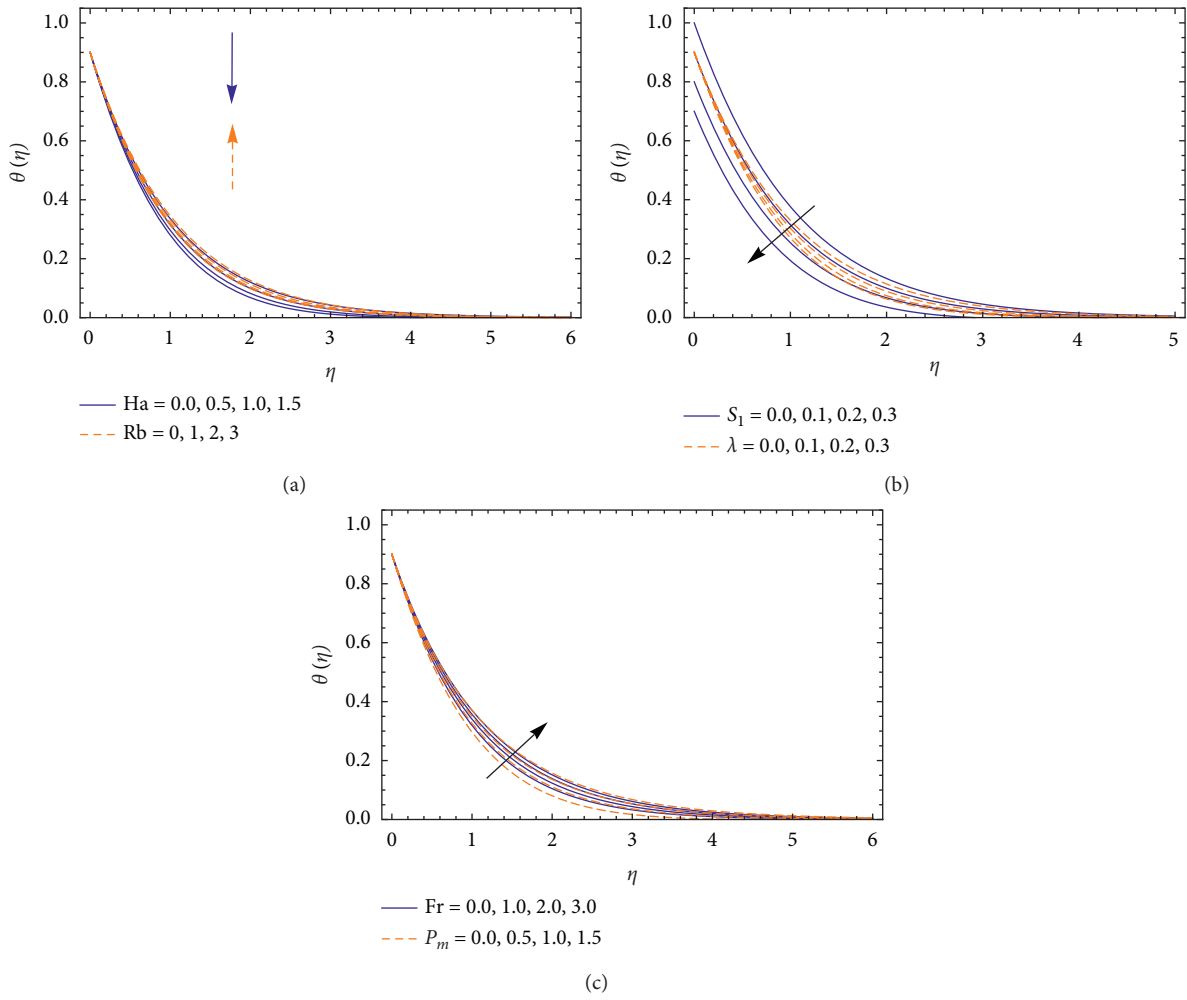


FIGURE 3: Temperature profile for different values of Ha , Rb , S_1 , λ , Fr , and P_m .

The boundary conditions are specified in the following manner:

$$\begin{aligned} f(0) &= 0, \\ f'(0) &= 1, \\ \theta(0) &= 1 - S_1, \\ \phi(0) &= 1 - S_2, \end{aligned}$$

$$\begin{aligned} \chi(0) &= 1 - S_3, \\ f'(\infty) &= 0, \\ \theta(\infty) &= 0, \\ \phi(\infty) &= 0, \\ \chi(\infty) &= 0, \end{aligned}$$

(10)

The nondimensional variables are

$$\begin{aligned} \text{Material parameters} &= \left(\alpha_1 = \frac{aA_1^*}{\nu}, \alpha_2 = \frac{aA_2^*}{\nu}, \beta = \frac{a\beta_1^*}{\nu} \right), \\ \text{Reynolds number (Re)} &= \frac{u_w x}{\nu}, \\ \text{Porous medium (} P_m \text{)} &= \frac{\nu}{k_p a}, \\ \text{Forchheimer number (Fr)} &= \frac{C_b}{\sqrt{k_p}} \end{aligned}$$

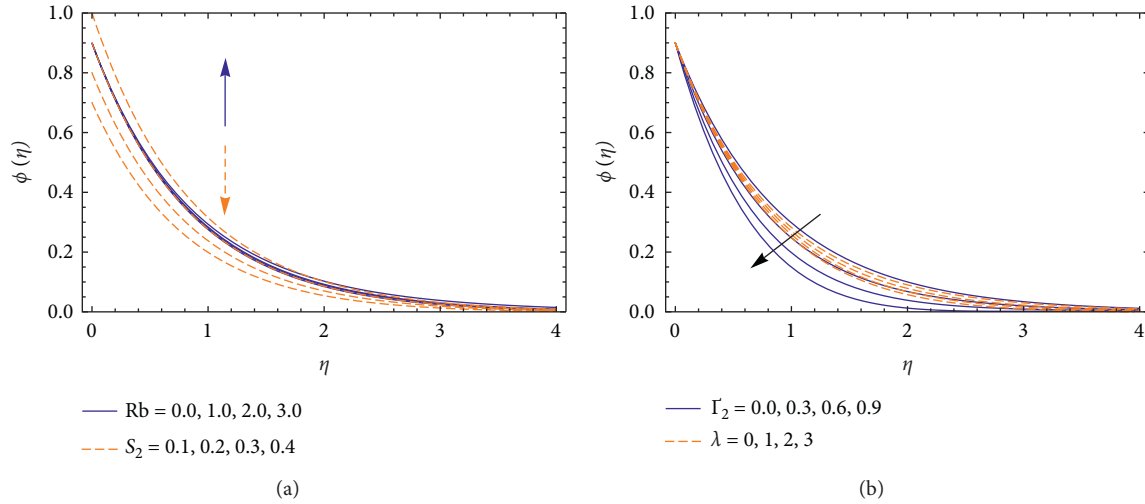


FIGURE 4: Nanoparticle concentration profile for different values of Ha, Rb, S_1, λ, Fr , and P_m .

$$\text{Prandtl number (Pr)} = \frac{\rho C_p}{k},$$

$$\text{Radiation parameter (Rd)} = \frac{(4\sigma^* T_\infty^3)}{(kk^*)},$$

$$\text{Heat generation parameter (Hg)} = \frac{Q_0}{\rho c_p},$$

$$\text{Heat thermal relaxation parameter } (\Gamma_1) = \lambda_T a,$$

$$\text{Mass thermal relaxation parameter } (\Gamma_2) = \lambda_C a,$$

$$\text{Mixed convection parameter } (\lambda) = \frac{\beta \gamma (1 - C_\infty)(T_w - T_0)}{a u_w},$$

$$\text{Buoyancy ratio parameter } (N_r) = \frac{(\rho_p - \rho_f)(C_w - C_0)}{\beta \rho_f (\hat{T}_w - \hat{T}_0)},$$

$$\text{Bioconvection Rayleigh number } (R_b) = \frac{\gamma (N_w - N_0)(\rho_m - \rho_f)}{\beta \rho_f (1 - C_\infty)(T_w - T_0)},$$

$$\text{Thermophoresis parameter } (N_t) = \frac{\tau D_T (T_w - T_0)}{\nu},$$

$$\text{Brownian motion parameter } (N_b) = \frac{\tau D_B (C_w - C_0)}{\nu},$$

$$\text{Lewis number } (Le) = \frac{\nu}{D_B},$$

$$\text{Bioconvection Lewis number } (L_b) = \frac{\nu}{D_m},$$

$$\text{Bioconvection Peclet number } (P_e) = \frac{b W_c}{D_m},$$

$$\text{Microorganisms concentration difference parameter } (\Omega) = \frac{N_\infty}{N_w - N_0},$$

$$\text{Thermal stratification parameter } (S_1) = \frac{b_2}{b_1},$$

$$\text{Mass stratification parameter } (S_2) = \frac{d_2}{d_1},$$

$$\text{Motile density stratification parameter } (S_3) = \frac{e_2}{e_1} \quad (11)$$

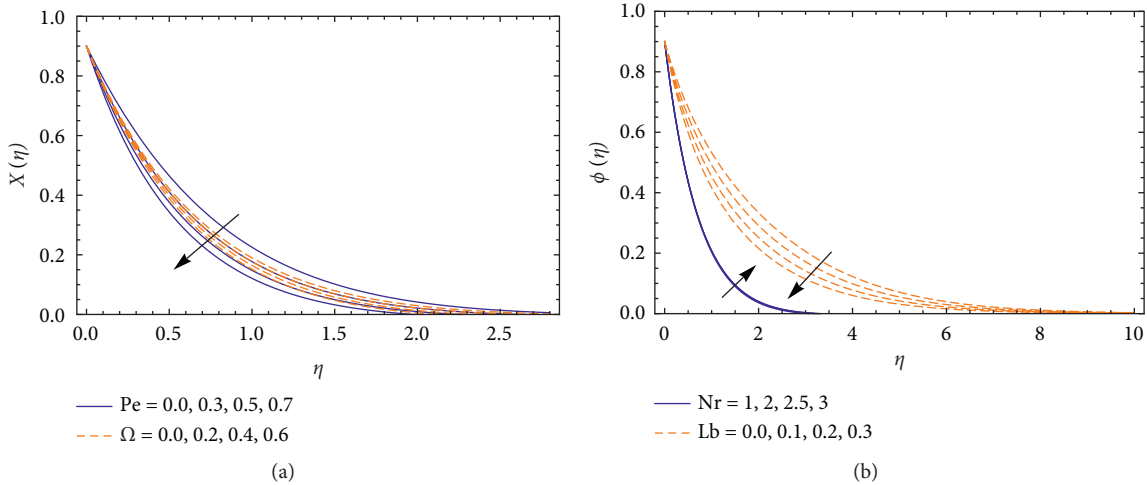


FIGURE 5: Microorganism profile for different values of P_e , Ω , Nr , and L_b .

Application of physical entitles are

$$\begin{aligned}
 C_f Re^{-0.5} &= f''(0) + \alpha_1 f'(0) f'''(0) + \beta Re [f''(0)]^3, \\
 Nu_x Re^{-0.5} &= -\left(1 + \frac{4}{3} Rd\right) \theta'(0), \\
 Sh_x Re^{-0.5} &= -\phi'(0), \\
 Nn_x Re^{-0.5} &= -\chi'(0).
 \end{aligned}
 \tag{12}$$

3. Modelling of Entropy Generation

For the third grade nanoliquid, the entropy generation rate is as follows:

$$\begin{aligned}
 S''_{gen} = & \left\langle \frac{K_1}{T_\infty^2} \left[\left(\frac{\partial T}{\partial x} \right)^2 + \left(\frac{\partial T}{\partial y} \right)^2 + \frac{16\sigma^* T_\infty^3}{3kk^*} \left(\frac{\partial T}{\partial y} \right)^2 \right] + \frac{\mu}{T_\infty} \left[2 \left(\frac{\partial u}{\partial x} \right)^2 + \left(\frac{\partial v}{\partial y} \right)^2 \right] + \left[\frac{\partial u}{\partial y} + \frac{\partial v}{\partial x} \right]^2 + \frac{RD}{C_\infty} \left[\left(\frac{\partial C}{\partial x} \right)^2 + \left(\frac{\partial C}{\partial y} \right)^2 \right] \right. \\
 & \left. + \frac{RD}{T_\infty} \left[\left(\frac{\partial T}{\partial x} \right) \left(\frac{\partial C}{\partial x} \right) + \left(\frac{\partial T}{\partial y} \right) \left(\frac{\partial C}{\partial y} \right) \right] + \frac{RD}{N_\infty} \left(\frac{\partial N}{\partial y} \right)^2 + \frac{RD}{T_\infty} \left[\left(\frac{\partial T}{\partial x} \right) \left(\frac{\partial N}{\partial x} \right) + \left(\frac{\partial T}{\partial y} \right) \left(\frac{\partial N}{\partial y} \right) \right] \right\rangle,
 \end{aligned}
 \tag{13}$$

Equation (13) was changed by using the boundary layer approximation.

$$\begin{aligned}
 S''_{gen} &= \left\langle \frac{K_1}{T_\infty^2} \left[\left(\frac{\partial T}{\partial y} \right)^2 + \frac{16\sigma^* T_\infty^3}{3kk^*} \left(\frac{\partial T}{\partial y} \right)^2 \right] + \frac{\mu}{T_\infty} \left(\frac{\partial u}{\partial y} \right)^2 + \frac{RD}{C_\infty} \left(\frac{\partial C}{\partial y} \right)^2 + \frac{RD}{T_\infty} \left(\frac{\partial T}{\partial y} \right) \left(\frac{\partial C}{\partial y} \right) + \frac{RD}{N_\infty} \left(\frac{\partial N}{\partial y} \right)^2 + \frac{RD}{T_\infty} \left[\left(\frac{\partial T}{\partial y} \right) \left(\frac{\partial N}{\partial y} \right) \right] \right\rangle, \\
 N_T &= \frac{K_1}{T_\infty^2} \left[\left(\frac{\partial T}{\partial y} \right)^2 + \frac{16\sigma^* T_\infty^3}{3kk^*} \left(\frac{\partial T}{\partial y} \right)^2 \right] = \text{“Entropy contribution due to heat transmission”}, \\
 N_f &= \frac{\mu}{T_\infty} \left(\frac{\partial u}{\partial y} \right)^2 = \text{“Entropy contribution due to fluid friction”}, \\
 N_C &= \frac{RD}{C_\infty} \left(\frac{\partial C}{\partial y} \right)^2 + \frac{RD}{T_\infty} \left(\frac{\partial T}{\partial y} \right) \left(\frac{\partial C}{\partial y} \right) = \text{“Entropy contribution due to mass transmission”}, \\
 S''_{gen} &= N_T + N_f + N_C + N_m.
 \end{aligned}
 \tag{14}$$

The typical entropy generation rate S''_0 is given by

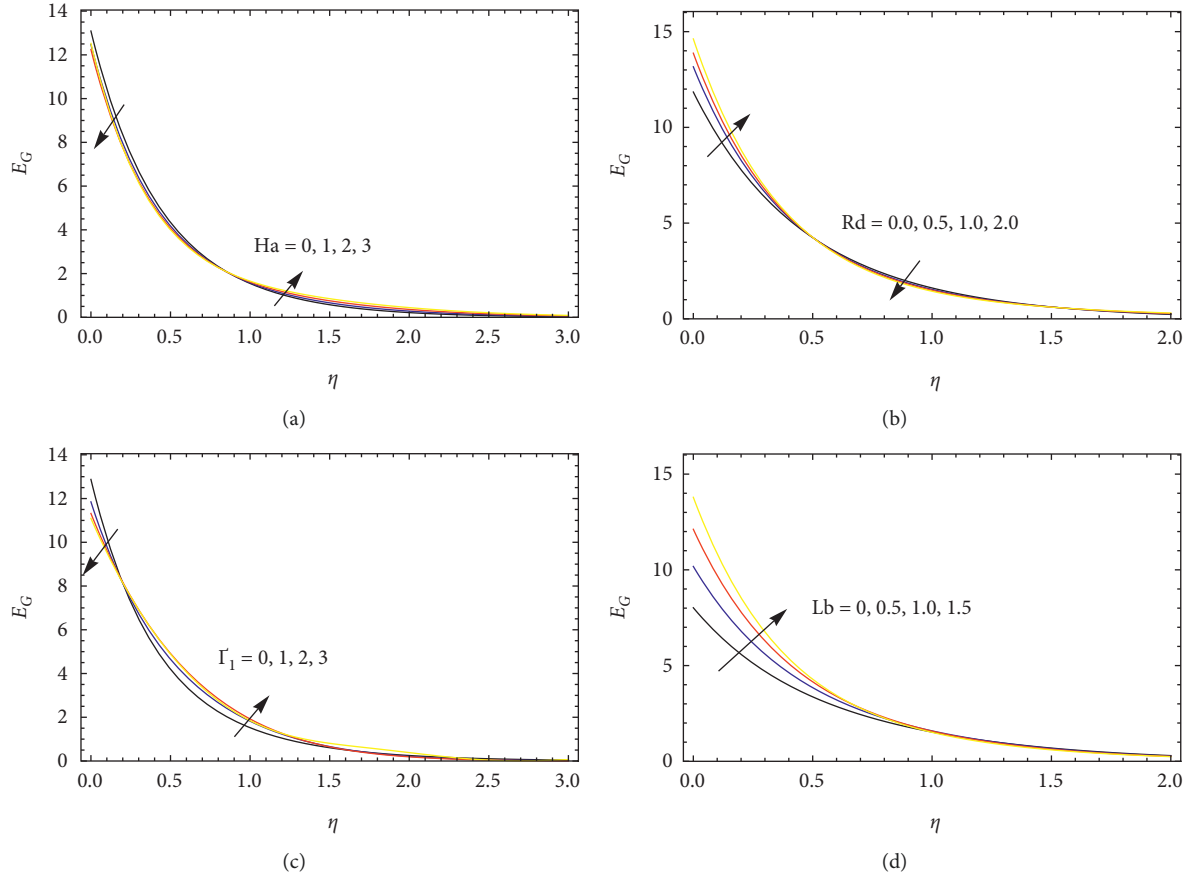


FIGURE 6: Entropy generation profile for different values of Ha , Rd , Γ_1 , and Lb .

$$S_0'' = \left\langle \frac{K_1}{T_\infty^2} \frac{(\Delta T)^2}{l^2} \right\rangle. \quad (15)$$

As a consequence, the dimensionless entropy generation number may be calculated by using the following formula:

$$E_G = \frac{S_0''^{\text{gen}}}{S_0''}. \quad (16)$$

As a result, the total entropy generation number has the corresponding dimensionless form:

$$E_G = \text{Re} \left(1 + \frac{4}{3} Rd \right) \theta'^2 + \text{Re} \frac{Br}{\Omega} f''^2 + \text{Re} \left(\frac{\zeta}{\Omega} \right)^2 \lambda \phi'^2 \\ + \text{Re} \frac{\zeta}{\Omega} \lambda \phi' \theta' + \text{Re} \lambda \left(\frac{\zeta}{\Pi} \right)^2 \chi'^2 + \text{Re} \lambda \left(\frac{\zeta}{\Pi} \right) \chi' \theta'. \quad (17)$$

Expression of the Bejan number is

$$Be = \frac{N_T + N_C + N_m}{E_G}. \quad (18)$$

4. Homotopy Solutions

The governing equations are solved analytically by applying the HAM scheme [18, 22–32]. In this regard, initially, we fix the initial approximation

$$\begin{aligned} f_0(\eta) &= [1 - e^{-\eta}], \\ \theta_0(\eta) &= [(1 - S_1)e^{-\eta}], \\ \phi_0(\eta) &= [(1 - S_2)e^{-\eta}], \\ \chi_0(\eta) &= [(1 - S_3)e^{-\eta}]. \end{aligned} \quad (19)$$

The linear operator is

$$\begin{aligned} \hat{L}_f &= \frac{\hat{d}^3 f}{d\eta^3} - \frac{df}{d\eta}, \\ \hat{L}_\theta &= \frac{\hat{d}^2 \theta}{d\eta^2} - \theta, \\ \hat{L}_\phi &= \frac{\hat{d}^2 \phi}{d\eta^2} - \phi, \\ \hat{L}_\chi &= \frac{\hat{d}^2 \chi}{d\eta^2} - \chi, \end{aligned} \quad (20)$$

with the property

$$\begin{aligned} \hat{L}_f [\Psi_1 + \Psi_2 e^\eta + \Psi_3 e^{-\eta}] &= 0, \\ \hat{L}_\theta [\Psi_4 e^\eta + \Psi_5 e^{-\eta}] &= 0, \\ \hat{L}_\phi [\Psi_6 e^\eta + \Psi_7 e^{-\eta}] &= 0, \\ \hat{L}_\chi [\Psi_8 e^\eta + \Psi_9 e^{-\eta}] &= 0. \end{aligned} \quad (21)$$

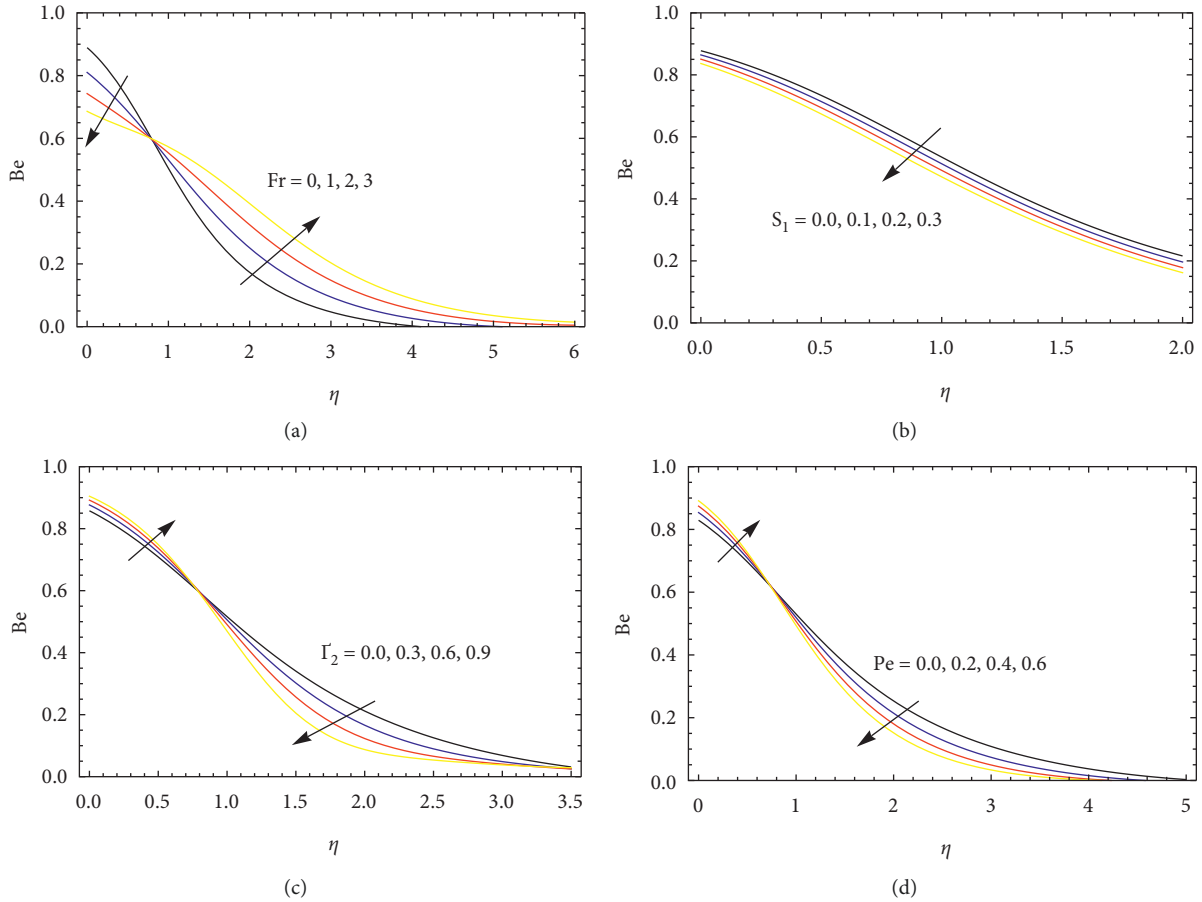


FIGURE 7: Bejan number profile for different values of Fr, S_1, Γ_2 , and Pe .

Here, $\Psi_i [i = 1 - 9]$ are the arbitrary constants.

After utilizing the j th order HAM, we get

$$\begin{aligned}
 f_j(\eta) &= f_j^*(\eta) + \Psi_1 + \Psi_2 e^\eta + \Psi_3 e^{-\eta}, \\
 \theta_j(\eta) &= \theta_j^*(\eta) + \Psi_4 e^\eta + \Psi_5 e^{-\eta}, \\
 \phi_j(\eta) &= \phi_j^*(\eta) + \Psi_6 e^\eta + \Psi_7 e^{-\eta}, \\
 \chi_j(\eta) &= \chi_j^*(\eta) + \Psi_8 e^\eta + \Psi_9 e^{-\eta}.
 \end{aligned} \tag{22}$$

Here, $f_j^*(\eta), \theta_j^*(\eta), \phi_j^*(\eta)$, and $\chi_j^*(\eta)$ are the particular solutions.

The HAM includes the auxiliary parameters (h_f, h_θ, h_ϕ , and h_χ), and these are the responsible for solution convergence.

5. Convergence Analysis

The convergence values are of h_f, h_θ, h_ϕ , and h_χ , are plotted in Figure 1. The range of convergence is $-0.4 \leq h_f \leq -0.1$, $-0.5 \leq h_\theta, h_\phi \leq -0.1$, $-0.5 \leq h_\phi \leq 0.0$, and $-0.55 \leq h_\chi \leq -0.2$. Table 1 observes $f''(0), \theta'(0), \phi'(0)$, and $\chi'(0)$ for the 15th order of estimation. The convergence range of the current solution is $h_f = 0.35$ and $h_\theta = h_\phi = h_\chi = -0.30$.

6. Results and Discussion

This section focused on the effects of divergent physical factors on fluid velocity, fluid temperature, nanoparticle volume fraction, motile microbe density, skin friction coefficients, local Nusselt number, and local Sherwood number. Table 1 provides the validation of the present analysis with previously published results [18, 22]. From this comparison, we found that the current computation is an optimum one.

In this section, we focused on the variations of fluid velocity, fluid temperature, nanoparticle volume fraction, motile microorganism density, skin friction coefficients, local Nusselt number, and local Sherwood number for divergent physical parameters. Figures 2(a)–2(d) provide the impact of $\alpha_1, \alpha_2, Ha, P_m, P_e, N_r, R_b$, and S_1 on the velocity profile. It is detected that the fluid velocity enriches when escalating the quantity of α_1, α_2, Ha , and P_e , and it downfalls when enhancing the quantity of P_m, N_r, R_b , and S_1 . Physically, the modified Hartmann number leads to strengthening the external electric field, and this causes to increase the fluid velocity. The temperature variations of $Ha, R_b, S_1, \lambda, Fr$, and P_m are presented in Figures 3(a)–3(c). It is seen that the fluid temperature escalates when raising the quantity of R_b, Fr , and P_m , and the opposite behaviour was attained when varying the values of Ha, S_1 , and λ . Figures 4(a) and

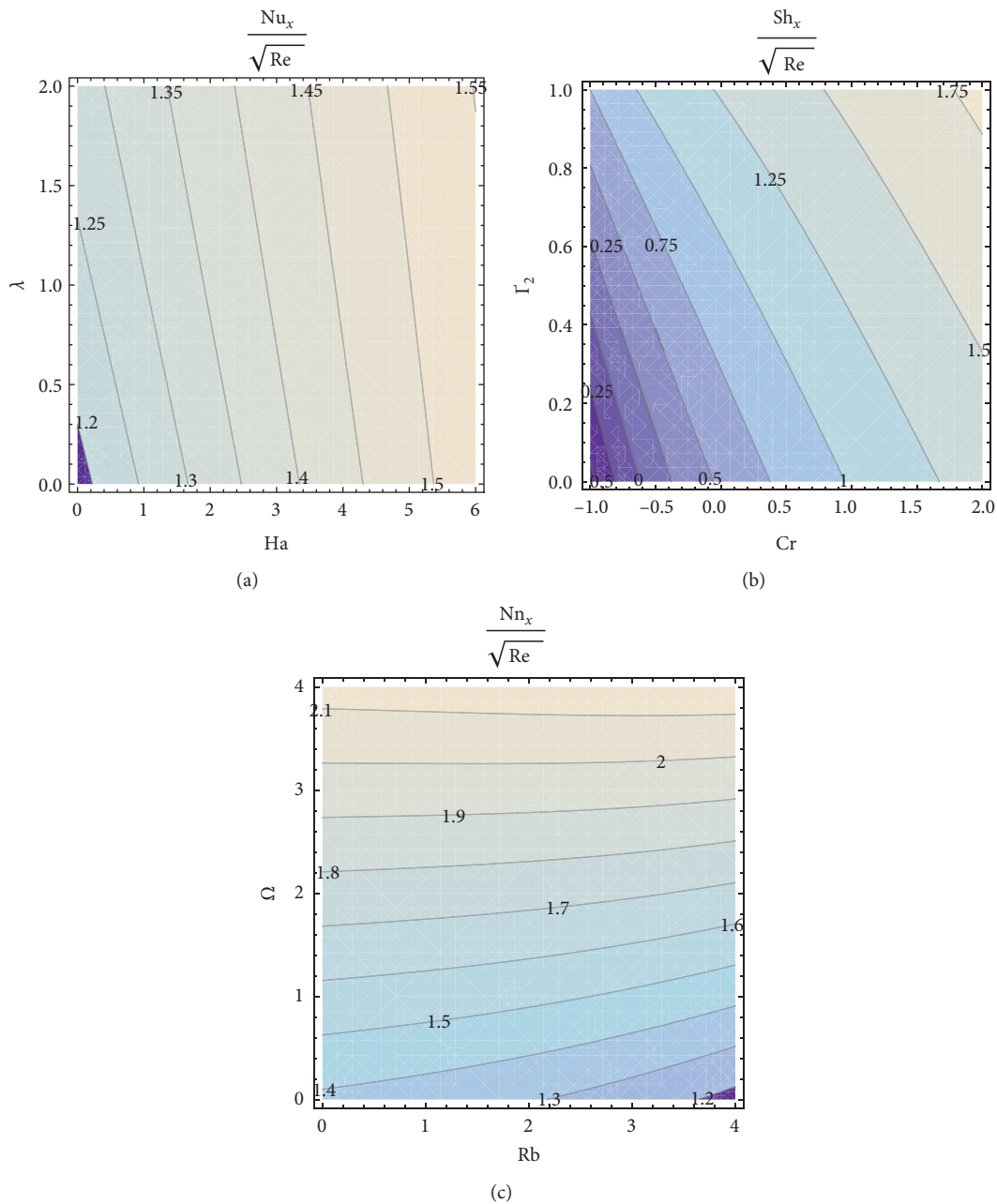


FIGURE 8: (a) “Nusselt number” for Ha and λ , (b) “Sherwood number” for Γ_2 and Cr , and (c) “Microorganism density number” for Ω and Rb .

4(b)) portray the consequences of R_b, S_2, Γ_2 , and λ on the concentration profile. It is concluded that the fluid concentration increases when rising the quantity of R_b , and it reduces when strengthening the values of S_2, Γ_2 , and λ . The microorganism profile for various values of P_e, Ω, Nr , and L_b is illustrated in Figures 5(a) and 5(b) and found that the microorganism profile suppresses when enhancing the P_e, Ω , and L_b quantities, and it escalates when escalating the values of Nr .

Figures 6(a)–6(d) display the consequences of Ha, Rd, Γ_1 , and Lb on the entropy generation profile. It is seen that the entropy generation diminishes near the plate and upturns away from the plate for varying the Ha and Γ_1 values, and the opposite behavior occurs for enhancing the

Rd values. In addition, the Lb leads to enrich the entropy generation. The changes of the Bejan number for different values of Fr, S_1, Γ_2 , and Pe are presented in Figures 7(a)–7(d) and seen that the Bejan number upturns near the plate and downfalls away from the plate for changing the Γ_2 and s values. The quite opposite trend attains for varying the Fr values. The S_1 values lead to reduce the Bejan number.

Fig. 8(a) reveals the collective effect of Ha and λ on $[Nu]_x$ with other parameters are kept fixed heat transfer rate $[Nu]_x$ is abridged with growing amounts of both Ha and λ . Figure 8(b) explores the graphical assessment of Sherwood number Sh_x against the variations in Cr and Γ_2 with other parameters are retained fixed. The Sherwood number Sh_x is improved with the enhancement in Cr and Γ_2 . Figure 8(c)

TABLE 1: Comparison of $C_f Re^{-0.5}$ for the limiting conditions. $P_m = Fr = Hm = \lambda = N_r = R_b = 0$.

α_1	α_2	β	Re	Imtiaz et al. [22]	Loganathan et al. [18]	Present
0.0	0.1	0.1	0.1	0.04605	0.04605	0.04605
0.1				1.06680	1.06680	1.06680
0.2				1.17470	1.17470	1.17470
	0.0	0.1	0.1	1.12010	1.12010	1.12010
0.1	0.1			1.06680	1.06680	1.06680
	0.2			1.01830	1.01830	1.01830
	0.1	0.0		1.06290	1.06290	1.06290
		0.1		1.06680	1.06680	1.06680
		0.2		1.07030	1.07030	1.07030
0.1		0.1	0.0	1.06290	1.06290	1.06290
			0.1	1.06680	1.06680	1.06680
			0.2	1.07060	1.07060	1.07060

describes the graphical evaluation of the microorganism density number Nn_x against the variations in Rb and Ω with other parameters as taken fixed. The microorganism density number Nn_x is improved with the enhancement in Rb and Ω .

7. Conclusions

In this article, we analyse the performance of heat-mass effects of third grade nanofluid flow through a triply stratified medium with swimming of nanoparticles, and gyrostatic microorganisms are swum into this flow. The non-Fourier heat and mass flux's theory were used to frame the energy and nanoparticle concentration equations. The reduced models were analytically solved by applying the HAM scheme. The major outcomes are summarized as follows:

- (i) The fluid velocity enhances when raising the modified Hartmann number, and it suppresses for a larger quantity of the thermal relaxation parameter.
- (ii) The fluid temperature rises when enhancing the Forchheimer number and downfalls when increasing the bioconvection parameter.
- (iii) The fluid concentration decays when strengthening the solutal relaxation time and stratification parameters.
- (iv) The microorganism profile reduces when improving the quantity of P_e , Ω , and L_b , and it escalates when escalating the values of Nr .
- (v) The entropy rate is enhanced for higher values of the heat thermal relaxation parameter and bioconvection Lewis number.
- (vi) The Bejan number diminishes for the solutal thermal relaxation parameter, thermal stratification, and bioconvection Peclet number.

Data Availability

"The raw data supporting the conclusion of this report will be made available by the corresponding author without undue reservation."

Conflicts of Interest

The author declares that there are no conflicts of interest.

References

- [1] S. U. S. Choi, "Enhancing thermal conductivity of fluids with nanoparticles," *Proceedings of the ASME International Mechanical Engineering Congress and Exposition*, vol. 66, pp. 99–105, 1995.
- [2] W. A. Khan and I. Pop, "Boundary-layer flow of a nanofluid past a stretching sheet," *International Journal of Heat and Mass Transfer*, vol. 53, no. 11-12, pp. 2477–2483, 2010.
- [3] P. Barnoon and D. Toghraie, "Numerical investigation of laminar flow and heat transfer of non-Newtonian nanofluid within a porous medium," *Powder Technology*, vol. 325, pp. 78–91, 2018.
- [4] M. Ghalambaz, A. Noghrehabadi, and A. Ghanbarzadeh, "Natural convection of nanofluids over a convectively heated vertical plate embedded in a porous medium," *Brazilian Journal of Chemical Engineering*, vol. 31, no. 2, pp. 413–427, 2014.
- [5] A. Aziz and W. A. Khan, "Natural convective boundary layer flow of a nanofluid past a convectively heated vertical plate," *International Journal of Thermal Sciences*, vol. 52, pp. 83–90, 2012.
- [6] R. Ahmad, M. Mustafa, and S. Hina, "Buongiorno model for fluid flow around a moving thin needle in a flowing nanofluid: a numerical study," *Chinese Journal of Physics*, vol. 55, no. 4, pp. 1264–1274, 2017.
- [7] B. C. Prasannakumara, M. R. Krishnamurthy, B. J. Gireesha, and R. S. R. Gorla, "Effect of multiple slips and thermal radiation on MHD flow of Jeffery nanofluid with heat transfer," *Journal of Nanofluids*, vol. 5, no. 1, pp. 82–93, 2016.
- [8] H. Waqas, A. Kafait, T. Muhammad, and U. Farooq, "Numerical study for bio-convection flow of tangent hyperbolic nanofluid over a Riga plate with activation energy," *Alexandria Engineering Journal*, vol. 61, no. 2, pp. 1803–1814, 2022.
- [9] M. J. Uddin, Y. Alginahi, O. A. Bég, and M. Kabir, "Numerical solutions for gyrotactic bioconvection in nanofluid-saturated porous media with Stefan blowing and multiple slip effects," *Computers & Mathematics with Applications*, vol. 72, no. 10, pp. 2562–2581, 2016.
- [10] A. S. Alshomrani, M. Z. Ullah, and D. Baleanu, "Importance of multiple slips on bioconvection flow of cross nanofluid past a wedge with gyrotactic motile microorganisms," *Case Studies in Thermal Engineering*, vol. 22, Article ID 100798, 2020.
- [11] T. Muhammad, S. Z. Alamri, H. Waqas, D. Habib, and R. Ellahi, "Bioconvection flow of magnetized Carreau nanofluid under the influence of slip over a wedge with motile microorganisms," *Journal of Thermal Analysis and Calorimetry*, vol. 143, no. 2, pp. 945–957, 2021.

- [12] J. Fourier, "Theorie analytique de la chaleur, par M.," *Fourier, Chez Firmin Didot, pre et fils*, 1822.
- [13] C. Cattaneo, "Sulla conduzione del calore," *Proceedings of the Mathematical and Physical Seminar of the University of Modena and Reggio Emilia*, vol. 3, Article ID 83101, 1948.
- [14] C. J. Christov, "On frame indifferent formulation of the maxwell-Cattaneo model of finite speed heat conduction," *Mechanics Research Communications*, vol. 36, no. 4, pp. 481–486, 2009.
- [15] T. Salahuddin, M. Awais, M. Khan, and M. Altanji, "Analysis of transport phenomenon in cross fluid using Cattaneo-Christov theory for heat and mass fluxes with variable viscosity," *International Communications in Heat and Mass Transfer*, vol. 129, Article ID 105664, 2021.
- [16] U. Farooq, H. Waqas, M. Imran, A. Albakri, and T. Muhammad, "Numerical investigation for melting heat transport of nanofluids due to stretching surface with Cattaneo-Christov thermal model," *Alexandria Engineering Journal*, vol. 61, no. 9, pp. 6635–6644, 2022.
- [17] H. Waqas, T. Muhammad, S. Noreen, U. Farooq, and M. Alghamdi, "Cattaneo-Christov heat flux and entropy generation on hybrid nanofluid flow in a nozzle of rocket engine with melting heat transfer," *Case Studies in Thermal Engineering*, vol. 28, Article ID 101504, 2021.
- [18] K. Loganathan, K. Mohana, M. Mohanraj, P. Sakthivel, and S. Rajan, "Impact of third-grade nanofluid flow across a convective surface in the presence of inclined Lorentz force: an approach to entropy optimization," *Journal of Thermal Analysis and Calorimetry*, vol. 144, no. 5, pp. 1935–1947, 2020.
- [19] R. S. Rivlin and J. Ericksen, "Stress-deformation relations for isotropic materials," *Collected Papers of RS Rivlin*, pp. 911–1013, Springer, Berlin, Germany, 1997.
- [20] R. Fosdick and K. Rajagopal, Eds., *Proceedings of the Royal Society of London A: Mathematical, Physical and Engineering Sciences* The Royal Society, London, UK, 1980.
- [21] M. Pakdemirli, "The boundary layer equations of third-grade fluids," *International Journal of Non-linear Mechanics*, vol. 27, no. 5, pp. 785–793, 1992.
- [22] M. Imtiaz, A. Alsaedi, A. Shafiq, and T. Hayat, "Impact of chemical reaction on third grade fluid flow with Cattaneo-Christov heat flux," *Journal of Molecular Liquids*, vol. 229, pp. 501–507, 2017.
- [23] T. Hayat, M. Ijaz Khan, S. Qayyum, and A. Alsaedi, "Modern developments about statistical declaration and probable error for skin friction and Nusselt number with copper and silver nanoparticles," *Chinese Journal of Physics*, vol. 55, no. 6, pp. 2501–2513, 2017.
- [24] M. Farooq, M. Javed, M. Ijaz Khan, A. Anjum, and T. Hayat, "Melting heat transfer and double stratification in stagnation flow of viscous nanofluid," *Results in Physics*, vol. 7, pp. 2296–2301, 2017.
- [25] M. Waqas, M. Farooq, M. I. Khan, A. Alsaedi, T. Hayat, and T. Yasmeen, "Magnetohydrodynamic (MHD) mixed convection flow of micropolar liquid due to nonlinear stretched sheet with convective condition," *International Journal of Heat and Mass Transfer*, vol. 102, pp. 766–772, 2016.
- [26] K. Loganathan and S. Rajan, "An entropy approach of Williamson nanofluid flow with Joule heating and zero nanoparticle mass flux," *Journal of Thermal Analysis and Calorimetry*, vol. 141, no. 6, pp. 2599–2612, 2020.
- [27] T. Hayat, F. Shah, M. I. Khan, and A. Alsaedi, "Framing the performance of heat absorption/generation and thermal radiation in chemically reactive Darcy-Forchheimer flow," *Results in Physics*, vol. 7, pp. 3390–3395, 2017.
- [28] T. S. Karthik, K. Loganathan, A. N. Shankar et al., "Zero and nonzero mass flux effects of bioconvective viscoelastic nanofluid over a 3D Riga surface with the swimming of gyrotactic microorganisms," *Advances in Mathematical Physics*, vol. 2021, Article ID 9914134, 13 pages, 2021.
- [29] I. Ahmad, M. Faisal, K. Loganathan, M. Z. Kiyani, and N. Namgyel, "Nonlinear mixed convective bidirectional dynamics of double stratified radiative Oldroyd-B nanofluid flow with heat source/sink and higher-order chemical reaction," *Mathematical Problems in Engineering*, vol. 2022, 16 pages, Article ID 9732083, 2022.
- [30] S. Eswaramoorthi, K. Loganathan, R. Jain, and S. Gyltshen, "Darcy-forchheimer 3D flow of glycerin-based carbon nanotubes on a Riga plate with nonlinear thermal radiation and cattaneo-christov heat flux," *Journal of Nanomaterials*, vol. 2022, Article ID 5286921, 20 pages, 2022.
- [31] S. Eswaramoorthi, K. Loganathan, M. Faisal, T. Botmart, and N. A. Shah, "Analytical and numerical investigation of Darcy-Forchheimer flow of a nonlinear-radiative non-Newtonian fluid over a Riga plate with entropy optimization," *Ain Shams Engineering Journal*, Article ID 101887, 2022.
- [32] K. Loganathan, N. Alessa, K. Tamilvanan, and F. S. Alshammari, "Significances of Darcy-Forchheimer porous medium in third-grade nanofluid flow with entropy features," *The European Physical Journal - Special Topics*, vol. 230, pp. 1293–1305, 2021.

Research Article

A Class of Symmetric Fractional Differential Operator Formed by Special Functions

Ibtisam Aldawish ¹, Rabha W. Ibrahim ², and Suzan J. Obaiys ³

¹Department of Mathematics and Statistics, College of Science, IMSIU (Imam Mohammad Ibn Saud Islamic University), Riyadh, Saudi Arabia

²The Institute of Electrical and Electronics Engineers(IEEE): 94086547, Portland 13765, NY, USA

³Department of Computer Systems and Technology, Faculty of Computer Science and Information Technology, University Malaya, Kuala Lumpur 50603, Malaysia

Correspondence should be addressed to Rabha W. Ibrahim; rabhaibrahim@yahoo.com

Received 16 May 2022; Accepted 4 July 2022; Published 2 August 2022

Academic Editor: Arzu Akbulut

Copyright © 2022 Ibtisam Aldawish et al. This is an open access article distributed under the Creative Commons Attribution License, which permits unrestricted use, distribution, and reproduction in any medium, provided the original work is properly cited.

In light of a certain sort of fractional calculus, a generalized symmetric fractional differential operator based on Raina's function is built. The generalized operator is then used to create a formula for analytic functions of type normalized. We use the ideas of subordination and superordination to show a collection of inequalities using the suggested differential operator. The new Raina's operator is also used to the generalized kinematic solutions (GKS). Using the concepts of subordination and superordination, we provide analytic solutions for GKS. As a consequence, a certain hypergeometric function provides the answer. A fractional coefficient differential operator is also created. The geometric and analytic properties of the object are being addressed. The symmetric differential operator in a complex domain is shown to be a generalized fractional differential operator. Finally, we explore the characteristics of the Raina's symmetric differential operator.

1. Introduction

Symmetry is both an abstract basis of attractiveness and an applied tool for resolving convoluted problems. As a consequence, symmetry is a well-known foundation in numerous fields of physics. Despite a well-developed abstract theory of analytic symmetry, symmetry in real-world complex networks has established little attention [1]. Many scientists in many domains of mathematical sciences have been interested in learning more about the theory of symmetric operators. A special class of symmetric operators is defined by using some special functions, which are satisfying the symmetric behavior. The Mittag-Leffler function and its extensions, including Raina's functions, are solutions for all categories of fractional differential equations (see [2–8]).

We examine how Raina's function may utilize to expand a symmetric fractional differential operator in a complex domain in this research. A range of new normalized analytic

functions are explained using the fractional symmetric operator. The idea of differential subordination and superordination is applied to study a collection of differential inequalities. The geometric behavior of the generalized kinematic solution (GKS), a family of analytic solutions, is also studied. A variety of applications employ the new convolution linear operator.

2. Methods and Techniques

We will go through the strategies we used in this part.

2.1. Geometric Concepts. We start by the following definition [9]:

Concept 2.1. The analytic functions ψ_1, ψ_2 in $\mathbb{U} = \{\xi \in \mathbb{C} : |\xi| < 1\}$ are subordinated $\psi_1 \prec \psi_2$ or

$$\psi_1(\xi) < \psi_2(\xi), \quad \xi \in \mathbb{U}. \tag{1}$$

If for an analytic function $v, |v| \leq |\xi| < 1$ owning

$$\psi_1(\xi) = \psi_2(v(\xi)), \quad \xi \in \mathbb{U}. \tag{2}$$

Concept 2.2. Consider the subclass of analytic functions Λ by

$$\psi(\xi) = \xi + \sum_{n=2}^{\infty} \varphi_n \xi^n, \quad \eta \in \mathbb{U}, \tag{3}$$

satisfying $\psi(0) = 0, \psi'(0) = 1$.

Furthermore, the functions $\psi_1, \psi_2 \in \Lambda$ are called convoluted $(\psi_1 * \psi_2)$ if they admin the operation [10]

$$\begin{aligned} (\psi_1 * \psi_2)(\xi) &= \left(\xi + \sum_{n=2}^{\infty} \phi_n \xi^n \right) * \left(\xi + \sum_{n=2}^{\infty} \varphi_n \xi^n \right) \\ &= \xi + \sum_{n=2}^{\infty} \phi_n \varphi_n \xi^n. \end{aligned} \tag{4}$$

Concept 2.3. The \mathcal{S}^* class of star-like functions and the \mathcal{C} class of convex univalent functions are both related to the class of normalized analytic functions (Λ). In addition, we require the class of analytic functions

$$\mathcal{P} := \{ \varrho: \varrho(\xi) = 1 + \varrho_1 \xi + \varrho_2 \xi^2 + \dots, \xi \in \mathbb{U} \}. \tag{5}$$

2.2. *Modified Special Function.* Special functions include integrals and the outputs of many different types of differential equations. Therefore, most integral sets include special duty descriptions, and these duties include the elementary integrals. Since symmetries are important in real life, the philosophy of special functions is tightly linked to various mathematical physics topics [11]. We will start with a well-known special function, the Mittag–Leffler function.

Concept 2.4. The extended Mittag–Leffler function is formulated by the series [12]

$$\mathcal{F}_{\alpha, \beta}^v(\xi) = \sum_{n=0}^{\infty} \left(\frac{(v)_n}{\Gamma(\alpha n + \beta)} \right) \frac{\xi^n}{n!}, \tag{6}$$

such that $(v)_n = \Gamma(v + n)/\Gamma(v)$. Clearly, for $v = 1$, implies that

$$\mathcal{F}_{\alpha, \beta}^1(\xi) = \sum_{n=0}^{\infty} \frac{\xi^n}{\Gamma(\beta + \alpha n)}. \tag{7}$$

After that, we will go through Raina’s function.

Concept 2.5. Raina’s function is determined by the power series as follows [12]:

$$\mathcal{F}_{\alpha, \beta}^v(\xi) = \sum_{n=0}^{\infty} \frac{v(n)}{\Gamma(\alpha n + \beta)} \xi^n, \quad \xi \in \mathbb{U}, \tag{8}$$

such that $\alpha \in (0, \infty), \beta \in [1, \infty)$ and $v := \{v(0), v(1), \dots, v(n)\}$ is a collection of real or complex numbers.

Notice 2.6. We have the following well-known special cases:

- (i) $v(n) = 1 \implies \mathcal{F}_{\alpha, \beta}^1(\xi)$
- (ii) $v(n) = ((v)_n/n!) \implies \mathcal{F}_{\alpha, \beta}^v(\xi)$
- (iii) $\alpha = 1, \beta = 1, v(n) = ((x)_n (y)_n / (s)_n) \implies {}_2\Theta_1(x, y; s; \xi) = \sum_{n=0}^{\infty} ((x)_n (y)_n / (s)_n) (\xi^n / \Gamma(n + 1))$

Employing the functional $\mathcal{F}_{\alpha, \beta}^v(\xi)$, we get the convolution operator, for $\psi \in \Lambda$

$$\begin{aligned} \mathbb{I}_{\alpha, \beta}^v \psi(\xi) &= \left(\frac{\Gamma(\alpha + \beta)}{v(1)} \right) (\mathcal{F}_{\alpha, \beta}^v * \psi)(\xi) \\ &= \left(\frac{\Gamma(\alpha + t\beta)}{v(1)} \right) v(0) + \xi \\ &\quad + \sum_{n=2}^{\infty} \left(\frac{\Gamma(\alpha + \beta)}{v(1)} \right) \left(\frac{v(n)}{\Gamma(\alpha n + \beta)} \right) \xi^n * \left(\xi + \sum_{n=2}^{\infty} a_n \xi^n \right) \\ &= \xi + \sum_{n=2}^{\infty} \left(\frac{\Gamma(\alpha + \beta)}{\Gamma(\beta + \alpha n)} \right) \left(\frac{v(n)}{v(1)} \right) a_n \xi^n \\ &:= \xi + \sum_{n=2}^{\infty} s_n a_n \xi^n, \end{aligned} \tag{9}$$

such that

$$\begin{aligned} s_n &:= \left(\frac{\Gamma(\alpha + \beta)}{\Gamma(\beta + \alpha n)} \right) \left(\frac{v(n)}{v(1)} \right) \\ &(\xi \in \mathbb{U}, \psi \in \Lambda, \alpha \in (0, \infty), \beta \in [1, \infty), v = \{v(0), \dots, v(n)\}). \end{aligned} \tag{10}$$

Clearly, $\mathbb{I}_{\alpha, \beta}^v \psi(\xi) \in \Lambda$. From the above structure, the fractional differential operator can be viewed geometrically.

Note that the operator $\mathbb{I}_{\alpha, \beta}^v \psi(\xi)$ is a new type of the convoluted Carlson–Shaffer operator [13] satisfying $\alpha = \beta = 1$, and $v(n) = ((1)_n (y)_n / (s)_n), \forall n$, with

$$\mathbb{I}_{\alpha, \beta}^v \psi(\xi) = \sum_{n=0}^{\infty} \left(\frac{(1)_n (y)_n}{\Gamma(n + 1) (s)_n} \right) a_n \xi^n. \tag{11}$$

Moreover, when $v(n) = \Gamma(\beta + \alpha n)$ for all $n \geq 1$, we have the Sal agean operator [14]:

$$\mathbb{I}_{\alpha, \beta}^v \psi(\xi) = \xi + \sum_{n=2}^{\infty} n a_n \xi^n. \tag{12}$$

2.3. *Arguments.* The following precursors are utilized to develop the results of this inquiry into differential subordination theory:

Argument 2.7 (see [9]). Suppose that $f_1(\xi)$ and $f_2(\xi)$ are convex univalent in \mathbb{U} with $f_1(0) = f_2(0)$. Then, for a fixed value $\eta \neq 0$, $\Re(\eta) \geq 0$, the subordination

$$f_1(\xi) + \left(\frac{1}{\eta}\right)\xi f_1'(\xi) \prec f_2(\xi), \tag{13}$$

gives

$$f_1(\xi) \prec f_2(\xi). \tag{14}$$

Argument 2.8 (see [9]). Consider the class of holomorphic functions as follows:

$$\Pi[b, n] = \left\{ \varphi: \varphi(\xi) = b + b_n \xi^n + b_{n+1} \xi^{n+1} + \dots \right\}, \tag{15}$$

where $b \in \mathbb{C}$ and $n \in \mathbb{Z}^+$. The condition $1 \in \mathbb{R}$ implies

$$\Re\{\varphi(\xi) + i\xi\varphi'(\xi)\} > 0 \Rightarrow \Re(\varphi(\xi)) > 0. \tag{16}$$

In addition, if $1 > 0$ and $\varphi \in \Pi[1, n]$, then for $\eta_1, \eta_2 \in (0, \infty)$ satisfying

$$\varphi(\xi) + i\xi\varphi'(\xi) \prec \left(\frac{1+\xi}{1-\xi}\right)^{\eta_1} \Rightarrow \varphi(\xi) \prec \left(\frac{1+\xi}{1-\xi}\right)^{\eta_2}. \tag{17}$$

Argument 2.9 (see [15]). Let $h, \varphi \in \Pi[b, n]$, where $\varphi \in \mathcal{C}$ and for $w_1, w_2 \in \mathbb{C}, w_2 \neq 0$. Then, the subordination

$$w_1 h(\xi) + w_2 \xi h'(\xi) \prec w_1 \varphi(\xi) + w_2 \xi \varphi'(\xi), \tag{18}$$

yields

$$h(\xi) \prec \varphi(\xi). \tag{19}$$

Argument 2.10 (see [16]). Let $\varphi, \phi \in \Pi[b, n]$, where $\phi \in \mathcal{C}$ and the functional $\varphi(\xi) + v\xi\varphi'(\xi)$ is univalent for some positive fixed number v . Then the differential inequality

$$\phi(\xi) + v\xi\phi'(\xi) \prec \varphi(\xi) + v\xi\varphi'(\xi), \tag{20}$$

implies

$$\phi(\xi) \prec \varphi(\xi). \tag{21}$$

3. Consequences

The next class of normalized analytic functions is defined in this paper, and its features are investigated employing differential subordination and superordination theory.

Concept 3.1. A function $\psi \in \Lambda$ aims to be in the class $\Omega_{\alpha, \beta}^{\mu}(\lambda, \rho)$ if it fulfills the inequality

$$\left(\frac{1-\lambda}{\xi}\right) \left[\mathbb{I}_{\alpha, \beta}^{\nu} \psi(\xi) \right] + \lambda \left[\mathbb{I}_{\alpha, \beta}^{\nu} \psi(\xi) \right]' \prec \rho(\xi), \tag{22}$$

$(\xi \in \mathbb{U}, \lambda \in (0, 1], \rho(0) = 1, \alpha \in (0, \infty), \beta \in [1, \infty)),$

whenever $\rho \in \mathcal{C}$.

Eventually, the convexity of the univalent function

$$\rho(\xi) = \frac{A\xi + 1}{B\xi + 1}, \tag{23}$$

implies that

$$\rho \in \mathcal{D} := \left\{ \rho \in \mathbb{U}: \rho(\xi) = 1 + \sum_{n=1}^{\infty} \rho_n \xi^n \right\}. \tag{24}$$

Consider the functional $\Sigma_{\psi}^{\lambda}: \mathbb{U} \rightarrow \mathbb{U}$, as in the following structure:

$$\Sigma_{\psi}^{\lambda}(\xi) := \left(\frac{1-\lambda}{\xi}\right) \left[\mathbb{I}_{\alpha, \beta}^{\nu} \psi(\xi) \right] + \lambda \left[\mathbb{I}_{\alpha, \beta}^{\mu} \psi(\xi) \right]'. \tag{25}$$

Consequently, in view of Concept 3.1, we get the next inequality

$$\Sigma_{\psi}^{\lambda}(\xi) \prec \frac{A\xi + 1}{B\xi + 1}, \quad \xi \in \mathbb{U}. \tag{26}$$

We proceed to investigate the geometric possessions of the suggested operators.

3.1. Results of Subordination Formula. We begin with the following outcome.

Proposition 1. Assume that $\psi \in \Omega_{\alpha, \beta}^{\mu}(\lambda, \rho)$. If

$$\Re\left\{ \Sigma_{\psi}^{\lambda}(\xi) \right\} = \Re \left\{ \left(\frac{1-\lambda}{\xi}\right) \left[\mathbb{I}_{\alpha, \beta}^{\nu} \psi(\xi) \right] + \lambda \left[\mathbb{I}_{\alpha, \beta}^{\nu} \psi(\xi) \right]' \right\} := \Re \left\{ 1 + \sum_{n=1}^{\infty} c_n \right\} > 0, \tag{27}$$

then the upper bound of the coefficients c_n is determined by the probability measure $d\omega$:

$$\frac{|c_n|}{2} \leq \int_0^{2\pi} |e^{-in\tau}| d\omega(\tau). \tag{28}$$

In addition, if

$$\Re\left(e^{i\tau} \Sigma_{\psi}^{\lambda}(\xi) \right) > 0, \quad \xi \in \mathbb{U}, \tau \in \mathbb{R}, \tag{29}$$

then $\psi \in \Omega_{\alpha, \beta}^{\mu}(A\xi + 1/B\xi + 1)$ and

$$\Sigma_{\psi}^{\lambda}(\xi) = \frac{A\xi + 1}{B\xi + 1}, \quad \xi \in \mathbb{U}. \tag{30}$$

Proof. Suppose that

$$\Re\left(\Sigma_{\psi}^{\lambda}(\xi) \right) = \Re \left(1 + \sum_{n=1}^{\infty} c_n \xi^n \right) > 0. \tag{31}$$

Continuously, the Carathéodory positivist lemma entails

$$|c_n| \leq 2 \int_0^{2\pi} |e^{-in\tau}| d\omega(\tau), \tag{32}$$

where $d\omega$ is a probability measure. Besides, if

$$\Re(e^{i\tau} \Sigma_\psi^\lambda(\xi)) > 0, \quad \xi \in \mathbb{U}, \tau \in \mathbb{R}, \tag{33}$$

then according to Theorem 1.6 in [10] and for a fixed number $\tau \in \mathbb{R}$, we have

$$\Sigma_\psi^\lambda(\xi) = \frac{A\xi + 1}{B\xi + 1}, \quad \xi \in \mathbb{U}. \tag{34}$$

Hence, $\psi \in \Omega_{\alpha,\beta}^\mu(\lambda, (A\xi + 1/B\xi + 1))$.

The following findings reveal the functional sandwich theory's required and adequate methodology. \square

Proposition 2. *Suppose that*

$$\lambda \xi [\mathbb{I}_{\alpha,\beta}^\nu \psi(\xi)]'' + [\mathbb{I}_{\alpha,\beta}^\nu \psi(\xi)]' < F_2(\xi) + \xi F_2'(\xi), \tag{35}$$

where $F_2(0) = 1$ and convex in \mathbb{U} . Moreover, let $\Sigma_\psi^\lambda(\xi)$ be univalent in \mathbb{U} with $\Sigma_\psi \in \Pi[F_1(0), 1] \cap \mathbb{D}$, where \mathbb{D} indicates the class of all univalent analytic functions F having the limit $\lim_{\xi \in \partial \mathbb{D}} F \neq \infty$ and

$$F_1(\xi) + \xi F_1'(\xi) < \lambda \xi [\mathbb{I}_{\alpha,\beta}^\nu \psi(\xi)]'' + [\mathbb{I}_{\alpha,\beta}^\nu \psi(\xi)]'. \tag{36}$$

Then

$$F_1(\xi) < \Sigma_\psi^\lambda(\xi) < F_2(\xi), \tag{37}$$

and $F_1(\xi)$ is the best subdominant and $F_2(\xi)$ is the best dominant.

Proof. Putting

$$\Sigma_\psi^\lambda(\xi) = \left(\frac{1-\lambda}{\xi}\right) [\mathbb{I}_{\alpha,\beta}^\nu \psi(\xi)] + \lambda [\mathbb{I}_{\alpha,\beta}^\nu \psi(\xi)]', \tag{38}$$

a calculation yields

$$\begin{aligned} \Sigma_\psi^\lambda(\xi) + \xi(\Sigma_\psi^\lambda(\xi))' &= \lambda [\mathbb{I}_{\alpha,\beta}^\nu \psi(\xi)]' \\ &+ \frac{\xi(\lambda \xi [\mathbb{I}_{\alpha,\beta}^\nu \psi(\xi)]'' - (\lambda - 1) [\mathbb{I}_{\alpha,\beta}^\nu \psi(\xi)]') + (\lambda - 1) [\mathbb{I}_{\alpha,\beta}^\nu \psi(\xi)]}{\xi} \\ &+ \frac{(1 - \lambda) [\mathbb{I}_{\alpha,\beta}^\nu \psi(\xi)]}{\xi} \\ &= \lambda \xi [\mathbb{I}_{\alpha,\beta}^\nu \psi(\xi)]'' + [\mathbb{I}_{\alpha,\beta}^\nu \psi(\xi)]'. \end{aligned} \tag{39}$$

As a consequence, the double inequality produced is as follows:

$$F_1(\xi) + \xi F_1'(\xi) < \Sigma_\psi^\lambda(\xi) + \xi(\Sigma_\psi^\lambda(\xi))' < F_2(\xi) + \xi F_2'(\xi). \tag{40}$$

Finally, Arguments 2.9 and 2.10 provide the required outcome. \square

Proposition 3. *Assume that*

$$\Sigma_\psi^\lambda(\xi) = \frac{(1-\lambda)}{\xi} [\mathbb{I}_{\alpha,\beta}^\nu \psi(\xi)] + \lambda [\mathbb{I}_{\alpha,\beta}^\nu \psi(\xi)]'. \tag{41}$$

Then this leads to

$$\begin{aligned} &\left(\frac{[\mathbb{I}_{\alpha,\beta}^\nu \psi(\xi)]'}{\xi}\right) \varepsilon_1 + [\mathbb{I}_{\alpha,\beta}^\nu \psi(\xi)] [\varepsilon_1 + 3\varepsilon_2] + \varepsilon_2 \xi [\mathbb{I}_{\alpha,\beta}^\nu \psi(\xi)]'' < \left(\frac{1+\xi}{1-\xi}\right)^{\gamma_1} \\ &\Rightarrow \Sigma_\psi^\lambda(\xi) < \left(\frac{1+\xi}{1-\xi}\right)^{\gamma_2}, \\ &(\gamma_1 > 0, \gamma_2 > 0, \varepsilon_1 = 1 - \lambda, \varepsilon_2 = \lambda > 0). \end{aligned} \tag{42}$$

Proof. A calculation gives that

$$\begin{aligned} \Sigma_{\psi}^{\lambda}(\xi) + \xi(\Sigma_{\psi}^{\lambda}(\xi))' &= \frac{(1-\lambda)}{\xi} [\mathbb{I}_{\alpha,\beta}^{\nu} \psi(\xi)] + \lambda [\mathbb{I}_{\alpha,\beta}^{\nu} \psi(\xi)]' \\ &\quad + \xi \left(\frac{(1-\lambda)}{\xi} [\mathbb{I}_{\alpha,\beta}^{\nu} \psi(\xi)] + \lambda [\mathbb{I}_{\alpha,\beta}^{\nu} \psi(\xi)]' \right)' \\ &= \left(\frac{[\mathbb{I}_{\alpha,\beta}^{\nu} \psi(\xi)]'}{\xi} \right) \varepsilon_1 + [\varepsilon_1 + 3\varepsilon_2] [\mathbb{I}_{\alpha,\beta}^{\nu} \psi(\xi)] + \varepsilon_2 \xi [\mathbb{I}_{\alpha,\beta}^{\nu} \psi(\xi)]'' \\ &< \left(\frac{1+\xi}{1-\xi} \right)^{\gamma_1}. \end{aligned} \tag{43}$$

In view of Argument 2.8, we obtain

$$\Sigma_{\psi}^{\lambda}(\xi) < \left(\frac{1+\xi}{1-\xi} \right)^{\gamma_2}. \tag{44}$$

□

3.2. Fractional Differential Equation with Kinematic Solutions. We will use the generalized differential operator to continue our research in this section. A generalized formula for the kinematic solutions (GKS) is presented using the suggested operator. Kinematic behaviors describe the motion of an item with constant acceleration in a dynamic system.

We aim to utilize the class $\Omega_{\alpha,\beta}^{\mu}(\lambda, (1 + \xi/1 - \xi))$ to extend GKSs. We deal with the upper bound solution, for the fractional differential equation

$$\begin{aligned} \left(\frac{1-\lambda}{\xi} \right) [\mathbb{I}_{\alpha,\beta}^{\nu} \psi(\xi)] + \lambda [\mathbb{I}_{\alpha,\beta}^{\nu} \psi(\xi)]' &= \frac{A\xi + 1}{B\xi + 1}, \\ ([\mathbb{I}_{\alpha,\beta}^{\nu} \psi(0)] &= 0, c \in [0, 1], \xi \in \mathbb{U}). \end{aligned} \tag{45}$$

The outcome of (45) is formulated as follows.

Proposition 4. Let $\xi \in \Omega_{\alpha,\beta}^{\nu}(c, (1 + \xi/1 - \xi))$. Then (45) has a solution expressed by

$$\begin{aligned} [\mathbb{I}_{\alpha,\beta}^{\nu} \psi(\xi)] &= c\xi^{(\lambda-1)/\lambda} + \frac{2\xi^2 {}_2\Theta_1(1, 1 + 1/\lambda; 2 + 1/\lambda; \xi)}{\lambda + 1} \\ &\quad + \frac{\lambda\xi}{\lambda + 1} + \frac{\xi}{\lambda + 1}, \end{aligned} \tag{46}$$

where c is a constant and ${}_2\Theta_1(x, y, s; \xi)$ is the hypergeometric function.

Proof. Let $\xi \in \Omega_{\alpha,\beta}^{\nu}(c, (1 + \xi/1 - \xi))$. Thus, we obtain

$$\left(\frac{1-\lambda}{\xi} \right) [\mathbb{I}_{\alpha,\beta}^{\nu} \psi(\xi)] + \lambda [\mathbb{I}_{\alpha,\beta}^{\nu} \psi(\xi)]' = \frac{\varphi(\xi) + 1}{1 - \varphi(\xi)}, \tag{47}$$

where $|\chi| \leq |\xi| < 1$ and $\chi(0) = 0$. As a result, we get the integral formula

$$[\mathbb{I}_{\alpha,\beta}^{\nu} \psi(\xi)] = \xi^{(\lambda-1)/\lambda} \int_0^{\xi} -\eta^{1/(\lambda-1)} \left(\frac{\chi(\eta) + 1}{\lambda(\chi(\eta) - 1)} \right) d\eta. \tag{48}$$

In view of Schwarz lemma, we get $\chi(\xi) = \omega\xi, |\omega| = 1$ (see Theorem 5.34 in [17]). Therefore, by assuming $\chi(\xi) = \xi$, we obtain the differential equation

$$\left(\frac{1-\lambda}{\xi} \right) [\mathbb{I}_{\alpha,\beta}^{\nu} \psi(\xi)] + \lambda [\mathbb{I}_{\alpha,\beta}^{\nu} \psi(\xi)]' = \frac{1+\xi}{1-\xi}. \tag{49}$$

If we reorganize the previous equation, we conclude that

$$[\mathbb{I}_{\alpha,\beta}^{\nu} \psi(\xi)]' + \frac{1-\lambda}{\lambda\xi} [\mathbb{I}_{\alpha,\beta}^{\nu} \psi(\xi)] = \left(\frac{1}{\lambda} \right) \left(\frac{1+\xi}{1-\xi} \right). \tag{50}$$

Then multiplying by the functional

$$\mathbb{T}(\xi) = \exp\left(\int \frac{1-\lambda}{\lambda\xi} d\xi \right) = \xi^{1/(\lambda-1)}, \tag{51}$$

we obtain

$$\begin{aligned} \xi^{1/(\lambda-1)} [\mathbb{I}_{\alpha,\beta}^{\nu} \psi(\xi)]' - \frac{[\mathbb{I}_{\alpha,\beta}^{\nu} \psi(\xi)]((1-\lambda)\xi^{1/(\lambda-2)})}{\lambda} \\ = \left(\frac{\xi^{1/(\lambda-1)}}{\lambda} \right) \left(\frac{1+\xi}{1-\xi} \right). \end{aligned} \tag{52}$$

As a result, we receive the solution

$$\begin{aligned} [\mathbb{I}_{\alpha,\beta}^{\nu} \psi(\xi)] &= c\xi^{(\lambda-1)/\lambda} + \frac{2\xi^2 {}_2\Theta_1(1, 1 + 1/\lambda; 2 + 1/\lambda; \xi)}{\lambda + 1} \\ &\quad + \frac{\lambda\xi}{\lambda + 1} + \frac{\xi}{\lambda + 1}. \end{aligned} \tag{53}$$

□

Example 1. Let $\psi \in \Omega_{\alpha,\beta}^{\nu}(\lambda, (1 + \xi/1 - \xi))$, where $\lambda = 1/2$ and $c = 0$. According to Proposition 5, we have

$$\begin{aligned} [\mathbb{I}_{\alpha,\beta}^{\nu} \psi(\xi)] &= \xi \left(\frac{2\xi {}_2\Theta_1(1, 1 + (1/\lambda), 2 + (1/\lambda), \xi)}{\lambda + 1} + 1 \right), \\ c = 0 &= \xi \left(\frac{4\xi {}_2\Theta_1(1, 3, 4, \xi)}{3} + 1 \right), \end{aligned}$$

$$\lambda = \frac{1}{2} = \xi + \xi^2 + \xi^3 + \xi^4 + \dots + O(\xi^7), \quad |\xi| < 1. \tag{54}$$

Let $\psi(\xi) = (\xi/1 - \xi)$. Then

$$[\mathbb{I}_{\alpha,\beta}^v \psi(\xi)] = \xi + \sum_{n=2}^{\infty} \left(\frac{\Gamma(\alpha + \beta)}{\Gamma(\beta + \alpha n)} \right) \left(\frac{v(n)}{v(1)} \right) \xi^n. \tag{55}$$

Comparing the right sides of the above equations, we obtain that $v(n) = \Gamma(\beta + \alpha n), \forall n$. But $\psi(\xi) = (\xi/1 - \xi)$ is the optimal convex function in the open unit disk; thus, the

operator $[\mathbb{I}_{\alpha,\beta}^v \psi(\xi)]$ is convex whenever ψ is convex (see Figure 1).

3.3. *Symmetric Differential Operator.* The Raina's convoluted operator is assumed to present an extended symmetric differential operator.

$$\begin{aligned} \mathcal{M}_\ell^0 [\mathbb{I}_{\alpha,\beta}^v \psi(\xi)] &= [\mathbb{I}_{\alpha,\beta}^v \psi(\xi)] \\ \mathcal{M}_\ell^1 [\mathbb{I}_{\alpha,\beta}^v \psi(\xi)] &= \ell \xi [\mathbb{I}_{\alpha,\beta}^v \psi(\xi)]' - (1 - \ell) \xi [\mathbb{I}_{\alpha,\beta}^v \psi(-\xi)]' \\ &= \ell \left(\xi + \sum_{n=2}^{\infty} n a_n c_n \xi^n \right) - (1 - \ell) \left(-\xi + \sum_{n=2}^{\infty} n (-1)^n a_n c_n \xi^n \right) \\ &= \xi + \sum_{n=2}^{\infty} [n(\ell - (1 - \ell)(-1)^n)] a_n c_n \xi^n \\ \mathcal{M}_\ell^2 [\mathbb{I}_{\alpha,\beta}^v \psi(\xi)] &= \mathcal{M}_\ell^1 [\mathcal{M}_\ell^1 [\mathbb{I}_{\alpha,\beta}^v \psi(\xi)]] \\ &= \xi + \sum_{n=2}^{\infty} [n(\ell - (1 - \ell)(-1)^n)]^2 a_n c_n \xi^n \\ &\vdots \\ \mathcal{M}_\ell^k [\mathbb{I}_{\alpha,\beta}^v \psi(\xi)] &= \mathcal{M}_\ell^1 [\mathcal{M}_\ell^{k-1} [\mathbb{I}_{\alpha,\beta}^v \psi(\xi)]] \\ &= \xi + \sum_{n=2}^{\infty} [n(\ell - (1 - \ell)(-1)^n)]^k a_n c_n \xi^n. \end{aligned} \tag{56}$$

When $c_n = 1, \forall n$, we have the symmetric operator in [18]. Moreover, when $c_n = 1$ and $\ell = 1$, we receive the Sălăgean integral operator [14].

The following classes will be studied:

Concept. Let $\psi \in \Lambda$. Then, we define the subclass of star-like functions:

- (i) $\psi \in S_{\alpha,\beta,\ell}^{*v,k}(\mathfrak{h})$ if and only if there occurs a convex function $\mathfrak{h} \in \mathcal{C}$ satisfying the subordination

$$\frac{\xi (\mathcal{M}_\ell^k [\mathbb{I}_{\alpha,\beta}^v \psi(\xi)])'}{\mathcal{M}_\ell^k [\mathbb{I}_{\alpha,\beta}^v \psi(\xi)]} \prec \mathfrak{h}(\xi). \tag{57}$$

- (ii) $\psi \in \mathbb{J}_\ell^{\mathfrak{h}}(A, B, k)$ if and only if

$$1 + \frac{1}{\mathfrak{h}} \left(\frac{2 \mathcal{M}_\ell^{k+1} [\mathbb{I}_{\alpha,\beta}^v \psi(\xi)]}{\mathcal{M}_\ell^k [\mathbb{I}_{\alpha,\beta}^v \psi(\xi)] - \mathcal{M}_\ell^k [\mathbb{I}_{\alpha,\beta}^v \psi(-\xi)]} \right) \prec \frac{1 + A\xi}{1 + B\xi}, \tag{58}$$

$(\xi \in \mathbb{U}, -1 \leq B < A \leq 1, k = 1, 2, \dots, \mathfrak{h} \in \mathbb{C} \setminus \{0\}, \ell \in [0, 1]).$

Proposition 5. Consider $\psi \in S_{\alpha,\beta,\ell}^{*v,k}(\mathfrak{h})$. Then

$$\mathcal{M}_\ell^{k+1} [\mathbb{I}_{\alpha,\beta}^v \psi(\xi)] \prec \xi e^{\left(\int_0^\xi (\mathfrak{h}(y(z)) - 1/z) dz \right)}, \tag{59}$$

where $y(\xi)$ is analytic in \mathbb{U} with $y(0) = 0$ and $|y(\xi)| < 1$. Additionally, for $|\xi| = \aleph$, $\mathcal{M}_\ell^{k+1} [\mathbb{I}_{\alpha,\beta}^v \psi(\xi)]$ satisfies the inequality

$$\begin{aligned} \exp \left(\int_0^1 \frac{\mathfrak{h}(y(-\aleph)) - 1}{\aleph} d\aleph \right) &\leq \left| \frac{\mathcal{M}_\ell^{k+1} [\mathbb{I}_{\alpha,\beta}^v \psi(\xi)]}{\xi} \right| \\ &\leq \exp \left(\int_0^1 \frac{\mathfrak{h}(y(\aleph)) - 1}{\aleph} d\aleph \right). \end{aligned} \tag{60}$$

Proof. Because $\psi \in S_{\alpha,\beta,\ell}^{*v,k}(\mathfrak{h})$, then we conclude that

$$\left(\frac{\xi (\mathcal{M}_\ell^{k+1} [\mathbb{I}_{\alpha,\beta}^v \psi(\xi)])'}{\mathcal{M}_\ell^{k+1} [\mathbb{I}_{\alpha,\beta}^v \psi(\xi)]} \right) \prec \mathfrak{h}(\xi), \quad \xi \in \mathbb{U}. \tag{61}$$

This leads to the existence of a Schwarz function with $y(0) = 0$ and $|y(\xi)| < 1$ such that

$$\frac{\xi (\mathcal{M}_\ell^{k+1} [\mathbb{I}_{\alpha,\beta}^v \psi(\xi)])'}{\mathcal{M}_\ell^{k+1} [\mathbb{I}_{\alpha,\beta}^v \psi(\xi)]} = \mathfrak{h}(y(\xi)), \quad \xi \in \mathbb{U}, \tag{62}$$

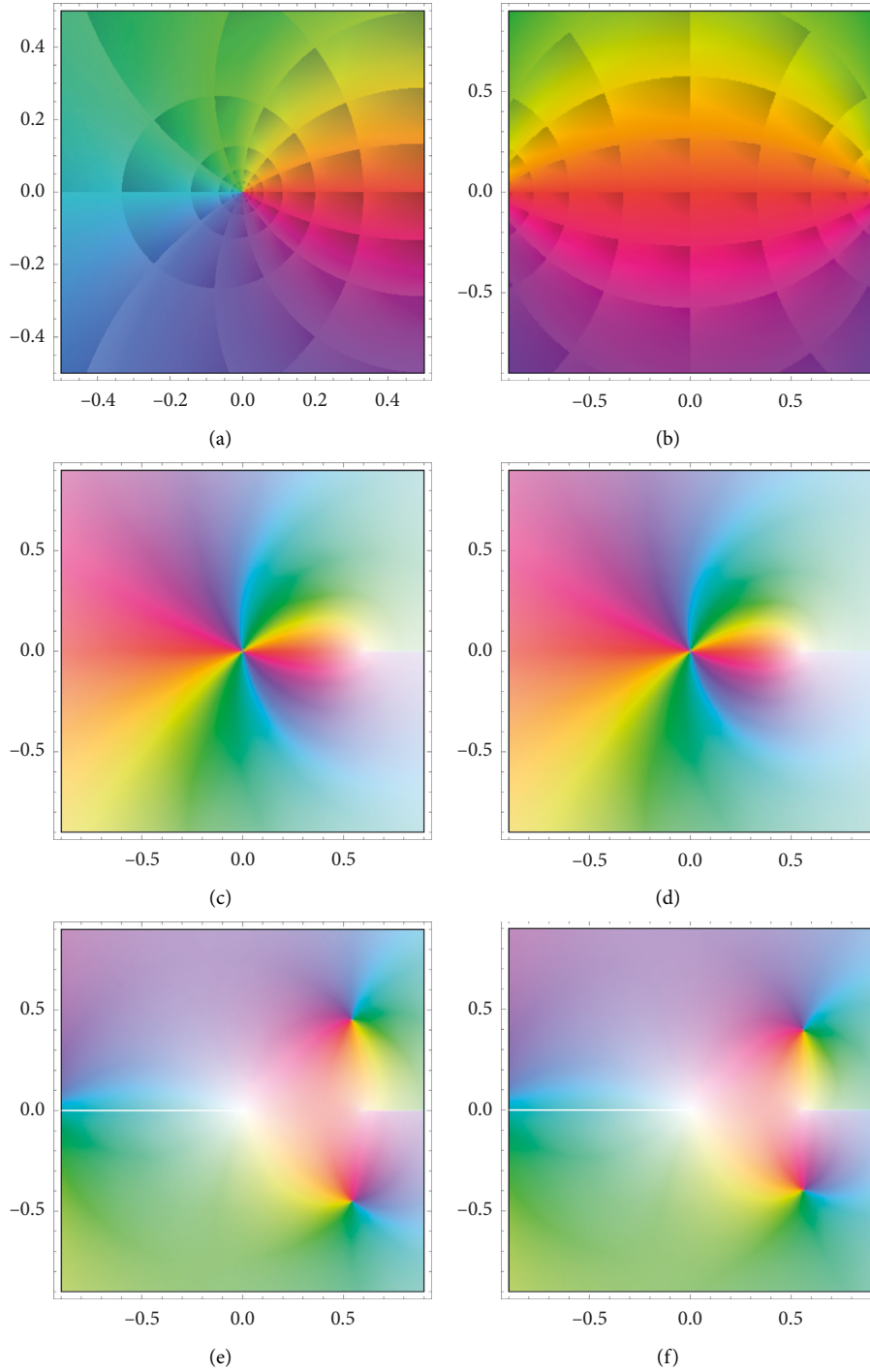


FIGURE 1: Plots of GKS of equation (45). (a) $\psi(\xi) = \xi/(1 - \xi)$. (b) $(1 + \xi)/(1 - \xi)$. (c) $[\mathbb{I}_{\alpha,\beta}^{\nu}\psi(\xi)]$, when $\lambda = 0.5, c = 0$. (d) $[\mathbb{I}_{\alpha,\beta}^{\nu}\psi(\xi)]$, when $\lambda = 0.25, c = 0$. (e) $[\mathbb{I}_{\alpha,\beta}^{\nu}\psi(\xi)]$, when $\lambda = 0.5, c = 1$. (f) $[\mathbb{I}_{\alpha,\beta}^{\nu}\psi(\xi)]$, when $\lambda = 0.25, c = 1$.

which implies that

$$\frac{(\mathcal{M}_{\ell}^{k+1}[\mathbb{I}_{\alpha,\beta}^{\nu}\psi(\xi)])'}{\mathcal{M}_{\ell}^{k+1}[\mathbb{I}_{\alpha,\beta}^{\nu}\psi(\xi)]} - \frac{1}{\xi} = \frac{\hbar(y(\xi)) - 1}{\xi}. \quad (63)$$

Integration implies that

$$\log \mathcal{M}_{\ell}^{k+1}[\mathbb{I}_{\alpha,\beta}^{\nu}\psi(\xi)] - \log \xi = \int_0^{\xi} \frac{\hbar(y(z)) - 1}{z} dz. \quad (64)$$

A computation brings

$$\log\left(\frac{\mathcal{M}_{\ell}^{k+1}[\mathbb{I}_{\alpha,\beta}^{\nu}\psi(\xi)]}{\xi}\right) = \int_0^{\xi} \frac{\hbar(y(z)) - 1}{z} dz. \quad (65)$$

The subordination yields

$$\mathcal{M}_\ell^{k+1}[\mathbb{J}_{\alpha,\beta}^v \psi(\xi)] < \xi \exp\left(\int_0^\xi \frac{\hbar(y(z)) - 1}{z} dz\right). \quad (66)$$

Moreover, the disk is mapped by $\hbar(\xi)$. When we apply $0 < |\xi| < \aleph < 1$ to an area that is convex and symmetric with respect to the real axis, we get

$$\hbar(-\aleph|\xi|) \leq \Re(\hbar(y(\aleph\xi))) \leq \hbar(\aleph|\xi|), \quad \aleph \in (0, 1), \quad (67)$$

which brings

$$\begin{aligned} \hbar(-\aleph) &\leq \hbar(-\aleph|\xi|), \quad \hbar(\aleph|\xi|) \leq \hbar(\aleph), \\ \int_0^1 \frac{\hbar(y(-\aleph|\xi|)) - 1}{\aleph} d\aleph &\leq \Re\left(\int_0^1 \frac{\hbar(y(\aleph)) - 1}{\aleph} d\aleph\right) \leq \int_0^1 \frac{\hbar(y(\aleph|\xi|)) - 1}{\aleph} d\aleph. \end{aligned} \quad (68)$$

Employing equation (65), we obtain

$$\int_0^1 \frac{\hbar(y(-\aleph|\xi|)) - 1}{\aleph} d\aleph \leq \log\left|\frac{\mathcal{M}_\ell^{k+1}[\mathbb{J}_{\alpha,\beta}^v \psi(\xi)]}{\xi}\right| \leq \int_0^1 \frac{\hbar(y(\aleph|\xi|)) - 1}{\aleph} d\aleph. \quad (69)$$

As a result, we get the inequality

$$\exp\left(\int_0^1 \frac{\hbar(y(-\aleph|\xi|)) - 1}{\aleph} d\aleph\right) \leq \left|\frac{\mathcal{M}_\ell^{k+1}[\mathbb{J}_{\alpha,\beta}^v \psi(\xi)]}{\xi}\right| \leq \exp\left(\int_0^1 \frac{\hbar(y(\aleph|\xi|)) - 1}{\aleph} d\aleph\right). \quad (70)$$

Hence, we receive

$$\exp\left(\int_0^1 \frac{\hbar(y(-\aleph)) - 1}{\aleph} d\aleph\right) \leq \left|\frac{\mathcal{M}_\ell^{k+1}[\mathbb{J}_{\alpha,\beta}^v \psi(\xi)]}{\xi}\right| \leq \exp\left(\int_0^1 \frac{\hbar(y(\aleph)) - 1}{\aleph} d\aleph\right). \quad (71)$$

Proposition 6. Suppose that $\psi \in \mathbb{J}_\ell^{\natural}(A, B, k)$ then the odd function

$$\mathfrak{Q}(\xi) = \frac{1}{2} [\psi(\xi) - \psi(-\xi)], \quad \xi \in \mathbb{U}, \quad (72)$$

fulfills the inequality

$$\begin{aligned} 1 + \frac{1}{\natural} \left(\frac{\mathcal{M}_\ell^{k+1}[\mathbb{J}_{\alpha,\beta}^v \mathfrak{Q}(\xi)]}{\mathcal{M}_\ell^k[\mathbb{J}_{\alpha,\beta}^v \mathfrak{Q}(\xi)]} - 1 \right) &< \frac{1 + A\xi}{1 + B\xi}, \\ \Re\left(\frac{\xi \mathfrak{Q}(\xi)'}{\mathfrak{Q}(\xi)}\right) &\geq \frac{1 - \eta^2}{1 + \eta^2}, \quad |\xi| = \eta < 1, \end{aligned} \quad (73)$$

$$(\xi \in \mathbb{U}, -1 \leq B < A \leq 1, k = 1, 2, \dots, \natural \in \mathbb{C} \setminus \{0\}, \ell \in [0, 1]).$$

Proof. By the condition $\psi \in \mathbb{J}_\ell^{\natural}(A, B, k)$, we obtain the existence of a function $G \in \mathbb{J}(A, B)$ such that

$$\begin{aligned} \mathfrak{h}(G(\xi) - 1) &= \left(\frac{2\mathcal{M}_\ell^{k+1} [\mathbb{I}_{\alpha,\beta}^\nu \Psi(\xi)]}{\mathcal{M}_\ell^k [\mathbb{I}_{\alpha,\beta}^\nu \Psi(\xi)] - \mathcal{M}_\ell^k [\mathbb{I}_{\alpha,\beta}^\mu \Psi(-\xi)]} \right), \\ \mathfrak{h}(G(-\xi) - 1) &= \left(\frac{-2\mathcal{M}_\ell^{k+1} [\mathbb{I}_{\alpha,\beta}^\nu \Psi(-\xi)]}{\mathcal{M}_\ell^k [\mathbb{I}_{\alpha,\beta}^\nu \Psi(\xi)] - \mathcal{M}_\ell^k [\mathbb{I}_{\alpha,\beta}^\mu \Psi(-\xi)]} \right). \end{aligned} \tag{74}$$

This leads to

$$1 + \frac{1}{\mathfrak{h}} \left(\frac{\mathcal{M}_\ell^{k+1} [\mathbb{I}_{\alpha,\beta}^\nu \mathfrak{Q}(\xi)]}{\mathcal{M}_\ell^k [\mathbb{I}_{\alpha,\beta}^\nu \mathfrak{Q}(\xi)]} - 1 \right) = \frac{G(\xi) + G(-\xi)}{2}. \tag{75}$$

Also, because

$$G(\xi) \prec \frac{1 + A\xi}{1 + B\xi}, \tag{76}$$

where $(1 + A\xi/1 + B\xi)$ is univalent, then the above subordination yields

$$1 + \frac{1}{\mathfrak{h}} \left(\frac{\mathcal{M}_\ell^{k+1} [\mathbb{I}_{\alpha,\beta}^\nu \mathfrak{Q}(\xi)]}{\mathcal{M}_\ell^k [\mathbb{I}_{\alpha,\beta}^\nu \mathfrak{Q}(\xi)]} - 1 \right) \prec \frac{1 + A\xi}{1 + B\xi}. \tag{77}$$

Additionally, the function $\mathfrak{Q}(\xi)$ is star-like in \mathbb{U} , which gives the inequality

$$\frac{\xi \mathfrak{Q}(\xi)'}{\mathfrak{Q}(\xi)} \prec \frac{1 - \xi^2}{1 + \xi^2}. \tag{78}$$

As a consequence, we confirm the existence of Schwarz function $\wp \in \mathbb{U}$, $|\wp(\xi)| \leq |\xi| < 1$, $\wp(0) = 0$ such that

$$Y(\xi) := \frac{\xi \mathfrak{Q}(\xi)'}{\mathfrak{Q}(\xi)} \prec \frac{1 - \wp(\xi)^2}{1 + \wp(\xi)^2}, \tag{79}$$

which yields that there is ξ , $|\xi| = \eta < 1$ such that

$$\wp^2(\xi) = \frac{1 - Y(\xi)}{1 + Y(\xi)}, \quad \xi \in \mathbb{U}. \tag{80}$$

By rearranging the above inequality, we receive

$$\left| \frac{1 - Y(\xi)}{1 + Y(\xi)} \right| = |\wp(\xi)|^2 \leq |\xi|^2. \tag{81}$$

Hence, we have the following conclusion:

$$\left| Y(\xi) - \frac{1 + |\xi|^4}{1 - |\xi|^4} \right| \leq \frac{4|\xi|^4}{(1 - |\xi|^4)^2}, \tag{82}$$

or

$$\left| Y(\xi) - \frac{1 + |\xi|^4}{1 - |\xi|^4} \right| \leq \frac{2|\xi|^2}{(1 - |\xi|^4)}. \tag{83}$$

This yields

$$\Re(Y(\xi)) \geq \frac{1 - \eta^2}{1 + \eta^2}, \quad |\xi| = \eta < 1. \tag{84}$$

As a result, we obtain the next outcomes. □

Corollary 1 (see [18]). *Let $\mu(n) = \Gamma(\alpha n + \beta)$ in Proposition 6. Then*

$$1 + \frac{1}{\mathfrak{h}} \left(\frac{\mathcal{M}_\ell^{k+1} [\mathbb{I}_{\alpha,\beta}^\nu \mathfrak{Q}(\xi)]}{\mathcal{M}_\ell^k [\mathbb{I}_{\alpha,\beta}^\nu \mathfrak{Q}(\xi)]} - 1 \right) = 1 + \frac{1}{\mathfrak{h}} \left(\frac{\mathcal{M}_\ell^{k+1} [\mathfrak{Q}(\xi)]}{\mathcal{M}_\ell^k [\mathfrak{Q}(\xi)]} - 1 \right) \prec \frac{1 + A\xi}{1 + B\xi}. \tag{85}$$

Corollary 2 (see [19]). *Let $\ell = 1$ and $v(n) = \Gamma(\alpha n + \beta)$ in Theorem 3.9. Then*

$$1 + \frac{1}{\mathfrak{h}} \left(\frac{\mathcal{M}_1^{k+1} [\mathbb{I}_{\alpha,\beta}^\nu \mathfrak{Q}(\xi)]}{\mathcal{M}_1^k [\mathbb{I}_{\alpha,\beta}^\nu \mathfrak{Q}(\xi)]} - 1 \right) = 1 + \frac{1}{\mathfrak{h}} \left(\frac{\mathcal{M}_1^{k+1} [\mathfrak{Q}(\xi)]}{\mathcal{M}_1^k [\mathfrak{Q}(\xi)]} - 1 \right) \prec \frac{1 + A\xi}{1 + B\xi}. \tag{86}$$

Corollary 3 (see [20]). *Let $\ell = 1, k = 1$ and $v(n) = \Gamma(\alpha n + \beta)$ in Theorem 3.9. Then*

$$1 + \frac{1}{\mathfrak{h}} \left(\frac{\mathcal{M}_1^2 [\mathbb{I}_{\alpha,\beta}^\mu \mathfrak{Q}(\xi)]}{\mathcal{M}_1^1 [\mathbb{I}_{\alpha,\beta}^\mu \mathfrak{Q}(\xi)]} - 1 \right) = 1 + \frac{1}{\mathfrak{h}} \left(\frac{\mathcal{M}_1^2 [\mathfrak{Q}(\xi)]}{\mathcal{M}_1^1 [\mathfrak{Q}(\xi)]} - 1 \right) \prec \frac{1 + A\xi}{1 + B\xi}. \tag{87}$$

Corollary 4. *Let $k = 0, \ell = 1$ and $v(n) = \Gamma(\alpha n + \beta)$ in Theorem 3.9. Then*

$$1 + \frac{1}{\mathfrak{h}} \left(\frac{\mathcal{M}_1^1 [\mathbb{I}_{\alpha,\beta}^\nu \mathfrak{Q}(\xi)]}{[\mathbb{I}_{\alpha,\beta}^\nu \mathfrak{Q}(\xi)]} - 1 \right) \prec \frac{1 + A\xi}{1 + B\xi}. \tag{88}$$

4. Conclusion

The preceding study used symmetric derivative and Jackson’s calculus to generalize Raina’s transformations in \mathbb{U} . We used the suggested linear convolution operator on the normalized subclass. The operator is utilized to analyze the outcome of a specific form of GKS, which is utilized as an application. The hypergeometric function was used to determine the behavior of solutions. We further stressed that the answer belongs to the normalized analytic functions category.

Data Availability

Data sharing is not applicable to this article as no datasets were generated or analyzed during the current study.

Conflicts of Interest

The authors declare that they have no conflicts of interest.

Authors' Contributions

All authors contributed equally and significantly to writing this article. All authors read and agreed to the published version of the manuscript.

References

- [1] H. Weyl, "Symmetry," in *Symmetry* Princeton University Press, Princeton, NY, USA, 2015.
- [2] H. J. Seybold and R. Hilfer, "Numerical results for the generalized Mittag-Leffler function," *Fractional Calculus and Applied Analysis*, vol. 8, no. 2, pp. 127–139, 2005.
- [3] F. Mainardi, "Why the mittag-leffler function can be considered the queen function of the fractional calculus?" *Entropy*, vol. 22, no. 12, p. 1359, 2020.
- [4] R. Gorenflo and F. Mainardi, "The Mittag-Leffler function in the thinning theory for renewal processes," 2018, <https://arxiv.org/abs/1808.06563>.
- [5] R. W. Ibrahim, "Normalized symmetric differential operators in the open unit disk," in *Approximation and Computation in Science and Engineering*, pp. 417–434, Springer, Berlin, Germany, 2022.
- [6] R. W. Ibrahim, "Analytic solvability of a class of symmetric nonlinear second order differential equations," *Montes Taurus Journal of Pure and Applied Mathematics*, vol. 4, no. 3, pp. 80–92, 2022.
- [7] R. W. Ibrahim and D. Baleanu, "Convolutated fractional differentials of various forms utilizing the generalized Raina's function description with applications," *Journal of Taibah University for Science*, vol. 16, no. 1, pp. 432–441, 2022.
- [8] A. Tassaddiq and A. Alruban, "On modifications of the gamma function by using Mittag-Leffler function," *Journal of Mathematics*, vol. 2021, p. 1, 2, 2021.
- [9] S. S. Miller and P. T. Mocanu, *Differential Subordinations: Theory and Applications*, CRC Press, Baco Raton, FL, USA, 2000.
- [10] S. Ruscheweyh, *Convolutions in Geometric Function Theory*, Les Presses De L'Universite De Montreal, 1982.
- [11] A. Gil, J. Segura, and M. Nico, "Numerical methods for special functions," *Society for Industrial and Applied Mathematics*, 2007.
- [12] R. K. Raina, "On generalized wright's hypergeometric functions and fractional calculus operators," *East Asian Mathematical Journal*, vol. 21, pp. 191–203, 2015.
- [13] B. C. Carlson and D. B. Shaffer, "Starlike and prestarlike hypergeometric functions," *SIAM Journal on Mathematical Analysis*, vol. 15, no. 4, pp. 737–745, 1984.
- [14] G. S. Sălăgean, "Subclasses of univalent functions, complex analysis-fifth Romanian-Finnish seminar, part 1 (Bucharest, 1981)," *Lecture Notes in Math*, vol. 1013, pp. 362–372, Springer, Berlin, Germany, 1983.
- [15] T. N. Shanmugam, S. Sivasubramanian, and H. M. Srivastava, "Differential sandwich theorems for certain subclasses of analytic functions involving multiplier transformations," *Integral Transforms and Special Functions*, vol. 17, no. 12, pp. 889–899, 2006.
- [16] S. S. Miller and P. T. Mocanu, "Subordinants of differential superordinations," *Complex Variables, Theory and Application: An International Journal*, vol. 48, no. 10, pp. 815–826, 2003.
- [17] R. E. Rodriguez, I. Kra, and J. P. Gilman, *Complex Analysis: In the Spirit of Lipman Bers*, Springer, Berlin, Germany, 2013.
- [18] R. W. Ibrahim and M. Darus, "New symmetric differential and integral operators defined in the complex domain," *Symmetry*, vol. 11, no. 7, p. 906, 2019.
- [19] M. Arif, K. Ahmad, J. L. Liu, and J. Sokol, "A new class of analytic functions associated with Salagean operator," *Journal of Function Spaces*, pp. 1–8, 2019.
- [20] R. N. Das and P. Singh, "On subclasses of Schlicht mapping," *Indian Journal of Pure and Applied Mathematics*, vol. 8, pp. 864–872, 1977.

Research Article

A Semianalytical Approach for the Solution of Nonlinear Modified Camassa–Holm Equation with Fractional Order

Jiahua Fang ¹, Muhammad Nadeem ², and Hanan A. Wahash ³

¹Yibin University, Yibin 644000, China

²Faculty of Science, Yibin University, Yibin 644000, China

³Department of Mathematics, Albaydaa University, Albaydaa, Yemen

Correspondence should be addressed to Muhammad Nadeem; nadeem@yibinu.edu.cn and Hanan A. Wahash; hawahash@baydaauniv.net

Received 28 May 2022; Revised 8 June 2022; Accepted 9 June 2022; Published 29 June 2022

Academic Editor: Arzu Akbulut

Copyright © 2022 Jiahua Fang et al. This is an open access article distributed under the Creative Commons Attribution License, which permits unrestricted use, distribution, and reproduction in any medium, provided the original work is properly cited.

This paper presents the approximate solution of the nonlinear acoustic wave propagation model is known as the modified Camassa–Holm (mCH) equation with the Caputo fractional derivative. We examine this study utilizing the Laplace transform (\mathcal{L} T) coupled with the homotopy perturbation method (HPM) to construct the strategy of the Laplace transform homotopy perturbation method (\mathcal{L} T-HPM). Since the Laplace transform is suitable only for a linear differential equation, therefore \mathcal{L} T-HPM is the suitable approach to decompose the nonlinear problems. This scheme produces an iterative formula for finding the approximate solution of illustrated problems that leads to a convergent series without any small perturbation and restriction. Graphical results demonstrate that \mathcal{L} T-HPM is simple, straightforward, and suitable for other nonlinear problems of fractional order in science and engineering.

1. Introduction

In the recent century, fractional differential problems have caught much attention towards the researchers and scientists due to their precise representation of the physical appearance. Many physical phenomena have been reported across the nonlinear models such as engineering, geophysics, astronomy, medicine, hydrology, chemical engineering, and astrophysics [1–4]. Most of the nonlinear problems of fractional order are difficult to solve. Therefore, these models are very much important to examine the exact and numerical solutions. Currently, many authors have examined the direct correlation and interrelated work on nonlinear problems and symmetry [5]. Integral transform methods are extremely effective in reducing the complexity of these nonlinear fractional problems. There are a number of popular and effective schemes to tackle the nonlinear appearance of these models with fractional order such as the Laplace transform [6], Fourier series approach [7], F -Expansion scheme [8], Residual power series method [9], (G/G) -expansion approach

[10], Trial equation approach [11], Sinc–Bernoulli collocation method [12], Variational iteration scheme [13], Subequation [14], Homotopy perturbation method [15], spline collocation approach [16], and so on.

In this paper, we consider a family of modified β -model of the aspect [17].

$$D^\alpha u_t - u_{xxt} + (\beta + 1)u^2 u_x - \beta u_x u_{xx} - uu_{xxx} = 0, \quad (1)$$

Setting $\beta = 2$ in equation (1), and we obtain the fractional modified Camassa–Holm (mCH) model of the shape.

$$D^\alpha u_t - u_{xxt} + 3u^2 u_x - 2u_x u_{xx} - uu_{xxx} = 0, \quad (2)$$

where u represents the horizontal component of the fluid velocity, x and t indicate the spatial and temporal elements. The mCH model appears in shallow water that was discovered to be entirely integrable with a Lax pair as an approximation to the incompressible Euler equation [18]. Islam et al. [19] obtained the solitary wave solution of the simplified modified Camassa–Holm equation. Zulfikar and

Ahmad [20] used the Exp-function scheme to investigate the solitary wave solutions of the fractional simplified mCH model. Khatun et al. [21] studied the explicit solutions of the mCH equation with fractional order. Labidi and Omrani [22] studied the variational iteration method and the homotopy perturbation method for solving the mCH equation and found the results in good agreement.

Another powerful technique was introduced to solve the nonlinear problem by He [23, 24] with some recent developments. Kashkari and El-Tantawy [25] applied the homotopy perturbation method for the dissipative soliton collisions in a collisional complex unmagnetized plasma. Later many authors showed the validity and accuracy of this approach [26, 27]. Gupta et al. [28] obtained the approximate solution of the family of the mCH equation with fractional time derivative. Khuri and Sayfy [29] introduced a strategy for specific kinds of differential problems. Later, Anjum and He [30] adopted this scheme for the solution of the nonlinear oscillator problem. Nadeem and Li [31] present a hybrid approach for the solution of nonlinear vibration systems and then Zhang et al. [32] extended this approach for obtaining the solution of nonlinear time fractional differential problems but all these have some limitations and assumptions.

In the present study, we propose an approach, called \mathcal{L} T-HPM which removes these disadvantages and elaborates our scheme to achieve the approximate solution of this nonlinear problem. The implementation of \mathcal{L} T coupled with HPM makes them easier for the construction of this approach for the solution of mCH with fractional order. This approach can also be considered for fractals theory [33, 34]. This article is summarized as follows: in Section 2, we recall the definition of fractional calculus theory. In Section 3, we

construct the idea of \mathcal{L} T-HPM to solve the mCH equation. In Section 4, we test the validity and accuracy of \mathcal{L} T-HPM illustrating a numerical problem with the help of graphs. At last, we represent the conclusion in Section 5.

2. Basic Concept of Fractional Theory

In this section, we present some fractional properties to understand the physical nature of calculus theory.

Definition 1. The fractional view of $u(t)$ is described as follows [32]:

$$D^\alpha u(x) = J^{h-\alpha} D^h u(x) = \frac{1}{\Gamma(h-\alpha)} \int_0^t (t-\tau)^{h-\alpha-1} f^h(\tau) d\tau, \quad \text{for } h-1 < \alpha \leq h, h \in \mathbb{N}, t > 0, u \in C_{-1}^h. \tag{3}$$

Definition 2. The fractional view of $\mathcal{L}[u(t)]$ is [1, 35]

$$\mathcal{L}[D_x^{n\alpha} u(x, t)] = s^{n\alpha} F(s) - \sum_{k=0}^{n-1} s^{n\alpha-k-1} u_x^{(k)}(0, t), \quad n-1 < \alpha \leq n. \tag{4}$$

Definition 3. Let $u(t) = t^\alpha$, so $\mathcal{L} T$ is [32]

$$\mathcal{L}[t^\alpha] = \int_0^\infty e^{-st} t^\alpha dt = \frac{\Gamma(\alpha+1)}{s^{(\alpha+1)}}. \tag{5}$$

Definition 4. The Caputo-sense becomes as for order $\alpha > 0$,

$$D^\nu u(x, t) = \begin{cases} \frac{1}{\Gamma(h-\alpha)} \int_0^t (t-\tau)^{h-\alpha-1} \frac{\partial^h u(x, t)}{\partial \tau^h} d\tau, & h-1 < \alpha < h, \\ \frac{\partial^h u(x, t)}{\partial t^h}, & \alpha = h \in \mathbb{N}. \end{cases} \tag{6}$$

3. Fundamental Concept of \mathcal{L} T-HPM

In this segment, we construct the fundamental concept of \mathcal{L} T-HPM. Let us consider the following FPDEs:

$$D_t^\alpha u(x, t) = T_1[u(x, t)] + T_2[u(x, t)] + g(x, t), \quad x \in \mathbb{R}, n-1 < \alpha \leq n, \tag{7}$$

where $D_t^\alpha = (\partial^\alpha / \partial t^\alpha)$ is taken in Caputo sense, T_1 and T_2 are linear and nonlinear operators whereas $g(x, t)$ represents as a source term.

By applying $\mathcal{L} T$ to equation (7), it follows,

$$\mathcal{L}[D_t^\alpha u(x, t)] = \mathcal{L}[T_1 u(x, t) + T_2 u(x, t) + g(x, t)]. \tag{8}$$

Applying $\mathcal{L} T$, we obtain the following equation:

$$s^\alpha \mathcal{L}[u(x, t)] - s^{\alpha-1} [u(x, 0)] = \mathcal{L}[T_1 u(x, t) + T_2 u(x, t) + g(x, t)]. \tag{9}$$

On applying Inverse $\mathcal{L} T$, we receive,

$$u(x, t) = W(x, t) + \mathcal{L}^{-1} \left[\frac{1}{s^\alpha} \mathcal{L} \{T_1 u(x, t) + T_2 u(x, t)\} \right], \tag{10}$$

where $W(x, t) = \mathcal{L}^{-1} [(1/s)u(x, 0) + (1/s^\alpha)\mathcal{L}\{g(x, t)\}]$.

The approximate solution of equation (7) can be expressed in terms of the following power series:

$$u(x, t) = \sum_{n=0}^\infty p^n u_n(x, t), \tag{11}$$

where p is called the homotopy parameter. According to HPM [23], The nonlinear terms can be calculated as follows:

$$T_2 u(x, t) = \sum_{n=0}^{\infty} p^n H_n(u). \tag{12}$$

Then, He's polynomials $H_n(u)$ can be obtained using the following formula:

$$H_n(u_0 + u_1 + \dots + u_n) = \frac{1}{n!} \frac{\partial^n}{\partial p^n} \left(T_2 \left(\sum_{i=0}^{\infty} p^i u_i \right) \right)_{p=0}, \quad n = 0, 1, 2, \dots \tag{13}$$

Now putting equations (11) and (12) in equation (10), we obtain the following equation:

$$\sum_{n=0}^{\infty} p^n u_n(x, t) = W(x, t) + p \left[\mathcal{L}^{-1} \left\{ \frac{1}{s^\alpha} \mathcal{L} \left(T_1 \sum_{n=0}^{\infty} p^n u_n(x, t) + \sum_{n=0}^{\infty} p^n H_n(u) \right) \right\} \right]. \tag{14}$$

Equating the values of p , we obtain the following equation:

$$\begin{aligned} p^0: u_0(x, t) &= W(x, t), \\ p^1: u_1(x, t) &= -\mathcal{L}^{-1} \left[\frac{1}{s^\alpha} \mathcal{L} \{ T_1 u_0(x, t) + H_0 \} \right], \\ p^2: u_2(x, t) &= -\mathcal{L}^{-1} \left[\frac{1}{s^\alpha} \mathcal{L} \{ T_1 u_1(x, t) + H_1 \} \right], \\ p^3: u_3(x, t) &= -\mathcal{L}^{-1} \left[\frac{1}{s^\alpha} \mathcal{L} \{ T_1 u_2(x, t) + H_2 \} \right], \\ &\vdots \end{aligned} \tag{15}$$

by continuing this process, we are able to identify the exact solution of this problems such as

$$u(x, t) = \lim_{N \rightarrow \infty} \sum_{n=0}^N u_n(x, t). \tag{16}$$

Generally, this series converges very rapidly.

4. Numerical Applications

In this section, we implement the idea of \mathcal{L} T-HPM for obtaining the smooth solitary wave and singular wave solutions. We see that this scheme presents good results only after a few terms. We compute the values of iterations with the help of Mathematical Software 11.0.1. We present some 2D and 3D graphs for a better understanding of the behavior of the mCH model.

4.1. Example 1. Considering the mCH equation with fractional order α such as

$$\frac{\partial^\alpha u}{\partial t^\alpha} - \frac{\partial}{\partial t} \left(\frac{\partial^2 u}{\partial x^2} \right) + 3u^2 \frac{\partial u}{\partial x} - 2 \frac{\partial u}{\partial x} \frac{\partial^2 u}{\partial x^2} - u \frac{\partial^3 u}{\partial x^3} = 0, \tag{17}$$

with initial condition

$$u(x, 0) = \frac{1}{3} \left[1 - 4 \operatorname{sech}^2 \left(\frac{x}{\sqrt{6}} \right) \right]. \tag{18}$$

Employing the \mathcal{L} T on equation (17), we get the following equation:

$$\begin{aligned} \mathcal{L} \left[\frac{\partial^\alpha u}{\partial t^\alpha} \right] &= \mathcal{L} \left[\frac{\partial}{\partial t} \left(\frac{\partial^2 u}{\partial x^2} \right) - 3u^2 \frac{\partial u}{\partial x} + 2 \frac{\partial u}{\partial x} \frac{\partial^2 u}{\partial x^2} + u \frac{\partial^3 u}{\partial x^3} \right], \\ s^\alpha \mathcal{L} [u(x, t)] - s^{\alpha-1} [u(x, 0)] &= \mathcal{L} \left[\frac{\partial}{\partial t} \left(\frac{\partial^2 u}{\partial x^2} \right) - 3u^2 \frac{\partial u}{\partial x} + 2 \frac{\partial u}{\partial x} \frac{\partial^2 u}{\partial x^2} + u \frac{\partial^3 u}{\partial x^3} \right], \\ \mathcal{L} [u] &= \frac{u(x, 0)}{s} + \frac{1}{s^\alpha} \mathcal{L} \left[\frac{\partial}{\partial t} \left(\frac{\partial^2 u}{\partial x^2} \right) - 3u^2 \frac{\partial u}{\partial x} + 2 \frac{\partial u}{\partial x} \frac{\partial^2 u}{\partial x^2} + u \frac{\partial^3 u}{\partial x^3} \right]. \end{aligned} \tag{19}$$

Using the inverse $\mathcal{L} T$ property,

$$u = u(x, 0) + \mathcal{L}^{-1} \left[\frac{1}{s^\alpha} \mathcal{L} \left\{ \frac{\partial}{\partial t} \left(\frac{\partial^2 u}{\partial x^2} \right) - 3u^2 \frac{\partial u}{\partial x} + 2 \frac{\partial u}{\partial x} \frac{\partial^2 u}{\partial x^2} + u \frac{\partial^3 u}{\partial x^3} \right\} \right]. \tag{20}$$

The description of $\mathcal{L} T$ -HPM presents as follows:

$$\sum_{n=0}^{\infty} p^n u_n = u(x, 0) + \mathcal{L}^{-1} \left[\frac{1}{s^\alpha} \mathcal{L} \left\{ \sum_{n=0}^{\infty} p^n \frac{\partial}{\partial t} \left(\frac{\partial^2 u_n}{\partial x^2} \right) - 3 \sum_{n=0}^{\infty} p^n u_n^2 \sum_{n=0}^{\infty} p^n \frac{\partial u_n}{\partial x} + 2 \sum_{n=0}^{\infty} p^n \frac{\partial u_n}{\partial x} \sum_{n=0}^{\infty} p^n \frac{\partial^2 u_n}{\partial x^2} + \sum_{n=0}^{\infty} p^n u_n \sum_{n=0}^{\infty} p^n \frac{\partial^3 u_n}{\partial x^3} \right\} \right]. \tag{21}$$

Equating the values of p , we obtain the following equation:

$$\begin{aligned} p^0: u_0 &= u(x, 0) \\ &= \frac{1}{3} \left[1 - 4 \operatorname{sech}^2 \left(\frac{x}{\sqrt{6}} \right) \right], \\ p^1: u_1 &= \mathcal{L}^{-1} \left[\frac{1}{s^\alpha} \mathcal{L} \left\{ \frac{\partial}{\partial t} \left(\frac{\partial^2 u_0}{\partial x^2} \right) - 3u_0^2 \frac{\partial u_0}{\partial x} + 2 \frac{\partial u_0}{\partial x} \frac{\partial^2 u_0}{\partial x^2} + u_0 \frac{\partial^3 u_0}{\partial x^3} \right\} \right] \\ &= -\frac{1}{27} \sqrt{\frac{2}{3}} \left[\sin h \left(\sqrt{\frac{3}{2}} x \right) + 25 \sin h \left(\frac{x}{\sqrt{6}} \right) \right] \operatorname{sech}^5 \left(\frac{x}{\sqrt{6}} \right) \frac{t^\alpha}{\Gamma(1 + \alpha)}, \\ &\vdots \end{aligned} \tag{22}$$

Thus, all the findings are expressed as follows:

$$\begin{aligned} u(x, t) &= u_0 + u_1 + u_2 \dots, \\ u(x, t) &= \frac{1}{3} \left[1 - 4 \operatorname{sech}^2 \left(\frac{x}{\sqrt{6}} \right) \right] - \frac{1}{27} \sqrt{\frac{2}{3}} \left[\sin h \left(\sqrt{\frac{3}{2}} x \right) + 25 \sin h \left(\frac{x}{\sqrt{6}} \right) \right] \operatorname{sech}^5 \left(\frac{x}{\sqrt{6}} \right) \frac{t^\alpha}{\Gamma(1 + \alpha)} + \dots \end{aligned} \tag{23}$$

Finally, This series of solutions provide the smooth solitary wave solution for $\alpha = 1$.

$$u(x, t) = \frac{1}{3} \left[1 - 4 \operatorname{sech}^2 \frac{1}{\sqrt{6}} \left(x - \frac{t}{3} \right) \right]. \tag{24}$$

It is noted that we calculate the results only up to two terms for obtaining the smooth solitary wave solution of equation (17) with initial condition (18). In Figure 1, we provide the graphical comparison between the obtained results of $\mathcal{L} T$ -HPM and the exact solution at $-5 \leq x \leq 5$ and $t = 1$. We see that only two term solutions by using $\mathcal{L} T$ -HPM are near with the exact solution at $\alpha = 1$. We also sketch a 2D plot of $\mathcal{L} T$ -HPM and the exact solution at

$t = 0.05$ to show the graphical error in Figure 2. Hence we remark that the solutions with $\mathcal{L} T$ -HPM are in good agreement.

4.2. Example 2. Considering equation (17) with the initial condition,

$$u(x, 0) = \frac{1}{3} \left[-3 + 4 \cot h^2 \left(\frac{x}{\sqrt{6}} \right) \right]. \tag{25}$$

Applying $\mathcal{L} T$ -HPM as described in equation (21) and equating the values of p , we obtain the following equation:

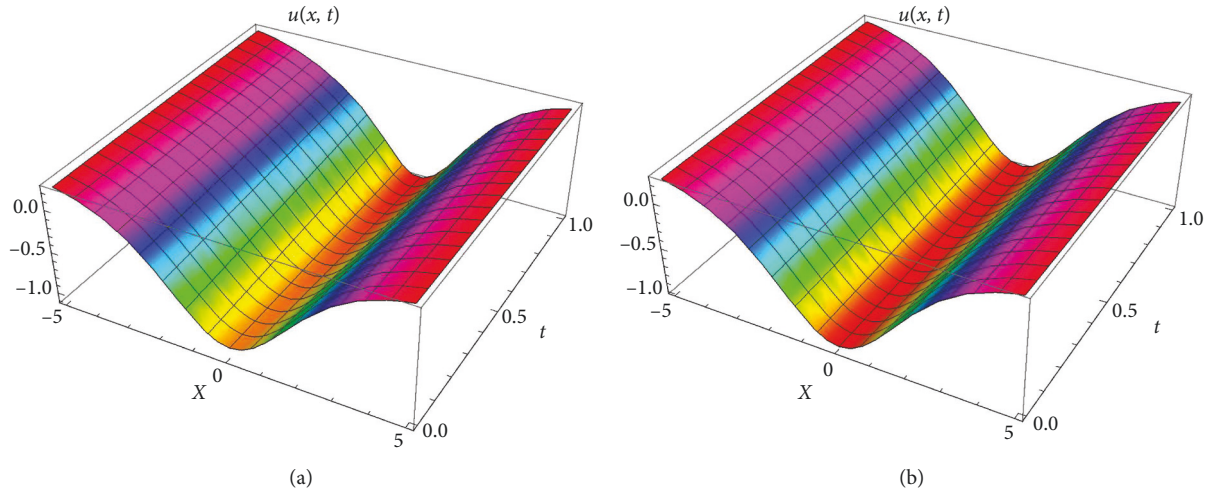


FIGURE 1: Surface solution between the proximate and the exact solutions w.r.t initial condition (18), when $\alpha = 1$. (a) Approximate solution. (b) Exact solution.

$$\begin{aligned}
 p^0: u_0 &= u(x, 0) \\
 &= \frac{1}{3} \left[-3 + 4 \cot h^2 \left(\frac{x}{\sqrt{6}} \right) \right], \\
 p^1: u_1 &= \mathcal{L}^{-1} \left[\frac{1}{s^\alpha} \mathcal{L} \left\{ \frac{\partial}{\partial t} \left(\frac{\partial^2 u_0}{\partial x^2} \right) - 3u_0^2 \frac{\partial u_0}{\partial x} + 2 \frac{\partial u_0}{\partial x} \frac{\partial^2 u_0}{\partial x^2} + u_0 \frac{\partial^3 u_0}{\partial x^3} \right\} \right] \\
 &= \frac{1}{27} \sqrt{\frac{2}{3}} \left[\cosh \left(\sqrt{\frac{3}{2}} x \right) - 25 \cosh \left(\frac{x}{\sqrt{6}} \right) \right] \operatorname{csch} \left(\frac{x}{\sqrt{6}} \right)^5 \frac{t^\alpha}{\Gamma(1 + \alpha)}, \\
 &\vdots
 \end{aligned} \tag{26}$$

Thus, all the findings are expressed as follows:
 $u(x, t) = u_0 + u_1 + u_2 \dots$,

$$\begin{aligned}
 u(x, t) &= \frac{1}{3} \left[-3 + 4 \cot h^2 \left(\frac{x}{\sqrt{6}} \right) \right] \\
 &+ \frac{1}{27} \sqrt{\frac{2}{3}} \left[\cosh \left(\sqrt{\frac{3}{2}} x \right) - 25 \cosh \left(\frac{x}{\sqrt{6}} \right) \right] \\
 &\times \operatorname{csch} \left(\frac{x}{\sqrt{6}} \right)^5 \frac{t^\alpha}{\Gamma(1 + \alpha)} + \dots
 \end{aligned} \tag{27}$$

Finally, This series of solutions provide the singular wave solution for $\alpha = 1$.

$$u(x, t) = \frac{1}{3} \left[-3 + 4 \cot h^2 \frac{1}{\sqrt{6}} \left(x - \frac{t}{3} \right) \right]. \tag{28}$$

It is noted that we calculate the results only up to two terms for obtaining the smooth solitary wave solution of equation (17) with initial condition (25). In Figure 3, we provide the graphical comparison between the obtained results of \mathcal{L} T-HPM and the exact solution at $-5 \leq x \leq 5$ and $t = 1$. We see that only two term solutions by using \mathcal{L} T-HPM are near with the exact solution at $\alpha = 1$. We also sketch a 2D plot of \mathcal{L} T-HPM and the exact solution at $t = 0.05$ to show the graphical error in Figure 4. Hence, we remark that the solutions with \mathcal{L} T-HPM are in good agreement.

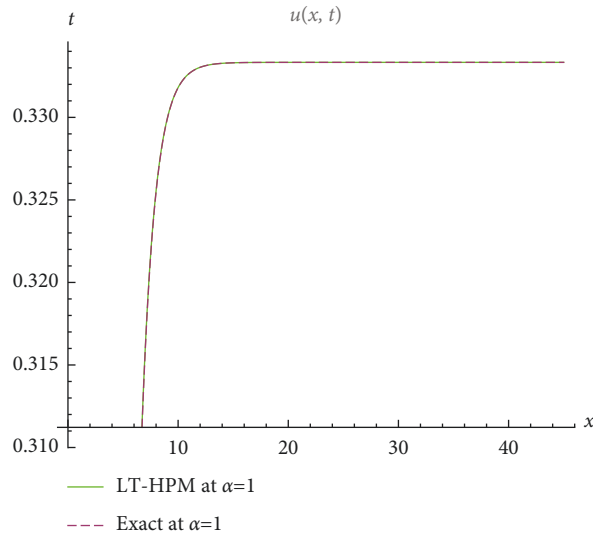


FIGURE 2: Error distribution between the approximate solution and the exact solution at $\alpha = 1$.

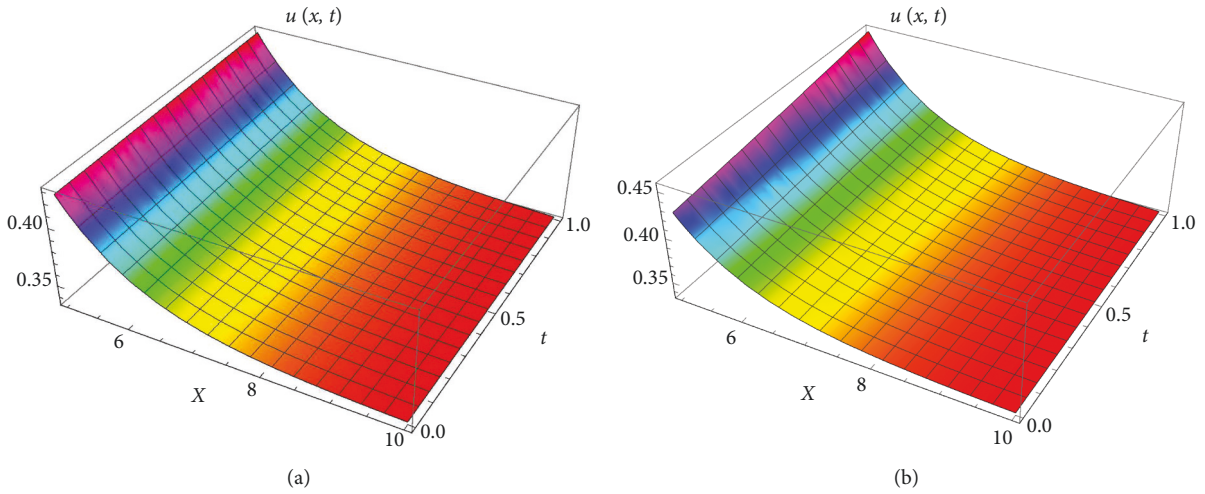


FIGURE 3: Surface solution between the proximate and the exact solutions w.r.t initial condition (25), when $\alpha = 1$. (a) The approximate solution. (b) The exact solution.

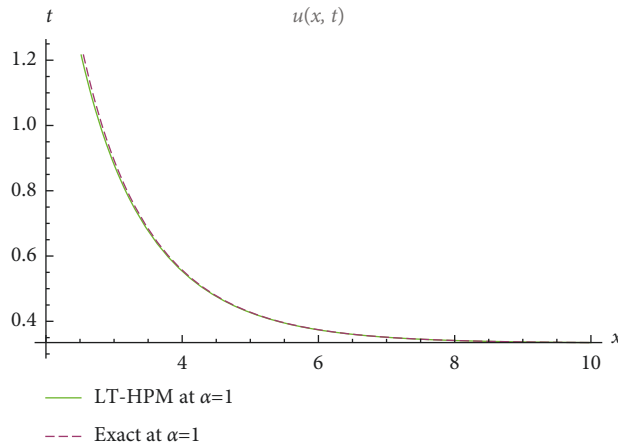


FIGURE 4: Error distribution between the approximate solution and the exact solution at $\alpha = 1$.

5. Conclusion

In this study, we successfully applied \mathcal{L} T-HPM to obtain the approximate solution of the mCH equation with fractional order. The most important benefit of this approach is that it does not consider any trivial perturbation and restrictions of variables for the solution of nonlinear problems with fractional order but also maintains an extreme authenticity of the solution. We observe that the obtained results are very close to the exact solution that confirms the accuracy and validity of this approach. We also present our solution results both in two-dimensional and three-dimensional graphs to show the accuracy of \mathcal{L} T-HPM. On the other hand, \mathcal{L} T-HPM plays a significant meaning in finding the simple solution process. This scheme can also be applied to other differential equations including fractal derivatives in our future applications.

Data Availability

The data used to support the study are included in the paper.

Conflicts of Interest

The authors declare that they have no conflicts of interest.

References

- [1] K. S. Miller and B. Ross, *An Introduction to the Fractional Calculus and Fractional Differential Equations*, Wiley, New York, NY, USA, 1993.
- [2] A. Akgül and S. A. Khoshnaw, "Application of fractional derivative on non-linear biochemical reaction models," *International Journal of Intelligent Networks*, vol. 1, pp. 52–58, 2020.
- [3] R. M. Jena, S. Chakraverty, S. K. Jena, and H. M. Sedighi, "On the wave solutions of time-fractional sawada-kotera-ito equation arising in shallow water," *Mathematical Methods in the Applied Sciences*, vol. 44, no. 1, pp. 583–592, 2021.
- [4] N. Attia, D. Seba, A. Akgül, and A. Nour, "Solving duffing-vander pol oscillator equations of fractional order by an accurate technique," *Journal of Applied and Computational Mechanics*, vol. 7, no. 3, pp. 1480–1487, 2021.
- [5] K. Karthikeyan, P. Karthikeyan, D. N. Chalishajar, D. S. Raja, and P. Sundararajan, "Analysis on ψ -hilfer fractional impulsive differential equations," *Symmetry*, vol. 13, no. 10, p. 1895, 2021.
- [6] L. Kexue and P. Jigen, "Laplace transform and fractional differential equations," *Applied Mathematics Letters*, vol. 24, no. 12, pp. 2019–2023, 2011.
- [7] K.-L. Wang, "Novel approach for fractal nonlinear oscillators with discontinuities by Fourier series," *Fractals*, vol. 30, no. 01, Article ID 2250009, 2022.
- [8] Y. Pandir and H. H. Duzgun, "New exact solutions of time fractional gardner equation by using new version of f-expansion method," *Communications in Theoretical Physics*, vol. 67, no. 1, p. 9, 2017.
- [9] R. M. Jena, S. Chakraverty, S. K. Jena, and H. M. Sedighi, "Analysis of time-fractional fuzzy vibration equation of large membranes using double parametric based residual power series method," *ZAMM-Journal of Applied Mathematics and Mechanics*, owing-sibling:*[4]), "publisher-name")+0^(?/^!"name(following-sibling:*[5]),"fpage")+0^(?/^!"name(following-sibling:*[6]),"lpage")+0^(?/^!"name(following-sibling:*[7]),"comment")+0^(?/^!"name(following-sibling:*[8]),"pub-id"), \$^!"content-markup(following-sibling:comment)", \$^!"content-markup(following-sibling:publsher-name)", [?--]>, vol. 101, no. 4, Article ID e202000165, 2021.
- [10] M. Ali Akbar, N. Hj Mohd Ali, and M. Tarikul Islam, "Multiple closed form solutions to some fractional order nonlinear evolution equations in physics and plasma physics," *AIMS Mathematics*, vol. 4, no. 3, pp. 397–411, 2019.
- [11] T. Liu, "Exact solutions to time-fractional fifth order kdv equation by trial equation method based on symmetry," *Symmetry*, vol. 11, no. 6, p. 742, 2019.
- [12] N. Moshtaghi and A. Saadatmandi, "Numerical solution of time fractional cable equation via the sinc-bernoulli collocation method," *Journal of Applied and Computational Mechanics*, vol. 7, no. 4, pp. 1916–1924, 2021.
- [13] D. Ziane and M. H. Cherif, "Variational iteration transform method for fractional differential equations," *Journal of Interdisciplinary Mathematics*, vol. 21, no. 1, pp. 185–199, 2018.
- [14] B. Tang, Y. He, L. Wei, and X. Zhang, "A generalized fractional sub-equation method for fractional differential equations with variable coefficients," *Physics Letters A*, vol. 376, no. 38–39, pp. 2588–2590, 2012.
- [15] A. Goswami, J. Singh, D. Kumar, S. Gupta, and Sushila, "An efficient analytical technique for fractional partial differential equations occurring in ion acoustic waves in plasma," *Journal of Ocean Engineering and Science*, vol. 4, no. 2, pp. 85–99, 2019.
- [16] Z. Alijani, D. Baleanu, B. Shiri, and G.-C. Wu, "Spline collocation methods for systems of fuzzy fractional differential equations," *Chaos, Solitons & Fractals*, vol. 131, Article ID 109510, 2020.
- [17] A.-M. Wazwaz, "Solitary wave solutions for modified forms of degasperis-procesi and camassa-holm equations," *Physics Letters A*, vol. 352, no. 6, pp. 500–504, 2006.
- [18] J. S. Kamdem and Z. Qiao, "Decomposition method for the camassa-holm equation," *Chaos, Solitons & Fractals*, vol. 31, no. 2, pp. 437–447, 2007.
- [19] M. N. Islam, M. Asaduzzaman, and M. S. Ali, "Exact wave solutions to the simplified modified camassa-holm equation in mathematical physics," *Aims Math*, vol. 5, no. 1, pp. 26–41, 2019.
- [20] A. Zulfiquar and J. Ahmad, "Exact solitary wave solutions of fractional modified camassa-holm equation using an efficient method," *Alexandria Engineering Journal*, vol. 59, no. 5, pp. 3565–3574, 2020.
- [21] M. A. Khatun, M. A. Arefin, M. Hafiz Uddin, and M. Inc, "Abundant explicit solutions to fractional order nonlinear evolution equations," *Mathematical Problems in Engineering*, vol. 202116 pages, Article ID 5529443, 2021.
- [22] M. Labidi and K. Omrani, "The use of variational iteration method and homotopy perturbation method for solving two nonlinear equations," *International Journal of Numerical Methods for Heat and Fluid Flow*, vol. 21, no. 4, pp. 377–398, 2011.
- [23] J.-H. He, "Homotopy perturbation method: a new nonlinear analytical technique," *Applied Mathematics and Computation*, vol. 135, no. 1, pp. 73–79, 2003.

- [24] J.-H. He, "Recent development of the homotopy perturbation method," *Topological Methods in Nonlinear Analysis*, vol. 31, no. 2, pp. 205–209, 2008.
- [25] B. S. Kashkari and S. A. El-Tantawy, "Homotopy perturbation method for modeling electrostatic structures in collisional plasmas," *The European Physical Journal Plus*, vol. 136, no. 1, p. 121, 2021.
- [26] U. Biswal, S. Chakraverty, and B. Ojha, "Application of homotopy perturbation method in inverse analysis of jeffery-hamel flow problem," *European Journal of Mechanics - B: Fluids*, vol. 86, pp. 107–112, 2021.
- [27] M. Qayyum, F. Ismail, S. I. Ali Shah, M. Sohail, E. R. El-Zahar, and K. C. Gokul, "An application of homotopy perturbation method to fractional-order thin film flow of the johnson-segalman fluid model," *Mathematical Problems in Engineering*, vol. 202217 pages, Article ID 1019810, 2022.
- [28] P. Gupta, M. Singh, and A. Yildirim, "Approximate analytical solution of the time-fractional camassa-holm, modified camassa-holm, and degasperis-procesi equations by homotopy perturbation method," *Scientia Iranica*, vol. 23, no. 1, pp. 155–165, 2016.
- [29] S. A. Khuri and A. Sayfy, "A laplace variational iteration strategy for the solution of differential equations," *Applied Mathematics Letters*, vol. 25, no. 12, pp. 2298–2305, 2012.
- [30] N. Anjum and J.-H. He, "Laplace transform: making the variational iteration method easier," *Applied Mathematics Letters*, vol. 92, pp. 134–138, 2019.
- [31] M. Nadeem and F. Li, "He-laplace method for nonlinear vibration systems and nonlinear wave equations," *Journal of Low Frequency Noise, Vibration and Active Control*, vol. 38, no. 3-4, pp. 1060–1074, 2019.
- [32] H. Zhang, M. Nadeem, A. Rauf, and Z. Guo Hui, "A novel approach for the analytical solution of nonlinear time-fractional differential equations," *International Journal of Numerical Methods for Heat and Fluid Flow*, vol. 31, no. 4, pp. 1069–1084, 2020.
- [33] K.-L. Wang, "Fractal solitary wave solutions for fractal nonlinear dispersive Boussinesq-like models," *Fractals*, vol. 30, no. 04, Article ID 2250083, 2022.
- [34] K.-L. Wang, "A study of the fractal foam drainage model in a microgravity space," *Mathematical Methods in the Applied Sciences*, vol. 44, no. 13, pp. 10530–10540, 2021.
- [35] L. Debnath, "Recent applications of fractional calculus to science and engineering," *International Journal of Mathematics and Mathematical Sciences*, vol. 2003, Article ID 753601, 30 pages, 2003.